NOTICE
PORTIONS OF THIS REPORT ARE ILLEGIBLE.
It has been reproduced from the best available copy to permit the broadest possible availability.

Distribution Categories:
Magnetic Fusion Energy (UC-20)
MFE--Fusion Systems (UC-20d)

ANL/FPP-84-1

ANL/FPP--84-1-Vol.3

DE85 005868

ARGONNE NATIONAL LABORATORY
9700 South Cass Avenue
Argonne, Illinois 60439

BLANKET COMPARISON AND SELECTION STUDY - FINAL REPORT

Contributors

D. L. Smith (ANL) G. D. Morgan (MDAC)

M. A. Abdou (UCLA)
C. C. Baker (ANL)
D. H. Berwald (TRW)
M. Billone (ANL)
W. D. Bjorndahl (TRW)
R. F. Bourque (GA)
D. A. Bowers (MDAC)
Y. S. Cha (ANL)
E. T. Cheng (GA)
R. Clemmer (ANL)
R. L. Creedon (GA)
C. F. Dahms (GA)
J. W. Davis (MDAC)
G. Deis (EG&G)[1]
J. DeVan (ORNL)
D. Diercks (ANL)
P. Finn (ANL)
A. Fischer (ANL)
J. Foley (ANL)[2]
K. Furuta (ANL)[3]
J. K. Garner (TRW)
Y. Gohar (ANL)
J. D. Gordon (TRW)
C. Gung (UCLA)
A. Hassanein (ANL)
S. Herring (EG&G)
G. Hollenberg (LLNL)
C. Johnson (ANL)
J. Jung (ANL)
T. Lechtenberg (GA)
J. D. Lee (LLNL)
R. Leonard (ANL)
Y. Y. Liu (ANL)
B. Loomis (ANL)
S. Majumdar (ANL)
R. C. Maninger (LLNL)
H. C. Mantz (MDAC)
R. F. Mattas (ANL)
I. Maya (GA)
T. J. McCarville (TRW)
R. Micich (Grumman)
B. Misra (ANL)
R. W. Moir (LLNL)
W. S. Neef, Jr. (LLNL)
B. Picologlou (ANL)
S. Piet (EG&G)
D. E. Ruester (MDAC)
R. Ryder (GA)
K. R. Schultz (GA)
A. E. Sherwood (LLNL)
K. Shin (UCLA)[4]
W. G. Steele (TRW)
D. K. Sze (ANL)
S.-W. Tam (ANL)
A. Tobin (Grumman)
P. Tortorelli (ORNL)
L. Turner (ANL)
D. Vasquez (GA)
S. Vogler (ANL)
E. Vold (UCLA)
L. M. Waganer (MDAC)
K. Wenzel (ANL)[5]
F. W. Wiffen (ORNL)
C. P. C. Wong (GA)
L. Yang (GA)
S. Yang (ANL)
M. Z. Youssef (UCLA)

September 1984

Study supported by
Office of Fusion Energy
U. S. Department of Energy

MASTER

[1]Presently with LLNL.
[2]Graduate Student, Princeton University.
[3]University of Tokyo.
[4]Kyoto University, Japan.
[5]Graduate Student, MIT.

DISTRIBUTION OF THIS DOCUMENT IS UNLIMITED

TABLE OF CONTENTS

ACKNOWLEDGMENTS

The BCSS Project gratefully acknowledges the support of A. L. Opdenaker, Program Administrator, Reactor Systems Design Branch, OFE/DOE, and P. Stone, Chief, Reactor Systems Design Branch, OFE/DOE.

The Project would also like to thank members of the BCSS Review Committee for their interest and comments during the course of the study: R. Krakowski (Chm.) (LANL), D. Cohn (MIT), C. Flanagan (W/FEDC), R. Gold (W), C. Henning (LLNL), G. Kulcinski (U of WI), R. Little (PPPL), J. Scott (ORNL), and F. Garner (HEDL).

The Project is also indebted to the management of all participating organizations, particularly C. Baker (Director, Fusion Power Program) and J. Roberts (Associate Laboratory Director) of Argonne National Laboratory, for their support and encouragement throughout the study.

We would like to acknowledge the outstanding effort of L. Ciarlette who coordinated the typing and assembly of this report and to C. Bury for administrative support. We would also like to express our appreciation to J. Ruettiger and R. Johns of ANL for their contributions to the typing of the final manuscript and to the secretarial staffs of MDAC, GA, TRW, EG&G, LLNL, and UCLA for their contributions to the typing of the report.

DISCLAIMER

This report was prepared as an account of work sponsored by an agency of the United States Government. Neither the United States Government nor any agency thereof, nor any of their employees, makes any warranty, express or implied, or assumes any legal liability or responsibility for the accuracy, completeness, or usefulness of any information, apparatus, product, or process disclosed, or represents that its use would not infringe privately owned rights. Reference herein to any specific commercial product, process, or service by trade name, trademark, manufacturer, or otherwise does not necessarily constitute or imply its endorsement, recommendation, or favoring by the United States Government or any agency thereof. The views and opinions of authors expressed herein do not necessarily state or reflect those of the United States Government or any agency thereof.

ABSTRACT

The Blanket Comparison and Selection Study (BCSS) was a two-year, multi-laboratory project initiated by the U.S. Department of Energy/Office of Fusion Energy (DOE/OFE) with the primary objectives of: (1) defining a limited number of blanket concepts that should provide the focus of the blanket R&D program, and (2) identifying and prioritizing critical issues for the leading blanket concepts. The BCSS focused on the mainline approach for fusion reactor (TMR) development, viz., the D-T-Li fuel cycle, tokamak and tandem mirror reactors for electrical energy production, and a reactor parameter space that is generally considered achievable with modest extrapolations from the current data base. The STARFIRE and MARS reactor and plant designs, with a nominal first wall neutron load of 5 MW/m^2, were used as reference designs for the study.

The study focused on:

- Development of reference design guidelines, evaluation criteria, and a methodology for evaluating and ranking candidate blanket concepts.
- Compilation of the required data base and development of a uniform systems analysis for comparison.
- Development of conceptual designs for the comparative evaluation.
- Evaluation of leading concepts for engineering feasibility, economic performance, and safety.
- Identification and prioritization of R&D requirements for the leading blanket concepts.

Sixteen concepts (nine TMR and seven tokamak) which were identified as leading candidates in the early phases of the study, were evaluated in detail. The overall evaluation concluded that the following concepts should provide the focus for the blanket R&D program:

(Breeder/Coolant/Structure)

Lithium/Lithium/Vanadium Alloy

Li_2O/Helium/Ferritic Steel

LiPb Alloy/LiPb Alloy/Vanadium Alloy

Lithium/Helium/Ferritic Steel

The primary R&D issues for the Li/Li/V concept are the development of an advanced structural alloy, resolution of MHD and corrosion problems, provision for an inert atmosphere (e.g., N_2) in the reactor building, and the development of non-water cooled near-plasma components, particularly for the tokamak. The main issues for the LiPb/LiPb/V concept are similar to the Li/Li/V blanket with the addition of resolving the tritium recovery issue. Furthermore, resolution of MHD and corrosion problems will be more severe for LiPb/LiPb/V than for the Li/Li/V; on the other hand, the LiPb blanket has reduced concerns with respect to chemical reactivity with environment. The R&D issues for Li_2O/He/FS concept include resolution of the tritium recovery/containment issue, achieving adequate tritium breeding and resolving other solid breeder issues such as swelling and fabrication concerns. Major concerns for the Li/He/FS concept are related to its rather poor economic performance. Improvement of its economic performance will be somewhat concept-dependent and will be more of a systems engineering issue.

BLANKET COMPARISON AND SELECTION STUDY

CHAPTER 7 - LIQUID METAL-COOLED BLANKET CONCEPTS

7. LIQUID METAL-COOLED BLANKET CONCEPTS

TABLE OF CONTENTS

LIST OF FIGURES FOR CHAPTER 7

LIST OF TABLES

7. LIQUID METAL-COOLED BLANKET CONCEPTS

7.1 Introduction

The liquid metal-cooled blankets for both tokamak and tandem mirror reactors are represented by two classes: (1) self-cooled system in which the same liquid metal serves as both breeder and coolant, and (2) separately-cooled liquid-metal blanket concepts in which two different liquid metals are used as breeder and coolant respectively. Preliminary evaluations of these two classes of blankets are reported in the Interim Report.[7-1] Emphasis here will be given to the self-cooled liquid-metal blankets for both the tokamak and the tandem mirror reactors.

The use of the same liquid metal as both tritium breeder and coolant greatly simplifies both materials and design considerations since the blanket requires only a structure and a breeder-coolant. Coolant-breeder compatibility/reactivity is not a factor and structure compatibility considerations are less restrictive. Heat transfer requirements are also reduced because most of the nuclear heating is deposited directly in the breeder-coolant. Lithium and LiPb both provide relatively high tritium breeding capability and tritium recovery with relatively low tritium inventory is feasible. Radiation effects on breeder are not important considerations for liquid metals. However, there are certain constraints related to the use of liquid metal in the blanket of a fusion reactor. For example, compatibility between the coolant and structural material will limit the coolant/structure interface temperature below a certain value. Pressure drop of liquid metal flow through a transverse magnetic field is much higher than that in the absence of a magnetic field. This will result in the requirement of relatively high strength structural material. These factors plus the relatively high heat (surface and nuclear heating) removal requirement make the design of the liquid-metal blanket a very challenging task.

Two liquid metals; lithium and lithium-lead (17Li-83Pb), and three structural materials: PCA, ferritic steel (HT-9), and vanadium alloy (V-15Cr-5Ti) are included in the evaluations for both the tokamak and the tandem mirror reactors. The major differences in relevant parameters between a tokamak and a tandem mirror reactor are shown in Table 7-1. It is apparent that the

design conditions are quite different for these two types of reactors. This will have significant impact on the design philosophy for the blankets.

TABLE 7-1. COMPARISON OF RELEVANT PARAMETERS BETWEEN A TOKAMAK AND A TANDEM MIRROR REACTOR (TMR)

	Tokamak	TMR
Surface Heat Flux (MW/m^2)	0.5, 1.0	0.05
First Wall Erosion Rate (mm/yr)	1.0	0.1
Magnetic Flux Density (Tesla)	7.5 (inboard)	~5.0

Summary of final rankings for various blanket concepts are presented in Section 7.2 and discussions of key factors and uncertainties generic to each concept are described in Section 7.3. Detailed descriptions of each blanket concept and justifications for the final rankings are presented in Sections 7.4 to 7.7. Analyses of special issues relevant to the self-cooled liquid-metal blanket are described in Section 7.8. Results of analysis of a liquid lithium-cooled limiter is described in Section 7.8.6. Safety concerns prohibit the use of a water-cooled limiter (reference limiter for the BCSS project) in the reactor if liquid lithium is the breeder/coolant in the blanket. So if liquid lithium is the breeder/coolant in the blanket, a lithium-cooled limiter will be assumed for the impurity control system of a tokamak reactor.

7.2 Summary of Final Rankings

Tables 7-2 and 7-3 summarize the final rankings for the self-cooled liquid-metal blankets of a tokamak reactor and a tandem mirror reactor, respectively. Detailed descriptions and justification for the ranking of each concept are presented in Sections 7.4 to 7.7. There are, however, several general observations which are quite helpful in understanding the rationales behind the rankings shown in Tables 7-2 and 7-3.

TABLE 7-2. SUMMARY OF FINAL RANKINGS FOR SELF-COOLED LIQUID-METAL BLANKET OF A TOKAMAK REACTOR

Concept	Ranking	Comments
Li/Li/V	1	Moderate design window and relatively high thermal efficiency (>40%).
Li/Li/HT-9	2A	No design window; structural temperature limit must be relaxed in order to have an attractive design; moderate thermal efficiency (~35%) can be achieved.
Li/Li/PCA	2B	No design window, structural and interface temperature limits must be relaxed simultaneously in order to have an attractive design, moderate thermal efficiency (~35%) can be achieved.
LiPb/LiPb/V	2A	No design window, this design can be attractive if the primary stress limit is relaxed, relatively high thermal efficiency (40%) can be achieved.
LiPb/LiPb/HT-9	2B	No design window, interface temperature is the most limiting factor. Both the interface and the structural temperature limits must be relaxed significantly in order to have a design window.
LiPb/LiPb/PCA	3	No design window, a mismatch between the coolant and the structural material which resulted in the most limiting interface temperature compared to other concepts.

TABLE 7-3. SUMMARY OF FINAL RANKINGS FOR SELF-COOLED LIQUID-METAL BLANKET OF A TANDEM MIRROR REACTOR

Concept	Ranking	Comments
Li/Li/V	1	A very large design window exists and relatively high thermal efficiency (>40%).
Li/Li/HT-9	1	A large design window exists and thermal efficiency can be sufficiently high (~40%).
Li/Li/PCA	2A	A moderate design window exists with moderately high thermal efficiency (~36%). Coolant ΔT is relatively small and piping cost will be high.
LiPb/LiPb/V	1	A large design window exist and thermal efficiency is high (>40%). Tritium containment may be a problem.
LiPb/LiPb/HT-9	2B	No design window, both the structural and the interface temperature limits have to be relaxed in order to have an attractive design.
LiPb/LiPb/PCA	3	No design window, a mismatch between the coolant and the structural material which resulted in the most limiting interface temperature compared to other concepts.

(1) From engineering design point of view, the blanket concepts of a TMR are ranked higher than those of a tokamak reactor. This is the result of lower surface heat flux, lower erosion rate of the first wall, and lower magnetic flux density of TMR compared to that of tokamak reactor.

(2) For the same structural material, a blanket using lithium as the coolant/breeder always has a larger design window than a blanket using lithium-lead as coolant/breeder. This is the result of relatively poor thermo-physical properties of lithium-lead and poor compatibility between the structural material and lithium-lead compared to lithium.

(3) The predicted structural temperature limit in a radiation environment and the coolant/structure interface temperature limit for the vanadium alloy is less restrictive than that of either ferritic steel or the PCA.

7.3 Key Factors

7.3.1 MHD Analysis

Because of the modest margins between allowable and calculated material stresses for the tokamak liquid metal blankets, the feasibility of the proposed designs depends heavily on the margin of error of the MHD pressure drop calculation. Although further improvements of the blanket can increase the design margin, the fact remains that if the pressure drop is underestimated by 20-50% the material stress cannot be maintained within allowable limits. This is because increasing the material thickness to reduce the stress will result in a further increase of the pressure. Current understanding of high interaction parameter, high Hartmann number MHD phenomena and the available data basis does not point in the direction of such large errors in the pressure estimates. Nonetheless, such errors cannot be strictly ruled out. Whereas there is little doubt that MHD analysis is highly reliable for single, straight conduits in uniform or slowly varying magnetic fields (as is the case of the tokamak field), analytical or experimental information concerning the rather complex manifolding arrangement of the tokamak design is insufficient for reliable prediction. For this reason the manifolding was designed on the basis of qualitative arguments and with a lack of detail commensurate with the lack of hard facts on MHD flows in such complex geometries. Thus the manifold

design should not be viewed as final. There is certainly room for improvement in this area in the future as more information becomes available.

When increased understanding of the associated phenomena is achieved and a more detailed design of the manifold, based on this understanding, is completed, the adequacy of the manifold design should still be verified by experiment, since it is highly unlikely that a realistic detailed analysis can be carried out for such a complex geometry. This, of course, is not peculiar to MHD analysis. Even in the absence of a magnetic field the fluid flow in the manifold cannot be fully treated with an analytical or numerical scheme. It should be pointed out that meaningful testing can only be carried out after a reasonable understanding of the phenomena involved is reached. Without such an understanding, if a manifold test vehicle exhibits excessive pressure drops, no rational decision for improving performance can be made.

The possibility that the pressure drop will be excessive, even with the best possible manifold design, cannot be eliminated at present. If this proves to be the case, an obvious and effective remedy of the situation is to use laminated insulated structures throughout most of the blanket, with the exception of the first wall. The use of laminated insulated structures and/or insulating coatings appears, as discussed elsewhere in this report, technically feasible. The use of laminated structures not only will result in smaller overall pressure drops but, what is more important, will make containment of even much higher pressures than those currently estimated easy to accomplish. In essence, the use of laminated structures changes the question of feasibility to that of efficiency. Also, the MHD pressure drop can be reduced by making the blanket thicker, at some economic penalty.

Use of laminated structures will also remove an additional uncertainty of the MHD analysis. Namely, the possibility of an increased pressure drop resulting from eddy current interaction between different parts of the blanket. The possibility of such interaction presents itself in the tokamak design because of the many changes of the direction of the flow relative to the magnetic field. Detailed analysis of such interaction is a formidable task because it may involve a large number of conduits whose flow distributions and pressure gradients are mutually coupled through currents flowing both in the liquid metal and the conducting walls. Such an undesirable interaction can realistically be substantiated and evaluated only through appropriate testing

of rather complex models of blanket segments. It is best that such interactions be minimized through appropriate design changes and use of insulators.

Most of the MHD pressure drop is proportional to the square of the magnetic flux intensity. As a result, the MHD problem depends strongly on the magnetic flux density. If future developments indicate a higher value for β, and thus a lower magnetic flux density, the problem of high pressures resulting from MHD interaction will be alleviated.

The discussion on the uncertainties in the MHD analysis is valid for both the tokamak and the tandem mirror designs. However, the configuration and the smaller design window margins for the tokamak reactor make the possibility of significant deviations from predicted behavior larger and the implications of such deviations more severe.

7.3.2 Thermal Hydraulics

The maximum structural temperature, the maximum structure/coolant interface temperature, and the temperature gradients in the first wall and blanket are all determined from thermal-hydraulic analysis. The accuracy of the thermal-hydraulic analysis is, therefore, critical to the design of the liquid-metal blankets. The uncertainty in heat transfer calculations comes primarily from the uncertainty in velocity profile in the blanket. In the heat transfer analysis described in Section 7.8.2, it was assumed that the velocity in the coolant channel is uniform as a result of the interaction between the liquid metal and the transverse magnetic field. Deviations from this assumption are likely as a result of either 3-dimensional effect or the complex geometry (especially for the blanket of of a tokamak reactor). It is also possible that secondary flow may be induced by the strong temperature gradient in the blanket. This may also have a significant impact on the heat transfer calculations. Finally, local hot spots due to flow mal-distribution could be a potentially serious problem. All of these problems must be resolved through experimental as well as analytical investigations before the uncertainties in heat transfer calculations can be reduced and before the design can be considered feasible.

It should be emphasized that although large uncertainties exist for the heat transfer analysis of a liquid-metal blanket, it does not necessarily mean that all uncertainties will have a negative effect on current design ranking.

For example, if secondary flow exists in the blanket, it will greatly improve heat transfer and thus reduce the maximum interface and structural temperatures.

The previously described uncertainties in thermal hydraulics are generic for both the tokamak and the tandem mirror reactors. The primary difference between the design of a tokamak reactor and that of a TMR is the blanket geometry. The blanket geometry of the tokamak reactor is apparently more complex than that of the TMR. This, plus the fact that the design window of the blanket (the size of which is an indication of the flexibility of the blanket in accommodating uncertainties in design calculations) of a tokamak reactor is, in general, smaller than that of a TMR, seems to imply that the feasibility of the blanket of a tokamak reactor is more at stake than that of a TMR. This suggests that future research and development effort should emphasize more towards tokamak reactors.

7.3.3 Stress Analysis

In order for any of the tokamak first wall designs to withstand a high surface heat flux and a high erosion rate, the first wall will very likely have to be grooved. There are a lot of uncertainties as to whether such a design will work. The crack growth analysis for the first wall reported here is based on assumed properties of vanadium which need to be verified by crack growth testing. The effect of radiation on material properties is also a concern. Detailed discussion of this issue is presented in Section 7.7.

The lithium cooled reference tokamak blanket has a complex geometry. Although an effort has been made in the present study to simulate some of the complexities by treating the first wall as part of a composite anisotropic plate, a detailed finite element analysis will be necessary to verify the simplified analysis, particularly near the ends because all end effects have been ignored in the present analysis. Similarly, a detailed global structural dynamics analysis will be needed to verify the ability of the design to withstand dynamically applied loadings due to plasma disruptions and seismic events and also to help design suitable supports for the blanket. Preliminary analysis of the inboard blanket has shown that in order to keep the bending stresses during a plasma disruption within allowable limits, one or more radial supports will be needed at the inboard vertical wall to carry a radial

force (directed towards the plasma) of 12MN per sector. Since space is at a premium at the inboard wall, a potential structural design problem will be to provide these supports together with adequate attachments to the shield. The problem is complicated by the fact that these forces are directed away from the central post of the reactor and not towards it. Hence an active rather than passive system of restraints will be required to hold the sectors in position. A final key factor for the liquid metal cooled designs, which was discussed in detail in the Interim BCSS Report, is the coupling between the MHD pressure drop and the primary stress in the manifold side walls. A possible decoupling between these two by using insulators would greatly enhance the attractiveness of the liquid metal cooled design.

The reference TMR blanket is relatively easy to analyze because of its axisymmetric geometry. It is also stressed much less severely than the tokamak blanket because the pressures and temperature gradients are smaller. However, since the actual geometries are not complete ring and the manifolds are assumed to provide the necessary ring continuity, the junction between the various zones and the manifold will need careful design. The only concern raised by the present analysis is that the 17Li-83Pb cooled design does not meet the conservative seismic stress criterion used in the study, particularly in the thin walled 8 cm outside diameter regions of the front tube where it is attached to the manifold at the top and bottom of the blanket. A detailed structural dynamics analysis will be needed to verify the ability of the design to meet the seismic requirements.

7.3.4 Neutronics

Four key neutronics issues for the liquid metal-cooled blanket concepts require future effort to assess their impacts on the blanket performance; uncertainty in kinetic energy release in material atoms (kerma) and nuclear heating profiles, neutrons and photons streaming through the lithium or lithium-lead manifolds and between reactor segments, blanket heterogeneity, and tritium breeding ratio changes resulted from the temperature distribution profiles.

Thermal hydraulics, stress analysis, and MHD analyses need an accurate prediction of the nuclear responses in each reactor component. The main nuclear responses are the nuclear heating, the tritium breeding, the gas produc-

tion, and the atomic displacement. The evaluation of these responses require accurate nuclear response functions. MACKLIB-IV[7-2] generated from ENDF/B-IV has served this function since 1978 for the national fusion program and other applications as well. However, due to cross section measurements over the last ten years and major corrections in the nuclear data, an updated ENDF/B-V version was developed to serve as a data base for the national fusion and fission programs. This version of ENDF/B has major changes for many key fusion elements which will have a strong impact on the kerma factors required for the nuclear heating profiles and the tritium breeding ratio. For example, the major updates in the photon production data and the new cross section evaluations for Fe, Ni, Mn, Cr and Pb will change nuclear heating profiles and neutron multiplication significantly. A generation of a new response library for fusion activities is strongly recommended to reduce the uncertainty and overall device cost by allowing less design conservatism.

Lithium and lithium-lead are not good shielding materials, for example, the neutron leakage from one meter lithium zone is half neutron per DT neutron source. This high level of leakage is expected to occur through the blanket manifolds which reduces the blanket tritium breeding ratio, increases the radiation damage and heat load in the superconductor coils, and the dose equivalent in the reactor building. A comprehensive analysis is needed to assess impacts on reactor designs and identify design solutions.

Lithium and lithium-lead blanket designs depend on the reflector zone to achieve the required performance, tritium breeding ratio and energy multiplication, which has a large volume fraction of solid reflector material. This leads to a heterogenous reflector zone which has different characteristics from the homogenous reflector analyzed in the different blanket concepts. Also, the segmentation of the reactor torus through the use of "pie-shaped" segments for tokamaks or cylinder segments for mirrors results in streaming problems which reduces the blanket performance, causes shielding problems, and hot spots in the structure materials and superconductor coils. These types of heterogeneities require detailed analyses to predict the blanket performance and develop blanket design solutions for such problems.

The temperature distribution has an effect on the nuclear cross section (Doppler effect) and the material density. Such changes need to be taken into consideration in the neutronics analyses to reduce the uncertainty in the blanket tritium breeding ratio and nuclear heating profiles.

7.3.5 Tritium Recovery

7.3.5.1 Tritium Recovery from 17Li-83Pb

There are no experimental results available to varify the tritium recovery scheme presented in Section 7.8.5.1. Although the theory is correct, the material properties used, such as the diffusivity of tritium in 17Li-83Pb, the resistance due to the surface recombination effect are highly uncertain. The effect of isotope, without which the purge gas flow rate will be just too high to be realistic is critical to the validity of the recovery concept. The assumed isotope effect has yet to be verified.

The tritium recovery concept is critical to the viability of the self-cooled 17Li-83Pb blanket. If the tritium partial pressure is $\sim 10^{-2}$ Pa, as was the case for the MARS design, the tritium containment problem may not be solvable. It should be noted that some of the problems encountered here are generic problems in some other blanket.

The uncertainty of the tritium recovery scheme is associated with the ability to reduce the tritium partial pressure to such a low level that containment can be accomplished. The only way to resolve this issue is by experiments. The tritium inventory is not an issue because it will certainly be low.

7.3.5.2 Tritium Recovery from Lithium

It has been demonstrated experimentally that molten-salt extraction of tritium from liquid lithium is a feasible process. The distribution coefficients of tritium between the lithium and the salt are favorable and other chemical and mechanical considerations do not indicate any serious constraints. Although the efficiency factor that accounts for nonequilibrium tritium distribution during the mixing process is not yet known, it is believed that values as high as 50% could be easily achieved. However, a potentially serious problem with the molten salt extraction scheme is the solution of the LiF, LiCl, and LiBr in liquid lithium. These dissolved halides, if transported back to the blanket region, would adversely affect both the corrosion characteristics and radioactivity of lithium. Solubility data of different halides in lithium, and the resulting effect of these

halides transported back to the blanket on the overall blanket neutronic performance and on the long-lived radioactive-isotope production need to be studied carefully and resolved before final approval of using molten-salt to extract tritium from liquid lithium. Another tritium recovery method based on yttrium adsorption has also been verified experimentally on laboratory scale.

7.4 Tokamak R=1 Concepts

The only concept that is ranked No. 1 in the liquid-metal cooled blanket of a tokamak reactor is the self-cooled, liquid-lithium blanket with vanadium alloy as the structural material (Li/Li/V). This section summarizes the mechanical design, the integral analyses, and the design parameters of this concept.

7.4.1 Mechanical Design

Mechanical design depends on factors such as system maintainability, reliability, and fabrication. It also depends strongly on the various constraints imposed from neutronic, thermal hydraulic, MHD, structural and material consideration. For the self-cooled liquid-metal blanket of a tokamak reactor, a number of design options were considered and reported in the Interim Report.[7-1] The advantages and disadvantages of each design were discussed. The toroidal/poloidal flow configuration was selected as the reference design. A schematic of such a design is shown in Fig. 7-1. This reference design is composed of slightly slanted poloidal manifolds and relatively small toroidal channels. Each manifold supplies a number of toroidal channels. The toroidal channels are exposed to both the surface heat flux and the relatively high nuclear heating rate, while the poloidal manifold is heated mainly by nuclear heating. The poloidal manifold is protected by the toroidal channels both thermally from the surface heat flux and structurally from radiation damage. A large cross-sectional area is maintained for the poloidal manifold to keep the velocity low which will reduce the MHD pressure drop through the manifold. Since the pressure drop through the manifold is the single largest pressure drop of the entire blanket, its reduction will significantly reduce the overall pressure drop of the blanket. A second advantage of the toroidal/poloidal flow blanket is that the the walls of the poloidal manifold can take higher stress (primary and thermal) levels than the first wall since the former is not exposed to the surface heat flux and receives less radiation

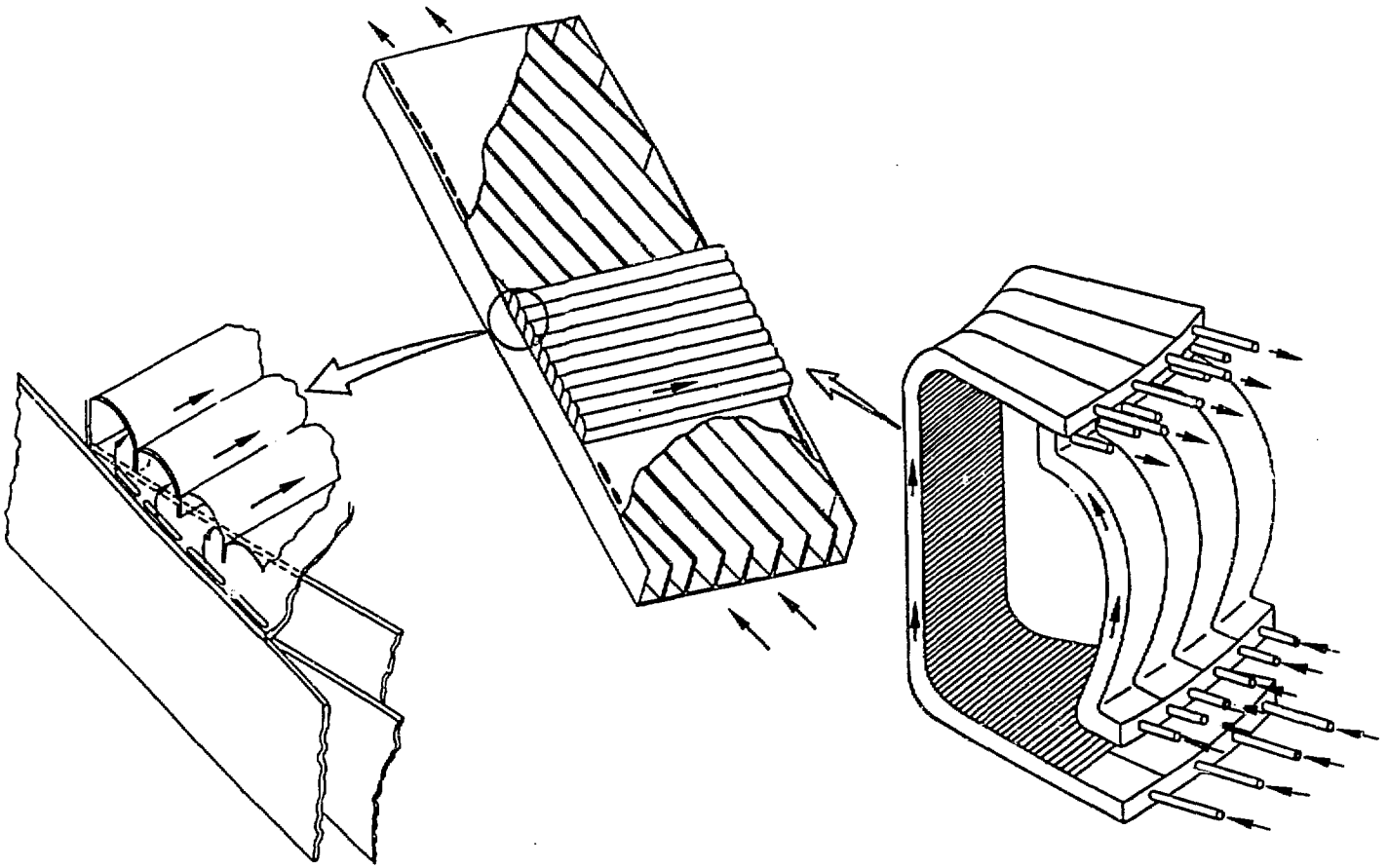

Figure 7-1. Reference design for the self-cooled liquid-metal blanket (poloidal/toroidal flow) of a tokamak reactor.

dosage than the latter. The first wall is cooled by the coolant flowing through the small toroidal channels which are parallel to the toroidal magnetic field. The flow in the toroidal channels is perpendicular to the poloidal field which is much smaller than the toroidal field. Thus, the velocity in the toroidal channels can be increased considerably over that in the poloidal manifold without increasing significantly the overall pressure drop through the blanket. It is this relatively high velocity in the toroidal channels (compared to the velocity in the manifold) and the relatively short length of the toroidal channels (compared to the full length of the manifold in the poloidal direction) that could reduce the maximum structure and interface temperatures to an acceptable level.

Figure 7-2 shows the cross-sectional view of the toroidal/poloidal flow blanket. The blanket can be divided into three regions in the direction, i.e., the toroidal channels, the poloidal manifolds, and the reflector. The partitions shown in Fig. 7-2 are not partitions for coolant flow. These partitions are perforated plates and thus there is communication between the manifold and the reflector regions. Therefore, pressure drops are the same in the manifold and the reflector region. In the thermal-hydraulic and MHD analyses, no distinction was made between the manifold and the reflector. The full cross section for coolant flow is utilized for heat removal. At the back of the blanket, a 4 cm thick structure is provided for additional high-temperature shielding and structural support. In this region, the nuclear heating rate is relatively low and the temperature of the reflector material, which is the same as the structural material, can be maintained at the acceptable level by the coolant flow.

In the current design, the outboard is geometrically similar to the inboard blanket. The only difference is that the overall blanket thickness in the radial direction is 84 cm for the outboard blanket, while it is 64 cm for the inboard blanket (including the high temperature shield).

7.4.2 Integral Analysis and Design Window

Once a reference design is selected, as shown in Fig. 7-1, various analyses described in Section 7.8 are performed. However, each analysis may not be independent of the other analyses, since common parameters exist among them. For example, the coolant inlet and exit temperatures are common parameters between MHD and heat transfer analyses. These two parameters also

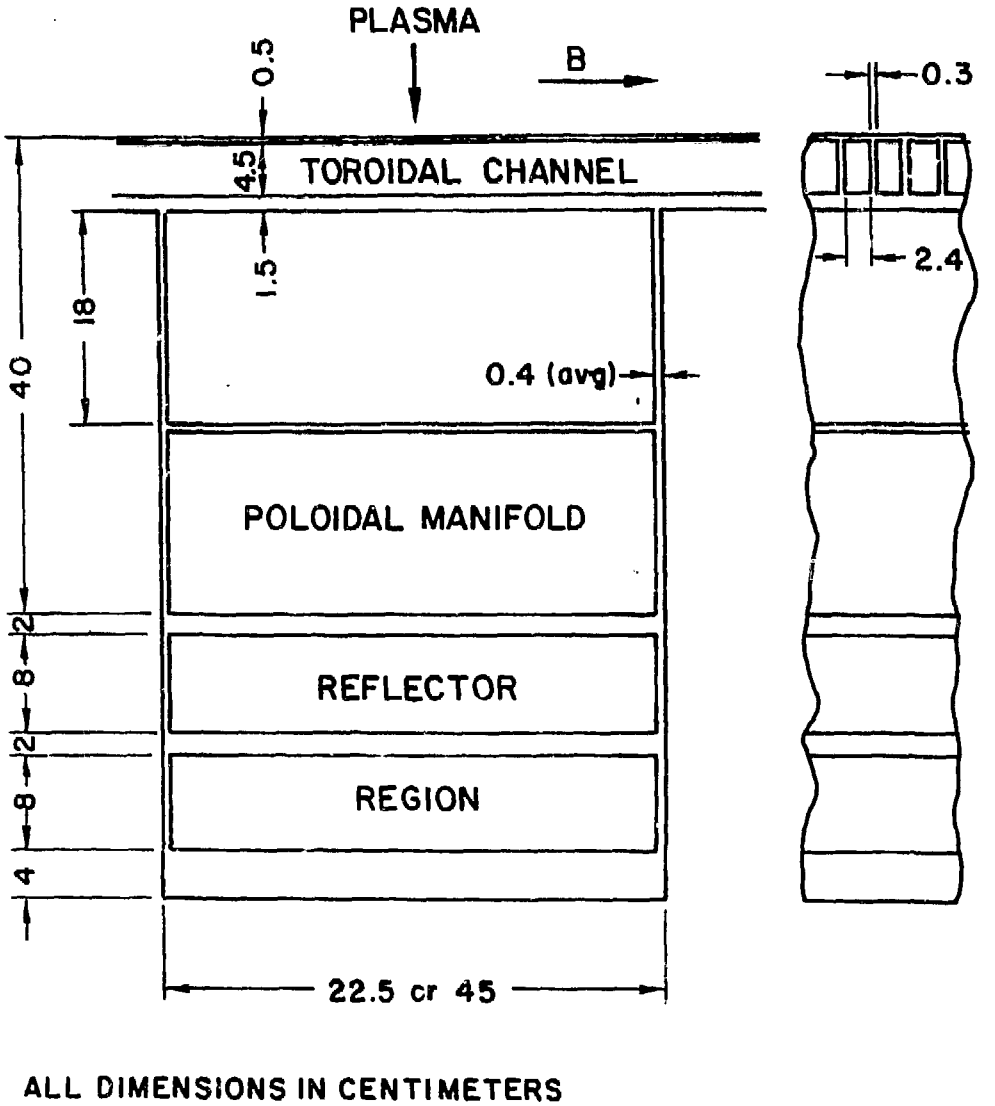

Figure 7-2. Cross-sectional view and dimensions of the toroidal/poloidal blanket.

affect the thermal efficiency of the plant. Another example is that the temperature distributions in the first wall and the blanket affect the thermal stress and the MHD pressure drop affects the primary stress in the structural material. A summary of the relations among various calculations is shown in Fig. 7-3, which includes heat transfer, MHD, stress, and power conversion analyses as well as corrosion and structural temperature limitations. Neutronic and tritium recovery calculations, although are not included in Fig. 7-3, are not independent of the various analyses shown in Fig. 7-3. They, nevertheless, can be conveniently addressed separately. Neutronic analysis depends on the coolant/structure fractions in the blanket and provides input (nuclear heating rate distributions) to heat transfer calculations. Tritium recovery has a strong impact on safety analysis and can usually be addressed separately.

A convenient and quite useful way of expressing the relations among various calculations (Fig. 7-3) is shown in Fig. 7-4, in which the limitations from various analyses are expressed in terms of two common parameters, the average coolant temperature rise through the blanket (ΔT_b) and the average coolant temperature at the outlet of the blanket (T_{out}). The limits shown in Fig. 7-4 are obtained by converting the results of those analyses described in Section 7.8 into the two common variables ΔT_b and T_{out}. The arrows in Fig. 7-4 indicate the regions of acceptable operation for each individual limitations imposed on the blanket. The shaded area in Fig. 7-4 represents the design window for this particular situation (surface heat flux of 0.5 MW/m^2 and first wall thickness of 5 mm). Any point within the design window is acceptable and will not violate the constraints imposed by the various analyses shown in Fig. 7-4.

There are a total of five different constraints shown in Fig. 7-4 and these limitations will be briefly explained below. The primary stress limit is the result of MHD pressure drop and the hoop stress in the duct. For the reference design of the tokamak reactor, the maximum stress with respect to the allowable stress occurs in the manifold at the inlet of the blanket. The higher the average coolant temperature rise through the blanket (ΔT_b), the lower the coolant average velocity and thus the lower the pressure drop through the blanket. The pinch point limit is calculated by assuming a pinch point $\Delta T > 20°C$ in the steam generator. With a small coolant temperature rise (ΔT_b), the pumping power becomes excessive since both volumetric flow rate and

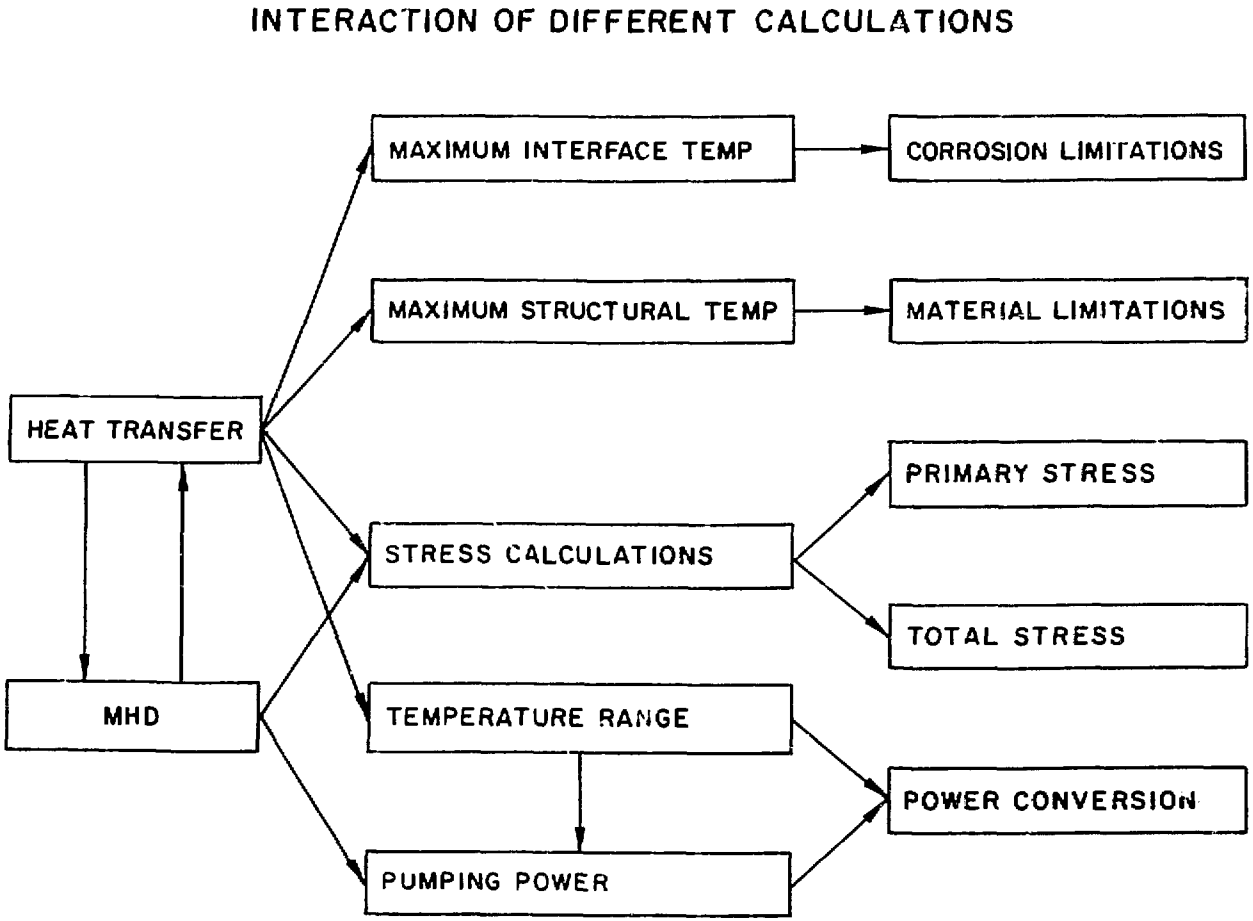

Figure 7-3. Relation among various calculations.

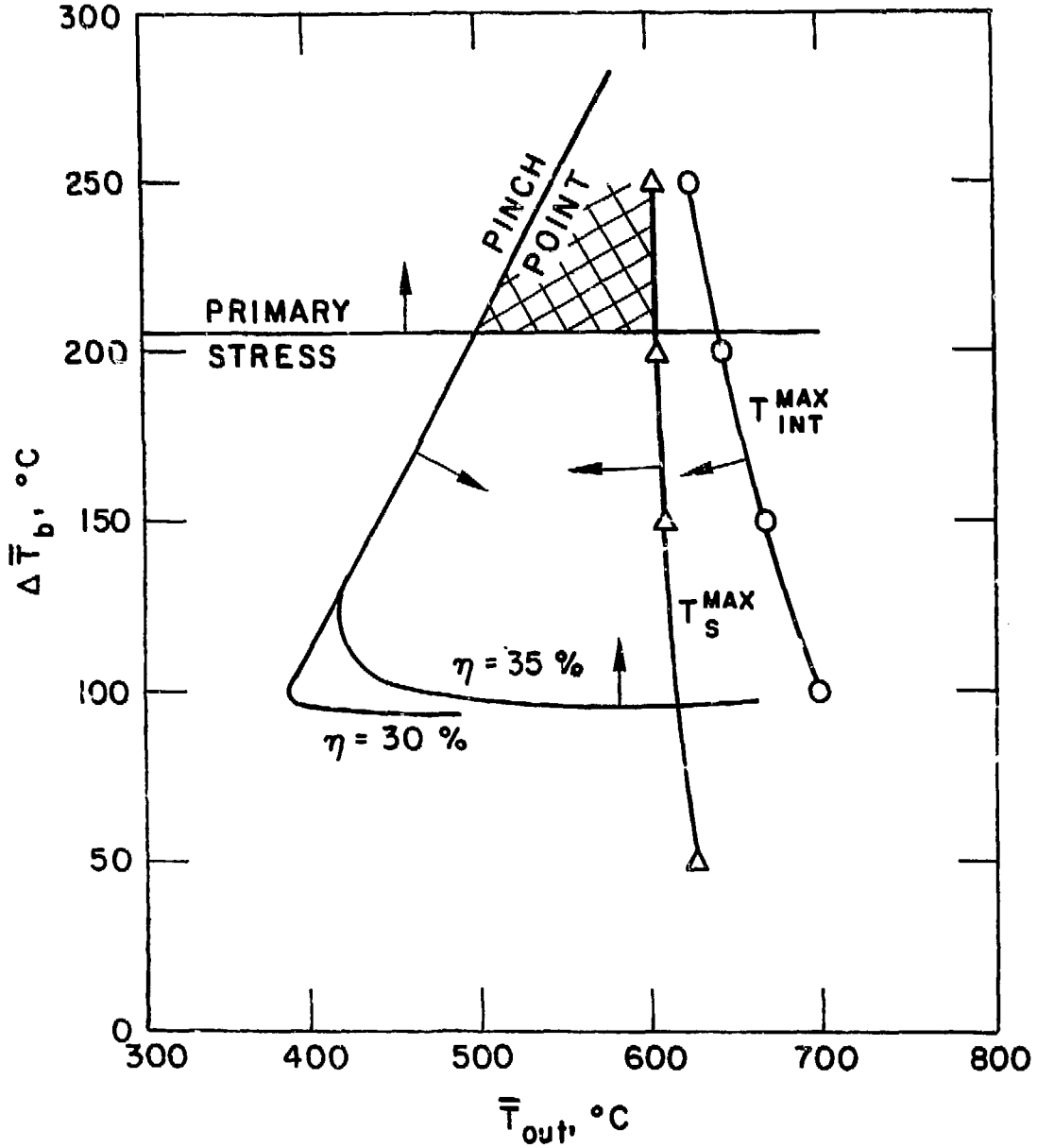

Figure 7-4. Design window for a vanadium structure, Li cooled blanket with a surface heat flux of 0.5 MW/m^2 and a first wall thickness of 5 mm.

pressure drop are inversely proportional to ΔT_b. Since coolant pumping power is directly proportional to the coolant flow rate and pressure drop, pumping power becomes a significant fraction of thermal power and the thermal efficiency decreases sharply at relatively low ΔT_b as shown in Fig. 7-4. The maximum structure (T_s^{max}) and coolant/structure interface (T_{INT}^{MAX}) temperature limits are derived from the heat transfer calculations described in Section 7.8.2. The maximum allowable temperature for vanadium alloy is 750°C as is the maximum allowable interface temperature between vanadium alloy and liquid lithium.

There are several important implications which are made evident by examining the results shown in Fig. 7-4:

(1) The relative size of the design window is an indication of the flexibility of the design in accommodating the uncertainties in various calculations. A designer can choose a design point (within the desing window) that will optimize among thermal efficiency and uncertainties associated with various analyses. This will become more clear when a design point is selected for the reference design of the tokamak reactor (Section 7.4.3).

(2) It is immediately evident from Fig. 7-4 which factors are more limiting than others and where improvement can be made, as far as the design is concerned. For example, in the particular case shown in Fig. 7-4 (q = 0.5 MW/m^2 and t_w = 5 mm), the maximum structural temperature is certainly more limiting than the maximum structure/coolant interface temperature. It is also obvious that thermal efficiency is not of major concern here whereas the primary stress is the limiting factor as far as ΔT_b is concerned. Thus, immediate improvement of the design should come from factors that affect primary stress and maximum structural temperature.

Figure 7-5 shows the results of the integral analyses for the Li/Li/V blanket of a tokamak reactor with a surface heat flux of 1 MW/m^2 and a first wall thickness of 2 and 3 mm. It is obvious that the maximum structure temperature (750°C), the primary stress, and the pinch point are the more limiting factors. The thermal efficiency limit is not shown in Fig. 7-5 since

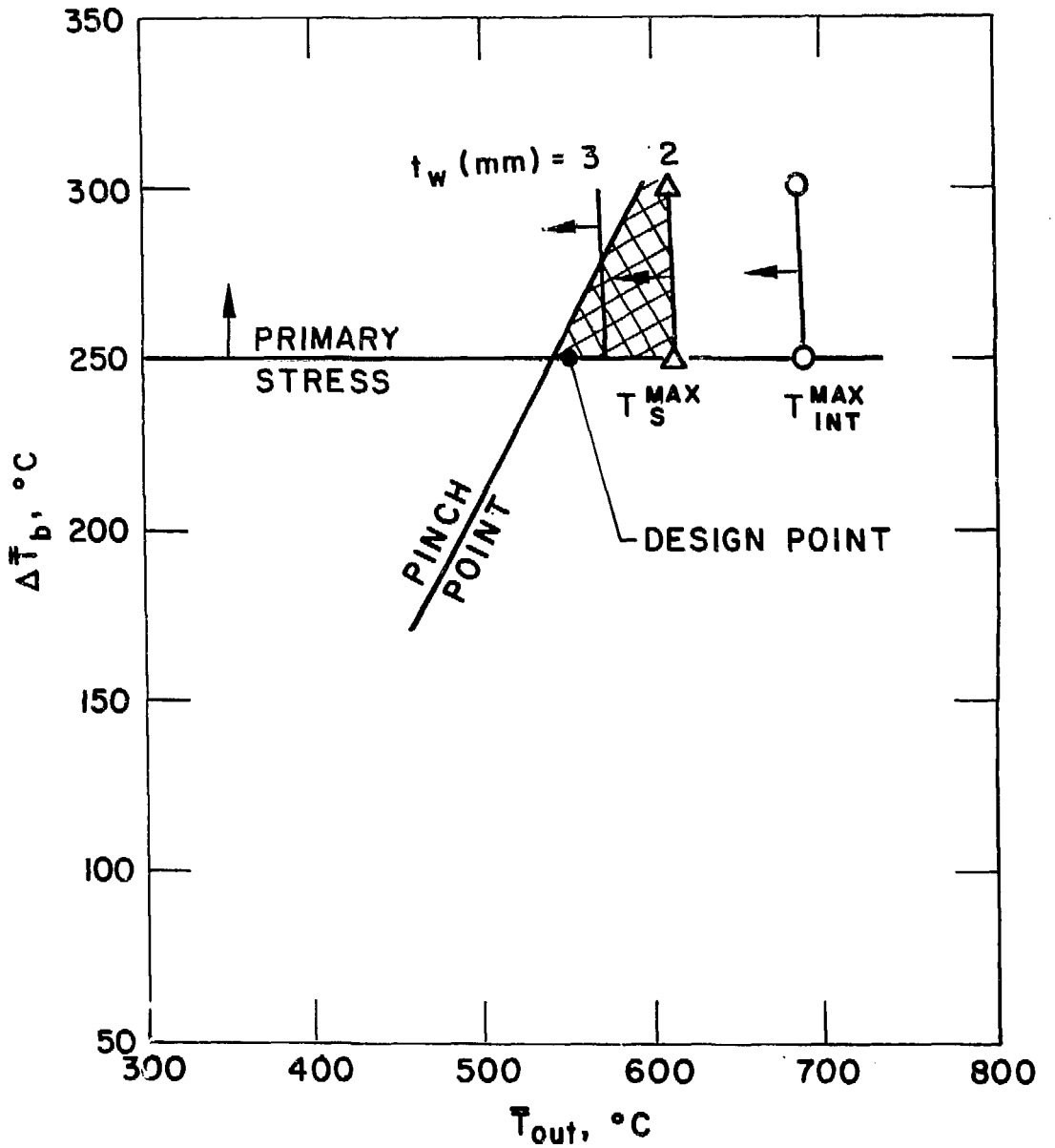

Figure 7-5. Design window for the Li/Li/V_2blanket of a tokamak reactor with a surface heat flux of 1 MW/m^2.

it is far below the limit imposed by the primary stress. There is a moderate design window if the first wall is 2 mm thick. The size of the window decreased somewhat if the thickness of the first wall is increased to 3 mm. MHD and stress calculations indicate that a minimum of 250°C is required for ΔT_b, as shown in Fig. 7-5.

Figure 7-6 shows the result of a Li/Li/V blanket with a surface heat flux of 1.2 MW/m^2. It is seen that a design window exists when the first wall is 2 mm thick. However, if the thickness of the first wall is increased to 3 mm, a design window no longer exists.

Two other types of stress calculations (see Section 7.8.3) although not shown in Fig. 7-5, need to be performed for a particular design. The first one is the bending stress in the walls of the toroidal channel (including the first wall) as a result of coolant pressures in the manifold and the toroidal channels. The results of these calculations indicate that a minimum thickness of 3 mm is required for the first wall. Figures 7-5 and 7-6 indicate that a design window exist for q = 1 MW/m^2 and the design window disappears for q = 1.2 MW/m^2 if the first wall thickness is 3 mm. The second calculation refers to the thermal stress in the first wall and blanket, which depends primarily on the radial temperature gradient from the manifold to the first wall. For vanadium structure, the thermal stress is well within the allowable limit (see Sectio 7.8.3).

The erosion rate of the first wall of a tokamak reactor is 1 mm per year. Since stress consideration requires a minimum thickness of 3 mm, the first wall thickness must be 6 mm at B-O-L (Beginning of Life) in order to have a three-year life. However, Fig. 7-5 indicate that a 6 mm first wall is not acceptable. The remedy is to use grooved wall which is discussed in detail in Section 7.7. For the reference design of the tokamak reactor, the first wall is assumed to be grooved and is 6 mm at B-O-L and 3 mm at E-O-I (End of Life). The maximum vanadium temperature for a 6 mm thick first wall is ~850°C which is well below the melting point of vanadium alloy (1866°C).

7.4.3 Design Summary

Based on the mechanical design and the integral analyses described previously, a desigr point can be selected. Such a point is shown in Fig. 7-5 and corresponds to the following conditions.

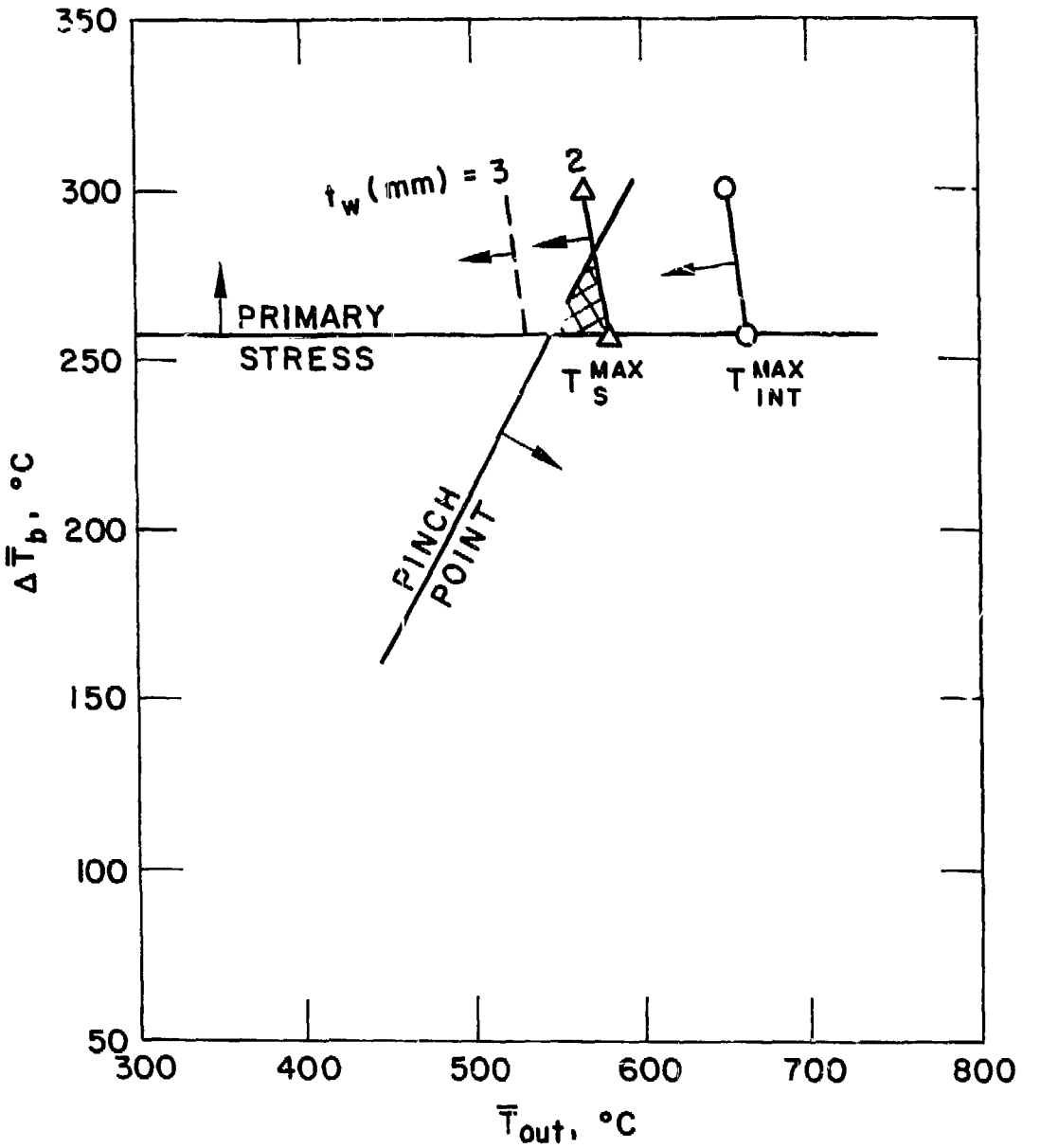

Figure 7-6. Design window for a Li/Li/V blanket of a tokamak reactor with a surface heat flux of 1.2 MW/m^2.

Surface heat flux	1 MW/m^2
First wall thickness	
at B-O-L (grooved)	6 mm
at E-O-L	3 mm
Average temperature rise through coolant	250°C
Average blanket outlet temperature	550°C

Based on these values, other parameters such as pressure drop, coolant flow rate, maximum structure temperature, maximum coolant/structure interface temperature, thermal efficiency, etc.; can be obtained from the results of the analyses described in Section 7.8. A summary of all the major parameters and features of the reference design of the blanket of tokamak reactor is listed in Table 7-4.

The choice of the design point shown in Fig. 7-5 is the result of the relatively large uncertainties in heat transfer calculations compared to other calculations. As described previously, any point within the design windown shown in Fig. 7-5 represent an acceptable design. The margins in maximum structural temperature and maximum coolant/structure interface temperature are the largest by choosing the lowest ΔT_b allowable. The primary stress limit shown in Fig. 7-5 is obtained by considering the allowable stress which already included some safety margin. The heat transfer calculations do not provide any margin of safety and this is the primary reason that the design point is selected right on the boundary of stress limit as shown in Fig. 7-5. For similar reasons, the blanket outlet temperature is selected to be on the lower end of the window. The outlet temperature of 550°C also satisfies the corrosion temperature limit for ferritic steel which is selected as the structural material outside the magnet for economic considerations. The thermal efficiency is fairly high (~42%) anywhere within the design window and thus is not a determining factor for this particular concept.

TABLE 7-4. KEY PARAMETERS FOR A Li/Li/V BLANKET OF A TOKAMAK REACTOR

Neutral Wall Load	5 MW/m^2
FW Surface Heat Flux	1 MW/m^2
Coolant Inlet/Outlet Temperature	300°C/550°C
Maximum Pressure	3.0 MPa
Coolant ΔP	2.85 MPa
Maximum Structural Temperature	690°C
Maximum Coolant/Structure Interface Temperature	610°C
Tritium Breeding Ratio	1.31
Blanket Thickness	
Inboard	0.64 m
Outboard	0.74 m
Coolant Flow Rate	
Inboard	5.9×10^6 kg/h
Outboard	1.4×10^7 kg/h
First Wall (Grooved)	
Erosion Rate	1 mm/y
Thickness at Beginning of Life	6 mm
Thickness at End of Life	3 mm
Calculated Life	3 years
Gross Thermal Efficiency	42.3%

7.5 Tandem Mirror R=1 Concept

The methodology used to rank the TMR blankets are identical to that for tokamak. The results of the calculation are used to establish a design window, from which a set of operation parameters can be selected. Since the methodology is the same, the discussion here is abbreviated. There are three coolant and structural material combinations to be rated R=1 as shown in Table 7-5. The reasons that the TRM has more candidates than the tokamak in number 1 ranking are the lower magnetic field and low surface heating load. Therefore, both MHD and heat transfer problems are less severe.

TABLE 7-5.
COOLANT MATERIAL COMBINATIONS FOR P=1 SELF-COOLED LIQUID METAL CONCEPT FOR TMR

Blanket Structure	Coolant/Breeding Material	Thermal Loop
V	Li	Ferritic Steel
Ferritic Steel	Li	Ferritic Steel
V	17Li-83Pb	Ferritic Steel

The reference design of the TMR blanket is similar to that of WITAMIR-1[7-3] and MARS design[7-4]. It is judged by the design team that the simplicity of the configuration outweighted some of the drawback such as large void fraction in the blanket and poor first wall heat transfer characteristics. However, if the first wall surface heat flux is considerably higher than 5 W/cm^2, the blanket configuration will have to be modified.

The cross-sectional views of the reference design of the self-cooled liquid metal blankets are shown on Figs. 7-7 and 7-8. The blanket basically consists of banks of tubes, which are bent to follow the contour of the circular plasma in the central cell. A single header feeds the coolant/breeding material (Li or 17Li-83Pb) to the manifold. The coolant flows through the blanket and reflector, into the exit manifold and exit through a single exit header. The coolant velocities in the tubes and reflector can be controlled by using different tube wall thicknesses which resulted in uniform radial temperature distribution within the blanket at any azimuthal angle.

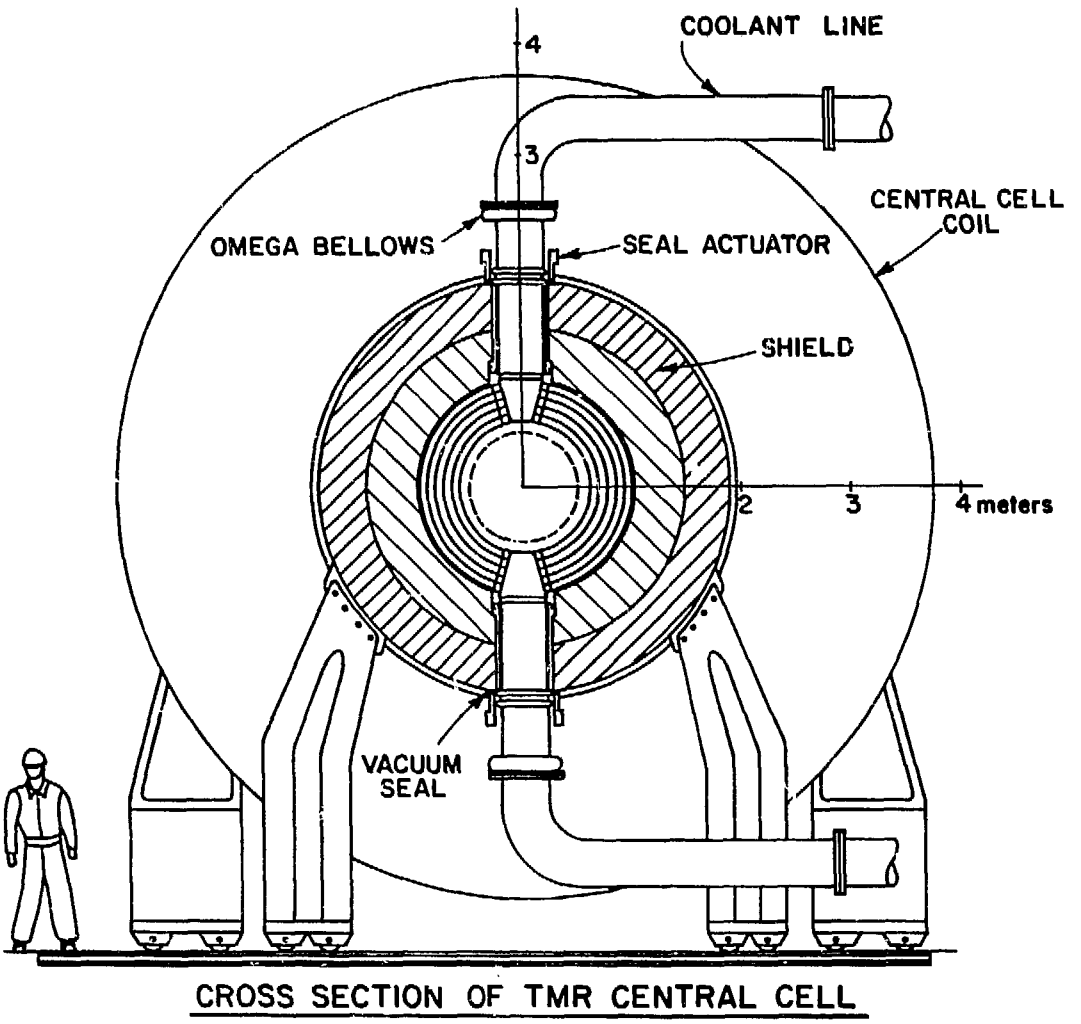

Figure 7-7. Cross-section of TMR central cell.

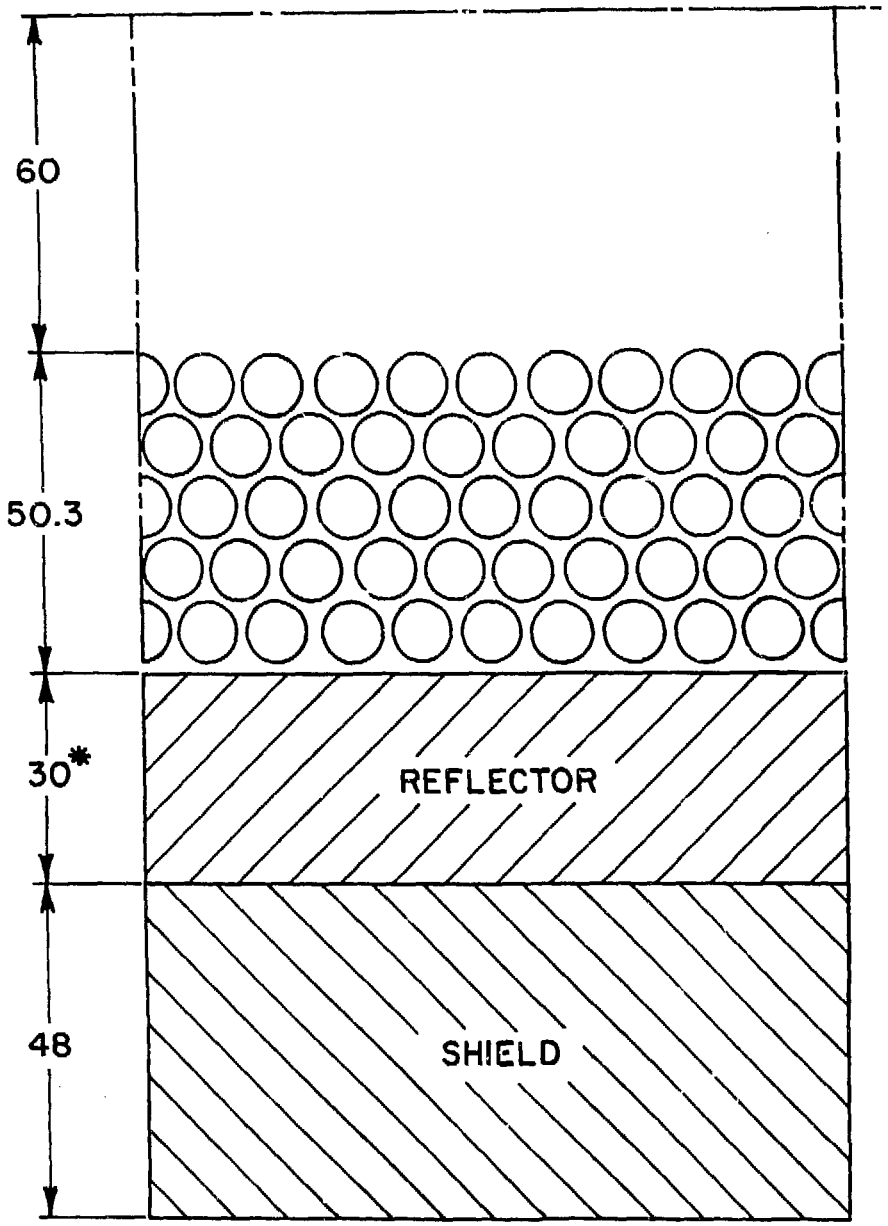

Figure 7-8. Horizontal section of TMR central cell.

The neutronic design of the blanket is a tradeoff between tritium breeding ratio, blanket energy multiplication, lithium enrichment and blanket thickness. The design goal of the tritium breeding ratio is set at 1.2, although this value can be increased significantly, if required. For lithium breeding, no enrichment is needed. For the 17Li-83Pb system, it was found that high enrichment is very costly due to the large 17Li-83Pb inventory in the piping system.[7-4] Therefore, 30% enrichment is used with a relatively thick blanket.

The effect of MHD, heat transfer and stress problems are closely related. The dominant force on a conducting fluid moving across a magnetic field lines is the MHD effects generated by $\vec{V} \times \vec{B}$, which increases the pressure drop and retards heat transfer by suppressing turbulence. The consequences of the relatively large pressure drop are higher blanket pressure and higher pumping power. The methodology of calculating the MHD pressure drop has been discussed in the interim report[7-1] and summarized in Section 7.8.1. The heat transfer problem in the blanket is simplified by the fact that velocity is always perpendicular to the magnetic field. The velocity profile is the classical Hartman flow, namely, it is laminar with a uniform velocity profile and a very thin boundary layer. Heat transfer in such a system is dominated by conduction. An exact solution to the problem of conducting heat transfer with both surface heating and non-uniform volumetric heating cannot be obtained. However, a numerical solution is available by using finite difference techniques. The summary of the neutronics, MHD, stress and heat transfer calculations is given on Table 7-6.

In ranking of the different material/coolant combinations, the concept of design window described in Section 7.4 will also be used here. The design window concept is a useful tool not only in judging the viability of the design, but also in choosing the proper design parameters, optimizing the system, and identifing the key design limitations. The design windows for Li/Li/V, Li/Li/FS and LiPB/LiPb/V systems are shown in Figs. 7-9, 7-10, 7-11 respectively. It can be seen that very comfortable design margins exist for all three cases. A set of design parameters can be chosen for each design which will provide reasonable heat transfer, pressure drop, pumping power, as well as efficient power conversion. The design margins are so large that some

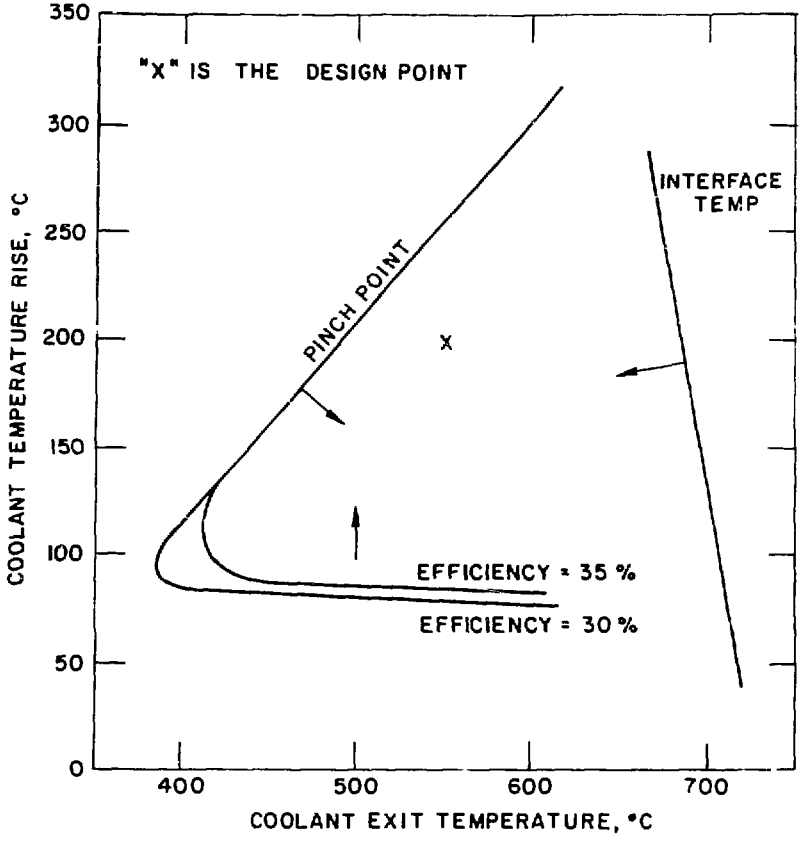

Figure 7-9. Design window for Li/V system.

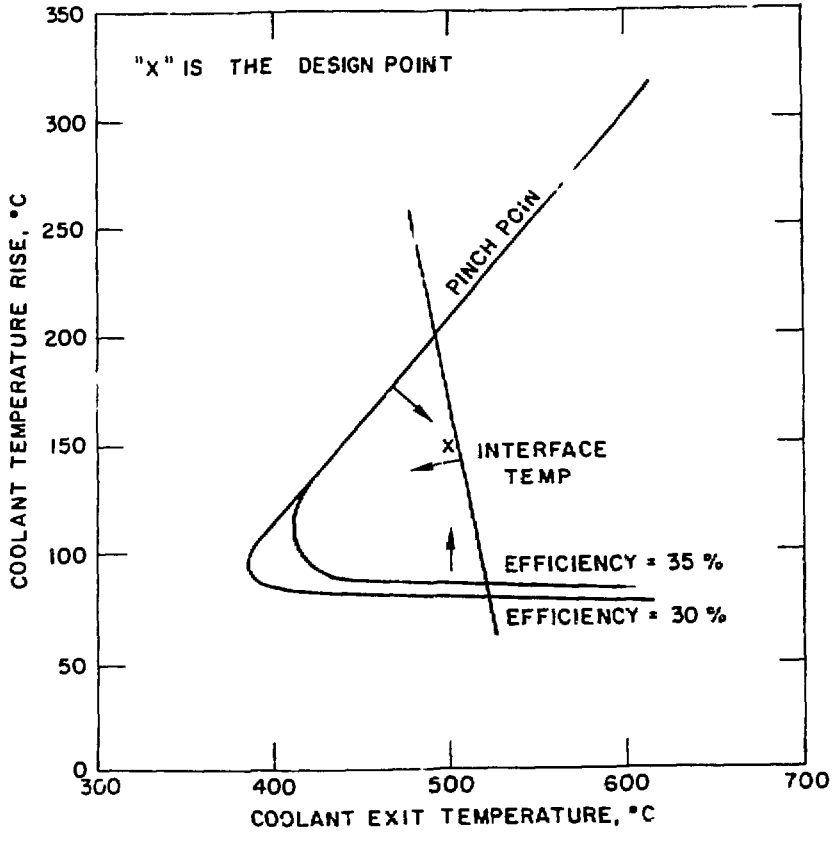

Figure 7-10. Design window for Li/HT-9 system.

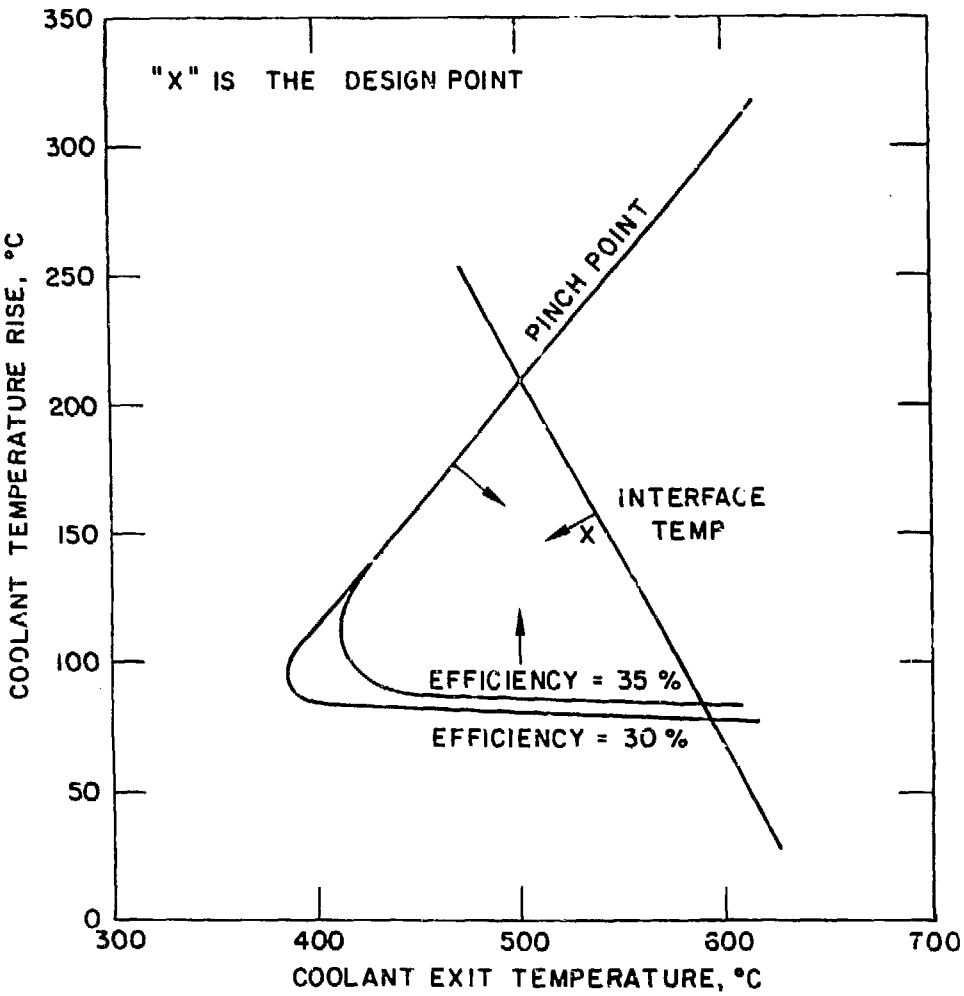

Figure 7-11. Design window for LiPb/V system.

uncertainties in certain calculations will not have major impact on the viability of the concepts.

There are some significant differences between the TMR and tokamak design windows. Due to the low surface heat flux on the first wall in TMR, the maximum structural temperature ceased to be a key factor in TMR design. The upper bound temperature limit is governed by the maximum allowable interface temperature, which is determined by 20 μm/y corrosion limit. Therefore, corrosion is a much more important issue to TMR than to a tokamak. Another interesting point is that the MHD pressure drop is lower in TMR and, consequently, the internal pressure is also lower. Therefore, primary stress effects are small.

TABLE 7-6. KEY PARAMETERS FOR R = 1 BLANKET CONCEPTS OF A TMR

System	Li/Li/V	Li/Li/HT-9	LiPb/LiPb/V
Blanket Thickness, cm	80.3	80.3	90.3
Li Enrichment	Natural	Natural	30%
T Breeding Ratio	1.26	1.21	1.33
Energy Multiplication	1.25	1.31	1.30
Blanket Thermal Power, MW	3063	3210	3534
Coolant Temperature, °C	350/550	350/500	380/530
Maximum Blanket Temperature, °C	605	550	650
Coolant Flow Rate, kg/hr	1.32×10^7	1.85×10^7	4.8×10^8
MHD Pressure Drop, MPa	.78	.75	2.15
Pumping Power, MW	8	13	38
Gross Thermal Efficiency, %	42.3	40.5	42.3

7.6 Concepts Ranked R=2A

7.6.1 Tokamak

There are two concepts ranked 2A for the self-cooled liquid-metal blanket. These are the Li/Li/HT-9 and the LiPb/LiPb/V blankets.

7.6.1.1 Li/Li/HT-9

Figure 7-12 show the results of the integral analyses of a Li/Li/HT-9 blanket for a tokamak reactor. A design window does not exist for this concept. The primary restriction comes from the structural temperature limitation, which is 550°C for ferritic steel. Note that the results shown in Fig. 7-12 are for a surface heat flux of 0.5 MW/m^2 and a first wall thickness of 5 mm. If a grooved first wall is used with an E-O-L thickness of 3 mm (minimum thickness required from bending stress calculation), the structural temperature limit shown in Fig. 7-12 will be relaxed somewhat. However, when the surface heat flux is increased to 1 MW/m^2, the structural temperature limit will remain close to where it is in Fig. 7.6-1 even if grooved first wall is used. In order to make the Li/Li/HT-9 blanket a viable and attractive concept, improvement must come from factors that relax the structural temperature limit shown in Fig. 7-12. These factors include higher allowable structural temperature (>550°C), lower surface heat flux (<1 MW/m^2), better heat transfer, and thinner grooved first wall (<3 mm). Another option may come from relaxing the primary stress limit. If the primary stress limit is reduced from a ΔT_b of 140°C shown in Fig. 7-12, to ~100°C, a narrow design window might exist. However, the thermal efficiency will be 30% or less. This low efficiency and the very narrow design window make this option rather unattractive. Simultaneous improvements in both the structural temperature limit and the primary stress limit will, of course, make the Li/Li/HT-9 blanket feasible and attractive.

7.6.1.2 LiPb/LiPb/V Blanket

Figure 7-13 show the results of the integral analyses for the LiPb/LiPb/V blanket of a tokamak reactor with a surface heat flux of 0.5 MW/m^2 and a first wall thickness of 5 mm. No design window exists for such a blanket. It is interesting to compare the LiPb/LiPb/V blanket with the Li/Li/V blanket since the latter does have a design window and is ranked No. 1. Comparison between Fig. 7-13 and Fig. 7-4 indicates that structural temperature and interface temperature limits are much more restrictive for the LiPb/LiPb/V blanket than the Li/Li/V blanket while other limits remain about the same for these two blankets (primary stress limit for LiPb/LiPb/V blanket is slightly more stringent than the Li/Li/V blanket because pressure drop for lithium-lead

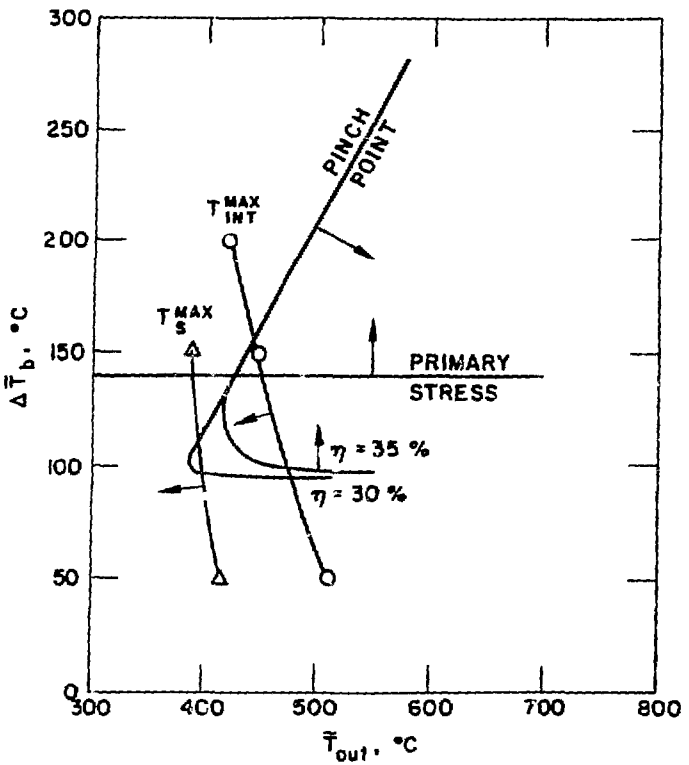

Figure 7-12. Results of integral analyses for a Li/Li/HT-9 blanket of tokamak reactor with a surface heat of 0.5 MW/m^2 and a first wall thickness of 5 mm.

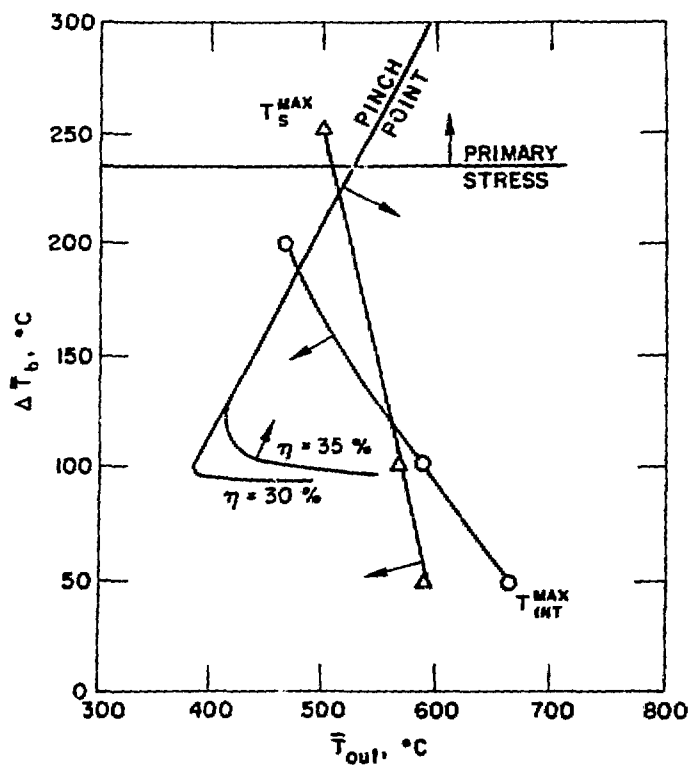

Figure 7-13. Results of integral analyses for a LiPb/LiPb/V blanket of a tokamak reactor with a surface heat flux of 0.5 MW/m^2 and a first wall thickness of 5 mm.

is slightly higher than that for lithium). This is the result of the relatively poor thermo-physical properties for lithium-lead, which result in poor heat transfer performance compared to lithium.

Improvement for LiPb/LiPb/V blanket can be made via the following two routes. The first one is through the relaxation of the primary stress limit. Referring to Fig. 7-13, a design window will appear if the stress limit is reduced from an equivalent ΔT_b of 235°C to 150°C. This can be accomplished by using electrical insulators to reduce the pressure drop through the blanket. Insulated wall is needed in the poloidal manifold in addition to the inlet and outlet pipes of the blanket. The feasibility of insulated poloidal manifold will be a key issue for the LiPb/LiPb/V blanket if this option is adopted.

The second route is through the improvements in both the structural temperature and the interface temperature limits. This is not going to be an easy task since it requires simultaneously raising significantly the corrosion temperature limit and the maximum allowable structural temperature (or other factors that will relax the structural temperature limit).

7.6.2 Tandem Mirror

Figure 7-14 shows the design window for the self-cooled Li/PCA blanket (R=2A) for TMR. The maximum coolant exit temperature is 425°C, with a coolant ΔT of 130°C. The low coolant exit temperature is caused by the relatively low corrosion temperature limit of 480°C. The lower corrosion limit in PCA comparing to HT-9 is due to the higher Ni content in PCA. In addition, the expected blanket life will also be much shorter than the HT-9 blanket of similar design due to the swelling characteristics of PCA.

A design point is available, as shown on Fig. 7-14. However, the expected thermal efficiency is low. With the low ΔT of the coolant, the volumetric flow rate is high. This will have impact on both the pumping power, as well as the cost of the primary loop. In addition, the design margin is small so that uncertainties in calculation may have major impact on the design window.

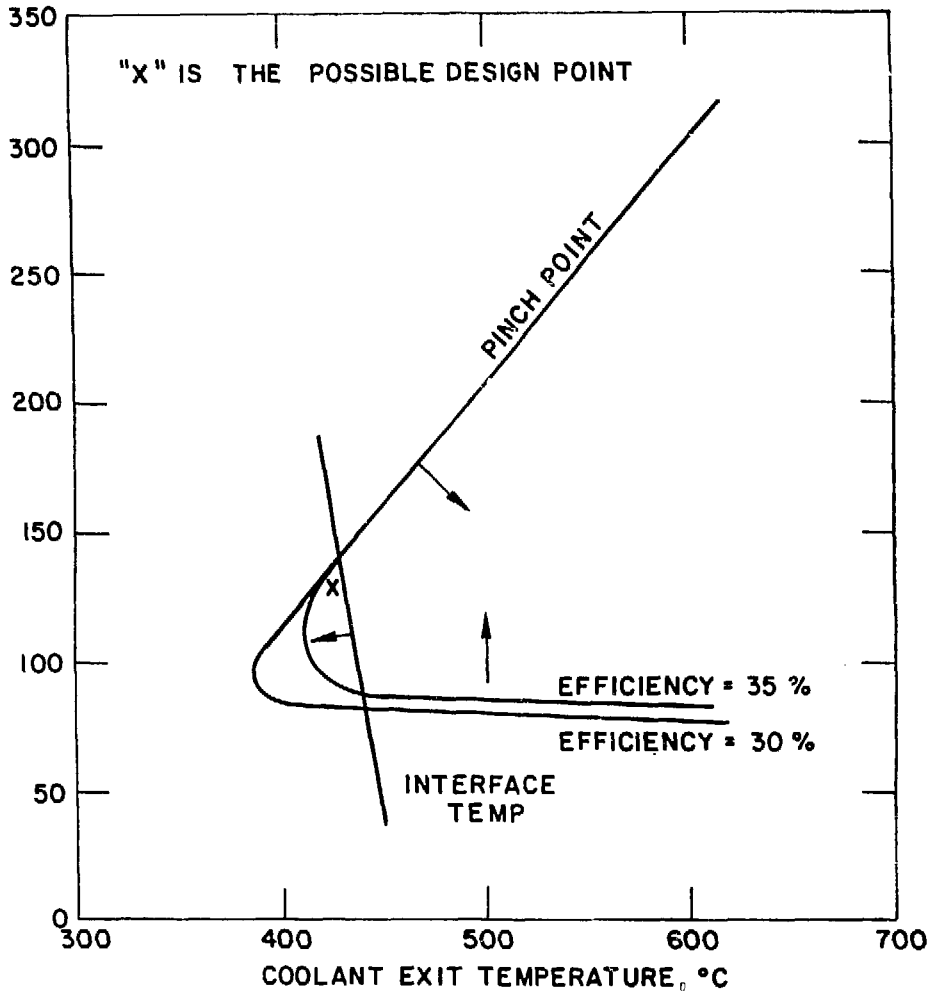

Figure 7-14. Design window for Li/PCA system.

7.7 Concepts Ranked R=2B/3

7.7.1 Tokamak

The Li/Li/PCA concept and the LiPb/LiPb/HT-9 concept are ranked No. 2B while the LiPb/LiPb/PCA concept is ranked No. 3 for the self-cooled liquid-metal blanket. The sodium-cooled Li-Pb blanket is ranked No. 3 and belongs to the category of separately-cooled liquid-metal concept.

7.7.1.1 Li/Li/PCA Blanket

Figure 7-15 shows the results of integral analyses for the Li/Li/PCA blanket of a tokamak reactor with a surface heat flux of 0.5 MW/m^2 and a first wall thickness of 5 mm. A design window does not exist for this concept. A design window will not exist even if grooved first wall is used since the surface heat flux has to be elevated to 1 MW/m^2. The most restricting factors are the structural temperature and the interface temperature limits as shown in Fig. 7-15. These two limits must be relaxed significantly and simultaneously in order to have a design window. If the primary stress limit is reduced somewhat (~20%), a design window may appear if both the structural temperature and the interface temperature limits are relaxed moderately. However, the thermal efficiency will be rather low (~30%) and the concept will not be attractive. Furthermore, this concept is inferior to either the Li/Li/HT-9 or the Li/Li/V blankets. Thus, a rank of 2B is assigned to this concept.

7.7.1.2 LiPb/LiPb/HT-9 Blanket

Figure 7-16 shows the results of the integral analyses for the LiPb/LiPb/HT-9 blanket of a tokamak reactor with a surface heat flux of 0.5 MW/m^2 and a first wall thickness of 5 mm. There is no design window available for this concept. The most limiting factor is the structural/coolant interface temperature as shown in Fig. 7-16. This is the result of the combination of relatively poor heat transfer performance of lithium-lead (which resulted in relatively high interface temperature) and a relatively low allowable interface temperature between lithium-lead and ferritic steel (~450°C). The heat transfer performance (which affects both the structural temperature and the interface temperature limits in Fig. 7-16), the pressure drop, and the corrosion

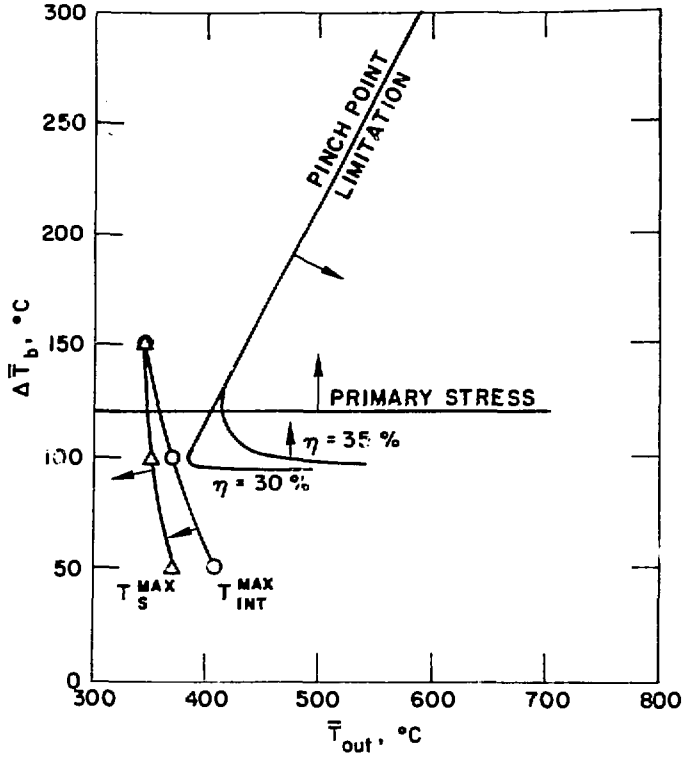

Figure 7-15. Results of integral analyses for the Li/Li/PCA blanket of a tokamak reactor with a surface heat flux of 1 MW/m^2 and a first wall thickness of 5 mm.

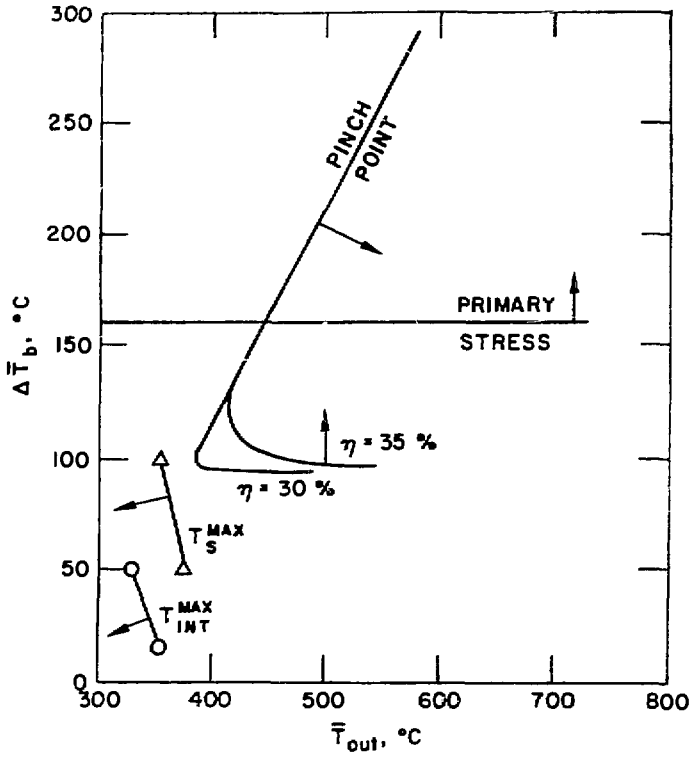

Figure 7-16. Results of integral analyses for the LiPb/LiPb/HT-9 blanket of a tokamak reactor with a surface heat flux of 1 MW/m^2 and a first wall thickness of 5 mm.

temperature limit, all must be improved significantly in order to make this concept feasible and attractive. This requires the use of electrical insulator in the blanket, redesign of the blanket towards better heat transfer performance (the current reference design is aimed toward minimizing the pressure drop), and the implementation of ways for relaxing the corrosion temperature limit. This concept is inferior to the Li/Li/HT-9 blanket primarily for the two reasons described previously (heat transfer and corrosion). Thus, the LiPb/LiPb/HT-9 blanket is ranked 2B.

7.7.1.3 LiPb/LiPb/PCA

The maximum allowable temperature for PCA is the same as that for ferritic steel (550°C). However, the maximum allowable corrosion temperature between LiPb and PCA is ~410°C which is lower than that between LiPb and HT-9. Furthermore, the thermal conductivity of PCA is lower than that of HT-9. These two factors will make the maximum structural temperature and maximum interface temperature limits of the LiPb/LiPb/PCA blanket more restrictive than that shown in Fig. 7-16 for the Li/Li/PCA blanket. Thus, the LiPb/LiPb/PCA blanket constitutes an even worse mismatch than the Li/Li/PCA blanket which is ranked 2B. Consequently, the LiPb/LiPb/PCA blanket is given a rank of 3.

7.7.2 Tandem Mirror

7.7.2.1 LiPb/LiPb/HT-9

The reference design of MARS, LiPb/HT-9, is rated 2B mainly due to the lower corrosion limit used here. In the MARS design, it was assumed that the maximum corrosion temperature limit is 550°C. However, new experimental results become available after the completion of the MARS work redefined the corrosion rate for this study. If 20 μm/y is used as the upper limit, the maximum allowable interface temperature reduces to 465°C. This maximum allowable interface temperature basically closes the design window, as shown in Fig. 7-17.

There are ways to increase the corrosion temperature limit, such as use of an inhibitor, or a corrosion product cleanup system. If a practical way can be found to increase this temperature to 550°C, as was assumed in MARS, a very comfortable design window is available, as seen in Fig. 7-17. The impact

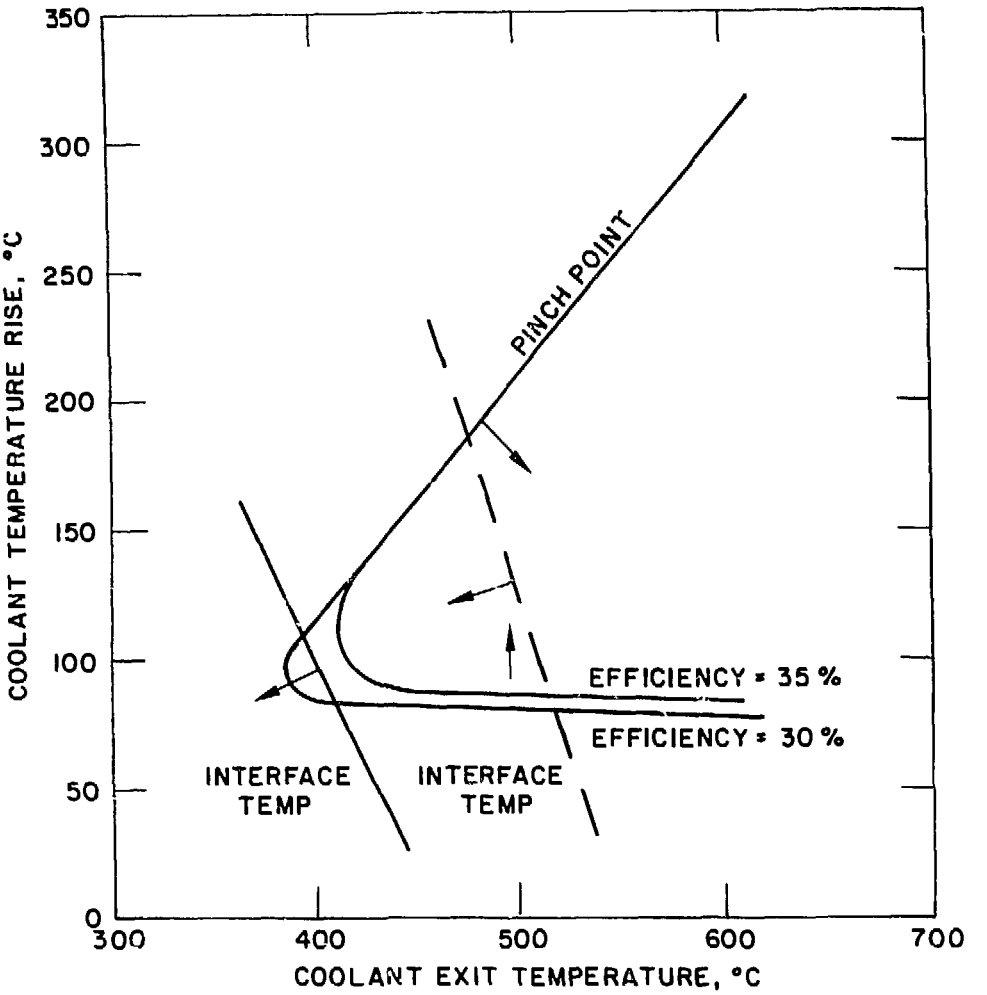

Figure 7-17. Design window for LiPb/HT-9 system.

of this temperature limit to the rating of the concept is, therefore, obvious.

7.7.2.2 17Li-83Pb/17Li-83Pb/PCA

The LiPb/PCA design is rated 3 because there is simply no design window as shown in Fig. 7-18. The corrosion temperature limit is so low that an attractive system is not possible.

7.8. Analysis of Special Issues

7.8.1 MHD Analysis

7.8.1.1 Introduction

The poloidal manifold/toroidal first wall coolant channel liquid metal blanket for a tokamak reactor, presented in Ref. 7-1, was the result of an effort to achieve the high coolant velocities needed for adequate cooling of the first wall, without prohibitively high MHD pressure drops. This was accomplished by orienting the high velocity coolant channels in the toroidal direction so that they will be parallel to the large toroidal magnetic field. At the same time, the manifolds, which are by necessity transverse to the toroidal field were made large to minimize the MHD pressure drop. In addition, the manifold walls, whose thickness affects the local MHD pressure gradient, were tapered so that they were thicker near the inlet and thinner near the outlet. Such tapering, if done properly, reduces the maximum material stresses in the conduit walls.

Since the Interim BCSS report, more careful neutronics calculations and the increase in first wall heat flux to 1 MW/m^2 resulted in an increased effective heat deposition in the blanket. At the same time, thermodynamic considerations led to a choice of higher coolant temperatures in the blanket and, thus, to a choice of a vanadium alloy as a structural material. Finally, the technical feasibility of laminated wall construction was established, thus opening the possibility of significant reductions in MHD pressure drops. As a result of these developments the reference design has evolved to the currently proposed design.

Magnetohydrodynamic considerations were also paramount in determining the configuration of a liquid-metal-cooled limiter. In both the inboard blanket

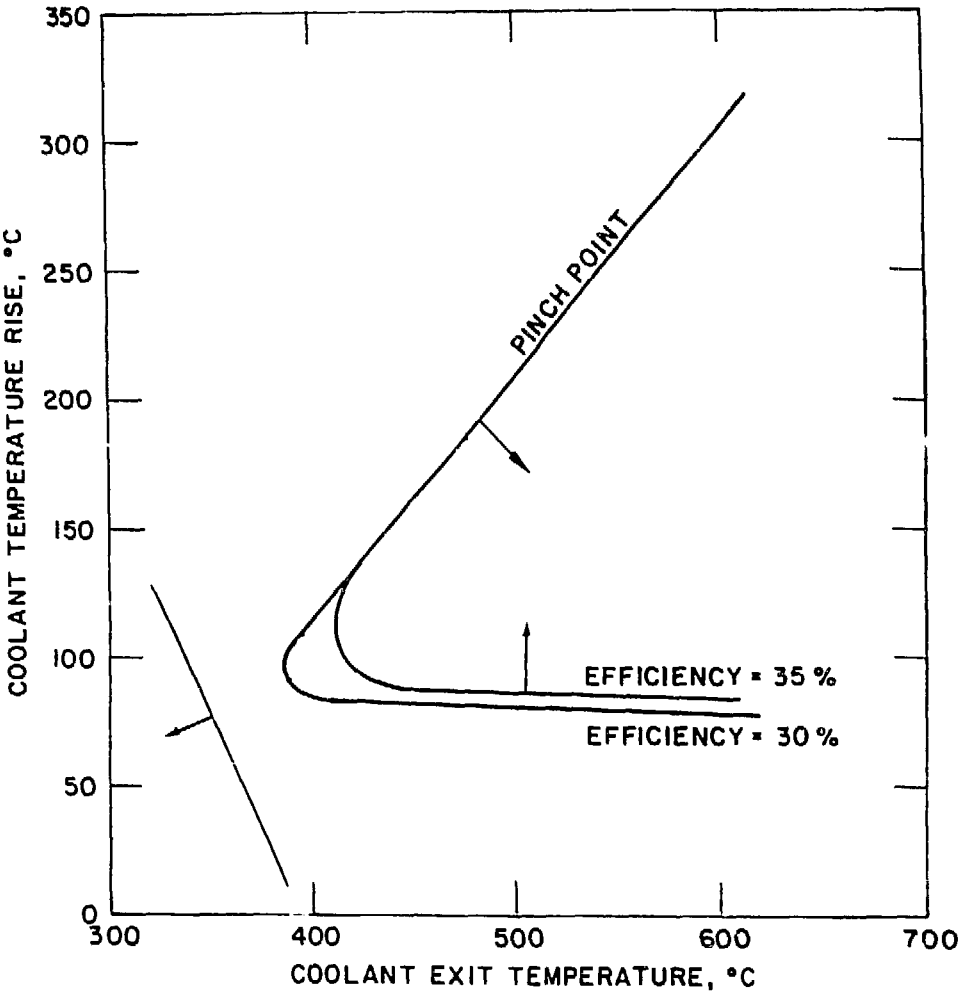

Figure 7-18. Design window for LiPb/PCA system.

and the limiter, laminated wall conduits were employed in areas where the heat and neutron fluxes were low. Because the electrical conductivity requirements of the insulators were satisfied by several orders of magnitude, further improvements in the blanket designs could be made by using laminated walls in the poloidal manifold conduits. Although such a design would offer significant improvements, the use of laminated structures in the poloidal manifolds was not deemed necessary and was not adopted. If in the future new developments in MHD analysis show that some of the MHD pressure drop formulae employed have been underestimating the pressure drop, the use of laminated wall construction at the poloidal manifolds would be an obvious improvement in an effort to compensate for the larger pressure drops.

Laminated wall construction in areas of low neutron and heat fluxes was also used in the design of a liquid-metal blanket for a tandem mirror reactor. Because of the different geometric constraints imposed by the two reactor types the mirror design is simpler but certainly non trivial.

In the following, a summary of the formulae employed in the MHD analysis and a discussion on the feasibility and insulating requirements of laminated structures is given first. Then, descriptions of the improved tokamak blanket and tandem mirror blanket designs and the associated pressure distributions are presented.

7.8.1.2 MHD Analysis

The study of magnetohydrodynamics involves the simultaneous solution of the Navier-Stokes equations for fluid motion (including a pondermotive force term) and Maxwell's equations. This formidable task is made possible by considering various regimes over which the equations are greatly simplified. These regimes are characterized by the following non-dimensional numbers.

Magnetic Reynolds number	$Re_m = B_{ind}/B$
Hartmann number	$M = aB\sqrt{\sigma/\mu}$
Interaction Parameter	$N = aB^2\sigma/V\rho$
Conductivity Ratio	$\phi = \sigma_w t_w/\sigma a$

where B is the magnetic flux density, a is the pipe radius or channel half width in the direction parallel to B, σ and μ are the electrical conductivity and viscosity of the fluid, σ_w and t_w are the electrical conductivity and thickness of pipe wall or of wall normal to B, V is the average fluid velocity, and B_{ind} is the induced magnetic flux density.

For the reference design these non-dimensional numbers are of the following order of magnitude.

$$R_{e_m} \sim O(10^{-3}),\ M \sim O(10^4),\ N \sim O(10^4),\ \Phi \sim O(10^{-2} - 10^{-3})$$

The smallness of the magnetic Reynolds number makes it possible to neglect the induced magnetic field and set the total magnetic field equal to the applied one.

As a result of the large value of M, the fluid flow and current density are uniform throughout most of the flow cross section, with variations confined in thin layers near the walls.

The large value of N makes inertial effects negligible; turbulence is also suppressed everywhere, with the possible exception of fluctuations that may exist in thin shear layers under some special circumstances.

Finally, the condition $\Phi << 1$ combined with $M\,\Phi >> 1$ defines the "thin wall" regime, in which the induced currents and, thus, the pressure drops are controlled by the wall resistance.

Fully developed flow in circular or rectangular ducts has been, since the mid-thirties, the subject of several investigations both analytical and experimental. The analyses available cover the whole range of M (the interaction parameter, N, is irrelevant for a fully developed flow, since there are, by definition, no inertial effects). The analyses pertinent to the fusion reactor are those for high M and $\phi << 1$. It can be stated, with considerable certainty, that fully developed MHD flow is well understood and that existing analyses, validated through experiments up to $M \sim O(10^3)$, are expected to be valid for $M \sim O(10^4)$ and higher.

At high Hartmann numbers, the pressure gradient for a uniform channel segment in a uniform transverse magnetic field is given by:

$$\frac{dp}{dz} = \sigma V B^2 \frac{\Phi}{1 + \Phi} \quad . \qquad [7\text{-}1]$$

The pressure gradient in rectangular ducts with unequal wall thicknesses and wall conductivities, as will be the case for the reference design, was examined in some detail in Ref. 7-1. It was shown that Eq. [7-1] provides an adequate and conservative estimate of the pressure gradient. It was also shown that high velocity sidewall layers exist but that the mass flow rates associated with these side layers are small. As a result, the effect of these layers on mass transfer, and thus on corrosion, are small.

In both the tokamak and mirror reactors the magnetic field changes sufficiently slowly with distance to make Eq. [7-1] valid locally. Thus, the overall pressure drop is simply obtained by integrating the pressure gradient equation over the length of the segment in question.

Three dimensional flow perturbations result from changing magnetic field (direction or magnitude), changing cross sectional area dimensions, changing wall thickness, bends, manifolds, etc. Such variations set up axial electric field gradients which, in turn, set up circulating currents within the liquid. These currents interact with the magnetic field and result in pressure drop over and above that predicted by fully developed flow theory.

Analyses that have been carried out to date predict stagnant regions at the center of the conduit with most of the flow rate carried in layers adjacent to the walls. Also, theory predicts significantly different behavior for rectangular and for circular conduits, with the rectangular ones being more prone to the adverse three dimensional effects.

Unlike the case for a straight duct normal to a uniform magnetic field, analysis of three dimensional effects is highly case specific, involved, and, for some cases, not amenable to solution with currently available analytical tools. Nevertheless, fair estimates of the pressure drop associated with a number of three dimensional effects exist, and are supported by limited experimental data albeit at much lower values of M and N than those prevailing in the blanket.

It was assumed in the analysis of the MHD pressure drop in the fusion blanket that the variation of magnetic field strength is sufficiently gradual, so that the associated three dimensional effects are minimal. The other

remaining three dimensional effects are associated with the abrupt change of the magnetic field at the inlet and outlet regions, the effects associated with abrupt changes in wall thickness and those associated with conduit bends, either on a plane normal to B or, as is the case of the reference design manifolds, from a direction normal to B to a direction parallel to B.

The pressure drop associated with abrupt changes in B (or equivalently with abrupt changes in wall thickness or cross-sectional areas), has been analyzed for thin wall circular ducts. This pressure drop is found to be equal to

$$\Delta p = C\ \sigma V a B^2 \sqrt{\Phi} \qquad [7\text{-}2]$$

with the coefficient C depending on the magnitude of the discontinuity. The peak value of C was computed to be 0.16. A conservative value of 0.2 is adopted in the analysis of the blanket. The pressure drop for a bend in a plane normal to B can also be estimated by the same equation for lack of a better alternative.

The blanket designs are such that the fluid turns from a direction normal to a large magnetic field to a direction essentially parallel to the field vector. This change in direction is combined with a manifold so that flow in a single conduit turns into a number of smaller conduits. Clearly this is a very complicated situation, even in the absence of MHD effects. When MHD effects are present the pressure drop will depend on the detailed manner the manifolding is accomplished, the presence of insulators, wall thickness distributions etc. Even for the case of a single conduit with such bend only a semiempirical correlation exists, namely

$$\begin{aligned} \Delta p &= 0.5\ \sigma V B^2 a N^{-1/3} \\ &= 0.5\ V^{4/3} B^{4/3} \sigma^{2/3} \rho^{1/3} a^{2/3} \end{aligned} \qquad [7\text{-}3]$$

where N is the interaction parameter $= \frac{\sigma a B^2}{\rho V}$, ρ is the coolant density, and "a" and V are the channel half width and coolant velocity associated with the channel normal to B. The pressure drop, as computed from Eq. [7-3], may indeed have little relation to the actual pressure drop. However, the latter

will depend so strongly on the details of the actual configuration that any speculation on its magnitude can neither be defended nor rejected until the design is specified to a much greater degree than the guidelines of the BCSS warrant and the understanding on 3-D MHD effects is increased beyond the present state-of-the-art. For the time being, it should be understood that the pressure drop associated with the manifolding from the poloidal manifolds to the toroidal first wall cooling channels represents the biggest uncertainty in the overall MHD pressure drop. It should also be understood that, although the pressure drop may be larger than that given by Eq. [7-3], there is confidence that careful design of the manifold and other improvements of the overall design will keep the material stresses within allowable limits. Finally, it should be stated that the different manifolding arrangement in the mirror design makes the possibility of large pressure drops in their manifolds less likely.

7.8.1.3 Laminated Wall Construction with Insulators

The fundamental difficulty in designing liquid metal blankets without insulators is that the MHD pressure drop is essentially proportional to the duct wall thickness, whereas the hoop stress in the duct wall is proportional to the pressure and inversely proportional to the wall thickness. As a result, the material hoop stress is essentially independent of the wall thickness and cannot be reduced, as is usually the practice, by increasing the wall thickness. Although designing a blanket with thicker walls where the pressure is higher, and thinner walls where it is lower can reduce the maximum hoop stress, the fundamental problem of coupling the pressure drop to the wall thickness remains. An obvious way of bypassing this difficulty is to decouple the load bearing structure from MHD pressure drop. This can be accomplished either by insulating coatings of the inner duct surfaces or by laminated wall construction with an insulating layer sandwiched between two metal layers.

Insulators were not originally considered because it was thought that their insulating properties would rapidly deteriorate in the presence of strong neutron fluxes. In addition there were concerns about the effect of unavoidable faults that may develop in the severe thermomechanical environment of the blanket. There were also concerns that the normal and shear forces to which the insulating bonding layer would be subjected would lead to delamination.

Despite these reservations, the spectacular improvements in blanket design that could be made, if insulators were used, dictated a closer look at their technical feasibility. A careful consideration of both insulating coatings and insulating laminated wall construction revealed the following.

1. Insulated Coatings

For maximum benefit in pressure drop reduction the resistivity of the insulating layer (thickness 20 μm) must be much larger than 10^2 ohm-m. The integrity of the insulating coating should be such that the total surface area of cracks that extend through the entire insulator thickness, is much smaller than 10^{-3} mm^2 per square meter of insulated surface. Not withstanding the fact that the latter criterion was obtained using very conservative assumptions, it appears that the integrity of insulating coatings will be a critical feasibility issue, unless a rapidly self-healing coating can be developed. The required resistivity of the insulators is several orders of magnitude smaller than that of candidate insulating materials. Thus, even if the resistivity is dramatically decreased under neutron irradiation the electrical performance of the insulators would in all likelyhood be adequate.

2. Laminated Construction

For maximum benefit in pressure drop reduction, the insulating layer materials (thickness 0.3 mm) should have electrical resistivity larger than 1.0 ohm-m. The integrity of the insulating layer is not critical unless the following three conditions are simultaneously satisfied: a) the surface area of the insulator cracks per surface area of insulator exceeds 1.0 mm^2/m^2, b) the liner fails at multiple locations, and c) as a result of (a) and (b) the cracks are filled with liquid-metal breeder. Both the electrical resistivity and the integrity requirements do not appear to be technically challenging.

In addition, estimates of the shear and normal stresses to which the insulator will be subjected as a result of MHD phenomena indicate that both stresses do not exceed a few psi. As a result, delamination is not considered a problem.

For the above reasons laminated wall construction appears to be feasible. Indeed, such construction can probably be utilized in high neutron flux environments since neutron irradiation will not reduce the electrical resistivity

of the insulator by six orders of magnitude. It is unlikely, however, that laminated structures will be suitable for areas of high heat flux (such as the first wall) because of the low thermal conductivity of the electrical insulators.

7.8.1.4 Tokamak Reactor

The reference design presented in the interim report of the BCSS has been modified to accommodate increased energy deposition rates in the blanket. Also, the inlet and outlet conduit geometry, the transition pieces between these conduits and the inboard blanket, and the end walls of the sector have been addressed in more detail that was done in the earlier design. The most significant changes involve a) the inlet conduit to the inboard blanket, b) the number of manifolds per sector, and c) the use of laminated wall construction in the inlet and outlet conduits, in areas where the surface heat flux is nonexistent and the neutron fluxes are low. The modified blanket configuration is shown in Fig. 7-19. The plasma dimensions are identical to those of the STARFIRE reactor except that the lower half of the plasma chamber has been enlarged to accommodate the limiter. Figure 7-20 shows the inboard blanket in relation to the magnet coils. In the modified configuration the coolant/breeder enters from the top to take advantage of the hydrostatic head and reduce the peak coolant pressure. The inlet segment is inclined at 45°. This is the most obvious configuration if the upper horizontal segment of the blanket is to become part of the outboard blanket. This change reduces the total energy deposited in the inboard blanket and thus the necessary mass flow rate for energy removal and, consequently, the pressure drop through the inboard blanket.

The modified design addresses in more detail the design of the inlet and outlet conduits, and the transition segments needed to connect these conduits to the inboard blanket. The inlet and outlet conduits (segments 7-8 and 1-2 in the figures) are circular in cross section, to be able to sustain the internal pressures effectively, with internal diameter 0.70 m and wall thickness of 2 mm at the inlet and 1 mm at the outlet. The conduits are small enough to be accommodated in the space between the magnet coils. The wall thickness has been made small to minimize MHD pressure drop. Load bearing sleeves, electrically insulated from the conduit walls are used to sustain the coolant pressures.

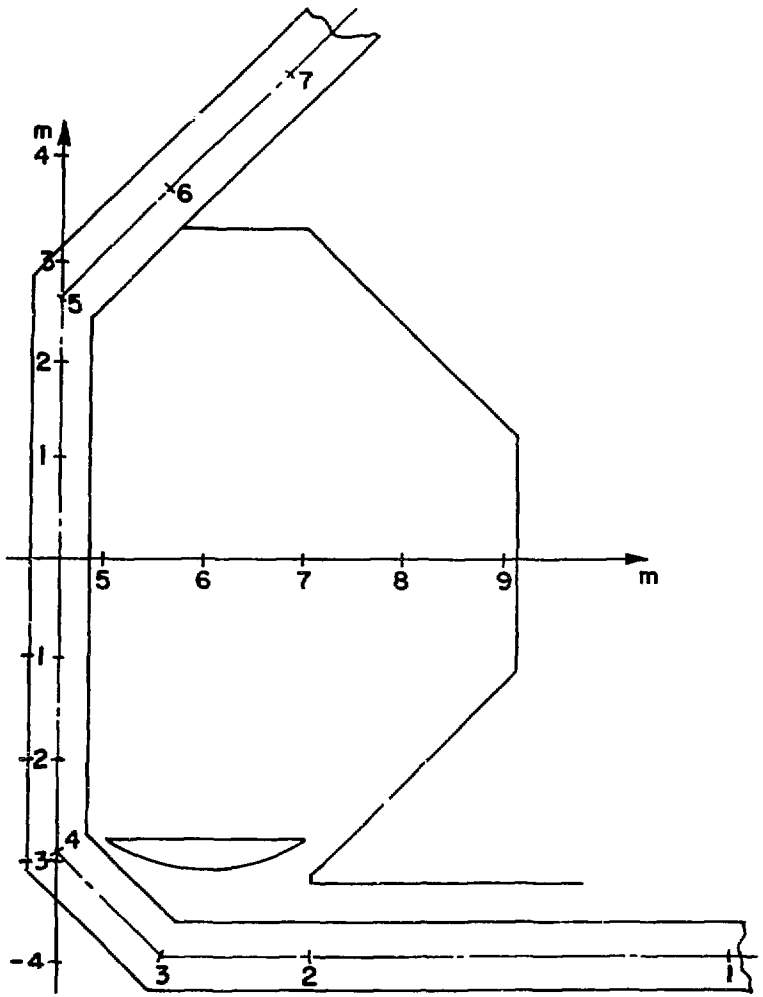

Figure 7-19. Inboard blanket configuration.

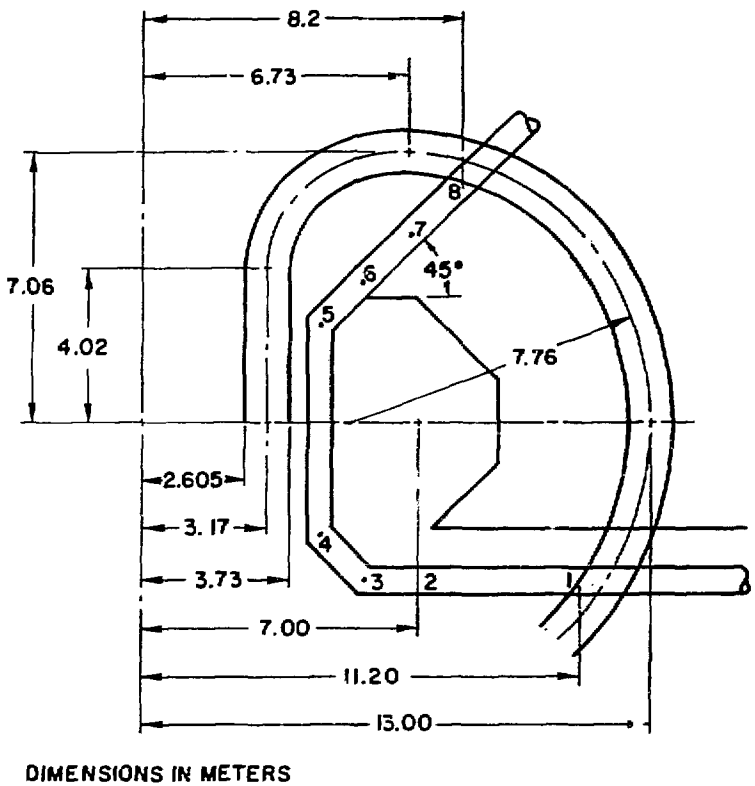

Figure 7-20. Special relationship of the inboard blanket to the coil/helium vessel.

There are two transition pieces (6-7 and 2-3 in the figures). These segments make the transition from a circular conduit of 0.7 m in diameter to a rectangular conduit of dimensions 0.59 m × 0.65 m. The inner wall thickness is 2 mm at the inlet and 1 mm at the outlet and a load bearing exterior wall structure sustains the coolant pressure.

The toroidal-poloidal design extends from point 3 to point 6. A development of the first wall of this segment is shown in Fig. 7-21. The increased duct dimensions between points 5 and 6, and 3 and 4, resulting from the increasing radial position is shown in that figure. These segments are trapezoidal in shape, to provide a transition from a cross section of 0.59 m × 0.65 m to a cross section 0.45 m × 0.50 m. The wall thickness of the 5-6 segment is 4 mm and that of the 3-4 segment is 2 mm.

The wall thickness of the blanket segment from point 5 to point 4 changes, as shown in Fig. 7-21, in a stepwise fashion instead of being tapered as originally conceived. The stepwise variation is, of course, easier to manufacture. The step sizes are small enough to make additional pressure drops due to 3-D effects negligible.

Figure 7-21 also shows that additional webs are incorporated in the blanket from point 6 to the mid point of the inboard blanket. These additional webs are necessary to reduce both the hoop stress at the webs, and the bending stress of the first wall to allowable levels. Although the presence of these webs causes a doubling of the local pressure gradient the overall effect is that the peak stress levels in the blanket are reduced. The possibility that such a transition in the number of webs will cause significant 3-D MHD effects and, consequently, excessive pressure drops has been considered. It was found that such a transition will have a miniscule effect on 3-D effects because the average velocity of the coolant does not change as a result of the transition and no axial voltage gradients are generated. The transition in the manifold width does not have an effect on the heat transfer as well, because the coolant velocity changes only slightly with the number of webs.

Variation of the web thickness and the number of webs in the axial direction can be used to minimize the material stresses resulting from MHD pressure drops. The modified reference design presents such an improvement over the original design. It should be mentioned that the proposed thickness and web number distribution do not necessarily represent the optimum configuration,

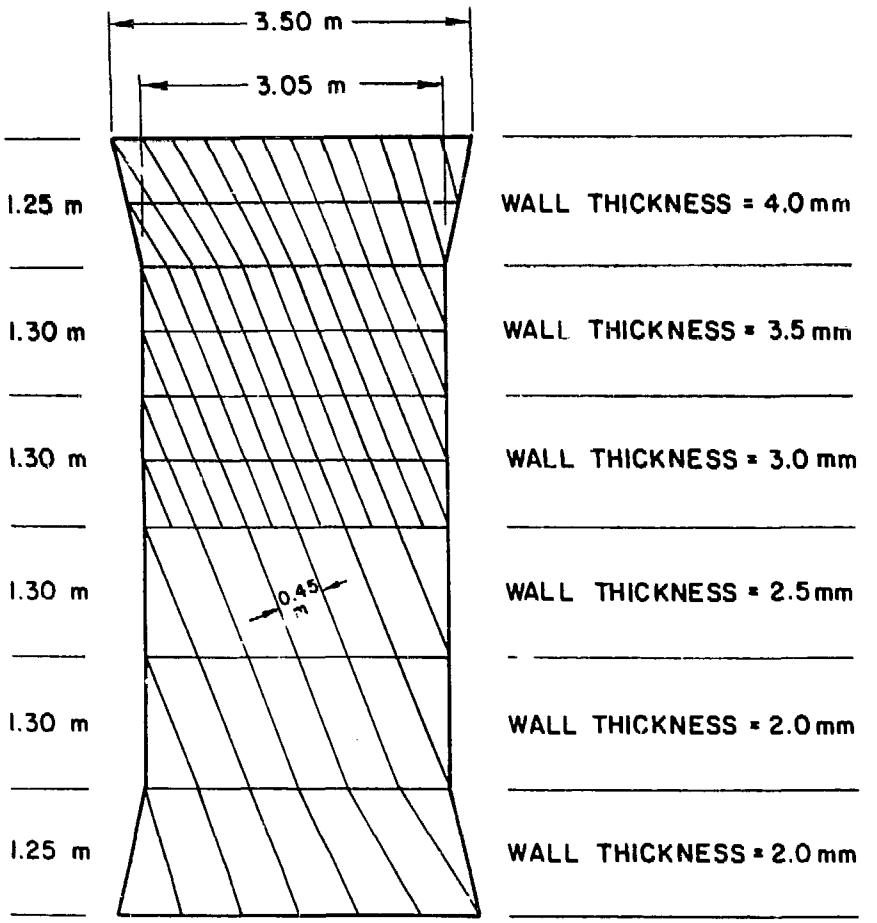

Figure 7-21. Inboard blanket first wall and manifold development.

and that further modest improvements are possible with different distributions.

Figure 7-22 illustrates a cross section of a manifold at the end of the sector. The end wall is comprised of semicylindrical surfaces of radius of 9 cm. The wall thickness is the same as that of the corresponding webs at the same axial location. The two thick (2 cm) reflector plates and the thinner plate near the first wall are perforated and allow coolant to flow between the various compartments. The first wall coolant channels communicate with the manifold in a manner similar to that shown in the figure. The state-of-the-art of MHD analysis does not allow detailed design of this connection. When more is known in the future about manifolding of liquid metals in thin conducting walls in the presence of strong magnetic fields, a more complete design, which will minimize MHD pressure drop and the possibility of hot spots, can be produced. At any rate, present understanding of MHD theory indicates that such manifolding will not present any unsurmountable problems.

7.8.1.5 Tandem Mirror Reactor

The easy access to the blanket, the shorter inlet and outlet duct lengths, and the lower magnetic flux densities involved make the design of the mirror blanket more straightforward. Two different designs were considered a) a configuration involving circumferential manifolds in conjuction with radial modules, and b) a configuration involving single circumferential coolant channels. In both cases the inlet and outlet ducts were straight circular conduits. Although both designs were feasible, the configuration involving circumferential coolant channels was selected as the reference design because of its simplicity.

The reference design involves modules, 2 m long in the axial direction, containing circumferential tube banks, as shown in Fig. 7-7. The circumferential tubes are fed by a manifold connected to a vertical inlet conduit. An identical outlet manifold and outlet conduit are located 180° from the inlet manifold.

The inlet and outlet conduits are circular in cross section with internal diameter of 36 cm. The walls are of laminated construction with an internal liner of 1 mm.

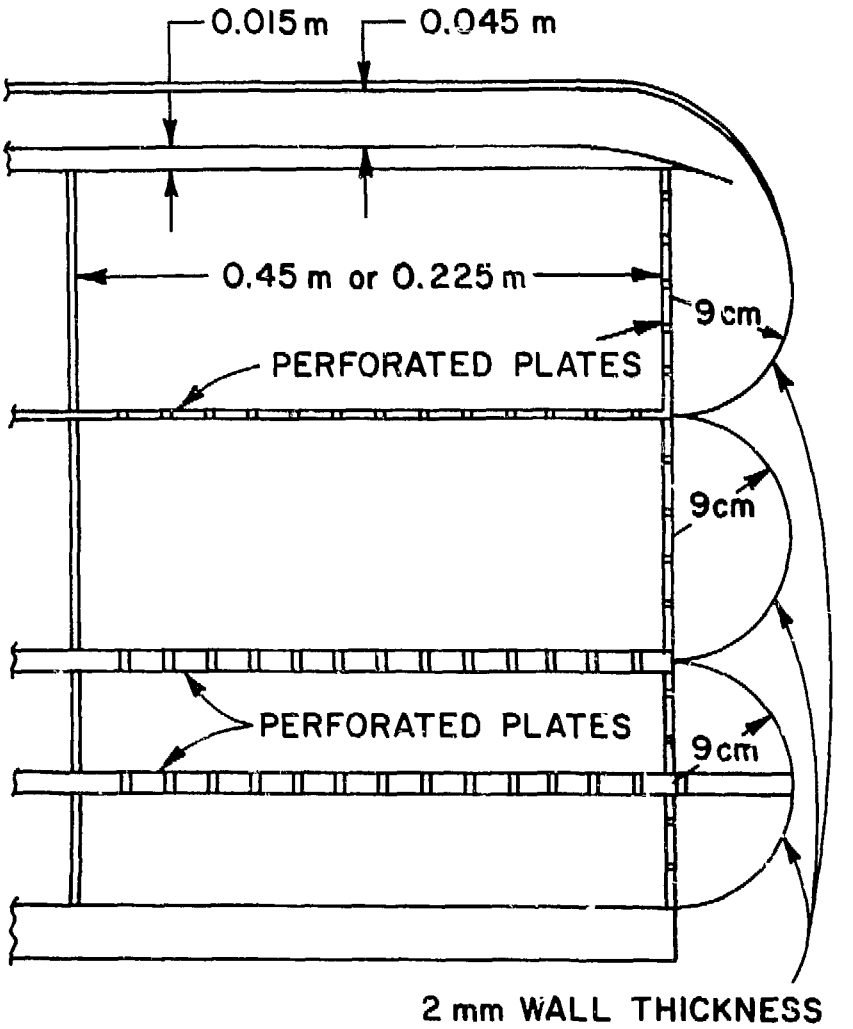

Figure 7-22. Section of the blanket showing first wall channel, poloidal manifolds and end module design for pressure containment.

For the purposes of MHD analysis only the first wall tubes need be considered. The remaining tube layers are designed with different wall thicknesses so that the pressure drops and the temperature rises through the various tube layers are identical.

The first wall tubes have a wall thickness of 2 mm and an ID of 9.75 cm. These dimensions determine the pressure drop through the bank of circumferential tubes and thus the overall pressure drop through the blanket.

The MHD analysis for the tandem mirror reactor is similar to that carried out for the tokamak. The main uncertainty in the MHD calculation involves, as for the tokamak, the pressure drop in the manifold. However, because the geometry is much simpler, the possibility for unexpectedly large pressure drops caused by electrical interaction between the manifold and the coolant channels is diminished.

7.8.1.6 Pressure Drop Calculations

Tokamak

The calculations for the tokamak reactor with a vanadium alloy structure are based on a total energy deposition/sector equal to 170 MW. Of that energy, 20 MW is the result of a 1 MW/m^2 heat flux on the first wall.

For a bulk temperature rise through the inboard blanket of 250°C the mass flow rate for each of the six manifolds of a given sector is 26.7 kg/s. The corresponding distributions of coolant velocity (average) and pressure is given in Table 7-7A. The pressure distribution given in Table 7-7A is for a manifolds which feeds a toroidal set of coolant channels between locations 6 and 7. The peak hoop stress in the blanket occurs in the intermanifold wall at point 6 and is equal to 160 MPa.

Tandem Mirror

The MHD analysis for the mirror design was performed for a number of structural materials and first wall coolant velocities. The results are given in Table 7-7B. The outlet pressure for all the cases shown in Table 7-7B was kept at 1.5 atm. In all the cases, inlet was at the higher elevation. For this reason, the inlet pressure shown is calculated as the outlet pressure

TABLE 7-7A.

Location	Velocity, m/s	Pressure, MPa
inlet	0.14	3.00
8	0.14	2.96
7	0.14	2.90
6	0.14	2.81
toroidal channel	1.06	
5	0.23/0.34	1.85
4'	0.34	0.73
4	0.34/0.23	0.34
3	0.14	0.23
2	0.14	0.20
1	0.14	0.16
outlet	0.14	0.15

TABLE 7-7B. SUMMARY OF MHD ANALYSES FOR TMR

First Wall Velocity mm/s	Inlet Temperature °C	ΔT °C	ΔP_{MHD} MPa	Inlet Pressure MPa	Maximum Hoop Stress MPa
0.1	250	150	0.49	0.60	<15
0.2	250	75	1.00	1.11	<28
0.3	250	50	1.52	1.63	<41
0.1	250	150	0.55	0.66	<17
0.2	250	75	1.14	1.25	<32
0.3	250	50	1.73	1.84	<46
0.1	250	150	0.73	0.84	<21
0.2	250	75	1.52	1.63	<41
0.3	250	50	2.30	2.41	<61
0.2	300	200	0.81	0.26	<7
0.4	300	100	1.66	1.11	<28
0.6	300	67	2.51	1.96	<49
0.2	300	200	0.90	0.35	<9
0.4	300	100	1.86	1.31	<33
0.6	300	67	2.82	2.27	<57
0.2	300	200	1.20	0.65	<17
0.4	300	100	2.50	1.95	<49
0.6	300	67	3.80	3.25	<82

increased by the MHD pressure drop and decreased by the hydrostatic head, which for the case of 17Li-83Pb can be substantial. Of course having the inlet at the higher elevation will not reduce the pumping power requirements since these are determined by the pressure losses. It will, however, decrease the stresses in the blanket conduits. As shown in Table 7-7B, the maximum hoop stresses for all the cases analyzed, is much smaller than the allowable material stress.

7.8.2 Thermal Hydraulic Analysis

The primary objectives of the thermal hydraulic analysis are to determine the temperature distributions in the blanket and the first wall under steady-state conditions. These temperature distributions can be used to determine the maximum structural temperature and maximum structure/coolant interface temperature in the first wall and blanket. These temperature distributions will also be utilized to perform thermal-stress calculations for the first wall and blanket. Another parameter which affects the results of thermal-hydraulic calculations is the average temperature rise through the blanket. This average ΔT also affects the MHD and the power cycle design.

7.8.2.1 Analyses

Calculations of the first wall temperature distributions are straightforward. It is assumed that the first wall is relatively thin and the temperature gradient in the radial direction is large compared to that in other directions and the one-dimensional, steady-state, heat conduction equation is employed.[7-1]

It is not easy to determine accurately the temperature distributions in the liquid metal blanket because interaction of liquid-metal flow with the magnetic field modifies the velocity distributions in the blanket. Certain assumptions have to be made in order to obtain quantitative results. The following assumptions are made based on current understanding of liquid-metal flow in a transverse magnetic field.

1. The flow is laminar and the velocity fluctuations carried from upstream (in absence of a magnetic field) is completely suppressed in the blanket by the magnetic field.

2. Natural circulation induced by temperature gradient is completely suppressed by the magnetic field.

3. The flow and temperature fields are two-dimensional.

4. The boundary layers in the duct are extremely thin and the velocity is essentially uniform over the entire cross section of the duct (slug flow).

Deviations from these assumptions could significantly affect the results of the heat transfer calculations and thus could have significant impact on the design of the blanket. For example, if a secondary flow exists, as a result of temperature gradients in the blanket, heat trasnfer near the first wall could be improved. The assumption of slug flow is valid only if the flow is fully developed and the Hartmann number is relatively large. In the reference design of the tokamak reactor, the flow in the manifold is perpendicular to the toroidal field (B = 7.5 Tesla in the inboard region) and that in the toroidal channel is perpendicular to the poloidal field (B ~ 0.5 Tesla). The resulting Hartmann numbers for lithium blanket are $\sim 10^5$ in the manifolds and ~600 in the toroidal channels. Thus, the Hartmann numbers in both the manifolds and the toroidal channels are high enough to ensure very thin boundary layers in the ducts provided that the flow is fully-developed. There still may be some uncertainties associated with the flow turning from the poloidal manifold to the toroidal channels or vice versa. This could violate the assumption of fully-developed flow to a certain extent. However, the flow fields in these regions are extremely complicated, and certainly better understanding is needed before accurate calculations can be performed.

For the tokamak reactor, thermal-hydraulic calculations are carried out for both the poloidal manifolds and toroidal channels. In the manifold, nuclear heating is the only heat source while the duct walls are assumed to be insulated. In the toroidal channels, both the surface heat flux and the nuclear heating are included. Additional description can be found in Ref. 7-1.

The thermal-hydraulic calculations for the tandem mirror reactor are carried out in a similar manner. Here, the geometry of the reference design is similar to MARS, i.e., the tube configuration. From the thermal-hydraulic point of view, the most critical area is the first row of tubes which are subjected to high nuclear heating rate.

7.8.2.2 Results

Figure 7-23 shows the maximum structural (vanadium alloy) temperature versus first wall thickness for various structure/coolant interface temperatures with a surface heat flux of 1 MW/m^2. Similar results are obtained for PCA and ferritic steel and some of the results are reported in the Interim Report.(7-1) These results are used to determine the maximum structural temperature in the first wall when the structure/coolant interface temperature is known.

Figure 7-24 shows the temperature distribution in the toroidal channel with a surface heat flux of 1 MW/m^2 and a coolant (lithium) average velocity of 1.06 m/s. Figure 7-25 shows the temperature distribution in the manifold with an average coolant velocity of 0.235 m/s, assuming that the flow in the manifold is not disturbed by the toroidal flow. The results shown in Figs. 7-24 and 7-25 corresponds to an average ΔT rise through the lithium blanket of 250°C. Results similar to those shown in Figs. 7-24 and 7-25 are available for various average ΔT's across the lithium blanket which corresponds to various velocities in the manifold and the toroidal channels. Calculations were also performed for a surface heat flux of 0.5 MW/m^2 and some of these results were reported in Ref. 7-1.

Similar calculations have also been performed for the lithium-lead blanket and the results are not reported here. However, the difference between lithium and lithium-lead coolants can be understood qualitatively by examining the thermo-physical properties in Table 7-8. Because there is still a lack of material properties for lithium-lead in general, the property values for lithium-lead are estimated. Lithium has higher thermal conductivity and higher product of density and specific heat than lithium-lead. Both these factors result in lower temperature gradient in the lithium blanket than that in the lithium-lead blanket. Furthermore, the higher density of lithium-lead resulted in steeper nuclear heating profile which also results in higher tem-

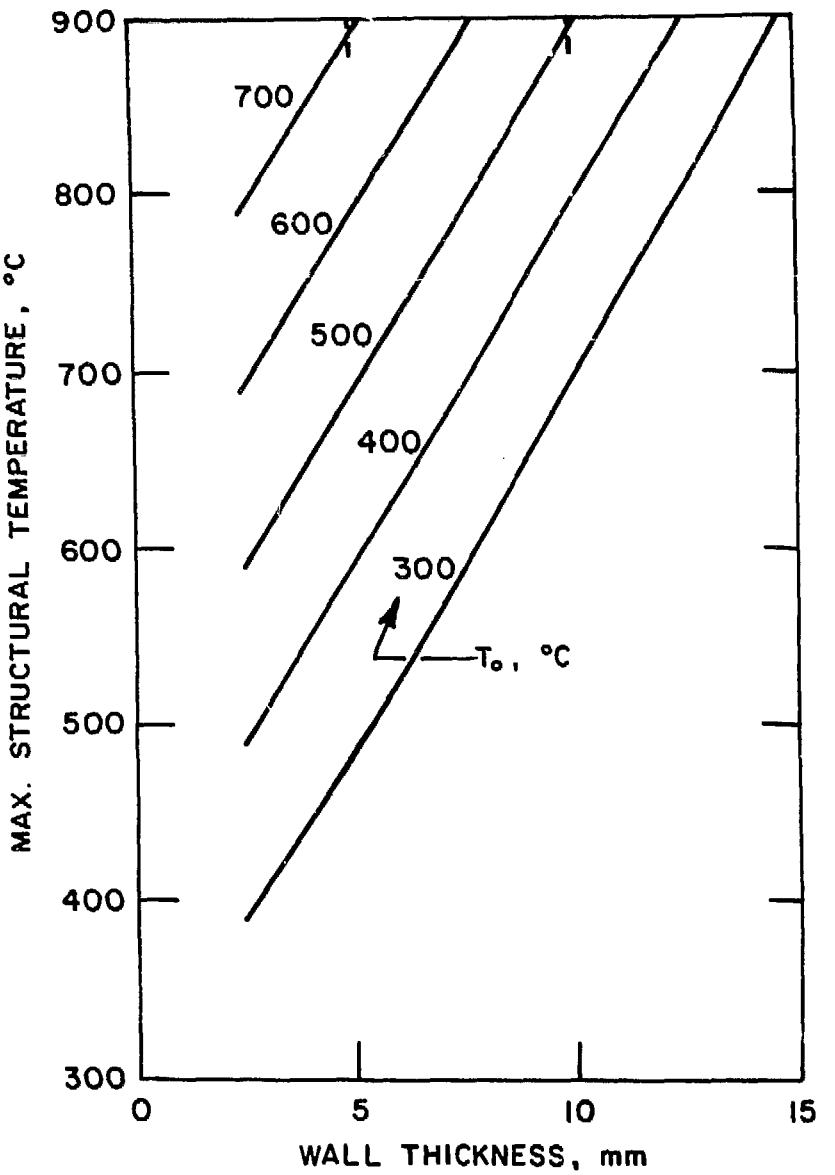

Figure 7-23. Variations of maximum structural (vanadium alloy) temperature with wall thickness for various coolant/structure interface temperatures and for a surface heat flux of 1 MW/m^2.

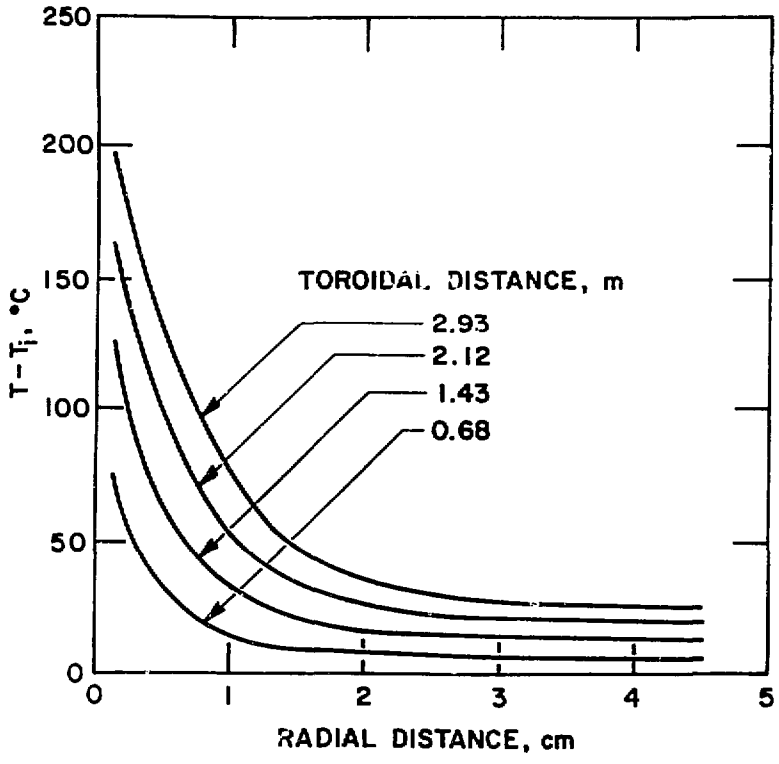

Figure 7-24. Radial temperature distributions at various axial locations in the toroidal channels of a tokamak reactor.

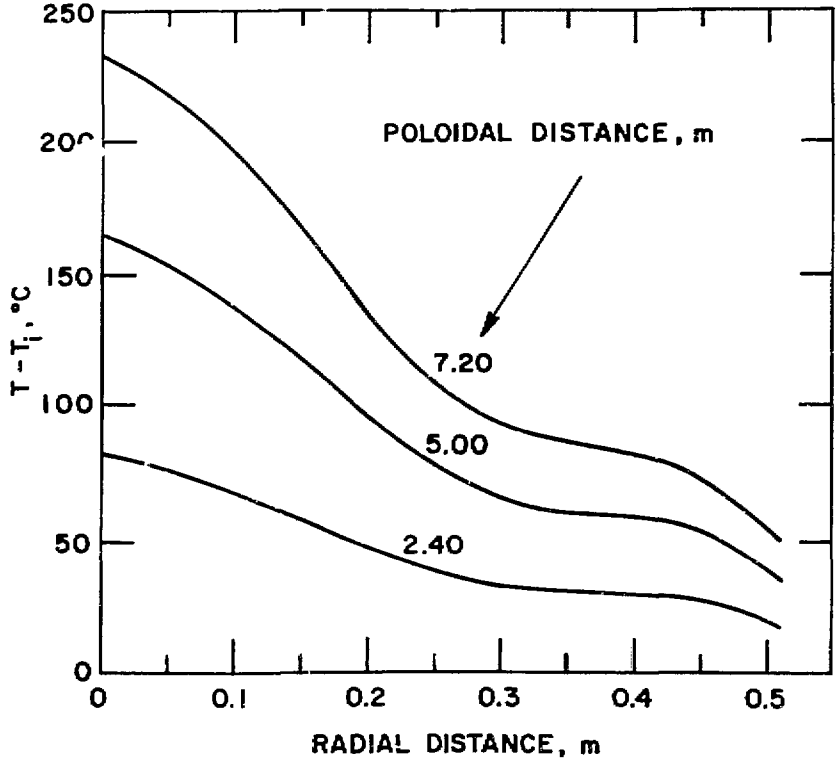

Figure 7-25. Radial temperature distributions at various radial distances in the poloidal manifold of a tokamak reactor.

perature gradient in the lithium-lead blanket than those in the lithium blanket. Thus, from the thermal-hydraulic point of view, lithium is obviously a better coolant than lithium-lead.

TABLE 7-8. SOME THERMO-PHYSICAL PROPERTIES OF LIQUID LITHIUM AND LITHIUM-LEAD (17Li-83Pb)

	Lithium (500°C)	Lithium-Lead (estimated)
Thermal Conductivity (W/m-k)	49.6	22
Specific Heat (J/kg-k)	4,200	130-150
Density (kg/m^3)	485	9,330

Results like those shown in Figs. 7-24 and 7-25 are used to estimate the maximum coolant/structure interface temperature for all the self-cooled liquid-metal blankets of tokamak reactors. Estimation of the maximum coolant/structure interface temperature is made in the following manner. Figure 7-26 shows the flow paths of the first and the last manifolds. The maximum interface temperature could occur either in the toroidal channel or in the poloidal manifold depending on which coolant (lithium or lithium-lead) is flowing in the blanket and on the magnitude of the surface heat flux (0.5 - 1.0 MW/m^2) imposed on the first wall. The maximum interface temperature always occurs at the discharge end of the blanket no matter whether the flow is through the first or the last manifold. For the flow through the first manifold, it is assumed that the temperature of the coolant is uniform after it passes through the toroidal channels near the top and just before it begins to move downward in the manifold (Fig. 7-26b). In other words, it is assumed that the flow is completely mixed after it turns from the toroidal channels to the manifold. The mixed-mean temperature is equal to the inlet temperature plus the mean ΔT rise through the toroidal channels. Using this mixed-mean temperature as the initial coolant temperature for the manifold, the results shown in Fig. 7-25 are used to estimate the maximum interface temperature at the discharge of the first manifold. For the last manifold, Fig. 7-26a, it is assumed that the coolant temperature is uniform after it turned from the

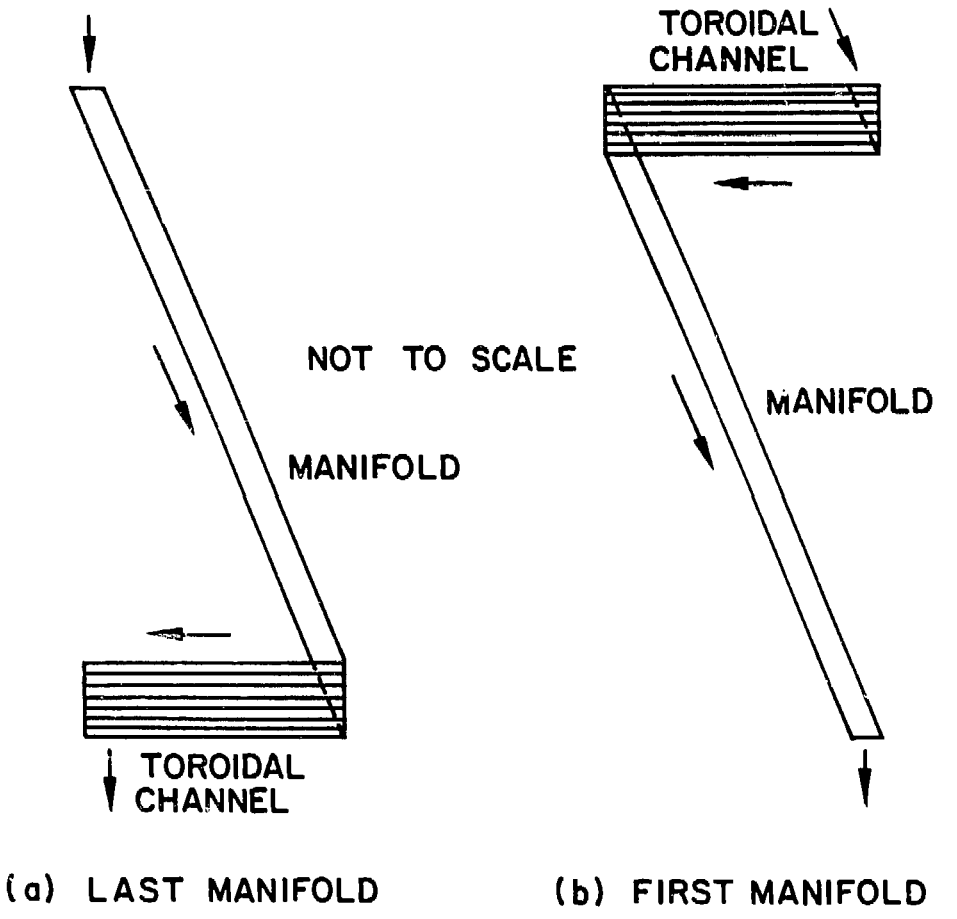

Figure 7-26. Flow path through the first and the last manifolds of a tokamak reactor.

manifold to the toroidal channels. The inlet temperature of the toroidal channels is assumed to be equal to the mixed-mean temperature rise through the manifold. The results shown in Fig. 7-24 are then used to estimate the maximum interface temperature of the flow through the last manifold. It should be noted that the maximum interface temperature for the flow through the first manifold occurs in the manifold while that of last manifold occurs in the toroidal channels. The higher of these two maximum temperatures is taken to be the absolute maximum interface temperature of the blanket. There are other paths that the coolant can and will go through (between the first and last manifolds shown in Fig. 7-26). However, the maximum interface temperature is assumed to be bounded by the two extreme cases described above.

For the tandem mirror reactors, the thermal-hydraulic calculations are straight-forward since the geometry (tube configuration) is relatively simple compared to the reference design of the tokamak blanket reactors. The critical area is the first row of tubes facing the plasma. The surface heat flux is 0.05 MW/m^2 and the erosion rate is 0.1 mm per year. The combination of low surface heat flux and low erosion rate greatly reduces the first-wall cooling problem as compared to that of the tokamak reactors. Since the erosion rate is low, the thickness of the first wall can be maintained relatively thin (2-3 mm). Figure 7-27 shows the radial temperature rise in the first wall (ferritic steel) of a tandem mirror reactor as a function of wall thickness. For a wall thickness of 3 mm, the temperature rise in the first wall is only about 14°C which is one order of magnitude smaller than that of a tokamak reactor.

Figures 7-28 and 7-29 show the maximum and average temperature rise through the first row of tubes in the lithium and the lithium-lead blanket for TMR, respectively. These temperature rises are primarily the result of nuclear heating in the blanket since surface heat flux is relatively small. Figure 7-28 shows that, for a lithium blanket with an average coolant velocity of 0.2 m/s, the difference between the average ΔT and the maximum ΔT is ~30°C for a tandem mirror reactor. The difference between maximum and average ΔT in a tandem mirror reactor is the result of the combination of relatively low surface heat flux (0.05 MW/m^2) and short heated length (1.9 m) in the azimuthal direction. This relatively small difference in maximum and average ΔT in the coolant plus the small ΔT rise in the first wall greatly reduces the heat

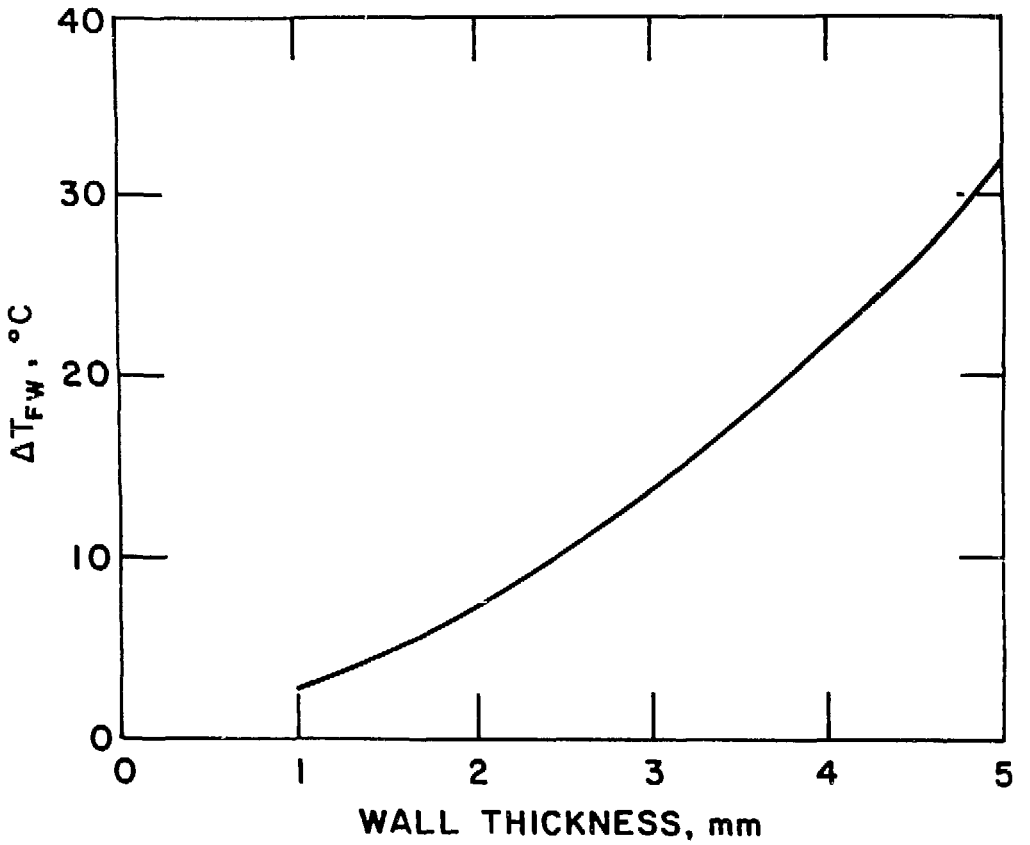

Figure 7-27. Temperature rise of the first wall as a function of wall thickness for ferritic steel and for a surface heat flux of 0.05 MW/m^2.

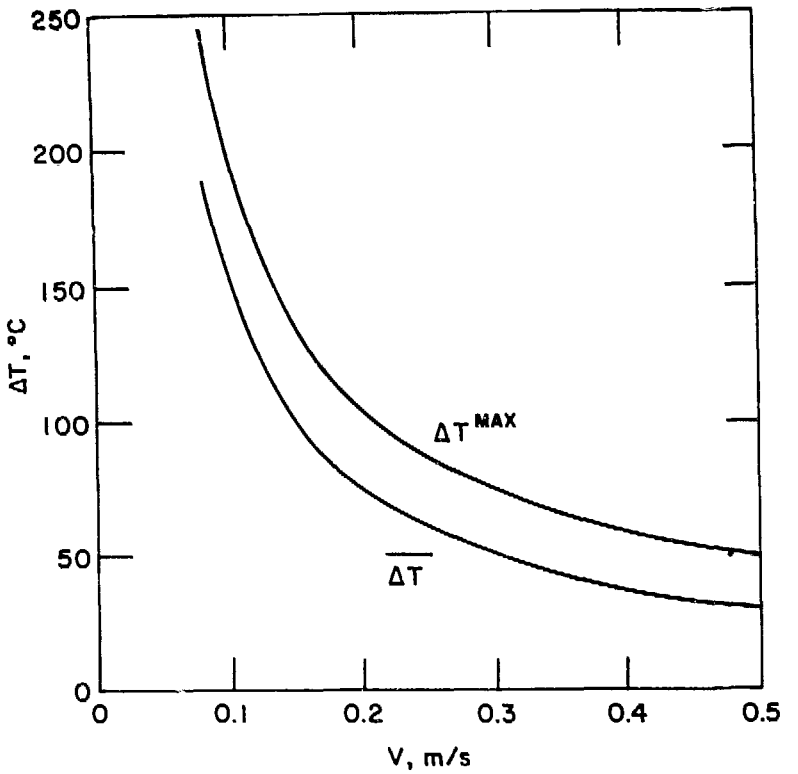

Figure 7-28. Variations of maximum and average temperature rise with average coolant velocity in the lithium blanket of a tandem mirror reactor.

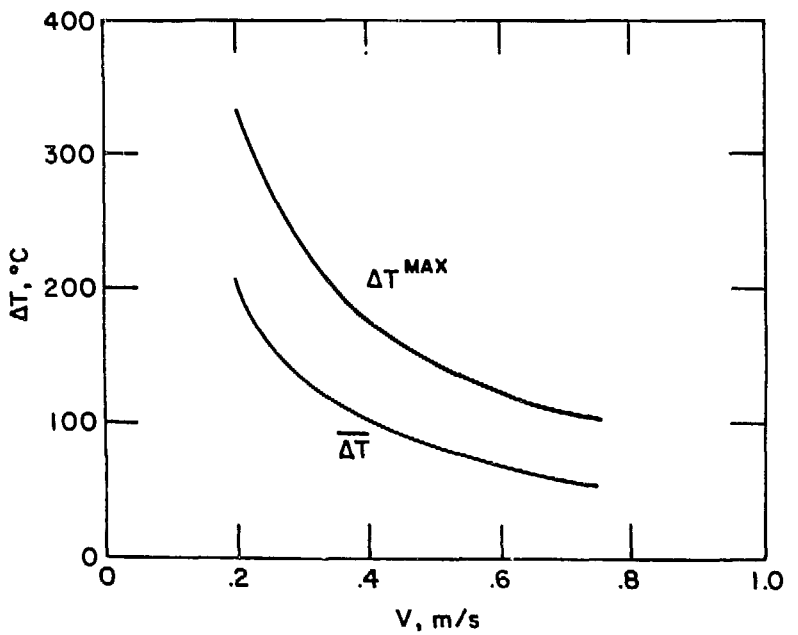

Figure 7-29. Variations of maximum and average temperature rise with average coolant velocity in the lithium-lead blanket of a tandem mirror reactor.

transfer problem in a tandem mirror reactor as compared to that of a tokamak reactor. Comparison between Figs. 7-28 and 7-29 shows that the difference between maximum and average ΔT of a lithium blanket is much smaller than that of lithium-lead blanket for the same average coolant velocity. This is the result of the relatively poor thermo-physical properties of lithium-lead compared to those of lithium as described previously.

The maximum structural and coolant/structure interface temperatures described here are used to determine the design windows in Sections 7.4 - 7.7.

7.8.3 Stress Analysis

Details of the stress analysis procedure were given in the BCSS Interim Report. Results of stress analyses for pressure, thermal, seismic and plasma disruption induced loadings are included here.

7.8.3.1 Tokamak Design (Lithium Cooled Vanadium Structure)

The first wall of the reference design has been analyzed as part of a composite plate as discussed in the interim report. In addition to stresses due to pressure from the manifold side, stresses are generated because of bending of the first wall itself due to coolant pressure in the first wall coolant channels. Figure 7-30a shows the variation of the maximum bending stress in the first wall of the reference design as functions of the first wall thickness and the coolant pressure. Also included in the figure, by dashed lines, are the allowable stresses corresponding to various fluence levels based on a maximum allowable radiation induced creep strain of 5%. Thus for a first wall thickness of 3.25 mm (exclusive of grooves) and coolant pressure of 3 MPa, the maximum allowable fluence is 150 dpa. Since there is a pressure gradient in the manifold, it is not necessary to design for the maximum pressure everywhere. Similarly, the manifold sidewall spacing need not be the same everywhere in the blanket and can be increased to 45 cm wherever the coolant pressure is reduced to 1 MPa. This will further help reduce the MHD pressure drop in the blanket. Figure 7-30b shows the variation of primary membrane stresses in a poloidal flow design as functions of the wall thickness and pressure. Note that in this case the minimum thickness necessary for a design life of 150 dpa exceeds that for the reference design.

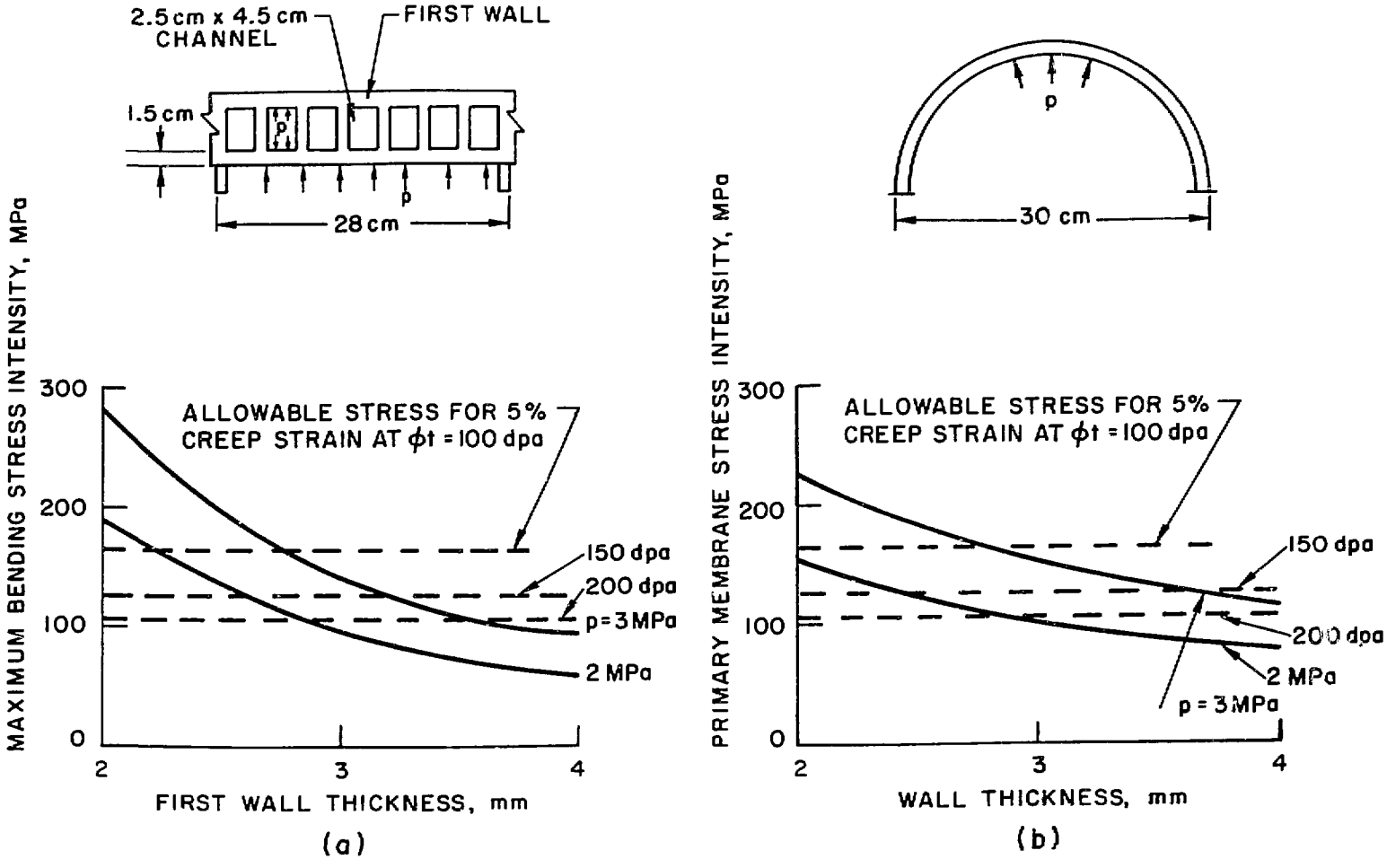

Figure 7-30. Variation of maximum primary stresses with wall thickness and pressure for a) the reference Li cooled tokamak reactor blanket design and b) alternated poloidal flow design.

A detailed thermal stress analysis showed that the maximum stress intensity in the first wall (ignoring the grooves), corresponding to a surface heat flux of 1 MW/m^2, volumetric nuclear heating rate of 20 MW/m^3 and coolant pressure of 3 MPa is 655 MPa which is well within the 3 S_m limit. A detailed radiation creep analysis indicated that the maximum displacement of the first wall is about 0.024 mm/dpa so that at the end of life (150 dpa) the maximum displacement is 3.6 mm. However, this is not the total displacement of the first wall with respect to the back wall because the stretching of the manifold side walls, which is about 10.4 mm, has to be added to it giving a maximum displacement of the first wall with respect to the back wall as 14 mm.

The end wall of the manifold poses a special problem because it has pressure acting only on one side causing large bending stress if a flat plate is used. To avoid the high bending stress, the end wall has been designed to be curved with a radius of about 9 cm and thickness of 2 mm giving a membrane stress of 135 MPa which is within the allowable limit.

A crack growth analysis of the grooved first wall (see Section 6.7 for details) with a total thickness of 6 mm and groove depth of 3 mm was carried out. For a surface heat flux of 1 MW/m^2 the allowable number of fatigue cycles is 35000 which is adequate for a three year lifetime.

For evaluating the effects of loadings due to disruptions or earthquake, a structural dynamics analysis of the complete blanket together with its supports is required. For the purposes of the present study a simple model of the inboard blanket together with a possible scheme for supports, as shown in Fig. 7-31, is used. The blanket is supported at the bottom (C) by a continuous support and is given lateral supports at the middle (B) of the inboard vertical wall and the middle (A) of the upper inlet segment. In reality the support A has to be inclined at a different angle with respect to the blanket segment from that shown in order to minimize the thermal stress due to a uniform temperature rise of the blanket with respect to the shield. However, for simplicity of calculations, the supports are assumed to provide no constraint to any movement of the blanket segment parallel to itself. Further, the blanket is assumed to be clamped (i.e., prevented from rotating or displacing normal to the blanket segment) at location C. The stress analysis follows by treating the blanket as a laterally supported cantilevered beam. To cover all possible loadings two cases were run; one with vertical loading and the other

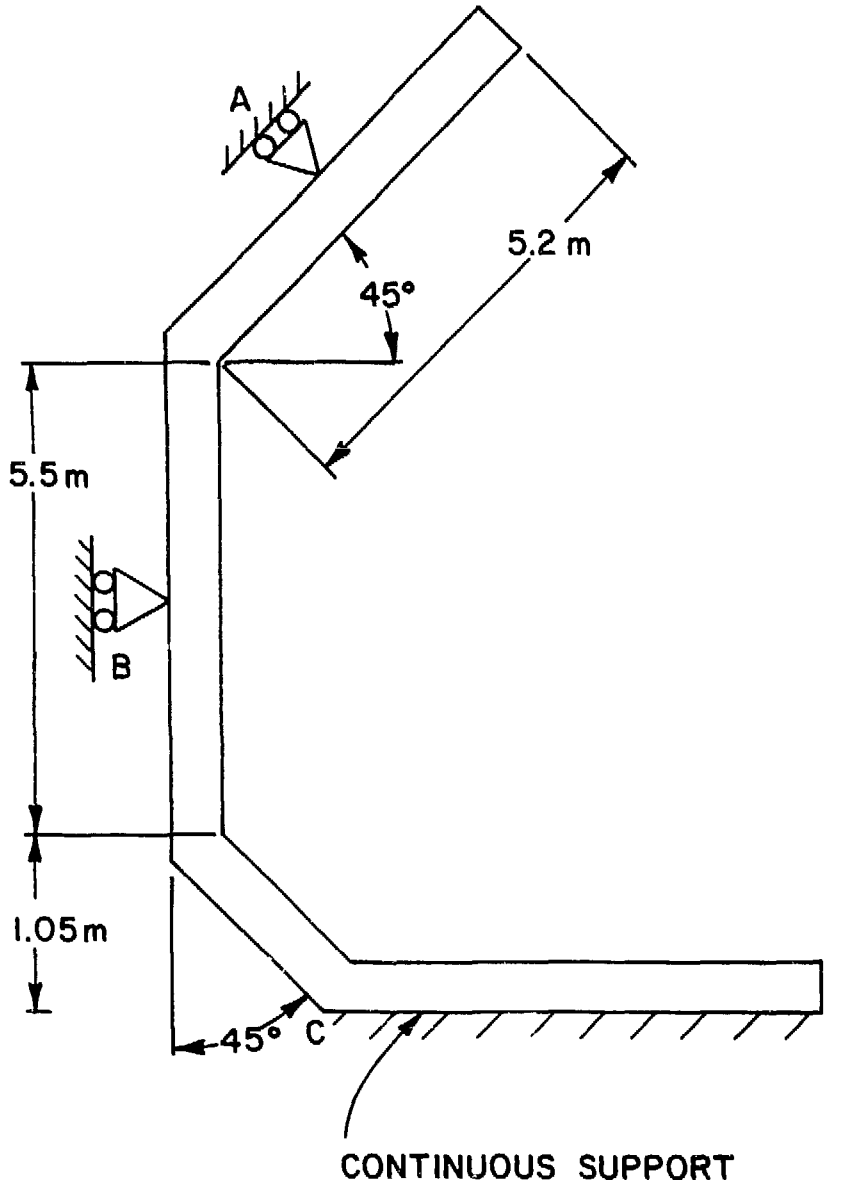

Figure 7-31. Idealized geometry of the reference liquid metal cooled tokamak inboard blanket.

with horizontal loading on all three segments of the blanket. The statically indeterminate problem is solved using the energy method, i.e., by minimizing the strain energy of the system with respect to the one unknown reaction P_A at A. Denoting the total vertically downward force in the top blanket segment by V_1, the vertical segment by V_2, and the bottom segment by V_3, and similar quantities for the horizontal forces (positive towards the plasma) by H_1, H_2, and H_3, the reactions at the supports A, B, and C can be shown to be related by

$$P_B = -P_A/\sqrt{2} - (H_1 + H_2 + H_3)$$

$$P_C = P_A/\sqrt{2} + (V_1 + V_2 + V_3) \quad .$$

The bending moments at all points can then be easily obtained by statics. The bending stiffness of the blanket has been assumed constant (0.012 m^4) equal to that at the inboard vertical wall by considering the contributions from the 3 mm thick first wall, 1.5 cm thick second wall, the two 2 cm thick walls parallel to the second wall and the 4 cm thick back wall (Fig. 7-2). The contribution of the manifold side walls was found to be negligible. The cross-sectional area for carrying axial loads and shear forces is 0.32 m^2. The distance of the first wall from the neutral axis is estimated to be 0.41 m. The disruption loading and gravity loading are shown in Fig. 7-32.

Table 7-9 shows the reactions at the three supports corresponding to the dead weight of the combined structure (V), coolant (Li) and steel in the reflector zone, seismic load (4.4 g) acting vertically and radially, and plasma disruption including effects of loss of plasma diamagnetism. It is evident that the reactive forces due to plasma disruptions are significantly larger than those due to the other sources of loading. These reactions can be reduced by providing additional supports at the inboard wall. However, this may prove to be difficult because of lack of available space behind the inboard vertical wall. A complicating factor in designing the supports for the inboard blanket is the fact that the radial forces on the central post of the reactor or the toroidally continuous shield, whichever will ultimately carry

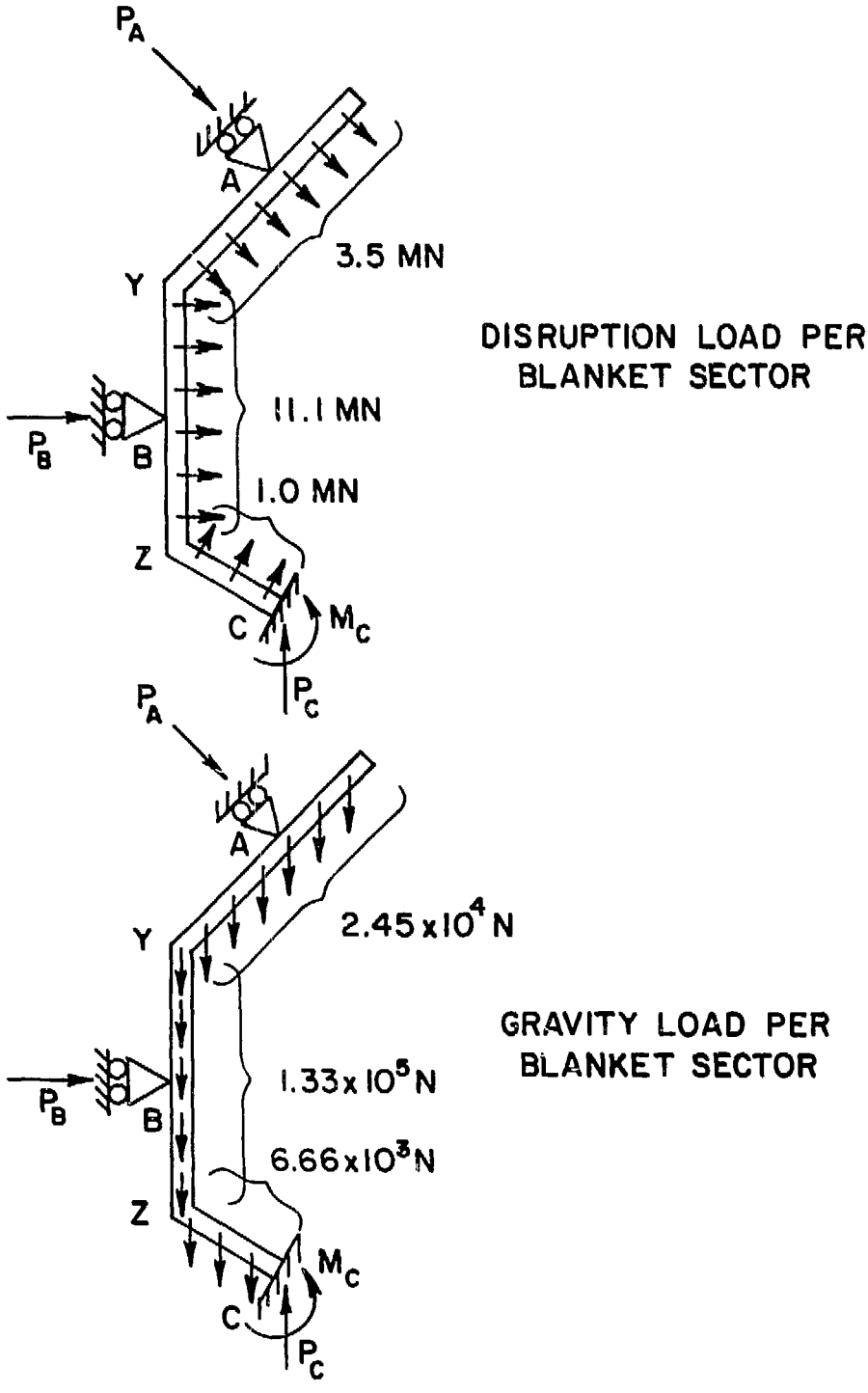

Figure 7-32. Summary of loadings on the reference liquid metal cooled inboard blanket due to gravity and plasma disruption.

the reactive force, are directed radially outwards. This will require the inboard blanket segments to be restrained actively from displacing radially outwards rather than by passive means, as was done in STARFIRE, had the forces been directed inwards. An additional large force on the supports will be induced during disruptions if the first walls of adjacent sectors are not electrically connected. Tangential pressures (2.7 MPa) acting vertically upwards on one side of a sector and downwards on the other do not produce any net force but subjects each sector to a couple (28.5 MN-m) about a radial axis tending to tip each sector in the toroidal direction. This torque in each sector will be reacted by a pair of equal and opposite vertical reaction forces of magnitude 10 MN primarily acting on support C. The average in-plane shear stress produced by these shear forces in the first wall and the other walls parallel to it is only 16 MPa.

The maximum primary and secondary stresses in the first wall produced by various loading mechanisms are summarized in Table 7-10. A maximum primary stress intensity of 235 MPa occurs at location B and is mostly due to plasma disruption loading. The allowable primary stress intensity for vanadium at the relevant temperature is also 235 MPa. Thermal stress at location A is negligible because it is shaded from the plasma by the outboard wall. The maximum total stress intensity in the Table 7-10 is obtained by combining stresses from one or more loading mechanisms and is within the 3 S_m limit of 705 MPa at all locations except at B where the stress limit is exceeded by a relatively small amount. However, the thermal stress at B is very likely smaller than the number reported in the table which is based on a uniform temperature gradient equal to the worst temperature gradient in the blanket occuring near the inlet where the coolant temperature in the manifold is the lowest in the system.

7.8.3.2 Tandem Mirror Design

Both the beam and the tube zones of the TMR designs have been analyzed as complete toroidal shells. The primary stress intensity due to coolant pressure, and dead weight loading of 17Li-83Pb and the structure has been estimated to be 124 MPa in the beam zone and 44 MPa in the tube zone both of which are less than the allowable limit of 125 MPa for vanadium corresponding to a radiation creep of 5% in 150 dpa. The primary stresses in the lithium cooled designs are smaller.

TABLE 7-9. COMPARISON OF REACTIVE FORCES ON THE INBOARD BLANKET DUE TO LOADINGS CAUSED BY DEAD WEIGHT, 4.4 g SEISMIC ACCELERATIONS IN THE VERTICAL AND RADIAL DIRECTION, AND PLASMA DISRUPTION INCLUDING EFFECTS OF LOSS OF PLASMA DIAMAGNETISM

Type of Loading	Reactive Forces (MN) at			Reactive Bending Moment (MN - m) at C
	A	B	C	
Dead Weight	-0.008	0.006	0.176	-0.158
Seismic	±0.132	±0.760	±0.840	±0.911
Plasma Disruption	-4.100	-11.300	-1.100[a]	4.200

[a]Reaction forces of ±10 MN have to be added to this to balance the couple acting on each blanket sector if adjacent sectors are not connected electrically at the first wall.

TABLE 7-10. COMPARISON OF MAXIMUM STRESSES IN THE FIRST WALL DUE TO LOADING CAUSED BY DEAD WEIGHT, 4.4 g SEISMIC ACCELERATION IN THE VERTICAL AND RADIAL DIRECTIONS, PLASMA DISRUPTION, COOLANT PRESSURE AND GRADIENT TEMPERATURE

Type of Loading	Maximum Stress (MPa) at				
	A	Y	B	Z	C
Dead Weight	-0.4	-0.8	-0.4	-0.5	5.4
Seismic	±3.4	±5.2	±19.1	±10.4	±31.4
Plasma Disruption	-78.7	53.4	-168.8	157.5	142.9
Coolant Pressure	+ 59.2 -118.3	+47.3 -94.6	+23.7 -47.3	+11.7 -23.7	+ 5.9 -11.7
Total Maximum Primary Stress	-200.8	+105.1	-235.6	+179.1	+185.6
Maximum Thermal Stress	0	-510	-510	-510	-510
Maximum Total Stress Intensity[a]	200.8	610.6	745.6	544.6	548.7

[a]Stress intensity is equal to twice the maximum shear stress.

Following a rapid plasma dump (in 100 ms), the first wall will experience a pressure much less than 0.016 MPa causing negligible stresses. The added radially inward force in the lithium cooled systems arising from loss of plasma diamagnetism is 56000 N/m MPa which causes a toroidal stress of about -42 MPa in the front tubes. In the case of 17Li-83Pb cooled systems, the total radially inward force is about 31000 N/m which is shared equally by the first four layers of tubes causing a stress of only 6 MPa.

In the case of lithium cooled design using HT-9 as the structural material, a body force due to magnetostatic interactions is generated in the structure. The body force on the front tube of the TMR design has been estimated to be about 27 gm/cc acting radially inwards at the magnets and radially outwards in between the magnets. The primary stress due to this body force has been estimated by treating the front tubes as toroidal circular tubes of toroidal radius 70 cm having a circular cross-section of diameter 10 cm with a wall thickness of 3 mm. The toroidal hoop stress due to a radial pressure p on such a toroidal tube is given by:

$$\sigma_H = pD/(2A)$$

where

D = diameter of the torus

A = solid cross-sectional area of the tube.

Substituting D=140 cm, A=3π cm^2, and p=27A gm/cm, the average hoop stress in the tube is only 0.2 MPa and can be neglected.

Since the weight of the 17Li-83Pb is a concern, an earthquake analysis of 17Li-83Pb cooled TMR blanket was carried out using the conservative equivalent static analysis method. As discussed in Section 7.7, earthquake induced loads of 4.4 g were applied simultaneously in three orthogonal directions. The model for the beam zone, shown in Fig. 7-33 for the vertical loading case, assumes the beam zone to be a complete ring supported at the locations indicated. For the vertical loading case, the unknowns are the horizontal reaction force H, and the stress resultants N_1 and M_1 which can be determined by

minimizing the strain energy of the system with respect to the three unknowns as in the case for the tokamak.

$$\left(1 + \frac{3\pi}{4}\right)M_1 + \left[1 + \frac{\sqrt{2}}{4} + \frac{3\pi}{4}\left(1 + \frac{\sqrt{2}}{2}\right)\right] r\, N_1 + \frac{3\sqrt{2}}{4}(\pi + 1)\, rH$$

$$- \left(1 + \frac{3\sqrt{2}}{4}\right)\frac{r}{2} P - \left(\frac{\pi}{4} - 1 - \frac{\sqrt{2}}{2}\right)r^2 w + \left(1 + \frac{\sqrt{2}}{4} - \frac{3\sqrt{2}\,\pi}{8}\right)rR = 0$$

$$\frac{\pi}{2} r\, N_i + \left(1 + \frac{3\pi}{2}\right)\frac{r}{4} H + \frac{\pi r^2}{4} w - \frac{r}{4} R = 0$$

$$M_1 + r\, N_1 + \frac{\sqrt{2}}{2}\left(\frac{3}{4} + \frac{1}{\pi}\right) rH - \frac{r}{\pi} P + r\left(\frac{1}{\pi} + \frac{\sqrt{2}}{2\pi} - \frac{3\sqrt{2}}{8}\right)R = 0$$

where

$$R = P + \pi r w.$$

For the horizontal loading case (Fig. 7-34), the only unknown is the vertical shear V_1 which can be solved for as before giving

$$V_1 = P(0.75 - 1/\pi) + wr(0.75\,\pi - 0.5) \quad .$$

For the axial loading case, the beam zone is assumed to be in a state of uniform tension or compression carried by the flanges.

The geometrical parameters and loadings for the 17Li-83Pb cooled design were taken from the preliminary MARS stress report.

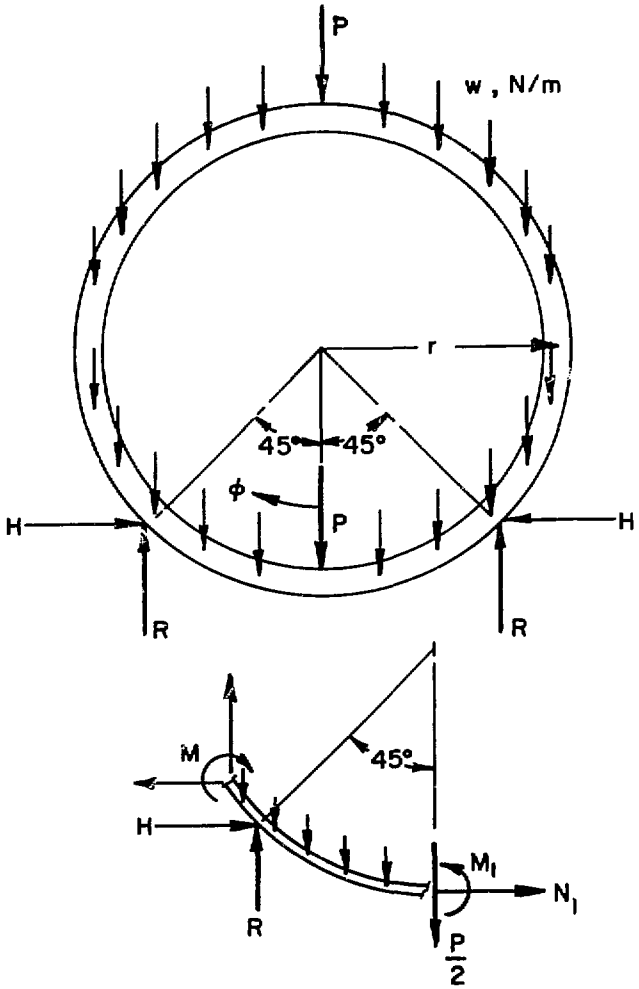

Figure 7-33. Geometry and loading of the beam zone of the reference liquid metal cooled tandem mirror reactor blanket for the vertical component of seismic loading.

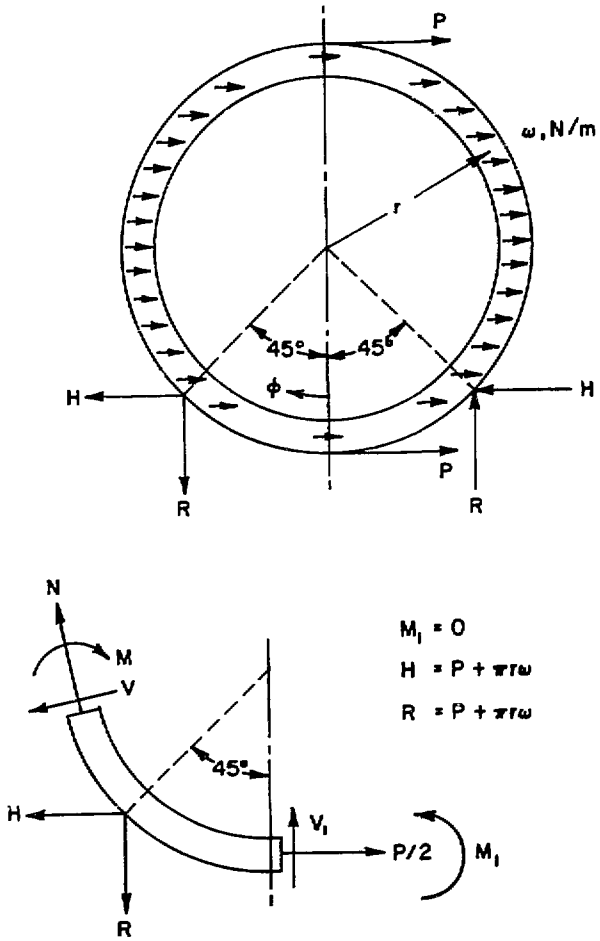

Figure 7-34. Geometry and loading of the tube zone of the reference liquid metal cooled tandem mirror reactor blanket for the vertical component of seismic loading.

$r = 0.895$ m

$I = 2.37 \times 10^{-4}$ m^4

$A = 0.0413$ m^2

$t = 0.007$ m

$P = 72418 \times 4.4$ N

The stresses in the beam zone arising from various sources are listed in Table 7-11. The bending stresses were found to be the largest being equal to ±149 MPa occurring at the top ($\phi = \pi$) for the vertical loading case and ±116 MPa occurring at the supports ($\phi = \pi/4$) for the horizontal loading case. The uniform axial stress due to the third component of seismic loading is ±39 MPa. For combined loading, a maximum stress intensity of 230 MPa occurs both at the top and at the supports. If this stress is added to the bending stress in the flanges due to the coolant pressure, and dead weight, the maximum primary bending stress intensity is 354 MPa, which exceeds the S_m value of 235 MPa. Although the allowable primary bending stress intensity is KS_m, where K=1.5 for a solid rectangular section, for a box beam as used in the TMR design, K is more like 1.1 and does not help in satisfying the primary stress criterion. The stresses in the Li-cooled designs are much smaller and easily meet the primary stress criterion.

The tube zone of the TMR blanket has been modelled as a complete ring clamped at both ends as shown in Fig. 7-35 for the vertical loading case. Proceeding as in the beam zone analysis, the maximum bending moment is

$$M_1 = 1.5\ wr^2$$

for the vertical loading case and

$$M_1 = \pi/2\ wr^2$$

TABLE 7-11. COMPARISON OF MAXIMUM STRESSES (MPa) IN THE BEAM ZONE OF THE TANDEM MIRROR REACTOR BLANKET DUE TO VARIOUS LOADING MECHANISMS

Type of Loading	17Li-83Pb Cooled V-Structure		Li-Coolant V-Structure		Li-Coolant HT-9 Structure	
	Toroidal	Axial	Toroidal	Axial	Toroidal	Axial
Dead Weight	±35	0	±4	0	±4	0
Seismic (±4.5g)	±191	±39	±34	±6	±24	±6
Coolant Pressure	14	+103 -63	7	+52 -32	7	+52 -32
Maximum Total Primary Stress Intensity[a]	354		79		79	

[a]Stress Intensity is equal to twice the maximum shear stress.

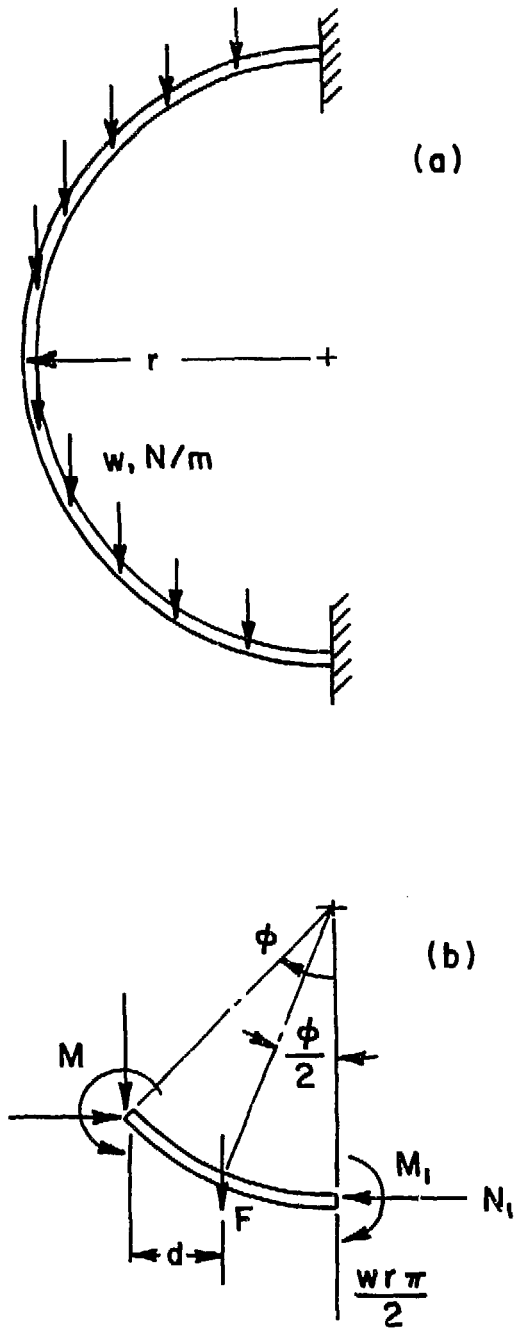

Figure 7-35. Geometry and loading of the tube zone of the reference liquid metal cooled tandem mirror reactor blanket for the vertical component of seismic loading.

for the horizontal loading case, both occurring at the supports.

The maximum bending moment caused by the third component of loading occurs at the support about an axis at right angles to the two previously calculated moments and is equal to

$$M_2 = wr^2 \quad .$$

In addition, there is a torque at the support equal to

$$T_2 = (\pi/2 - 4/\pi)\, wr^2 \quad .$$

The following loading and geometrical parameters for the 17Li-83Pb cooled design were taken from the preliminary MARS stress report

$w = 839 \times 4.4$ N/m
$r = 0.65$ m
$d = 0.1$ m
$t = 0.0023$ m.

The stresses in the tube zone for the various designs are summarized in Table 7-12. The maximum earthquake stresses in the tube zone are 265 MPa bending and 15 MPa shear. Adding to this the toroidal and poloidal hoop stress due to the coolant pressure, the bending stress due to dead weight, and the stresses due to plasma loss, the maximum stress intensity in the tube zone is 315 MPa which again exceeds the allowable S_m value of 235 MPa. As before, the primary stress intensity in the Li cooled designs are much smaller and easily meet the primary stress criterion. The thermal gradient in the front tube is 150 Deg C for the 17Li-83Pb cooled design and about 75 Deg C for the Li cooled designs. These gradients generate very small thermal stresses and the primary plus secondary stress criterion is satisfied by all designs.

TABLE 7-12. COMPARISON OF MAXIMUM STRESSES (MPa) IN THE TUBE ZONE OF THE TANDEM MIRROR REACTOR BLANKET DUE TOVARIOUS LOADING MECHANISMS

Type of Loading	17Li-83Pb Cooled V-Structure		Li-Coolant V-Structure		Li-Coolant HT-9 Structure	
	Toroidal	Axial	Toroidal	Axial	Toroidal	Axial
Dead Weight	±29	0	±4	0	±4	0
Seismic (± 4.4g)	±265	0	±35	0	±35	0
Plasma Loss	-6	0	-42	0	-42	0
Magnetostatic	0	0	0	0	±0.2	0
Coolant Pressur	15	30	8	15	8	15
Total Maximum Primary Stress Intensity	315		88		88.2	
Maximum Thermal Stress Intensity	90		45		45	
Maximum Total Stress Intensity	405		133		133.2	

The inability to meet the primary stress limits in both the tube and the beam zones of the 17Li-83Pb cooled design under earthquake loading imply that a detailed structural dynamics analysis will be needed to validate the ability of this design to withstand earthquake loadings. It should also be noted that the primary stress in the 8 cm OD regions of the front tube where it is attached to the manifold at the top and bottom of the blanket is computed to be in excess of 500 MPa if the wall thickness in these regions is 1.5 mm. If a detailed structural dynamics analysis shows this wall thickness to be unacceptable then the wall thickness should be increased to 3 mm in order to meet the primary stress criterion. Finally, additional thermal stresses occur in the front tube at the point of attachment to the manifold due to a temperature gradient between the manifold and the front tube. These stresses have not been computed in the present study.

7.8.4 Nucleonic Analyses

Nucleonic analyses were carried out to define and study the performance of the self-cooled liquid blanket concepts with respect to the main blanket neutronics functions.[7-1,7-5] These functions are to convert the kinetic energy of the DT neutrons to recoverable heat and produce sufficient tritium to supply the tritium fuel requirement during the whole reactor lifetime as well as generate enough surplus tritium to start another reactor within a reasonable period of time. From the reactor design point of view, it is desirable to maximize the recoverable heat produced in the blanket which is defined as the energy deposited in the first wall, breeder, reflector, and plenum per fusion neutron. Another important function of the blanket is to perform as a part of the reactor bulk shield.

In the nucleonic analyses, three performance parameters are used to compare the different blanket designs; the tritium breeding ratio (TBR), the blanket energy multiplication factor, and the energy fraction lost to the shield. The analyses were done in a systematic way to study the performance changes due to the following variables: a) the breeder material selection (Li or 17Li-83Pb), b) the lithium-6 enrichment, c) the breeder zone thickness, d) the reflector material selection, e) the reflector zone thickness, and f) the reflector zone composition.

The main concern in these analyses is to improve the reactor economics by maximizing the blanket energy multiplication factor and reducing the capital cost of the blanket materials. No effort was given to maximizing tritium production, however, the analyses does show the potential for achieving a high TBR with minor design changes. The other key parameter is the energy deposition in the shield which is recovered at low temperature, low pressure, and cannot be used for generating electrical power. This energy loss should be limited to about 3% of the energy produced per DT neutron to improve the plant efficiency and reduce the shielding system capital cost.

The tritium breeding characteristics, the energy deposition in the blanket and the reactor shield, the tritium breeding benchmark calculations, and the liquid metal reference blankets are discussed in this section.

7.8.4.1 Tritium Breeding

Analyses were performed to study the tritium breeding potential of the self-cooled concepts for a wide range of blanket parameters. Lithium and lithium-lead (17Li-83Pb) breeders were considered in the analyses. Table 7-13 gives the blanket parameters considered for the analyses. The first wall has a composition of 50% steel structure and 50% liquid metal coolant (Li or 17Li-83Pb) by volume with a 1 cm total thickness. The tritium breeding zone has a variable thickness and a constant composition with 7.5% steel structure and 92.5% breeder. Both the first wall and the tritium breeding zone compositions are dictated by thermal hydraulic, structure, and MHD considerations as discussed in the other sections. Different reflector materials (C, Al, Cu, Zr, Mo, W, Pb, H_2O, PCA steel type, and V15Cr5Ti alloy) were analyzed. The thickness and the composition of the reflector zone were varied in the analyses. The ^6Li enrichment changed from natural abundance to 90% for the 17Li-83Pb breeder. Only natural abundance was considered for the liquid lithium breeder. In general, the blanket does not benefit from lithium-6 enrichment unless a neutron multiplier or a large structural fraction is used in the breeding zone. A shielding zone is included in the calculational blanket model to get the correct boundary conditions at the outer surface of the reflector zone. The one-dimensional discrete ordinates code ANISN[7-6] was used to perform the transport calculations with a P_3 approximation for the scattering cross sections and an S_8 angular quadrature set. A 67-coupled

group cross section data library (46-neutron and 21-gamma) based on ENDF/B-IV was employed for these calculations. This data library is based on the VITAMIN-C[7-7] and MACKLIB-IV[7-2] libraries.

Lithium and lithium-lead blankets require a reflector zone which has good neutron moderators combined with high Z-material to absorb the secondary gamma rays. The reflector materials soften the neutron spectrum which increase $^{6}Li(n,\alpha)t$ reaction and the tritium production rate per fusion neutron. The high Z-reflector materials absorb the secondary gamma rays generated from the blanket and the front section of the shield causing an increase in the blanket energy multiplication factor. So, the use of the reflector zone improves the blanket performance in the following manner: a) reduces the blanket thickness to achieve a specific tritium breeding ratio, b) increases the blanket energy multiplication factor, c) reduces the energy deposition in the bulk shield, and d) reduces the total blanket and shield thickness for a specific blanket performance. The impact on the TBR will be analyzed in this section. The other aspects will be discussed in the next sections.

TABLE 7-13. BLANKET PARAMETERS FOR THE NUCLEONIC ANALYSES

Zone Description	Zone Thickness (cm)	Zone Composition (Vol. %)
First Wall	1	50% steel structure 50% liquid metal (Li[a] or 17Li-83Pb[b])
Breeder	A[c]	7.5% steel structure 92.5% liquid metal (Li[a] or 17Li-83Pb[b])
Reflector	B[c]	C%[c] steel structure D%[c] liquid metal (Li[a] or 17Li-83Pb[b]) (100-C-D)% reflector material
Shield	60	90% type Fe1422 steel 10% water

a) Natural lithium.

b) ^{6}Li enrichment is a variable.

c) A, B, C, and D are variables.

A natural lithium-lead blanket without a reflector zone was considered to demonstrate the undesirable characteristics of this blanket configuration. A ferritic steel structure (HT-9) was employed for the analysis. For this blanket, a 1.0 m breeder zone thickness is required to achieve a 1.24 TBR. At this thickness, about 7% of the total energy is deposited in the shield zone and 0.17 neutrons per fusion neutron leaves the blanket to the shield zone. Increasing the breeding zone thickness to 1.2 m reduces the neutron leakage and the energy deposition in the shield by a factor of two and increases the TBR from 1.24 to 1.31. Thus, a 1.2 m thick blanket is required to achieve a 96% of the total energy deposited in the blanket with adequate tritium breeding. Such blanket thicknesses have undesirable effects on the reactor design. For a natural liquid lithium breeder, the neutron leakage is greater than the leakage for the lithium-lead case. For the 1 m blanket, the neutron leakage from the lithium breeder zone is about 0.5 neutron per fusion neutron which is a large value. The lead material is more effective in slowing down the fusion neutrons relative to lithium.

In order to compare and select a reflector material, several materials were used with the same blanket. The blanket has a 50 cm lithium-lead breeder zone with a PCA structural material which is 5% by volume. The reflector zone is 30 cm thick with a 5% lithium-lead coolant and another 5% PCA structure by volume. The ^{6}Li enrichment is 90% to ensure adequate ^{6}Li absorption for tritium breeding. The other blanket parameters are given in Table 7-13. The TBR obtained from this analysis is given in Table 7-14 as well as the blanket energy deposition per fusion neutron for each blanket. The water reflector gives the highest TBR due to the excellent slowing down properties of hydrogen.[7-8] The carbon reflector is second with a 4% lower tritium production relative to water. The high Z-reflector materials produce lower TBRs relative to water or carbon. This is due to more parasitic absorption and less slowing down by the reflector materials. The use of a high pressure water reflector with the self-cooled liquid metal concepts produces an undesirable combination from a safety point of view. The carbon reflector is the choice if a high TBR is the main criterion for the design. The other reflector materials (Cu, Cr, Mo, W, Pb, type PCA steel, and V15Cr5Ti alloy) have about the same TBR as shown in Table 7-14. Each of these materials has at least one disadvantage from a reactor design point of view. For example,

Cu, Zr, and Mo have long-term radioactive products and lead has a low melting point. The V-15Cr-5Ti alloy and W are expensive relative to other materials. For these reasons and others, carbon and steel type reflectors were considered for more detail analyses.

TABLE 7-14. IMPACT OF THE DIFFERENT REFLECTOR MATERIALS ON THE LITHIUM-LEAD BLANKET[a] PERFORMANCE

Reflector Material	Tritium Breeding Ratio	Blanket Energy Per DT Neutron
Mo	1.54	18.06
Cu	1.55	17.82
W	1.51	17.63
Type PCA Steel	1.59	17.36
H_2O	1.75	17.36
V15Cr5Ti Alloy	1.60	17.28
Zr	1.60	17.05
C	1.68	16.96
Pb	1.59	16.48
Al	1.57	16.47

[a]Blanket parameters are listed in Table 7-12 with following modifications: 49 cm breeding zone thickness (95% 17Li-83Pb, 5% type PCA steel), 30 cm reflector (5% 17Li-83Pb, 90% reflector, 5% type PCA steel) and 90% ^{6}Li enrichment.

Carbon and steel were used with the natural lithium-lead breeder to compare in more detail their performance from the TBR point of view. A ferritic steel structure (HT-9) was employed for this analysis. Figures 7-36 and 7-37 show the TBR as a function of the reflector zone thickness for different breeding zone thicknesses. The blankets with the steel reflector do not achieve a TBR greater than 0.9 for a 90 cm maximum blanket thickness (50 cm breeder and 40 cm reflector). The same blanket with a carbon reflector has a TBR greater than 1.2. This difference in performance is related to the macroscopic cross section ratio of the lithium-6 to the total absorption in the reflector zone. This ratio is close to unity for the carbon reflector because it is dominated by ^{6}Li(n,α)t cross section. The carbon absorption cross section for low energy neutrons is four to six order of magnitudes lower than ^{6}Li(n,α)t. For a steel reflector, this ratio is less than one because the macroscopic absorption cross section of steel is comparable to the lithium-6

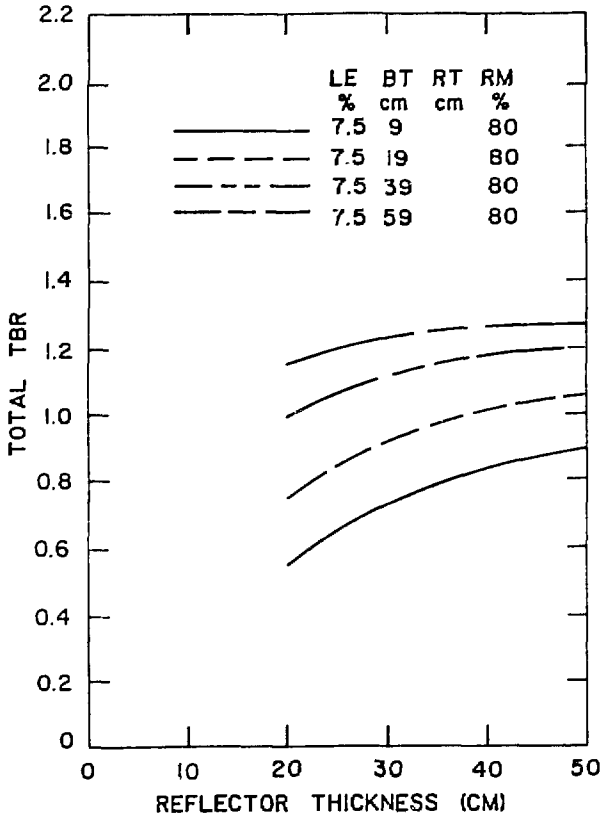

Fig. 7-36. Tritium breeding ratio as a function of the carbon reflector zone thickness for different lithium-lead breeding zone thicknesse. with natural lithium enrichment.

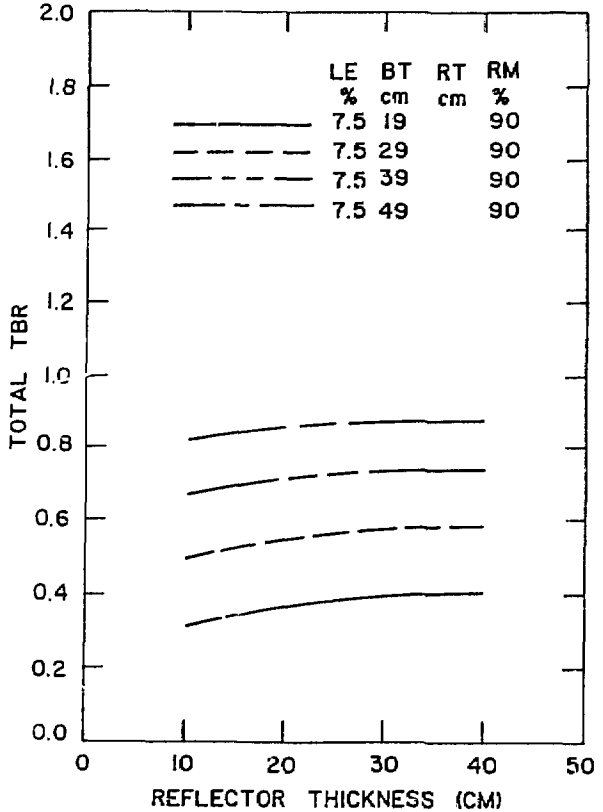

Figure 7-37. Tritium breeding ratio as a function of the steel reflector zone thickness for different lithium-lead breeding zone thicknesses with natural lithium enrichment.

which leads to a competition between the steel and the lithium-6 for the available neutrons in the reflector zone. This point is clearly demonstrated when lithium-6 enrichment is increased in the blanket. The TBR increases from 0.9 to 1.5 when a 90% lithium-6 enrichment is used instead of the natural enrichment for the same blanket as shown in Figs. 7-37 and 7-38.

Based on the above analysis, the natural lithium lead blanket with carbon reflector can achieve a TBR greater than 1.2. The same blanket with a steel reflector instead of the carbon requires lithium-6 enrichment to obtain a similar TBR. However, the steel reflector has an advantage related to the blanket energy multiplication which is the subject of the next section. Similar behavior is observed with the liquid lithium breeder except both reflectors can achieve a TBR greater than 1.2 with natural lithium enrichment.

The higher energy multiplication factor of a steel reflector motivated further in-depth analysis for the liquid metal blankets to address the potential of this concept. The results will also apply to other high Z-materials (Cu, Mo, and W). The blanket parameters in Table 7-13 were considered with the lithium-lead breeder where the lithium-6 enrichment (LE) was varied from natural to 90% in steps. The breeder zone thickness (BT) changed from 20 to 50 cm for different reflector zone thicknesses (RT). The TBR results are shown in Figs. 7-39 through 7-44 for a 90% (RM) ferritic steel, 10% 17Li-83Pb reflector zone composition. Other reflector compositions were used in the analysis which show similar trend to the results displayed in Figs. 7-39 through 7-44.

With respect to the tritium breeding results, the following observation can be made: a) a TBR up to 1.65 is achievable with a total blanket thickness less than 90 cm, b) the TBR of the natural lithium-lead blanket increases linearly with the breeding zone thickness for any reflector zone thickness up to about 1.2 meter total blanket thickness, c) for a specific breeding zone thickness, the TBR ratio reaches a saturation level at about a 30 cm reflector zone thickness, d) at about 30% lithium-6 enrichment, a tritium breeding ratio of 1.2 to 1.4 is achievable with a blanket thickness less than one meter, and e) for a specific tritium breeding ratio, the total blanket thickness decreases as the lithium-6 enrichment or the breeding zone thickness increases.

The carbon reflector with the lithium-lead breeder gives similar results to the steel reflector. Figure 7-45 gives the TBR as a function of the breed-

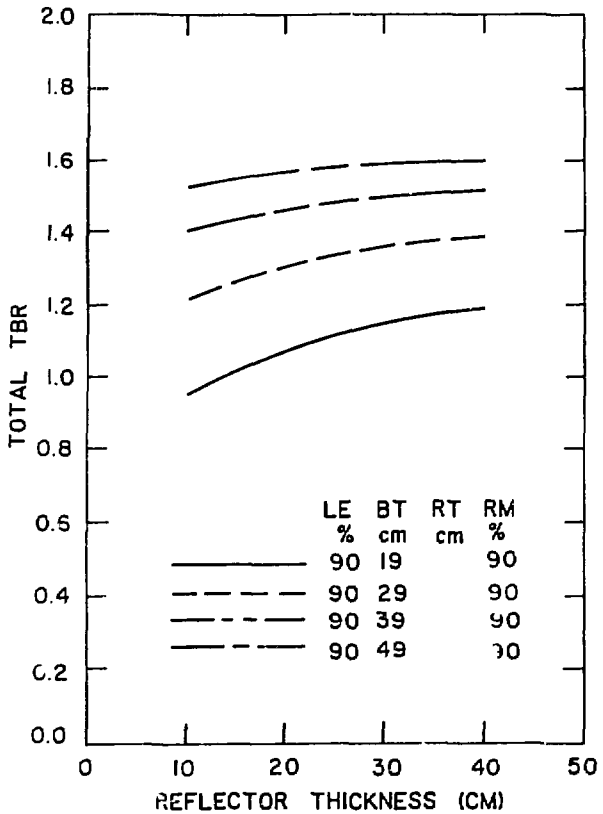

Fig. 7-38. Tritium breeding ratio as a function of the steel reflector zone thickness for different lithium-lead breeding zone thicknesses with 90% lithium-6 enrichment.

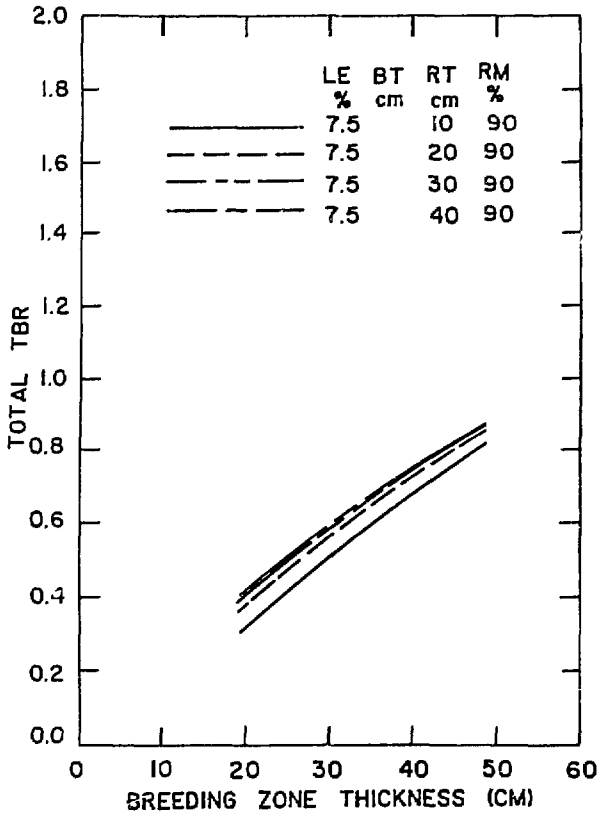

Fig. 7-39. Tritium breeding ratio as a function of the lithium-lead breeding zone thickness for different steel reflector zone thicknesses with natural lithium enrichment.

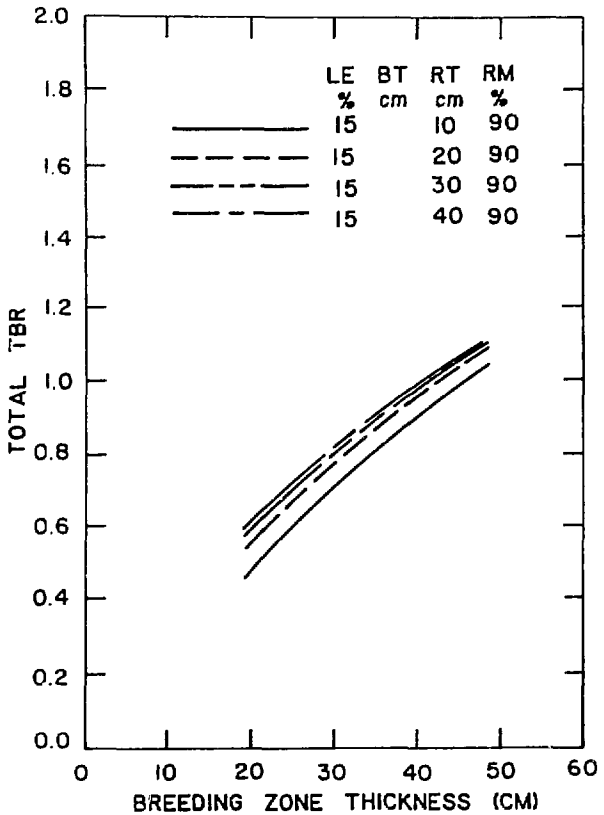

Fig. 7-40. Tritium breeding ratio as a function of the lithium-lead breeding zone thickness for different steel reflector zone thicknesses with 15% lithium-6 enrichment.

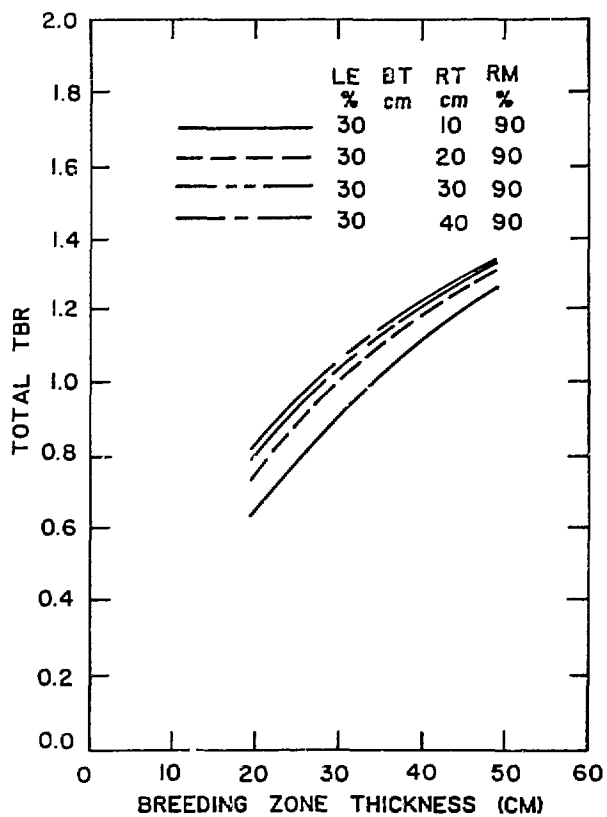

Figure 7-41. Tritium breeding ratio as a function of the lithium-lead breeding zone thickness for different steel reflector zone thicknesses with 30% lithium-6 enrichment.

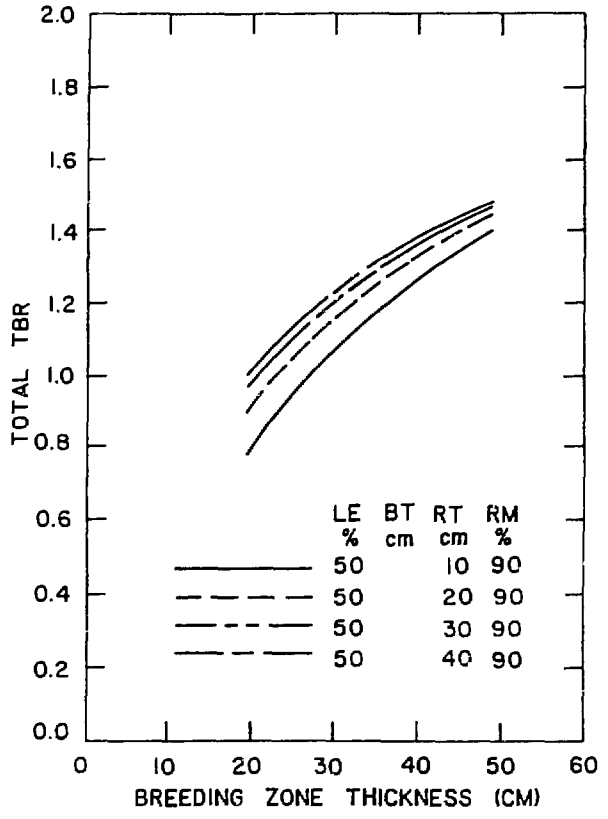

Figure 7-42. Tritium breeding ratio as a function of the lithium-lead breeding zone thickness for different steel reflector zone thicknesses with 50% lithium-6 enrichment.

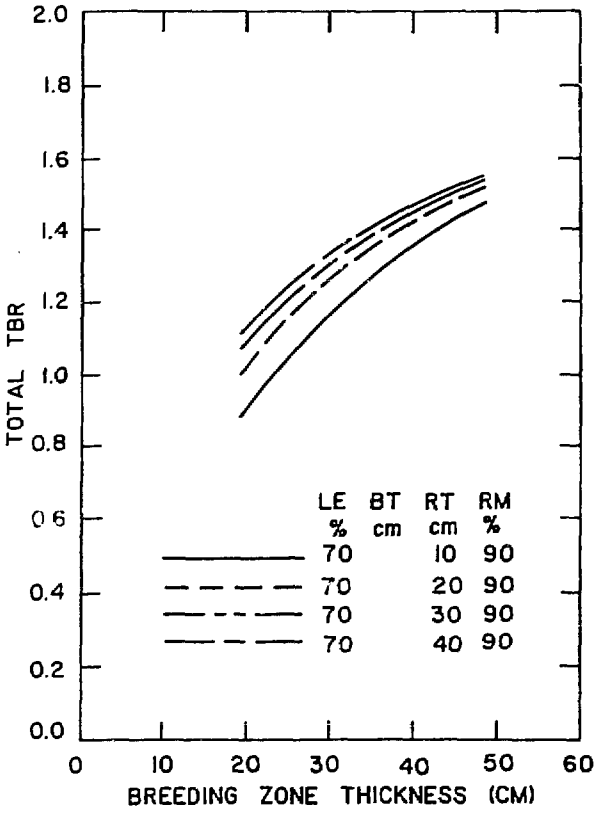

Fig. 7-43. Tritium breeding ratio as a function of the lithium-lead breeding zone thickness for different steel reflector zone thicknesses with 70% lithium-6 enrichment.

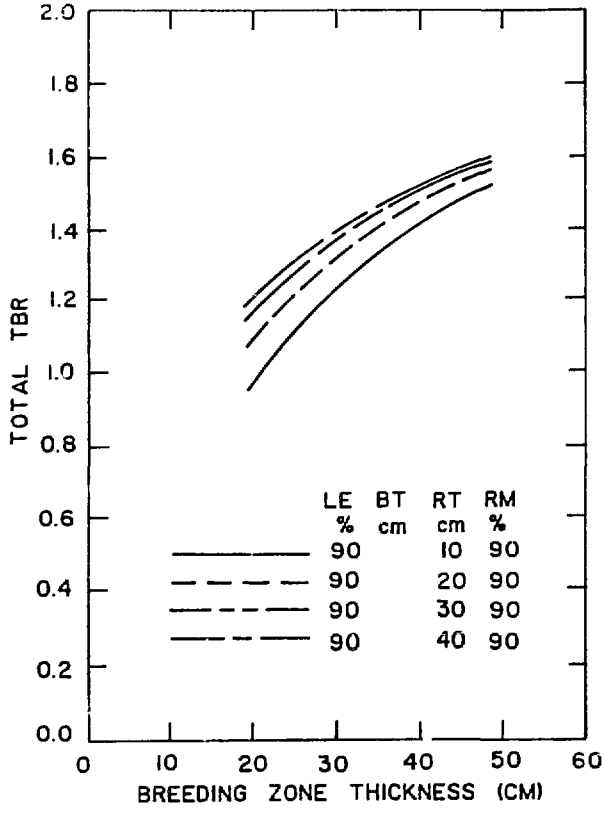

Fig. 7-44. Tritium breeding ratio as a function of the lithium-lead breeding zone thickness for different steel reflector zone thicknesses with 90% lithium-6 enrichment.

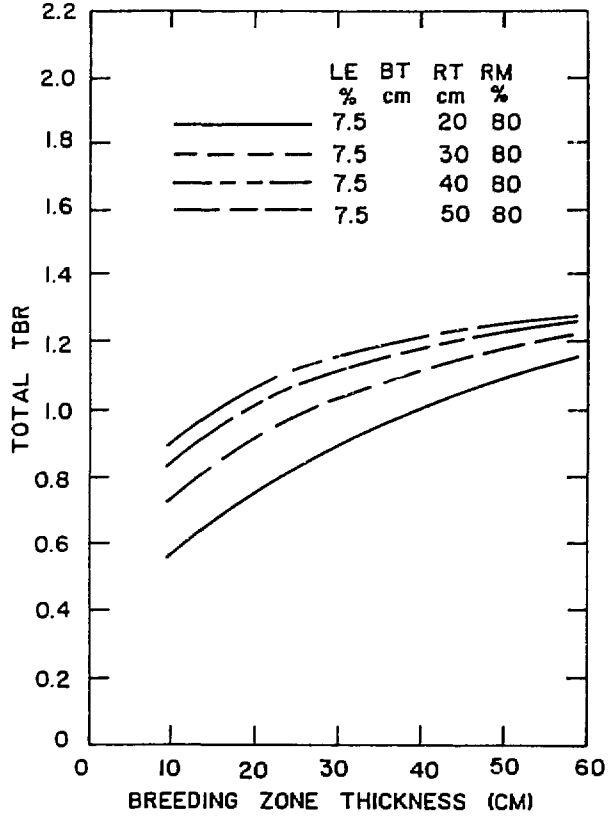

Fig. 7-45. Tritium breeding ratio as a function of the lithium-lead breeding zone thickness for different carbon reflector zone thicknesses with natural lithium enrichment.

ing zone thickness for different carbon reflector thicknesses with a natural lithium-6 enrichment. The carbon reflector requires a 40 cm zone thickness to achieve the TBR saturation value of a specific breeding zone thickness instead of the 30 cm for the steel reflector. Also, the natural lithium blanket with a carbon reflector has a higher tritium breeding potential than the corresponding blanket with a steel reflector as shown in Figs. 7-39 and 7-45.

A similar analysis was performed for the lithium breeder with a steel reflector. Natural liquid lithium is only used because the small steel fraction in the blanket does not require high lithium-6 concentration to achieve the highest possible TBR. Also, the use of natural lithium reduces the breeder material cost. Figure 7-46 shows the TBR as a function of the breeding zone thickness for different reflector zone thicknesses. The results show that a 60 cm blanket thickness is not adequate from the blanket energy multiplication point of view. The next section will address this issue in detail. Again, it appears that about 30 cm steel reflector zone is adequate to achieve the maximum TBR.

7.8.4.2 Blanket Energy Multiplication

The main function of the blanket is to produce recoverable heat in suitable conditions for the plant thermal cycle. So, it is desirable to maximize the recoverable heat and just satisfy the other requirements, such as the tritium breeding. Two factors determine the blanket energy multiplication, these are the blanket materials and the TBR required. Four materials (breeder, structure, coolant, and reflector material) are required for the blanket. For the self-cooled liquid metal concepts, the breeder and the coolant are the same material. The structural material choice is based on material compatibility considerations with the breeder material (Li or 17Li-83Pb) as discussed in the material sections. This leads to consider the ferritic steel and the V15Cr5Ti alloys as structural materials. The reflector material is the only material choice that can be defined based on the desire to improve the blanket energy multiplication.

As mentioned before, several materials were considered to define the reflector material. Table 7-14 gives the energy produced per fusion neutron in the blanket for these reflector materials. Molybdenum, copper, and tungsten material produce the highest energy deposition in the blanket.

Among these three materials, tungsten is the preferred material for two reasons. It has a good shield performance which reduces the total blanket and shield thickness. Also, tungsten does not produce long-term activation and it can be recycled without difficulty. Steel and water reflectors deposit the same amount of energy in the blanket through different mechanism as can be seen from the corresponding TBR. The blanket with vanadium for the reflector zone produces less energy than the corresponding blanket with steel. The other reflector materials (Zr, C, Pb, and Al) are in a lower rank in terms of the energy deposition per fusion neutron but they have high TBRs due to their low absorption cross sections. Again steel and carbon were used for more detail analyses for the same reasons discussed in the previous section.

Figures 7-47 through 7-52 show the blanket energy multiplication as a function of the lithium-lead breeding zone thickness for different reflector zone thicknesses and several lithium-6 enrichments. The blanket energy multiplication factor decreases as the lithium-6 enrichment increases. As shown before for the lithium-lead breeder in the previous section, the $^{6}Li(n,\alpha)t$ reaction rate increases with the lithium-6 enrichment because So more neutrons are absorbed in the lithium-6 with a 4.8 MeV energy release instead of about 7 to 8 MeV from neutron capture in the steel structure. As a result, the lithium-6 enrichment should be reduced to increase the blanket energy multiplication. For all the blankets, an increase in the reflector zone thickness increases the blanket energy multiplication and the TBR. So, it is always desirable to increase the reflector zone thickness to about 30 to 40 cm to improve the blanket performance. For blankets with reflector zone thicknesses less than 30 cm, an increase of the breeding zone thickness improves the blanket energy multiplication factor and the TBR. As the reflector zone thickness exceeds 30 to 40 cm, the blanket energy multiplication decreases with the increase of the breeding zone thickness as shown in Figs. 7-47 through 7-52.

Figure 7-53 shows similar results for the carbon reflector with a natural lithium-lead breeder. For the same blanket, the use of the carbon reflector results in less blanket energy multiplication and higher TBR relative to the use of the steel reflector. The blanket energy multiplication increases to

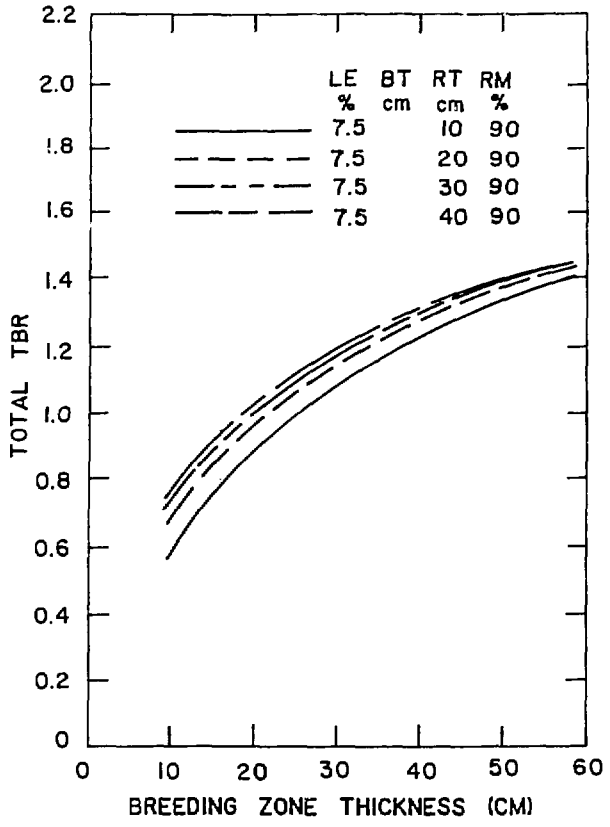

Figure 7-46. Tritium breeding ratio as a function of the lithium zone thickness for different steel reflector zone thicknesses with natural lithium enrichment (ENDF/B-IV data for ^{7}Li).

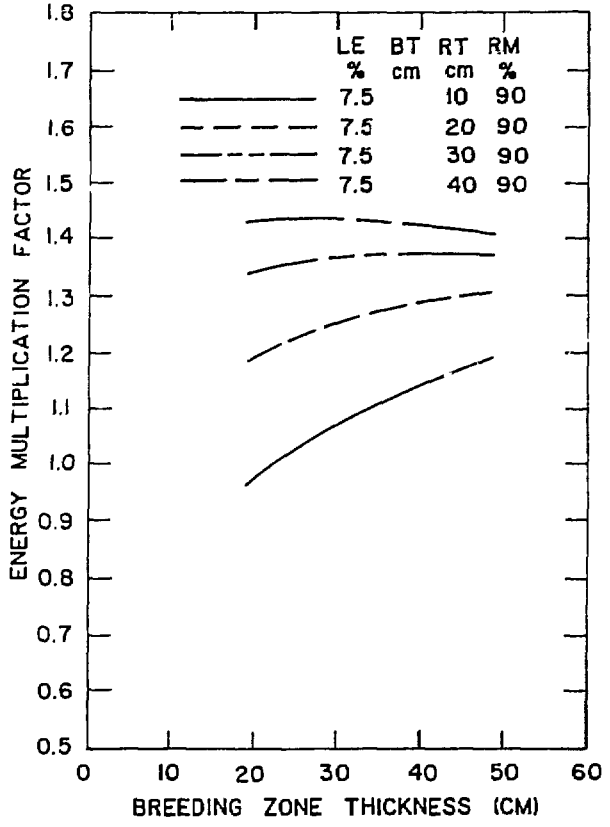

Fig. 7-47. Blanket energy multiplication factor as a function of the lithium-lead zone thickness for different steel reflector zone thicknesses with natural lithium enrichment.

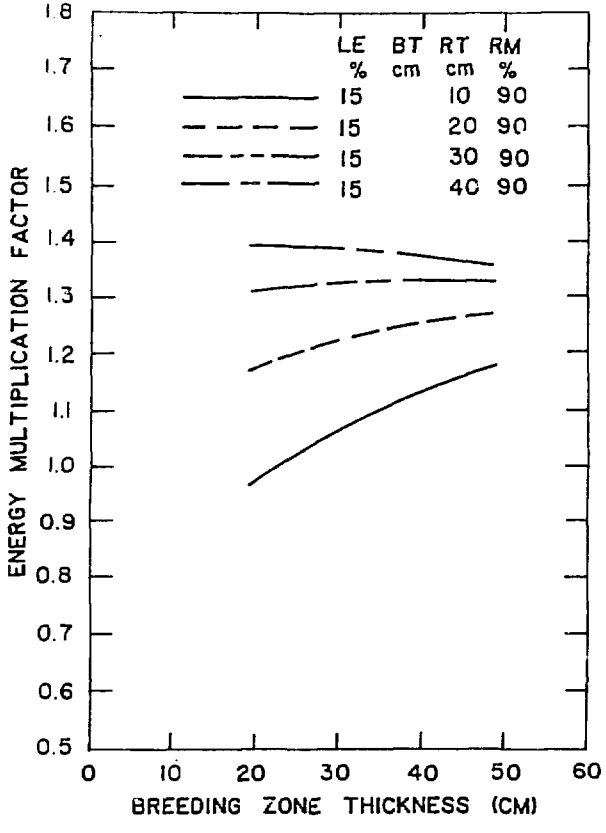

Fig. 7-48. Blanket energy multiplication factor as a function of the lithium-lead zone thickness for different steel reflector zone thicknesses with 15% lithium-6 enrichment.

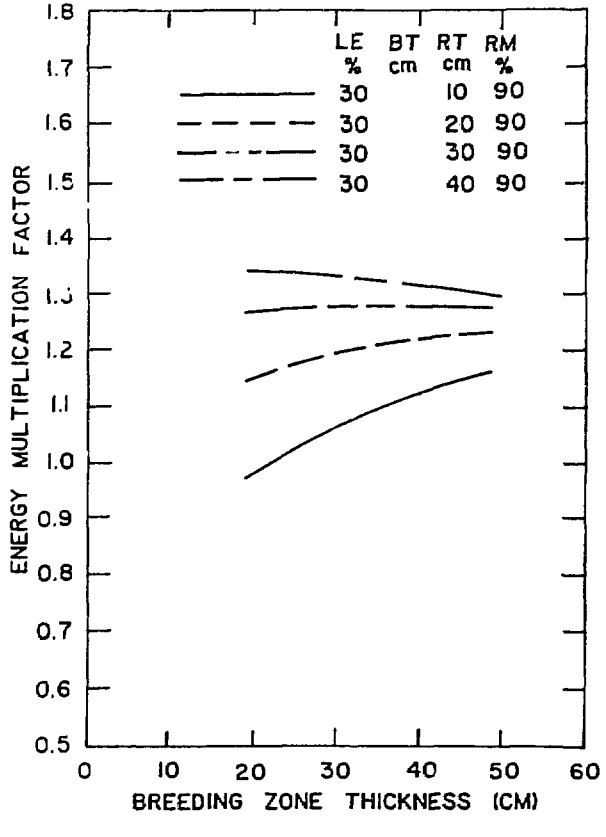

Fig. 7-49. Blanket energy multiplication factor as a function of the lithium-lead zone thickness for different steel reflector zone thickness with 30% lithium-6 enrichment.

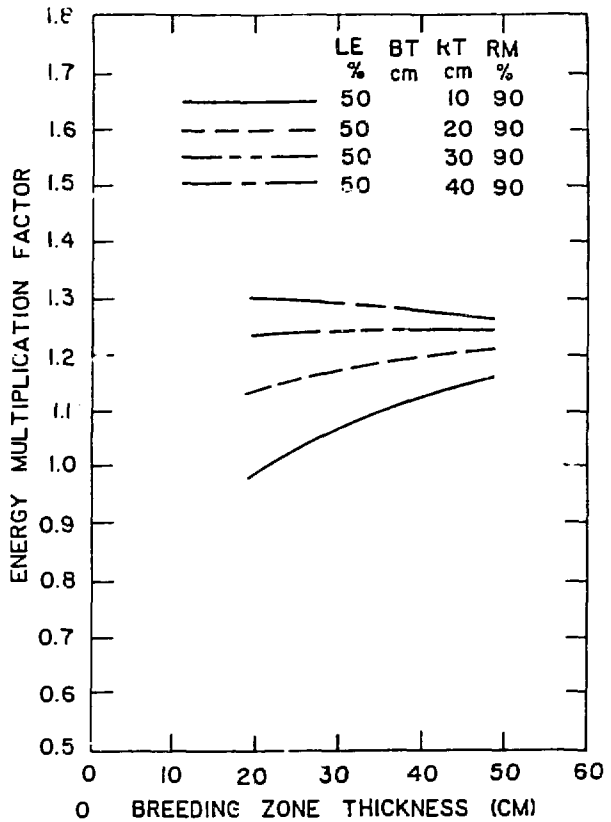

Fig. 7-50. Blanket energy multiplication factor as a function of the lithium-lead zone thickness for different steel reflector zone thicknesses with 50% lithium-6 enrichment.

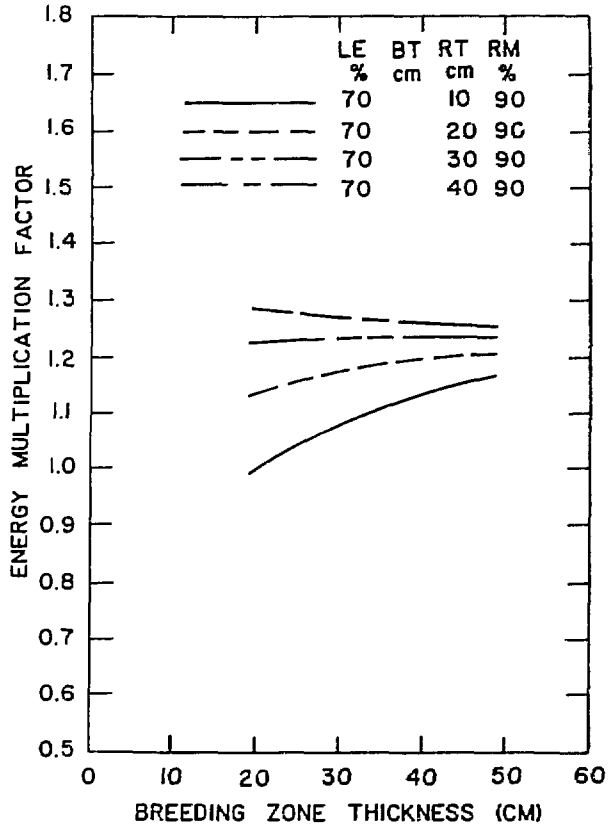

Fig. 7-51. Blanket energy multiplication factor as a function of the lithium-lead zone thickness for different steel reflector zone thicknesses with 70% lithium-6 enrichment.

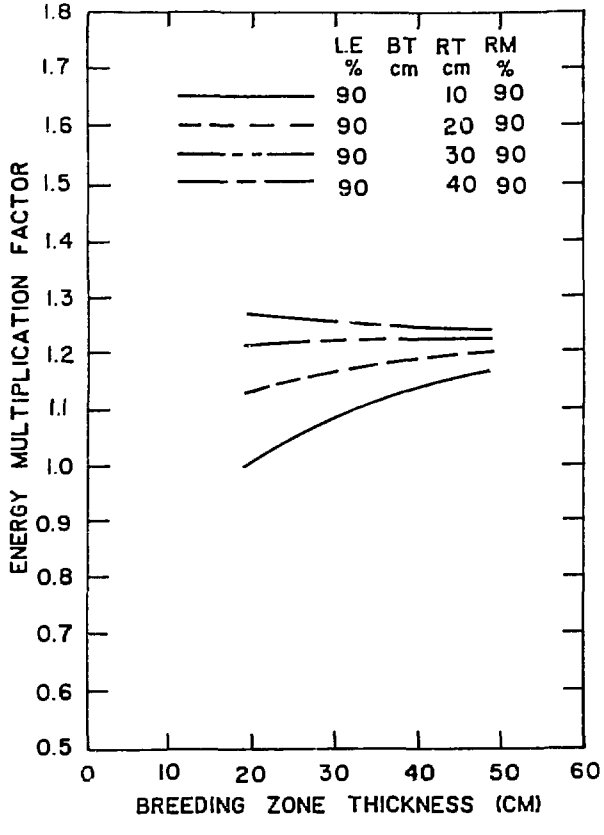

Fig. 7-52. Blanket energy multiplication factor as a function of the lithium-lead zone thickness for different steel reflector zone thicknesses with 90% lithium-6 enrichment.

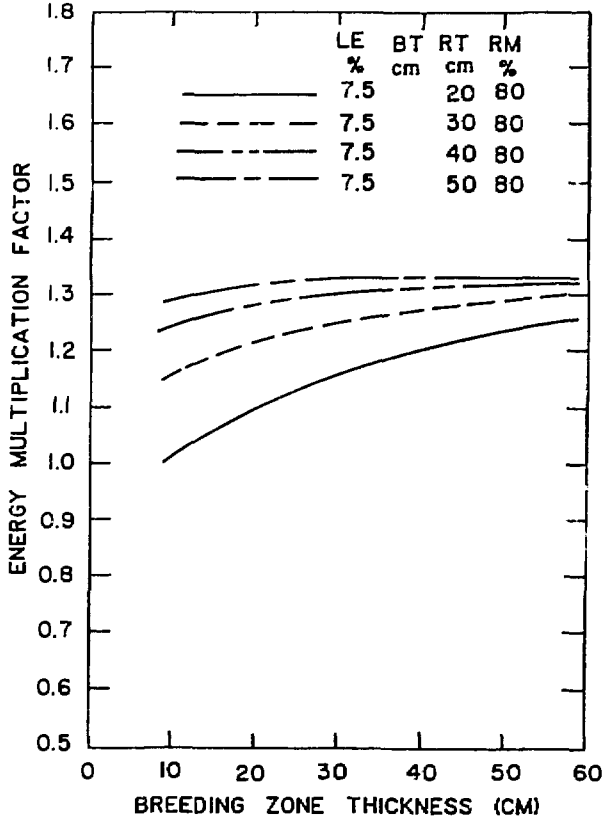

Fig. 7-53. Blanket energy multiplication factor as a function of the lithium-lead zone thickness for different carbon reflector zone thicknesses with natural lithium enrichment.

reach a saturation value as the breeding zone thickness increases for any reflector zone thickness. This observation is different from the steel reflector case. In fact, the carbon reflector increases the neutron absorption rate in lithium-6 and reduces the neutron leakage from the blanket. This causes a continuous increase in the TBR and the blanket energy multiplication. In the case of the steel reflector, lithium-6 has to compete with the parasitic absorption in the steel. In this case, the use of a high lithium-6 enrichment can lead to an increase in the TBR but reduces the blanket energy multiplication as explained before.

Figure 7-54 shows the blanket energy multiplication for the natural liquid lithium breeder as a function of the breeding zone thickness for different reflector zone thicknesses. The results are similar to the lithium-lead breeder with steel reflector.

7.8.4.3 Shield Energy Deposition

The energy deposited in the shield system is lost because it is not suitable for power generation. This energy should be minimized to improve the reactor economics by adjusting the blanket dimensions and/or compositions. The plant efficiency drops by about 1% for every 3% of the total energy deposited in the shield. Figures 7-55 through 7-62 give the energy fraction of the total energy deposited in the shield for the same range of the blanket parameters discussed in the previous two sections.

In order to reduce the energy deposition in the shield to about 3% for the blanket with the lithium-lead breeder and the steel reflector, the total blanket thickness should be about 80 to 90 cm thick depending on the lithium-6 enrichment. The blanket with natural lithium requires about 90 cm total blanket thickness. The use of 90% lithium-6 enrichment reduces the blanket thickness to 80 cm. This shows that the use of the 90% lithium-6 enrichment instead of the natural lithium reduces the total blanket thickness only by 10 cm. However, this reduction in thickness is accompanied by more than a 6% reduction in the blanket energy multiplication factor. The corresponding dimensions for the same blanket with the carbon reflector are 60 to 70 cm as shown in Fig. 7-61 for natural lithium enrichment. These dimensions indicate that the use of carbon reflector results in a 20 cm reduction in blanket

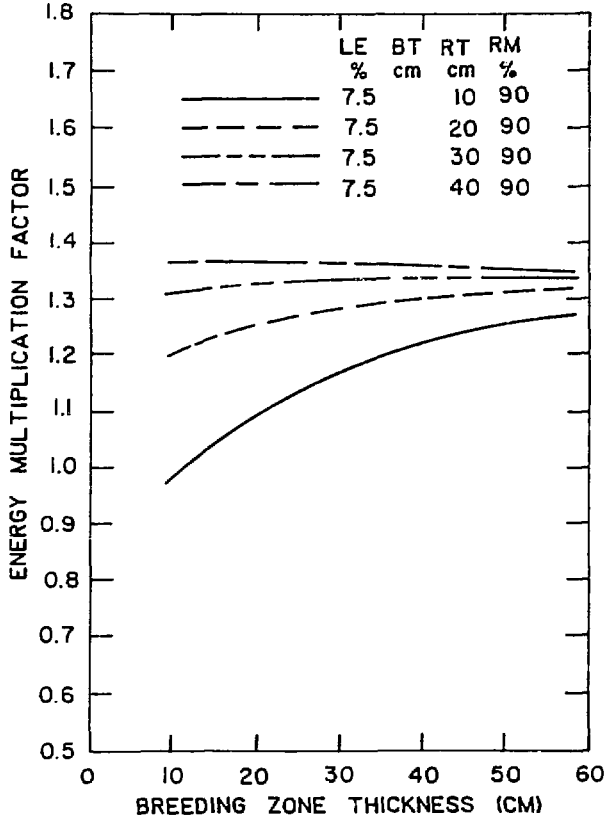

Fig. 7-54. Blanket energy multiplication factor as a function of the lithium breeder zone thickness for different steel reflector zone thicknesses with natural lithium enrichment.

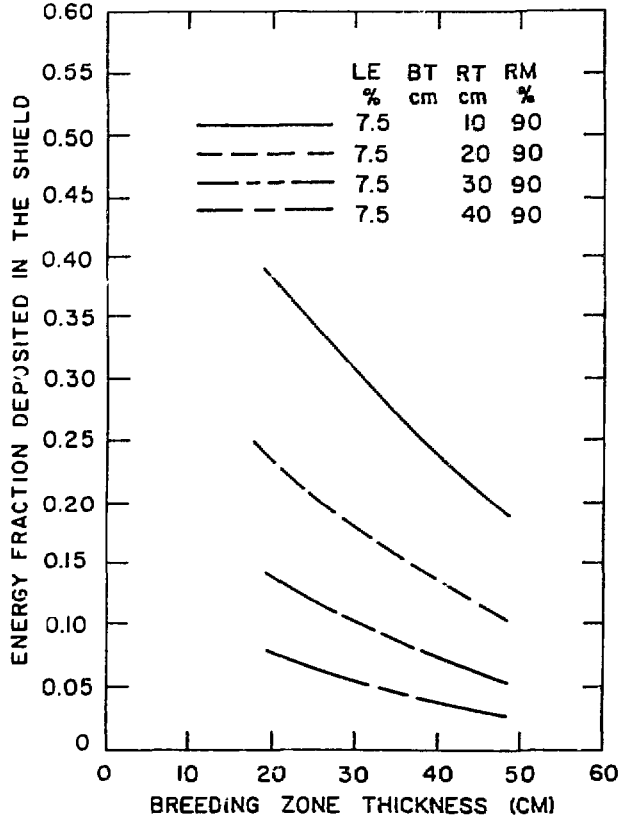

Fig. 7-55. Fraction of the total energy deposited in the shield as a function of the lithium-lead breeder zone thickness for different steel reflector zone thicknesses with natural lithium enrichment.

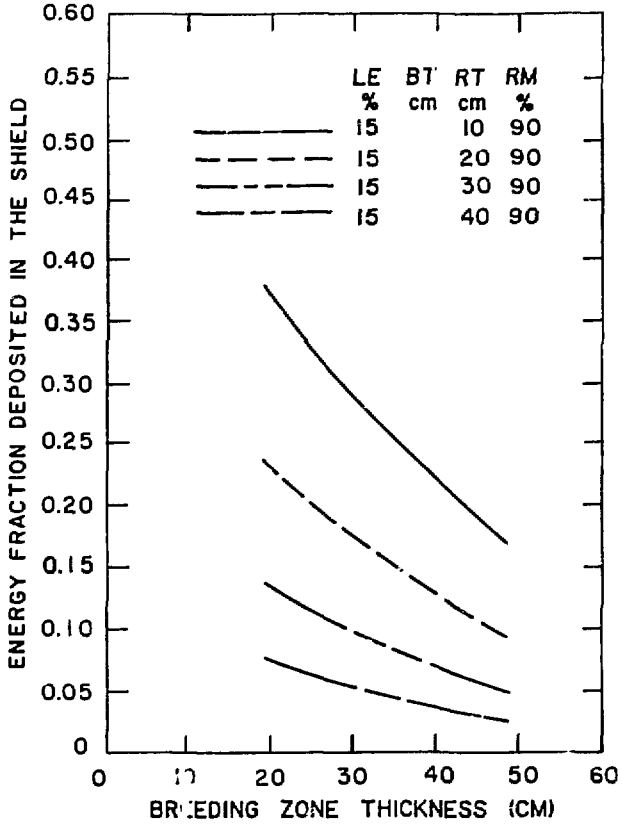

Fig. 7-56. Fraction of the total energy deposited in the shield as a function of the lithium-lead breeder zone thickness for different steel reflector zone thicknesses with 15% lithium-6 enrichment.

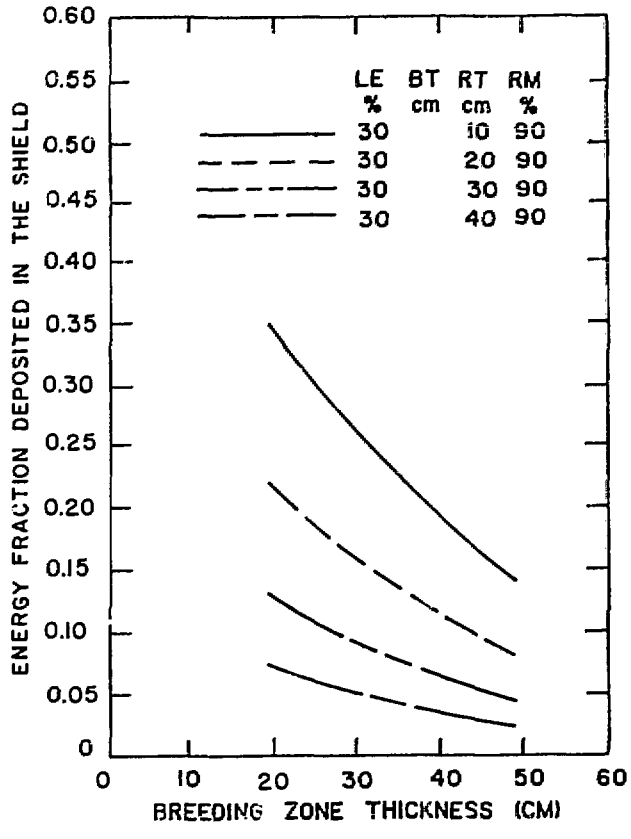

Fig. 7-57. Fraction of the total energy deposited in the shield as a function of the lithium-lead breeder zone thickness for different steel reflector zone thicknesses with 30% lithium-6 enrichment.

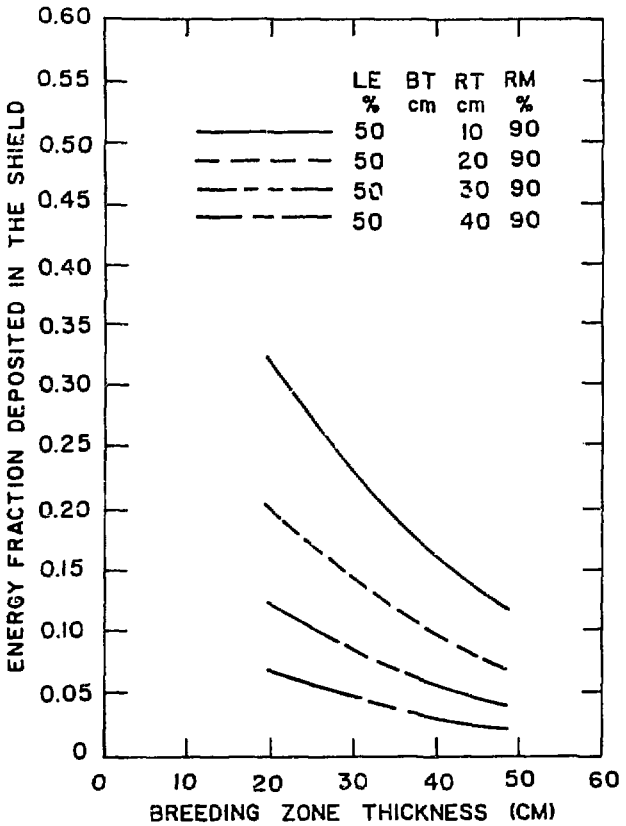

Fig. 7-58. Fraction of the total energy deposited in the shield as a function of the lithium-lead breeder zone thickness for different steel reflector zone thicknesses with 50% lithium-6 enrichment.

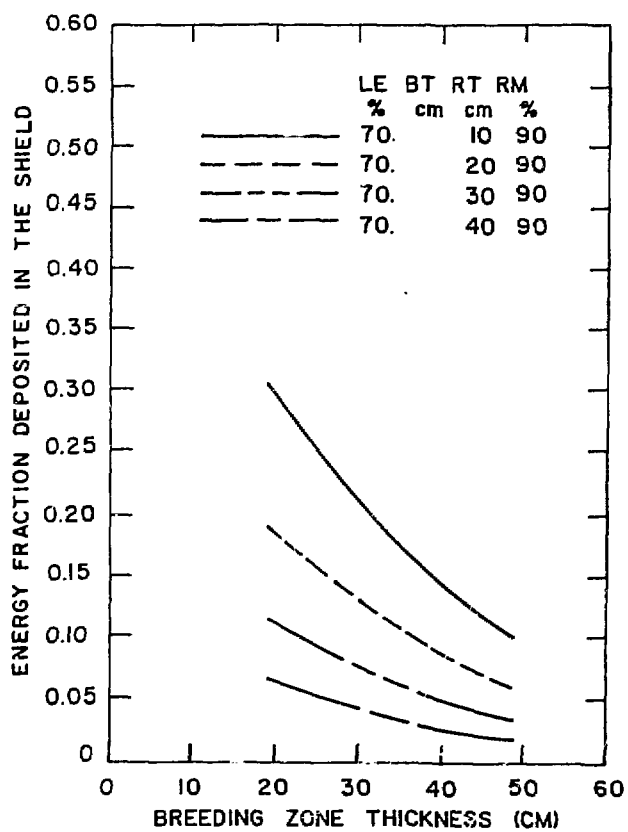

Fig. 7-59. Fraction of the total energy deposited in the shield as a function of the lithium-lead breeder zone thickness for different steel reflector zone thicknesses with 70% lithium-6 enrichment.

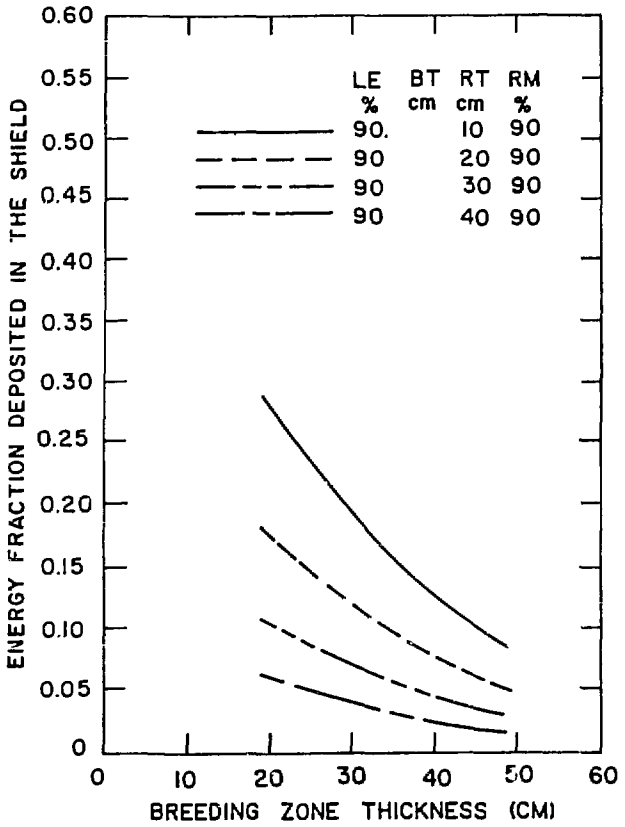

Fig. 7-60. Fraction of the total energy deposited in the shield as a function of the lithium-lead breeder zone thickness for different steel reflector zone thicknesses with 90% lithium-6 enrichment.

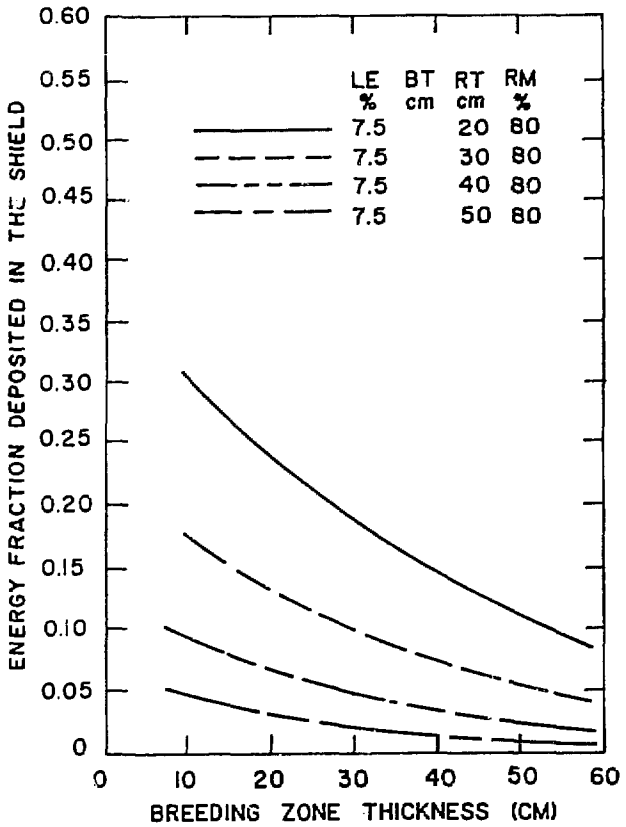

Fig. 7-61. Fraction of the total energy deposited in the shield as a function of the lithium-lead breeder zone thickness for different carbon reflector zone thicknesses with natural lithium enrichment.

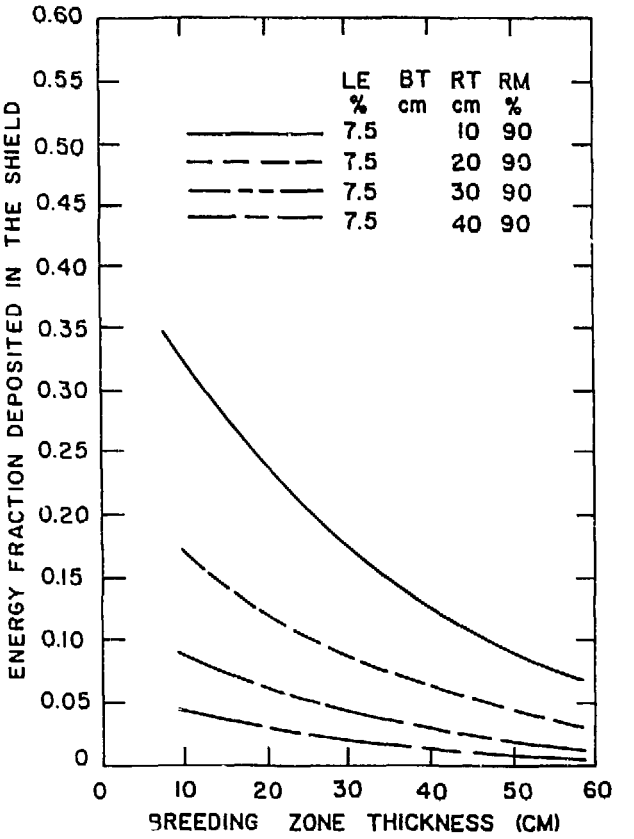

Figure 7-62. Fraction of the total energy deposited in the shield as a function of the lithium breeder zone thicknesses for different steel reflector zone thicknesses with natural lithium enrichment.

thickness. Again, a blanket with carbon reflector has a higher TBR and lower blanket energy multiplication than the same blanket with steel reflector.

Figure 7-62 shows the energy deposition in the shield of the liquid lithium blanket. It appears from the energy loss point of view that a 60 cm blanket thickness is required. This dimension is equivalent to the lithium-lead blanket with carbon reflector.

Also, it should be noted that another energy fraction of 0.01 to 0.03 will be lost to the shield. This leakage is due to radiation streaming from blanket manifolds, slots between blanket segments, and other reactor penetrations (limiter or divertor, choke coil, or instrumentation). Thus about 6% of the total energy is expected to be lost to the shield.

7.8.4.4 Tritium Breeding Benchmark Calculations for Liquid Lithium Blanket Concept

Accurate prediction of the tritium breeding ratio is a key parameter in the blanket design process. Thus it is desirable to compare the TBR values calculated by different transport codes and data libraries. ANISN[7-6] and MCNP[7-9] transport codes were employed for the benchmark calculations. ANISN is a one-dimensional, multi-group, neutron/photon transport code using the discrete ordinates method and the legendre expansion approximation for the scattering cross sections. MCNP is a three-dimensional, continuous energy, neutron/photon transport code using the Monte Carlo method. Four nuclear data libraries based on ENDF/B version IV and V were used for the calculations. Vitamin-C[7-7] and MACKLIB-IV[7-2] libraries were collapsed to a 46-neutron groups structure with a 1/E neutron spectrum for ENDF/B-IV multigroup ANISN calculations. Also, the Vitamin-E[7-10] library was collapsed to the same group structure with its spectrum (DT +1/E + LMFBR + 1/E + Maxwillian) for the ENDF/B-V ANISN calculations. MCNP uses two continuous energy libraries based on the ENDF/B version IV and V.

A natural liquid lithium blanket with PCA as a structural and reflector material was used for the benchmark. The geometrical model for this blanket is shown in Table 7-15 as well as the number of intervals for the discrete coordinate calculations. The ANISN calculations were performed with an S_8 symmetrical angular quadrature set shown in Table 7-16 and a P_3 approximation for the scattering cross sections. The neutron source distribution is uniform in

the plasma volume and the energy range of the first neutron group (13.499 to 14.918 MeV) for all the calculations. The atomic density of each blanket material is shown in Table 7-16. The fractional standard deviation in the MCNP results for the tritium breeding is less than 1.5% for all these blankets.

The breeding zone thickness was varied from 39 to 79 cm with a 20 cm step. The TBR was calculated for each blanket four times using the different combinations of the transport codes and the data libraries. Table 7-18 gives the TBR results for the three blankets. The relative differences between the TBR results for each liquid lithium blanket are given in Table 7-19. For the same data base (ENDF/B-IV or V), the TBRs calculated by MCNP or ANISN have a good agreement as shown in Table 7-18. The differences between MCNP and ANISN results have a maximum value of 1.33%. This maximum difference is less than the 1.5% statistical error in the MCNP results.

However, the difference between ENDF/B version IV and V is about 4.6 to 5.6% which is mainly related due to the correction in the lithium-7 cross section. These results lead one to conclude that the uncertainty in the TBR for this liquid lithium blanket concept is about 1% due to nuclear data processing, multigroup treatment, and numerical errors from the transport codes. Also, a similar conclusion was found for the lithium-lead blanket with a total thickness less than 80 cm.(7-11)

TABLE 7-15. BLANKET GEOMETRICAL MODEL

Zone Description	Radius, cm		No. of Invervals Per Zone	Composition Vol. %
	From	To		
Plasma	0	130	5	Vacuum
Scrape-off	130	150	1	Vacuum
First Wall	150	151	1	50% PCA, 50% Li
Breeding	151	190	39	7.5% PCA, 92.5% Li
Reflector	190	210	20	90% PCA, 10% Li
Shielding	210	270	50	90% Fe1422, 10% H_2O

TABLE 7-16. S_8 SYMMETRICAL ANGULAR QUADRATURE SET

Cosine (mu)	Weight
-2.79004e-01	0
-1.83435e-01	4.53355e-02
1.83435e-01	4.53355e-02
-6.04419e-01	0
-5.25532e-01	5.22844e-02
-1.83435e-01	4.53355e-02
1.83435e-01	4.53355e-02
5.25532e-01	5.22844e-02
-8.50774e-01	0
-7.96666e-01	5.55953e-02
-5.25532e-01	5.22844e-02
-1.83435e-01	4.53355e-02
1.84335e-01	4.53355e-02
5.25532e-01	5.22844e-02
7.96666e-01	5.55953e-02
-9.83032e-01	0
-9.60290e-01	5.06143e-02
-7.96666e-01	5.55953e-02
-5.25532e-01	5.22844e-02
-1.83435e-01	4.53355e-02
1.83435e-01	4.53355e-02
5.25532e-01	5.22844e-02
7.96666e-01	5.55953e-02
9.60290e-01	5.06143e-02

TABLF 7-17. ATOMIC DENSITY OF THE BENCHMARK BLANKET MATERIALS

Material	Element	Atom/b-cm
H_2O	H	0.0670
	O	0.0335
Li	^{6}Li	3.450-3
	^{7}Li	4.255-2
PCA Steel	Cr	1.274-2
	Ni	1.290-2
	Fe	5.499-2
	C	1.971-4
Fe1422 Alloy	C	2.309-3
	Cr	1.843-3
	Mn	1.219-2
	Fe	6.953-2
	Ni	1.580-3

TABLE 7-18. TRITIUM BREEDING BENCHMARK RESULTS FOR LIQUID LITHIUM BLANKET CONCEPTS

Data Base	Transport Code	Blanket Thickness, cm (First Wall & Breeding Zone Thickness/ Reflector Zone Thickness)		
		40/20	60/20	80/20
ENDF/B-IV	ANISN	1.2832	1.4471	1.5333
ENDF/B-IV	MCNP	1.2695	1.4338	1.5288
ENDF/B-V	ANISN	1.2103	1.3735	1.4626
ENDF/B-V	MCNP	1.1984	1.3656	1.4434

TABLE 7-19. RELATIVE DIFFERENCES BETWEEN THE TRITIUM BREEDING RATIO RESULTS FOR EACH LIQUID LITHIUM BLANKET

Relative Difference %	Blanket Thickness, cm (First Wall & Breeding Zone Thicknesses/Reflector Zone Thickness)		
	40/20	60/20	80/20
(ANISN - MCNP) × 100/MCNP with ENDF/B-IV	1.08	0.[illegible]	0.29
(ANISN - MCNP) × 100/MCNP with ENDF/B-V	0.99	0.58	1.33
(ENDF/B-V - ENDF/B-IV) × 100/MCNP with ENDF/B-V	-5.68	-5.09	-4.61
(ENDF/B-V - ENDF/B-IV) × 100/ANISN with ENDF/B-V	-5.60	4.76	-5.59

7.8.4.5 Optimum Design Range for the Liquid Metal Blanket Concepts

From a reactor design point of view, the blanket parameters should be defined to achieve the following goals: a) satisfy the tritium breeding, thermal hydraulic, and mechanical requirements; b) achieve the highest possible energy multiplication; c) reduce the energy deposition in the shield to less than 3% of the total energy produced per fusion neutron; and d) use low cost and natural materials to reduce the reactor capital cost.

The design range defined in this section is based on the neutronics considerations of the above requirements list. Other design aspects will narrow this design range as discussed in the other sections. A 1.2 tritium breeding ratio based on a one-dimensional analysis is the design goal; the potential for a higher TBR is also considered.

For the lithium-lead blanket concept, the steel reflector produces a higher blanket energy multiplication factor than carbon. The blanket energy multiplication factor shows a continuous decrease as the lithium-6 enrichment increase. Thus it is desirable to have the lowest possible lithium-6 enrichment subject to achieving tritium breeding. In fact, the 1.2 TBR is achievable with a 30% lithium-6 enrichment as shown in Figs. 7-41 through 7-44. Figure 7-49 shows that the blanket energy multiplication saturates at about a 40 cm reflector zone thickness. At this reflector thickness, the energy deposi-

tion in the shield is about 3% with the 40 cm breeder zone thickness. This blanket configuration (40 cm breeder and 40 cm reflector) has the potential to achieve a 1.5 TBR if the lithium-6 enrichment is increased to 90% as shown in Fig. 7-44. Also, a 10 cm increase in the breeding zone thickness changes the TBR from 1.2 to 1.35 for the same lithium-6 enrichment. However, for both cases the blanket energy multiplication decreases as the lithium-6 enrichment or the breeding zone thickness increases. Also, the increase of the lithium-lead concentration in the reflector zone increases the TBR and reduces the blanket energy multiplication factor. Table 7-20 gives the main parameters for the reference blanket based on the above analyses for the mirror reactor. The replacement of the ferritic structure in the reference blanket by vanadium structure results in about a 6% increase in the TBR and about a 2% decrease in the blanket energy multiplication factor. The blanket parameters with the vanadium structure are also given in Table 7-20.

TABLE 7-20. LITHIUM-LEAD REFERENCE BLANKET FOR MIRROR REACTOR

A. Ferritic Structure	
First Zone (50% 17Li-83Pb, 50% Ferritic) thickness, cm	1.00
Breeding Zone (92.5% 17Li-83Pb, 7.5% Ferritic) thickness, cm	39.00
Reflector Zone (20% 17Li-83Pb, 80% Ferritic) thickness, cm	40.00
Lithium-6 Enrichment, %	30.00
Blanket Energy Multiplication Factor	1.30
Total Energy Multiplication Factor	1.35
Energy Deposition in the Blanket Per Fusion Neutron, MeV	18.26
Total Energy Deposition in the Reactor Per Fusion Neutron, MeV	19.00
Tritium Breeding Ratio	1.26
B. Vanadium Structure	
First Wall Zone (50% 17Li-83Pb, 50% V15Cr5Ti) thickness, cm	1.00
Breeding Zone (92.5% 17Li-83Pb, 7.5% V15Cr5Ti) thickness, cm	39.00
Reflector Zone (20% 17Li-83Pb, 10% V15Cr5Ti, 70% Ferritic) Thickness, cm	40.00
Lithium-6 Enrichment, %	30.00
Blanket Energy Multiplication Factor	1.27
Total Energy Multiplication Factor	1.31
Energy Deposition in the Blanket Per Fusion Neutron, MeV	17.87
Total Energy Deposition in the Reactor Per Fusion Neutron, MeV	18.45
Tritium Breeding Ratio	1.33

A similar analysis was performed to define the lithium blanket parameters. Figure 7-46 shows that a 40 cm breeder zone thickness is required to achieve a 1.2 TBR after a 6% correction factor was assumed to account for the change in the lithium-7 nuclear data. The blanket energy multiplication factor in Fig. 7-54 shows that a reflector zone thickness exceeding 30 cm is required. The energy deposition in the shield is about 3% of the total energy deposition per fusion neutron for the 30 cm reflector zone thickness as shown in Fig. 7-62. The reference blanket parameters for the lithium blanket with ferritic structure is given in Table 7-21 for the mirror reactor. The blanket has a potential to achieve a 1.4 TBR by increasing the breeder zone thickness to about 60 cm. The same blanket dimension was used with the vanadium structure. The previous observations about the increase in the TBR and the decrease in the blanket energy multiplication are observed as shown in Table 7-21.

For a tokamak reactor, the lithium blanket with vanadium structure was modified in the inboard section to accommodate the large flow crosssectional area required by MHD and thermal hydraulic considerations. The lithium fraction in the reflector zone was increased to 50%. In the outboard blanket, the lithium fraction was reduced to get more energy per fusion neutron and reduce the TBR. Table 7-21 gives the main parameters for the inboard and the outboard blankets.

7.8.5 Tritium Recovery

7.8.5.1 Tritium Recovery from LiPb

One of the attractive features of using 17Li-83Pb as a breeding material is its low tritium solubility. Although low solubility, reduces blanket tritium inventory, it often results a high tritium partial pressure, which causes excessive leakage problem. To reduce tritium leakage to an acceptable level, the tritium partial pressue in the 17Li-83Pb has to be kept around 10^{-7} Pa.

A 17Li-83Pb tritium recovery scheme has been developed during the study. The principle of the scheme is based on a multiple stage gas-liquid extraction system, as has been used in chemical industry for decades. The system is shown schematically on Fig. 7-63. The cross-sectional view of the stage is

TABLE 7-21. LITHIUM REFERENCE BLANKET FOR MIRROR REACTOR

A. Ferritic Structure	
First Wall Zone (50% Li, 50% Ferritic) thickness, cm	1.00
Breeding Zone (92.5% Li, 7.5% Ferritic) thickness, cm	39.00
Reflector Zone (10% Li, 90% Ferritic) thickness, cm	30.00
Lithium-6 Enrichment	Natural
Blanket Energy Multiplication Factor	1.30
Total Energy Multiplication Factor	1.37
Energy Deposition in the Blanket Per Fusion Neutron, MeV	18.32
Total Energy Deposition in the Reactor Per Fusion Neutron, MeV	19.24
Tritium Breeding Ratio (1.28 Based on ENDF/B-IV)	1.21
B. Vanadium Structure	
First Wall Zone (50% Li, 50% V15Cr5Ti) thickness, cm	1.00
Breeding Zone (92.5% Li, 7.5% V15Cr5Ti) thickness, cm	39.00
Reflector Zone (10% Li, 10% V15Cr5Ti, 80% Ferritic) Thickness, cm	30.00
Lithium-6 Enrichment	Natural
Blanket Energy Multiplication Factor	1.25
Total Energy Multiplication Factor	1.31
Energy Deposition in the Blanket Per Fusion Neutron, MeV	17.57
Total Energy Deposition in the Reactor Per Fusion Neutron, MeV	18.42
Tritium Breeding Ratio (1.33 Based on ENDF/B-IV)	1.26

TABLE 7-22. LITHIUM REFERENCE BLANKET FOR TOKAMAK REACTOR

A. Inboard Blanket	
First Wall Zone (50% Li, 50% V15Cr5Ti) thickness, cm	1.00
Breeding Zone (92.5% Li, 7.5% V15Cr5Ti) thickness, cm	39.00
Reflector Zone (50% Li, 10% V15Cr5Ti, 40% Ferritic) thickness, cm	20.00
Lithium-6 Enrichment	Natural
Blanket Energy Multiplication Factor	1.18
Total Energy Multiplication Factor	1.30
Energy Deposition in the Blanket Per Fusion Neutron, MeV	16.52
Total Energy Deposition in the Reactor Per Fusion Neutron, MeV	18.35
Tritium Breeding Ratio (1.43 Based on ENDF/B-IV)	1.35
B. Outboard Blanket	
First Wall Zone (50% Li, 50% V15Cr5Ti) thickness, cm	1.00
Breeding Zone (92.5% Li, 7.5% V15Cr5Ti) thickness, cm	39.00
Reflector Zone (10% Li, 10% V15Cr5Ti, 80% Ferritic) thickness, cm	30.00
Lithium-6 Enrichment	Natural
Blanket Energy Multiplication Factor	1.26
Total Energy Multiplication Factor	1.31
Energy Deposition in the Blanket Per Fusion Neutron, MeV	17.68
Total Energy Deposition in the Reactor Per Fusion Neutron, MeV	18.42
Tritium Breeding Ratio (1.37 Based on ENDF/B-IV)	1.30

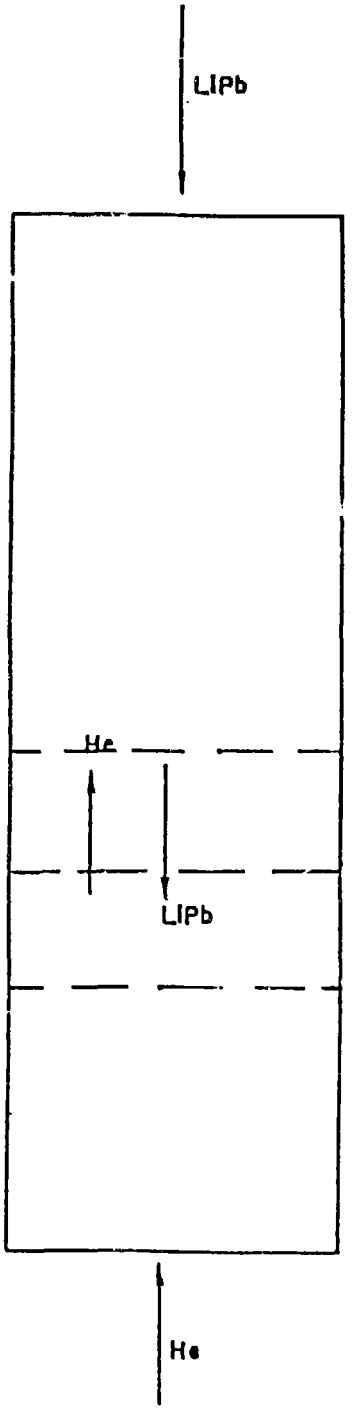

Figure 7-63. Counter current extraction tritium recovery system.

shown in Fig. 7-64. At each stage, flow passages are provided for both downward LiPb flow and upward helium purge flow. The counter-current flow of LiPb and helium in between two stages is where the mass transfer mechanism occurs. Multiple stages are used here to facilitate tritium diffusion process from the liquid.

To reduce the tritium leakage through the steam generator to an accept able level, a tritium partial pressure less than $<10^{-7}$ Pa has to be maintained in the primary coolant in the steam generator. By mass balance, it can be calculated that the tritium partial pressure in the LiPb stream at the outlet of the reactor is 76.5×10^{-4} Pa. A purge gas flow rate of in excess of 10^{7} liter/sec will be required to recover 600 g/day of tritium. Such a purge flow rate appears to be excessive.

To alleviate the tritium problem, hydrogen is added to the purge. The effects of the isotopes to permeation was summarized by Hickman.(7-12) In addition, the hydrogen isotopes will also increase the HT pressure, and will thus reduce the purge gas volumetric flow rate requirement. The hydrogen partial pressure will also enhance the surface recombination, which will reduce the resistance of tritium release from the 17Li-83Pb droplets. The effects of hydrogen isotopes are summarized on Table 7-23.

A sample calculation which shows the effect of isotopes is summarized in Table 7-24. By adding 10 Pa of hydrogen in the purge gas, the P_{HT} increases to 9.3×10^{-2} Pa, from a T_2 pressure of 6.5×10^{-4} Pa. As a consequence, the required purge gas flow rate reduces from 10^{7} liter/sec to 1.5×10^{5} liter/sec. The allowable HT pressure in the steam generator is 1.45×10^{-3} Pa, compared to T_2 pressure of 1.3×10^{-7} Pa. Therefore, 98.5% of the tritium in 17Li-83Pb has to be recovered from the tritium recovery system before it reaches the steam generator.

The fractional recovery $(1-\theta)$ of each stage in the tritium recovery system is plotted as a function of the Fourier No., F_o as shown on Fig. 7-65.

$$F_o \equiv Dt/r^2$$

in which

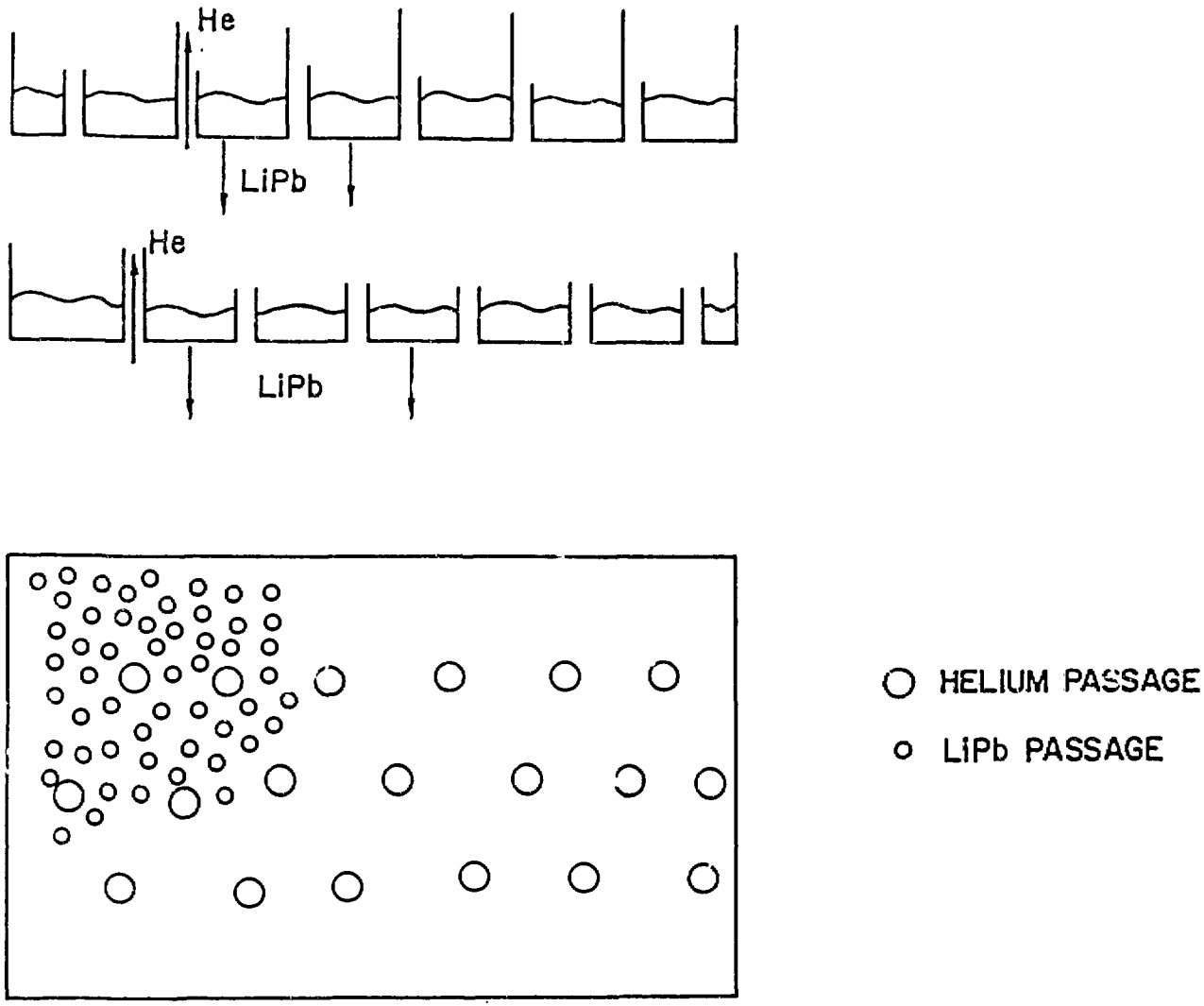

Figure 7-64. Conceptual design of the extraction system.

TABLE 7-23. EFFECTS OF HYDROGEN ISOTOPES ON PERMEATION, RECOVERY, AND RECOMBINATION

PERMEATION

Without Isotopes

$$T_2 \underset{\leftarrow}{\rightarrow} 2T$$

$$T \quad \alpha \quad P_{T_2}{}^{1/2}$$

OR

$$\dot{M} = DS \left(P_{T_2}{}^{1/2} - P'_{T_2}{}^{1/2} \right)$$

With Isotopes and H >> T

$$HT \underset{\leftarrow}{\rightarrow} H + T$$

AND

$$H_2 \underset{\leftarrow}{\rightarrow} 2H$$

$$T \quad \infty \quad P_{HT}/P_{H_2}{}^{1/2}$$

$$\dot{M} = DS \left[\left(P_{HT}/P_{H_2}{}^{1/2} \right)_1 - \left(P_{HT}/P_{H_2}{}^{1/2} \right)_2 \right]$$

PARTIAL PRESSURE

With No Isotopes

$$P_{T_2} = K_s{}^2 X_T{}^2$$

With Isotope and H >> T

$$P_{DT} = K_s{}^2 X_D X_T$$

RECOMBINATION

With No Isotopes

$$T + T \rightarrow T_2$$

With Isotopes

$$H + T \rightarrow HT$$

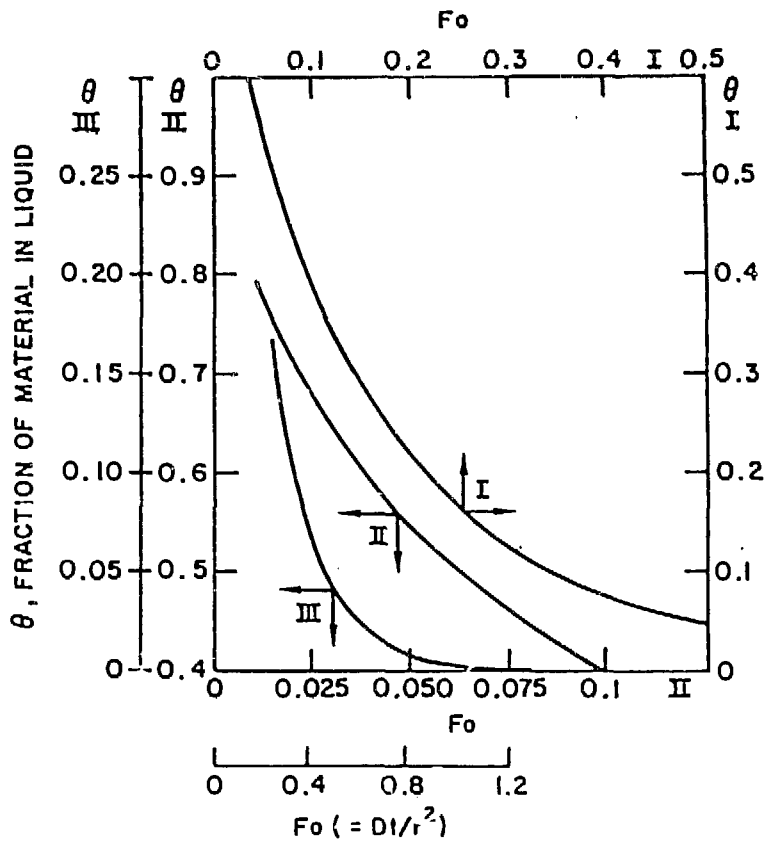

Figure 7-65. Mass transfer rate as a function of Fourier number.

TABLE 7-24. AN EXAMPLE OF THE EFFECT OF ISOTOPES

	No Isotopes	.01 kPa H_2 Added
H_2 Pressure	0	.01 kPa
P_{T_2}/P_{HT} at Reactor Outlet	6.5×10^{-7} kPa (T_2)	9.3×10^{-5} kPa (HT)
Purge Gas Flow Rate	10^7 liter/sec	1.45×10^5 liter/sec
Maximum P_{T_2}/P_{HT} Allowable at SG	$1/3 \times 10^{-10}$ kPa	1.45×10^{-6} kPa
Mass H_2 Added	0	42.5 kg/day
Tritium Recovery System Efficiency	99.98%	98.5%

D is the mass diffusivity

t is the drop time from one stage to next

r is the radius of 17Li-83Pb droplet.

The diffusivity of tritium in 17Li-83Pb is not available but is estimated to be 1×10^{-3} cm^2/sec.[7-13] If the distance between two stage is 10 cm, the drop time is .225 cm. The size of the droplet is determined by the size of the hole and is assumed to be r = .1 cm. F_o is .0225 and the θ = .7. Therefore, each stage can theoretically recover 30% of the tritium. Fig. 7-66 shows the number of recovery stage required as a function of single stage recovery efficiency. For 30% recovery from each stage, 11 recovery stages are needed for 98.5% total recovery. The parameters of the tritium recovery system are summarized in Table 7-25.

The total hydrogen added is 42.5 kg/day, this has to be separated from 600 g/day of tritium. An isotope separation system has been designed[7-14] to serve this function. The flow diagram is shown on Fig. 7-67. The additional capital cost of the separation system is estimated to be less than 10 million.

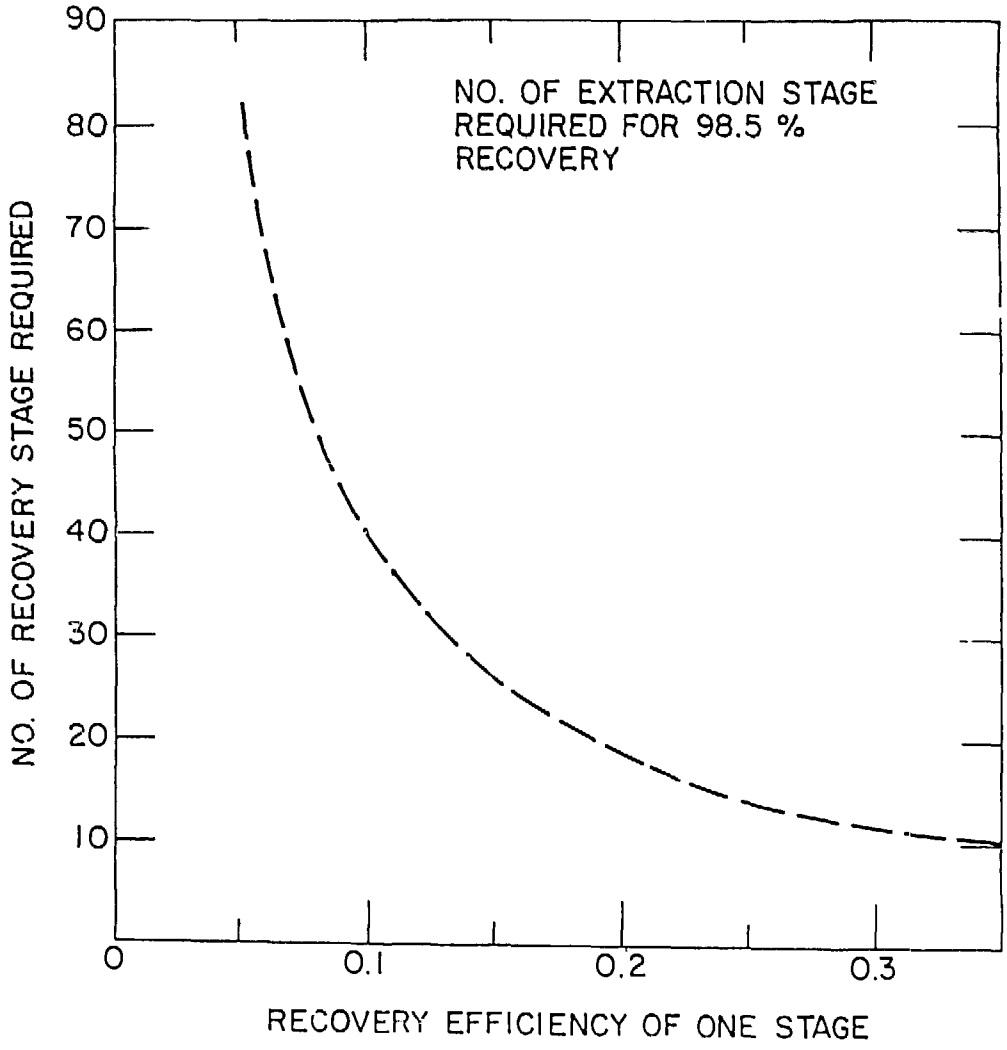

Figure 7-66. Number of recovery stage required as a function of the single stage recovery efficiency.

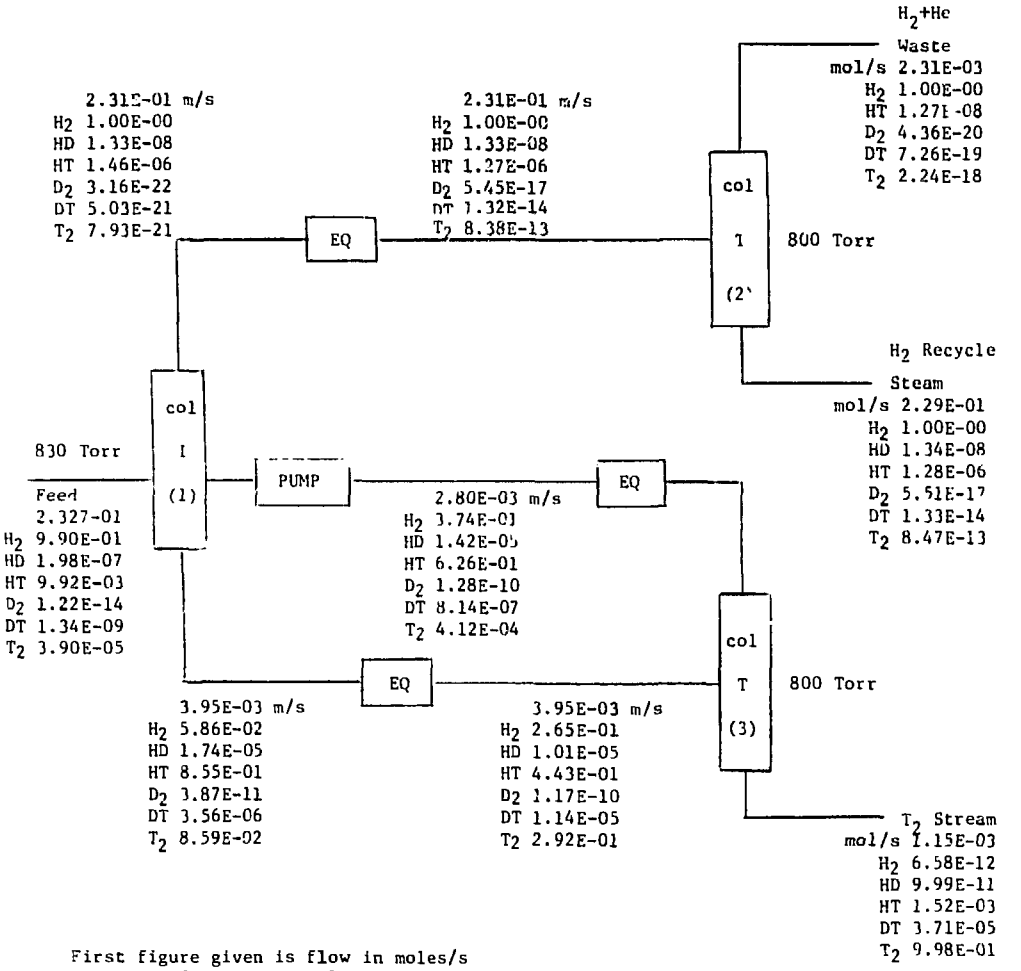

Figure 7-67. Breeding blanket tritium recovery system.

TABLE 7-25. TRITIUM RECOVERY SYSTEM PARAMETERS

LiPb Flow Rate	1.7×10^8 g/sec
Purge Gas Flow Rate	1.45×10^5 liter/sec
Hydrogen Pressure	.01 KPa
Tritium Recovery System Efficiency	98.5%
Purge Gas Velocity	30 m/sec
Purge Gas Pressure	100 KPa
Cross-sectional Area of Extraction Column	20 m^2
Number of Ectraction Stage	15
Distance Between Two Stages	10 cm
Extraction Column Height	1.8 m
HT Pressure at the Exit of the Extraction System	1.45×10^{-6} KPa
Tritium Leakage Rate in Steam Generator	10 Curie/d

7.8.5.2 Tritium Recovery from Liquid Lithium

An efficient processing system is required to recover tritium from a lithium blanket at a rate equal to the breeding rate, and at the same time maintains a low steady state inventory of tritium throughout the blanket region. Low tritium inventory in the blanket is required for both economic and safety reasons. If large amounts of tritium is allowed to build up in the blanket it will be necessary to start the operation of the reactor with very high tritium supply for fueling. In addition, high tritium concentration in the blanket increases the rate of tritium permeation through the blanket structure and the primary heat exchanger.

Among all the methods proposed to extract tritium from liquid lithium, the use of molten alkali halide salts, such as LiF-LiCl-LiBr appears to be the most attractive. This process has shown considerable promise for removing hydrogen isotopes at the ppm level from liquid lithium.[7-9] In this method, a stream of lithium from the fusion blanket is in contact with the molten salt which has a higher affinity for tritium than the lithium does. As a result, tritium is extracted from the lithium by the salt during the mixing process. Lithium is about a factor of three less dense than these halide salts, therefore it can be easily separated from molten salts by gravity and returned to

the blanket. The salt is then electrolyzed to yield T_2 at an emf voltage less than that required to decompose the salt itself.

In a system where equal volumes of salt and lithium are brought into contact, the quantity of the lithium processed per unit time, X, is given by:(7-16)

$$X = \frac{R_b}{I_{ss}} \left(\frac{\varepsilon D_v \eta + 1}{\varepsilon D_v \eta}\right) I_L$$

where

R_b = tritium breeding rate,

ε = efficiency of tritium recovery from the salt,

D_v = volumetric distribution coefficient of tritium between the lithium and the salt,

η = efficiency factor that accounts for nonequilibrium tritium distribution during contacting,

I_L = lithium inventory, and

I_{ss} = steady-state tritium inventory.

The efficiency factor that accounts for non-equilibrium tritium distribution during contact is not yet known but it is believed that values as high as 50% could easily be achieved. A reasonable value of ηD_v is about 2. For a fusion power of 4000 MW and a tritium breeding ratio of 1.2, the tritium breeding rate is about 900 g/d. Table 7-26 shows the required lithium fraction processed per second for two different tritium removal efficiencies in order to keep the tritium inventory at the values given. It can be seen that

the fraction that needs to be processed is very small, even for low tritium removal efficiency and low tritium inventory. The amounts of in-plant space and recirculating electrical power needed for continuous extraction using centrifugal contactors were shown to be acceptably small.

TABLE 7-26. REQUIRED FRACTION PROCESSED OF LITHIUM COOLANT FOR DIFFERENT TRITIUM INVENTORIES

Tritium Inventory	Tritium Removal Efficiency	Fraction Processed per Sec
1 Kg	1) 30%	2.7×10^{-5}
	2) 90%	1.6×10^{-5}
5 Kg	1) 30%	5.5×10^{-6}
	2) 90%	3.24×10^{-6}

7.8.6 Liquid-Metal-Cooled Limiter for Tokamaks

7.8.6.1 Introduction

Safety considerations make the water-cooled reference design limiter of the BCSS incompatible with the lithium-cooled blanket of the liquid metal reference design of a tokamak reactor. As a result, the feasibility of either an gas-cooled or a liquid-metal-cooled limiter is closely related to the feasibility of a lithium cooled blanket.

In the following, an acceptable design of a liquid-metal-cooled limiter is presented. In addition to the liquid-metal-cooled design, a helium-cooled design and a graphite-gas two-phase coolant design were also considered. The two-phase coolant design was analyzed in some detail because of its attractive heat transfer characteristics, compared to those of the helium-cooled design. However, concerns about possible extensive erosion, caused by the graphite particles, and lack of data to resolve such concerns, led to shelving the two-phase coolant concept. The helium-cooled design was not pursued extensively, because it was thought that it does not have a clear-cut advantage over the liquid-metal-cooled design, whereas the latter is more compatible with the liquid-metal-cooled blanket.

7.8.6.2 Mechanical Design

The design proposed here is an evolution of a preliminary design, developed for an INTOR study on impurity control. The high coolant velocity channels are aligned with the large toroidal magnetic field to minimize MHD pressure drop, and are made as short as possible to minimize peak interface and material temperatures. The balance of the limiter, i.e., the manifolds and the inlet and outlet conduits are designed so as to minimize MHD pressure drop within the geometric constrains and material stress limitations.

Each of the 63 limiter modules is 2 m wide and 0.6 m long (in the toroidal direction). It is made entirely of vanadium alloy, except for the 10 mm thick beryllium tile lining of the collector plates and the tantalum lining of the leading edges.

Coolant enters a limiter module through a circular inlet conduit of internal diameter of 20 cm. After a right angle bend the inlet conduit feeds a horn-shaped manifold, as shown in Figs. 7-68 and 7-69. The inlet conduit and the inlet manifold are of laminated wall construction with an inner liner thickness of 0.2 mm. The outer load bearing sleeve, which is electrically insulated from the lines, is made thick enough to sustain the coolant pressure.

The coolant is distributed to the 156 coolant channels through 156 circular ducts of internal diameter of 8 mm and wall thickness of 1.0 mm. The 5 mm × 12 mm coolant channels are rectangular in cross section and they share 1.5 mm thick webs. The thickness of the channel walls facing the plasma are made as thin as possible (1.0 mm) to minimize peak material temperatures. The thickness of the opposite wall has no effect on MHD or heat transfer calculations and can be designed to satisfy structural requirements. A cross section of a segment of the limiter showing, in addition to the coolant channels, the beryllium lining and the tantalum-lined leading edge is shown in Fig. 7-70.

The inlet manifold feeds the coolant channels at their mid-toroidal point. In this fashion the effective heated length of the limiter is reduced to 30 cm, leading to a reduction of peak interface and material temperatures. The coolant leaves the channels through circular ducts of 8 mm diameter and 1.0 mm thickness, is collected into two identical outlet manifolds and leaves

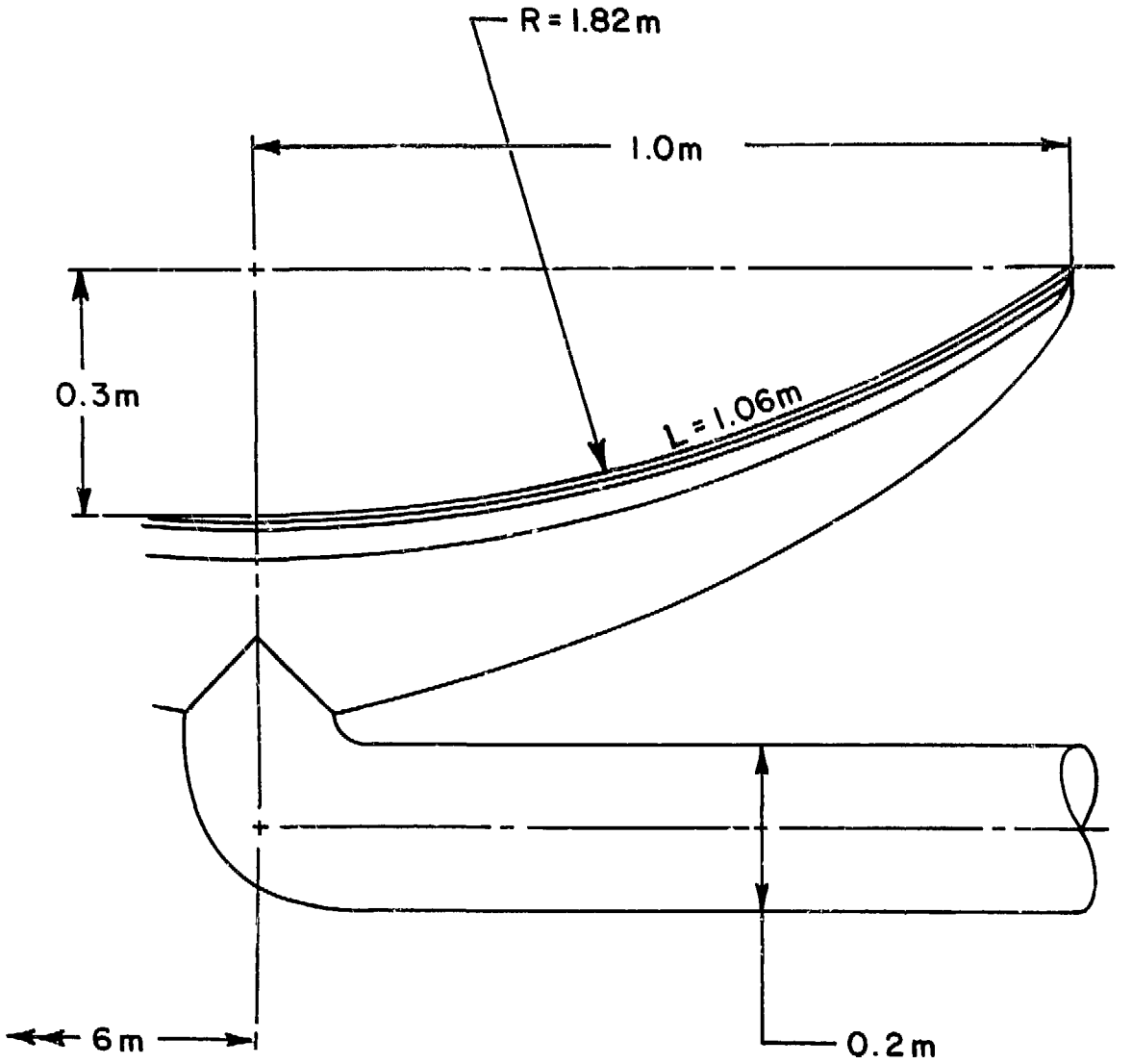

Figure 7-68. End view of limiter showing inlet pipe and manifold.

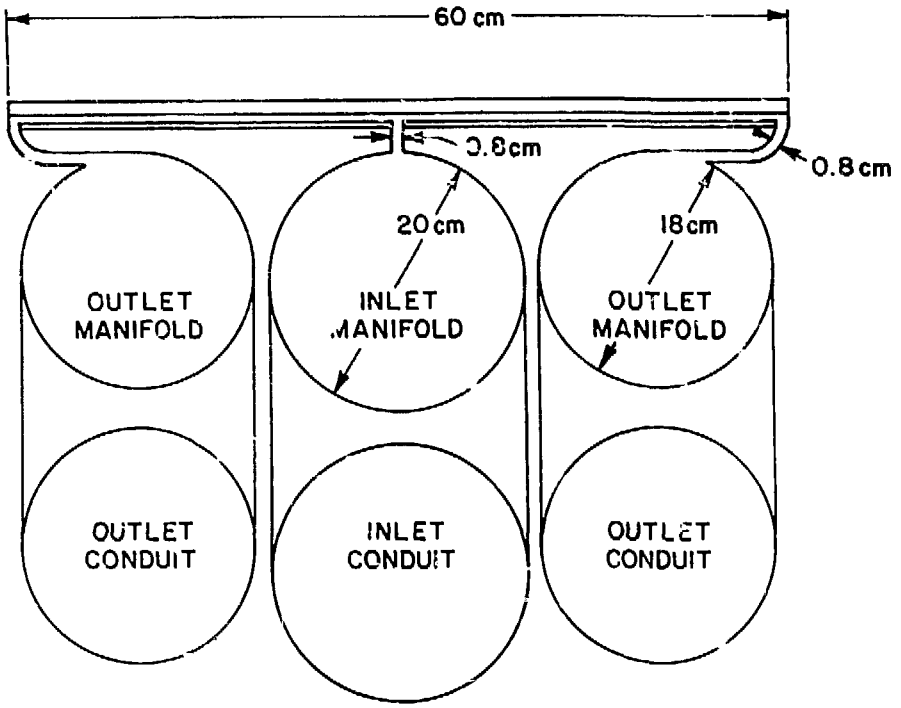

Figure 7-69. Section of the limiter module by a toroidal plane showing the inlet and outlet conduits and manifolds and the collector plate.

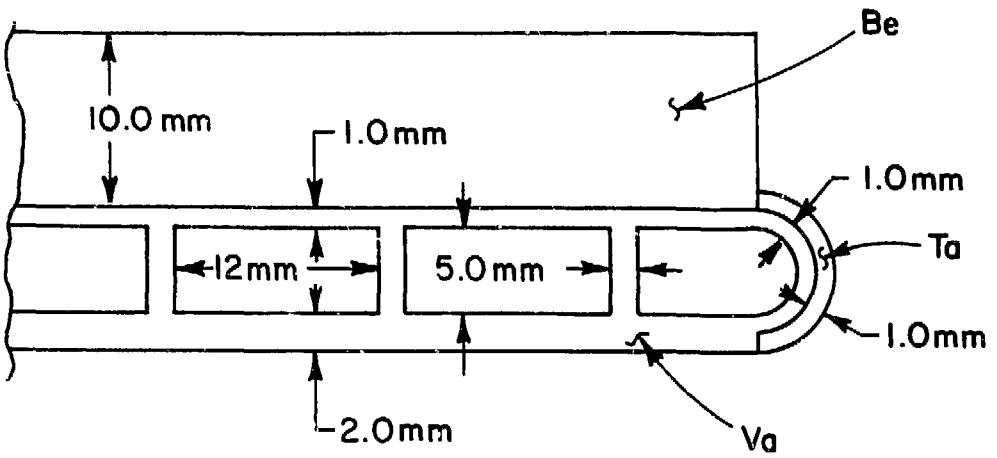

Figure 7-70. Cross section of the limiter module collector plate showing typical coolant channels and leading edge detail.

the module through two outlet conduits. The conduits have a diameter of 18 cm (the two outlet manifolds are similarly scaled down from the inlet manifold). The outlet manifolds and conduits are of laminated wall construction identical to that at the inlet side.

The limiter collector plates extend from a radial position of 5.0 m to a radial position of 7.0 m. Such placement results in the most demanding design circumstances, i.e., high magnetic flux density and small surface area (high heat flux and high erosion).

The velocity in the coolant channels is set at 10.0 m/s. This corresponds to velocities of 6.0 m/s and 3.4 m/s in the inlet and outlet conduits, in that order. The velocities in the 8.0 mm connecting ducts are 24 m/s and 12 m/s. These velocities (and the associated pressure drops) can be made smaller, if connecting ducts of elliptical cross section are employed.

For the assumed placement, the surface area of the limiter is 80 m^2. The average heat flux is 3.5 MW/m^2, resulting in a total energy deposition of 280 MW. The energy deposition is increased by 290 MW to account for the volumetric energy deposition in the limiter collector plates, manifolds and inlet and outlet ducts. The figure of 290 MW is consistent with the assumed reduction in energy deposition in the inboard blanket resulting from the presence of the limiter. The mass flow rate per limiter module, corresponding to a coolant channel velocity of 10 m/s is 94 kg/s. This mass flow rate, and the total energy deposition per limiter module of 9 MW results in a mean temperature rise in the coolant of 22°C.

7.8.6.3 MHD Analysis

The basic design concept of the limiter, of high coolant velocity channels aligned with the large toroidal magnetic field and low velocity manifolds transverse to it, is identical to that of the blanket design, although, because of different geometric limitations, the manifolding here is more conventional. The MHD analysis is therefore similar. The results of the analysis indicate that the pressure at the module inlet is 5.5 MPa for an outlet pressure of 0.15 MPa. The maximum pressure at the first wall coolant channel is about 2.5 MPa at the channel inlet. This pressure is important from the structural analysis point of view because it must be sustained by the relatively thin webs and first wall plate. The pressure in the manifolds and in-

let and outlet conduits is essentially immaterial because it is sustained by thick outer load-bearing walls. The critical pressure in the coolant channels can be further decreased, at the expense of the overall pressure drop, by enlarging the manifolds and conduits at the outlet side and diminishing them at the inlet side.

7.8.6.4 Thermal Hydraulic Analysis

The method of analysis adopted here is similar to that described in Section 7.8.2. The critical area is the top surface of the limiter which is exposed to high surface heat fluxes (peak heat flux is ~4.1 MW/m^2). The inlet temperature of the liquid lithium coolant is assumed to be 230°C. In the flow path of 30 cm which is exposed to surface heat flux, i.e., near the top surface of the limiter, the contribution due to nuclear heating is usually much smaller than that of surface heat flux. However, nuclear heating is also present in the inlet and discharging manifolds and pipes. Since the velocities in these manifolds and pipes are kept at relatively low values (to reduce MHD pressure drop), the coolant could be heated up somewhat before and after it passes through the top surface. Accurate account of these effects requires detailed information of the velocities and nuclear heating rates in the manifolds and pipes, and is not available at present. Instead, a 50°C temperature rise is assumed as a result of nuclear heating. This temperature rise is conservatively much larger than the 22°C temperature rise corresponding to total heat deposition per module of 9 MW.

Figure 7-71 shows the variation of the maximum structural (vanadium alloy) temperature with surface heat flux for three different coolant velocities. The dashed line in Fig. 7-71 is the maximum allowable temperature (750°C) for the vanadium alloy. It can be seen that this temperature requirement is easily satisfied, as long as the surface heat flux is not excessive (<5 MW/m^2). There is also a corrosion temperature limit (750°C for vanadium and lithium) at the coolant/structure interface anywhere in the limiter. Since the maximum interface temperature is always less than the maximum structural temperature, the corrosion temperature requirement is satisfied as long as the structural temperature limit is satisfied.

Figure 7-72 shows the variation of the maximum coating (beryllium) temperature with surface heat flux for three different coolant velocities. The

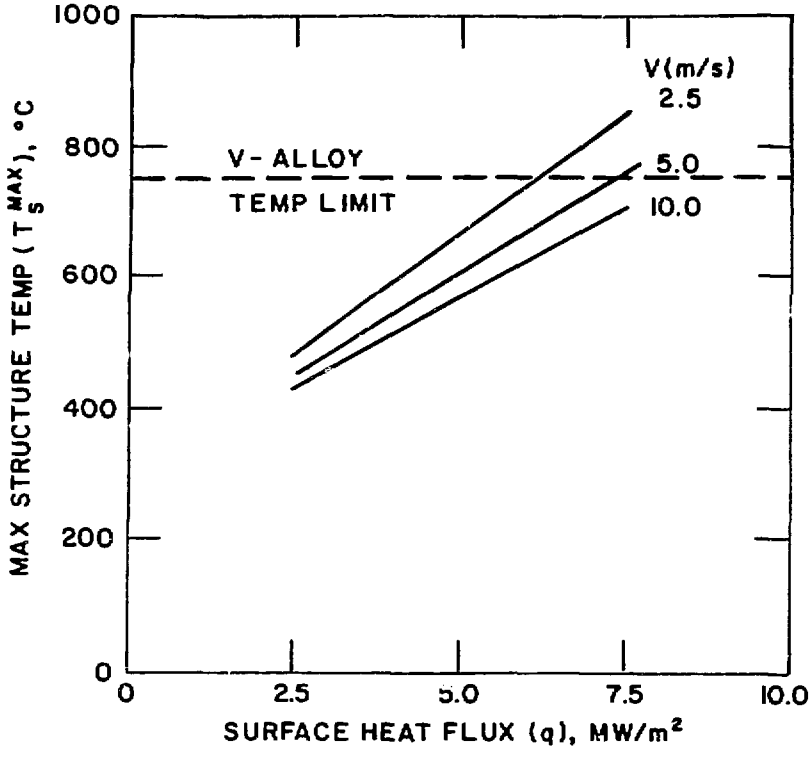

Figure 7-71. Variation of maximum structural temperature with surface heat flux for various coolant velocities.

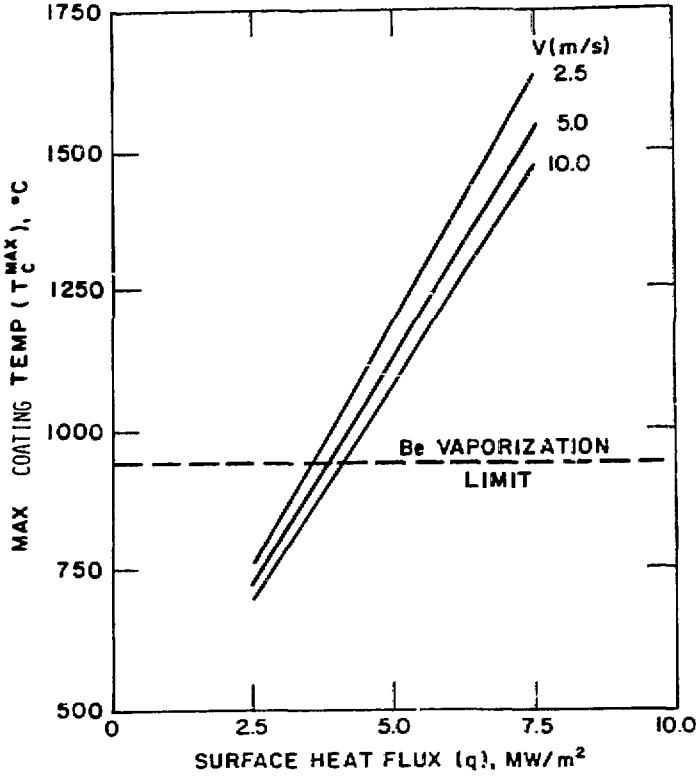

Figure 7-72. Variation of maximum coating temperature with surface heat flux for various coolant velocities.

dashed line in Fig. 7-72 is the estimated maximum allowable temperature for beryllium. The operating temperature limit for Be is dependent upon the vaporization rate. Material that is vaporized from the surface is assumed to act in a manner similar to that of sputtered particles which enter the plasma scrape-off region, are ionized, and then return to the limiter surface along magnetic field lines. It is believed that, if the vaporization rate is less than the gross sputtering rate, then, the vaporization losses should have little effect on lifetime. For this study, a vaporization rate of 10 mm/y has been used to establish a temperature limit. The temperature corresponding to this vaporization rate is calculated to be ~940°C.(7-17)

The results shown in Fig. 7-72 indicate that, for a velocity of 10 m/s, the maximum surface heat flux allowable, without exceeding the vaporization temperature limit of beryllium, is ~4.1 MW/m^2. Thus, among the three temperature limits (structure/coolant interface, structural material, and coating material), the vaporization temperature limit of the coating material is the most restrictive. The coolant velocity can be increased beyond 10 m/s to allow higher surface heat flux. However, the pay-off is relatively small while the penalty in pressure drop may be rather large.

Improvements in the thermal performance of the limiter can be made by: 1) Using a different liquid metal coolant with lower melting point. NaK can be used at least down to room temperature; a more appropriate temperature, so that heat rejection is possible, would be about 100°C. In that case all temperatures will decrease by 130°C. 2) Using a structural material (niobium or tantalum) with higher thermal conductivity. 3) Reducing the thickness of the beryllium tiles. Although such improvements can lead to substantial reduction of the peak temperatures and may be adopted in the future, they did not prove to be necessary at this time.

Finally, it should be noted that the uncertainties associated with the results described here is of the same order of magnitude as that for the blanket, and are generic to all the heat transfer analyses for liquid-metal systems in a fusion reactor.

7.8.6.5 Stress Analysis

The limiter is constrained by the two 18 cm diameter outlet pipes and the 20 cm diameter inlet pipe from expanding in either the toroidal or the poloi-

dal direction. The extent of the toroidal constraint depends on the relative toroidal stiffness of the main limiter and the bending stiffness of the 18 cm diameter pipes. The toroidal stiffness of the limiter is given by:

$$K_L = [E_s\ h_s/(1 - \nu_s^2) + E_c\ h_c/(1 - \nu_c^2)]\ 2b/\ell \qquad [7\text{-}4]$$

where E and ν are the elastic modulus and Poissons ratio, h is the thickness, 2b and 2ℓ are the lengths of the limiter in the poloidal and toroidal directions respectively. Subscripts s and c represent structure (vanadium alloy) and coating (beryllium) materials respectively. Putting in the appropriate values of the geometric and material parameters, the stiffness of the limiter in the toroidal direction is 10^4 MN/m or 3×10^3 MN/m, if the beryllium coating is cracked. On the other hand the bending stiffness of the 18 cm diameter pipes is given by:

$$K_M = 3EI/L^3 \qquad [7\text{-}5]$$

where E is the elastic modulus, I is the moment of inertia and L is the length of the cantilevered span of the outlet pipes. Putting in the appropriate values of the parameters, the bending stiffness of the inlet pipe is only 33 MN/m, which is negligible compared to the toroidal stiffness of the limiter. Thus, for all practical purposes the main limiter may be assumed to be unconstrained toroidally. For computing the poloidal stiffness of the composite plate, the axial stiffnesses of the horn shaped inlet and outlet pipes are added to the poloidal stiffness of the plate. For simplicity the poloidal curvature of the limiter is ignored. The in-plane stiffnesses of the composite plates can be shown to be as follows (denoting the poloidal and the toroidal directions by X and Y respectively):

$$K_y = 3\ E_s\ h_s/(1 - \nu_s^2) + E_c\ h_c/(1 - \nu_c^2) \qquad [7\text{-}6]$$

$$K_x = K_y + E_s (A_I + 2 A_o)/(2\ell) \qquad [7\text{-}7]$$

$$K_{xy} = 3\nu_s E_s h_s/(1 - \nu_s^2) + \nu_c E_c h_c/(1 - \nu_c^2) \qquad [7\text{-}8]$$

where $E_s = 1.2 \times 10^5$ MPa, $E_c = 10^5$ MPa, $\nu_s = .36$, $\nu_c = .07$, $h_s = .001$ m, $h_c = .01$ m, and $2\ell = 0.6$ m. A_I and A_o are the average solid cross-sectional areas of the inlet and outlet pipes. Assuming, for simplicity, that all structures, except the front wall facing the plasma, are at the reference stress-free temperature equal to the temperature of the inlet coolant, i.e., 230°C, the thermal force corresponding to the average surface heat flux of 3.5 MW/m^2 can be shown to equal:

$$N_T = E_s\alpha_s/(1 - \nu_s) \int_S T\, dz + E_c\alpha_c/(1 - \nu_c) \int_C T\, dz = 6.89 \text{ MPa - m} \qquad [7\text{-}9]$$

where the integral S and C denote integration of the temperature over the vanadium alloy structure thickness and the beryllium coating thickness respectively. For computing the thermal stresses it is conservatively assumed that although the limiter is free to expand in the toroidal and the poloidal directions, it is constrained from bending in either direction. The uniform strain of the limiter in the poloidal and toroidal directions can be shown to equal

$$\bar{\varepsilon}_x = \frac{K_y - K_{xy}}{K_x K_y - K_{xy}^2} N_T = 3.28 \times 10^{-3} \qquad [7\text{-}10]$$

$$\bar{\varepsilon}_y = \frac{K_y - K_{xy}}{K_x K_y - K_{xy}^2} N_T = 4.35 \times 10^{-3} \qquad [7\text{-}11]$$

The stresses in the structure and the coating are then given by:

$$\sigma_x(Z) = \frac{E(Z)}{1 - \nu^2(Z)} [\bar{\varepsilon}_x + \nu(Z)\, \bar{\varepsilon}_y] - \frac{E(Z)\, \alpha(Z)\, T(Z)}{1 - \nu(Z)} \qquad [7\text{-}12]$$

$$\sigma_y(Z) = \frac{E(Z)}{1 - \nu^2(Z)} [\bar{\varepsilon}_y + \nu(Z)\, \bar{\varepsilon}_x] - \frac{E(Z)\, \alpha(Z)\, T(Z)}{1 - \nu(Z)} \qquad [7\text{-}13]$$

The elastically computed maximum stress intensity in the vanadium alloy structure occurring at the inlet is 762 MPa which slightly exceeds the allowable 3 S_m value of 705 MPa. Similarly, the maximum elastically computed stress intensity in the coating is 883 MPa occurring at the location of maximum surface heat flux (4 MW/m^2). Since the yield strength of the beryllium coating is expected to be of the order of 240-290 MPa and that of vanadium is about 450 MPa, such high stresses will not be sustained in either the coating or the structure and they will both yield. If the coating is cracked so that it does not offer any constraint on the deformation of the underlying structure, the maximum stress intensity in the structure, including the primary bending stress (160 MPa) due to the coolant pressure, occurs at the location of maximum surface heat flux (4 MW/m^2) and equals 610 MPa which is easily within the allowable stress limit. The allowable fatigue cycles of the vanadium structure, even in the absence of cracking of the coating, is in excess of 10^5 cycles and is considered adequate.

The leading edge of the limiter was analyzed (generalized plane strain) for a slightly different geometry (Fig. 7-73) using the ANSYS Finite Element Code. The coating thickness for the top surface is 10 mm (Be) and for the leading edge is 1 mm (Ta). It is realized that in reality such an abrupt change in coating thickness cannot be maintained and is undesirable because of stress concentration effects. Therefore the finite element model was not refined at the top surface, near the leading edge, in order to capture this stress concentration effect in the poloidal direction. The maximum thermal stress which occurs in the toroidal direction is adequately represented in the present analysis.

Figure 7-74 shows the thermal and pressure loadings assumed for the analysis. The top surface was subjected to a constant surface heat flux of 2 MW/m^2 and the leading edge was subjected to a cosinusoidally decreasing surface heat flux beginning with 1.7 MW/m^2 at the top surface. The coolant pres-

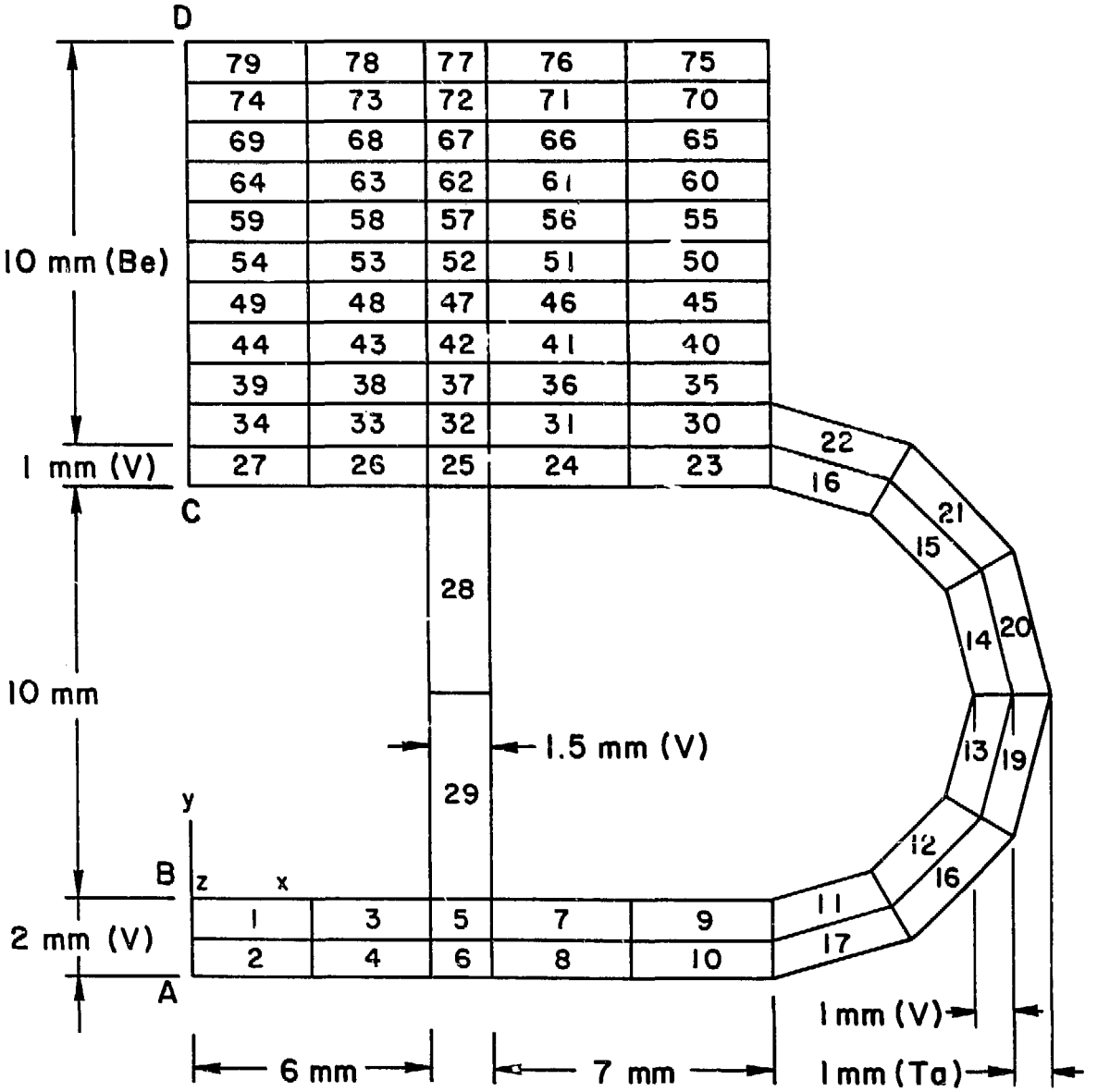

Figure 7-73. Geometry and finite element model of the leading edge of the BCSS limiter.

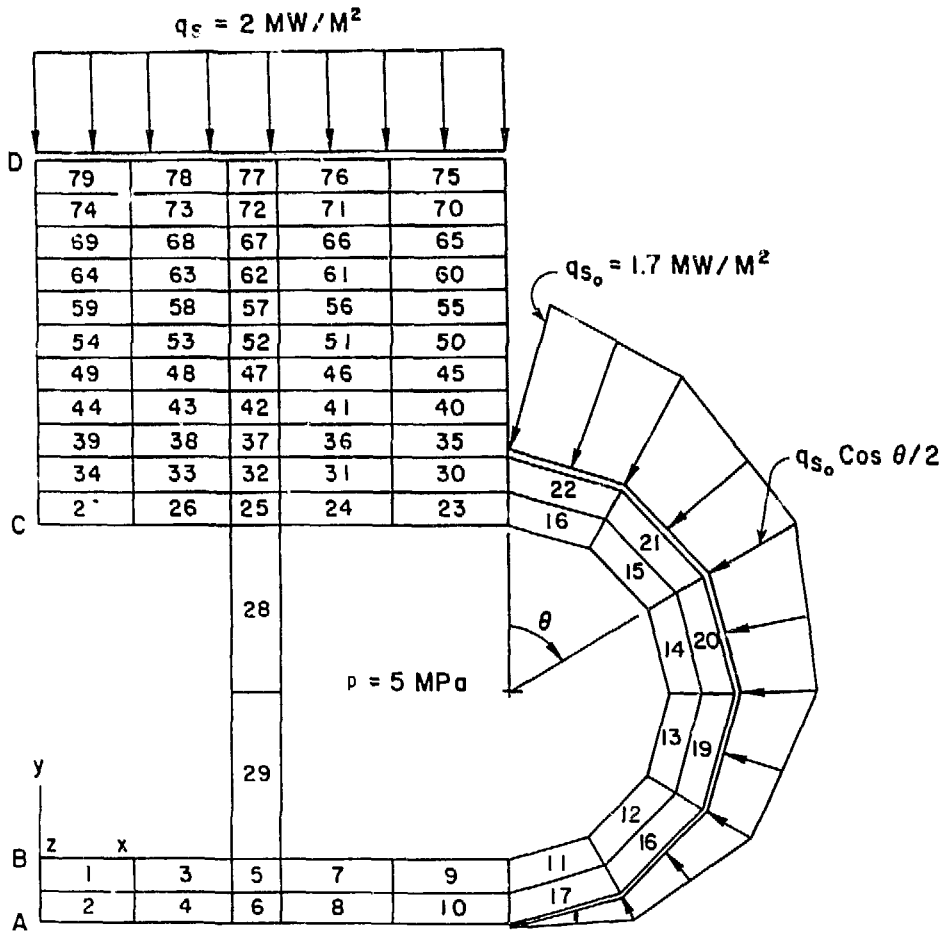

Figure 7-74. Loading on the leading edge of the BCSS limiter.

sure was conservatively assumed to be 5 MPa. The nodal temperatures at the coolant interface was set equal to 250°C and the bottom surface away from the plasma was assumed to be insulated. The boundary conditions for the stress analysis was as follows: Point B was assumed fixed in space, edge AB was free to expand in the veritical direction but not in the poloidal direction, edge CD was constrained to be vertical but otherwise free to displace.

Figure 7-75 shows the computed temperature distribution in the limiter. The maximum temperature of the vanadium alloy structure beryllium coating and the tantalum coating are 340°C, 454°C and 370°C respectively. Figure 7-76 shows a summary of the magnitude and location of the maximum primary membrane stress intensity (P_L), primary bending stress intensity (P_B) and thermal stress intensity (Q). A maximum stress intensity of 380 MPa in the structure occurs not at the leading edge but on the top surface and is easily within the allowable limit. The maximum stress in the structure at the leading edge is 310 MPa. The maximum stresses in the beryllium and tantalum coatings are 415 MPa and 475 MPa respectively. These stresses are, in general, much smaller than the stresses at the top surface.

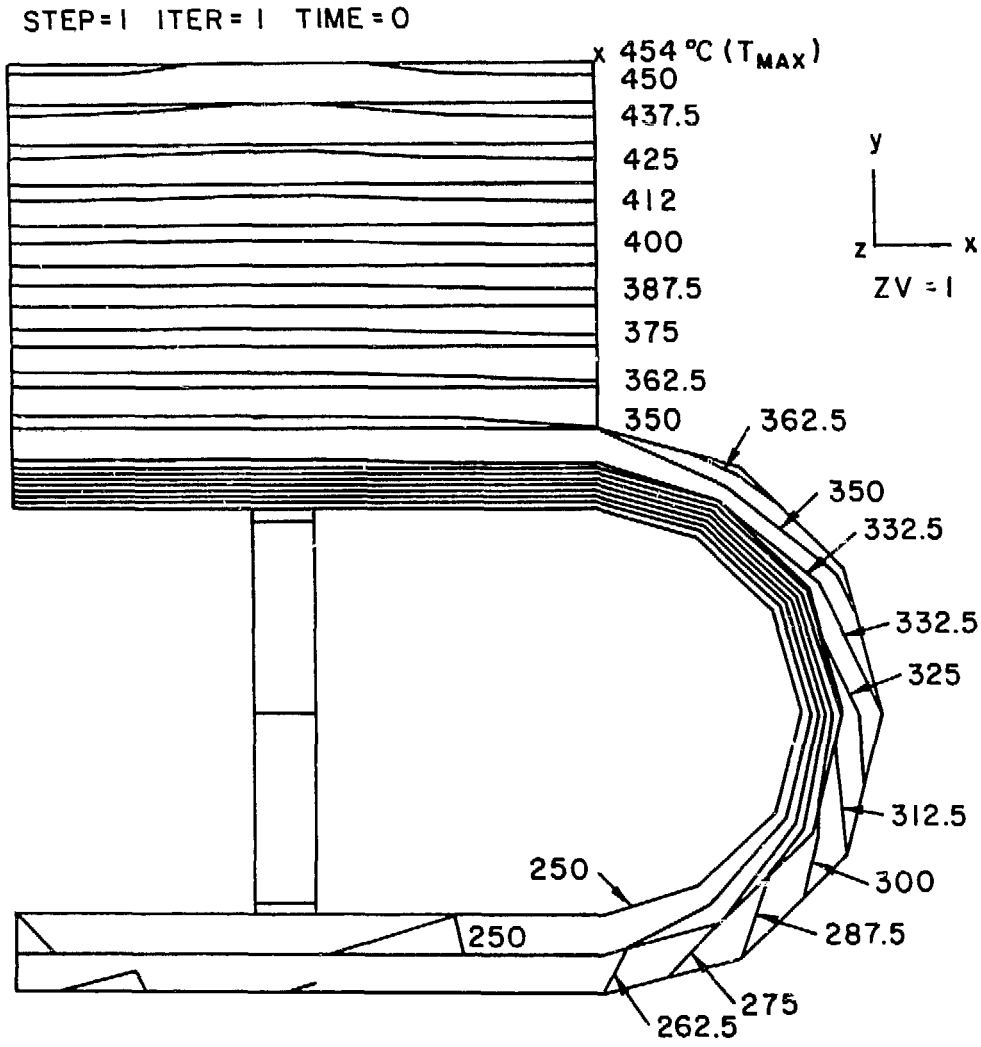

Figure 7-75. Temperature distribution in the leading edge of the BCSS limiter.

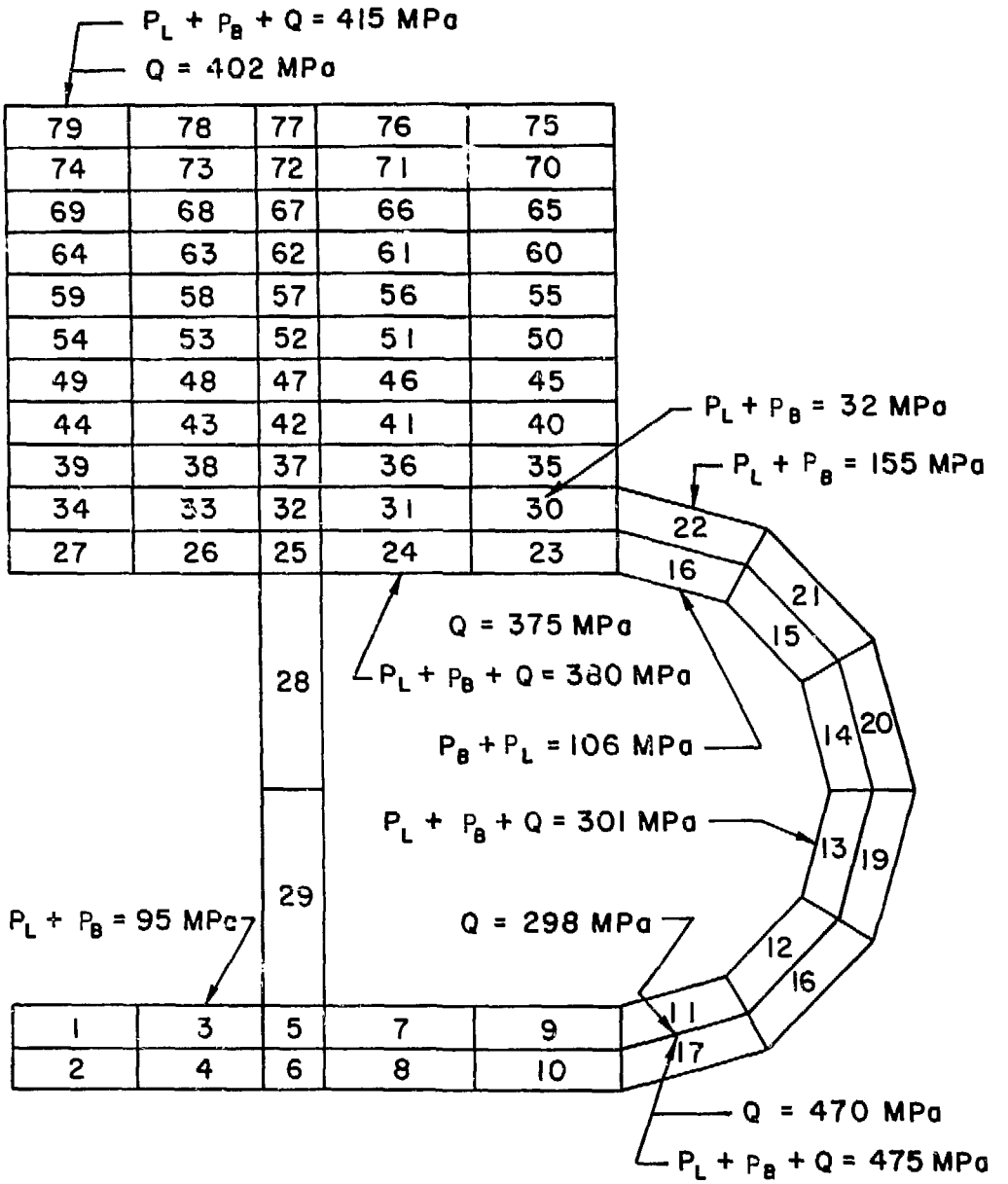

Figure 7-76. Summary of maximum stress intensities at the leading edge of the BCSS limiter.

REFERENCES FOR CHAPTER 7

7-1 M. Abdou et al., "Blanket Comparison and Selection Study," ANL/FPP-83-1, October 1983.

7-2 Y. Gohar and M. A. Abdou, MACKLIB-IV: A Library of Nuclear Response Functions Generated with MACK-IV Computer Program from ENDF/B-IV," Argonne National Laboratory, ANL/FPP/TM-106 (1978).

7-3 B. Badger et al., "WITAMIR-1, A Tandem Mirror Fusion Power Plant," UWFDM-400 (1980).

7-4 G. Logan et al., "Mirror Advanced Reactor Study (MARS) - Interim Report," UCAL-53333, LLNL (1982) (Final report to be published September, 1984).

7-5 Y. Gohar and M. A. Abdou, "Neutronics Optimization of Solid Breeder Blankets for STARFIRE Design," Proceedings of the Fourth Topical Meeting on the Technology of Controlled Nuclear Fusion, King of Prussia, PA, October 14-17, 1980.

7-6 W. W. Engle, Jr., "A User's Manual for ANISN, A One Dimensional Discrete Ordinates Code with Anisotropic Scattering," Oak Ridge Gaseous Diffusion Plant, ORGDP-K-1963 (1967).

7-7 R. W. Roussin et al., "The CTR Processed Multigroup Cross Section Library for Neutronics Studies," Oak Ridge National Laboratory ORNL/RSCIC-37.

7-8 J. H. Huang and M. E. Sawan, "Neutronics Analysis for the MARS Li-Pb Blanket and Shield," Journal of Nuclear Technology/Fusion, Vol. 6, No. 2, 883 (1983).

7-9 LASL Group X-6, "MCNP - A General Monte Carlo Code for Neutron and Photon Transport, Version 2B," Los Alamos National Laboratory, LA-7396-M, Revised (April 1981).

7-10 C. R. Weisbin et al, "VITAMIN-E: An ENDF/B-V Multigroup Cross-Section Library for LMFBR CORE and Shield, LWR Shield, DOSIMETRY and Fusion Blanket Technology," Oak Ridge National Laboratory, ORNL-5505 (February 1979).

7-11 J. H. Huang and M. E. Sawan, "Benchmark Calculations of Tritium Breeding in a $Li_{17}Pb_{83}$ Fusion Reactor Blanket," Transactions of the American Nuclear Society, Vol. 44, 142 (1983).

7-12 R. G. Hickman, "Some Problems Associated with Tritium in Fusion Reactors," Technology of Controlled Thermonuclear Fusion Experiments and the Engineering Aspects of Fusion Reactors, Austin, Texas, November 1972.

7-13 M. Ortman, Private Communication.

7-14 R. Sherman and J. Anderson, Los Alamos National Laboratory, Private Communication.

7-15 V. A. Maroni, R. D. Wolson, and G. E. Strahl, "Some Preliminary Considerations of a Molten-Salt Extraction Process to Remove Tritium from Liquid Lithium Fusion Reactor Blankets," Nucl. Tech., 25, 83 (1975).

7-16 W. F. Calaway, "Electrochemical Extraction of Hydrogen from Molten LiF-LiCl-LiBr and its Application to Liquid-Lithium Fusion Reactor Blanket Processing," Nucl. Tech., 39, 63 (1978).

7-17 C. C. Baker et al., "STARFIRE - A Commercial Tokamak Fusion Power Plant Study," ANL/FPP-80-1 (1980).

CHAPTER 8

TABLE OF CONTENTS

LIST OF FIGURES FOR CHAPTER 8

LIST OF TABLES FOR CHAPTER 8

8. HELIUM-COOLED BLANKET CONCEPTS

This chapter presents the technical details of the helium-cooled blanket concepts that were developed by the BCSS teams from GA Technologies Inc., and Lawrence Livermore National Laboratories. The work presented here is the continuation and logical conclusion of the work on helium-cooled blanket concepts presented in the BCSS interim report,[8.1-1] and presents a new helium-cooled FLiBe design which was developed in the second year.

8.1 Introduction

During the first year of the BCSS effort, helium-cooled blanket concepts were identified as attractive candidates for selection by the study. Because helium is totally inert, it offers the possibility of blanket designs with a very low level of corrosion and radioactive material transport concerns. Safety problems associated with use of coolant materials that could react with air, water, or concrete can be eliminated. Being a nonelectrical conductor, helium will not support electrical or magnetic effects, eliminating coolant MHD concerns. Helium-cooled power conversion systems offer high efficiency and the use of well-developed technologies. Helium cooling appears to be well-suited to the requirements and unique environment of a fusion reactor blanket. Helium does have low density and low volumetric heat capability, leading to the need for high pressures (40 to 80 atm) and large coolant temperature differentials. In the design of a helium-cooled fusion reactor blanket, these characteristics must be accommodated in the design.

During the first year of the BCSS effort[8.1-1] we reviewed the past efforts on helium-cooled fusion reactor blanket design and selected the pressurized lobe concept as the most attractive configuration for both the tokamak and the tandem mirror reactor. We developed design concepts that are attractive for both solid and liquid breeder materials and identified special issues that required investigation and resolution for these concepts. We

performed initial screening of helium-cooled blanket concepts to ensure that only viable, potentially attractive candidates were pursued.

The work done during the second year of the BCSS effort is reported here. From the initial screening work done during the first year, a number of promising choices had emerged for the choice of structural material, tritium breeder, and neutron multiplier. Three structural materials, six tritium breeders, and three neutron multipliers, shown on Table 8.1-1, appeared attractive. A total of ($3 \times 6 \times 3 = 54$) potential helium-cooled blanket options are possible. We have explored these options, developing sufficient information to narrow the list to four R=1 concepts that were then analyzed in enough depth to allow full evaluation of their technical feasibility, economic potential, safety characteristics, and R&D needs. These evaluations are presented in Sections 3.1 through 3.4 of this report.

The detailed information associated with the design and selection process is presented in this chapter. Of the 54 possible options, four were selected as R=1, attractive designs selected for detailed evaluation. These are:

Li_2O/He/FS
Li/He/FS
$LiAlO_2$/He/FS/Be
FLiBe/He/FS/Be

These designs are described in detail in Sections 8.4 through 8.7 below. Thirteen concepts were judged to be attractive, but slightly less so than the four R=1 concepts. These 13 were rated as "1B" or "2A" and were not pursued further at this time. These concepts do appear to be attractive, however, and could be considered for future design and investigation, particularly as additional information becomes available on the various materials and technologies used in them. If any of the four R=1 options are found to have a design concern, it is possible that one or more of the R=1B/2A designs could be used instead. Further, if one of the R=1 designs is found to look very attractive in the detailed evaluation, it is possible that one or more of the R=1B/2A concepts would also share these favorable characteristics and should

TABLE 8.1-1
POSSIBLE HELIUM-COOLED BLANKET DESIGN OPTIONS

Structure	Breeder	Multiplier
• Modified 316 austenitic stainless steel (Prime Candidate Alloy)	• Solid breeders Li_2O Li_8ZrO_6 Ternary ceramics ($LiAlO_2$)	• None • Beryllium • Lead
• 9-12Cr Ferritic Stainless Steel (HT-9)		
• Vanadium Alloy (V-15Cr-5Ti)	• Liquid breeders Li $Li_{17}Pb_{83}$ FLiBe	

Total number of potential options: (3 × 6 × 3 = 54)

be included in the R=1 category in the future. Similarly, the reason for the unattractiveness of an R=1 concept may also apply to similar R=1B and/or 2A concepts. These concepts, attractive but not pursued further in the BCSS project, are described in Section 7.8.

Of the remaining 37 potential options, 13 were found to be technically infeasible for one or more reasons and were ranked R=3. It is the project's judgment that these concepts simply will not work and should not be pursued further. The final 24 concepts were judged, for a variety of reasons, to be inferior to the 17 R=1 and R=1B/2A concepts. They were ranked R=2B. It is possible, as additional information becomes available about the materials and technologies required, that these R=2B concepts may emerge as attractive. A specific example of this situation is the use of vanadium alloy. Vanadium alloy has many attractive features for use with helium-cooled liquid-metal breeder blankets. At present, however, concerns about oxidation of the vanadium was sufficient to relegate V/He/Li or V/He/ LiPb concepts to the R=2B category. With additional information, this situation could be changed. The R=2B/3 concepts are discussed in Section 8.9.

The development of the helium-cooled blanket designs for the BCSS resulted in analysis of a number of special issues that are critical to the design and evaluation of these concepts. These special issues are generally of concern for more than one blanket concept. The analysis of the special issues for helium-cooled blankets is discussed in Section 8.10.

Reference

8.1-1. "Blanket Comparison and Selection Study," ANL/FPP-83-1, October, 1983.

8.2 Summary of Final Ranking

A summary of the final ranking of the helium-cooled blanket concepts into the various categories is presented in Table 8.2-1. The ranking terms are described as:

- Favored concepts

  R=1 Attractive, selected for detailed evaluation

  R=1B Attractive, but appears similar to an R=1 concept, not evaluated in detail

  R=2A Appears less attractive than an R=1 concept.

- Concepts not pursued further

  R=2B Appears inferior to R=1, 1B, or 2A concepts

  R=3 Appears infeasible.

Discussion on all of the helium-cooled blanket concepts is presented below. The R=1 concepts have their own sections, 8.4 Li_2O/He/FS, 8.5 Li/He /FS, 8.6 $LiAlO_2$/Be/He/FS, and 8.7 FLiBe/Be/He/FS. The other attractive concepts, ranked 1B and 2A, are discussed in Section 8.8, and the less attractive and infeasible concepts, ranked 2B and 3, are discussed in Section 8.9. The full matrix of preliminary rankings for the helium-cooled concepts is shown in Table 8.2-2 and a brief summary of the ranking rationale is presented below.

Structural Material. Austenitic steel (PCA) has much lower thermal conductivity than ferritic steel or vanadium. As a result, it is thermal-stress-limited to about half the wall load that FS or V are capable of carrying. This relegates the PCA designs to a lower score than the same blanket concept using FS. Vanadium is highly intolerant of oxygen at elevated temperatures. For the oxide ceramic solid breeders, which release tritium at least partially as T_2O, vanadium will not be allowed. For the liquid breeders, the issue is less clear-cut. It should be readily possible to ensure

TABLE 8.2-1
SUMMARY OF HELIUM-COOLED BLANKET RANKINGS
(Breeder/Structure/Multiplier)

Ranking	Solid Breeder	Liquid Breeder
R=1	Li_2O/FS, $LiAlO_2$/FS/Be	Li/FS, FLiBe/FS/Be
R=1B	$LiAlO_2$/PCA/Be, $LiAlO_2$/FS/Pb	Li/FS/Pb, LiPb/FS Li/FS/Be
R=2A	Li_2O/PCA, Li_2O/PCA/Be, Li_2O/FS/Be, $LiAlO_2$/PCA/Pb	Li/PCA, Li/PCA/Be, or Pb, FLiBe/PCA/Be
R=2B	Li_2O/FS/Pb, Li_2O/PCA/Pb, Li_8ZrO_6 - all	LiPb/PCA, LiPb/FS or PCA/Be or Pb, FLiBe/FS or PCA/Pb V-all
R=3	$LiAlO_2$/PCA or FS Oxygen-Containing Solid Breeder/V - all	FLiBe/PCA or FS or V

TABLE 8.2-2
HELIUM-COOLED BLANKET RANKINGS

Breeder	Multiplier	Structure PCA	FS	V
Solid Breeders				
Li_2O	None	2A	1	3
	Be	2A	2A	3
	Pb	2B	2B	3
Li_8ZrO_6	None	2B	2B	3
	Be	2B	2B	3
	Pb	2B	2B	3
$LiAlO_2$	None	3	3	3
	Be	1B	1	3
	Pb	2A	1B	3
Liquid Breeders				
Li	None	2A	1	2B
	Be	2A	1B	2B
	Pb	2A	1B	2B
$Li_{17}Pb_{83}$	None	2B	1B	2B
	Be	2B	2B	2B
	Pb	2B	2B	2B
FLiBe	None	3	3	3
	Be	2A	1	2B
	Pb	2B	2B	2B

low oxidant levels in helium and thus allow use of vanadium. The oxidation concerns, however, prompted the BCSS to judge the vanadium-structured designs less desirable than ferritic steel.

Li_8ZrO_6. The materials group elevation showed it to have no advantages over Li_2O or $LiAlO_2$ with or without a neutron multiplier.

Neutron Multiplier. The helium-cooled Li_8ZrO_6, $LiAlO_2$, and FLiBe blankets simply cannot breed adequate tritium without a neutron multiplier. Those blankets that can breed adequately without additional multiplier (Li, LiPb, Li_2O) are simpler and thus were judged more desirable than the same blanket with a multiplier. Solid breeder ($LiAlO_2$) is better suited to solid multiplier (Be) than liquid multiplier (Pb). Lead was judged more difficult to implement in all cases and to raise concerns about corrosion.

LiPb. Lithium-lead has numerous attractive features, but the ferritic steel-LiPb interface compatibility temperature limit is fairly low. This results in low outlet helium temperature and low thermal efficiency.

When the feasibility issues and preferences discussed above are applied to Table 8.2-2, the rankings given emerge. The four top concepts are Li_2O/He/FS, $LiAlO_2$/Be/He/FS, Li/He/FS, and FLiBe/Be/He/FS.

There are additional combinations of the materials options shown on Table 8.1-1 that could be possible. Use of multiple structural materials and use of a different option for the inboard blanket of a tokamak than is used for the outboard blanket are two examples. These are discussed briefly in Sections 8.8 and 8.9, below.

It should be noted that all the helium-cooled blanket concepts appear to be equally applicable to a tandem mirror reactor as to a tokamak. The blanket internals and pressure boundary configuration would be essentially identical. Only the overall mechanical structure would change somewhat. The first wall design for a tandem mirror is greatly simplified by the absence of any significant level of particle erosion or surface heat flux.

8.3 Key Factors

This section presents the key factors affecting the helium-cooled blanket designs for tokamak and tandem mirror reactors (TMR), namely, the reactor configuration, the surface loading and erosion of the first wall, the helium flow thermodynamics, tritium breeding, and tritium control. Helium-cooled blankets were configured and designed for these factors and they are presented for tokamak reactor and TMR in Sections 8.3.1 and 8.3.2, respectively.

8.3.1 Tokamak Reactor

In the design of blanket modules for helium-cooled tokamak reactor, care was taken to fit the module into the toroidal geometry and to design the first wall to withstand the high surface heat loading and erosion rate.

Figure 8.3-1 shows the proposed arrangement of the helium-cooled pressurized module to fit the tokamak reactor sector. The modules are placed in the toroidal direction. The coolant inlet and outlet plena are at the back of the module, and the flow is across the modules in a poloidal direction, as illustrated in Figs. 8.3-1 and 8.4-1. Two inlet helium pipes are located at the bottom of the tokamak sector and the coolant is collected at the top. The inlet and outlet coolant is distributed and collected by the inlet and outlet circular ring ducts placed at the bottom of the reactor. The estimated sizes of these pipes are indicated in Fig. 8.3-1. For a 36-degree module sector, two sets of the inlet and outlet pipes will be needed between the module and the ring ducts.

For the BCSS study, tokamak modules are to be designed for neutron and surface loadings of 5 and 1 MW/m^2, respectively. In addition, a first wall erosion rate of 1 mm/yr must be accommodated. To handle the relatively high surface loading, an internally-finned first wall cooling channel will be needed. This concept is presented in detail in Sections 8.4 to 8.6. To design for first wall erosion, a first wall with orthogonally grooved erodable material (see Section 6.7) is proposed. The additional material on the

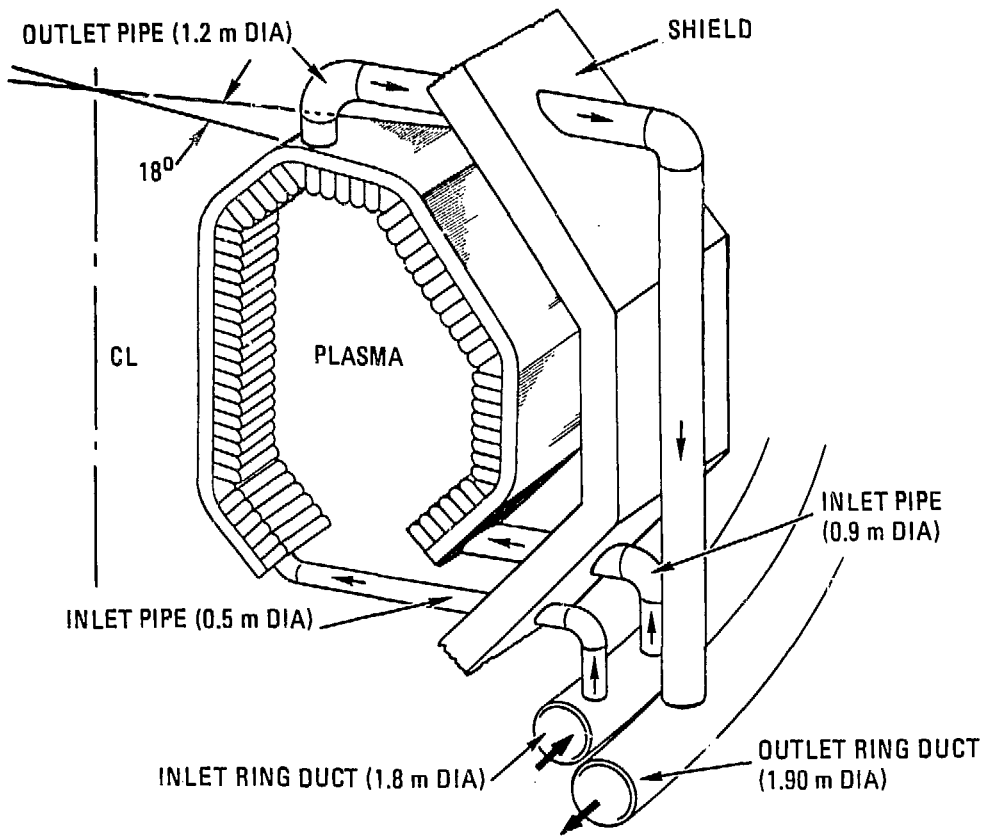

Figure 8.3-1. Tokamak module and piping arrangement

first wall is allowed to operate beyond the HT-9 material structural design limit of 550°C. More details of the grooved first wall analysis are presented in Section 6.7. For the helium-cooled tokamak design, the module life is defined by the thickness of the added erodable layer. The erodable layer thickness was set at 2 mm, based on a 700°C temperature limit for the material in the erodable layer. At an erosion rate of 1 mm/yr, this sets a two year first wall lifetime. The creep stress limit was thus set to a two year limit. Subsequently, the 700°C limit was found to not be applicable. Thus additional erodable material could be added to the first all. A 4 mm layer (four year lifetime) appears possible. This would require some redesign to accommodate a longer creep lifetime, which has not been done, but again appears possible.

8.3.2 Tandem Mirror Reactor

The design of the helium-cooled blanket module for the TMR is conceptually much simpler than that of the tokamak reactor because of the simple cylindrical geometry, as shown in Fig. 8.3-2. As illustrated, the modules are aligned axially. The coolant inlet and outlet pipes are grouped at one end of the module and are connected by ring ducts. Figure 8.3-2 illustrates how the blanket modules can be removed without moving the hefty solenoid coils. Because of the tapered geometry of an individual submodule, the solid breeder plates are also arranged in a tapered fashion, as discussed in Section 8.4.2.

For the first wall design, there is no problem in handling the relatively low surface loading of 0.05 MW/m^2 and erosion rate of 0.1 mm/yr. The blanket lifetime of the module is then defined not by erosion, but by the HT-9 irradiation damage limit of 190 dpa, which corresponds to a module life of at 3.2 years of continuous operation at the reference neutron wall loading of 5 MW/m^2. (12 dpa ≈ 1 MW/m^2 was assumed.)

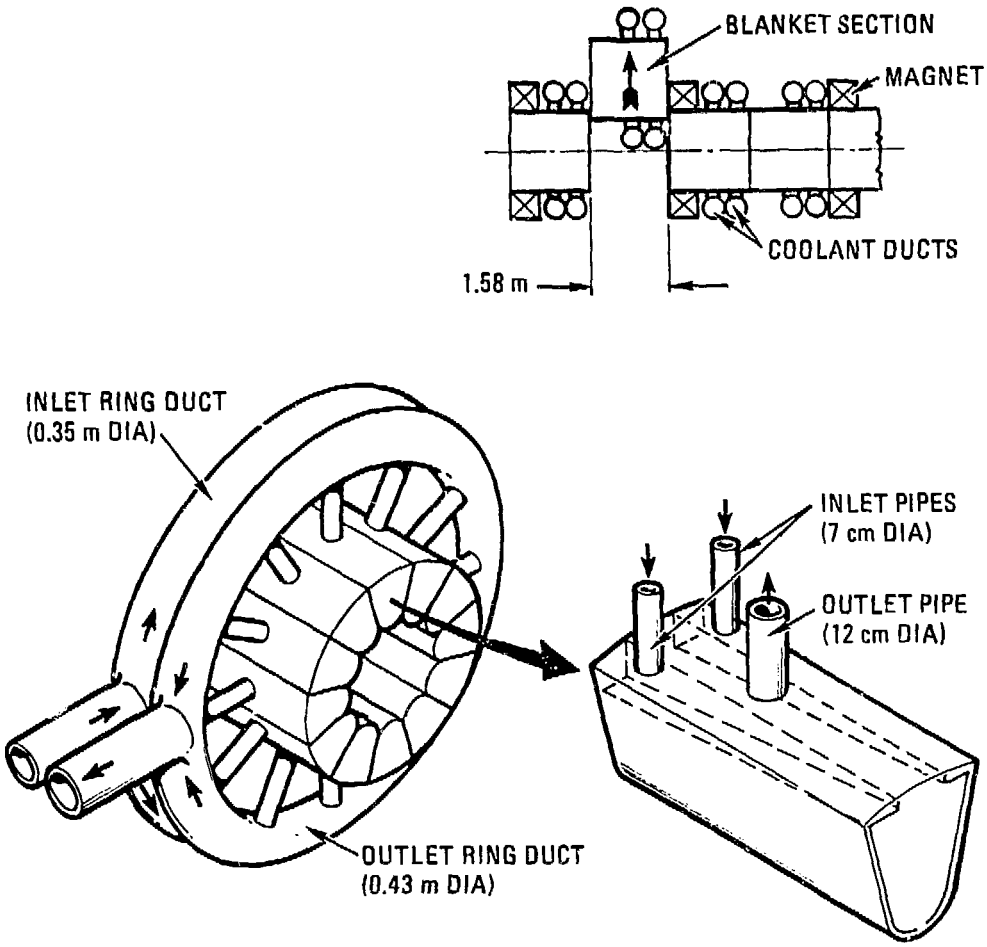

Figure 8.3-2. TMR blanket module and piping arrangement

8.3.3 Helium Flow Thermodynamics

A key factor common to all the helium-cooled designs is the low volumetric heat capacity of helium. In order to keep the pumping power down, a high gas pressure is used (~40 to 80 atm) to increase density, and a large helium temperature rise through the blanket is used to reduce the flow rate required. Materials temperature limits restrict the helium outlet temperature to ~500°C to 550°C. Steam generator pinch point concerns limit the blanket helium inlet temperature to about 250°C or above. The high outlet temperature dictates that the coolant flow radially outward through the blanket. Cool inlet helium is directed to the first wall and front of the blanket where the power density is highest.

The pressure chosen for the four reference helium-cooled designs is 5 MPa for both tokamak and tandem mirror reactors. The pumping power for the eight designs is about 2% to 4% of the blanket thermal power, which translates into about 5% to 10% of the plant electric power. Although most of this power is returned to the coolant as heat, the conversion losses are lost. A higher helium pressure would reduce the pumping power requirement and should be investigated in the future. This is discussed further in Section 8.11.

8.3.4 Tritium Breeding

It should be noted that for helium-cooled blankets designed by the GA Technologies design team for the BCSS, the design philosophy was to design for minimum blanket thickness with adequate tritium breeding ratio (TBR). Because of the importance that was subsequently placed on TBR, this approach may give designs which are not necessarily optimized. The design point was chosen to be a one-dimensional calculated TBR of 1.21. This decision was based on the corresponding three-dimensional TBRs equal to ~1.15 for different R=1 helium-cooled designs as indicated in the BCSS interim report. As the requirement of three-dimensional TBR for fusion reactor blankets becomes more firmly known due to resolution of the many uncertainties associated with TBR calculations, detailed designs for different helium-cooled blankets can

then be adjusted to meet the specified TBR requirement. Examples of potential adjustments are changes of blanket thickness and/or the reduction or addition of neutron multiplier zone thickness. For different blanket concepts, the sensitivities of TBR to these changes are different and will be discussed in the summary and issues sections.

8.3.5 Tritium Control

Tritium control in the helium purge flow and coolant streams would be quite straightforward if chemical equilibrium could be relied upon. If ~10 appm excess oxygen is maintained in the helium streams, at equilibrium chemical thermodynamics should force virtually all of the tritium present into the form of T_2O. Preliminary results from the TRIO-01 experiment, however, indicate that a significant fraction of the tritium may be released in the T_2 form. Further, a study of $T_2 \rightarrow T_2O$ conversion kinetics suggests that equilibrium may require too much time to achieve, although the effect of oxide layers and other possible oxidizing mechanisms is unknown. Because of this concern, it was assumed in the BCSS that all the tritium appears and stays as T_2. This assumption makes tritium control much more difficult, requiring larger clean-up systems and isotopic dilution by adding H_2 to the helium streams. The tritium oxidation behavior in the helium streams is a critical R&D need and is discussed further in Section 6.6.

8.4 Li_2O/Helium/HT-9 (R=1)

This section presents the design of the R=1 Li_2O, helium-cooled blanket using ferritic steel as the structural material. The tokamak version is described in Section 8.4.1, and the mirror version is described in Section 8.4.2.

8.4.1 Tokamak

8.4.1.1 Blanket Configuration

The helium-cooled/Li_2O/HT-9 design for tokamak reactors is illustrated in Fig. 8.4-1. It is a pressurized module design containing the 5 MPa (50 atm) helium and arranged in the toroidal direction as illustrated in Fig. 8.3-1. Li_2O may be the only solid breederthat will be able to breed adequate tritium without the use of a neutron multiplier. The breeder Li_2O is in plate geometry and clad in HT-9 in order to maximize the blanket breeder volume fraction. A separate purge stream of helium flows through the breeder plates for tritium extraction. Hydrogen is added to the purge stream for tritium permeation control. Coolant helium flows through the module side inlet channels toward the plasma, cools the first wall, turns at the apex of the module, and then flows radially outward to cool the breeder plates.

To enhance the first wall cooling for the tokamak reactor, finned cooling channels are needed to remove the heat resulting from surface loading and volumetric power generation. The total blanket thickness, including the plenum, was selected to be different at inboard and outboard locations, being 0.41 and 0.85 m, respectively. This choice would allow the minimum overall reactor dimension while providing adequate tritium breeding. This observation was based on the trade-off between shield and blanket thickness. In general, the blanket is not as effective as a specifically design shield to perform the function of shielding.

During the BCSS study, the swelling of Li_2O at high neutron fluence was identified as a potentially critical problem for the design as discussed in

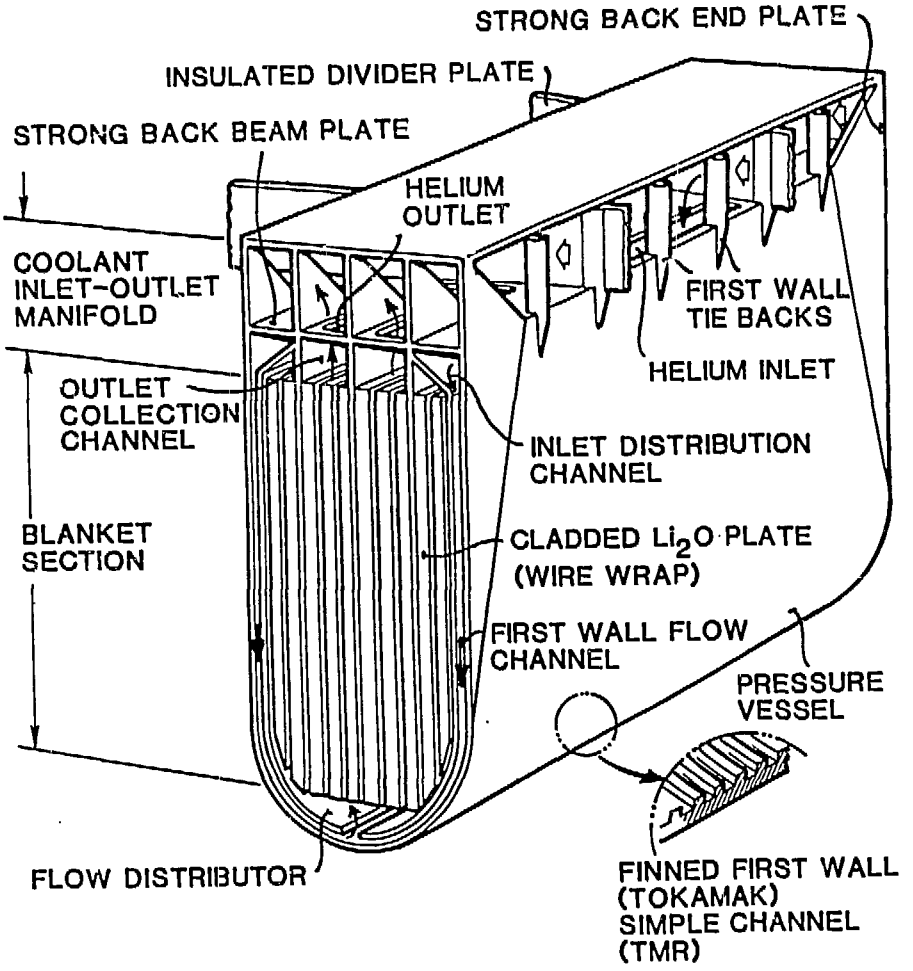

Figure 8.4-1. Tokamak/He/Li_2O blanket design

Section 6.3. The magnitude of the induced swelling and how much of it can be relaxed by material creep still has to be determined. A swelling-tolerant plate design was proposed to accommodate volumetric swelling up to 10%. Mechanical, neutronics, and thermal-hydraulics details of this blanket design, and the consideration of tritium inventory, extraction and control are presented in Section 8.10.

8.4.1.2 Design Summary and Issues

This section presents the design summary of the tokamak helium-cooled Li_2O design. Its favorable design features are identified, as are the issues that need to be addressed in future studies.

Table 8.4-1 summarizes the design characteristics of the tokamak helium-cooled Li_2O design. The following favorable characteristics of the reference design can be identified:

- Compared to liquid-lithium designs, this design has relatively low chemical energy content.

- No neutron multiplier is needed for this design to breed adequate tritium.

- No ^6Li enrichment will be required.

- With the purge flow design, it has double-wall tritium containment (breeder clad and heat exchanger). The chemistry of the purge helium stream can be adjusted relatively easily for tritium extraction and/or control; and for the control of breeder and cladding material interaction.

TABLE 8.4-1
MAJOR PARAMETERS AND FEATURES OF
THE TOKAMAK HELIUM-COOLED Li_2O DESIGN

General Description	
Materials	
Coolant	Helium @ 5 MPa (50 atm)
Breeder	Li_2O
Neutron multiplier	None
Structure	HT-9
Major Design Parameters	
Reactor blanket thermal power, MW	5382
Average neutron wall load, MW/m^2	5.0
Average first wall surface heat flux, MW/m^2	1.0
Coolant	
Inlet/outlet temperature, °C/°C	275/510
Maximum pressure, MPa	5.0
Breeder	
Minimum/maximum temperature, °C/°C	510/795
Purge stream pressure, MPa	0.1
Structure	
First wall/blanket maximum temperature, °C	547 (first wall) 649 (erodable surface at beginning of life)
Minimum/maximum temperature at:	
Coolant interface, °C/°C	275/515
Breeder interface, °C/°C	442/515
Neutronics	
Tritium breeding ratio	
1-D, 100% coverage	1.21
Net (3-D with all geometrical details and penetration)[a]	1.113
Maximum nuclear heating rates	
Breeder, W/cc	47
Structure, W/cc	50

TABLE 8.4-1 (Continued)

Energy (1-D calculation)	
Multiplication factor	1.18[b]
Deposited in heat recovery zone, MeV	16.65
Deposited in heat loss zone, MeV	0.44
First Wall/Blanket Design Description	
Inboard first wall/blanket	
Thickness (including manifolds), m	0.41
Manifold thickness, m	0.11
Percent structure/% coolant in manifold region, %/%	20/80
Coolant ΔP (total), MPa	0.095
Outboard first wall/blanket	
Thickness (including manifolds), m	0.85
Manifold thickness, m	0.22
Percent structure/% coolant in manifold region, %/%	20/80
Coolant ΔP (total), MPa	0.122
Primary coolant loop pumping power, MW	237
First Wall	
Description	Internal fins
Minimum/maximum coolant temperature, °C/°C	275/334
Maximum structure temperature, °C	547 (first wall) 649 (erodable surface at beginning of life)
Blanket	
Description	Pressurized module, Li_2O clad in 1.1-cm-thick plates
^6Li enrichment, %	7.4 (natural)
Minimum/maximum coolant temperature, °C/°C	334/507
Maximum structure temperature, °C	515
Tritium removal from breeder	
Method	Purge flow
Steady-state breeder tritium inventory, g	133.6
Purge gas	
Material	Helium

TABLE 8.4-1 (Continued)

Temperature, °C	300–500
Pressure, MPa	0.1
Tritium barriers	Natural oxide on main helium coolant side[d]
Power Conversion System	
Thermal storage provision (tokamak)	
Technique	Packed bed thermal storage
Storage medium	Steel balls
Steam generator	
Type	Helical wound tube and shell
Single or double wall tubes	Single
Steam	
Inlet/outlet temperature, °C/°C	204/460
Maximum pressure, MPa	8.3
Tritium barriers	Natural oxide on both sides of steam generator wall[d]
Thermal efficiency	
$\eta = \frac{(MW_e)_{out} - (MW_e)_{pump}}{MW_{th\ TOTAL}}$, %	36.4
Gross (MW_e/MW_{th}), %	39.2
Steady-State Tritium Losses, Ci/d	43.6 (100% T_2)[c,e]

[a]As calculated by Tritium Breeding Task Group.

[b]Neutron energy multiplication only.

[c]Hydrogen is added into the purge stream at a rate equal to 100 times the mass generation rate of tritium.

[d]Barrier factor of 100 was assumed on the surface of the wall or clad, as discussed in Section 6.6.

[e]Tritium influx from the first wall at 0.22 g/day.

Generic issues for the helium-cooled HT-9 blanket designs are identified in Section 3.4 and 8.3. Potential issues that need to be addressed specifically for the helium-cooled Li_2O HT-9 design are the following:

- Irradiation-induced swelling of Li_2O is a potentially critical issue. Radiation-induced swelling of Li_2O needs to be quantified. The effect should be studied in a constrained design such that the material creep property can be coupled into the swelling effects. The swelling-tolerant design as described in Section 8.10.1 should be studied experimentally.

- The issues of tritium extraction and containment need to be addressed further by experiment. Such a program would include qualification and quantification of purge flow design under an in-situ simulated fusion reactor environment. Tritium permeation data under reference design operating conditions are critical for predicting and controlling the bred tritium.

- Understanding of LiOH mass transfer is needed. Experiments will be needed to simulate the LiOH mass transfer in the tritium purge stream under the recommended flow conditions of the reference design.

- The tritium breeding ratio of Li_2O is modest, but adequate. This quantity should be reviewed with further understanding of the TBR requirements for the tokamak reactor.

- Mechanical properties of Li_2O are needed. These properties are needed in order to project breeder behavior under thermal stresses and irradiation gradient conditions. Simulation of the breeder/clad mechanical interaction is also needed.

8.4.2 Tandem Mirror Reactor

8.4.2.1 Blanket Configuration

The helium-cooled/Li_2O/HT-9 design for tandem-mirror reactors is similar to the design illustrated in Fig. 8.4-1. The differences between these designs are in the coolant routing in the plenum design and in the design of the first wall. As illustrated in Fig. 8.3-2, the coolant in the plenum of the TMR module flows in the module axial direction, which fits the mirror reactor geometry. The inlet/outlet piping is on one side of the module to ensure that the module segment can be removed without moving the hefty solenoid coils. Since the surface heat loading for the TMR is 0.05 MW/m^2, which is much smaller than the 1.0 MW/m^2 for the tokamak reactor, a simple channel first wall is adequate to cool the first wall structure as indicated in Fig. 8.4-1. Similarly, because of the small surface heat load and negligible first wall erosion rate for the TMR, no grooving of the first wall or erosion layer will be needed.

This may also be the only solid breeder for TMR that can breed adequate tritium without the use of a neutron multiplier. The module is pressurized to 5 MPa (50 atm) and can be arranged in the axial direction, as illustrated in Fig. 8.3-2. The breeder Li_2O is in tapered plates to fit the cylindrical configuration. They are clad in HT-9 in order to maximize the blanket breeder volume fraction. A separate purge stream of helium is fed through the breeder plates for tritium extraction. Hydrogen is added to the purge stream for permeation control. Coolant helium flows through the module side inlet channels toward the plasma, cools the first wall, turns at the apex of the module and then flows radially outward to cool the breeder plates. The total blanket thickness, including the plenum, was selected to be 0.62 m. This thickness would allow the minimum overall reactor dimension while providing for adequate tritium breeding.

During the BCSS study, the swelling of Li_2O at high neutron fluence was identified as a potentially critical problem for the design. The magnitude of the induced swelling and how much of it can be relaxed by material creep

still has to be determined. A swelling-tolerant plate design was proposed to accommodate volumetric swelling up to 10%. Mechanical, neutronics, and thermal-hydraulics details of this blanket design, and the consideration of tritium inventory, extraction, and control are given in Section 8.10.

8.4.2.2 Design Summary and Issues

This section presents the design summary of the TMR helium-cooled Li_2O design. Its favorable design features are identified, as are the issues that need to be addressed in future studies.

Table 8.4-2 summarizes the design characteristics of the TMR helium-cooled Li_2O design. The following favorable characteristics of the reference design can be identified:

- Compared to liquid-lithium designs, this design has relatively low chemical energy content.
- No neutron multiplier is needed for this design to breed adequate tritium.
- No ^6Li enrichment will be required.
- With the purge flow design, it has double wall tritium containment (breeder clad and heat exchanger). The chemistry of the purge helium stream can be adjusted relatively easily for tritium extraction and/or control; and for the control of breeder and cladding material interaction.

Generic issues for the helium-cooled HT-9 blanket designs are identified in Sections 3.4 and 8.3. Potential issues that need to be addressed specifically for the helium-cooled Li_2O HT-9 design are the following:

- Irradiation-induced swelling of Li_2O is a potentially critical issue. Radiation-induced swelling of Li_2O needs to be quantified.

TABLE 8.4-2
MAJOR PARAMETERS AND FEATURES OF
THE TMR HELIUM-COOLED Li_2O DESIGN

General Description	
Materials	
Coolant	Helium @ 5 MPa (50 atm)
Breeder	Li_2O
Neutron multiplier	None
Structure	HT-9
Major Design Parameters	
Reactor blanket thermal power, MW	2958
Average neutron wall load, MW/m^2	5.0
Average first wall surface heat flux, MW/m^2	0.05
Coolant	
Inlet/outlet temperature, °C/°C	275/540
Maximum pressure, MPa	5.2
Breeder	
Minimum/maximum temperature, °C/°C	519/782
Maximum pressure, MPa	0.1
Structure	
First wall/blanket maximum temperature, °C	546 (cladding)
Minimum/maximum temperature at	
Coolant interface, °C/°C	275/546
Breeder interface, °C/°C	437/546
Neutronics	
Tritium breeding ratio	
1-D, 100% coverage	1.19
Net (3-D with all geometrical details and penetration)[a]	1.176
Maximum nuclear heating rates	
Breeder, W/cc	47
Structure, W/cc	50

TABLE 8.4-2 (Continued)

Energy (1-D calculation)	
Multiplication factor	1.19[b]
Deposited in heat recovery zone, MeV	16.72
Deposited in heat loss zone, MeV	0.45
First Wall/Blanket Design Description	
Blanket thickness (including manifolds), m	0.63
Manifold thickness, m	0.10
Percent structure/% coolant in manifold region, %/%	20/80
Coolant ΔP (total), MPa	0.03
Primary coolant loop pumping power, MW	62
First Wall	
Description	Simple channel
Minimum/maximum coolant temperature, °C/°C	275/303
Maximum structure temperature, °C	448
Blanket	
Description	Pressurized module, Li_2O clad in 1.1 to 1.9-cm-thick tapered plates
^6Li enrichment, %	7.6 (natural)
Minimum/maximum coolant temperature, °C/°C	303/538
Maximum structure temperature, °C	546
Tritium removal from breeder	
Method	Purge flow
Steady-state breeder tritium inventory, g	130.7
Purge gas	
Material	Helium
Temperature, °C	300-500
Pressure, MPa	0.1
Tritium barriers	Natural oxide on main helium coolant side[d]

TABLE 8.4-2 (Continued)

Power Conversion System	
Steam generator	
Type	Helical wound tube and shell
Single or double wall tubes	Single
Steam	
Inlet/outlet temperature, °C/°C	204/490
Maximum pressure, MPa	8.3
Tritium barriers	Natural oxide on both sides[d]
Thermal efficiency	
$\eta = \frac{(MW_e)_{out} - (MW_e)_{pump}}{MW_{th\ TOTAL}}$, %	38.4
Gross (MW_e/MW_{th}), %	40.2
Steady-State Tritium Losses, Ci/d	40.5 (100% T_2)[c,e]

[a]As calculated by Tritium Breeding Task Group.

[b]Neutron energy multiplication only.

[c]Hydrogen is added into the purge stream at a rate equal to 100 times the mass generation rate of tritium.

[d]Barrier factor of 100 was assumed on the surface of the wall or clad, as discussed in Section 6.6.

[e]Tritium influx from the first wall at 0.2 g/day.

The effect should be studied in a constrained design such that the material creep property can be coupled into the swelling effects. The swelling tolerant design as described in Section 8.10.1 should be studied experimentally.

- The issues of tritium extraction and containment will need to be addressed further by experiment. Such a program would include qualification and quantification of purge flow design under in-situ simulated fusion reactor environment. Tritium permeation data under reference design operating conditions are critical for predicting and controlling the bred tritium.

- Understanding of LiOH mass transfer is needed. Experiments will be needed to simulate the LiOH mass transfer in the tritium purge stream under the recommended flow conditions of the reference design.

- Tritium breeding ratio. The tritium breeding ratio of Li_2O is marginally adequate at this point. This should be reviewed with further understanding on the requirements of TBR for the TMR.

- Mechanical properties of Li_2O are needed. These properties are needed in order to project breeder behavior under thermal stresses and irradiation gradient conditions. Simulation of the breeder/clad mechaical interaction is also needed.

8.5 Li/Helium/HT-9 (R=1)

This section presents the design of the R=1 liquid lithium, helium-cooled blanket using ferritic steel as the structural material. The tokamak version is described in Section 8.5.1, and the mirror version is described in Section 8.5.2.

8.5.1 Tokamak

8.5.1.1 Blanket Configuration

The design developed for detailed comparative evaluations and investigations of critical issues of the liquid lithium, helium-cooled tokamak blanket concept is shown in Fig. 8.5-1. It consists of a pressurized module containing 5 MPa (50 atm) helium and arranged in the toroidal direction as illustrated in Fig. 8.3-1. This mechanically simple configuration features an HT-9 lobed first wall of the internal-fin type, HT-9 tube fuel elements containing very slowly circulating liquid lithium breeder, and a plate-type HT-9 reflector/hot shield region. Helium coolant entering the blanket at 275°C is directed initially along side inlet channels to the first wall region and then radially cross-flowed through the lithium tube bank and reflector plates. The helium outlet temperature is 510°C, allowing a net power conversion system efficiency of 36.0% including pumping power losses.

8.5.1.2 Design Summary and Issues

The key features and parameters of the helium-cooled, liquid lithium tokamak blanket design are presented in Table 8.5-1 and summarized in this section. Details of the mechanical, neutronic and thermal-hydraulic design, and considerations of tritium extraction and control are provided in Section 8.10.

To enhance the first wall cooling for the tokamak reactor, finned cooling channels are needed to remove the heat from surface loading and volumetric power generation. Total blanket inboard/outboard thicknesses of 0.61/1.20 m were selected to minimize overall reactor cost while designing for adequate tritium breeding. Inboard/outboard lithium breeding zone thicknesses are 0.24/0.78 m. The lithium is contained in 4.7 cm o.d. 1.1 mm thickness HT-9 tubes in a triangular 5.1 cm pitch. Tritium is recovered by slow circulation of the lithium (0.092 m^3/s for the reactor) to a molten salt extractor.(8.5-1) One cm thick inlet/outlet plena for lithium distribution

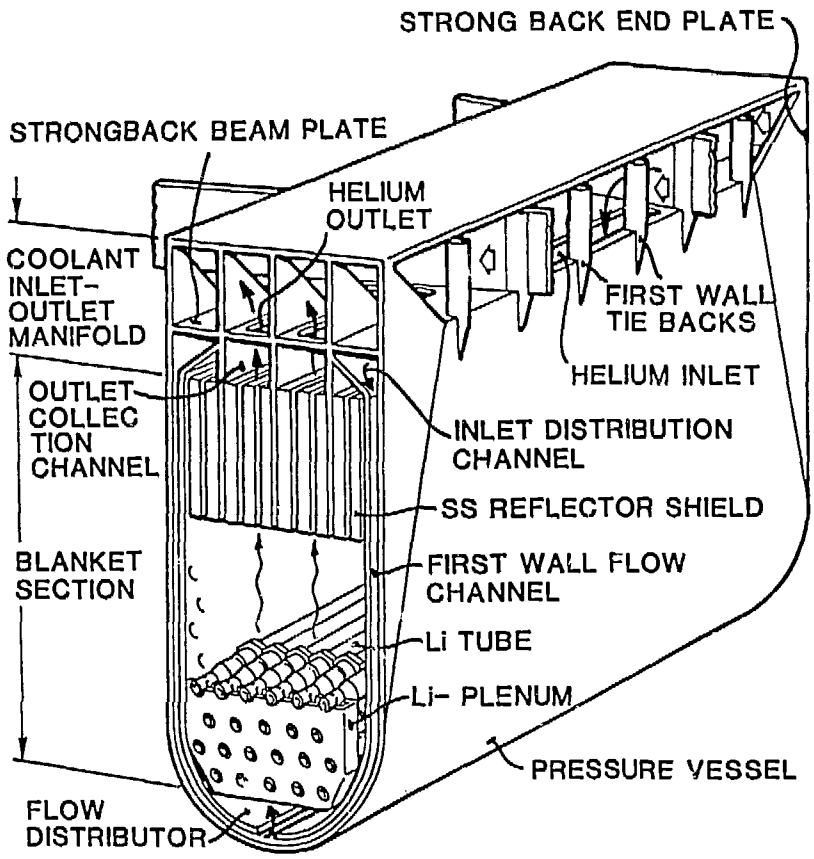

Figure 8.5-1. Liquid lithium/He blanket design

TABLE 8.5-1
MAJOR PARAMETERS AND FEATURES OF
THE TOKAMAK HELIUM-COOLED LIQUID LITHIUM DESIGN

General Description	
Materials	
Coolant	Helium @ 5 MPa (50 atm)
Breeder	Li
Neutron multiplier	None
Structure	HT-9
Major Design Parameters	
Reactor blanket thermal power, MW	5577
Average neutron wall load, MW/m^2	5.0
Average first wall surface heat flux, MW/m^2	1.0
Coolant	
Inlet/outlet temperature, °C/°C	275/510
Maximum pressure, MPa	5.0
Breeder	
Minimum/maximum temperature, °C/°C	500/560
Maximum pressure, MPa	5.0
Structure	
First wall/blanket maximum temperature, °C	547 (first wall) 649 (erodable surface at beginning of life)
Minimum/maximum temperature at:	
Coolant interface, °C/°C	275/533
Breeder interface, °C/°C	500/535
Neutronics	
Tritium breeding ratio	
1-D, 100% coverage	1.16
Net (3-D with all geometrical details and penetration)[a]	1.12
Maximum nuclear heating rates	
Breeder, W/cc	23
Structure, W/cc	50

TABLE 8.5-1 (Continued)

Energy (1-D calculation)	
Multiplication factor	1.23[b]
Deposited in heat recovery zone, MeV	17.4
Deposited in heat loss zone, MeV	0.2
First Wall/Blanket Design Description	
Inboard first wall/blanket	
Thickness (including manifolds), m	0.61
Manifold thickness, m	0.11
Percent structure/% coolant in manifold region, %/%	20/80
Coolant ΔP (total), MPa	0.101
Outboard first wall/blanket	
Thickness (including manifolds), m	1.20
Manifold thickness, m	0.22
Percent structure/% coolant in manifold region, %/%	20/80
Coolant ΔP (total), MPa	0.142
Primary coolant loop pumping power, MW	262
First Wall	
Description	Internal fins
Minimum/maximum coolant temperature, C/°C	275/334
Maximum structure temperature, °C	547 (first wall) 649 (erodable surface at beginning of life)
Blanket	
Description	Pressurized module, Li in HT-9 tubes
^{6}Li enrichment, %	7.4 (natural)
Minimum/maximum coolant temperature, °C/°C	328/507
Maximum structure temperature, °C	515
Steady-state breeder tritium inventory, g	330
Tritium Recovery	
Total MHD lithium ΔP (inboard), MPa	1.01

TABLE 8.5-1 (Continued)

Power Conversion System	
Thermal storage provision (tokamak)	
Technique	Packed bed thermal storage
Storage medium	Steel balls
Steam generator	
Type	Helical wound tube and shell
Single or double wall tubes	Single
Steam	
Inlet/outlet temperature, °C/°C	204/460
Maximum pressure, MPa	8.3
Tritium barriers	Natural oxide on water side of steam generator wall
Thermal efficiency	
$\eta = \frac{(MW_e)_{out} - (MW_e)_{pump}}{MW_{th\ TOTAL}}$, %	36.0
Gross (MW_e/MW_{th}), %	39.2
Steady-State Tritium Losses, Ci/d	16.1 d

[a]As calculated by Tritium Breeding Task Group.

[b]Neutron energy multiplication only.

[c]Tritium barrier factors of 2 and 100 are assumed to be on the wall/clad of the main helium coolant and water side of the steam generator, respectively.

[d]Hydrogen is added into the main helium coolant stream at 22 gm/day, which is 100 times the tritium influx rate from the first wall at 0.22 gm/day.

are located at both ends of the lithium tubes. Inlet/outlet lithium collector piping is located inside the helium plenum at the back of the module, occupying less than 10% of the flow space and increasing the plenum thickness accordingly. The tritium inventory in the lithium is 330 g, resulting in a tritium loss rate via permeation through the steam generator of 16.1 Ci/d. Total MHD pressure drop in the inboard blanket loop resulting from the lithium circulation is 0.01 MPa.

Considering the reference design, the following favorable characteristics can be identified for the helium-cooled liquid lithium blanket design:

- Conceptually simple mechanical, neutronic, and thermal-hydraulic design.
- No ^{6}Li enrichment required.
- Lower lithium inventory than self-cooled concepts.
- Lithium is circulated slowly only for tritium recovery with moderately low attendant MHD pressure drop, making it less vulnerable than self-cooled concepts.
- Low inventory and double containment of tritium (blanket breeder tubes and heat exchanger).
- Inherent safety features described below.

The present design offers multiple safety features. It incorporates a multiple containment approach to liquid breeder release, and since the coolant is helium, the inventory of liquid breeder is minimized to that required only from neutronics considerations. There is no appreciable potential for breeder-coolant chemical interaction due to the low level of impurities in the helium. In a depressurization event, the design allows for rapid communication between submodules. The design is projected to withstand the maximum

forces expected without propagation to adjacent submodules. With gas coolant, the capability exists to circulate the depressurized coolant for heat removal during accident conditions, which will prevent module failure from excessive temperatures. The capability also exists to provide a redundant and diverse auxiliary cooling circuit via recirculation of the liquid breeder. Under complete loss of cooling, the blanket has a large heat capacity (Li) and offers good heat conduction for heat removal from the first wall region.

The critical feasibility issue in this concept is that of liquid metal corrosion and compatibility with the containment tube material. The maximum structural interface temperature is the critical design constraint on the thermal-hydraulics. The tradeoff between this temperature limit and the maximum acceptable pumping power through the breeder zone establishes the tube dimensions and pitch.

Though not a critical issue, a significant design constraint is the neutronic distribution of energy between the inboard and outboard blankets. The economic tradeoff of minimizing the inboard blanket thickness while maintaining adequate neutronic protection of the magnet versus maximizing the total energy recovered at useful temperatures establishes the relative inboard/outboard blanket thicknesses. Though the resultant blanket design exhibits relatively low power density, its performance can be significantly improved by incorporating a neutron multiplier (Be or Pb).

8.5.2 Tandem Mirror Reactor

8.5.2.1 Blanket Configuration

The TMR helium-cooled liquid lithium, HT-9 design is similar to the design shown in Fig. 8.5-1. The differences are in the design of the coolant routing in the plenum and in the design of the first wall. The module is also tapered to fit the cylindrical geometry. As illustrated in Fig. 8.3-2, the coolant in the plenum of a TMR module flows in the module axial direction, which fits the mirror reactor geometry. The module inlet/outlet piping

is on one side of the module to make sure that the module segment can be removed without moving the solenoid coils. Since the surface loading for the TMR is 0.05 MW/m^2, which is much smaller than the 1.0 MW/m^2 for the tokamak reactor, a simple channel first wall is adequate to cool the first wall structure, as indicated in Fig. 8.4-1. The design offers a mechanically simple configuration and features, in addition to the simple channel HT-9 lobed wall, HT-9 tube fuel elements containing slowly circulating liquid lithium breeder, and a plate-type HT-9 reflector/hot shield region. Helium coolant entering the blanket at 275°C is directed initially to the first wall region by a flow baffle and subsequently cross flowed through the lithium tube bank and reflector plates. The helium outlet temperature is 540°C, allowing a net power conversion system efficiency of 38.5%, including pumping power losses.

8.5.2.2 Design Summary and Issues

The key features and parameters of the helium-cooled, liquid lithium TMR blanket design are presented in Table 8.5-2 and summarized in this section. Details of the mechanical, neutronic, and thermal-hydraulic design, and considerations of tritium extraction and control are provided in Section 8.10.

As discussed earlier, a simple channel first wall is adequate for removing the heat from surface loading and volumetric power generation. A total blanket thickness of 1.08 m was selected to minimize overall reactor cost while designing for adequate tritium breeding. The lithium breeding zone thickness is 0.78 m. The lithium is contained in 4.8 cm o.d. 1.1 mm thickness HT-9 tubes in a triangular 5.1 cm pitch. Tritium is recovered by slow circulation of the Li (0.11 m^3/s) to a molten salt extractor. The tritium inventory in the Li is 330 g. The tritium loss rate via permeation through the steam generator is 10.2 Ci/d. Total MHD pressure drop resulting from the Li circulation is 0.2 MPa.

TABLE 8.5-2
MAJOR PARAMETERS AND FEATURES OF
THE TMR HELIUM-COOLED LIQUID LITHIUM DESIGN

General Description	
Materials	
Coolant	Helium @ 5 MPa (50 atm)
Breeder	Li
Neutron multiplier	None
Structure	HT-9
Major Design Parameters	
Reactor blanket thermal power, MW	3056
Average neutron wall load, MW/m^2	5.0
Average first wall surface heat flux, MW/m^2	0.05
Coolant	
Inlet/outlet temperature, °C/°C	275/540
Maximum pressure, MPa	5.0
Breeder	
Minimum/maximum temperature, °C/°C	470/560
Maximum pressure, MPa	5.0
Structure	
First wall/blanket maximum temperature, °C	547 (cladding)
Minimum/maximum temperature at:	
Coolant interface, °C/°C	275/548
Breeder interface, °C/°C	470/550
Neutronics	
Tritium breeding ratio	
1-D, 100% coverage	1.28
Net (3-D with all geometrical details and penetration)[a]	1.13
Maximum nuclear heating rates	
Breeder, W/cc	23
Structure, W/cc	50

TABLE 8.5-2 (Continued)

Energy (1-D calculation)	
Multiplication factor	1.24[b]
Deposited in heat recovery zone, MeV	17.5
Deposited in heat loss zone, MeV	0.3
First Wall/Blanket Design Description	
Inboard first wall/blanket	
Thickness (including manifolds), m	1.08
Manifold thickness, m	0.10
Percent structure/% coolant in manifold region, %/%	20/80
Coolant ΔP (total), MPa	0.059
Primary coolant loop pumping power, MW	80
First Wall	
Description	Simple channel
Minimum/maximum coolant temperature, °C/°C	275/303
Maximum structure temperature, °C	448
Blanket	
Description	Pressurized module, Li in HT-9 tubes
^{6}Li enrichment, %	7.6 (natural)
Minimum/maximum coolant temperature, °C/°C	303/538
Maximum structure temperature, °C	546
Steady-state breeder tritium inventory, g	330
Tritium Recovery	
Total MHD lithium ΔP, MPa	0.2
Power Conversion System	
Steam generator	
Type	Helical wound tube and shell
Single or double wall tubes	Single
Steam	
Inlet/outlet temperature, °C/°C	204/490
Maximum pressure, MPa	8.3
Tritium barriers	Natural oxide on water side of steam generator wall[c]

TABLE 8.5-2 (Continued)

Thermal efficiency $\eta = \frac{(MW_e)_{out} - (MW_e)_{pump}}{MW_{th\ TOTAL}}$, %	38.5
Gross (MW_e/MW_{th}), %	40.2
Steady-State Tritium Losses, Ci/d	10.2[d]

[a]As calculated by Tritium Breeding Task Group.

[b]Neutron energy multiplication only.

[c]Tritium barrier factor of 2 and 100 are assumed to be on the wall/clad of the main helium coolant and water side of the steam generator, respectively.

[d]Hydrogen is added into the main helium coolant stream at 20 gm/day, which is 100 times the tritium influx rate from the first wall of 0.20 gm/day.

Considering the reference design, the following favorable characteristics can be identified for the helium-cooled liquid lithium blanket design:

- Conceptually simple mechanical, neutronic, and thermal-hydraulic design.
- No neutron multiplier needed for adequate tritium breeding and energy multiplication.
- No ^{6}Li enrichment required.
- Lower lithium inventory than self-cooled concepts.
- Lithium is circulated slowly only for tritium recovery with moderately low attendant MHD pressure drop, making it less vulnerable than self-cooled concepts.
- Low inventory and double contaiment of tritium (blanket breeder tubes and heat exchanger).
- Inherent safety features described below.

The present design offers multiple safety features. It incorporates a multiple containment approach to liquid breeder release, and since the coolant is helium, the inventory of liquid breeder is minimized to that required only from neutronics considerations. There is no appreciable potential for breeder-coolant chemical interaction due to the low level of impurities in the helium. In a depressurization event, the design allows for rapid communication between submodules. The design is projected to withstand the maximum forces expected without propagation to adjacent submodules. With gas coolant, the capability exists to circulate the depressurized coolant for heat removal during accident conditions, which will prevent module failure from excessive temperatures. The capability also exists to provide a redundant and diverse auxiliary cooling circuit via recirculation of the liquid

capacity (Li) and offers good heat conduction through the blanket for heat removal from the first wall region to the shield.

The critical feasibility issue in this concept is that of liquid metal corrosion and compatibility with the containment tube material. The maximum structural interface temperature is the critical design constraint on the thermal-hydraulics. The tradeoff between this temperature limit and the maximum acceptable pumping power through the breeder zone establishes the tube dimensions and pitch.

Though not a critical issue, a significant design concern is the relatively low power density of the blanket. This issue could be addressed and the blanket and reactor performance improved by incorporating a neutron multiplier (Be or Pb) in the design.

Reference

8.5-1. "Blanket Comparison and Selection Study," ANL/FPP-83-1, October, 1983.

8.6 $LiAlO_2$/Be/Helium/HT-9 (R=1)

This section presents the design of the R=1 $LiAlO_2$ helium-cooled blanket using beryllium rods as the neutron multiplier and ferritic steel as the structural material. The tokamak version is described in Section 8.6.1, and the mirror version is described in Section 8.6.2.

8.6.1 Tokamak

8.6.1.1 Blanket Configuration

The helium-cooled/$LiAlO_2$/Be/HT-9 design for tokamak reactors is illustrated in Fig. 8.6-1. It is a pressurized module design containing the 5 MPa (50 atm) helium and arranged in the toroidal direction, as illustrated in Fig. 8.3-1. In order to provide adequate tritium breeding, bare beryllium rods are placed in front of the $LiAlO_2$ region for neutron multiplication. In order to maximize the blanket breeder volume fraction, the breeder $LiAlO_2$ is in plate geometry and clad in HT-9. A separate purge stream of helium passes through the breeder plates for tritium extraction. Hydrogen is added in the purge stream for permeation control and for the control of potential surface tritium inventory, as explained in Section 6.3. Coolant helium flows through the module side inlet channels toward the plasma, cools the first wall and turns at the apex of the module, then flows radially outward to cool the beryllium rods and the breeder plates.

To enhance the first wall cooling for the tokamak reactor, finned cooling channels, as shown in Fig. 8.4-1, are needed to remove the heat from surface loading and volumetric power generation. The total blanket thickness, including plenum, was selected to be different at inboard and outboard locations, with thicknesses of 0.41 and 0.70 m, respectively. This would allow the minimum inboard thickness and thus the minimum overall reactor dimension, while designing for adequate tritium breeding. To maintain minimum inboard thickness and reduce the use of beryllium, no beryllium is utilized in the inboard blanket. Details of the mechanical, neutronics, thermal-hydraulics

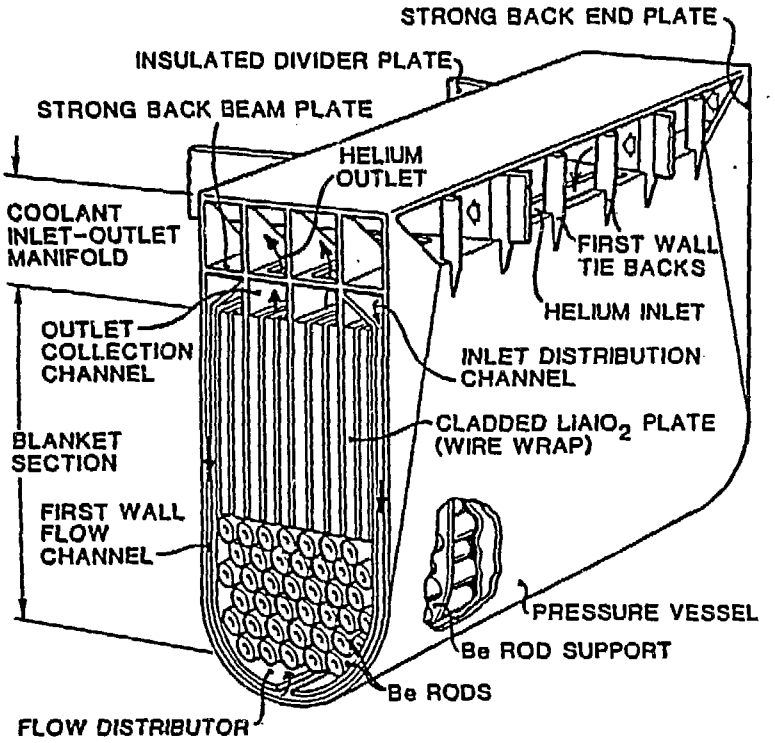

Figure 8.6-1. $LiAlO_2$/Be/He blanket design

design of the blanket module, and the considerations of tritium inventory, extraction, and control are presented in Section 8.10.

8.6.1.2 Design Summary and Issues

This section presents the design summary of the tokamak helium-cooled $LiAlO_2$/Be design. Its favorable design features are identified, as are the issues that need to be addressed in future studies.

Table 8.6-1 summarizes the design characteristics of the helium-cooled $LiAlO_2O$/Be design. The following favorable design characteristics of the reference design can be identified:

- Compared to liquid-lithium designs, this design has relatively low chemical energy content.

- Compared to Li_2O, $LiAlO_2$ is a much easier material to handle.

- With the purge flow design, it has double wall tritium containment (breeder clad and heat exchanger). The chemistry of the purge helium stream can be adjusted relatively easily for tritium extraction and/or control; and for the control of breeder and cladding material interaction compatibility.

- The tritium breeding potential for this design has not been reached. If it is necessary, 10 cm of beryllium can be added to the inboard blanket allowing a TBR increase of 6%, or the thickness of the outboard-$LiAlO_2$ zone can be increased by 10 cm to also obtain an increase of tritium breeding by 6%. Use of both inboard beryllium and a thicker $LiAlO_2$ zone would increase TBR by over 10%. A configuration change to allow mixing of the beryllium and $LiAlO_2$ zones would increase TBR by an additional 10% to 15%.

TABLE 8.6-1
MAJOR PARAMETERS AND FEATURES OF
THE TOKAMAK HELIUM-COOLED $LiAlO_2$/Be DESIGN

General Description	
Materials	
Coolant	Helium @ 5 MPa (50 atm)
Breeder	$LiAlO_2$
Neutron multiplier	Beryllium
Structure	HT-9
Major Design Parameters	
Reactor blanket thermal power, MW	5499
Average neutron wall load, MW/m^2	5.0
Average first wall surface heat flux, MW/m^2	1.0
Coolant	
Inlet/outlet temperature, °C/°C	275/510
Maximum pressure, MPa	5.0
Breeder	
Minimum/maximum temperature, °C/°C	520/1000
Maximum pressure, MPa	0.1
Structure	
First wall/blanket maximum temperature, °C	544 (first wall) 646 (erodable surface at BOL)
Minimum/maximum temperature at:	
Coolant interface, °C/°C	275/521
Breeder interface, °C/°C	509/521
Neutronics	
Tritium breeding ratio	
1-D, 100% coverage	1.21
Net (3-D with all geometrical details and penetration)[a]	1.04
Maximum nuclear heating rates	
Breeder, W/cc	64
Neutron multiplier	30
Structure, W/cc	52

TABLE 8.6-1 (Continued)

Energy (1-D calculation)	
Multiplication factor	1.21[b]
Deposited in heat recovery zone, MeV	17.12
Deposited in heat loss zone, MeV	0.84
First Wall/Blanket Design Description	
Inboard first wall/blanket	
Thickness (including manifolds), m	0.41
Manifold thickness, m	0.11
Percent structure/% coolant in manifold region, %/%	20/80
Coolant ΔT (total), MPa	0.099
Outboard first wall/blanket	
Thickness (including manifolds), m	0.70
Manifold thickness, m	0.22
Percent structure/% coolant in manifold region, %/%	20/80
Coolant ΔP (total), MPa	0.127
Primary coolant loop pumping power, MW	179
First Wall	
Description	Internal fins
Minimum/maximum coolant temperature, °C/°C	275/332
Maximum structure temperature, °C	544 (first wall) 646 (erodable surface at beginning of life)
Blanket	
Description	Pressurized module, bare beryllium rods and $LiAlO_2$ clad in 0.9 cm thick plates
^6Li enrichment, %	60
Minimum/maximum coolant temperature, °C/°C	332/507
Maximum structure temperature, °C	520
Tritium removal from breeder	
Method	Purge flow
Power loss (thermal), % total	~0
Steady-state breeder tritium inventory, g	38.2

TABLE 8.6-1 (Continued)

Purge gas	
Material	Helium
Temperature, °C	300-500
Pressure, MPa	0.1
Tritium barriers	Natural oxide on main helium coolant side[d]
Power Conversion System	
Thermal storage provision (tokamak)	
Technique	Packed bed thermal storage
Storage medium	Steel balls
Steam generator	
Type	Helical wound tube and shell
Single or double wall tubes	Single
Steam	
Inlet/outlet temperature, °C/°C	204/460
Maximum pressure, MPa	8.3
Tritium barriers	Natural oxide on both sides of steam generator wall[d]
Thermal efficiency	
$\eta = \frac{(MW_e)_{out} - (MW_e)_{pump}}{MW_{th\ TOTAL}}$, %	36.2
Gross (MW_e/MW_{th}), %	39.2
Steady-State Tritium Losses, Ci/d	24.0 (100% T_2)[d,f]

[a] As calculated by Tritium Breeding Task Group.

[b] Neutron energy multiplication only.

[c] Hydrogen is added into the purge stream at a rate equal to 100 times the mass generation rate of tritium.

[d] Barrier factor of 100 was assumed on the surface of the steam generator wall or breeder clad.

[e] BOL - beginning of life.

[f] Tritium influx from the first wall at 0.22 g/day.

Generic issues for the helium-cooled-HT-9 blanket designs are identified in Sections 3.4 and 8.3. Potential issues that need to be addressed specifically for the helium-cooled $LiAlO_2$/Be HT-9 design are the following:

- The issues of tritium extraction and containment will need to be addressed further by experiment. Such a program would include qualification and quantification of the tritium system design under an in-situ simulated fusion reactor environment. Tritium permeation data under reference design operating conditions are critical for the predicting and controlling of the bred tritium.

- Beryllium resources limitation is still a concern. The beryllium rods have been designed to allow recycling of the beryllium to help to ease the problem. Demonstration of recycling is needed.

- Irradiation damage of beryllium. In our design, care was taken to allow the bare beryllium rods to take the thermal and swelling stresses as presented in Section 8.10.1. More detailed analysis and simulated experiments will be needed to confirm and improve the design.

- Tritium generation in beryllium. In the use of beryllium as the neutron multiplier, tritium will be generated through the (n,T) reaction at 0.3% of the blanket tritium production rate. Potentially, the accumulated tritium in the bare beryllium rod can be diffused out to the main coolant helium. At close to equilibrium, the tritium outflux from the beryllium rod can be significant. If such an outflux is too high, impacting permeation leakage to steam generator, the beryllium rod may need to be clad. Tritium can then be purged through the clad beryllium rods.

- Module refabrication. The procedure in the assembly of hot refabricated beryllium rods into the blanket module will need to be developed.

8.6.2 Tandem Mirror Reactor

8.6.2.1 Blanket Configuration

The helium-cooled/$LiAlO_2$/Be/HT-9 design for tandem mirror reactors is similar to the design illustrated in Fig. 8.6-1. The differences between the two designs are in the coolant routing in the plenum design and in the design of the first wall. As illustrated in Fig. 8.3-2, the coolant in the plenum of the TMR module flows in the module axial direction which fits the mirror reactor geometry. The inlet/outlet piping is on one side of the module to assure that the module segment can be removed without moving the hefty solenoid coils. Since the surface loading for the TMR is 0.05 MW/m^2, which is much smaller than the 1.0 MW/m^2 for the tokamak reactor, a simple channel first wall is adequate to cool the first wall structure as indicated in Fig. 8.4-1. Similarly, because of the negligible first wall erosion rate for TMR, no first wall grooving will be needed.

The module is pressurized to 5 MPa (50 atm) and can be arranged in the axial direction, as illustrated in Fig. 8.3-2. In order to provide adequate tritium breeding, beryllium rods are placed in front of the $LiAlO_2$ region for neutron multiplication. The breeder $LiAlO_2$ is in tapered plates to fit the cylindrical configuration, in order to maximize the blanket breeder volume fraction. They are clad in HT-9. A separate purge stream of helium is fed through the breeder plates for tritium extraction. Hydrogen is added in the purge stream for permeation control and for the control of potential surface tritium inventory, as explained in Section 6.3. Coolant helium flows through the module side inlet channels toward the plasma, cools the first wall and turns at the apex of the module, then flows radially outward to cool the beryllium rods and the breeder plates. The total blanket thickness, including the plenum, was selected to be 0.58 m. This thickness would allow the minimum overall reactor dimension while designing for adequate tritium breeding. Details of this blanket mechanical, neutronics, and thermal-hydraulics design, and the consideration of tritium inventory, extraction, and control are given in Section 8.10.

8.6.2.2 Design Summary and Issues

This section presents the design summary of the TMR helium-cooled $LiAlO_2$/Be design. Its favorable design features are identified, as are the issues that need to be addressed in future studies.

Table 8.6-2 summarizes the design characteristics of the helium-cooled Li_2O design. The following favorable characteristics of the reference design can be identified:

- Compared to liquid-lithium designs, this design has relatively low chemical energy content.

- Compared to Li_2O, $LiAlO_2$ is a much easier material to handle.

- With the purge flow design, it has double wall tritium containment (breeder clad and heat exchanger). The chemistry of the purge helium stream can be adjusted relatively easily for tritium extraction and/or control; and for the control of breeder and cladding material interaction.

- The tritium breeding potential for this design is relatively high. If it is necessary, beryllium zone thickness can be increased to obtain higher tritium breeding than indicated in this design.

Generic issues for the helium-cooled HT-9 blanket designs are identified in Sections 3.4 and 8.3. Potential issues that need to be addressed specifically for the helium-cooled $LiAlO_2$/Be design are the following:

- The issues of tritium extraction and containment will need to be addressed further by experiment. This would mean qualification and quantification of the purge flow design under an in-situ simulated fusion reactor environment. Tritium permeation data under reference design operating conditions are critical for the understanding and control of the bred tritium.

TABLE 8.6-2
MAJOR PARAMETERS AND FEATURES OF
THE TMR HELIUM-COOLED $LiAlO_2$/Be DESIGN

General Description	
Materials	
Coolant	Helium @ 5 MPa (50 atm)
Breeder	$LiAlO_2$
Neutron multiplier	Beryllium
Structure	HT-9
Major Design Parameters	
Reactor blanket thermal power, MW	3106
Average neutron wall load, MW/m^2	5.0
Average first wall surface heat flux, MW/m^2	0.05
Coolant	
Inlet/outlet temperature, °C/°C	275/540
Maximum pressure, MPa	5.2
Breeder	
Minimum/maximum temperature, °C/°C	520/1000
Maximum pressure, MPa	0.1
Structure	
First wall/blanket maximum temperature, °C	550 (cladding)
Minimum/maximum temperature at	
Coolant interface, °C/°C	275/550
Breeder interface, °C/°C	473/550
Neutronics	
Tritium breeding ratio	
1-D, 100% coverage	1.26
Net (3-D with all geometrical details and penetration)[a]	1.186
Maximum nuclear heating rates	
Breeder, W/cc	64
Neutron multiplier	30
Structure, W/cc	52

TABLE 8.6-2 (Continued)

Energy (1-D calculation)	
Multiplication factor	1.25[b]
Deposited in heat recovery zone, MeV	17.57
Deposited in heat loss zone, MeV	0.66
First Wall/Blanket Design Description	
Inboard first wall/blanket	
Thickness (including manifolds)[b], m	0.58
Manifold thickness, m	0.1
Percent structure/% coolant in manifold region, %/%	20/80
Coolant ΔP (total), MPa	0.059
Primary coolant loop pumping power, MW	84
First Wall	
Description	Simple channel
Minimum/maximum coolant temperature, °C/°C	275/302
Maximum structure temperature, °C	450
Blanket	
Description	Pressurized module, bare beryllium rods and $LiAlO_2$ breeder in 1.1-1.9 cm tapered plates
^6Li enrichment, %	60
Minimum/maximum coolant temperature, °C/°C	302/538
Maximum structure temperature, °C	550
Tritium removal from breeder	
Method	Purge flow
Power loss (thermal), % total	~0
Steady-state breeder tritium inventory, g	24.1
Purge gas (if applicable)	
Material	Helium
Temperature, °C	300-500
Pressure, MPa	0.1
Tritium barriers	Natural oxide on main helium coolant side[d]

TABLE 8.6-2 (Continued)

Power Conversion System	
Steam generator	
Type	Helical wound tube and shell
Single or double wall tubes	Single
Steam	
Inlet/outlet temperature, °C/°C	204/490
Maximum pressure, MPa	8.3
Tritium barriers	Natural oxide on both sides of the steam generator wall[d]
Thermal efficiency	
$\eta = \frac{(MW_e)_{cut} - (MW_e)_{pump}}{MW_{th\ TOTAL}}$, %	38.2
Gross (MW_e/MW_{th}), %	40
Steady-State Tritium Losses, Ci/d	27.6 (100% T_2)[c,e]

[a]As calculated by Tritium Breeding Task Group.

[b]Neutron energy multiplication only.

[c]Hydrogen is added into the purge stream at a rate equal to 100 times the mass generation rate of tritium.

[d]Barrier factor of 100 was assumed on the surface of the steam generator wall or breeder clad.

[e]Tritium influx from the first wall at 0.2 g/day.

- Beryllium resources limitation is still a concern. The beryllium rods have been designed to allow recycling of the beryllium to help to ease the problem. Demonstration of recycling is needed.

- Irradiation damage of beryllium. In our design, care was taken to allow the bare beryllium rods to take the thermal and swelling stresses, as presented in Section 8.10.1. More detailed analysis and simulated experiments will be needed to confirm and improve the design.

- Tritium generation in beryllium. In the use of beryllium as the neutron multiplier, tritium will be generated through the (n,T) reaction at 0.3% of the blanket of the tritium production rate. Potentially, the accumulated tritium in the bare beryllium rod can be diffused out to the main coolant helium. At close to equilibrium, the tritium outflux from the beryllium rod can be significant. If such an outflux is too high, impacting from permeation leakage to steam generator, the beryllium rod may need to be clad. Tritium can then be purged through the clad beryllium rods.

- Module refabrication. The procedure in the assembly of hot refabricated beryllium rods into the blanket module will need to be developed.

8.7 Flibe/Be/He/FS Concept (R=1)

8.7.1 Design Choices

The blanket concept is shown in Fig. 8.7-1. Beryllium, in the form of pebbles nominally 1 cm diameter in a 20 cm thick bed, is employed to multiply neutrons. The multiplier zone is followed by a zone of silicon carbide (SiC) which slows neutrons. Neutrons are captured in the Lithium-6 carried in the molten fluoride salt (LiF+BeF- melting point, 363°C) to breed tritium and release extra energy in exothermic nuclear reactions. The salt flows slowly through tubes in the blanket and out to a simple flash separator where the tritium is removed. Helium flows radially through the Be pebble bed and SiC region carrying the heat out to the thermal conversion plant. The tubes are coated either on the inside or outside with a 10 μm tungsten barrier by chemical vapor deposition to cut down tritium permeation to the helium coolant circuit. With the tungsten barrier on the inside the tritium inventory in the tube walls is small and tungsten will contribute to corrosion inhibition. A 1-mm aluminum jacket on the steam generator tubes keeps the tritium permeation to the steam down to 30 curies per day. The design can be converted into a fission-suppressed fissile breeder by thickening the beryllium zone by a factor of 2 or so and adding ThF_4 to the salt in which case 6 tonnes of uranium - 233 would be produced per year.

Beryllium is chosen as the neutron multiplier because of its large (n,2n) nuclear reaction cross-section and low cross-section for competing side reactions. By comparison to other materials, beryllium significantly stands out as a neutron multiplier as can be seen in the infinite media results of Fig. 8.7-2. The material having the next largest neutron multiplication* is ^7Li. However, because its density is 3.8 times lower than beryllium, it requires a very thick blanket to approach its infinite media multiplication ability. The multiplication in Pb is much lower than in beryllium but is still quite appreciable.

Beryllium is a limited resource and some people have thought it inadvisable to use in fusion plant designs because then fusion power would

---

*^7Li is not truly a multiplier but has the same effect because of the $^7Li(n,n'T)^4He$ reaction which produces tritium and preserves the incident neutron.

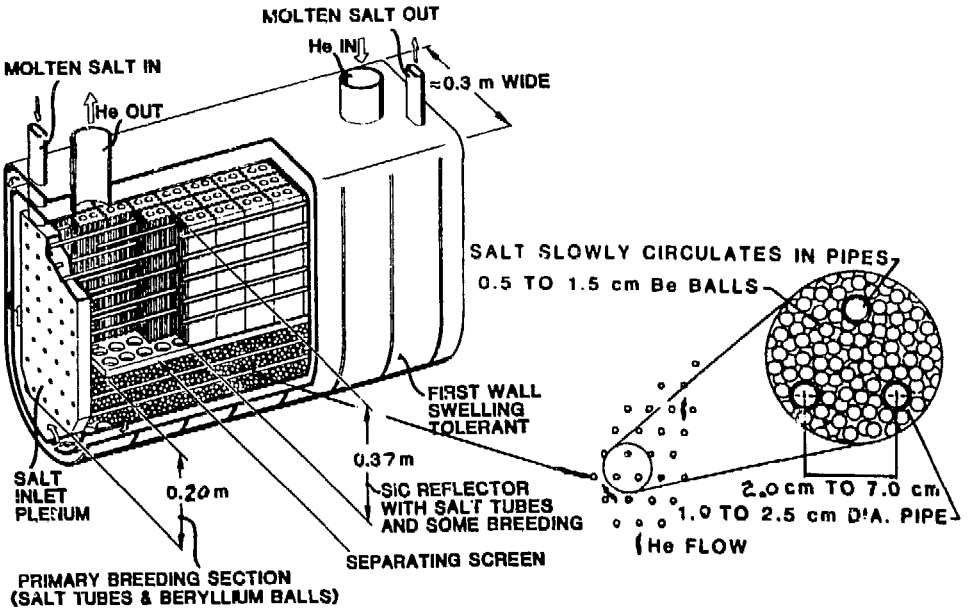

Figure 8.7-1

Helium cooled, flibe blanket configuration with beryllium as the neutron multiplier.

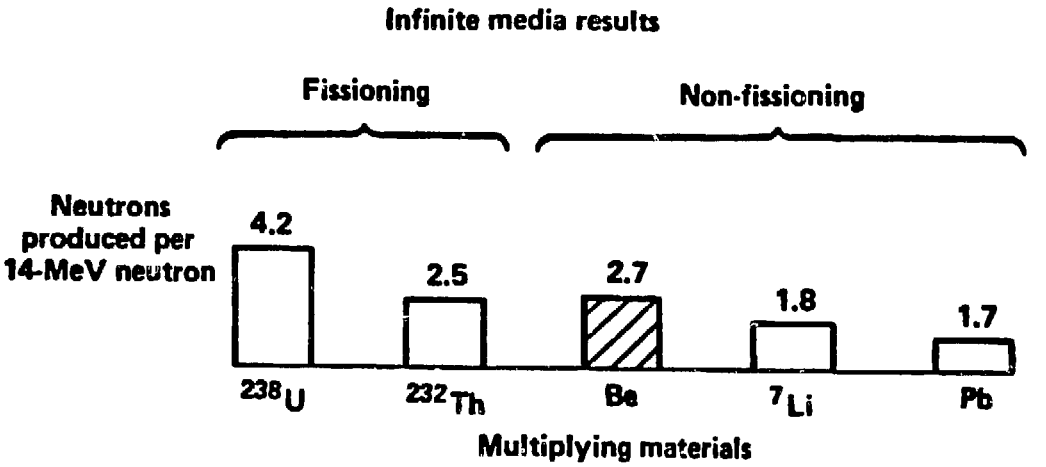

Figure 8.7-2

Neutron multiplication for various materials. We chose beryllium because its multiplication was the highest for nonfissioning materials.

not be inexhaustible. We find beryllium so advantageous that this question needs re-examining carefully. There is enough beryllium for many hundreds of plants and this would allow fusion to be deployed extensively enough for people to become familiar with the technology. After the first 50-70 years of introduction, the amount of beryllium employed in the blanket could be reduced by more neutronically efficient designs. Apparently, with careful design and full recycle of used beryllium, fusion power based on the use of beryllium can be considered semi-inexhaustible. Beryllium resources were discussed in last years report and elsewhere in this report.

We chose beryllium in the form of pebbles to facilitate recycle of irradiated beryllium. A bed of pebbles can potentially accommodate some swelling and relative thermal expansion, and can be loaded and unloaded by flowing. We envision blankets to be factory made, shipped to the plant and installed after testing and inspection. The recycled beryllium would have a contact dose rate that would not allow extensive personnel exposure. Therefore, the pebbles would be loaded into the blanket sometime after manufacturing, perhaps at the plant. If beryllium in a form not suitable for flowing were used, then the beryllium, or any other recycled material, would have to be loaded into the blanket during the manufacturing process and would require remote manufacturing of blankets. No one has shown how to fabricate something as complicated as a blanket by remote methods. Surely it can be done, but the cost may be prohibitive, not just double the usual manufacturing cost, for example.

Flibe was chosen as the tritium breeding material. It has been shown to have a very low corrosion rate with austenitic steel and is expected to be low with ferritic steel if the salt is kept in a reducing state (deficiency of flourine). Flibe is one of the few lithium bearing materials that will not react exothermically with air or water. Therefore, catastrophic accidents caused by such reactions are not possible.

The activation products for both flibe and Beryllium have a relatively short half-life so that they can be disposed of by shallow burial. After ten years, out-of-the-reactor worker protection is still needed; however, after 100 years flibe and beryllium can be handled without worker protection. Flibe has an extremely low tritium solubility which makes for very easy tritium removal but also leads to an increased tendency for tritium to permeate into the helium stream.

The blanket configuration shown in Fig. 8.7-1 was chosen for this study. This basic pod design for the helium pressure vessel forms the basis for most of the helium cooled designs and therefore, the first wall, manifolding, plena, and many other features are in common and do not come up as a unique issue when considering the flibe design.

We prefer to be able to gravity drain both the flibe and the beryllium pebbles. Both these objectives were achieved in the design developed for the tandem mirror. However, due to the non-commonality with the other helium cooled designs considered in the BCSS, we relegated this to a "backup" design. It is shown in Fig. 8.7-3. The end view is shown in Fig 8.7-4. An adaptation to the tokamak configuration has been worked out but is not shown.

8.7.2 Tokamak Blanket Configuration

The pod modules shown in Fig. 8.7-1 are arranged to fit the Tokamak configuration as shown in Fig. 8.3-1. The module ends, where one sector fits very close to the next sector, is not shown, but is discussed elsewhere in this report. Much more effort needs to be devoted to module end design as it has a major impact on blanket design and is not not just a perturbation to the design.

8.7.3 Tandem Mirror Blanket Configuration

The pod modules shown in Fig. 8.7-1 are arranged to fit the Tandem Mirror configuration as shown in Fig. 8.3-2. The dimensions are based on the MARS study (B.G. Logan et. al., "Mirror Advanced Reactor Study (MARS)", Lawrence Livermore National Laboratory Report UCRL-53563, (1984)). The first wall radius is 0.6 m and the center cell (blankets) is 130 m long. The vacuum magnetic field on axis is 4.7 T.

8.7.4 Design Summary and Issues

The key issue with the Flibe design is tritium control. The tungsten on the flibe tubes and the aluminum jacket including the oxide layer on the steam generator tubes must be shown to be workable and reliable as tritium barriers.

Another important issue is integrity of beryllium during its residence in the blanket. A limited amount of breakup could be tolerated to the point where flying particles would damage the helium circulator or plug the pebble bed. We speculate a two year residence time (8 MWy/m^2) might be economically

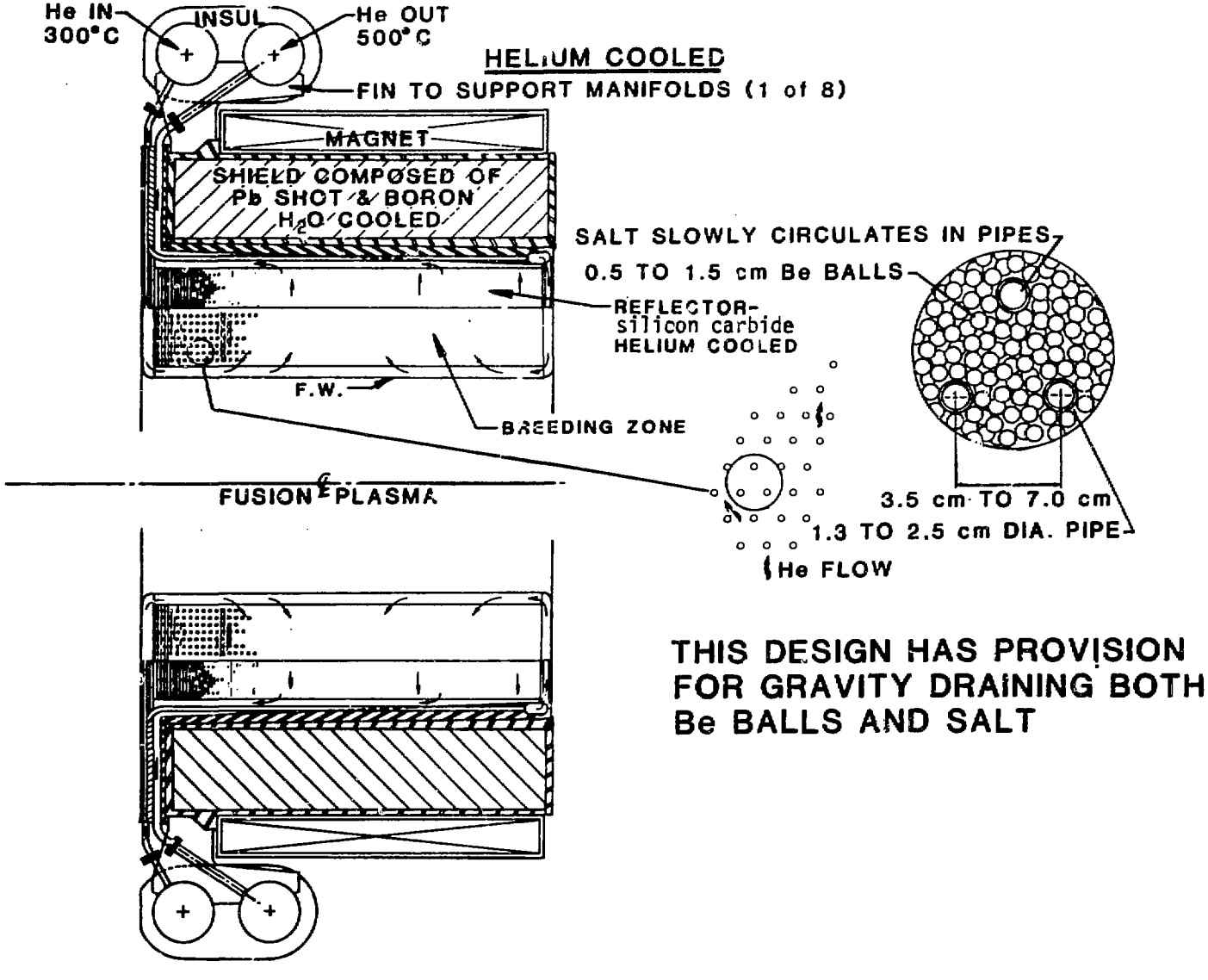

Figure 8.7-3

He/Flibe/Be--Tandem mirror backup design.

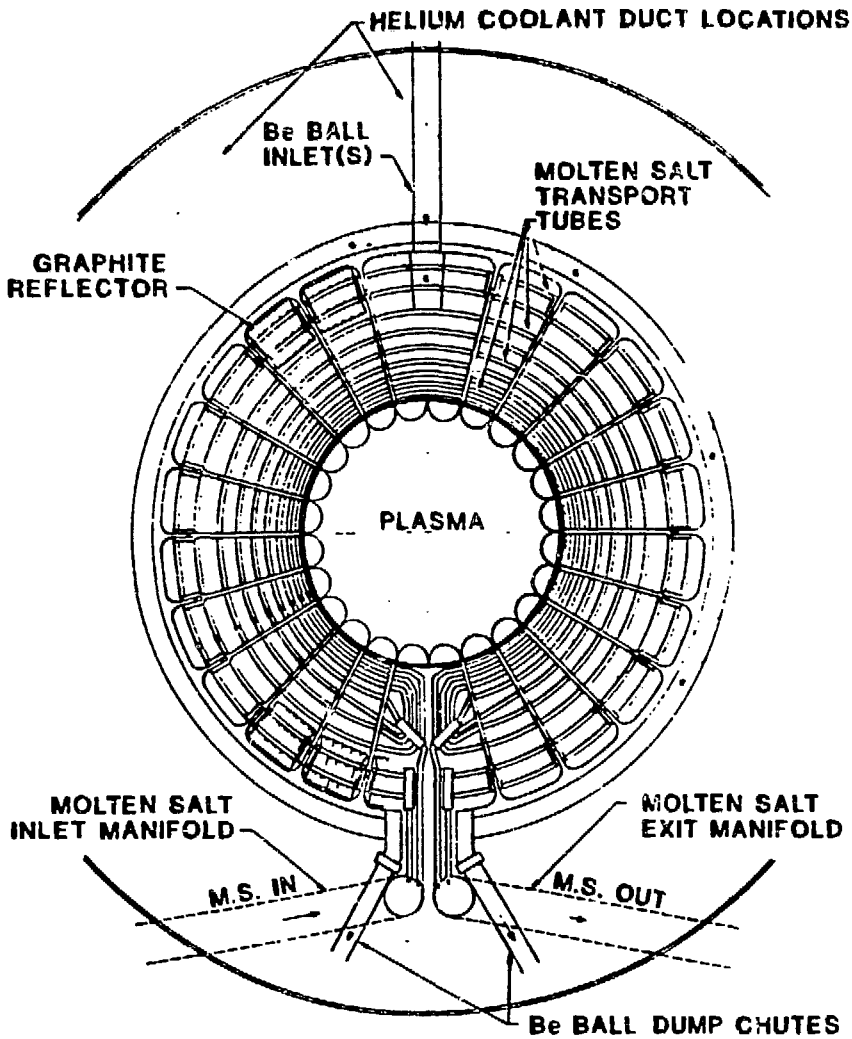

Figure 8.7-4

Molten salt blanket.

acceptable after which time the pebbles could be remanufactured especially with the back-up design in which the pebbles could be removed and replaced on a shorter time than the blanket changeout time.

The question of tritium which is generated in the beryllium being released into the helium was not addressed. Since only 1% of the tritium is produced in the beryllium, the problem was considered unimportant.

Some people believe the remanufacturing of beryllium pebbles will require a large development effort. We believe, however, that use of automated, free flowing powder techniques now being implemented in the beryllium industry will allow remanufacturing of these pebbles by straight forward but automated powder metallurgical techniques without a large developmental effort.

Hydrogen (tritium) embrittlement has been flagged as a special problem for the flibe design because the tritium concentration estimated for the HT-9 tubes is 1.5 wppm versus 0.3 to 0.6 wppm for the other designs not using flibe. This 1.5 wppm was appropriate for the tungsten layer on the outside of the tubes. With tungsten on the inside the tritium concentration should go down by a large factor. Experiments will be needed to determine under realistic operating conditions the actual tritium concentration and see if this is any problem whatsoever.

Corrosion of HT-9 tubes by flibe has been flagged as a significant problem for the flibe design by the BCSS. With austenitic steel the corrosion has been shown experimentally to be very small, and with ferritic steel we expect it to be very low. Pumped loop experiments will be needed to prove the corrosion rates are low, especially with realistic impurities. MHD and radiation effects are not predicted to be important.

8.8 Attractive Concepts, Ranked 1B and 2A

Seventeen of the 54 helium-cooled blanket concepts that were investigated as part of the BCSS were judged to be attractive concepts. Because of the limitations of time and effort available for the BCSS work, it was judged impractical to provide a full evaluation of all 17 of these attractive concepts. As a consequence, a further subdivision was made. The attractive concepts were divided into the R=1 category (full evaluation), the R=1B category (concepts judged to be equally attractive yet similar to the R=1 concepts and thus not evaluated at this time), and the R=2A category (concepts which were judged to be slightly less attractive than either the R=1 or R=1B concepts). Four of the helium-cooled blanket concepts were ranked as 1 and received full evaluation. These are described in detail in Sections 8.4 through 8.7 above. Five of the remaining concepts were judged to be R=1B and eight were judged to be R=2A. The 13 attractive concepts that could not be fully evaluated in the course of the BCSS are discussed briefly in the sections below.

Although these R=1B/2A concepts did not receive full evaluation, we believe them to be attractive. If any of the four R=1 concepts prove to have technical problems not shared by a similar R=1B/2A concept, a substitution could be made. If an R=1 concept proves to be particularly attractive, similar R=1B/2A concepts might also be elevated to R=1 status to receive full evaluation. Conversely, if an R=1 concept does not do well in the detailed evaluation, similar R=1B and/or 2A concepts may also not do well.

8.8.1 R=1B Concepts

Five of the 17 attractive helium-cooled blanket concepts were judged to be very similar to the four R=1 concepts, and thus, because of limitations of time and funding, it was decided that these five concepts would not receive full evaluation. It should be noted that these appear to be almost as attractive as the four R=1 concepts and should be given serious consideration in the future. These concepts are discussed briefly below.

8.8.1.1 Solid Breeders

$LiAlO_2$/PCA/Be. The ternary ceramic PCA/beryllium blanket is virtually identical to the ternary ceramic beryllium blanket using ferritic steel structure, the only difference being substitution of austenitic steel (PCA, prime candidate alloy) for the ferritic steel. All other characteristics would be identical. The principal difference between these blankets is the lower thermal conductivity of the PCA and its non-magnetic nature. For the tokamak reactor the low thermal conductivity of PCA results in higher thermal stresses at a given wall load, and this results in a limitation of approximately 0.6 MW/m^2 for the surface heat flux that the helium-cooled PCA first wall can tolerate. Although this design has not been fully optimized, it is clear that the use of ferritic steel significantly increases the first wall heat flux ability. On the other hand, the elimination of paramagnetic forces on the structural material with use of non-magnetic PCA results in a simpler design because, although the forces are quite modest, they must be accounted for in the design. These two effects tend to counterbalance one another; hence, it is felt that the ternary ceramic PCA/beryllium blanket is very similar in its overall desirability to the R=1 ranked ternary ceramic ferritic steel beryllium blanket. The radiation lifetime of both PCA and ferritic steel is subject to uncertainty. It is expected that both will be capable of total exposures in the range of 100-150 dpa, but this remains to be shown for both of these materials. If the PCA proves to have the sort of severe swelling problems that are found to be associated with 316-SS, it could result in a significantly shorter lifetime could result, causing this concept to be moved to a 2B category.

$LiAlO_2$/FS/Pb. This concept is very similar to the R=1 $LiAlO_2$/FS/Be blanket with the substitution of lead-filled tubes for the beryllium rods as the neutron multiplying material at the front of the blanket. The neutronic performance of this blanket would be very similar to that of the beryllium multiplier blanket, but would require a thicker lead zone than the roughly 10-cm-thick beryllium zone in the R=1 alternate. The use of lead, however, eliminates concern about beryllium resource limitations, although it would require a piping system to allow draining and filling of the lead to

prevent the stresses associated with thermal expansion from melting and freezing in the tubes. The piping system for the lead would be virtually identical to that used in the helium-cooled lithium blanket concepts.

8.8.1.2 Liquid Breeders

Li/FS/Pb. The use of a neutron multiplier with the helium-cooled lithium blanket is not required in order to achieve adequate tritium breeding. The use of the multiplier, however, would allow a thinner blanket to be achieved. The tritium breeding performance of the lithium blanket with a lead multiplier is very similar to the excellent performance achieved by the lithium lead blanket. Separation of the lithium and the lead into separate zones introduces additional complication in the blanket, and would require two separate piping systems, one for the lithium and the other for the lead. On the other hand, this separation would allow much better control of tritium than for the LiPb/FS concept (see below), in that the solubility of tritium in lithium is quite high, whereas the solubility in lithium lead is quite low. All told, it is expected that the additional complexity of this blanket would be well balanced by the potential for improved tritium control and improved tritium production.

Li/FS/Be. This concept adds beryllium multiplier to the front of the helium-cooled lithium/ferritic steel blanket. The addition of beryllium would significantly enhance the tritium production capability of the blanket and would allow use of a thinner blanket while still achieving adequate tritium production. A thinner blanket could achieve economic benefits relative to the lithium/ferritic steel blanket. The configuration of this blanket would be quite simple in that approximately 10 cm of the lithium-containing tubes at the front of the blanket would be replaced by beryllium rods virtually identical to those used in the lithium aluminate/ferritic steel/beryllium blanket that is rated as an R=1 concept. Because of the extreme importance placed upon tritium breeding ratio and tritium leakage in the engineering and safety evaluations, it is possible that the Li/FS/Be or Li/FS/Pb blankets

would rate even higher than the Li/FS blanket. These options should be explored further in the future.

LiPb/FS. This blanket is very similar to the R=1 lithium/ferritic steel blanket with the substitution of lithium lead for lithium. The use of lithium lead would allow better tritium production performance than is found in the lithium blanket case, thus allowing the use of a thinner blanket which could improve the overall economics. Use of the lithium lead will result in a higher leakage rate of tritium from the breeder into the helium coolant stream, but this should be manageable by use of a higher helium stream clean-up rate. The lithium lead does result in a lower materials compatibility temperature limit at the interface between the lithium lead and the ferritic steel than is found in the lithium/ferritic steel blanket. Because the lithium lead is circulating only very slowly in the helium-cooled concepts, the temperature restriction is not severe. The interface temperature limit is 475° C, which will allow reasonable helium outlet gas temperature and acceptable power conversion system efficiency. The reduction in efficiency is believed to be balanced by the economic benefits of a thinner blanket and higher tritium production rate.

8.8.2 R=2A Concepts

Eight of the 17 attractive helium-cooled concepts were judged to be less attractive than the 9 R=1 or 1B concepts that have been described in the sections above. Although less attractive, they are on an absolute scale still considered attractive blanket concepts. If information on the materials and technologies needed for these blankets that is developed during the development phases proves favorable, it is quite possible that some of these R=2A concepts could, in fact, be moved to R=1 status.

8.8.2.1 Solid Breeders

Li_2O/PCA. This blanket would be virtually identical to the R=1 Li_2O/FS blanket concept. For the tokamak reactor, the use of PCA instead of ferritic steel results in a lower allowed first wall heat flux load of approximately

0.6 MW/m^2, as compared with the capability of ferritic steel to exceed 1.0 MW/m^2. This difference is due to the lower thermal conductivity of PCA and the resulting higher thermal stresses. PCA has a lower total neutron fluence lifetime than ferritic steel, which is also a consideration in ranking this concept R=2A.

Li_2O/PCA and FS/Be. The use of beryllium as a multiplier with the lithium oxide breeding material appears to offer no advantages compared with the use of lithium aluminate ternary ceramic as the breeding material. If a beryllium neutron multiplier is added, ample tritium production can easily be achieved using lithium aluminate. The potential difficulties associated with use of the more chemically reactive lithium oxide as opposed to lithium aluminate thus appears to have little incentive. Thus, it appears that these concepts would be inferior to the lithium oxide blankets without a beryllium multiplier in terms of increased complexity and the beryllium resource concern, and would be slightly inferior to the lithium aluminate/beryllium concepts in terms of increased technical risk.

$LiAlO_2$/PCA/Pb. This concept is very similar to the R=1 $LiAlO_2$/FS/Be blanket and the R=1B $LiAlO_2$/FS/Pb blanket. In this case, however, the use of PCA is considered slightly inferior to use of ferritic steel, and the use of Pb as a neutron multiplier is considered slightly inferior for a solid breeder blanket to the use of solid beryllium. As a consequence, this concept is rated R=2A.

8.8.2.2 Liquid Breeders

Li/PCA. This concept is identical to the R=1 Li/FS blanket with the substitution of PCA for ferritic steel. In addition to the comments made above with regard to the relative desirability of PCA and ferritic steel for the first wall material, PCA also has a lower temperature limit than does ferritic steel for the interface between lithium and the structural material. The Li/PCA temperature limit is 495°C in slowly circulating lithium; that for Li/FS is 565°C. Although the 495°C temperature limit will allow acceptable power conversion system efficiency, it is clearly less desirable than the

temperatures which could be achieved with ferritic steel. Thus, due to the reduced potential for surface heat flux wall loading for the tokamak reactors and reduced outlet gas temperature, this concept is judged to be R=2A.

Li/PCA/Be or Pb. As was discussed in Section 8.8.1 above, the addition of a neutron multiplier to the helium-cooled lithium breeder blankets may result in very attractive blanket systems. This would apply for use of either beryllium or lead as the neutron multiplier. The limitations in terms of surface heat flux and outlet gas temperature discussed above for PCA in a lithium breeder blanket result in this concept being judged slightly inferior to the Li/FS/Be or Pb concepts. Thus, it is categorized as R=2A.

FLiBe/PCA/Be. This concept is very similar to the R=1 FLiBe/FS/Be blanket concept with the substitution of PCA for ferritic steel. As has been discussed above, PCA is considered somewhat inferior to ferritic steel due to its lower thermal conductivity that causes a lower surface heat flux limit and the concern about a lower radiation damage lifetime. Because of these considerations, this concept is rated R=2A, slightly inferior to the FLiBe/FS/Be concept.

8.8.2.3 Multiple Structural Materials

The helium-cooled blanket concepts appear to offer potential for advantageous use of multiple structural materials. A blanket concept could use one structural material for the first wall and a second structural material for the breeder containment material. This scheme could be particularly useful in the case of the liquid breeders where materials compatibility is the key consideration in breeder containment, whereas surface heat flux dictates the first wall structural material selection. A particularly attractive potential combination is the use of ferritic steel as the structural material and vanadium alloy as the breeder containment. Vanadium alloy offers a much higher compatability temperature limit (750°C) than either ferritic steel or PCA in contact with either Li or LiPb. Vanadium, on the other hand, is expensive and complex welding may be difficult to achieve. Use of simple tube geometry for the breeder containment could be easily achieved with the

vanadium alloy structural materials. The design could allow helium outlet gas temperatures approaching 700°C (similar to HTGR conditions), which, in turn, could result in higher efficiency and economic advantages. If ferritic steel were used for the first wall and balance of blanket structural material, the fabrication and cost concerns of vanadium could be avoided for the majority of the blanket structure. The concerns that are discussed in Section 8.9 below for use of vanadium alloys in a helium environment precluded this concept from being seriously pursued in the BCSS. We believe, however, that this concept of multiple structural materials (ferritic steel and vanadium alloy) in a helium-cooled blanket does warrant further investigation in the future. There appear to be no clear-cut advantages to using combinations of PCA and ferritic steel in a helium-cooled blanket. In all cases the ferritic steel appears to be superior to PCA for use as both the breeder containment material and the first wall material. As a consequence, the investigation of multiple structural materials was not carried out further and these concepts were rated as R=2A.

8.9 Concepts Ranked R=2B and R=3

Of the 54 helium-cooled blanket concepts that were investigated as part of the BCSS, 37 were judged to be either less attractive, R=2B, or infeasible, R=3. These concepts are discussed in this section and the reasons for the less favorable ranking are described. It is possible that, as further information is obtained on the materials and technologies needed for these blanket concepts the ranking could change upward. This is particularly the case in the R=2B concepts. Those concepts rated as infeasible, R=3 are highly unlikely to be moved into the more feasible category.

8.9.1 Less Attractive Concepts, Ranked R=2B

Twenty-three concepts were judged, for a variety of reasons, to be inferior to the R=1 and R=1B or 2A concepts. Although these were not rated as infeasible, they were considered very inferior to the more highly ranked concepts. They were ranked R=2B.

8.9.1.1 R=2B Solid Breeders

Li_2O/FS or PCA/Pb. The use of lead as a neutron multiplier with the lithium oxide blankets, using either ferritic steel or PCA structure, is clearly less desirable than either using the lithium oxide without a multiplier, using lithium oxide with a beryllium multiplier, or using lithium aluminate with a lead or beryllium multiplier. The use of a solid breeder with a liquid multiplier like lead requires the use of a double piping system: (1) for the purge flow into and out of the blanket; (2) for the lead-containing pipes. The piping system for the lead would be required to accommodate the expansion and contraction that will occur when the lead melts and freezes during start-up and shutdown. While these concepts are not infeasible from a technical point of view, they are clearly less desirable than the other alternatives. These two concepts appear to combine the worst features of both the solid breeder and liquid breeder concepts and to obviate several of the advantages of both.

Li_8ZrO_6 - All. Li_8ZrO_6 appeared to be an attractive potential solid breeder. It has a high lithium content and thus may not need a neutron multiplier, and it was hoped that it could be more chemically stable than lithium oxide. Investigations by the Solid Breeder Special Issues group during the BCSS, indicated that the chemical stability of Li_8ZrO_6 is not expected to be significantly better than lithium oxide. There appears to be a phase change at 660°C. Tritium breeding calculations as a result of the BCSS clearly indicated the desirability of higher tritium breeding ratios than Li_8ZrO_6 can provide. Thus, Li_8ZrO_6 appears to offer no advantages over lithium oxide, either with or without a neutron multiplier, and no advantages over lithium aluminate with a neutron multiplier. As a consequence, it was rated as clearly less desirable, and was not pursued further in the study.

8.9.1.2 R=2B Liquid Breeders

LiPb/PCA. The compatibility temperature limit for LiPb in contact with PCA, even with slowly flowing or static LiPb, is only 430°C. This low temperature limit imposes a severe restriction on the helium outlet temperature that can

be achieved, which, in turn, results in low power conversion sytem efficiency. As a result, this concept is clearly inferior to the LiPb/FS blanket concept, which is capable of temperatures up to 475°C. While not strictly infeasible, the low temperature allowed for this blanket means that it is not attractive for use with a helium-cooled power conversion system. This rank would be raised if high temperature limits are possible.

LiPb/FS or PCA/Be or Pb. Lithium lead contains the built-in neutron multiplier, lead, and is capable of achieving excellent tritium breeding performance. Thus, the use of beryllium or lead as an additional neutron multiplier, in conjunction with the LiPb breeding material, does not make any sense at all, and is rated as clearly less desirable than the use of lithium lead without a neutron multiplier.

FLiBe/PCA or FS/Pb. The use of a separate lead multiplier with a FLiBe breeding material blanket is clearly less desirable than the use of FLiBe with a beryllium multiplier. The lead would require a piping system separate from the FLiBe. Further, FLiBe requires buffering with excess beryllium to maintain tritium in the gaseous state and avoid production of tritium fluoride. Thus, the use of beryllium in direct contact with FLiBe is an attractive combination. Use of lead multiplier is clearly less desirable.

Liquid Breeder/V - All. The use of vanadium as a structural material in a helium-cooled liquid breeder blanket has a number of desirable characteristics. The high temperature capability of the vanadium, even in contact with liquid metals, can be fully utilized with the helium power conversion system to achieve higher efficiencies. Vanadium and vanadium alloys, however, are highly intolerant of an oxidizing environment at temperatures above ~250°-300°C. Although helium is completely chemically inert, and would not react with vanadium at any temperature, concern was raised that small levels of impurities in the helium stream would result in unacceptable oxidization of the vanadium structure. Work done during the first year of the BCSS (Ref. 8.9-1) shows that the partial pressure of oxygen or moisture in the coolant strem must be kept to very low levels, below 1 ppm. Oxidizing impurity levels in this range were routinely maintained during operation of the Peach

Bottom and Fort St. Vrain HTGRs, and very pure helium production on a laboratory scale basis is done routinely. Further, the techniques used in liquid metal coolant designs to prevent ingress of moisture or oxygen into the coolant stream could be used very easily with the helium-cooled vanadium structured design. These include use of a double-wall steam generator with a lower pressure in the space between the two walls than appear either in the helium or on the water side, and use of pumps and seals that do not contain water. Calculations were done which suggested that the moisture and oxygen that inevitably would get into the helium loop during shutdown for maintenance and repair could be readily accommodated within the oxygen content limits suggested by Gold and Bajaj (Ref. 7.9-2) without excessive oxidization or embrittlement of the vanadium structure. The BCSS Structural Materials group, however, ruled that use of vanadium in a helium-cooled blanket design had sufficient technical difficulties or uncertainties that it was ruled as less attractive than use of alternate structural materials. There are reasons to believe that, as further information on vanadium alloys and on helium power conversion systems is developed, it is quite possible the vanadium alloy-structured, helium-cooled blanket concepts will become very attractive contenders and can be moved to the R=1 or R=2A categories.

8.9.1.3 Different Inboard/Outboard Blanket

During the course of the BCSS investigations, it was suggested that use of different blanket concepts on the inboard and the outboard side of the tokamak reactor could offer some significant advantages. Use of a very thin blanket on the inboard side of the tokamak could allow a smaller major radius and economic savings. This could then be compensated for by use of a thicker blanket on the outboard side. It appears that the complications associated with using different helium-cooled blankets inboard and outboard do not give any significant advantages. It is possible that use of water-cooled blankets on the inboard or outboard side, and helium-cooled blankets on the other, would allow some very interesting coupling of power conversion systems with the net result of a very high efficiency. These sorts of investigations, however, are more closely related to overall reactor design than to blanket

concept investigation, and it was decided not to pursue the different inboard/outboard concepts any further during the BCSS.

8.9.2 Concepts Ranked 3, Infeasible

Fourteen of the helium-cooled blanket concepts were found to be technically infeasible for a variety of reasons. These concepts simply will not work with our present understanding of the technical limitations of the materials and technologies in the fusion reactor blanket environment. While it is possible that future developments in materials research or technology areas may improve the chances of these concepts, we believe it is highly unlikely they can be moved out of the R=3 category.

8.9.2.1 R=3 Solid Breeders

$LiAlO_2$/PCA or FS. The use of a ternary ceramic such as $LiAlO_2$ with any structural material requires the use of a neutron multiplier. Thus, blanket concepts using ternary ceramics without use of a separate neutron multiplier are clearly infeasible.

Solid Breeder/V - All. Tritium is released from solid breeders at least partially in the form of T_2O. Because of the vanadium oxidation concerns mentioned in Section 8.9.1.2 above, this raises a significant problem for use of vanadium structure. The helium-cooled designs will require breeding material temperatures in excess of 400°C. Use of the solid breeder releasing tritium in the form of T_2O in contact with the vanadium structure at these temperatures would surely result in excessive oxidization and embrittlement of the vanadium material. The nine concepts that combine solid breeders and multipliers with vanadium are thus ruled infeasible.

8.9.2.2 R=3 Liquid Breeders

FLiBe/PCA or FS or Vanadium. The use of FLiBe alone without an additional neutron multiplier results in tritium breeding ratios less than unity for any

credible reactor blanket design. As a consequence, these concepts are ruled R=3.

References

8.9-1. "Blanket Comparison and Selection Study," ANL/FPP-83-1, October, 1983.
8.9-2. R.E. Gold and R. Bajaj, "Mechanical Properties of Candidate Vanadium Alloys for Fusion Applications," Proceedings of the Third Topical Meeting on Fusion Reactor Materials, Albuquerque, NM, September, 1983.

8.10. Analysis of Special Issues

8.10.1 Mechanical Design

During the first year of the BCSS, the pressurized lobe design was identified as the most suitable structure for the helium-cooled designs.(8.10-1) Since then the strongback and plenum designs for the blanket module were analyzed. Radiation-induced swelling of Li_2O was identified to be a potential critical problem for the Li_2O designs. To accommodate a volumetric swelling up to 10%, a swelling-tolerant Li_2O-plate design was introduced. The first wall/module structural design was analyzed by considering loads from coolant pressure, thermal effects, and disruption. Bare beryllium rods were used for the $LiAlO_2$/Be design. The structural behavior of these rods under thermal and irradiation-induced swelling behavior was investigated. These design issues were studied in the second year of the BCSS and the results are presented in this section.

8.10.1.1 Solid and Lithium Breeder Designs

Furtner development of the strongback structural concept has been carried out and integrated into the configuration, which is little changed from that in Fig. IX.4-6 of Ref. 8.10-1. The blanket consists of lobed units with the first wall tied to a back structure which contains the gas coolant

distribution system. The front space in the lobe contains the breeding material in the form of plates between which coolant is circulated from front to rear.

Further development of the Li_2O breeder plates has also been carried out to ensure that the plate installation is swelling tolerant. Figure IX.4-6 in Ref. 8.10-1 shows the structural design as it existed at the beginning of FY-84 effort and Fig. IX.4-15 shows the breeder plates.

Figure 8.4-1 shows the presently-developed version of this design in its tokamak form. A version appropriate to the mirror configuration is shown in Fig. 8.4-2.

The mechanical design of the module with its gas distribution system tends to be independent of the breeder contents. Two other breeder types, one with lithium aluminate plates and beryllium rods, and the other with liquid lithium contained in tubes and stainless steel reflective plates, are described below.

The gas supply system shown in Fig. 8.4-1 is for the tokamak, with the gas entering and leaving the module through the rear region of the planes of the tieback walls. The tieback function is completed by the individual streamlined attachment points, as illustrated in Fig. 8.4-1. The hot and cold gas streams crossing through the module are divided by thermally insulated walls of ~05. cm thick. The thermal insulation is accomplished by simply providing 0.5 cm of stagnant helium (k_{th}=0.3 W/m-K at 500°C) between the hot and cold duct walls. If the detailed design shows natural convection within the stagnant helium to be a concern, the 0.5 cm gap may be filled with commercially available ceramic fiber insulation (Al_2O_3/SiO_2, service to 1260°C), virtually identical to the thermal barrier used on the HTGR.

Considering again Fig. 8.4-1, a major structural plate separates the crossflow streams from the breeder material, but penetrations are made in this plate to allow the coolant to circulate and a gas distribution plenum exists between the plate and the breeder material.

Figure 8.3-2 shows the simpler gas system associated with the mirror machines where the major gas flows are not required to penetrate the tieback planes. As is usual in these configurations, gas flow is down the tieback planes into the front region, cooling the first wall, thence diffusing back through the blanket to the outlet.

The blanket and first wall structural functions are to carry the weight of the blanket contents and to serve as the pressure containment in a fusion reactor environment. The back of the lobe consists of a structural frame, with gas passages and lobe ends which cantilever from the back to carry the end pressures, and can relieve the first wall of end load constraints due either to pressure, swelling, or thermal effects.

This strongback design concept places the structural functions of the blanket at the rear of the module. The pressure lobes, end walls, and blanket internal supports are then hung from the strongback structure. The advantages of this design are: (1) relief of the first wall from all structural requirements except containment of the coolant pressure; (2) protection of the structure located at the rear from the intense radiation; (3) absence of structure in front of the blanket to avoid attenuation of the neutron flux, which would reduce tritium breeding.

Figure 8.10-1 shows the simplest strong-back structure where the end forces are carried entirely in bending across the back. This type of structure is most suitable for the mirror machines where the gas does not flow through the tieback plates. In the tokamak design, the bending from the end forces is carried by the back plate and a plate between the manifold zone and the collection channel zone, as shown in Fig. 8.4-1. The breeder fuel elements ends (plates, tubes and rods) will have to be designed to fit the geometry indicated by the reinforcing plates.

The first wall is described in the BCSS interim report.(8.10-1) For both mirror and tokamak machines, the wall does not structurally interact with the end plates, being merely restrained at the tieback points. The

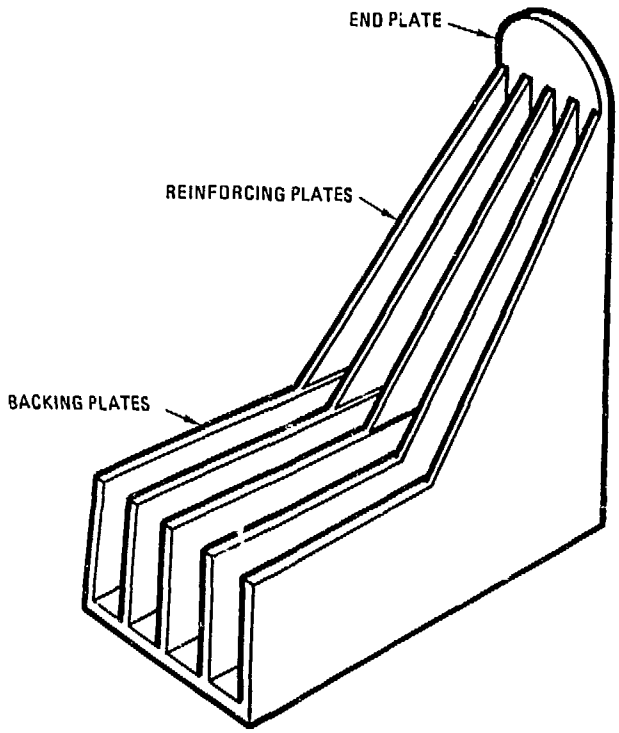

Figure 8.10-1. Blanket module structure.

tokamak first wall is essentially a two-dimensional grooved design on the outside to deal with erosion and is finned at the coolant side to accommodate surface load effects. The mirror wall is flat on the plasma side, with a simple channel for cooling inside.

Figures 8.10-2 and 8.10-3 show details of Li_2O breeder plates and their installation and represent development work on concepts shown in Ref. 8.10-1, Fig. IX.4-15. Metal honeycomb foil is crushed to accommodate swelling at the rear of a plate, as shown in Fig. 8.10-2 and the plate front is designed to be sufficiently convoluted to allow it to stretch a few percent without rupture. This design feature creates crushable zones which are part of the side insulation to allow plate front edge swelling, as shown in Fig. 8.10-3. As indicated, at the front end of the plates facing the plasma, maximum allowance in the crushing dimension change is expected, yet it couples well with the minimum requirement of the thermal insulation. On the other hand, at the back of the plates, where thermal insulation is needed to separate the inlet-outlet coolant, the swelling tolerant requirement is at a minimum. It was estimated that this swelling tolerant design can withstand volume swelling of up to 10%. The necessity for this crushable design will be clarified when more experimental information is available on the swelling and creep behavior of Li_2O under high fluence. Recent unpublished results from the FUBR experiments appear to indicate that Li_2O will creep readily under irradiation, thus relieving swelling.

Lithium-Helium Designs

The liquid-lithium helium designs differ from the solid breeder only in the blanket contents. Figure 8.5-1 shows the arrangement, simple stainless plates at the rear acting as a reflector with the front occupied by a tubular array filled with semi-stagnant lithium. The tubes will tend to curve and lengthen under irradiation, but the stresses induced by the restraint system to hold the geometry are small, since the side plena are not rigidly fixed and the tubes can grow in length with relatively little constraint and are only held against bending.

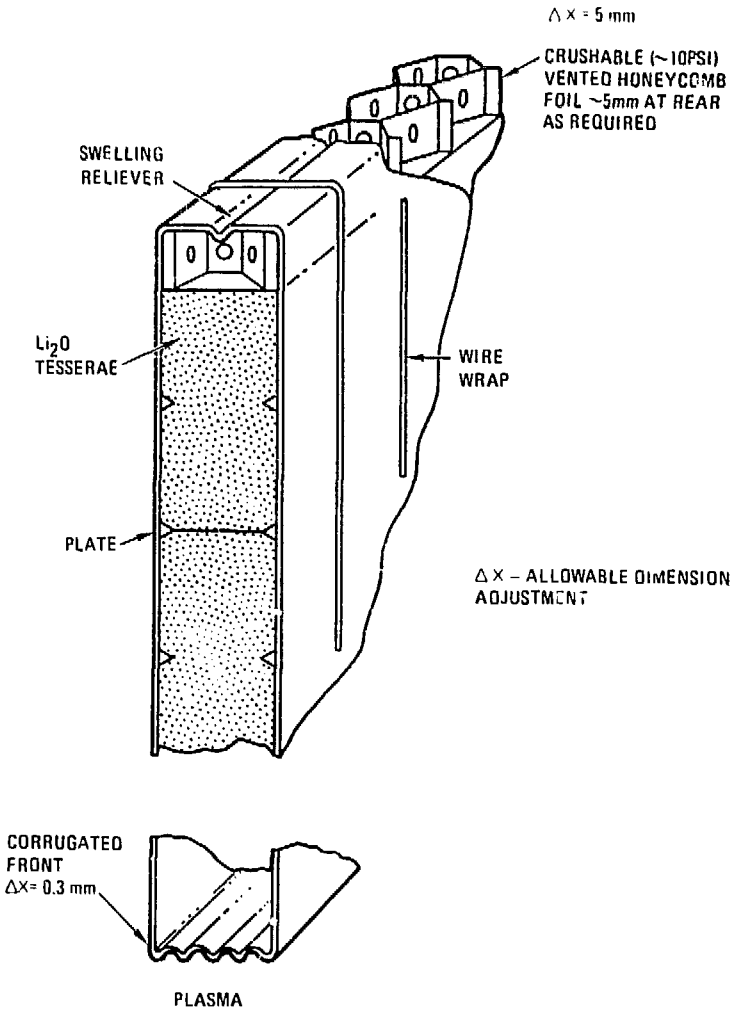

Figure 8.10-2. Li_2O swelling accommodation - Design I.

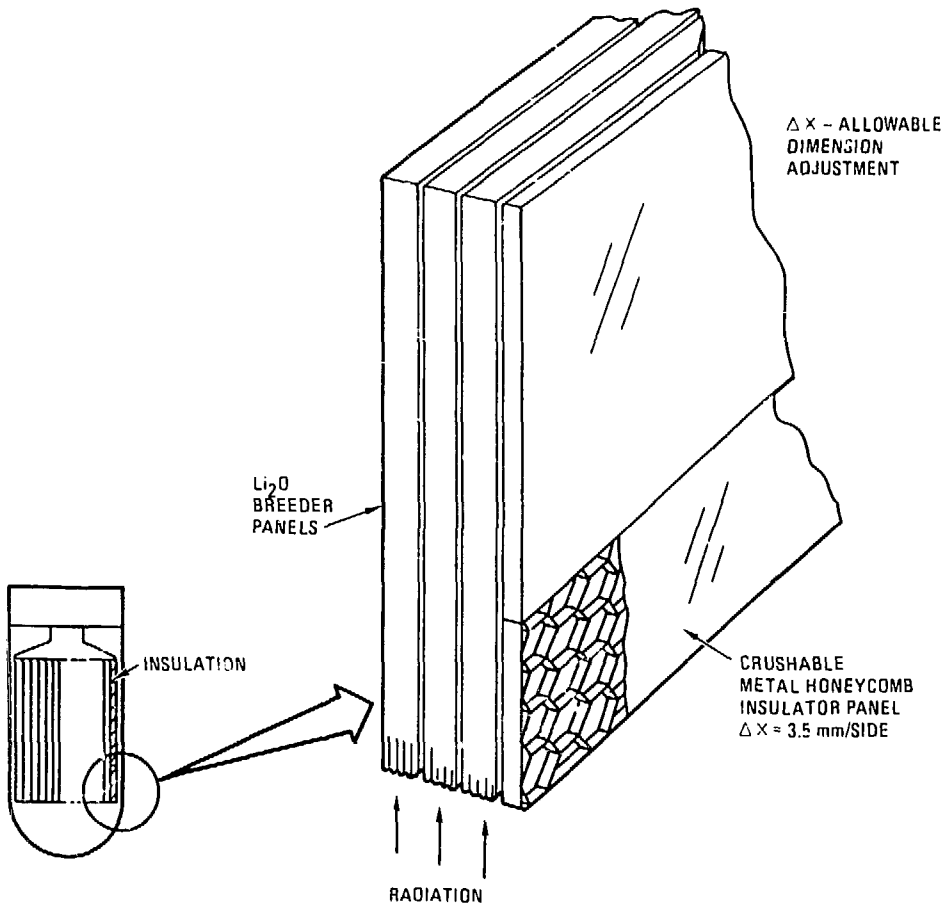

Figure 8.10-3. Li_2O swelling accommodation - Design II.

Coolant flow and structural aspects are similar to the solid Li_2O design above. An investigation was made into the stability of the lithium tubes under different depressurization conditions. When the module depressurizes, the tensile stress on the Li-tube is ~0.8 primary stress limit (Sm). When the lithium depressurizes, the loading to buckle the tube was calculated to be ~6.5 MPa, which is higher than the 5.0 MPa exerted by the coolant helium. Therefore, from the above observations, the lithium tubes for the Li-He/FS design should be stable under both module or lithium depressurization conditions.

First Wall/Module Structural Analysis

A parametric evaluation of the helium-cooled first wall design for the tokamak was carried out to determine the effects of primary loads, thermal constraints, and plasma disruptions. The structural criteria specified in the BCSS guidelines were used to assess the integrity of the first wall.

Stresses were calculated at the most critical point in the wall at the apex of the lobe nearest the plasma and at the base of the lobe, as illustrated in Fig. 8.10-4. An equivalent axisymmetric finite element model (referred to as "local analysis") was used after the conservatism of such an approach was verified by studying the overall thermal displacements of the structure in the poloidal direction (referred to as "lobe analysis").

Lobe Analysis

This analysis was done using the computer code MODSAP.(8.10-2) The model, shown in Fig. 8.10-4, consists of a cross-section of the structural part of the lobe module. Thermal loadings applied were wall temperature distribution (including strongback temperature and detailed distributions through the wall) and internal pressure. It was assumed that no constraint was imposed in the longitudinal (toroidal) direction by the strongback end plates. The stresses induced at the most critical location were compared with those obtained from an analysis assuming a fully axisymmetric structure (Fig. 8.10-5) having the same temperature distribution as at the critical

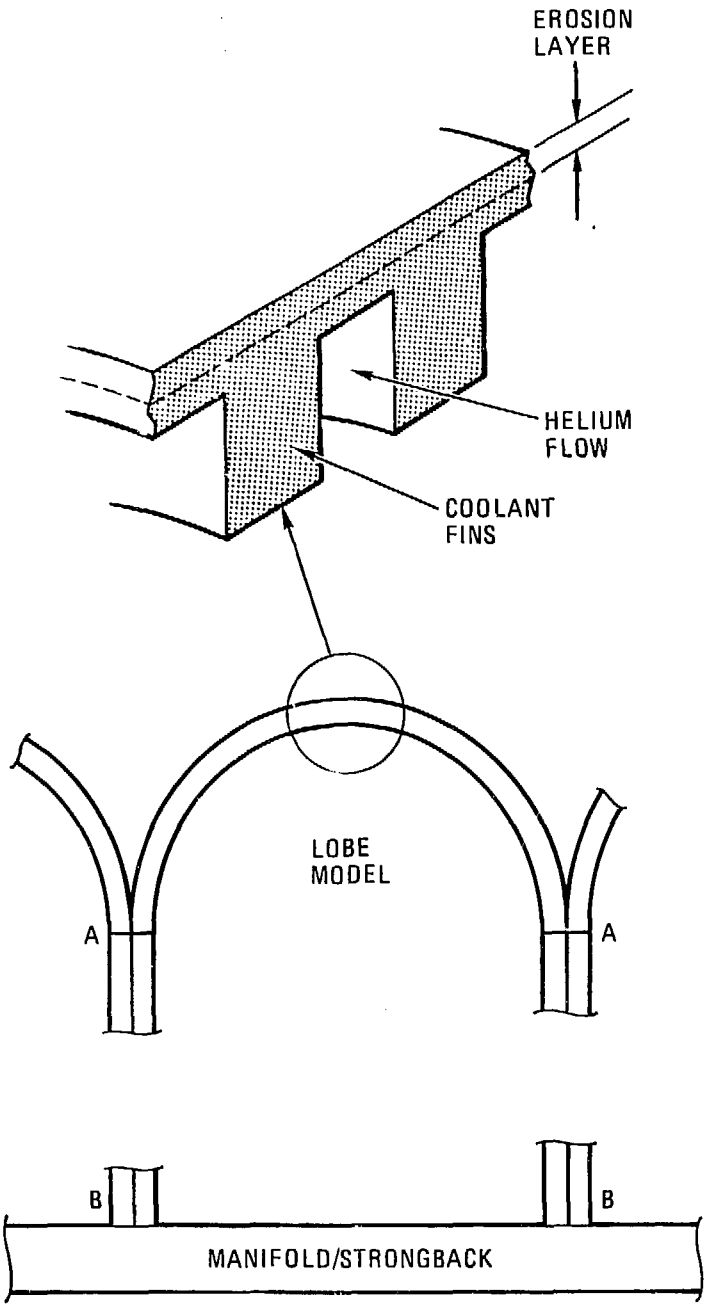

Figure 8.10-4. Lobe model and two-dimensional axisymmetric model for detailed analysis.

location. The stresses in the lobe model were found to be lower. All further stress analysis was, therefore, done with the axisymmetric model below.

Local Analysis (Axisymmetric Model)

Figure 8.10-5 shows the extent of finite element model used for the analysis. The computer code TEPC[8.10-3] (an in-house GA Technologies code) was used in this case.

A smooth surface was assumed for the plasma side incorporating an erodable layer which was consumed at the rate of 1 mm per year of operation. Stresses were calculated at both the beginning of life and at the end of two calender years of service.

Table 8.10-1 gives a summary of the stresses calculated for HT-9 and shows a comparison with the allowables from the design guidelines. Values are given for the top of the lobe nearest the plasma and for the base location where adjacent lobes meet. The wall was designed to a primary stress allowable (S_{mt}) of 163 MPa. This corresponds to a creep lifetime of 2 years (100 dpa). This is not an inherent limit, however, but rather a design choice made much earlier when an upper temperature limit of 700°C was applied to the first wall erodable layer. With this limit, the maximum erodable layer thickness is about 2 mm, corresponding to a lifetime of two years at 1 mm per year. With the lifetime thus specified, the structural design of the first wall was performed using two-year creep stress design limits. When the 700°C limit was relaxed late in the study, it appears that a 4 mm erodable layer could be used. If the additional 2 mm of material were included in the stress analysis, the resulting creep in two years will be less than the 5% allowable, but it would probably not last a full four years. This would result in a thicker non-erodable first wall and slightly reduced tritium breeding ratio.

TABLE 8.10-1
STRESS ANALYSIS RESULTS FROM THE HELIUM-COOLED LOBE MODULE CONSIDERING PRIMARY, THERMAL, AND DISRUPTION LOADINGS

Location		Time (yr)	Temperature °C	Pressure (MPa)		Pressure + Disruption (MPa)		Pressure + Disruption + Thermal (MPa)	
				P_L	1.0 S_{mt}	P_L+P_B	1.5 S_m	P_L+P_B+D[a]	3 S_m
Top of Lobe	Outside	0	649	112	155	175	263	176	330
	Midwall		497						
	Inside		344					353	615
Top of Lobe	Outside	2	549	157	163	244	284	87	480
	Midwall		444						
	Inside		340					312	615
Base of Lobe		0	344	109	163	230	308		
Base of Lobe		2	340	154	163	306	309		

[a] P_L - primary stress, P_B - thermal stress, D - disruption stress.

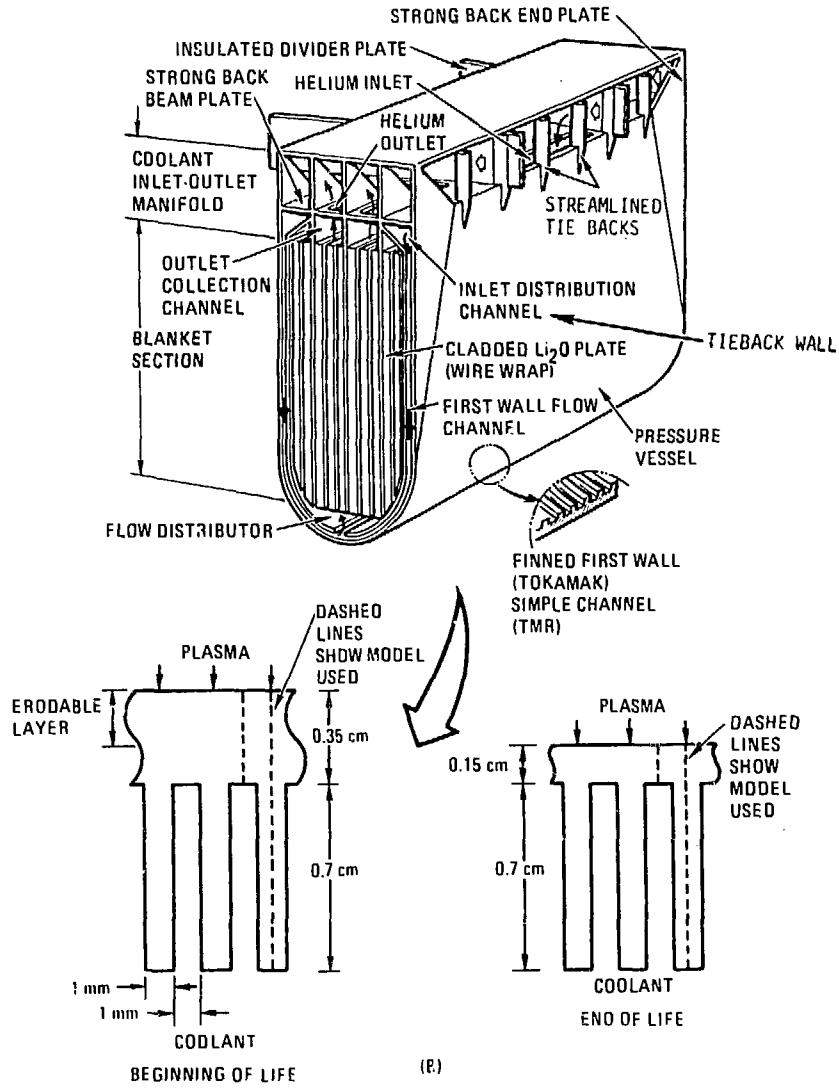

Figure 8.10-5. Helium-cooled blanket module with details

Conclusions

PCA was found to be unsatisfactory in this application because of the high thermal stresses induced with a 1 MW/m^2 surface heat flux. Lower heat fluxes ($\lesssim$0.6 $MW.m^2$) could be tolerated.

The stresses in the HT-9 material were below the allowables in the guidelines, but the metal temperature exceeded the allowable value at the beginning of life. This excessive temperature can be alleviated by using a grooved surface on the plasma side.

Further analysis is required to perform fatigue and crack propagation analyses for the grooved wall configuration.

Response to External Loadings

Zeroth-order analyses were performed for seismic loads and ferromagnetic forces for the helium-cooled pressurized module designs.

An individual 30-cm-wide module has to withstand an internal helium pressure of 5 MPa (730 psi). Calculating the section density of the module, it would have a loading of <70 KPa (10 psi) due to gravity. Even under an acceleration of 4.4 g, the maximum loading will be <303 KPa (44 psi), which is much less than the module design internal loading.

Considering the overall lobe assembly for the tokamak, which has to be constrained to a D-shape configuration, the moment generated by the pressurized modules on the D-ring would be about an order of magnitude higher than the moment generated by the seismic loadings. This indicates that, with proper support, the module structure can withstand the seismic loads. Correspondingly, no problem is expected for the TMR.

The ferromagnetic loadings for an HT-9 blanket structure in a STARFIRE-type tokamak magnetic field were calculated.(8.10-4) With the assumption

that all of the blanket internals are supported from the strongback structure, the overall load equivalent from ferromagnetic effects is approximately twice the weight of the module. Thus the ferromagnetic effects are of sufficient magnitude that they must be included in the design calculations, but do not appear to be of concern as a critical issue or problem for the design.

8.10.1.2 Flibe/He/FS/Be Concept

The following section discusses a number of special issues for the Flibe design. The salt tubes immersed in the bed of beryllium balls must be spaced so the balls can flow into or out of the tube region with no bridging resulting in flow stoppage. We have conducted flow tests which show that if the balls are no larger in diameter than one-half of the free space between tube walls, free flow will occur. Since some balls may crack or swell and develop imperfections of shape, we prefer that the ball diameter not exceed one-third of that free space. The pebble size is picked to be large enough to avoid excessive pumping power but small enough to freely flow between the tubes during pebble changeout and during periodic pebbles movement to allow for pebble swelling. The nominal values we have chosen are given in Table 8.10-2.

Table 8.10-2

NOMINAL PEBBLE/PIPE PARAMETERS

Pipe outside diameter	1.7 cm
Pipe spacing	4.7 cm
Pipe wall thickness	0.5 mm
Pebble diameter	1.0 cm

The tubes are held in place by clips attaching them to perforated grid spacers not shown in the figure.

The tube diameter is large enough so that freeze-up will not occur and small enough so that the centerline temperature will stay well below the boiling point (1300°C at one atmosphere). These limits are discussed in the thermal hydraulic section. The tube spacing is selected based on nucleonics. Too large a spacing will give parasitic loss of neutrons in the beryllium and too small a spacing will displace beryllium and reduce fast neutron multiplication. The tube wall thickness is selected to reduce parasitic absorption in the steel and yet be thick enough to avoid buckling caused by the helium pressure being higher than the salt pressure. Normally, the salt pressure is one atmosphere below the helium pressure, but abnormally the salt may be depressurized to one atmosphere in which case the tubes will not buckle.

Beryllium and Flibe Requirements

The salt volume is 9% of the blanket. The steel tube walls are 1% by volume and the structural fraction is 5% steel in the beryllium zone. The beryllium pebbles take up 53% and the Helium occupies 32%. In the reflector zone, the beryllium is replaced by SiC which occupies 75% of the volume. The beryllium zone is 20 cm thick and the SiC zone is 37 cm thick, except on the inside of the Tokamak where it is only 4 cm thick.

The beryllium zone volume is 0.2 m^3 per m^2 of first wall area in a Tokamak and 0.23 m^3 for the tandem mirror (larger due to the small first wall radius). The volume of the 37 cm thick SiC region is 0.59 m^3 in the mirror and 0.37 m^3 (assuming the same coverage on the inside as the outside) in the Tokamak. Taking 53% of the volume being beryllium and a full theoretical density of 1.84 g/cm^3 we get 0.20 tonnes/m^2 for a Tokamak and 0.22 tonnes/m^2 for a mirror. The salt volume is 0.033 m^3 per m^2 in a Tokamak and 0.053 m^3 in a mirror. For 3000 MW fusion and 5 MW/m^2 neutron, there are 480 m^2 of wall area. The salt volume in the blanket for a Tokamak is 16 m^3 and in a mirror is 25 m^3. The mass of beryllium is 96 tonnes in a Tokamak and 110 tonnes in a mirror. There are approximately 100 million pebbles of 1 cm diameter.

Tube Failure Rate

Breeder tube failure rate is a concern for this concept. With so many tubes, the question comes up of the failure rate. For the case of a tube nominal spacing of 4.7 cm on a triangular array, there would be 80,000 tubes in the blanket each having an average length of 11 m. If we can tolerate one failure per five years, then the failure rate per tube per hour of operation must be less than 4×10^{-10}. The helium pressure outside the tube is about 1 atmosphere higher than the pressure of the molten salt in the tube. Small cracks, at welds, for example, would result in leakage of helium into the salt and does not constitute a failure. Too large a crack would result in too large a helium leak rate and force a shut down and module change but have little overall consequence. An offset tube break could lead to molten salt contamination of the helium coolant loop. This would require shut down and a clean up procedure to follow. Analysis should be carried out to determine what size of crack is tolerable and then if an acceptable failure rate ($< 4 \times 10^{-10}$ per tube per hr) can be achieved.

Alternate Module End Design

An alternative module end design to that shown in Fig. 8.10-1 is presented here. The idea is to allow the end modules of one sector to support the end modules of the adjacent sector as shown in Fig. 8.10-6. The viewer is looking in the poloidal direction in a tokamak or the azimuthal direction in a tandem mirror. The direction of the lobes is shown here to be poloidal (azimuthal) but could be oriented toroidally (axially) and the idea is equally applicable. Consideration must be given to tolerance accumulation which can cause overstress of module sidewalls. Also, unintentional "cold welding" of walls in contact could occur. This would prevent disassembly without damaging the module end-wall in contact with a neighboring sector. Both of these unpleasant effects can be overcome by a simple expedient. An aluminum oxide plate (or several smaller pads) can be mounted on the end walls of modules in adjacent sectors. The aluminum oxide pad thickness can be selected just before final assembly to compensate for tolerance build-up in the manufactured condition. Alternatively, a pressurized cushion could be used in conjunction with the aluminum oxide plate to take up the tolerance. The ceramic pads will not weld inside the vacuum. Pad spacing and area must be controlled to minimize any local wall bending stresses in an unsupported area. The space occupied by these thin ceramic pads can be small so that valuable breeding volume is conserved and parasitic neutron capture minimized. Clearly, further work is needed on design of the module end support.

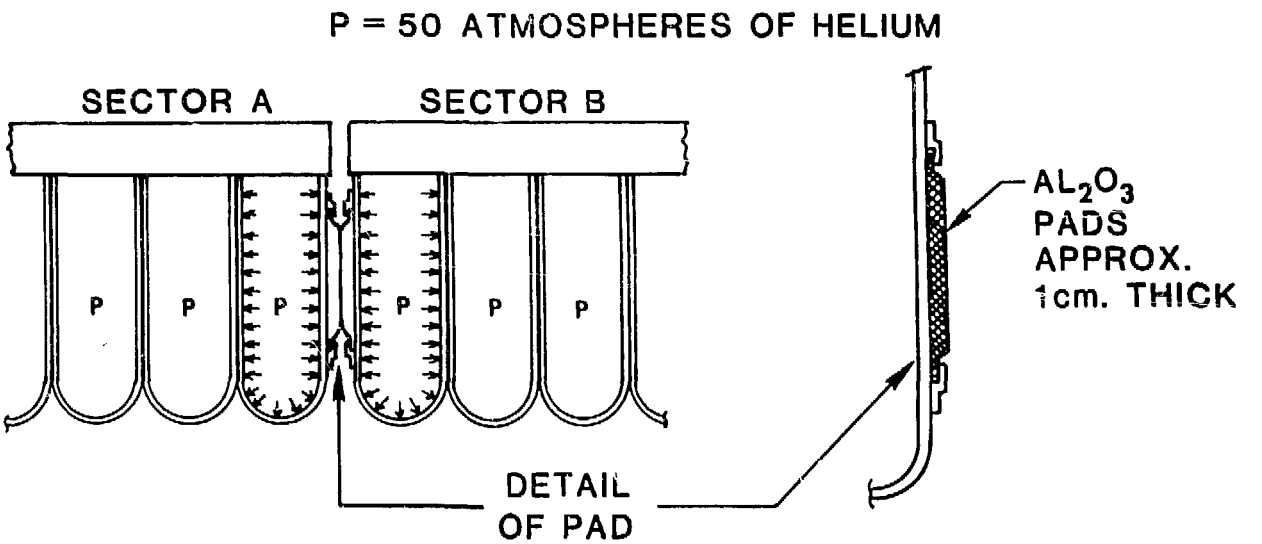

Figure 8.10-6

Alternate module end design.

$LiAlO_2$/Beryllium Rod Design

This design has gas-flow characteristics similar to the lithium oxide and liquid lithium designs. The plate design for lithium aluminate has not been extensively examined, since it was felt that the lithium oxide plate is a more difficult task and will encompass the aluminate design.

Figure 8.6-1 shows the beryllium rod configuration. Its design and support have been examined fairly closely in view of the poor swelling behavior of beryllium under neutron irradiation. Further, the swelling behavior is strongly temperature-dependent. If significant temperature gradients exist, the large differential swelling can result in the build-up of stresses.

Figure 8.10-7 shows a summary of this work. The lower view shows a plot of the temperature gradient, which is fairly small, across a 2-cm diameter beryllium rod having a maximum of 10°C from center to rear of rod. This and the flux difference gives rise to a swelling which is plotted on the same view. The rods are held as shown in the upper view, and gross swelling is allowed to slide out. The support points are arranged such that the differential swelling, which produces a circular curve in the unrestrained bar, gives an equal deflection of the bar toward and away from the plasma. The exponential swelling component, which is seen as the curvature in the swelling plot, is averaged by the curvature and a residuum of 0.03% trapped strain is left. Thus, assuming no creep, a stress of 82.7 MPa (12,000 psi) is trapped, versus a yield of 207 MPa (30,000 psi). Rods further from the plasma see progressively less movement as shown in the center view. It is concluded that this bare beryllium rod assembly is acceptable based on the beryllium-swelling data that are available.

8.10.2 Neutronics Designs

8.10.2.1 Solid Breeder Designs

In this section the neutronics designs are presented for the solid breeder blankets, namely, Li_2O/He and $LiAlO_2$/Be/He designs for both tokamak

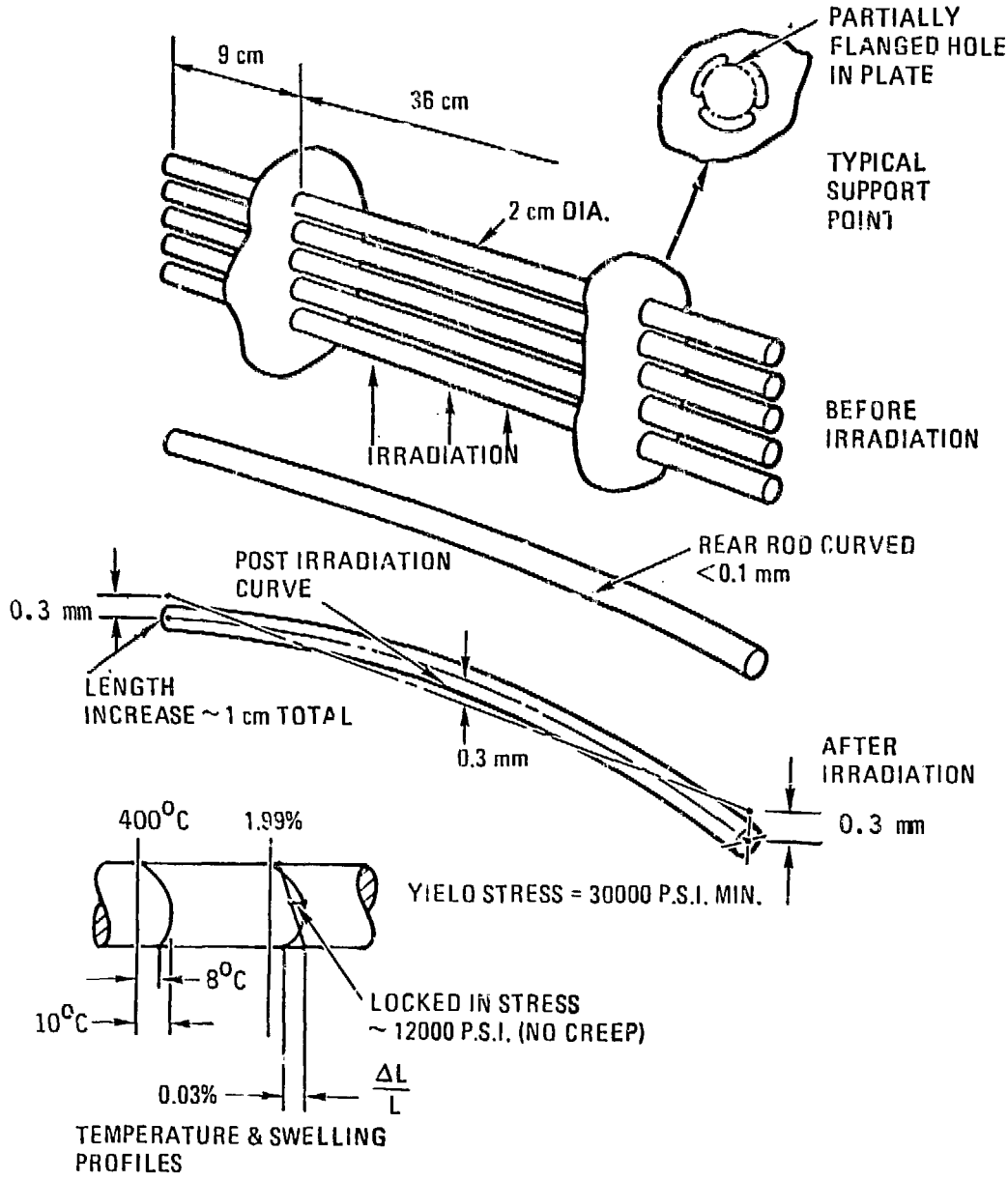

Figure 6.10-7. Beryllium rod and swelling effects.

and tandem mirror reactors (TMR). Only one-dimensional blanket models and neutronic results are discussed here, since they were provided as preliminary input to the overall blanket design evaluations. Subsequent three-dimensional neutronic results are discussed in Section 6.10. All neutronics calculations in this and the following section (Li/He designs) were performed using the one-dimensional transport code ANISN[8.10-5] with P_3S_8 approximation in cylindrical geometry. The nuclear data libraries used are the ENDF/B-IV-based VITAMIN-C[8.10-6] and MACKLIB-IV,[8.10-7], and the ENDF/B-V based, MATXS library[8.10-8]. The VITAMIN-C library was collapsed by ANL into 46 neutron group and 21 gamma-ray group structures. The LANL MATXS library was used only for tritium breeding calculations because of its capability of producing more accurate $^7Li(n,n'\alpha)$ reaction rates.

Li_2O/He Design -- Tokamak

Table 8.10-3 shows the zone thicknesses and compositions of the reference helium-cooled Li_2O blanket for a tokamak reactor system. As shown in this table, the inboard blanket consists of a 6 cm first wall zone, a 24-cm blanket zone, and an 11-cm plenum. The first wall is composed of only 11.7 vol. % ferritic steel, structure and the balance of helium, resulting in a net metal thickness of about 7 mm at the beginning of life (BOL) before any erosion occurs. The blanket is divided into two regions to include the effect of more supporting structure in the back region of the blanket. Blanket region-1, which is 12 cm thick in this design, consists of 7.9% HT-9, 50.6% Li_2O, and the balance of helium, all by volume. Blanket region-2, which is also 12 cm thick, consists of more structure (28.6%), less Li_2O (62.5%), and the balance of helium. The plenum zone is composed of 20% structural HT-9 alloy and the balance of helium. The zone thicknesses and compositions of the outboard blanket are essentially identical as those in the inboard blanket, except that in the outboard blanket, the blanket region-1 zone is 45 cm thick and the plenum is 22 cm thick. The total blanket thicknesses for the inboard and outboard blanket are 41 and 85 cm, respectively.

TABLE 8.10-3
ONE-DIMENSIONAL BLANKET ZONES AND MATERIAL COMPOSITIONS
FOR THE REFERENCE HELIUM-COOLED Li_2O BLANKET FOR TOKAMAK REACTOR

Zone	Component	Inboard (Thickness)	Outboard (Thickness)
1	First Wall	11.7% HT-9 + 88.3% Helium (6 cm)	11.7% HT-9 + 88.3% Helium (6 cm)
2	Blanket Region 1	7.9% HT-9 + 80.6% Li_2O[a] + 11.5% Helium (12 cm)	7.9% HT-9 + 80.6% Li_2O[a] + 11.5% Helium (45 cm)
3	Blanket Region 2	28.6% HT-9 + 62.5% Li_2O[a] + 8.9% Helium (12 cm)	28.6% HT-9 + 62.5% Li_2O[a] + 8.9% Helium (12 cm)
4	Plenum	20% HT-9 + 80% Helium (11 cm)	20% HT-9 + 80% Helium (22 cm)
5	Shield[b]	100% HT-9 (30 cm)	100% HT-9 (30 cm)

[a] 80% dense; natural lithium in Li_2O.

[b] Included in the calculation to simulate the albedo effect of the shield.

The neutronics calculations were performed using two one-dimensional models:

1. Poloidal model - an infinite cylinder with the centerline of the poloidal plasma as the centerline of the cylinder. This model is used to represent the top and bottom of the tokamak blanket geometry.

2. Toroidal model - also an infinite cylinder; however, with the centerline of the tokamak toroid as the centerline of the cylinder. This model is used to simulate the geometry representing the combination of inboard and outboard blankets, and allows the design of different inboard and outboard blanket thicknesses.

A combined performance, 0.4 × (poloidal model) + 0.6 × (toroidal model), is employed to simulate the 1-D full coverage blanket performance in a tokamak geometry. (The actual blanket performance should be calculated using a realistic 3-D geometry with a Monte Carlo transport code such as MCNP, as given in Section 5.7.) Table 8.10-4 gives the calculated neutronic results for the two models mentioned above. The combined performance for the full coverage tokamak geometry simulation, also given in Table 8.10-4, indicates that a tritium breeding ratio of 1.21 tritons per D-T neutron can be obtained for the helium-cooled Li_2O blanket with a blanket nuclear heating of about 16.7 MeV per D-T neutron, or a blanket energy multiplication of 1.18.

Li_2O Design - Tandem Mirror Reactor

Table 8.10-5 gives the one-dimensional blanket model for the helium-cooled Li_2O blanket for the tandem mirror reactor. The blanket consists of a 6-cm HT-9 first wall, a 35-cm region-1 breeding zone, a 12-cm region-2 breeding zone, and a 10-cm plenum. The component zone compositions are the same as those in a tokamak blanket except for the first wall which is 10.3% HT-9 structure instead of 11.7%, as designed for the tokamak reactor.

TABLE 8.10-4
TRITIUM BREEDING RATIOS (T/D-T NEUTRON) AND
NUCLEAR HEATING RATES (MeV/D-T NEUTRON)
IN THE REFERENCE HELIUM-COOLED Li_2O BLANKET
- TOKAMAK REACTOR

Calculation Model	I Poloidal	II Toroidal	I × 0.4 + II × 0.6
Simulation	Top and Bottom Blankets	Inboard and Outboard Blankets Combined	3-D Full Coverage Blanket
T_6	0.905	0.869	0.883
T_7	0.337	0.312	0.322
TBR	1.242	1.181	1.205
Blanket nuclear heating	16.5	16.6	16.7
Total nuclear heating	17.1	17.2	17.2

Neutronic calculations were performed using the one-dimensional infinite cylinder model with plasma and first wall radii of 49 and 60 cm, respectively. The calculated results for the reference blanket are presented in Table 8.10-6. Note that this blanket gives a tritium breeding ratio of 1.19 tritons per D-T neutron and a blanket nuclear heating of 16.6 MeV per D-T neutron.

$LiAlO_2$/Be/ Design - Tokamak

Table 8.10-7 describes the blanket zones and material compositions for the reference helium-cooled, beryllium-multiplier, $LiAlO_2$ blanket for a tokamak reactor. The beryllium zone (10 cm thick) is incorporated only in the outboard blanket in an attempt to minimize the total beryllium inventory needed for the tokamak reactor. The inboard blanket design is similar to that for the Li_2O/He inboard blanket as described previously, except that the breeder is replaced by $LiAlO_2$. The outboard blanket requires a 10-cm beryllium zone (blanket region-1), which consists of 4.7% HT-9, 54% beryllium and the balance of helium; and a $LiAlO_2$ breeding zone (blanket region-2). The breeding zone is composed of 15.7% HT-9, 75.3% $LiAlO_2$ and the balance of helium, all by volume. The total blanket thicknesses are 41 and 70 cm, respectively, for the inboard and outboard blankets.

Table 8.10-8 summarizes the neutronic results for the tokamak reactor system employing the models mentioned previously for the Li_2O/He system. As seen in Table 8.10-8, the combined 1-D full-coverage blanket estimate gives a tritium breeding of 1.21 tritons per D-T neutron. The nuclear heat deposited in the blanket is about 17.1 MeV per D-T neutron, which is equivalent to a blanket energy multiplication of 1.21.

$LiAlO_2$/Be Design - Tandem Mirror Reactor

The blanket zones and material compositions for the reference TMR helium-cooled beryllium-multiplier $LiAlO_2$ blanket are displayed in Table 8.10-9. Note that this design is essentially the same as that for the

TABLE 8.10-5
ONE-DIMENSIONAL BLANKET ZONES AND COMPOSITIONS
FOR THE REFERENCE HELIUM-COOLED Li_2O BLANKET
FOR TANDEM MIRROR REACTOR

Zone	Component	Composition and Thickness
1	First Wall	10.3% HT-9 + 89.7% Helium (6 cm)
2	Blanket Region 1	7.9% HT-9 + 80.6% Li_2O[a] + 11.5% Helium (35 cm)
3	Blanket Region 2	28.6% HT-9 + 62.5% Li_2O[a] + 8.9% Helium (12 cm)
4	Plenum	20% HT-9 + 80% Helium (10 cm)
5	Shield[b]	100% HT-9 (30 cm)

[a] 80% dense; natural lithium in Li_2O.

[b] Included in the calculation to account for the albedo effect of the shield.

TABLE 8.10-6
TRITIUM BREEDING RATIO (T/D-T NEUTRON)
AND NUCLEAR HEATING RATE (MeV/D-T NEUTRON)
IN THE REFERENCE HELIUM-COOLED Li_2O BLANKET
- TANDEM MIRROR REACTOR

Tritium Breeding	
T_6	0.854
T_7	0.338
TBR	1.192
Nuclear Heating	
Blanket	16.6
Total	17.2

TABLE 8.10-7
ONE-DIMENSIONAL BLANKET ZONES AND MATERIAL COMPOSITIONS FOR THE REFERENCE HELIUM-COOLED BERYLLIUM-MULTIPLIER $LiAlO_2$ BLANKET FOR TOKAMAK REACTOR

Zone	Component	Inboard (Thickness)	Outboard (Thickness)
1	First Wall	11.7% HT-9 + 88.3% Helium (6 cm)	11.7% HT-9 + 88.3% Helium (6 cm)
2	Blanket Region 1	7.9% HT-9 + 80.6% $LiAlO_2$[a] + 11.5% Helium (12 cm)	4.7% HT-9 + 54.0% Be[b] + 41.3% Helium (10 cm)
3	Blanket Region 2	28.6% HT-9 + 62.5% $LiAlO_2$[a] + 8.9% Helium (12 cm)	15.7% HT-9 + 75.3% $LiAlO_2$[a] + 9% Helium (32 cm)
4	Plenum	20% HT-9 + 80% Helium (11 cm)	20% HT-9 + 80% Helium (22 cm)
5	Shield[c]	100% HT-9 (30 cm)	100% HT-9 (30 cm)

[a]80% dense; 60% ^6Li in lithium.

[b]80% dense.

[c]Included in the neutronic calculation to account for the albedo effect of the shield.

TABLE 8.10-8
TRITIUM BREEDING RATIOS (T/D-T NEUTRON)
AND NUCLEAR HEATING RATES (MeV/D-T NEUTRON)
IN THE REFERENCE HELIUM-COOLED BERYLLIUM-MULTIPLIER $LiAlO_2$ BLANKET
FOR TOKAMAK REACTOR

Calculation Model	I Poloidal	II Toroidal	I × 0.4 + II × 0.6
Simulation	Top- and Bottom-Board Blanket	Inboard and Outboard Blankets Combined	3-D Full Coverage Blanket
T_6	1.225	1.158	1.185
T_7	0.025	0.027	0.026
TBR	1.250	1.185	1.211
Blanket nuclear heating	17.5	16.9	17.1
Total nuclear heating	18.3	17.8	18.0

TABLE 8.10-9
ONE-DIMENSIONAL BLANKET ZONES AND MATERIAL COMPOSITION FOR THE REFERENCE HELIUM-COOLED BERYLLIUM-MULTIPLIER $LiAlO_2$ BLANKET FOR TANDEM MIRROR REACTOR

Zone	Component	Composition and Thickness
1	First Wall	10.3% HT-9 + 89.7% Helium (6 cm)
2	Blanket Region 1	4.7% HT-9 + 54% Be[a] + 41.3% Helium (10 cm)
3	Blanket Region 2	15.7% HT-9 + 75.3% $LiAlO_2$[b] + 9% Helium (32 cm)
4	Plenum	20% HT-9 + 80% Helium (10 cm)
5	Shield[c]	100% HT-9 (30 cm)

[a] 80% dense.

[b] 80% dense; 60% ^6Li in lithium.

[c] Included in the neutronic calculation to account for the albedo effect of the shield.

tokamak outboard blanket except that the plenum needed for the TMR design is only 10 cm thick instead of 22 cm, as designed for the tokamak reactor. The total blanket thickness is thus only 58 cm.

Table 8.10-10 presents the calculated neutronic results for the reference $LiAlO_2$/Be TMR blanket. The tritium breeding ratio is 1.26 tritons per D-T neutron. The blanket nuclear heating is about 17.6 MeV per D-T neutron resulting in a blanket energy multiplication of 1.25.

8.10.2.2 Li/He Designs

In this section, the neutronics designs for the helium-cooled, liquid-lithium blankets are described for the tokamak reactor and TMR systems.

Li/He Design - Tokamak

Table 8.10-11 describes the blanket zones and material compositions for both inboard and outboard blankets. In this design, a high structure content zone (blanket region-2) was arranged behind the breeding zone (blanket region-1) to enhance the nuclear energy deposition in the blanket. Blanket region-1 consists of 8% HT-9 structure, 66% liquid lithium, and the balance of helium, all by volume; and blanket-2 zone consists of 88% HT-9 and the balance of helium. The thicknesses of these zones are 24 cm (blanket-1) and 20 cm (blanket region-2), and 78 and 14 cm, respectively, for inboard and outboard blankets. Including the plena, the total thickness for the inboard and outboard blankets are 0.61 and 1.2 m, respectively.

Table 8.10-12 gives the calculated neutronic performance for the Li/He reference blanket. As in the previous section, the neutronic results for poloidal, toroidal, and combined models for the tokamak system are given in this table. As seen in Table 8.10-12, the combined 1-D tokamak full coverage blanket performance gives a tritium breeding ratio of 1.22 tritons per D-T neutron. The blanket nuclear heating for the reference blanket is also about 17.4 MeV per D-T neutron based on ENDF/B-V, LANL processed nuclear data library. This is equivalent to a blanket energy multiplication of 1.23.

TABLE 8.10-10
TRITIUM BREEDING RATIO (T/D-T NEUTRON)
AND NUCLEAR HEATING RATE (MeV/D-T NEUTRON)
THE REFERENCE HELIUM-COOLED BERYLLIUM-MULTIPLIER
$LiAlO_2$ BLANKET FOR TANDEM MIRROR REACTOR

Tritium Breeding	
T_6	1.233
T_7	0.025
TBR	1.258
Nuclear Heating	
Blanket	17.6
Total	18.8

TABLE 8.10-11
ONE-DIMENSIONAL BLANKET ZONES AND MATERIAL COMPOSITIONS
FOR THE REFERENCE HELIUM-COOLED LITHIUM BLANKET
FOR TOKAMAK

Zone	Component	Inboard (Thickness)	Outboard (Thickness)
1	First Wall	11.7% HT-9 + 88.3% Helium (6 cm)	11.7% HT-9 + 88.3% Helium (6 cm)
2	Blanket Region 1	8% HT-9 + 66% Lithium[a] + 26% Helium (24 cm)	8% HT-9 + 66% Lithium + 26% Helium (78 cm)
3	Blanket Region 2	88% HT-9 + 12% Helium (20 cm)	88% HT-9 + 12% Helium (14 cm)
4	Plenum	20% HT-9 + 80% Helium (11 cm)	20% HT-9 + 80% Helium (22 cm)
5	Shield[b]	100% HT-9 (30 cm)	100% HT-9 (30 cm)

[a]Natural lithium.

[b]Included in the blanket neutronic calculation to account for the albedo effect from the shield.

TABLE 8.10-12
TRITIUM BREEDING RATIOS (T/D-T NEUTRON)
AND NUCLEAR HEATING RATES (MeV/D-T NEUTRON)
IN THE REFERENCE HELIUM-COOLED LITHIUM BLANKET
FOR TOKAMAK

Calculation Model	I Poloidal	II Toroidal	I × 0.4 + II × 0.6
Simulation	Top- and Bottom-Board Blanket	Inboard and Out-Board Combined Blankets	3-D Full Coverage Blanket
T_6	0.876	0.825	0.845
T_7	0.399	0.360	0.376
TBR	1.275	1.185	1.221
Blanket nuclear heating	17.5	17.4	17.4
Total nuclear heating	17.6	17.6	17.6

8.10.2.3 Flibe/He Design

Scoping Study

Initial scoping calculations were done by Lee at LLNL with the TART code and ENDL data to determine the tritium breeding potential of this blanket type. A radially zoned cylindrical nucleonics model was used and is described in Table 8.10-13. Note that the LiF and BeF_2 mole fractions of Flibe were inadvertently reversed but the effects of this error are insignificant. Results, local (100% blanket coverage) T and M vs Be zone thickness, are shown in Fig. 8.10-8. The tritium breeding ratio, T, is seen to vary between 0.5 with no Be to 1.7 with a 60-cm Be zone. Correspondingly, energy multiplication, M, varies between 1.1 and 1.4. The effects of less than 100% blanket coverage on T is shown in Fig. 8.10-9. For example, if the effective coverage is only 80, a 15-cm Be zone is needed for T = 1.01 compared to 10 cm at full coverage. Higher T can be achieved, of course, by increasing the Be zone thickness. Another possibly attractive use of the excess neutrons generated in Be is for higher M. While this was not the objective here it is clearly possible to include material in the blanket with significantly higher Q's than 4.8 MeV for the Li6(n,t) reaction. Also enriching the Li in Li6 can increase T.

TMR and Tokamak Reference Blankets

The next step in the nuclear analysis of this blanket was the 1-d calculations of reference blankets for the tokamak and the tandem mirror. This was done by Jung at ANL with the same codes and data used for the other candidate blankets.

The computation was carried out using: (1) ANISN (S_8P_3) with the VITAMIN-C/MACKLIB-IV libraries (both based on ENDF/B-IV); and (2) MCNP with ENDF/B-V. For the sake of comparison, additional Monte Carlo computations were made using MCNP along with the ENDF/B-IV data.

In the case of the TMR design, the MCNP-ENDF/B-V computation results in a TBR of $\sim$ 1.46 ($\pm$1%) while the ANISN-MACK computation yields a TBR of $\sim$ 1.40. For comparison on the basis of consistent data library of ENDF/B-IV, the ANISN TBR should be compared to $\sim$ 1.36 ($\pm$1%) of the corresponding MCNP calculation.

The blanket energy deposition was calculated only by ANISN/MACK and estimated to be 21.3 MeV/D-T (i.e., an energy multiplication factor of ∿ 1.5 per 14.06-MeV neutron). Evidently, such a high energy multiplication was brought about by the substantial neutron multiplication by the Be(n,2n) reaction in this design. Indeed, the Be(n,2n) reaction rate amounts of ∿ 0.95/D-T (ANISN estimate).

On the other hand, the tokamak Flibe design yields a TBR of ∿ 1.22 (± 1%) by the MCNP-ENDF/B-V computation, which is compared to ∿ 1.25 by ANISN-MACK and to ∿ 1.17 (± 1%) by MCNP-ENDF/B-IV. The reason for the substantial decrease of TBR in this design, relative to the TMR design is twofold: namely, the increased first wall thickness due to the sacrificial structural material against erosion and the substantially thinner inboard blanket than the outboard. In fact, the TBR increases to 1.44 (± 1%) by extending the inboard blanket as much as the outboard blanket.

The energy deposition is estimated to be ∿ 20.5 MeV/D-T and the Be(n,2n) reaction rate amounts to ∿ 0.87/D-T in this case.

A more detailed summary of these results is given in Table 8.10-14 while blanket material compositions and system dimensions and zonal material compositions are given in Tables 8.10-15 and 8.10-16.

Discussion of Nuclear Analysis

The blanket 1-d model given in Table 8.10-16 does not include structure needed to close the module ends.

Refined estimates of the composition of the He/Flibe/Be blankets for the tokamak and mirror are given in Table 8.10-17. These estimates include the structure for first wall, end plates, reinforcing plates and backing plates and lobe walls, by homogenizing these materials in the appropriate zones. The blanket module structural concept is GA's "book end" design; see Fig. 8.10-10 taken from Jan. 3 - Feb. 1, 1984 handouts distributed by G. D. Morgan with additional information from Clement Wong. The Flibe zones contain an additional 1 v/o structure to account for the tubes and manifolds.

The major change occurs in the back region of the SiC zone where the backing plates add 22 v/o additional structure. The plena zones also have increased structure (27 v/o) because of the backing plates. If this additional structure is found to reduce breeding significantly, a thicker Be zone and/or additional Flibe and/or Li6 enrichment can be used to counter

the increased structure. It is probably cost effective to just increase the Be zone thickness slightly and take advantage of the added structure for higher M.

These models do not account for penetrations such as divertors in tokamaks and end cells in mirrors. For the tandem mirror, end cell effects as determined in the MARS study result in an effective blanket coverage of 0.97. For the tokamak the effective blanket coverage is 0.90 based on Starfire with an INTOR-type limiter.

Fluorine Activation

Fluorine is a major element of Flibe [LiF (46.9 m/o) + BeF_2 (53.1 m/o)], the tritium breeding material we are proposing. One of the initial blanket neutronic calculations used to determine tritium breeding ratio is representative and used here to calculate activities and afterheat caused by fluorine activation. The mole frations of LiF and BeF_2 were inadvertently reversed, but the effect on the results is expected to be very small. The activation and decay chain evaluated is shown in Fig. 8.10-11. Results are listed in Table 8.10-18. Column 1 lists the 8 F(n,x)Y reactions calculated, 4 of which result in radioisotopes. The calculated reaction rates for these 8 reactions are given in column 2. The TART code with ENDL data was used for this calculation. Column 3 lists F reactions per F atom in the blanket per 1.0 MWY/m^2 exposure. Since the total is only 6 parts per million per unit exposure, chemical contamination is not expected to be a problem. Column 4 lists the products of the F(n,x)Y reactions, with column 5 listing the half-lives of the radioactive products. Column 6 lists the type, energy, and intensity of the radioactive produce decay. The beta energies listed are maximum values. Column 7 gives the equilibrium activities in $Curies/MW_f$ for the radioactive products. The final column (8) lists the stable end products of the 8 fluorine reactions.

Afterheat - The total energy release from the 4 radioactive products of the F(n,x)Y reactions is 0.117 MeV/DT neutrons. This is only 0.53% of the prompt energy release in the blanket. Thus, the afterheat level due to fluorine reactions at shutdown is 0.53% minus the fraction carried away by neutrinos. Five minutes after shutdown the afterheat level drops to 0.022% (again, minus the neutrino fraction).

Conclusion

Based on 3-D analysis to date we predict the reference Flibe blanket to perform as follows:

	Tokamak	Tandem Mirror
T	1.14	1.29
E (Blk)	22.3	21.6

And we can confidently predict that based on the initial scoping calculations we can significantly increase T and/or M by increasing Be zone thickness.

TABLE 8.10-13

NUCLEONICS MODEL FOR FLIBE BLANKET

CALCULATIONS (CYLINDRICAL)

ZONE	R_1 CM	Δ R, CM	COMPOSITION	
PLASMA	0	60		
FIRST WALL	199.5	0.5	FE	(100 v/o)
INNER BLANKET	200	0	FLIBE*	(9 v/o)
		TO		
		60	FE	(6 v/o)
			BE	(53 v/o)
OUTER BLANKET	200	100	FLIBE	(9 v/o)
	TO	TO		
	260	40	FE	(6 v/o)
			SIC	(53 v/o)
SHIELD	300	20	FE	(100 v/o)

*53.1 M/o LiF (NAT. LI) K+ 46.9 M/O BEF_2 - These mole fractions were mistakenly reversed

TRANSPORT CODE - TART MONTE CARLO

DATA - ENDL BASED 175 GOROUP LIBRARY

TABLE 8.10-14

SUMMARY OF NUCLEAR ANALYSIS 1-D RESULTS

	TBR		Energy Deposition
	MCNP-ENDF5	ANISN-MACK	ANISN-MACK
(A) TMR			
First wall (cm)	---	---	0.72
BANK-1 (20 cm)	0.946 (±1%)	0.943 (0.941)[a]	13.48
BANK-1 (37 cm)	0.512 (±1%)	0.457 (0.457)[a]	6.73
Plenum (22 cm)	---	---	0.38
TOTAL	1.458 (±1%) [1.375 (±140)][b]	1.400 (1.398)[a]	21.31 MeV/D-T
(B) TOKAMAK			
Inboard			
Plenum (11 cm)	---	---	0.33
BANK-2 (12 cm)	---	0.083 (0.083)[a]	1.55
BANK-1 (12 cm)	0.081 (±3%)	0.195 (0.195)[a]	2.93
First wall (6 cm)	---	---	0.41
Outboard			
First wall (6 cm)	---	---	0.97
BANK-1 (20 cm)	0.656 (±1%)	0.683 (0.682)[a]	9.96
BANK-2 (37 cm)	0.296 (±2%)	0.288 (0.288)[a]	4.12
Plenum (22 cm)	---	---	0.20
TOTAL	1.222 (±1%) [1.166 (±1%)][b]	1.248 (1.247)[a]	20.47 MeV/D-T

[a] $T_6 + 0.85\ T_7$.

[b] Based on MCNP-ENDF/B-IV.

TABLE 8.10-15

MATERIAL COMPOSITIONS

@ 100% T.D.		atom/b-cm
HT-9	Fe	7.058-2
	Cr	1.070-2
	Mo	4.833-4
Flibe	^{6}Li	1.135-3
(Natural lithium)	^{7}Li	1.420-2
	Be	1.729-2
	F	4.991-2
SiC	Si	4.834-2
	C	4.834-2
Beryllium	Be	1.236-1
Fe-2422	Fe	7.028-2
	Mn	1.219-2
	Cr	1.849-3
	Ni	1.581-3
H_2O	H	6.686-2
	O	3.348-2

TABLE 8.10-16

SYSTEM DIMENSIONS AND ZONAL MATERIAL COMPOSITIONS

Zone	Outer Radius (cm)	Composition
(A) TMR		
Plasma	46	---
Scrape-off	60	---
First wall	66	8.3% HT-9
BANK-1	86	6% HT-9 + 9% Flibe + 53% beryllium[a]
BANK-2	123	6% HT-9 + 9% Flibe + 75% SiC
Plenum	145	20% HT-9
Shield	175	Fe-1422 + 20% HO

Zone	Outer Major Radius (cm)	Composition
(B) Tokamak[b]		
Inboard		
Shield	(415-) 445	80% Fe-1422 + 20% H_2O
Plenum	456	20% HT-9
BANK-2	468	6% HT-9 + 9% Flibe + 75% SiC
BANK-1	480	6% HT-9 + 9% FLIBE + 53% beryllium[a]
First wall	486	11.7% HT-9
Scrape-off	506	---
Plasma	894	---
Outboard		
Scrape-off	914	---
First wall	920	11.7% HT-9
BANK-1	940	6% HT-9 + 9% Flibe + 53% beryllium[a]
BANK-2	977	6% HT-9 + 9% FLIBE + 75% Sic
Plenum	999	20% HT-9
Shield	1029	80% Fe-422 + 20% H_2O

[a]Beryllium: 100% T.D.

[b]Based on a major radius model at the reactor midplane.

TABLE 8.10-17

REFINED MODEL DIMENSIONS AND ZONAL MATERIALS COMPOSITIONS

	Zone	Outer Radius cm	Composition
(A)	TMR		
	Plasma	46	--
	Scrape-off	60	--
	First wall	66	8.7% HT-9
	BANK-1	86	6% HT-9 + 9% Flibe + 53% beryllium[a]
	BANK-2	98	6% HT-9 + 9% Flibe + 75% SiC
	BANK-3	123	28% HT-9 + 9% Flibe + 53% SiC
	Plenum	145	27% HT-9
	Shield	175	Fe-1422 + 20% H_2O

	Zone	Outer Major Radius (cm)	Composition
(B)	Tokamak[b]		
	Inboard		
	Shield	(415-) 445	80% Fe-1422 + 20% H_2O
	Plenum	456	27% HT-9
	BANK-2	460	6% HT-9 + 9% Flibe + 75% SiC
	BANK-1	480	6% HT-9 + 9% Flibe + 53% beryllium[a]
	First wall	486	11.7% Ht-9
	Scrape-off	506	--
	Plasma	894	--
	Outboard		
	Scrape-off	914	--
	First wall	920	11.7% HT-9
	BANK-1	940	6% HT-9 + 9% Flibe + 53% beryllium[a]
	BANK-2	952	6% HT-9 + 9% Flibe + 75% SiC
	BANK-3	977	28% HT-9 + 9% Flibe + 53% SiC
	Plenum	999	27% HT-9
	Shield	1029	80% Fe-1422 + 20% H_2O

[a] Beryllium: 100% T.D.

[b] Based on a major radius model at the reactor midplane

TABLE 8.10-18

NUCLEAR REACTOR RATES FOR FLUORINE

Reaction Type	Reactions per DT Neutron	Reaction per F Atom per MWY/m^2	Product	Halflife	Decay, Type, Energy (MeV) Intensity (%)	Equilibrium Activity (Curies/MW_f)	End Product
n,2n	2.84(-3)*	7.53(-6)	F-18	110 m	β^+(.635),ε	2.7(4)	O-18
					γ(.511) 200%		
n,n'p	7.40(-4)	1.96(-6)	O-18	--	--	--	O-18
n,n'a	4.37(-3)	1.16(-5)	N-15	--	--	--	N-15
n,p	2.62(-3)	6.94(-6)	O-19	27 s	β^-(4.6)	--	F-19
					γ(.2, 97%,		
					1.4, 59%)	2.5(4)	
n,d	1.03(-3)	2.73(-6)	O-18	--	--	--	O-18
n,t	5.98(-4)	1.59(-6)	O-17	--	--	--	O-17
n,a	8.03(-3)	2.13(-5)	N-16	7 s	β^-(10.4)		O-16
					γ(6.13, 69%)	7.7(4)	
n,g	2.21(-3)	5.86(-6)	F-20	11 s	β^-(5.4)	2.1(4)	Ne-20
					γ(1.63, 100%)		
Totals	0.022	5.75(-5)				1.5(5)	

*(-3) = x 10^{-3}

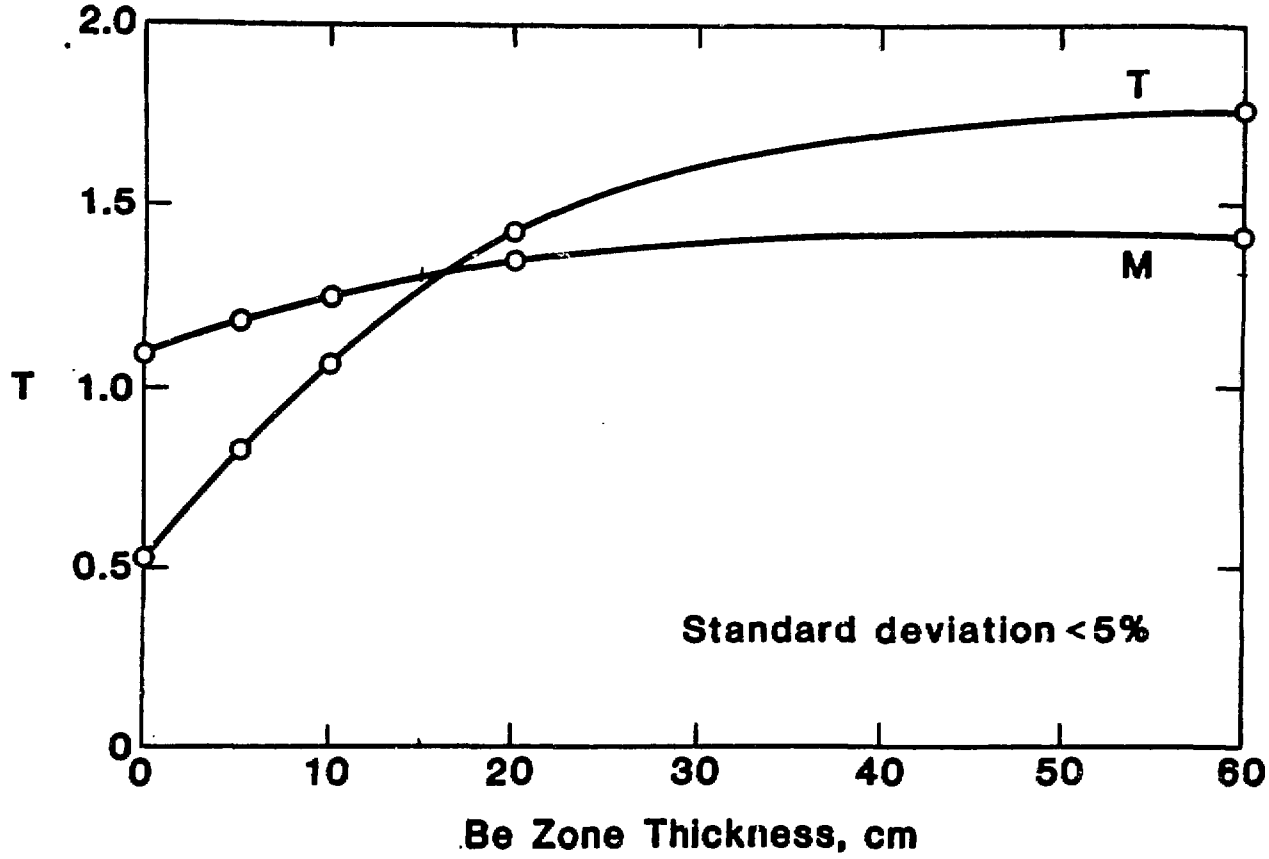

Local Tritium (T) and Energy Multiplication (M) for a FLIBE Blanket

Figure 8.10-8

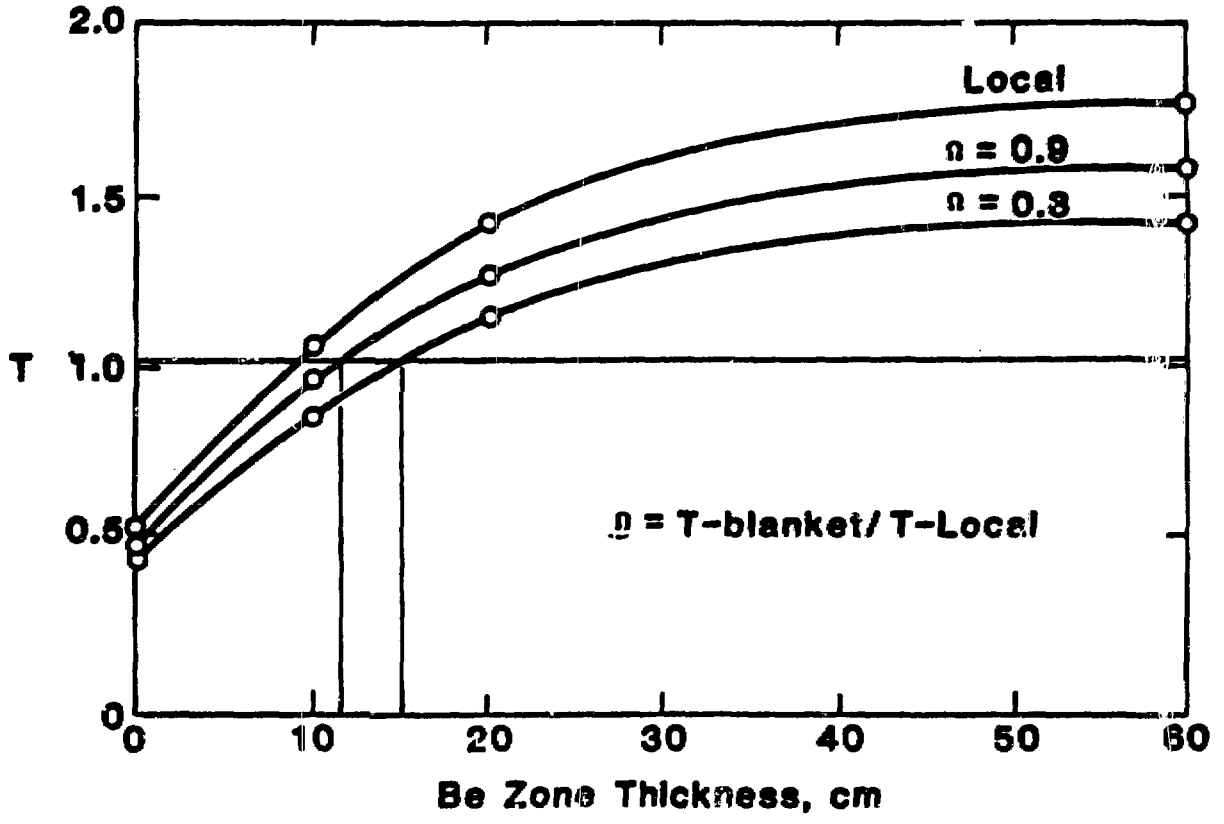

Tritium Breeding Ratio for FLIBE Blanket

Figure 8.10-9

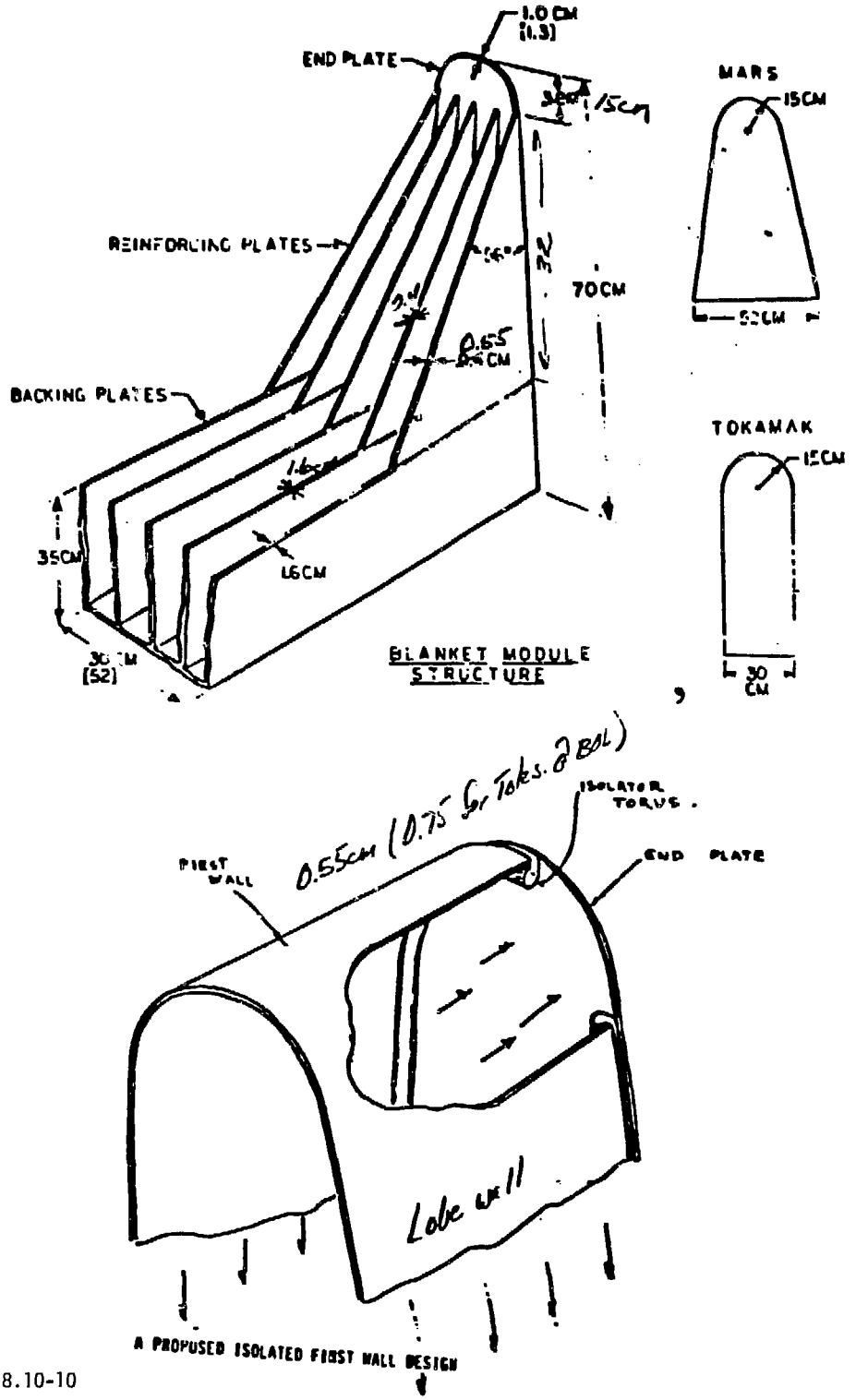

Figure 8.10-10

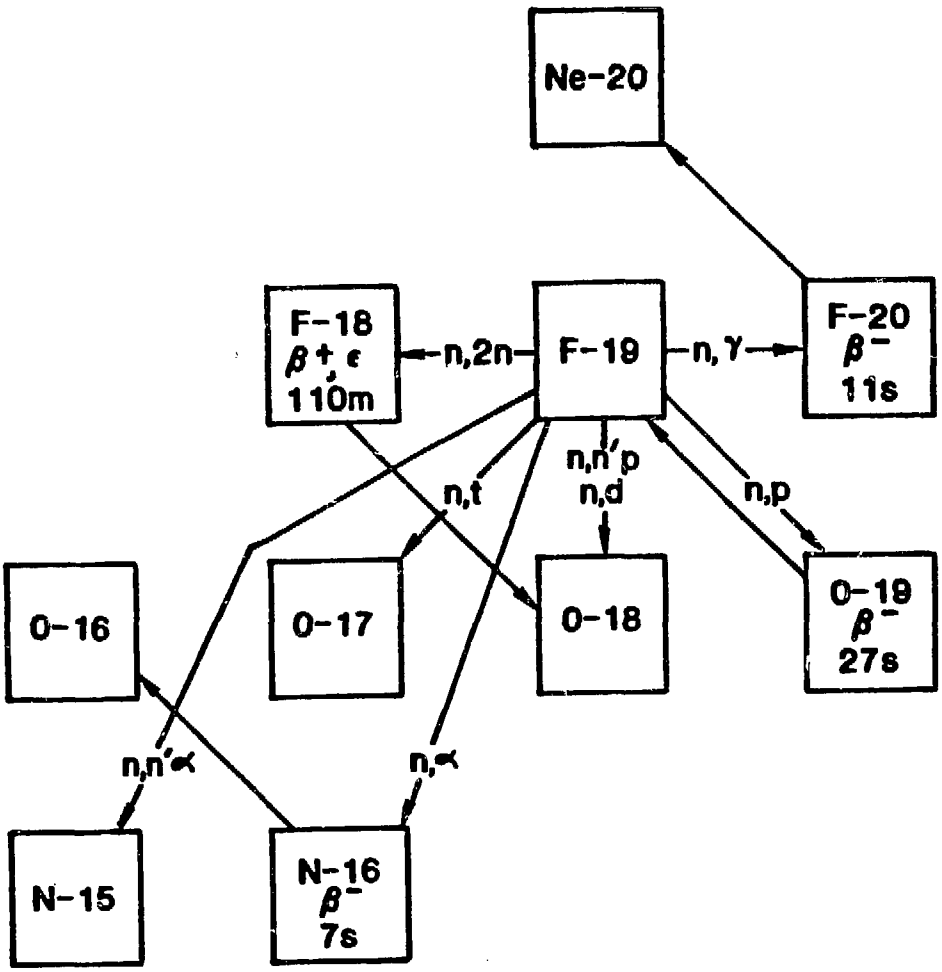

Figure 8.10-11. Nuclear reactions with Fluorine. The two hour half-life Fluorine-18 is the important one from a maintenance and safety point of view.

Li/He Design - Tandem Mirror Reactor

Table 8.10-19 gives the one-dimensional blanket zones and material compositions for the reference helium-cooled lithium blanket for the TMR system. They are similar to that for the tokamak outboard blanket, except for the first wall material composition, which is 10.3% HT-9 in this design, as opposed to 11.7% in the tokamak design, and the blanket region thicknesses, which are 78 cm (blanket region-1) and 14 cm (blanket region-2). The total blanket thickness, including plenum, is 1.08 m.

Table 8.10-20 shows the calculated neutronic performance for the reference TMR Li/He blanket. It provides a 1.28 tritium breeding ratio and 17.5 MeV/ D-T neutron blanket nuclear heating, or 1.24 blanket energy multiplication.

The above results were obtained using atom densities based on a lithium tube wall thickness of 0.6 mm. This thickness was increased to 1.1 mm late in the study in order to satisfy the structural design requirements of module and tube depressurization accidents. This increase in structure volume fraction would reduce the tritium breeding ratio by ~3.5% for both the tokamak and TMR designs. These final results were used for the BCSS design evaluations, but are not shown on the tables in this section.

8.10.3 Thermal-Hydraulics Design

The thermal-hydraulic design of a gas-cooled reactor system should design to high thermal efficiency and low pressure drop. The high efficiency requirement dictates a high coolant outlet temperature, restricted by the maximum operating temperature limits of the reactor materials. The low pressure drop requirement leads to high system operating pressure to obtain high coolant density, a large coolant inlet-to-outlet temperature differential, and restricted velocities of the coolant in various sections of the coolant

TABLE 8.10-19
ONE-DIMENSIONAL BLANKET ZONES AND MATERIAL COMPOSITIONS
FOR THE REFERENCE HELIUM-COOLED LITHIUM BLANKET
FOR TANDEM MIRROR REACTOR

Zone	Component	Composition and Thickness
1	First Wall	10.3% HT-9 + 89.7% Helium (6 cm)
2	Blanket Region 1	8.3% HT-9 + 68.4% Lithium[a] + 26% Helium (78 cm)
3	Blanket Region 2	88% HT-9 + 12% Helium (14 cm)
4	Plenum	20% HT-9 + 80% Helium (10 cm)
5	Shield[b]	100% HT-9 (30 cm)

[a]Natural lithium.

[b]Included in the neutronic calculation to account for the albedo effect from the shield.

TABLE 8.10-20
TRITIUM BREEDING RATIO (T/D-T NEUTRON)
AND NUCLEAR HEATING RATE (MeV/D-T NEUTRON)
THE REFERENCE HELIUM-COOLED LITHIUM BLANKET
FOR TANDEM MIRROR REACTOR

Tritium Breeding	
T_6	0.872
T_7	0.410
TBR	1.282
Nuclear Heating	
Blanket	17.5
Total	17.8

loop. On the other hand, the restrictions on material operating temperature limits lead to high coolant velocities to maintain high heat transfer coefficients. During the course of the blanket thermal-hydraulics design, close interaction was maintained with the mechanical design, neutronics analysis, and material selection efforts.

The material temperature and blanket pressure drop limits and general helium-cooled thermal-hydraulics design equations were presented in Refs. 8.10-9 and 8.10-10. The thermal-hydraulics design characteristics for different designs during the second year of this study are reported in this section. The blanket designs evaluated are the solid breeder designs, including Li_2O and $LiAlO_2$/Be; lithium breeder designs and the FLiBE/Be designs. All these were evaluated for both tokamak and mirror reactors.

8.10.3.1 Solid Breeder Designs

This section presents the thermal-hydraulics designs for the Li_2O and $LiAlO_2$/Be blankets. Results for the first wall, breeder plate, and helium loop pressure drop analyses are reported. Both tokamak and mirror reactors were considered.

First Wall Design

As described in the BCSS interim report for the tokamak reactor, a finned first wall design will be needed in order to handle the relatively high surface loading of 1 MW/m^2 and the corresponding volumetric power generation from the neutron wall loading of 5 MW/m^2. The finned first wall configuration is illustrated in Fig. 7.4.1 and is explained in more detail in the BCSS interim report.(8.10-1) Since the first wall erosion rate is projected to be at 1 mm/year for the BCSS, an erodable layer of 2 mm was added to the first wall for heat transfer analyses.

For the mirror reactor, a simple channel first wall design is adequate, since the projected surface loading is relatively low at 0.05 MW/m^2 even

though the neutron wall loading is the same at 5 MW/m^2. At a projected first wall erosion rate of 0.1 mm/yr, the difference in first wall thickness at the beginning of life (BOL) and at the end of life (EOL) was ignored in the analyses.

Since the first wall configuration for the helium-cooled pressurized lobe design is similar for all the solid breeder and lithium breeder designs, the respective design parameters and results for all the blankets are summarized in Tables 8.10-21 and 8.10.22.

It can be noted from Table 8.10-15 that at the EOL for the tokamak reactor and during the lifetime of the mirror reactor first wall, the structure maximum temperature is <550°C which is the design limit for HT-9 specified by the BCSS structural material design group. At the BOL, the first wall temperature is allowed to operate beyond 550°C at the nonstructural, erodable front face. It is likely that in order to relax some of the bending and thermal stresses, the erodable layer may need to be grooved.

Breeder Plate Design

As discussed in Sections 8.4 and 8.6, all the solid breeder designs are in plate geometry. This was selected to maximize the breeder volume fraction in the blanket, to minimize the structure volume fraction, and to reduce the overall blanket thickness. Plate design also has the property of minimizing the contact resistance between the clad and the breeder by relying on the pressure differential of 4.9 MPa (715 psi) between the helium coolant and the purge helium streams to press the clad against the solid breeder pellet. To fit the respective configurations, the tokamak reactor uses plates of uniform thicknesses and the mirror reactor uses tapered plates to fit the cylindrical geometry.

Table 8.10-23 summarizes the design characteristics for the solid breeder plate designs. The results for the Li-breeder tube design are presented in Section 8.10.3.2.

TABLE 8.10-21
HELIUM-COOLED FIRST WALL DESIGN PARAMETERS

	Tokamak			Mirror		
	Li_2O	$LiAlO_2$/Be	Li	Li_2O	$LiAlO_2$/Be	Li
Neutron wall loading, MW/m^2	5	5	5	5	5	5
Surface loading, MW/m^2	1	1	1	0.05	0.05	0.05
Wall configuration	Finned	Finned	Finned	Simple Channel	Simple Channel	Simple Channel
Fin height, mm	7	7	7	NA	NA	NA
Fin thickness, mm	1	1	1	NA	NA	NA
Coolant channel width (tokamak) height (TMR), mm	1	1	1	5	5	5
Minimum wall thickness[a] BOL/EOL, mm	3.5/1.5	3.5/1.5	3.5/1.5	6	6	6
Helium pressure, MPa (atm)	5 (50)	5 (50)	5 (50)	5 (50)	5 (50)	5 (50)
Coolant T_{in}/T_{out}, °C	275/510	275/510	275/510	275/540	275/540	275/540
Blanket energy multiplication[b]	1.18	1.21	1.24	1.24	1.25	1.24

[a]First wall erosion rate of 1 mm/year was assumed for the tokamak reactor.

[b]Results based on one-dimensional neutronics calculations.

TABLE 8.10-22
HELIUM-COOLED FIRST WALL DESIGN RESULTS

	Tokamak			Mirror		
	Li_2O	$LiAlO_2$/Be	Li	Li_2O	$LiAlO_2$/Be	Li
Coolant T_{max}, °C	334	332	328	303	302	302
Coolant velocity, m/sec	60	61	62	31	32	32
Reynolds number	13,226	13,529	21,001	21,001	22,079	21,900
Heat transfer coefficient,[a] W/m^2-K	7,831	7,105	3,437	3,437	3,573	3,551
Wall T_{max} BOL/EOL, °C	649/547	646/544	628/531	448	444	445
Pressure drop, kPa (psi)[a]	29.0(4.2)	29.6(4.3)	31.0(4.5)	2.7(0.39)	2.7(0.39)	27(0.39)

[a]A roughness factor of 1.5 was assumed in the calculations.

TABLE 8.10-23
SOLID BREEDER PLATE DESIGN CHARACTERISTICS

	Li_2O		$LiAlO_2$/Be	
	Tokamak	Mirror	Tokamak	Mirror
Neutron wall loading, MW/m^2	5	5	5	5
Surface loading, MW/m^2	1	0.05	1.0	0.05
Breeder plate configuration	Uniform thickness	Tapered	Uniform thickness	Tapered
Breeder thermal conductivity, W/m-K	2.7	2.7	1.9	1.9
Plate thickness, cm	1.1	1.1 to 1.9	0.9	1.1 to 1.9
Coolant gap width, mm	1	1	1	1
Helium pressure, MPa(atm)	5 (50)	5 (50)	5 (50)	5 (50)
Coolant T_{in}/T_{out}, °C	275/510	275/540	275/510	275/540
HT-9 clad thickness	0.25	0.25	0.25	0.25
Breeder maximum heating rate, W/cc	47	47	64	64
Breeder T_{max}	795	782	1000	1000
Breeder T_{min}	510	519	520	552
Cladding T_{max}	550	550	521	550

It can be noted in Table 8.10-23 that the T_{min}/T_{max} for Li_2O and $LiAlO_2$ are within the temperature limits for the respective breeders. The thermal conductivities used for the calculations are the irradiated values at the plate average temperature. The discussion on the effect of high fluence on the thermal conductivity for the sintered Li_2O and $LiAlO_2$ is presented in Section 6.3. During the course of the BCSS study, the blanket plate thickness changed as more information became available on the projected thermal conductivity of the solid breeders as functions of temperature, packing fraction, and neutron fluence. The trend was toward lower thermal conductivity. Therefore, thinner plates were used in order to design within the specified solid breeder temperature window. For a fixed module width, the module structure was optimized to minimize the structural volume fraction of the module wall and the first wall thickness. With a fixed coolant flow gap width of 1 mm, the flow cross-sectional area then increased with the reduction of plate thickness. This design variation drove the coolant flow through the plate gaps from the turbulent to the transition flow regime, having a Reynolds number of 4000 to 5000. It was noted that, based on this range of Reynolds numbers, the entry-length of the coolant was quite long, in the range of 20 to 30 cm. In such a flow regime, the laminar flow heat transfer coefficient (~1000 W/m^2-K) will be enhanced by a factor of 3 to 4. This effect increases the heat transfer coefficient to higher values than those obtained by turbulent flow (~2600 W/m^2-K). For simplicity, in the scoping calculations, a turbulent correlation was used. For more detailed design in the future, the module width and coolant gap width can be adjusted to maintain turbulent flow, or alternately, the transition flow regime with consideration of entry-effects could be studied in more detail.

Since beryllium has relatively high thermal conductivity, no detailed heat transfer calculation was performed and the design is supported by the following consideration. For a bundle of beryllium rods with rod separation of 2 mm and diameter of 2 cm at a volumetric power generation of 30 MW/m^2 for beryllium metal, the calculated rod centerline temperature is 426°C, which is quite acceptable. The coolant temperature at 330°C after cooling the tokamak first wall. The temperature drop through the beryllium solid is less than 8°C.

Helium Loop Pressure Drops

One of the drawbacks of using helium as the blanket coolant is its relatively high pumping power requirement. This section presents the pressure drop results for the solid breeder blankets from which pumping power can be calculated. The pressure drop considered encompasses the whole helium loop segment in the blanket, inlet/outlet piping, and steam generators. It also includes pressure drop contributions from frictional, turning, expansion, and contraction effects. Pressure drops and power conversion characteristics for the solid breeder designs are presented in Table 8.10-24 In general, the results show that when compared with water, the helium-cooled design pumping powers are relatively high. Nevertheless, when considering the relatively high gross thermal efficiency of helium blankets, the net thermal efficiency of the respective blankets are still quite acceptable.

8.10.3.2 Li/He Designs

This section presents the thermal-hydraulics designs of the helium-cooled Li blankets for tokamak and TMR reactors. Results are presented for the breeder tube zone and the helium loop pressure drop analysis. First wall thermal-hydraulics designs are as presented previously in Section 8.10.3.1.

Breeder Tube Zone

In the breeding zone, the thermal-hydraulics design is guided by liquid metal/structure compatibility concerns. Figure 8.5-1 shows a schematic of the breeder tube bank arrangement. The equations used in the analysis of cross-flow heat transfer through the tube bank are the same as those of the Interim Report.(8.10-1) The resultant thermal-hydraulics designs are summarized in Table 8.10-25. The designs satisfy the compatibility-limited interface temperature guideline with acceptable pumping power (presented in next section), high breeder volume fractions, and reasonable tube dimensions.

TABLE 8.10-24
HELIUM LOOP PRESSURE DROPS AND POWER CONVERSION CHARACTERISTICS
HELIUM-COOLED, SOLID BREEDER DESIGNS

	Li_2O		$LiAlO_2$/Be	
	Tokamak	Mirror	Tokamak	Mirror
Reactor thermal power, MW	5382	2958	5499	3106
Coolant pressure, MPa (atm)	5 (50)	5 (50)	5 (50)	5 (50)
Coolant T_{in}/T_{out}, °C	275/510	275/540	275/510	275/540
Pressure drops				
Blanket - Inboard/outboard, kPa	94.7/122.3	33.7	132/172	45.0
Inlet/outlet pipings, kPa[a]	36.9	36.9	36.9	36.9
Steam generator, kPa[a]	30	30	30	30
Total pumping power, MW_{th}	237	62	246	84
Gross thermal efficiency	39.2	40	39.2	40
Net thermal efficiency	36.4	38.4	36.2	38.2

[a]Estimated results by allowing adjustment in characteristic flow dimensions.

TABLE 8.10-25
Li/He/HT-9 BLANKET BREEDER ZONE THERMAL-HYDRAULICS DESIGN

	Tokamak	Tandem Mirror
Neutron wall loading, MW/m^2	5	5
Surface loading, MW/m^2	1	0.05
Coolant T_{in}/T_{out}, °C	275/510	275/540
Helium pressure, MPa	5	5
Tube pitch, cm	5.1	5.1
Tube outside diameter, cm	4.7	4.8
Tube wall thickness, cm	0.11	0.11
Maximum interface temperature, °C	531	547
(Maximum allowable interface temperature, °C)	(565)	(565)
Maximum breeder temperature, °C	544	560
Breeder volume fraction	0.71	0.74
Structure volume fraction	0.063	0.066

Helium Loop Pressure Drops

Calculations were performed of the total pressure drop of the cooling circuit, including the blanket, inlet/outlet piping, and steam generators. Included were pressure drop contributions from friction, turning, expansion, and contraction effects. Pressure drop and power conversion characteristics are presented in Table 8.10-26. The results show that though the pumping powers are high relative to water coolant, the relatively high gross thermal efficiency of helium blankets allows for acceptable net thermal power conversion efficiencies.

TABLE 8.10-26
HELIUM LOOP PRESSURE DROP AND POWER CONVERSION CHARACTERISTICS
HELIUM-COOLED LITHIUM BREEDER DESIGN

	Tokamak	Tandem Mirror
Reactor thermal power, MW	5577	3056
Coolant T_{in}/T_{out}, °C	275/510	275/540
Helium pressure, MPa	5	5
Pressure drops, kPa		
Blanket, inboard/outboard	101/142	58.8
Piping[a]	36.9	36.9
Steam generator[a]	30.0	30.0
Total pumping power, MW	262	80
Gross thermal efficiency, %	39.2	40.2
Net thermal efficiency, %	36.0	38.5

[a]Estimated results by allowing adjustment in characteristic flow dimensions.

8.10.3.3 Flibe/He Concept

As in all fusion blankets many physics and engineering parameters influence material temperature and heat transfer to the coolant. In performing thermal-hydraulics calculations for the Flibe/He concept, the first wall was assumed to be 5 MW/m^2. The coolant is helium with a nominal pressure of 50 atmospheres. To eliminate "pinch-point" steam generator problems a helium inlet temperature of 275°C was specified. Helium outlet temperature was limited to 500°C in order to not have structural HT-9 steel above 550°C. That limit for HT-9 has been imposed due to neutron damage effects which seriously detract from its ductility and strength above that temperature.

The blanket energy multiplication ratio has been calculated to be 1.51. Table 8.10-27 below shows energy deposition in the various blanket layers by nuclear analysis.

TABLE 8.10-27
BLANKET ENERGY DEPOSITION (ANISN-MACK)

First wall	0.72 MeV
Breeding zone (20 cm)	13.48 MeV
Reflector zone (37 cm)	6.73 MeV
Coolant plenum (22 cm)	0.38 MeV
Total	21.31 MeV per D-T
M = 21.31/14.1 = 1.51	

The blanket analyzed has a first-wall radius of 0.7 meters; so each meter of blanket length in a TMR produces 33.2 MW of thermal power. That power distributes itself through the blanket elements in accordance with Table 8.10-27. A curve (Fig. 8.10-12) was obtained by plotting the three zone points from Table 8.10-27 that pertained to zones where salt tubes would be present. The first-wall point was ignored because that region is not a breeding zone. The plenum point was used to better define the energy deposition near the back of the reflector. Power density estimates were made for crucial blanket locations. This allowed calculation of the salt tube

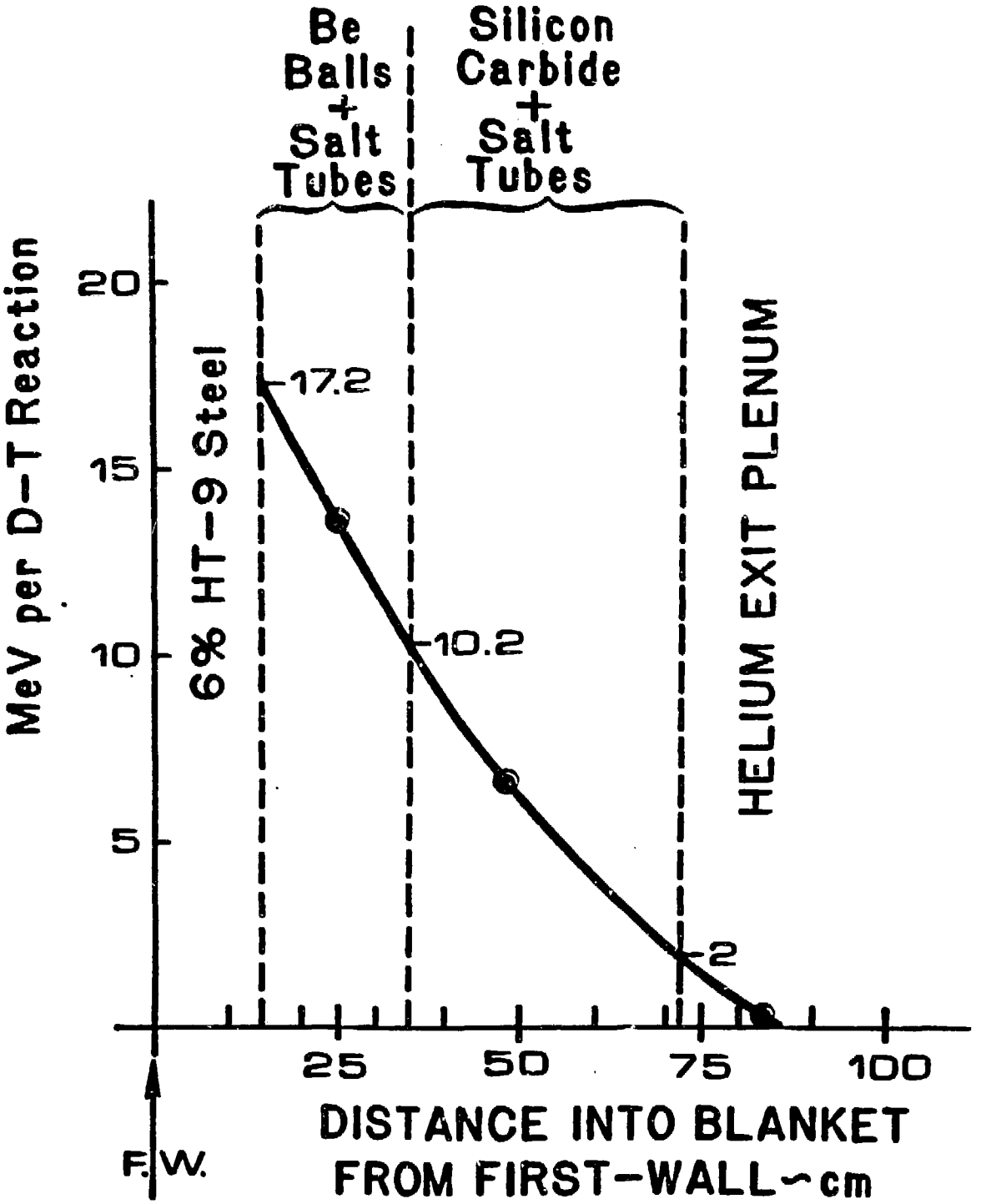

Figure 8.10-12. Neutron energy deposition in molten-salt breeding blanket.

diameters in those zones. One assumption that we made without detailed calculation was that the helium temperature would increase 50°C in moving from the plenum chamber to the front wall. This assumption is probably valid for a tokamak where there is considerable first wall cooling but is probably too large for the tandem mirror. The coolant passes the pod side walls and cools those structural elements first before cooling the first-wall. So the "blanket entrance temperature" (i.e., approach to first-wall) assumed is 325°C.

Table 8.10-28 shows volumetric heating rates at important blanket locations. These were obtained by plotting the data from Table 8.10-27 and interpolating. In order to insure adequate cooling of the salt we must know the division of neutron energy deposition between the salt and other blanket elements. Neutronics calculations for the two major zones reveal that in the breeding zone 70% of the energy is deposited in the salt and 30% in the beryllium; and in the reflector zone 75% of the energy is deposited in the salt and 25% in the silicon carbide. Table 8.10-29 summarizes the material fractions in those two zones. It can easily be shown neglecting heating in the structure that the ratio of volumetric heat production is the following:

$$q_{salt}/q_{Be} = 13.74$$

$$q_{salt}/q_{SiC} = 25$$

Hence,

$$q_{salt} \times .09 + q_{Be} \times .53 = 17.6 \times 1.0$$

$$q_{salt} = 136 \text{ watts/cm}^3$$

The graphs of Figs. 8.10-13 and 8.10-14 show the film temperature drop at the outside of the salt tube and the temperature drop across the wall of the salt tube. Both are linear functions of tube diameter as long as we assume a constant value for the film coefficient.

The key to control of the tube wall temperature lies in the film coefficient at the outside of the tubes. If the tubes have polished outsides, then the film coefficient will probably be in the range from .1 to .15 watts/cm^2 K. Intentionally roughened tubes with a knurled-like exterior are known to have film coefficients at least a factor of 2 higher.

Using the factor of 2 enhancement by surface roughening gives a range of h_f (in the tube size range of interest) varying from .25 to .19 watts/cm^2 K.

TABLE 8.10-28

VOLUMETRIC HEATING AT KEY BLANKET LOCATIONS.

	Volume cm^3	Average Volumetric Heating w/cm^3	Volumetric Heating at Front of Zone w/cm^3	Volumetric Heating at Back of Zone w/cm^3
Multiplier zone (beryllium balls and salt tubes)	1.19×10^6	17.6	22.1	13.1
Reflector zone (silicon carbide and salt tubes)	2.52×10^6	4.2	7.1	1.4

TABLE 8.10-29

BLANKET MATERIAL FRACTIONS.*

	Multiplier zone	Reflector zone
Beryllium	53 vol %	--
Silicon carbide	--	75 vol %
Flibe (salt)	9 vol %	9 vol %
Ferritic steel	6 vol %	6 vol %

*Based on GA Technologies structural design concept presented to BCSS meeting of Jan. 31, 1984.

Table 8.10-30

SUMMARIZES THESE CALCULATIONS FOR THE TWO IMPORTANT BLANKET ZONES.

Energy deposited in salt (W/cm^3)

Multiplier Zone		Reflector Zone	
Front	Back	Front	Back
172	192	85	17

This is good agreement with the bed-of-balls value.[8.10-11] We have chosen a value of .2 W/cm^2 K until experiments can be made on the case of tubes within packed ball beds.

If we decide to confine the salt to a region representing 9% of the multiplier zone volume, and further decide on a staggered tube array (i.e., triangular spacing), one can easily calculate the tube pitch (centerline to centerline) of 2.86 cm and a space between tubes of 1.86 cm. Our tests on ball flow between parallel tubes indicates that Be ball size should be no larger than 0.33 times the space between tubes. The beryllium balls could then be 0.62 cm in diameter and be counted on to "flow" freely into position around the tubes or be readily emptied from the bed when desired. Both the tube spacing and ball diameter turned out smaller than desired. Further design work should be done to come up with a consistent set of parameters with larger values of these two parameters.

It is possible to select smaller tube sizes to reduce the HT-9 tube's inside wall temperature. Tube bank (no balls) calculations show the increase in film coefficient as tube diameter is decreased (see Fig. 8.10-15). One pays twice for that higher film coefficient. First the number of tubes in the blanket becomes very large and they are closely spaced. Second, the beryllium ball diameter which will still flow through the spaces between tubes becomes very small and an enormous number must be manufactured to fill the blanket. Another approach is to increase the breeding salt volume percent. Since the same total energy is captured, the tube surface heat flux

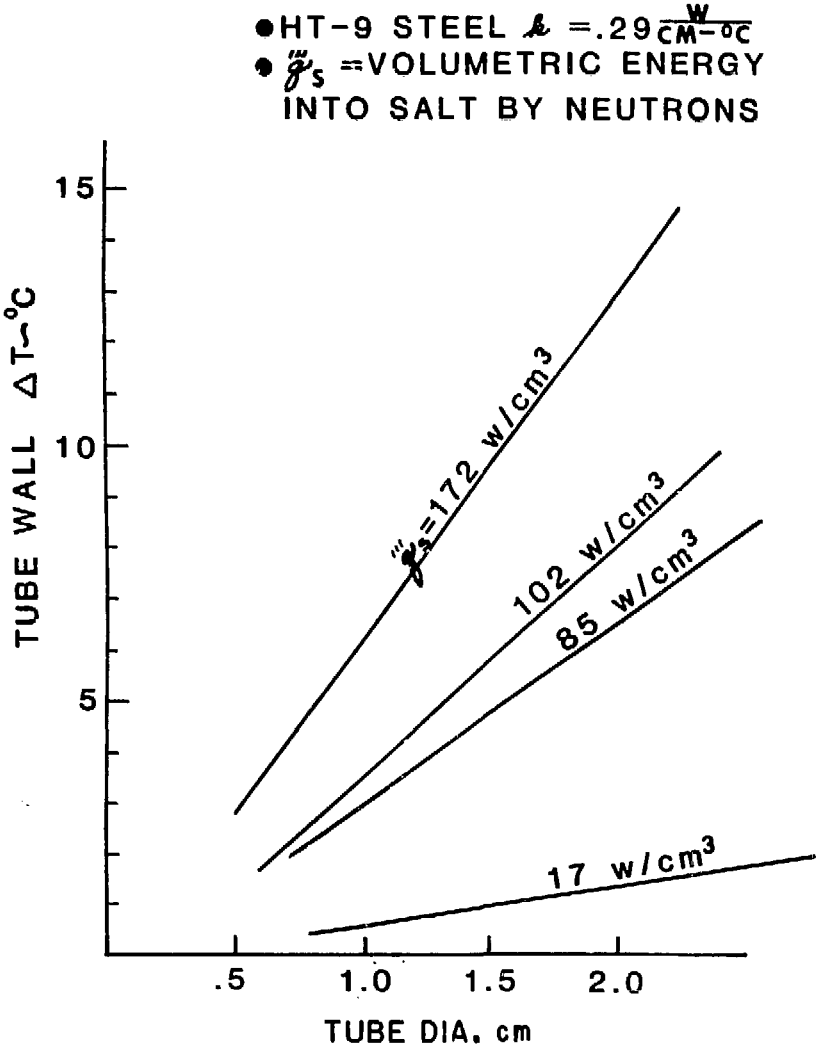

Figure 8.10-13

Temperature drop through tube wall of molten salt tube.

The wall thickness is 0.5 mm.

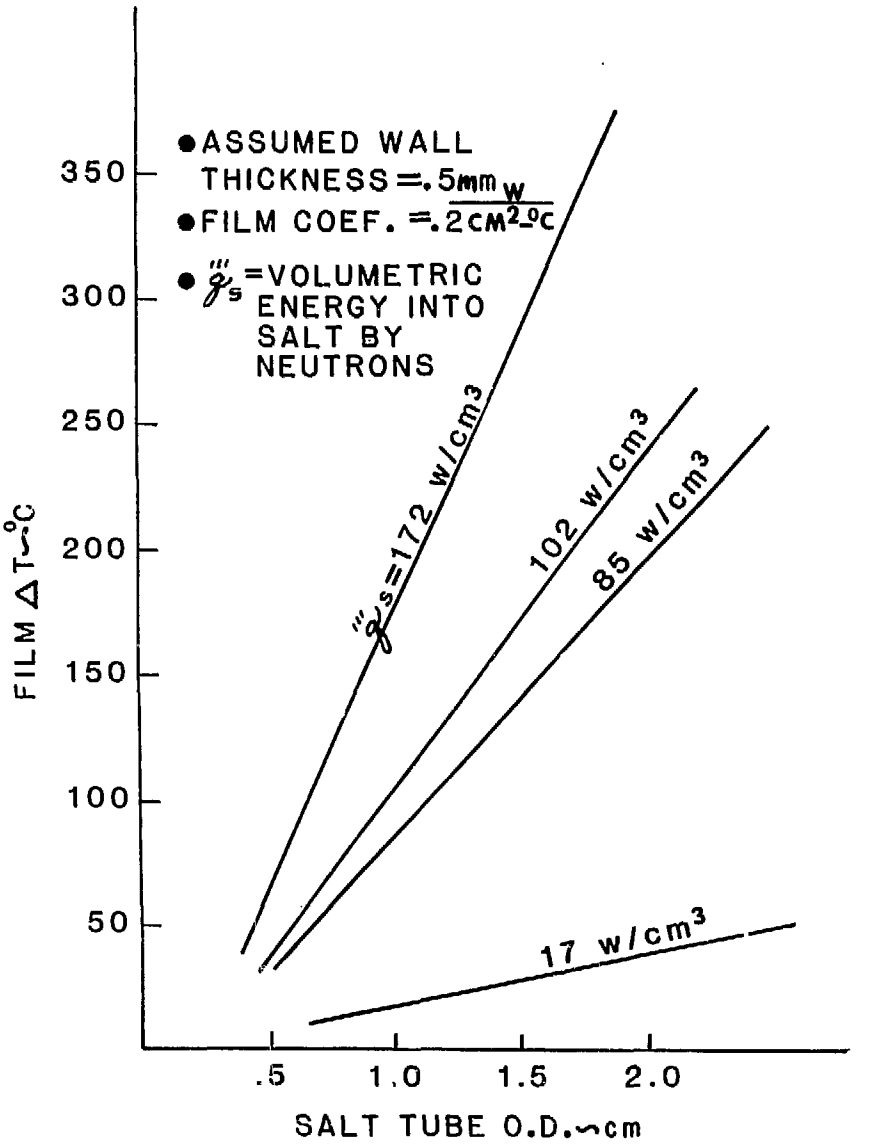

Figure 8.10-14

Temperature drop through outside coolant film on salt tube.

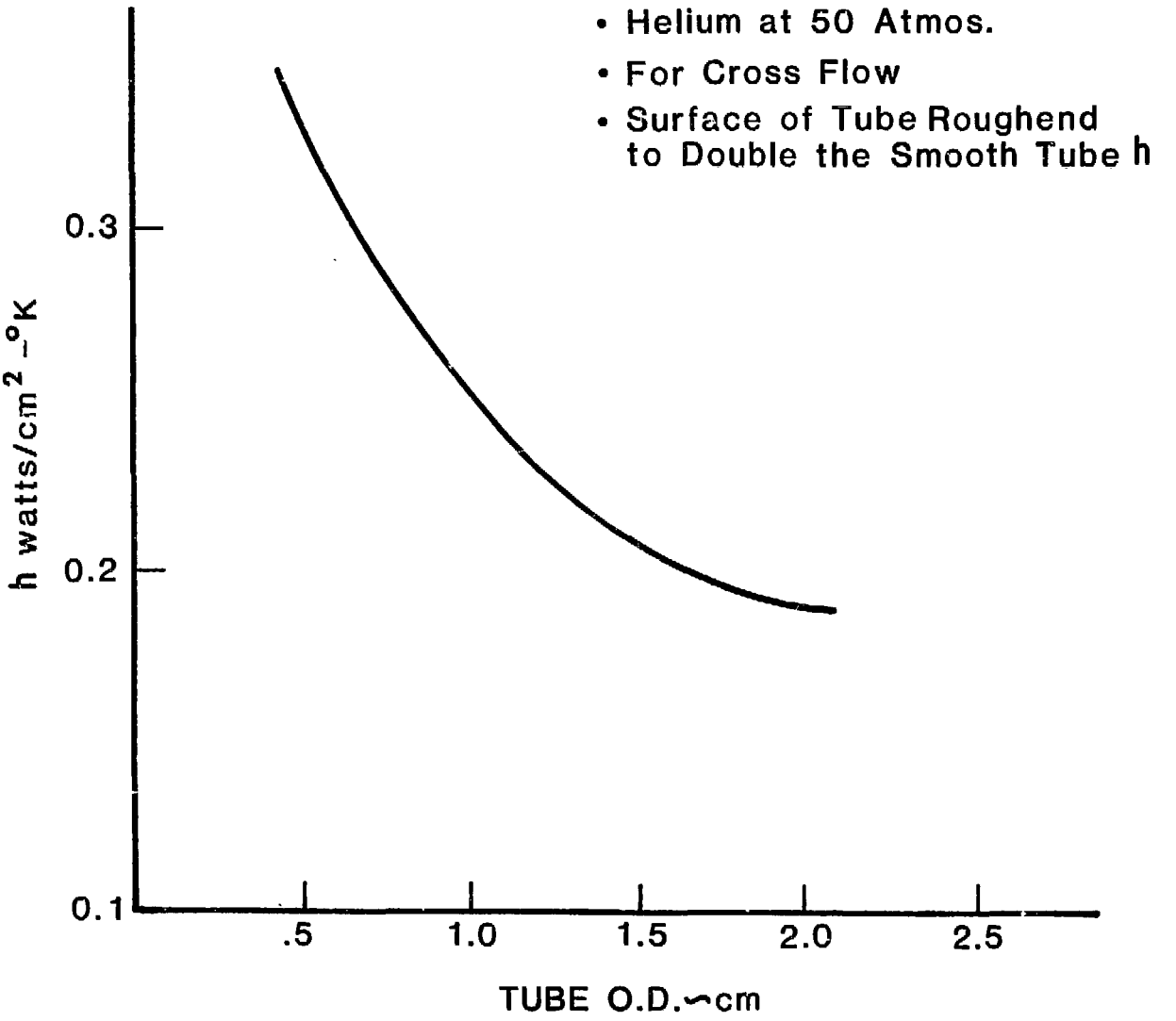

Figure 8.10-15

Surface film coefficient of heat transfer at outside diameter of tube versus tube diameter.

(hence, wall film drop) will decrease. Larger tube diameters at the same spacing require smaller beryllium balls. Optimization of the parameters, tube diameter, volume fraction of salt, maximum tube wall temperature and beryllium ball diameter must be obtained to yield lowest cost at acceptable material temperature.

We have constructed Table 8.10-31 to show the coolant temperature as it progresses through the blanket, and the resulting HT-9 temperature at the inside surface of the salt tubes. The charts of film and wall ΔT (Figs. 8.10-13 and 8.10-14) were employed and a tube diameter was chosen for each zone which yielded a temperature slightly lower than 550°C for the HT-9 salt tubes. Tube sizes vary from 1.0 to 2.0 cm diameter. It may prove most economical to settle on a single size, 1.0 cm o.d. and accept slightly conservative tube temperatures in the other blanket zones.

Discussion of Results and Suggestions for Design Improvement

As the coolant moves into the reflector zone its mean temperature has risen to 442°C. The film temperature drop on the outside of the salt tubes becomes severely limiting. If some of the salt tubes at the rear of the breeding zone and the front of the reflector could be eliminated, the breeding of tritium would be slightly reduced but the temperature limit for HT-9 tubes, 550°C, would not be encountered in that region of the blanket. This would allow the overall mass flow of coolant to be reduced. The outlet coolant temperature would be higher (closer to the 550°C structure temperature limit). This would both raise the thermodynamic efficiency and reduce pumping power due to lower coolant mass flow.

This design has a very large number of salt tubes. This number could be reduced by decreasing the fraction of beryllium and increasing the fraction of salt. The smaller neutron multiplication will result in less tritium bred. It will also decrease the neutron energy density released in molten salt and allow each tube to be a larger diameter. The spacing must be increased as the tube diameter is increased in a manner so that the pebble size can also be increased. The result is a smaller number of larger diameter salt tubes. The tritium breeding ratio in the present design is large enough that some reduction can be permitted.

The reduced fraction of beryllium and increased structure has one more beneficial effect. By capturing more neutrons in structural material we get

TABLE 8.10-31

HT-9 TUBE TEMPERATURE IN THE BLANKET.

Zone	Coolant Temp - ^{o}C	Salt Tube Diam. cm	ΔT ^{o}C (Film)	ΔT ^{o}C (Tube Wall)	HT-9 Temp. at Tube I.D.
Inlet Helium	275^{o}	--	--	--	--
	+50^{o} from pod side walls				
Entering First Wall	325^{o}	--	--	--	--
	+8^{o} from first wall				
Enter Multiplier Zone	333^{o}	1.1	194	7	534^{o}C
Exit Multiplier Zone	442^{o}	1.0	103	4	549^{o}C
Enter Reflector Zone	442^{o}	1.1	96	4	541^{o}C
Exit Reflector Zone	496^{o}	2.0	39	1	536^{o}C
Enter Helium Plenum	500^{o}				

Maximum acceptable tube wall temperature = 550^{o}C

a higher energy release, more than the 4.8 MeV released in the $^{6}Li(n,T)^{4}He$ reaction. This larger blanket energy multiplication further assists the economics.

Pressure Drop and Power Loss in Blanket

The velocity of helium coolant based on "empty column flow" is 144 cm/sec. Empty column flow is used by Ergun[8.10-12] to calculate pressure drop in packed beds such as our beryllium balls surrounding steel tubes which carry molten salt.

The Reynolds number for this flow is 736. A friction factor, $f_k = 2$, can be read from Fig. 9 of Ergun's paper. The void fraction in this bed of tubes and balls is estimated to be 35%. Using the relationship

$$f_k = \frac{D_p}{L} \frac{\epsilon^3}{1-\epsilon} \frac{\Delta P g_c}{\rho_m U_m^2}$$

one finds the pressure drop to be only .07 atmospheres in the beryllium ball multiplier zone, the 20-cm-deep region just behind the first wall.

The reflector zone, behind the multiplier zone, is 37-cm deep. It is composed of silicon carbide blocks with space between each block for helium flow. The block spacing is about 2 mm. Since 75% of the reflector is silicon carbide the gas velocity will be about 600 cm/sec. This modest velocity leads to pressure drop less than .01 atmospheres in this zone. In the back zone where there is more structure and only 53% SiC the power density is low and cooling becomes easier especially if we increase the salt volume as discussed previously.

Allowance for inlet and exit plenum flow losses as well as ball retention screens still leads to the conclusion that overall blanket pressure loss will not exceed 0.1 atmospheres.

If the total thermal power of the reactor is 4000 MW, we calculate that 3432 MW is developed in the blanket and 568 MW goes to the direct converter. If 225°C is the allowable helium temperature rise, it follows that $2.94(10)^6$ gms/sec of helium must flow through the blanket. This is 840 m^3/sec at a mean density of .0035 gms/cm^3. The power consumed in the blanket by the coolant pressure loss is estimated to be 8.4 MW.

8.10.4 Tritium Extraction and Control

This section presents the tritium extraction and control designs for the helium-cooled blankets. The solid breeder designs (Li_2O and $LiAlO_2$/Be) are presented in Section 8.10.4.1. A purge flow design was selected, which allows active control of the impurities and coolant chemistry in the purge stream and, at the same time, creates two barriers, the breeder plate clad and the steam generator wall, which reduce bred tritium loss through the steam generators. The lithium breeder design is presented in Section 8.10.4.2. The tritium bred in the lithium tubes is extracted in the lithium stream. The potentially large influx of tritium from the first wall into the main coolant stream of helium can be handled by the already existing helium cleanup system. The FLiBE/Be design is presented in Section 8.10.4.3. Because of the relatively low tritium solubility of FLiBe, most of the bred tritium will be extracted from the main coolant stream of helium.

8.10.4.1 Solid Breeder Designs

Steady-State Tritium Inventory and Permeation Losses

In the helium-cooled solid breeder blanket designs (Li_2O and $LiAlO_2$/Be), the bred tritium is extracted by a purge stream of helium through the solid breeder plates. This tritium extraction method permits positive control of tritium and impurity levels in the purge helium stream. Both of these levels have direct impacts on the blanket tritium migration and inventory. The purge flow loop was selected to operate at a helium pressure of 1 atm (compared with the main helium coolant pressure of 50 atm) to reduce the effect of clad-to-breeder contact resistance and to prevent distortion of the breeder cladding in case of blanket module depressurization. This section describes the TRIT4 code which was used for the calculation of tritium inventory and migration in the solid breeder blankets.

The release of tritium generated in the solid breeder to the extraction system (purge gas) is a critical concern for tritium recovery and inventory. The TRIT4 code developed at GA Technologies Inc., models the migration and

inventories of tritium in the breeder, purge helium loop, coolant loop, and steam generator loop at equilibrium.

The model assumed in the breeder is as follows:

1. Bulk diffusion was taken as the dominant mechanism for the migration of tritium from the solid breeder grains (100% theoretical density) to the grain boundaries. Temperature-dependent bulk diffusion coefficients for Li_2O and $LiAlO_2$ are given in Section 5.3.2. To minimize the diffusive tritium inventory contribution from $LiAlO_2$, a small grain size of 0.2 μm diameter was selected for the reference design. On the other hand, in order to reduce the solubility tritium inventory from Li_2O, its grain size was selected to be 20 μm in diameter. This choice would reduce the effect of high tritium partial pressure in the center of the pellet due to porous diffusior.

2. It was assumed that the release of tritium from grain boundaries to open pores in the breeder pellet occurs much faster than the mean bulk diffusion time. For the reference designs, potential surface inventory contribution as discussed in Section 5.3.3 is considered to be negligible when hydrogen is added into the helium purge stream as a means of controlling tritium leakage.

3. Through porous diffusion in the pellet, the bred tritium can then migrate out to the surface of the pellet into the purge stream. Only the effect of concentration diffusion was used in the porous diffusion calculation. The temperature effect on porous diffusion was found to be negligible and the pressure gradient effect on diffusion was consequently neglected. The release of T_2O from the grains and porous diffusion through the purge gas in the pores is included in the calculation. The appropriate mass transport properties are calculated allowing for Knudsen, transition, or ordinary diffusion in the pores of the breeder pellets. The tritium is then released from the breeder pellet to the purge gas stream.

4. The model calculates the temperature profile in the breeder pellet and the pressure and concentration distributions of T_2O in the pores of the breeder. The reduced thermal conductivities of Li_2O and $LiAlO_2$ due to high neutron fluence as indicated in Section 5.3.2 were used in the calculations. The temperature and pressure distributions were then used in the calculation of solubility and bulk diffusion inventories.

5. Experimentally determined activities[8.10-13] were used in the determination of breeder solubility inventory of LiOT in Li_2O as a function of temperature. Solubility tritium inventory in the $LiAlO_2$ was assumed to be negligible.

6. The pellet was assumed representative of the entire breeder and therefore, an average volumetric heating rate and an average volumetric tritium generation rate were used in the calculation.

The tritium inventories in the coolant and in the piping, and the permeation release rates were determined by iteration through the purge and coolant loops until equilibrium was reached. The coolant inventories in different purge/coolant segments were then determined as products of tritium concentration in the gas streams and gas volumes, respectively. Gas channel tritium inventories on metal surfaces were calculated by using the solubility data of stainless steel and the corresponding temperatures in different segments of the blanket loop. For the tritium permeation calculations, the permeability data for HT-9 as given in Section 6.6 was used. With the addition of hydrogen to the purge stream side, a barrier factor of 100 was used to account for the oxide barrier on the helium coolant side of the breeder cladding. At the steam generator, a barrier factor of 200 was used to account for oxide barriers on both sides of the wall separating the helium and water streams.

Tritium inventories for Li_2O and $LiAlO_2$/Be blankets for both tokamak and TMR reactors were calculated and the results are summarized in Table

8.10-32. As can be noted, all the tritium inventories are dominated by contributions in the breeders. For the Li_2O designs, the breeder inventories are dominated by solubility contributions. For the $LiAlO_2$ designs, the breeder inventories are dominated by bulk diffusive contribution in the breeder. The total inventories are in the range of 24 to 134 gm, which are quite acceptable.

Tritium permeation losses for these designs are presented in Table 8.10-33. Four cases were considered for different solid breeder designs of interest. Case 1 is the permeation losses when 1% of the tritium in the purge stream is assumed to be in the form of gaseous T_2. The leakages to the steam generator are high at >100 Ci/day. The losses increase if all the tritium in the purge stream is in the gaseous form, as indicated in Case 2. Case 3 shows how the leakage can be reduced to an acceptable level by the addition of hydrogen in the purge stream. All the leakage rates are <100 Ci/day. Further adjustments can be made by changing the amount of hydrogen added. Case 4 shows the reference cases when the influx of tritium from the first wall is going into the helium coolant streams. The leakages are higher than expected, yet they are still less than 100 Ci/day. Further studies will be needed to quantify the losses when better permeability and tritium coolant loop chemistry under a fusion environment is available. Reliable tritium barriers on metallic surfaces can be developed to relieve the problem.

Purge Flow Design - Solid Breeder - HT-9

In the helium-cooled solid breeder blanket designs (Li_2O, $LiAlO_2$/Be), the bred tritium is extracted by a purge stream of helium through the solid breeder plates. The general module configurations are given in the respective report sections for the Li_2O (tokamak and TMR) and $LiAlO_2$/Be (tokamak and TMR) designs. Figure 8.10-16 illustrates the schematic of the proposed purge breeder plate design. The connector mounts double as the helium purge flow inlet/outlet channels. The purge flow enters the purge plate, whence it flows along the plenum at one end of the plate. It then flows axially along the plate through the purge channels as illustrated in Fig. 8.4-1 for the

TABLE 8.10-32
SELECTED INPUTS/OUTPUTS FOR THE HELIUM-COOLED SOLID BREEDER BLANKET TRITIUM INVENTORIES

	Tokamak		TMR	
	Li_2O	$LiAlO_2$/Be	Li_2O	$LiAlO_2$/Be
Reactor thermal power, MW	5382	5499	2958	3106
Tritium production rate, gm/day	897	897	562	567
Breeder mass, 10^3 kg	519	522	494	512
Tritium inventories,[a] gm				
Breeder - Diffusive	0.04	38.3	0.02	24.1
- Solubility	133.6	Negligible	130.7	Negligible
- Porous	0.04	0.04	0.04	0.04
Metal	0.28	0.08	0.23	0.08
Helium coolant	0.33×10^{-4}	0.11×10^{-4}	0.38×10^{-4}	0.13×10^{-4}
Total, gm	134	38.4	131	24.2

[a]Hydrogen is added into the purge stream at the rate of 100 times the mass generation rate of tritium.

TABLE 8.10-33
HEAT EXCHANGER TRITIUM LOSSES (Ci/Day)

	Case 1 1% T_2	Case 2 100% T_2	Case 3[a] 100% T_2 H_2 Added in Purge Stream	Case 4[b] 100% T_2 H_2 Added + T_2 in Leakage From First Wall
Tokamak				
Li_2O/He	396	1,260	39.8	43.6
$LiAlO_2$/Be/He	177	566	18	24.0
Mirror				
Li_2O/He	372	1,180	37.3	40.5
$LiAlO_2$/Be/He	133	424	13.4	27.6

[a]Hydrogen is added into the purge stream at a rate equal to 100 times the mass generation rate of tritium; barrier factors of 100 and 200 assumed on the breeder clad and steam generator wall, respectively.

[b]T_2 added from first wall - 0.22 gm/day for tokamak reactor and 0.2 gm/day for mirror reactor.

TABLE 8.10-34
PURGE FLOW DESIGN CHARACTERISTICS
HELIUM-COOLED SOLID BREEDER

	Tokamak		Mirror	
	Li_2O	$LiAlO_2$/Be	Li_2O	$LiAlO_2$/Be
Reactor thermal power, MW	5382	5499	2958	3106
Coolant Helium				
Pressure, MPa (atm)	5 (50)	5 (50)	5 (50)	5 (50)
T_{in}/T_{out}, °C	275/510	275/510	275/540	275/540
Volume flow rate, m^3/s	1468	1500	716	751
Purge Helium				
Pressure, MPa (atm)	0.1 (1.0)	0.1 (1.0)	0.1 (1.0)	0.1 (1.0)
Volume flow rate, m^3/s	14.7	15	7.2	7.5
Purge flow channel				
Volume fraction % per breeder plate	2	2	2	2
Flow velocity, m/s	4	5.4	3.3	4.3
Flow frictional[a] pressure drop, Pa (psi)	1690 (0.24)	2939 (0.43)	1255 (0.18)	1953 (0.28)

[a] A purge flow channel length of 2 m was assumed.

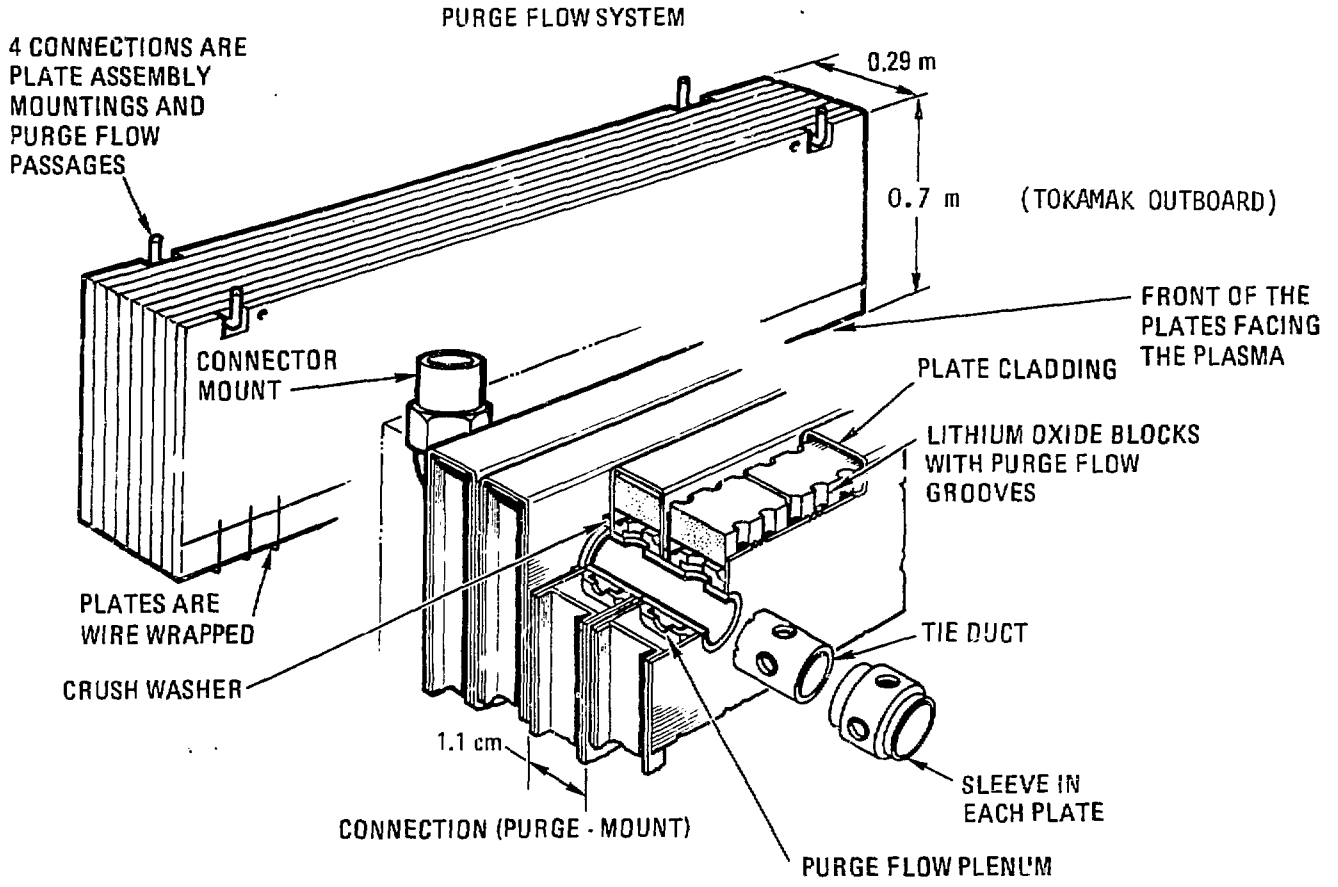

Figure 8.10-16. Purge flow system.

Li_2O designs. A similar arrangement is also selected for the $LiAlO_2$/Be designs.

The purge channel spacing was determined such that the porous diffusion path in the pellet would not be too long, in order to minimize purge flow tritium partial pressure. The channel size of 1.5 mm diameter was selected to ensure that the pressure differential between the purge and main coolant helium stream of 4.9 MPa (49 atm) would not fail the 0.25 mm HT-9 clad. As can be seen in Fig. 8.10-17, the purge flow channels are located at the edge of the plate so that the purge flow operates at the lower temperature region of the pellets in order to minimize mass transfer (which could be a significant problem for the Li_2O design at temperatures above approximately 800°C).

To check that the purge flow design is acceptable, the flow velocities and frictional pressure drops for the solid-breeder purge flow designs were calculated. The results are summarized in Table 8.10-34. The purge flow velocities are relatively high, yet acceptable; the frictional pressure drops for the 2 m long breeder plates are also acceptable for all the solid breeder helium-cooled designs.

We conclude from our purge fluid-flow analysis that the purge flow design is feasible. More detailed study is needed to describe the complete purge and extraction loop. At the same time, the effect of breeder thermal stress and the problem of breeder/clad mechanical interaction needs to be addressed. The mass transfer of solid breeder in the purge flow channels should also be considered in future designs.

8.10.4.2 Li/He Designs

Tritium management of the Li/He blanket designs consists of circulation of the liquid lithium and optional slipstream cleanup of the primary coolant. The tritium generated within the liquid lithium is recovered by slow circulation of the lithium to the tritium recovery system. Tritium can be extracted from the Li either by circulation to a yttrium bed at 450°C, extracting to

the 1.3 wppm level, or by molten salt extraction to the 1.0 wppm level. The latter was used for the reference design. Tritium which enters the primary coolant via the first wall is recovered two ways. First, by maintaining a sufficiently low tritium partial pressure in the lithium tubes, some of the tritium will permeate from the helium into the coolant and be recovered as described above. Second, if necessary, additional tritium can be recovered by the primary coolant slipstream cleanup system.

The requirements on the tritium management system are established by the safety guidelines adopted by this study. Since the majority of the tritium is recovered by circulation of the lithium, the safety guideline on tritium inventory trades off against the acceptable MHD pressure drop and diminishing returns on extraction efficiency. Since the only nonrecoverable tritium permeation loss is through the primary heat exchanger, the safety guideline on steam generator leakage trades off against the size and cost of the helium cleanup system. The resultant tritium management system design parameters are shown in Table 8.10-35.

The table shows that the tritium inventory can be kept to 330 gm via circulation of the lithium at rates of 0.092/0.12 m^3/s for the tokamak/TMR. The associated MHD pressure drops are 1.01/0.2 MPa. Faster circulation increases the pressure drop, but the inventory does not drop appreciably due to the partial pressure corresponding to the assumed minimum achievable tritium concentration of 1.0 wppm in Li. The table also shows that steam generator tritium loss rates of 16.1/10.2 Ci/d for the tokamak/TMR are achieved without any slipstream processing of the main helium flow. These losses include the influx of tritium from the first wall at 0.22 gm/day and 0.2 gm/day for the tokamak and TMR, rexpectively. More details on tritium influx from the first wall are given in Section 6.6. To obtain these steam generator leakage rates, hydrogen was added in the main helium coolant (for isotopic dilution) at the rate of 100 times of the first wall tritium influx rate. This reducing atmosphere inhibits the formation of the oxide scale on the helium side of the blanket and heat exchanger tubes. A barrier factor of two is assumed in the calculations.

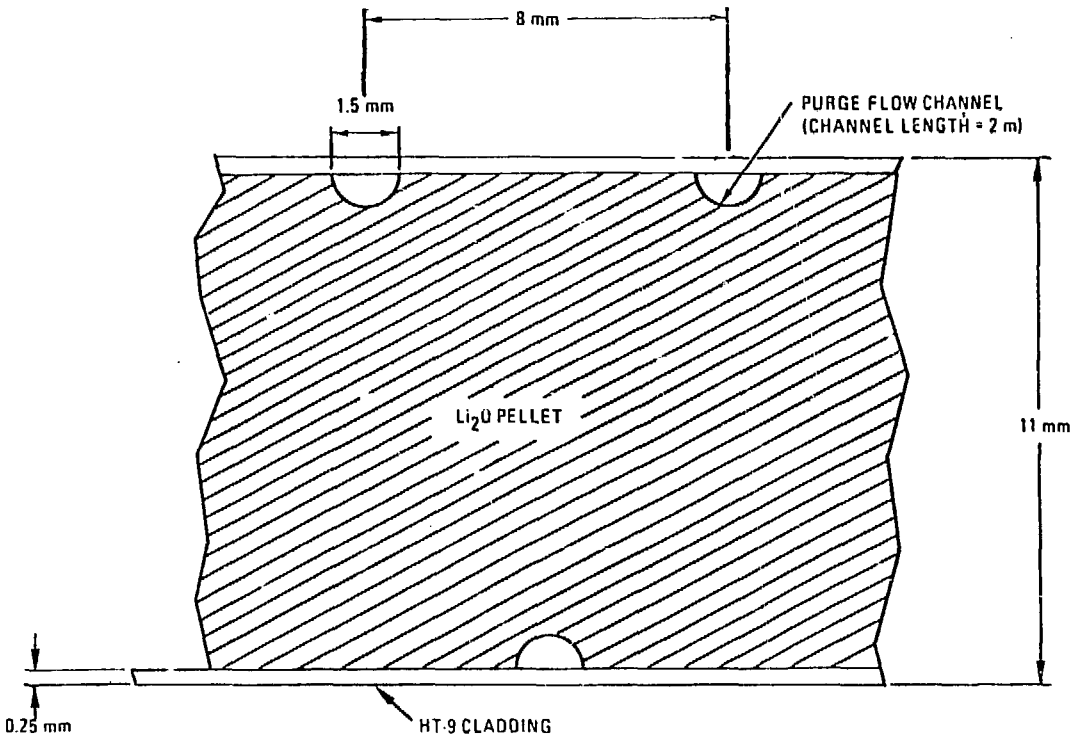

Figure 8.10-17. Details of the purge flow dimensions of the Li_2O - tokamak purge flow design.

TABLE 8.10-35
Li/He BLANKET TRITIUM MANAGEMENT
SYSTEM DESIGN PARAMETERS

	Tokamak	Tandem Mirror
Tritium production rate, g/day	973	533
Percentage of tritium in element form, %	100	100
Blanket heat transfer area, m^2	3.67×10^4	3.84×10^4
Heat transfer wall thickness, mm	1.1	1.1
Heat transfer wall temperature, °C	565	565
Li tube oxide barrier factor from the helium side	2	2
Primary coolant mass, kg	3.2×10^4	1.8×10^4
Tritium inventory in primary coolant, g	1.0×10^{-6}	4.8×10^{-7}
Tritium leakage to primary coolant (from first wall), g/day	0.22	0.2
Hydrogen addition to primary coolant, g/day	22	20
Tritium partial pressure in primary coolant, Pa	1.1×10^{-7}	9.3×10^{-8}
Hydrogen partial pressure in primary coolant, Pa	1.1×10^{-5}	9.3×10^{-6}
Primary coolant flow rate, l/s	1.5×10^6	8.3×10^5
Clean-up by-pass fraction, %	0	0
Clean-up efficiency, %	0	0
Tritium leakage from primary coolant to breeder tubes, Ci/day	2096	1910
Steam generator surface area, m^2	4.1×10^4	2.3×10^4
Steam generator wall thickness	2	2
Steam generator temperature, °C	510	540
Steam generator wall oxide barrier factor[a] (total from two sides)	102	102
Tritium leakage rate, Curie/day	16.1	10.2
Tritium recovery method	Li circulation to molten salt tritium extraction to 1.0 wppm	

TABLE 8.10-35 (Continued)

	Tokamak	Tandem Mirror
Extraction efficiency, %	20	10
Maximum tritium concentration in Li, wppm	1.25	1.11
Maximum tritium partial pressure in Li, Pa	8.7×10^{-8}	6.9×10^{-8}
Minimum tritium partial pressure (@1.3 wppm) in Li, Pa	5.6×10^{-8}	5.6×10^{-8}
Average effective tritium partial pressure in Li, Pa	7.1×10^{-8}	6.2×10^{-8}
Li inventory, m^3	590	640
, kg	2.9×10^{5}	3.1×10^{5}
Tritium inventory in Li (based on average effective partial pressure), g	330	330
Li flow rate (reactor), m^3/s	0.092	0.12
MHD pumping ΔP, MPa	1.01	0.2

[a]Barrier factors of 2 and 100 were assumed on the helium and water sides of the steam generator wall.

8.10.4.3 Tritium Permeation and Recovery for the Flibe/He Blanket Design

A study of tritium permeation and recovery for molten salt for the fusion breeder is reported in Ref. 8.10-14. The results are directly relevant to the fusion electric case. This study assumes tritium to be a gas dissolved in molten salt, with TF formation suppressed. Tritium permeates readily through the hot steel tubes of the reactor and steam generator and will leak into the steam system at the rate of about one gram per day in the absence of special permeation barriers, assuming that 1% of the helium coolant flow rate is processed for tritium recovery at 90 % efficiency per pass. Tritiated water in the steam system is a personnel hazard at concentration levels well below one part per million and this level would soon be reached without costly isotopic processing. Alternatively, including a combination of permeation barriers on reactor and steam generator tubes and molten salt processing is estimated to reduce the leak rate into the steam system by over two orders of magnitude. For the option with the lowest estimated leak rate, 55 Ci/d, it may be possible to purge the steam system continously to prevent tritiated water buildup. At best, isotopic separation of dilute tritiated water may not be necessary and for higher leak-rate options the isotopic processing rate can be reduced.

The proposed permeation barrier for the reactor tubes is a 10 μm layer of tungsten which, in principle, will reduce tritium blanket permeation by a factor of about 300 below the bare-steel rate. A research and development effort is needed to prove feasibility or to develop alternative barriers. The partial pressure of tritium gas dissolved in molten salt is high, easing the recovery process for which a flash-separator has been chosen. A 1 mm aluminum sleeve is proposed to suppress permeation through the steam generator tubes. This gives a calculated reduction factor of more than 500 relative to bare steel, including a factor of 30 due to an assumed oxide layer.

To gain a better understanding of permeation effects, equations describing steady-state tritium permeation without axial flow have been derived for a multi-layer tube wall within the blanket region. A layer of frozen salt is included, along with fluid boundary-layer resistances. Calculations of the partial-pressure distribution show significant differences for tubes irradiated at different power densities. Molten salt boundary-layer resistance can be important in the absence of a good

permeation barrier, or for a low-power tube coated with a nominal 1 μm tungsten barrier. Permeabilities of various metals are shown in Fig. 8.10-18. This nominal permeation barrier will dominate the flow resistance, however, for medium or high power-density tubes closer to the first wall. Examination of the radial flux equation shows a complicated dependence on upstream partial pressure, which reduces to a linear dependence at low pressures where Henry's Law materials become flux limiters and a square-root dependence at high tritium partial pressures where Sievert's Law materials are flux limiting.

An analytical model has been developed to establish the tritium split between wall permeation and reactor-tube flow. Permeation barriers are shown in Fig. 8.10-19. The barriers are shown on the outside of the tubes but could equally well be on the inside. For the molten salt tubes the inside barrier would greatly reduce the tritium inventory in the tube walls and further reduce the already very low corrosion rate. The tritium fraction escaping through the tube walls has been quantified for limiting cases of Henry's Law and Sievert's Law barriers as flux limiters. All parameters of design interest are explicitly included: tritium generation rates and solubility in salt, tube geometry, barrier permeation parameters, and molten salt processing rate and recovery efficiency.

The intermediate helium heat transfer loop has been treated as a well-mixed tank for analytical purposes, with input from the reactor, partial tritium recovery in a slipstream process loop, and Sievert's Law permeation loss to the steam system.

A combination of effective tritium permeation barriers are required on both blanket and steam generator tubes together with substantial process rates for molten salt and helium systems, in order to hold tritium permeation into the steam system to 55 Ci/d. If this can be done, it may be feasible to simply purge the steam system of incoming tritium with only minor environmental impact and personnel hazard from steam leaks, and without the necessity of costly and hazardous isotopic processing to separate tritiated and ordinary water.

A surprisingly thin (10 μm) tungsten coating will, in principle, provide a good permeation barrier on the blanket tubes. The feasibility of, in fact, reducing tritium blanket permeation by a factor of 300 or so below the bare steel tube rate for some 10^4 m^2 of tube area will require a

research and development effort. Other materials or alloys may prove to be superior, probably at the price of greater thickness of coating.

A relatively thick 1 mm aluminum sleeve was selected to suppress permeation through the steam generator tubes. This gave a calculated reduction factor of more than 500 relative to bare steel, including a factor of 30 due to an assumed oxide layer. This is essentially a brute force approach that may well be improved upon by the development of more sophisticated permeation barriers.

Although we have focused attention on a tungsten barrier due to a remarkably low tritium permeability, beryllium and other low-permeability materials such as ceramics and cermets should be considered in a barrier development problem.

The tritium recovery system flow sheet is shown in Fig. 8.10-20. Due to the low solubility of tritium in the reducing salt, a simple flash separator will allow removal of the tritium and other noncondensible gases, mainly helium. Tritium removal from helium is virtually a standard system. The bulk of the tritium is recovered as a hybride on a getter bed, with final cleanup accomplished by catalyzed oxidation and adsorption.

The diffusivity of tritium gas dissolved in molten salt will need to be measured, especially to verify whether or not the fluid boundary-layer barrier is realistic.

Finally, some definitive experimental work on the kinetics of tritium gas conversion to tritiated water at low concentrations in helium is called for. Popular opinion has oscillated over the last decade from an initial optimism that thermodynamics would reduce the gas concentration to nil, to a current pessimism that predicts no gas conversion at all in the main helium loop. The critical experiments remain to be done, both with "clean" walls and particulate-free helium, and in the presence of catalytic surfaces or other reaction promoters. The challenge is to demonstrate a method of drastically reducing tritium gas partial pressure in the intermediate helium loop, and thus suppress permeation into the steam system.

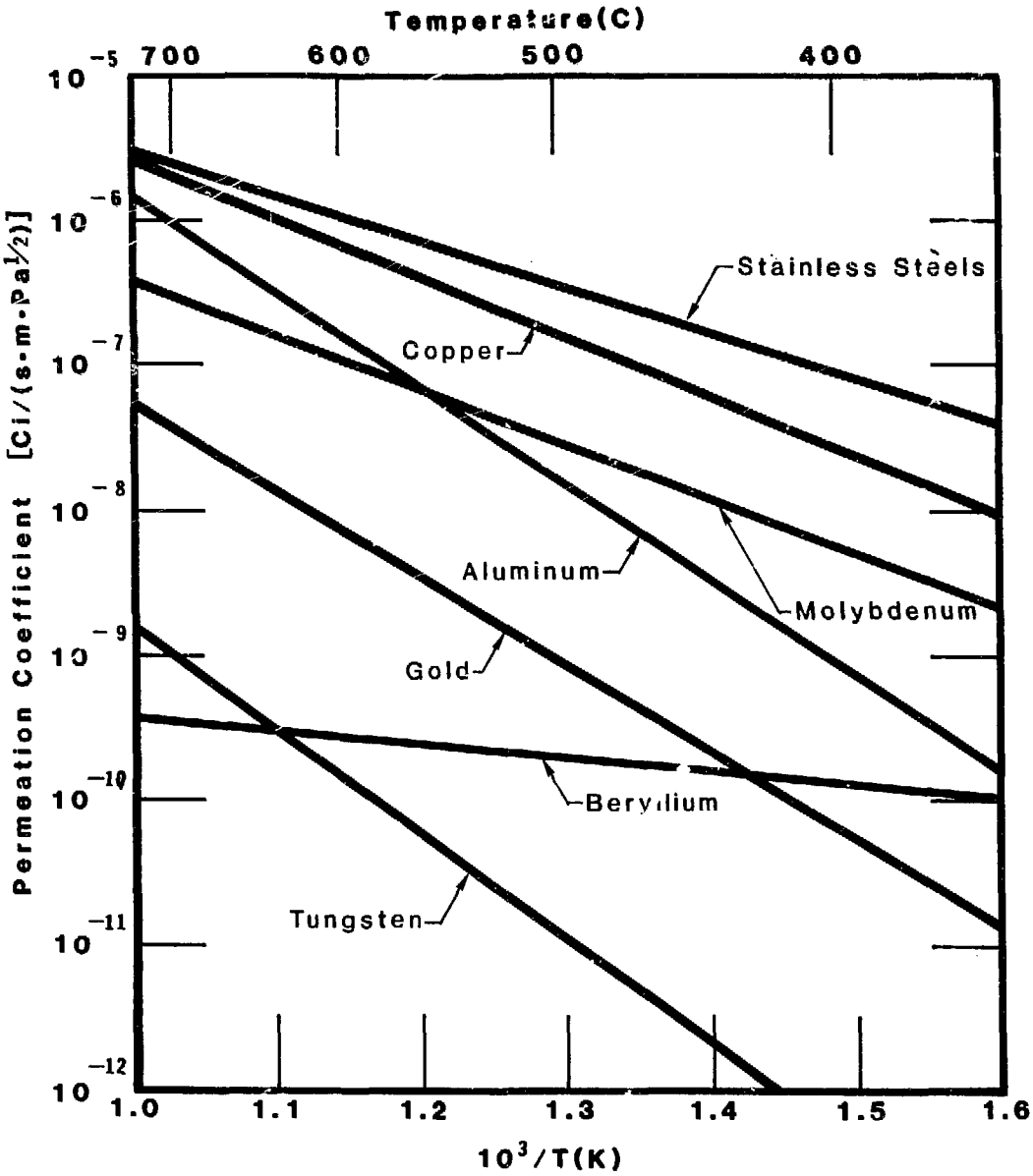

Figure 8.10-18

Permeation coefficient of tritium through metals.

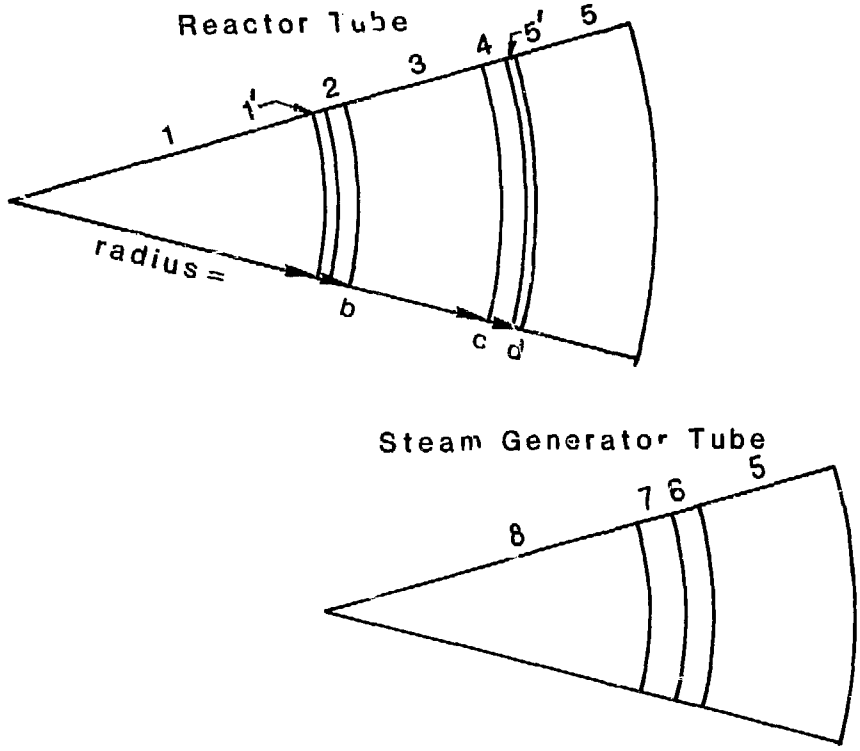

Figure 8.10-19

Permeation Geometry and Materials.

Reactor Tube:

1	molten salt
1'	molten salt boundary layer
2	frozen salt
3	stainless steel tube
4	permeation barrier (tungsten)
5'	helium gas boundary layer
5	helium gas

Steam Generator Tube:

5	helium gas
6	stainless steel tube
7	permeation barrier (aluminum)
8	water/steam

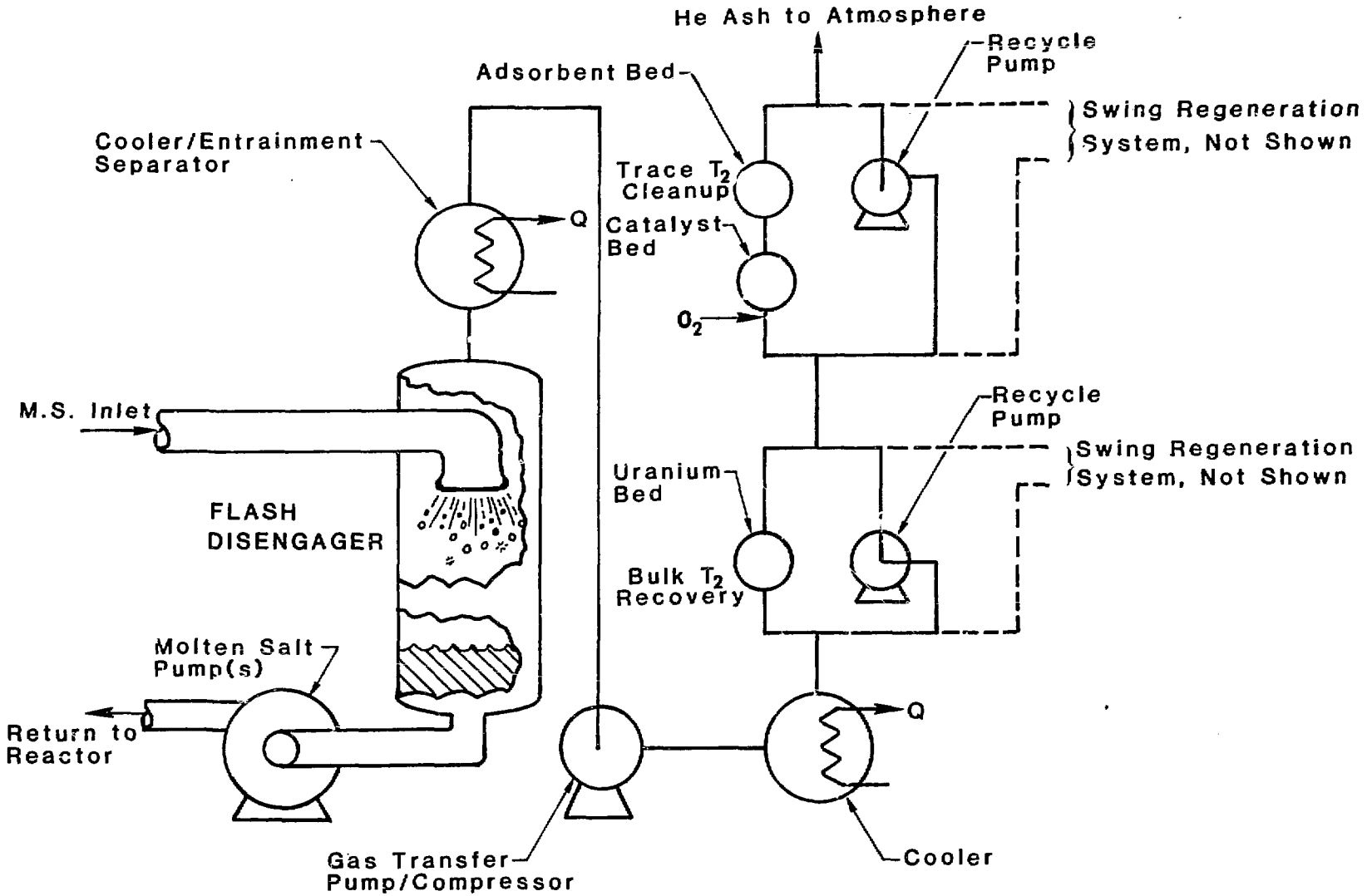

Figure 8.10-20. Molten salt tritium processing

8.10.4.4 Tritium Inventory/Containment Structure Corrosion in Oxidized FLIBE Environment

In the FLIBE breeder design, the tritium which is produced can be reduced to T_2 in the presence of added beryllium. The reaction which occurs is,

$$2\ TF + Be \rightarrow T_2 + BeF_2 \qquad (8.10\text{-}1)$$

In the absence of beryllium, the tritium is expected to exist as the positive tritium ion.[8.10-15] An advantage of having tritium ion rather than tritium in the FLIBE is the lower partial pressure of T_2 that would exist.[8.10-16] In a reducing salt, partial pressures of tritium can reach 0.1 atm while in an oxidizing salt, the partial pressure of tritium will be less than 10^{-15} atm (partial pressures of TF will be around 10^{-2} atm). Therefore lower permeation rates are expected in situations where tritium ion rather than tritium exists in the FLIBE breeder tubes, and the potential problem of excessive tritium leakage might be avoided.

Besides tritium leakage, another major problem is the corrosion by tritium ion of the FLIBE containing tubes. To determine the magnitude of corrosion, a computer program was written to keep track of the produced tritium. The tritium ion can diffuse to the wall of the FLIBE containing tube, where it is reduced, while at the same time, the wall material is oxidized (i.e., corrosion of the wall occurs). The tritium then permeates through the wall and into the helium coolant stream.

The fraction of tritium which diffuses to the wall is a function of the rate at which FLIBE is circulated through the blanket tube. There are two reasons for this. First of all, if it assumed that the tritium is reduced immediately as it reaches the wall, then the rate of transport of tritium to the wall is a function of the FLIBE velocity. In terms of the Nernst boundary layer model, higher velocities decrease the boundary layer thickness across which tritium must diffuse in order to reach the tube wall. The second reason is due to the fact that tritium is volumetrically produced in the FLIBE. Therefore, its bulk concentration is a function of the FLIBE residence time. The bulk concentration determines the driving force for mass transfer. Therefore, the longer the residence time, the greater the bulk concentration or driving force for mass transfer.

The computer program takes into account these considerations as it keeps track of the produced tritium and the extent of the wall recession. The mathematical model upon which it is based derives from a mass balance over a differential length of blanket tube. Included in the mass balance is a term containing a mass transfer coefficient. This mass transfer coefficient is calculated by the program using available engineering correlations.(8.10-17) The parameters and values investigated using the computer model are listed in Table 8.10-36. Note that a peak tritium breeding rate of $2 \cdot 10^{-10}$ g/s is expected in the BCSS FLIBE breeder blanket.

Figure 8.10-21 shows the tube wall recession rate as a function of temperature and FLIBE velocity. For FLIBE velocities of 0.1 cm/s the wall recession rate is about 10 μm/year, while at FLIBE velocities of 10 cm/s, the wall recession rate is less than 1μm/year. Either value is acceptable with respect to tube wall recession over 5 years. This behavior appears to contradict the Nernst boundary layer theory which would predict a mass transfer increase with increasing FLIBE velocity. However, the rate of mass transfer is also a function of the bulk concentration and the bulk concentration is a function of the FLIBE residence time (i.e., the FLIBE velocity). As FLIBE residence time is decreased (FLIBE velocity increased), bulk tritium ion concentrations should also decrease. Figure 8.10-22 shows the computer model predictions of how the bulk concentration of tritium in FLIBE decreases with increasing FLIBE velocity. It is assumed that tritium removal outside of the blanket is 100% efficient. The decrease in bulk tritium concentration due to an increase in FLIBE velocity more than balances the corresponding decrease in mass transfer resistance at the tube wall, and thus causes a decrease in tube wall recession rate.

The fraction of tritium which remains in the FLIBE blanket tube (i.e., the fraction which does not permeate into the helium purge stream), was also determined and the results are shown in Fig. 8.10-23. At a FLIBE velocity of 1.0 cm/s, about 5% of the produced tritium will permeate into the helium coolant stream while at a FLIBE velocity of 10 cm/s, only 1% of the produced tritium will permeate into the helium.

Outlines of two processing schemes to remove tritium from the FLIBE are shown in Fig. 8.10-24 and Fig. 8.10-25. In the first scheme (Fig. 8.10.4.3.4), the TF is outgassed into helium at low pressure from the FLIBE salt. The TF is then passed through a water scrubber where it is absorbed.

Electrolysis then removes the tritium from the water. In the second scheme (Fig. 8.10-25), tritium is reduced to T_2 which is then outgassed. An advantage of T_2 outgassing over TF outgassing is the higher partial pressure of T_2 which develops over the FLIBE. The T_2 is then oxidized to T_2O in an oxygen containing helium carrier gas. The tritiated water is then condensed and electrolyzed. Details of these processing schemes are further described in Reference 8.10-16.

Table 8.10-36. Parameters and Values Investigated using TRIFLIB

Parameter	Values Investigated
Tube diameter	2.8 cm
Tube length	700 cm
Temperature	500°C, 600°C
Tritium production rate	2×10^{-9} g/cc-sec
	2×10^{-10} g/cc-sec
	2×10^{-11} g/cc-sec
Velocity	0.1, 1, 10 cm/sec

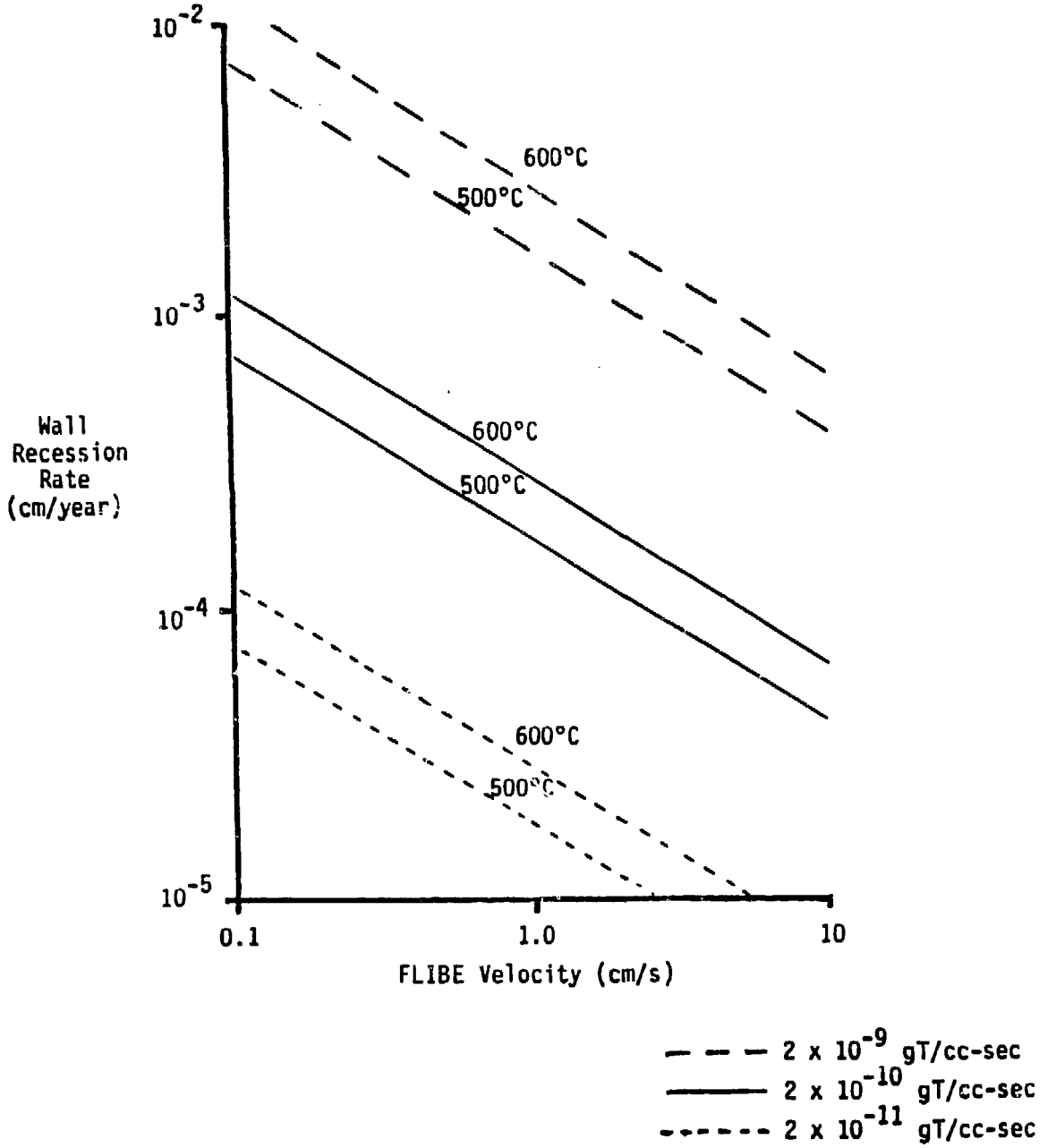

Figure 8.10-21. Wall Recession Rate as a Function of Wall Temperature FLIBE Velocity and Tritium Production Rate

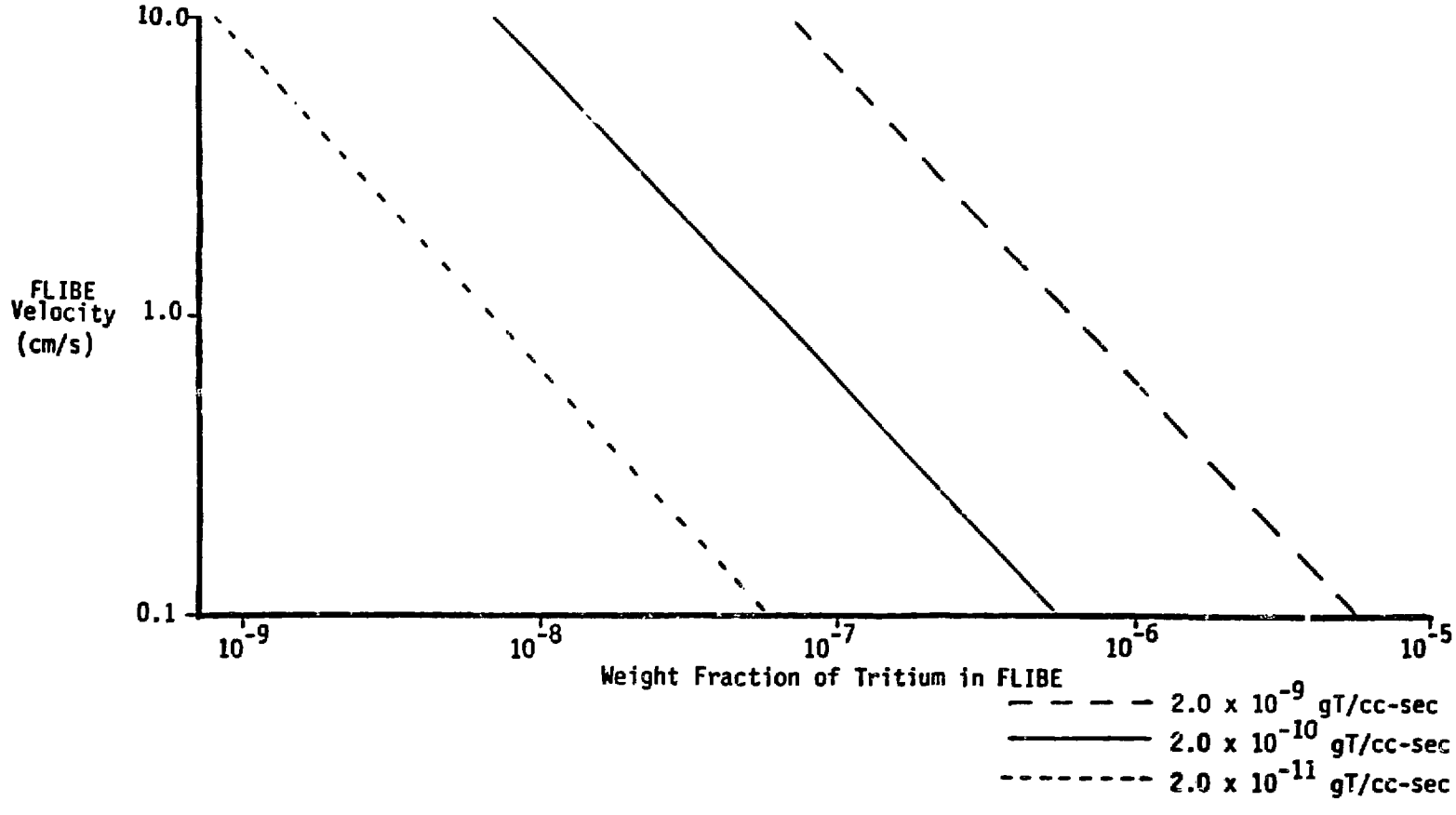

Figure 8.10-22. Bulk weight fraction of tritium in FLIBE exit stream as a function of FLIBE velocity and tritium production rate. 500°C and 600°C cases essentially fall on the same line. Natural and forced convection has been considered.

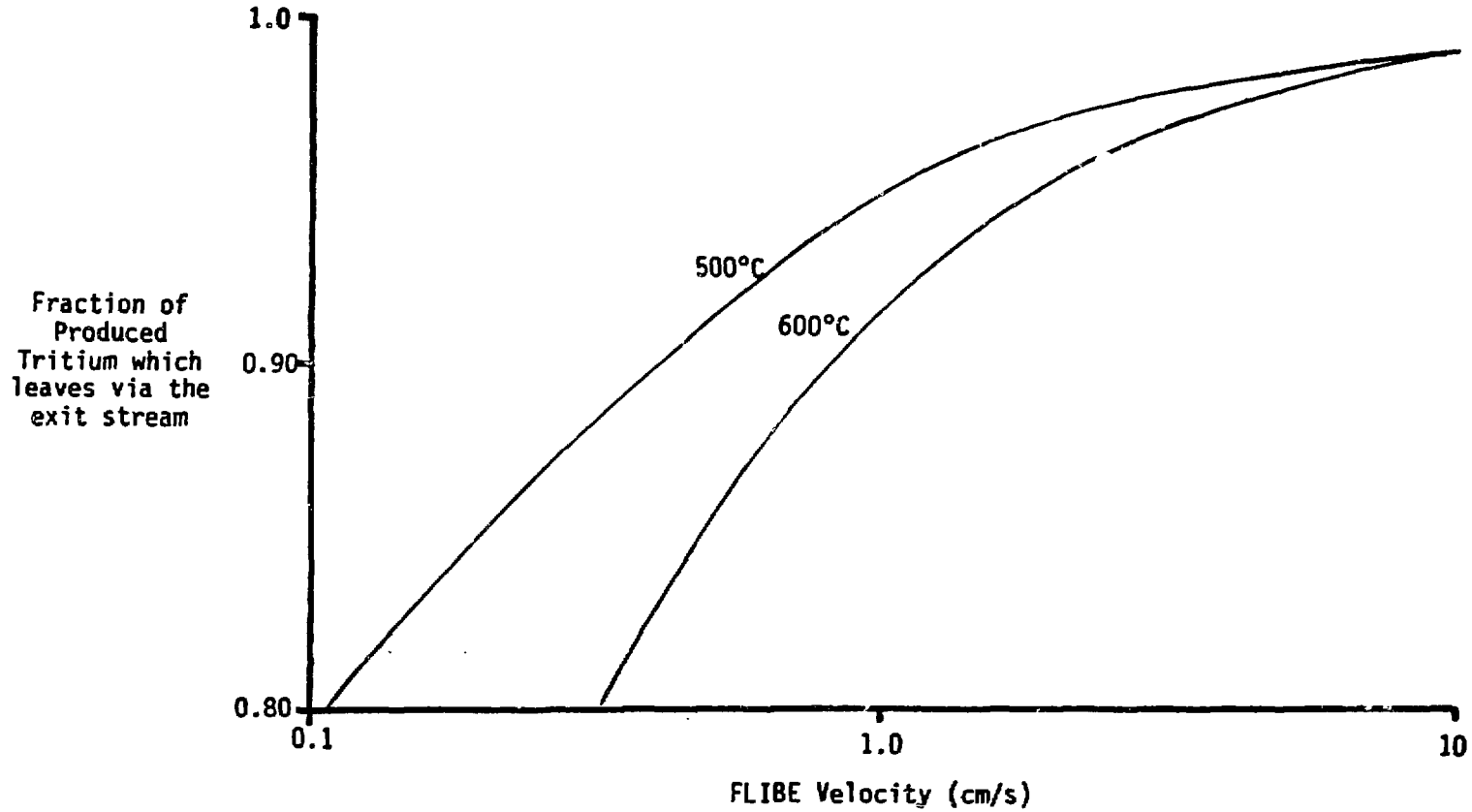

Figure 8.10-23. The velocity dependence of the fraction of produced tritium leaving the blanket tube via the FLIBE exit stream. The above curves are essentially independent of tritium production rate.

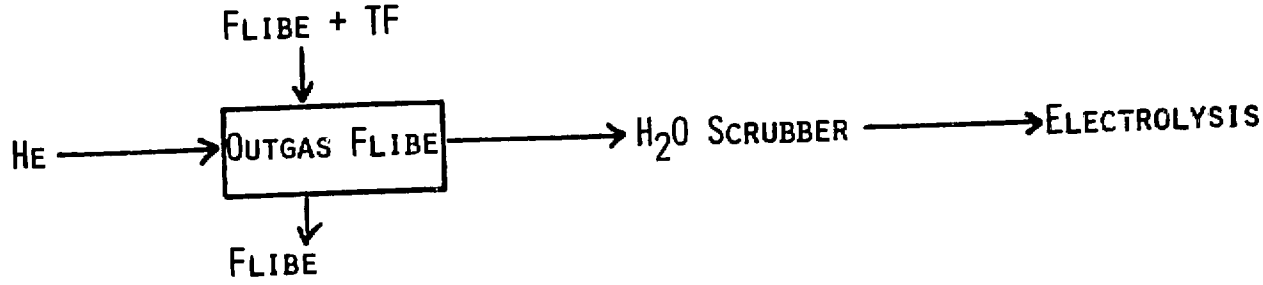

Figure 8.10-24. TF Processing Scheme

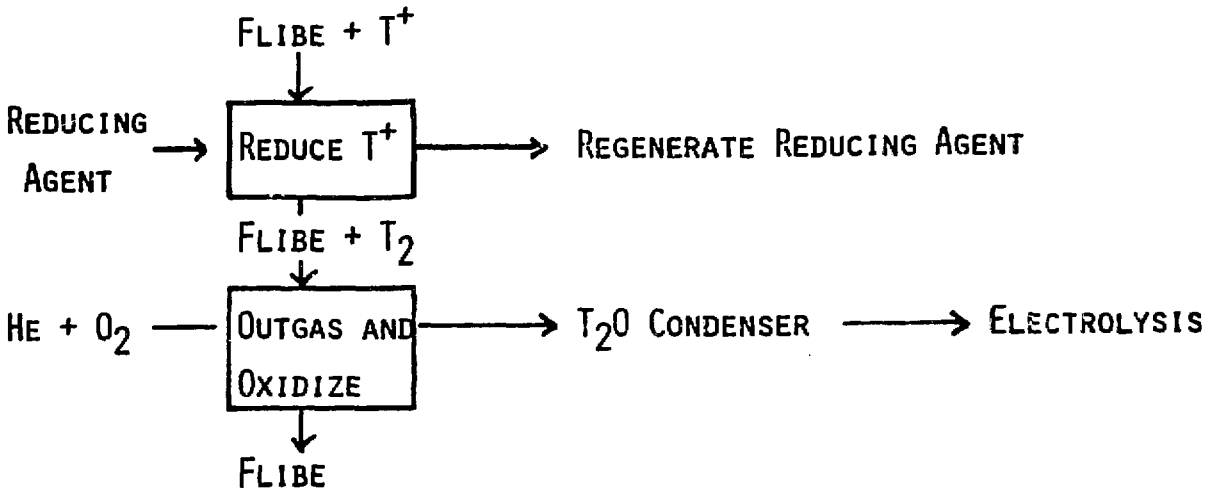

Figure 8.10-25. T^+-T_2 Processing Scheme

References

8.10-1. "Blanket Comparison and Selection Study," ANL/FPP-83-1, October, 1983.

8.10-2. J.J. Johnson, "MODSAP - A Modified Version of the Structural Analysis Program SAP4 for the Static and Dynamic Response of Linear and Localized Nonlinear Structures," GA Technologies Report, GA-A14006, UC-77 (January 1980).

8.10-3. C. Bharman and F. Tsung, "TEPC-2D - A Two-Dimensional Finite Element Computer Program for Thermal-Elastic-Plastic-Creep Analysis," GA Technologies Report, GA-A12753 (1974).

8.10-4. T.A. Lechtenberg and C.F. Dahns, "Magnetically-Induced Forces on a Ferromagnetic HT-9 First Wall/Blanket Module," Proceedings of the Third Topical Meeting on Fusion Reactor Materials, Albuquerque, NM, September 1983.

8.10-5. W.W. Engle, Jr., "A User's Manual for ANISN, A One-Dimensional Discrete Ordinates Transport Code with Anisotropic Scattering," K-1693, Oak Ridge Gaseous Diffusion Plant (1967).

8.10-6. R.W. Roussin, et al., "VITAMIN-C: The CTR Processed Multigroup Cross Section Library for Neutronics Studies," ORNL/RSIC-37 (DLC-41), Oak Ridge National Laboratory (1980).

8.10-7. Y. Gohar, M.A. Abdou, "MACKLIB-IV, A Library of Nuclear Response Functions Generated with the MACK-IV Computer Program from ENDF/B-IV," ANL/FPP/TM-106, Argonne National Laboratory (1978).

8.10-8. R.E. MacFarlane, Los Alamos National Laboratory, private communication (1983).

8.10-9. C.P.C. Wong, Y.S. Yang, and K.R. Schultz, "Thermal-Hydraulics Design Comparisons for the Tandem Mirror Hybrid Reactor Blanket," ANS Topical Meeting on the Technology of Controlled Nuclear Fusion, King of Prussia, October 1980; also, GA Technologies Report, GA-A16069, September 1980.

8.10-10. M. Huggenberger, "Helium-Cooled, Solid Breeder Blanket Design for a Tokamak Fusion Reactor," GA Technologies Report, GA-A16308, April 1981.

8.10-11. Stephen Whitaker, "Fundamental Principles of Heat Transfer," Pergamon Press, Inc. (1977).

8.10-12. Sabri Ergun, "Mass Transfer Rate in Packed Columns," Chemical Engineering Progress, Vol. 48, No. 5 (May 1952).

8.10-13. J.H. Norman and G.R. Hightower, "Measurements of the Activity Coefficient of LiOH Dissolved in $Li_2O(s)$ for an Evaluation of Li_2O as a Tritium Breeder Material," Journal of Nuclear Materials 122 and 123, p. 913-920, 1984.

8.10-14. A.E. Sherwood, "Tritium Permeation and Recovery for the Helium-Cooled Molten Salt Fusion Breeder," Lawrence Livermore National Laboratory Report UCID-20141 (1984).

8.10-15. E.F. Johnson, "Fuel Handling," in A Fusion Power Plant, R.G. Mills, ed., pp. 362-409.

8.10-16. W.D. Bjorndahl and W.C. Wong, "Tritium Inventory in FLIBE and Corrosion of Blanket Tubes," Lawrence Livermore National Laboratory Report UCID-20149 (1984).

8.10-17. D.K. Edwards, V.E. Denny and A.F. Mills, Transfer Processes, Holt, Rinchart and Winston Inc., New York (1973) pp. 142-145.

8.11 Potential Design Improvements

Design is an iterative process. The analysis and evaluation of a first design inevitably leads to ideas on how to improve it, leading to the second design, and so on. In the BCSS, little time or resources were available for iteration of the designs. Further, some of the design criteria and evaluation procedures changed during the course of the BCSS. As a result, although we believe the designs presented are technically sound, we have found areas where these blanket designs can be improved. This section is a summary of potential design improvements for the R=1 ranking helium-cooled blankets, that we believe would result in improving the score of respective blanket concepts. Section 8.11.1 presents the design improvements of the helium-cooled Li_2O, Li and $LiAlO_2$/Be blankets.

8.11.1 Li_2O, Li and $LiAlO_2$/Be Blankets

Table 8.11-1 summarizes the potential improvements for the helium-cooled Li_2O, Li and $LiAlO_2$/Be blankets. They are grouped in the four areas of evaluation, which are engineering feasibility, economics, safety and R&D. The more significant impacts on improving the score of helium-cooled designs are in the areas of tritium breeding ratio (TBR), safety and economics.

Tritium breeding ratio is a major part of the Engineering Feasibility evaluation, comprising 25% of the total maximum possible score. The helium-cooled blankets received relatively low scores in this area because they were initially designed to achieve the minimum required one-dimensional TBR of 1.2. In retrospect, this did not provide adequate margin. The evaluation procedure that evolved eventually required a three-dimensional TBR of >1.3 to get maximum tritium breeding score. When the requirement for TBR margin is better defined and the related uncertainties are better understood, the importance of TBR in the engineering evaluation may be reduced. For the selected designs with the present evaluation procedure, different design

TABLE 8.11-1
POTENTIAL DESIGN IMPROVEMENTS FOR HELIUM-COOLED BLANKETS

	Li_2O		Li		$LiAlO_2$/Be	
	Tokamak	TMR	Tokamak	TMR	Tokamak	TMR
I. ENGINEERING FEASIBILITY						
1. Tritium Breeding Ratio (Estimated improvements on 3-D TBR are indicated)						
• Use of metallic reflector (~30 cm) in the blanket, while keeping similar total blanket and shield thickness.	~ 2%	~ 2%	NA[a]	NA	~ 1%	~ 1%
• Increase blanket thickness by 10 cm.	~ 2%	~ 2%	~ 4%	~ 3%	~ 6%	~ 6%
• Incorporation of Be into inboard blanket.	NA	NA	NA	NA	~ 6%	NA
• Use of homogenized design of Be/Li-compound, with high ^6Li enrichment and minimizing the amount of Li-compound volume fraction.	~15%[b]	~15%[b]	~15%[c]	~15%[c]	~15%[b]	~15%[b]
2. Power Variation						
• First wall finned design can be optimized to lower the maximum temperature to ~500°C - thus a higher power variation could be tolerated.[d]	✓	NA	✓	NA	✓	NA

TABLE 8.11-1 (Continued)

	Li_2O		Li		$LiAlO_2$/Be	
	Tokamak	TMR	Tokamak	TMR	Tokamak	TMR
II SAFETY						
1. Tritium Inventory						
• A more accurate description of the radial breeder temperature profile can reduce tritium inventory from the reference design.(e)	✓	✓	NA	NA	NA	NA
2. Tritium Leakage						
• More accurate description of steam-generator tubing temperature can reduce tritium leakage.(f)	✓	✓	✓	✓	✓	✓
• Smaller lithium tubes with larger surface to volume ratio and thinner walls can reduce tritium leakage to steam generator.	NA	NA	✓	✓	NA	NA
III ECONOMICS						
• Increased helium pressure from 50→80 atm can reduce pumping power fraction from 4%→1%, increasing net efficiency by approximately 3 percentage points.	✓	✓	✓	✓	✓	✓

TABLE 8.11-1 (Continued)

	Li_2O		Li		$LiAlO_2$/Be	
	Tokamak	TMR	Tokamak	TMR	Tokamak	TMR
• Metallic reflector can increase blanket energy multiplication.	✓	✓	NA	NA	✓	✓
• Thicker blanket can increase blanket energy multiplication.	✓	✓	✓	✓	✓	✓
• An increase of 1-reheat in the power conversion cycle can increase efficiency by 1.5%-2%.	✓	✓	✓	✓	✓	✓
• Homogenized Be/Li-compound design as indicated above can potentially allow thinner blanket.	✓	✓	✓	✓	✓	✓
IV R&D						
• Tubular fuel elements as presented in footnote (b) can avoid complexity in the swelling tolerant plate design for Li_2O when creep is taken into consideration, which potential can relax swelling concerns for tubular elements.	✓	✓	NA	NA	NA	NA

TABLE 8.1-11 (Continued)

(a)NA - not applicable.
(b)A tubular fuel element containing Be and solid-Li-compound can be considered.
(c)A mixture of Li-in-tubes and Be-balls can be considered.
(d)The present reference designs are optimized to T_{max} ~550°C.
(e)Reference design numbers were conservatively calculated from average blanket radial temperature. This improvement would be useful to Li_2O designs, since its tritium inventory is controlled by tritium solubility in Li_2O.
(f)Reference designs conservatively used maximum coolant temperature to calculate tritium leakage to steam generator.

changes can be made to improve the TBR. As indicated in Table 8.11.1-1, TBR can be improved by increasing the blanket thickness for all the designs. For the solid breeder blankets, the use of metallic reflectors can help and for the $LiAlO_2$/Be Tokamak design, the addition of Be in the inboard blanket can improve the 3-D TBR by ~6%. If beryllium were to be incorporated into the blanket in a homogenized design, with the use of a maximum volume fraction of Be and an enriched lithium compound, the TBR could be improved by ~15%.

The safety evaluation is strongly influenced by tritium inventory and tritium leakage. The helium-cooled blankets and all the solid breeder blankets suffered due to the BCSS reference assumption that tritium is released into the helium coolant and purge streams as T_2, and that oxidation to T_2O will not be possible. The helium-cooled designs can obtain some benefit from use of more detailed, less conservative calculational models and from minor design changes. In particular, with the incorporation of the actual radial blanket temperature distribution, the average breeder temperature would be lowered from the peak values assumed in the reference design, thus reducing the tritium inventory in the Li_2O breeder. With a more detailed model of the heat exchanger wall temperatures, the average temperature would be much lower than the maximum coolant temperature assumed in the reference calculation. This can significantly reduce the tritium leakage rate through the steam generator. It is also important to point out that the perceived importance of the problem of tritium leakage is very sensitive to the allowable leakage rate per site, which is set at 100 Ci/day for the BCSS, independent of reactor power output.

In the area of economics, the major drawback of the reference helium-cooled designs is their required pumping power. This ranges from 2.1% to 4.7% of the blanket thermal power, but must be provided in the form of electrical power. Thus, it results in a reduction of about 3 percentage points in the net plant efficiency. This can be improved significantly by increasing the helium pressure. In the case of increasing the pressure from

50 to 80 atmospheres (the Gas-Cooled Fast Breeder reactor was designed to operate at 85 atmospheres), the pumping power fraction can be reduced from ~4% to ~1%, which can improve the net plant thermal efficiency by approximately two percentage points. This can have significant impact on the economics score of the helium-cooled blankets. Other changes that could improve on the economics score of the helium-cooled blankets are also given in Table 8.11-1.

The interactive nature between different areas of evaluation should be included in the incorporation of the improvements suggested in Table 8.11-1, e.g., the increase of helium pressure can lead to thicker first wall which can mean a reduction in TBR. To compensate for this, a thicker blanket may be needed which would then impact on the economics. Yet it is our judgment, after exercising the BCSS evaluation procedure, and following the rules set by BCSS, the design changes suggested in Table 8.11-1 would lead to improvement in the scores of the helium-cooled designs.

BLANKET COMPARISON AND SELECTION STUDY

CHAPTER 8 - HELIUM-COOLED BLANKET CONCEPTS

BLANKET COMPARISON AND SELECTION STUDY

CHAPTER 9 - WATER-COOLED BLANKET CONCEPTS

TABLE OF CONTENTS

CHAPTER 9 - WATER-COOLED BLANKET CONCEPTS

LIST OF TABLES FOR CHAPTER 9

LIST OF FIGURES FOR CHAPTER 9

9. WATER-COOLED BLANKET CONCEPTS

9.1 Introduction

The discussions in this chapter pertain to all those concepts considered within the BCSS which use high temperature pressurized water as a coolant for the first wall and blanket. The principal focus is on those concepts which have a solid tritium breeder, because all the higher-ranking blankets with water coolant were those with solid breeders.

The final rankings for all water-cooled concepts are discussed in Sec. 9.2. The rationale for the ranking assigned to each concept is summarized in that section, and discussed in more detail for each concept in Sections 9.4 through 9.7.

Key factors and issues generic to most of the water-cooled blanket concepts are discussed in Sec. 9.3 for both tokamak and tandem mirror reactors (TMR). The two top-rated (R=1) concepts, $LiAlO_2/H_2O/FS/Be$ (tokamak and TMR), are discussed in Sections 9.4 and 9.5 for those two reactors respectively. The blanket configurations are presented and design issues are discussed in depth.

Sections 9.6 and 9.7 present the concepts ranked R=2 and R=3 respectively, with decreasing amounts of detail given for blanket configurations and increasing emphasis on only the key issues for the specific concept.

Finally, the subsections of Sec. 9.8 present the summaries of work performed in specialized design and analysis areas:

- Sec. 9.8.1 - Thermal-Hydraulics Analyses for Solid Breeder Concepts
- Sec. 9.8.2 - Thermal-Hydraulics Analyses - First Wall
- Sec. 9.8.3 - Structural Analyses
- Sec. 9.8.4 - Neutronics Analyses

9.2 Final Rankings for Water-Cooled Concepts

The final rankings for all the water-cooled tokamak and TMR blanket concepts considered in the BCSS are listed in Table 9.2-1. A summary of the rationale for those rankings is presented in this section. A more complete discussion is presented in the specific subsection in Section 9.4 through 9.7 that pertains to any given concept. The evaluation and ranking process showed

TABLE 9.2-1. SUMMARY OF FINAL RANKINGS FOR WATER-COOLED BLANKET CONCEPTS

R=1: Attractive; submit to comparative evaluation

R=2A: Study to resolve key issues

R=2B: Severe fundamental problems or disadvantages

R=3: Not acceptable

CONCEPT	SEPARATE NEUTRON MULTIPLIER	STRUCTURE PCA	STRUCTURE FS	STRUCTURE V-ALLOY	COMMENTS
o LIQUID METALS					
o Li/H_2O	--	3	3	3	EXPLOSIVE
o $LiPb/H_2O$	--	2B	2B	2B	VERY REACTIVE
o SOLID BREEDERS					
o [a]TC/H_2O	--	3	3	3	NET BREEDING NOT POSSIBLE
o Li_2O/H_2O	--	2B	2B	2B	ADEQUATE BREEDING VERY UNCERTAIN; RADIATION DAMAGE CONCERN
o Li_8ZrO_6/H_2O	--	2B	2B	2B	NET BREEDING NOT POSSIBLE; HIGH ACTIVATION
o $Li_8ZrO_6/H_2O/Be$	Be	2B	2B	2B	LOW BREEDING RATIO; HIGH ACTIVATION
o $Li_2O/H_2O/Pb$	Pb	2B	2B	2B	Pb RESULTS IN MAJOR DESIGN PROBLEMS
o $TC/H_2O/Pb$	Pb	2B	2B	2B	Pb RESULTS IN MAJOR DESIGN PROBLEMS
o $Li_2O/H_2O/Be$	Be	2A	2A	2A	RADIATION DAMAGE CONCERNS
o $TC/H_2O/Be$	Be	1B[b]	1	1B[b]	CONCEPT WITH FERRITIC STEEL RECOMMENDED FOR COMPARATIVE EVALUATION

[a]TC = Ternary ceramic oxide solid breeder (e.g., $LiAlO_2$) other than Li_8ZrO_6.

[b]Not evaluated pending outcome of concept with ferritic steel.

that there were no essential differences in the relative attractiveness of each concept whether for the tokamak or the TMR. Therefore, the rankings shown apply for both reactor types.

9.2.1 General Conclusions for Water-Cooled Blanket Concepts

Some general conclusions from the BCSS can be made that relate to the attractiveness of water-cooled blanket concepts for tokamaks and TMR's:

- The two liquid metal coolants, Li and 17Li-83Pb (LiPb), are sufficiently reactive with water to preclude their use together in a blanket.
- None of the candidate solid breeders, including Li_2O, appear capable of achieving adequate TBR without the use of a neutron multiplier.
- Beryllium appears to be the only viable neutron multiplier for concepts using solid breeders.
- The low thermal conductivity and narrow range of allowable temperature are severe design handicaps for solid breeders.
- Tritium contamination of water coolant represents the most important concern as well as the largest uncertainty, with respect to safety and environment considerations.
- The sphere-pac fabrication approach for solid breeders appears to result in better temperature predictability as compared to sintered product.
- Ferritic steels (FS) as structural materials are superior overall to PCA because of better radiation damage resistance and higher tritium barrier factors for oxides, and to vanadium alloy because of lower tritium permeation rates and reduced concerns for corrosion.

9.2.2 Summary of Rationale for Rankings

- $Li/H_2O/(STRUC)$ - R=3; $LiPb/H_2O/(STRUC)$ - R=2B. Tests indicate reactivity between these liquid metal breeders and water coolant is too great to permit their use together in blanket modules in the case of Li, and probably in the case of LiPb as well.
- $LiAlO_2/H_2O/(STRUC)$ - R=3. Net tritium breeding cannot be achieved.

- o $Li_8ZrO_6/H_2O/(STRUC)$ - R=2B, with or without Be as neutron multiplier. Will probably not produce net TBR without an additional neutron multiplier. Phase transformation at ~660°C, serious waste management problems, and very low thermal conductivity make this breeder even less attractive than Li_2O for water-cooled blankets.
- o $Li_2O/H_2O/(STRUC)/Pb$; $LiAlO_2/H_2O/(STRUC)/Pb$ - R=2B. The use of molten Pb instead of solid Be as a neutron multiplier in water-cooled concepts results in a large number of serious design problems that relate to the proximity of lead's solidus temperature (327°C) and the desired operating temperature range of water coolant (280 to 320°C).
- o $Li_2O/H_2O/(STRUC)$ - R=2B. There are major uncertainties in the viability of Li_2O because of radiation-induced swelling observed in the FUBR experiments. The interactive effects with structure and the related effects on tritium release characteristics are unknown at this time, and require further R&D for resolution. In addition, Li_2O does not appear to be capable of breeding with an adequate margin (Sec. 6.8) in designs with water coolant developed using BCSS design guidelines, unless a neutron multiplier is included.
- o $Li_2O/H_2O/(STRUC)/Be$ - R=2A. The addition of Be as a neutron multiplier reduces the concern for achieving an adequate TBR. But the remaining concerns for Li_2O radiation damage are sufficient to keep this concept from being ranked R=1.
- o $LiAlO_2/H_2O/FS/Be$ - R=1. The concept gives adequate tritium breeding, and appears to give reasonable performance with no unacceptable safety risks. FS is superior to austenitic stainless steel (PCA) for this concept. Vanadium alloy is less attractive, and might ultimately be not acceptable because of high tritium permeation rates. The use of sphere-pac fabrication for the breeder should give acceptable breeder temperature predictability. $LiAlO_2$ breeder appears to be very stable under irradiation within specified allowable temperature range. The concept's tokamak and TMR versions were recommended for further development and comparative evaluation with all other concepts ranked R=1.

9.3 Key Factors for H_2O-Cooled Blanket Concepts

There are a number of very important issues for H_2O-cooled concepts using solid tritium breeders (SB/H_2O concepts) for which resolution is crucial to

eventual success of the concepts as power reactor blankets. (The emphasis in this section is on solid breeder blankets because, as a group, they were the more highly rated of all H_2O-cooled concepts.) These factors are essentially generic to SB/H_2O blankets, whether for tokamaks or TMR's. Differences between concepts for the two reactor types are more design- and configuration-related. Thus, the discussion in this section is divided into two main parts. First, the generic issues for SB/H_2O concepts are presented:

- o Sec. 9.3.1.1 - Reliability of Coolant Tubes
- o Sec. 9.3.1.2 - Tritium Control
- o Sec. 9.3.1.3 - Breeder Physical Integrity
- o Sec. 9.3.1.4 - Breeder Temperature Control
- o Sec. 9.3.1.5 - Breeder Allowable Temperature Limits
- o Sec. 9.3.1.6 - ^6Li Burnup Effects

The major differences between concepts for tokamaks and TMR's are then discussed in the next four subsections:

- o Sec. 9.3.2.1 - Blanket Thickness
- o Sec. 9.3.2.2 - First Wall
- o Sec. 9.3.2.3 - Module Shape Requirements
- o Sec. 9.3.2.4 - Manifolds

9.3.1 Key Factors Generic to H_2O-Cooled Blanket Concepts

9.3.1.1 Reliability of Coolant Tubes

During the first year of the BCSS[1], it was identified that the reliability of small diameter coolant tubes could be very important to the economics of the concepts, due to the effects on availability of the reactor if relatively high failure rates resulted in large amounts of machine downtime. Based on various tube failure rate data sets examined, it was estimated that the number of tube failures in a Starfire-size reactor could be between 1 to 100 or more per year. For Starfire[2], it was considered, based on availability analyses, that the occurrence of more than two tube failures per year for the entire reactor would probably be unacceptable from the standpoint of availability. Preferably, the number of tube failures per year should be much less than one, since total downtime to replace one blanket sector having a failed tube could be from one to four weeks.

The key problem is that any water leak into the solid breeder in the interior of the blanket is likely to force a reactor shutdown due to (1) a buildup of steam pressure inside the blanket, (2) effects of the H_2O carried by the helium purge gas on the tritium removal subsystem, or (3) the effects of H_2O on the solid breeder itself (especially Li_2O).

The approach taken for all SB/H_2O concepts, tokamak or TMR, was to replace the previous single wall tubes (SWT) with double wall tubes (DWT), with the tube ends double welded so as to form two separate pressure boundaries. Thus, for a given tube assembly, each of the two pressure boundaries would have to be breached before H_2O could contact the material inside the blanket module. Each tube and weld is sized to withstand the coolant design pressure as a normal operating load.

In theory, the reliability of SWT can be defined as

$$R_{swt} = 1 - \left(\frac{n_f}{n_t}\right) \qquad [9.3\text{-}1]$$

where R_{swt} is the reliability of SWT against leaks, n_f is the number of failures of tubes in a given period, and n_t is the number of tubes under consideration. Then for DWT, if no common mode failures occur, the reliability of DWT sized and welded as described above could be given by

$$R_{dwt} = 1 - \left(\frac{n_f}{n_t}\right)^2 \qquad [9.3\text{-}2]$$

where R_{dwt} is the reliability of DWT against leaks. The overall reliability of the blankets with DWT would thus be dramatically improved over that for blankets with SWT of similar configuration. For example, if $(n_f/n_t) = 10^{-4}$, then $R_{swt} = 0.9999$ and mean time between failures (MTBF) = 0.1 yr for 10^5 tubes. By changing to DWT, reliability could be increased to $R_{dwt} = 0.99999999$ with MTBF = 1000 yr.

The largest uncertainty at this time in determining the overall blanket reliability for DWT is the amount by which the theoretical reliability improvement over SWT is reduced by the occurrence of common mode failures. No assessment of this reduction has been made within the BCSS since necessary

information such as basic failure data for tubing made from the proper structural materials, effects of environment, and effects of radiation on the design details are virtually unknown.

9.3.1.2 Tritium Control

Controlling the degree to which tritium permeates into the water coolant in the FW and the blanket is the most important safety-related issue for H_2O-cooled blanket concepts. Tritium from the plasma can permeate into the H_2O coolant in the first wall (Sec. 6.6). For H_2O-cooled concepts with solid breeders, tritium in gaseous form within the breeder zone can permeate the coolant tubes and enter the H_2O coolant.

Recent experimental evidence tends to indicate that tritium from the solid breeders will remain for the most part in gaseous form while inside the breeder zone, since the kinetics of oxidation appear to be relatively slow. For all solid breeder concepts and all coolants, hydrogen gas is added to the helium purge gas to provide elemental hydrogen sufficient to permit rapid release of the tritium atoms from the breeder grain surface as HT. The key to acceptable tritium control in the breeding zone is to keep the HT concentration sufficiently low that permeation through the double wall coolant tubes is at levels which permit costs for tritium removal from the water to be affordable. The contamination level permitted for the primary coolant, 1 Ci/liter, is the maximum acceptable level given the assumption of 100 liter/day loss of primary coolant to the secondary side of the steam generator (all such leakage is considered lost to the environment).

There are a number of design details for the SB/H_2O concepts which were selected to keep contamination of the coolant at low levels. There are three oxide barriers on the ferritic steel structure: the films on the two annular surfaces of the DWT, and the film on the inside of the inner tube at the water interface which extends throughout the primary loop including the steam generator. Hydrogen is added to the helium purge gas as previously mentioned. Channels within the blanket for the purge gas were located at the coldest breeder regions, next to the coolant tubes, to enhance release. The 15% porosity among particles of the sphere-pac breeder facilitates migration of the helium purge gas through the breeder to the purge gas channels.

The tritium that permeates through the first wall into the coolant is implanted from the plasma. Tritium flux through the first wall into the water coolant is estimated to be approximately 2200 Ci/d. The oxide film on the coolant channel inside surface is the only effective barrier to the tritium. The largest unknowns in present estimates of the rate of tritium permeation through the first wall are the values for the recombination factors for the front (plasma-facing) and back (coolant-contacting) surfaces (Sec. 6.6).

The addition of an intermediate coolant loop and heat exchanger would greatly improve tritium control for H_2O-cooled concepts in terms of tritium losses to the environment. However, its use would make the thermal conversion efficiency of the concepts much lower and would, therefore, sharply increase the cost of electricity. Therefore, use of an IHX for tritium control in H_2O-cooled concepts is considered not acceptable.

9.3.1.3 Breeder Physical Integrity

In most previous studies of solid breeder blankets, the reference fabrication method for the solid breeder has been sintered product. The potential for cracking of sintered product was evaluated analytically within the BCSS[1]. It was determined that sintered Li_2O, and most likely other solid breeders as well, would be expected to crack at very low stress levels, of the order of ~12 to 20 MPa (~2 to 3 ksi).

Cracking of the solid breeder can affect blanket performance through two principal mechanisms. First, the creation of crack surfaces normal to the direction of heat flow produces additional impedances to such flow. A temperature gradient, ΔT_g, will exist across each such crack, the magnitude of which is primarily a function of the crack interface pressure or the crack gap width, and of the helium purge gas pressure. Each ΔT_g will raise the breeder maximum temperature by approximately that same magnitude. It is not possible to predict the number, orientation, and characteristics of such cracks in a given design. Second, if breeder fragments are allowed to shift their positions slightly relative to the surrounding breeder, the ΔT_g values will become far higher due to the opening up of much larger gaps at the irregular surfaces of the cracks. The danger also exists of continued motion and ratchetting of the fragments, and a progressive breaking-up of the breeder.

The sphere-pac breeder fabrication approach appears to offer a way to preclude breeder cracking or relative motion (shifting) while retaining the same overall porosity percentage and thermal conductivity (k_t) achievable with the sintered product. The sphere-pac approach uses a specific mixture of three different sizes of breeder spheres. The mixture can literally be poured into a cavity, with the desired %TD and k_t resulting with little additional effort.

Three key factors involved with sphere-pac solid breeder are expected to relieve the initial problems of cracking and of interface predictability (Sec. 9.3.1.4). First, if the 85% dense breeder is kept below the maximum allowable temperature, then sintering among pellets is not expected to occur, and therefore macroscopic cracking of the bulk breeder cannot occur. Second, the breeder is expected to expand with increasing temperature at a faster rate than the steel structure, so that the breeder, if properly confined, can be held in contact with the structure at all times. Third, the mixture is expected to remain "loose", given 15% porosity and no sintering, to accommodate the movements of the structure. In combination with the higher thermal expansion rate of the breeder, this is expected to keep reasonable breeder-to-structure interface contact pressure at all times during blanket operation.

9.3.1.4 Breeder Temperature Predictability

The degree of predictability of the heat conductance, h_g, across the breeder-to-structure (b/s) interface is of major importance in determining the range of breeder temperatures allowable for the design under normal operating conditions. If h_g is invariant and is known exactly at all points, then the full range of allowable breeder temperatures (Sec. 6.3) may be utilized for design conditions. However, any uncertainty in the nominal h_g value must be accounted for by increasing the design minimum and decreasing the design maximum breeder temperature by some amount, so that the breeder does not operate outside the allowable temperature range regardless of the true h_g value. As an example, for the DEMO Li_2O/H_2O blanket,[3] an uncertainty of only ±20% in h_g results in an increase and decrease of ~30^0C breeder T_{max} and T_{min}, respectively. The design temperature range for the breeder in the concept would thus have to be reduced by ~60^0C (about 15% of the allowable range for Li_2O, for example) just to accommodate such an uncertainty range.

Methods to accomplish the b/s interface were examined. The use of a discrete helium-filled gap greater than 0.1 mm is considered not feasible for power reactor conditions. The extreme sensitivity of h_g--and thus of breeder temperatures--to very small changes in gap width (Sec. IX.2 of Ref. 1) results in gap tolerance requirements that are unacceptable even for blanket fabrication, much less achievable during long-term blanket operation. The b/s metallurgical bond suggested for the DEMO blanket[3] is attractive and conceptually feasible, but the fracture stength of sintered product solid breeders is presently much too low to prevent fracture of the breeder at its interface with the compliant intermediate layer. Techniques to significantly increase breeder fracture strength, such as the addition of chopped fibers, need to be demonstrated before this interface method can be utilized. A third method is to place the breeder in direct contact with the structure or an intermediate layer, and to maintain some amount of compressive load at the interface. This method appears to yield a reasonable degree of predictability in h_g (Sec. IX.2 of Ref. 1). A key element is the method or process by which the interface compression is maintained.

9.3.1.5 Breeder Allowable Temperature Limits

All solid tritium breeders have allowable minimum and maximum temperature limits established for normal operation (Sec. 6.3). These limits are based principally on considerations of tritium release and tritium inventory buildup. Li_2O is a special case; the lower limit is established to prevent formation of LiOH in liquid form, and the upper limit to prevent excessive vaporization of LiOT or LiOH. Temperature limits for the solid breeders are shown in Table 9.3-1 together with lithium atom density and thermal conductivity.

The temperature limits result in a relatively narrow allowable temperature range for solid breeders. The amount of breeder that can be placed around a coolant cube, for a given nuclear heating rate in the breeder, is a function of the product $(\Delta T)(k_t)$, where ΔT is that part of the allowable breeder temperature range that can actually be utilized in a given blanket design. Since thermal conductivity, k_t, is quite low for most of the solid breeders of interest, irradiated or unirradiated, the available temperature window for design is small (Table 9.3-1) and thus the amount of breeder around

TABLE 9.3-1. SUMMARY OF BCSS DESIGN GUIDELINES FOR CANDIDATE SOLID BREEDERS[a]

Breeder	MP, °C	ρ Li_z, g/cm^3	k, W/m-K	T_{min}, °C	T_{max}, °C	ΔT, °C	Grain Dia., μm
Li_2O	1433	0.93	2.5[c] 1.27[d]	410	800	390	3.0
γ-$LiAlO_2$	1610	0.28	1.6[c] 1.1[d]	350	1000	650	0.2
Li_8ZrO_6	1295	0.68	1.8	350	760	410	2.0

[a] Estimates based on limited unirradiated and irradiated data for solid breeders and other ceramic materials. See Sec. 6.3.4 for complete discussion.

[b] Estimated for unirradiated, sintered materials of 85% theoretical density at 1000 K.

[c] Estimated for 85%-dense, sintered material at 1000 K after 0.7-2.8 MW yr/m^2 fusion neutron fluence.

[d] Estimated for 87% solid packing fraction, sphere-pac material made of high-density (~100% TD) particles with three sizes (30, 300, and 1200 μm diameters) at 1000 K (1 atm He pressure) and after 0.7-2.8 MW yr/m^2 fusion neutron fluence.

a coolant tube relative to the total amount of structure and coolant is also quite small near the front of the blanket where nuclear heating rates are highest. This is important because tritium breeding ratio (TBR) values for solid breeder blankets are not large, and there are limits to how much they can be improved by simply adding more neutron multiplier to the design. Thus the question of establishing allowable temperature limits for the breeders themselves is very important to the feasibility of solid breeder blanket concepts.

If solid breeder and beryllium neutron multiplier are mixed together, as in the $LiAlO_2/H_2O$/FS/Be concepts in which both the breeder and Be are in sphere-pac form in a 90:10 volume ratio, the situation changes to some extent since (1) the ΔT of the mixture is now governed by the minimum and maximum allowable temperatures of Be based on radiation damage considerations, and (2) the k_t of the mixture is now a function of the solid-breeder-to-Be (SB/Be) volume ratio as well as damage level (fluence) and the pressure of the helium purge gas. In general, thermal-hydraulics calculations (Sec. 9.8.1) indicate

the $(\Delta T)(k_t)$ product is not much changed compared to pure solid breeder. However, the sensitivity of the mixture's temperature limits to changes in the solid breeder temperature limits would be reduced.

9.3.1.6 ^{6}Li Burnup Effects

The potential effects of high levels of ^{6}Li burnup in regions near the first wall on blanket design lifetime and performance is a key issue for concepts with $LiAlO_2$ and water coolant, that requires further study both to determine the severity of the problem and to assess potential solutions.

Neutronics analyses of the Li_2O/H_2O/PCA blanket with natural Li during the first part of the BCSS[1] showed that lithium burnup effects on life and performance were minimal. As burnup increased with fluence, tritium production and nuclear heating decreased in regions close to the first wall but increased in regions further away. The net effects at end of life (EOL; 25 MW-yr/m^2) were a reduction in TBR of only 1%, and a reduction in nuclear heating rate immediately behind the first wall of ~7%. For this concept the TBR reduction was not significant and the nuclear heating rate reduction--only ~2.5% over the first 3 cm of the blanket--could either be accommodated by a slight increase in the breeder BOL design minimum temperature, or simply accepted as a slight reduction in the overall power output of the reactor.

The situation for $LiAlO_2$/Be systems may be more difficult, however. Initial neutronics estimates indicate that, for the $LiAlO_2/H_2O$/FS/Be reference design (Sec. 9.4, 9.5), TBR could drop by $\gtrsim$15% after four years of operation, a serious problem for this concept. Also, the maximum nuclear heating rate immediately behind the first wall drops from 61 to 45 W/cc at EOL, a reduction of >25% compared to ~7% for the Li_2O/H_2O/PCA concept. Heating rates deeper into the blanket increase somewhat over the blanket lifetime.

Accommodating these changes may be difficult. Reducing design lifetime from >4 years to ~2 years would moderate the reductions in TBR and nuclear heating but would increase cost of electricity (COE) for the concept because of higher annual blanket costs and possibly decreased reactor availability. Changing the Be:breeder mixture volume ratio from 90:10 to 80:20 would decrease the effects since twice as many breeder and ^{6}Li atoms would be available in the front of the blanket, but blanket TBR at BOL would be reduced (Sec. 9.8.4). Accommodating the changes in nuclear heating rate throughout

the blanket lifetime would probably require decreasing the breeder allowable design temperature range, which would decrease the amount of breeder relative to the structure and coolant, also degrading TBR.

Good potential solutions to the problems caused by high burnup rates are not obvious at this time. The importance of these effects was established only after the design work had been ended, and thus problem severity and potential design solutions could not be investigated in the BCSS. However, this work is required for future designs of $LiAlO_2/H_2O/(STRUC)/Be$ systems, to fully establish the feasibility of such concepts.

9.3.2 Differences for Tokamak and TMR Concepts

The principal differences between tokamaks and TMR's relating to the attractiveness of H_2O-cooled concepts are listed in Table 9.3-2, together with important factors in determining the most desirable configurations for H_2O-cooled concepts that are the same for both confinement approaches. The four areas of the first wall/blanket subsystem where the most significant differences in tokamak and TMR blanket concepts can occur are discussed in the following sections.

9.3.2.1 Blanket Thickness

In tokamaks, minimization of blanket thickness in the inboard region nearest the centerpost is of major importance. Any additions to blanket thickness over and above the minimum needed for reaching performance goals (TBR, shielding, power generation) add to magnet size, reactor size, and capital costs primarily since the plasma must be further away from the maximum toroidal field of the TF coils. An increase in outboard blanket thickness is not as important, because the increase has a minimum impact on the reactor major axis and there is relatively a much larger distance between the blanket and the inside of the TF coil outer leg.

For a TMR having the MARS configuration[4], with large discrete coils spaced a few meters apart, the effects of increases in blanket thickness are not as important as in the inboard region of a tokamak, except locally under the coils. Additional thickness adds to capital costs, through increased blanket and shield material costs and increased magnet bore size, but the plasma and the end cells are not affected.

TABLE 9.3-2. MAJOR DESIGN CONSIDERATIONS AFFECTING CONFIGURATIONS OF WATER-COOLED TMR AND TOKAMAK BLANKETS

	TMR	TOKAMAK
o FACTORS[a] WHICH COULD PRODUCE CONFIGURATION DIFFERENCES		
- FW SURFACE EROSION RATE, mm/yr	0.1	1.0
- FW SURFACE HEAT FLUX, mw/m^2	0.05	1.0
- PEAK DISRUPTION/SUDDEN-LOSS-OF-PLASMA LOAD, MPa	0.02	0.76
- BURN CYCLES, n/yr	~12[b]	~2500[c]
- FUSION CORE SHAPE	CYLINDRICAL	TOROIDAL
o FACTORS WHICH ARE THE SAME FOR TMR AND TOKAMAK		
- HIGH NEUTRON WALL LOAD (5 MW/m^2)		
- COOLANT TUBE RELIABILITY CONCERNS		
- BREEDER-TO-STRUCTURE INTERFACE PROBLEMS		
- TBR REQUIREMENT		
- TRITIUM CONTROL AND REMOVAL PROBLEMS		
- MATERIALS TEMPERATURE LIMITS		

[a] Assumed for BCSS.

[b] Startup/shutdown cycles.

[c] Burn cycle length = 10^4 s. Includes startup/shutdown cycles.

The inboard blanket for the top-ranked SB/H_2O concepts was designed to a thickness of 35 cm, including 7 cm of manifold thickness, compared to 70 cm for the outboard blanket. This is considered to be a reasonable compromise for power production and tritium breeding, without making the inboard shield excessively thick. For the TMR version, the full 70 cm thickness was used all around the plasma. The manifold thickness was unchanged from the 18 cm used for the tokamak outboard blanket, although the blanket in practice probably would be reconfigured to have the coolant in the manifold flow in an axial direction (lengthwise through the module) to be compatible with the location of coolant inlet/outlet pipes which would be located at the center of the module.

9.3.2.2 First Wall

Two fundamental differences between the tokamak and TMR confinement approaches can potentially result in signficant differences in the first wall design for H_2O-cooled concepts: (1) surface heat flux level; and (2) erosion rate of the plasma-facing surface. For the BCSS we have assumed that the surface heat flux and surface erosion rates are much higher for the tokamak than for the TMR, as shown in Table 9.3-2.

For first wall structure, thermal stresses are often the most critical factor in determining the maximum allowable thickness. Thermal stresses are a function of the difference between the outer and inner structural surface temperatures, ΔT. For first walls actively cooled by H_2O, the inner structural surface temperature is only 10 to 20^0C above the local coolant temperature (280 to 320^0C). Since for the BCSS, the T_{max} allowed for structure is 550^0C for ferritic steel, the resulting ΔT is relatively large, so that structure thickness is limited only by thermal stresses and not by the available ΔT. Other gaseous coolants such as helium, with higher first wall inside surface temperatures, do not have this advantage.

The first walls for tokamak SB/H_2O concepts were designed to accommodate surface heating from the plasma and nuclear heating from the breeder (or SB/Be mixture) in contact with the back face, as well as the nuclear heating of the first wall itself. Active cooling of tokamak first walls is mandatory. For TMR's, analyses were performed (Sec. 9.8.1) to determine if the very low surface heat flux, in combination with nuclear heat from a thin breeder layer behind the first wall, could be accommodated by the first bank of coolant

tubes in the breeding zone without violating any limits. The results showed that this approach was not feasible because the allowable breeder layer thicknesses became extremely thin and could not physically be attained, given the need for discrete coolant tubes of greater than 1 cm diameter. Thus, first walls for TMR versions of SB/H_2O concepts were required to be actively cooled.

Erosion thickness requirements for tokamak first walls are much higher than for TMR first walls. To achieve a life of approximately 4 or 5 operating years limited by radiation damage to the structure, an erosion thickness of 4 to 5 mm must be added to the minimum structural thickness of the first wall's plasma-facing surface. This thickness, if added directly to the structural thickness, would result in thermal stresses above the maximum allowable limit for many concepts. In tokamak SB/H_2O concepts, therefore, this additional thickness of erodable material is orthogonally grooved (Sec. 6.7) to keep the additional thermal stresses in the structural material to low levels, so that thermal stress limits are not violated. For TMR's, this approach is not needed since the additional 0.4-0.5 mm can be added directly to the structural material thickness without violating stress limits.

Verification of the orthogonal grooving approach for tokamak first walls is a key R&D issue for SB/H_2O concepts. Erosion thicknesses would have to be reduced to approximately 3 mm with a 3 year life resulting, if orthogonal grooving were shown to be unacceptable.

9.3.2.3 Module Shape

The configuration initially studied for SB/H_2O blankets was the rectangular-shaped or parallelepiped module with a flat first wall. Subsequently, lobe-shaped modules with semi-cylindrical noses (similar to the helium-cooled designs, Chapter 8) were studied and compared to rectangular modules for both tokamak and TMR reactors.

There are several important factors involved in determining the best module shape for SB/H_2O blanket concepts; three of these are discussed below.

Containment of Internal Pressure - Based on work done by EG&G Idaho on the Starfire blanket[5], it has been predicted that in the event of a coolant

tube break inside the module, the internal pressure could rise as high as ~11 MPa (~1600 psi) before being relieved by such passive measures as blowout plugs in the sides of the modules. These pressure levels would occur for both tokamak and TMR versions of the blanket concepts.

Plasma Disruption Loads - For plasma disruptions (or loss-of-plasma events in the case of TMR's), the forces produced on the first wall of a tokamak can be as high as ~0.8 MPa (~110 psi). The forces produced in TMR first walls would be only ~0.02 MPa, however (Sec. 5.1). These forces act as body loads on the first wall structure, forcing it toward the plasma.

Void Spaces - The creation of void spaces between the front portions of lobe-shaped modules results in ~20-25% reduction in the amount of breeder or neutron multiplier material that can be placed in this part of the blanket (up to a depth equal to the lobe radius) compared to rectangular modules which can be placed directly together in the poloidal direction with very little void region between them. All other factors being equal, for lobe-shaped modules the void region significantly reduces the TBR obtainable from a given blanket thickness.

These factors and others were considered in determining the best configuration for the SB/H_2O concepts, as described in Sec. 9.4.3.1. The lobe-shaped module was finally selected, for both tokamak and TMR blanket concepts, primarily on the basis of its more efficient accommodation of the most critical load, the internal presure due to a coolant tube rupture.

9.3.2.4 Manifolds

The differences between the tokamak and TMR reactor configurations can affect the manifolding for SB/H_2O blankets. In tokamaks, there is a premium on minimizing the inboard blanket thickness because of reactor economics considerations (Sec. 9.3.2.1), which forces the designer to minimize the manifold thickness in that blanket as well. The coolant main inlet and outlet lines are most conveniently directed radially outward away from the reactor centerline through openings between adjacent TF coils. The number of these lines is generally mininized to simplify maintenance operations. The manifold region in outboard blankets can be relatively thick since there is no strong economic penalty other than that associated with additional amounts of material.

In TMR's, the manifolds in all blanket modules around the plasma region would be similar. For the MARS magnet configuration[4], with two discrete large-cross-section magnets per cell, the inlet and outlet pipes would be directed radially outward from the axial center of the cell, so the magnets would not be trapped by the pipes. Flow direction in the manifolds would preferably be in the axial direction to minimize manifold thickness and to be consistent with use of inlet and outlet lines at the cell midpoint.

The top-ranked SB/H_2O concepts used the same basic blanket configuration for both tokamak and TMR for purposes of evaluation, with an 18-cm thick manifold behind 52 cm depth of first wall and breeding zone. It is recognized that in-depth analysis to optimize TMR concepts would likely lead to some changes in manifold flow direction and thickness, but these are not considered significant for purposes of comparative evaluations of blanket concepts within the BCSS.

9.4 $LiAlO_2/H_2O$/FS/Be Concept - Tokamak (R=1)

This section describes the water-cooled blanket concept for the tokamak reactor that uses lithium aluminate ($LiAlO_2$, gamma form) solid tritium breeder, HT-9 ferritic steel structure, and beryllium as a neutron multiplier. The reference blanket configuration (Table 9.4-1 and Fig. 9.4-1) is described zone by zone in Sec. 9.4.1. The concept is summarized in the discussions of Sec. 9.4.2, with the major emphasis on the key factors and issues for the concept. Blanket design detail selections and related issues are discussed in Sec. 9.4.3.

9.4.1 Reference Blanket Design Configuration

9.4.1.1 General Description

The reference design of the $LiAlO_2/H_2O$/HT-9/Be blanket concept for the tokamak reactor (Fig. 9.4-1) is modular in nature, with a lobe-shaped (semi-cylindrical) actively cooled first wall. Nominal dimensions are 30 cm width poloidally (15 cm radius for the first wall) and 70 cm depth measured radially away from the plasma. The interior of the blanket is all breeding zone. For outboard, top and bottom blanket modules of the blanket sector, the first 20 cm of the zone is a 90:10 volume mixture ratio of beryllium (Be) and the

TABLE 9.4-1.
MAJOR PARAMETERS AND FEATURES OF
$LiAlO_2/H_2O$/FS/Be CONCEPT - TOKAMAK

General Description	
Materials	
Coolant	Pressurized H_2O
Breeder	γ-$LiAlO_2$ @ 86% TD; 90% ^6Li
Neutron Multiplier	Be @ 86% TD
Structure	HT-9 Ferritic Steel
Purge Gas	Helium
Major Design Parameters	
Reactor blanket thermal power, MW_{th}	6056
Average neutron wall load, MW/m^2	5.0
Average first wall surface heat flux, MW/m^2	1.0
Coolant	
Inlet/outlet temperature, $^0C/^0C$	280/320
Maximum pressure, MPa	15.2
Breeder	
Minimum/maximum temperature, $^0C/^0C$	350/1000[c]
Maximum pressure, MPa	~0.6 (Purge Gas)
Structure	
First wall/blanket maximum temperature, $^0C/^0C$	~465/340
Minimum/maximum temperature at:	
Coolant interface, $^0C/^0C$	~290/330
Breeder interface, $^0C/^0C$	~350/350
Neutronics	
Tritium breeding ratio	
1-D, 100% coverage	1.21
Net (3-D with all geometrical details and penetration)[a]	1.16
Maximum nuclear heating rates (outboard)	
Be/breeder zone, W/cc	70
Breeder zone, W/cc	19
Structure, W/cc	66
Energy (1-D calculation)	
Multiplication factor	1.399
Deposited in heat recovery zone, MeV	1.372
Deposited in heat loss zone, MeV	0.027
First Wall/Blanket Design Description	
Inboard first wall/blanket	
Thickness (including manifolds), m	0.35
Manifold thickness, m	0.07
Percent structure/percent coolant in manifold region, %/%	25/75
Coolant ΔP (total), MPa	~0.2
Outboard first wall/blanket	
Thickness (including manifolds), m	0.70
Manifold thickness, m	0.18
Percent structure/percent coolant in manifold region	25/75
Coolant ΔP (total), MPa	0.2
Primary coolant loop pumping power, MW_e	49.5

TABLE 9.4-1 (Continued)

First Wall	
Description	Welded; rect. x-sec. channels
Minimum/maximum coolant temperature, $^0C/^0C$	280/320
Maximum structure temperature, ^0C	~465
Blanket	
Description	30-cm dia. lobular module. Double wall coolant tubes within Be/breeder (first 20 cm) or breeder (last 32 cm), in sphere-pac form.
^6Li enrichment, %	90
Minimum/maximum coolant temperature, $^0C/^0C$	280/320
Maximum structure temperature, ^0C	~340
Tritium removal from breeder	
Method	Purge gas flow
Power loss (thermal), % total	~0
Steady-state breeder tritium inventory, g	2300
Purge gas	
Material	He
Temperature, ^0C	~350-400
Pressure, MPa	0.1-0.6[d]
Tritium barriers	Natural oxides
Power Conversion System	
Thermal storage provision	
Technique	Circulating liquid
Storage medium	Pressurized water
Steam generator	
Type	Once-through horizontal
Single or double wall tubes	Single
Steam	
Inlet/outlet temperature, $^0C/^0C$	240/299
Maximum pressure, MPa	6.9
Tritium barriers	Natural oxides
Thermal efficiency	
$\eta = \frac{(MW_e)_{out} - (MW_e)_{pump}}{MW_{th\ TOTAL}}$, %	34.9
Gross (MW_e/MW_{th}), %	35.7
Steady-State Tritium Losses, Ci/d	100[e]

[a] As calculated by Tritium Breeding Task Group

[b] Neutron energy multiplication only.

[c] 650^0C maximum for Be/$LiAlO_2$ mixture.

[d] Variable, for changing breeder bulk k_t.

[e] Assumes 1 Ci/liter in primary coolant, with 100 liter/day losses to secondary side of steam generator.

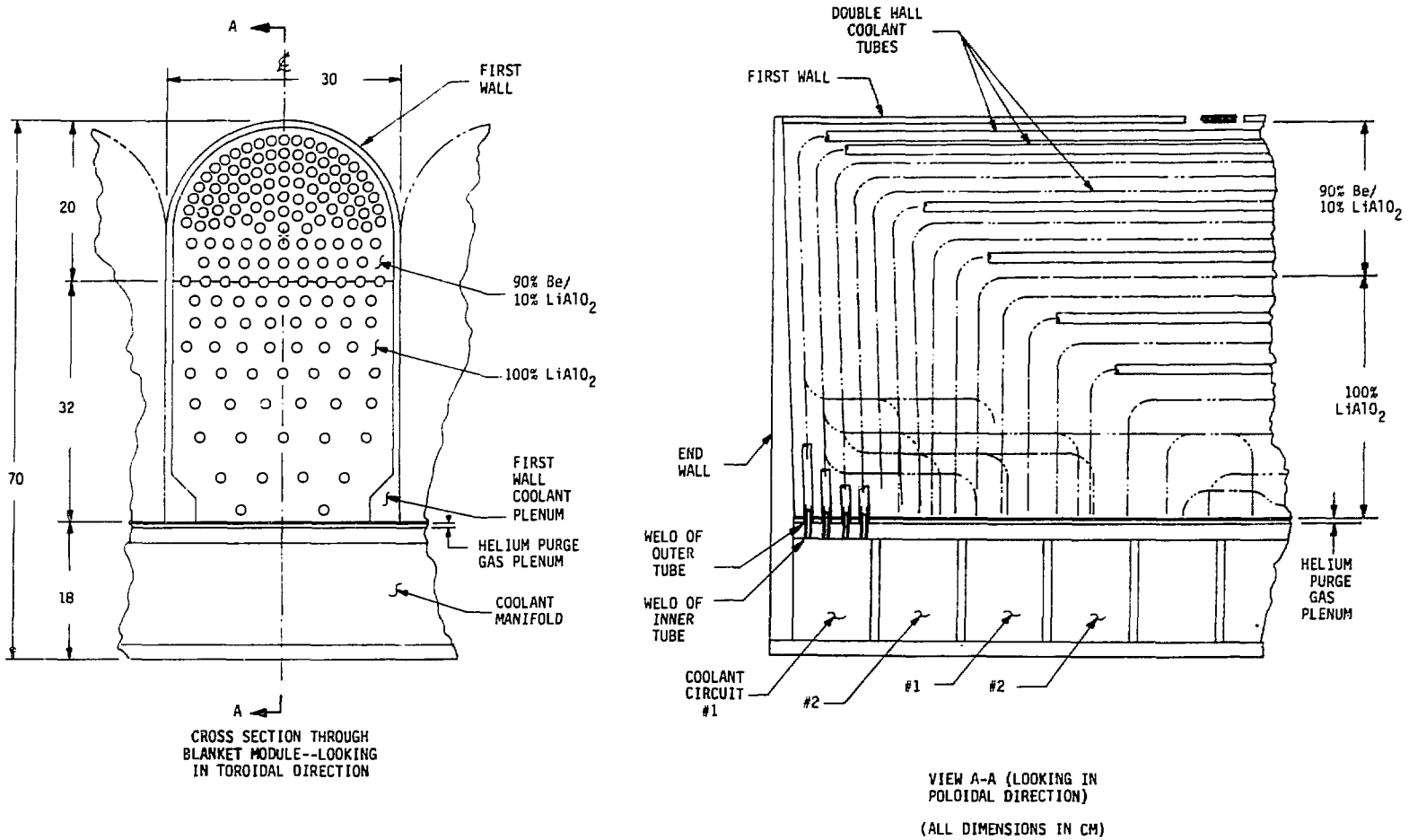

Fig. 9.4-1. Reference design configuration for $LiAlO_2/H_2O$/FS/ Be concept-tokamak

$LiAlO_2$ ternary ceramic solid breeder (SB). Both materials are fabricated in sphere-pac form. The Be is 100% dense. The individual SB spheres, comprised of grains ~0.2 μm in size, are approximately 100% dense. Packing density for the sphere-pac regions is 86%. The remaining 32 cm of the breeding zone is all $LiAlO_2$, again in sphere-pac form. The last 18 cm of the module depth is coolant inlet and outlet manifold which extends around all the blanket modules to form the blanket sector, with the manifold acting as sector structure. Inlet and outlet coolant lines for the dual circuit coolant loops are located at top and bottom of the outboard blanket region.

The inboard blanket modules are very similar to the outboard modules except for depth. The breeding zone plus first wall is 28 cm, and manifold depth is 7 cm. The SB/Be mixture depth is 20 cm as in the outboard modules, with the last 8 cm of the breeding zone being breeder only.

The individual blanket modules contact each other along their side walls from the juncture of adjacent lobes radially back to the manifold zone. The side walls bear against each other, providing mutual support to reduce structural requirements for reacting loads due to the 6-atm maximum internal pressure of the helium purge gas.

9.4.1.2 First Wall

The first wall is formed by the semi-cylindrical portion of the continuous actively cooled panel which extends from the back wall of the module to the front and returns along the other side of the module to the back wall. The panel, constructed of ferritic steel, forms the two side walls of the module as well as the first wall.

The coolant channels are rectangular in cross section (Fig. 9.4-2), formed by ribs which separate the front and rear walls of the panel. The coolant flows in the circumferential (poloidal) direction around the first wall. Small plenums are located at the panel ends next to the back wall for collecting inlet and outlet flow, to distribute the flow from the two coolant circuits into the small channels.

The first wall structure is sized to take the maximum 15.2 MPa coolant pressure from inside the blanket which might result as a peak pressure from a ruptured coolant tube in the breeding zone, as an emergency loading condition

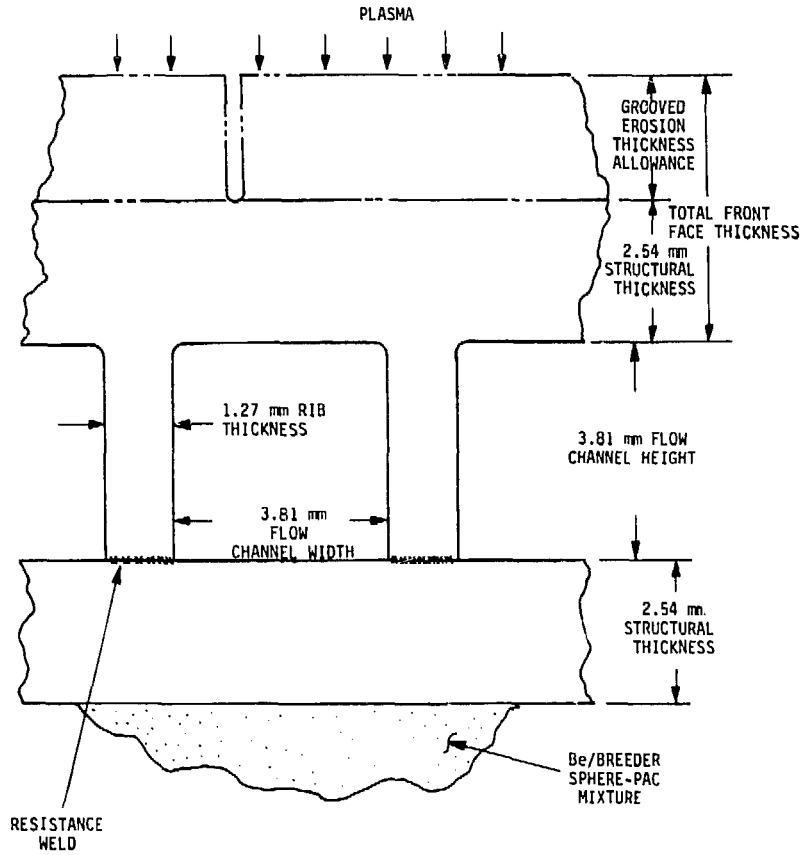

Fig. 9.4-2. First wall configuration, $LiAlO_2/H_2O$/FS/Be concept (tokamak)

(stress equal to or less than ultimate strength) without failing or rupturing. A nominal 3 mm thickness is added to this structure as orthogonally grooved material continuous with the structual material, to permit 3 years of erosion lifetime. A lifetime of 4.8 years, based on first wall radiation damage, was actually used for the economics evaluation (Sec. 5.3). Up to 10 mm of erosion thickness could be used without violating design guidelines, with the only penalty being a loss in tritium breeding ratio of ~.005-.010 at BOL per mm of additional erosion material.

9.4.1.3 Neutron Multiplier and Breeding Zone

The breeding zone for the concept comprises the full 52 cm depth of the blanket from the back face of the first wall to the back wall of the module. The first 20 cm consists of a 90:10 volume ratio mixture of Be neutron multiplier and $LiAlO_2$ solid tritium breeder. Both the Be and the ternary ceramic are in sphere-pac form, in a graded mixture of 30, 300 and 1200 micron diameter spheres. The Be spheres are each at 100% of theoretical density (TD), and the breeder spheres are approximately 100% TD. The overall density of the sphere-pac is approximately 86%. The last 32 cm of depth in the zone is filled with breeder only, again in sphere-pac form.

The zone is cooled by double walled coolant tubes of ferritic steel, each in the shape of a U with 90-degree bends near each end. The tubes connect to the inlet and outlet channels of the manifold. The inner tube is 10 mm inside diameter; the walls of both inner and outer tubes are 0.75 mm thick. The tubes are in direct contact at their annular sufaces to provide good heat transfer characteristics. The annular region is sealed under 1 atm of helium. The tube ends are double welded at the rear wall (Fig. 9.4-3) to form two independent boundaries against the coolant pressure, each sized to withstand the full coolant pressure as a primary load. The breeder and SB/Be mixture are each in direct contact with the outer surface of the tube assemblies over their full length. Lateral and depthwise spacing of the tubes (Table 9.4-1) is graded in accordance with local nuclear heating rate q_n, breeder or SB/Be bulk k_t, and allowable temperature limits of the surrounding material.

The end walls (toroidally) of the module are welded to the side walls and to the back wall of the module, and are sized to withstand the full pressure of the coolant as an emergency loading condition in the event of a coolant tube rupture. The design is similar to that used for the He-cooled modules (Chapter 8).

9.4.1.4 Tritium Purge

Tritium removal from the breeder zone is accomplished through the use of dry helium purge gas, with 1% hydrogen added to facilitate the formation of HT at the surface of the $LiAlO_2$ grains. Flow channels are provided for the purge gas at each coolant tube by a perforated thin walled steel tube which is

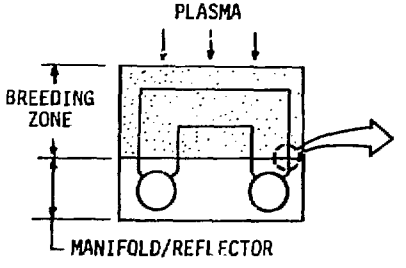

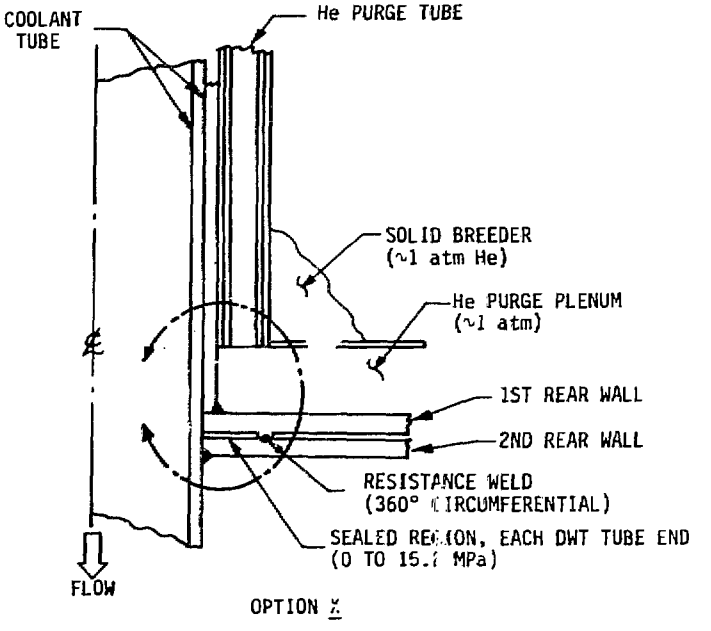

OPTION X

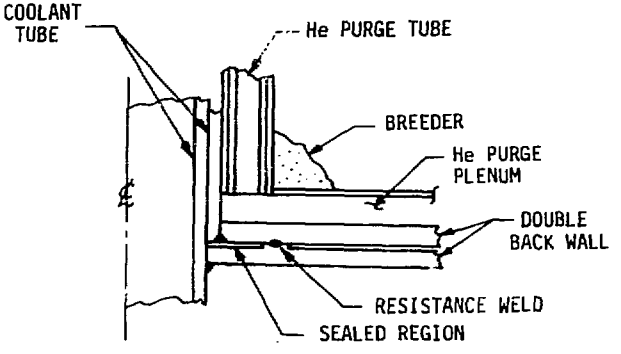

VIEW A - OPTION Y

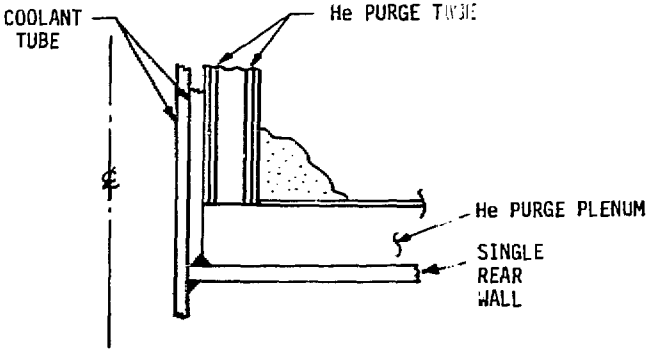

VIEW A - OPTION Z

Fig. 9.4-3. Configuration options for welds at ends of double-walled coolant tubes

coverd by a thin sleeve of woven steel mesh (Fig. 9.4-4). The perforations in

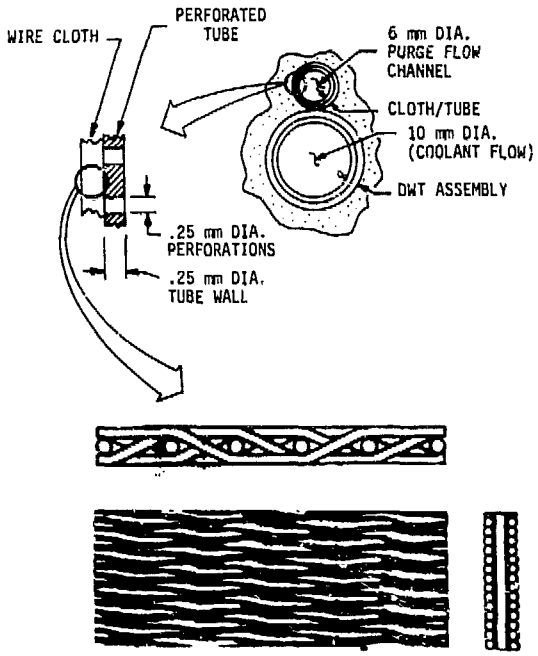

WIRE CLOTH SPECIFICATIONS[a]:

- SS OR FS MATERIAL
- T ≈ 0.25 mm (.010 IN.)
- 58% ∅D
- 80 x 700 MESH, TWILLED DUTCH WEAVE
- OPENINGS ARE TRIANGULAR, 20-25 μm WIDTH (<30 μm SPHERE-PAC MINIMUM PELLET SIZE)

TUBE SPECIFICATIONS:

- 6 mm I.D. (≈0.19 IN.)
- 0.25 mm DIA. PERFORATIONS, ≈10% OF SURFACE AREA
- t_w = .25 mm (.010 IN.)

[a]TETKO CO., NEW YORK

Fig. 9.4-4. Helium purge gas system-design details within breeding zone

the tube permit helium to flow in and out of the tube through the breeder or SB/Be mixture. The mesh is sized to keep the smallest of the sphere-pac particles out of the perforated tube to prevent flow blockage.

The tubes are welded to a shallow-depth helium plenum region at the back wall. The plenum is divided in half toroidally into separate inlet and outlet regions. The integrity of the tube weld at the plenum is not important, and the weld can be slightly "leaky." The purge tube assemblies wrap around the coolant tubes over their full length in a shallow spiral, to provide support and to keep the purge tubes at the coldest part of the breeder, i.e., nearest the coolant tube.

9.4.1.5 Manifold Region

For the outboard blanket, the last 18 cm of the blanket module is made up of the coolant manifold (Fig. 9.4-5). The region, which includes the purge helium plenum (Sec. 9.4.1.4), provides a path for coolant flow and also serves

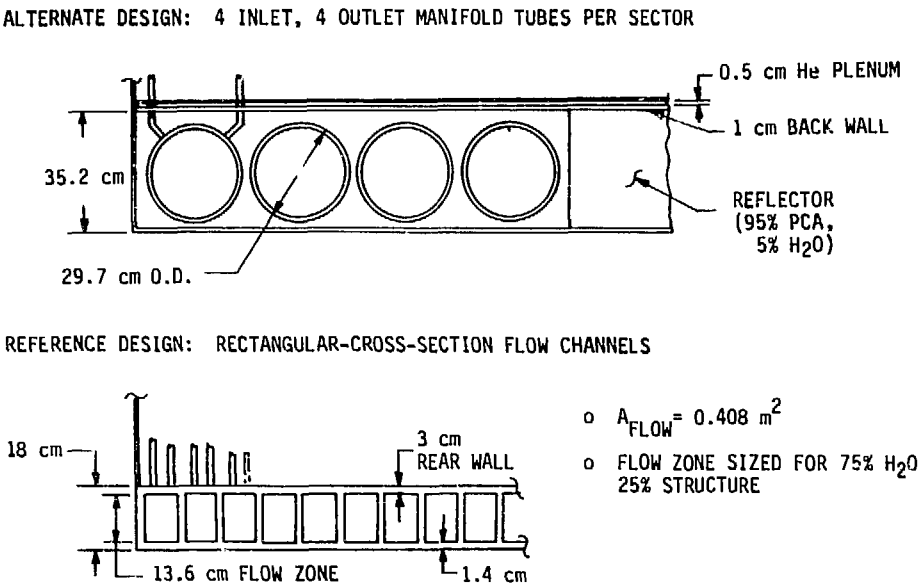

Fig. 9.4-5. Reference design and alternate for SB/H_2O reflector/manifold zone

as major structure for the blanket sector. It also acts as a neutron reflector for the breeding zone to enhance tritium breeding.

The region is sized on the basis of maximum volumetric flowrate requirements, at a maximum allowable coolant velocity of 6 m/s and an arbitrary water:steel volume ratio of 3:1. The required equivalent coolant thickness is 13.5 cm, which results in 18 cm total zone thickness after 4.5 cm equivalent thickness of ferritic steel structure is added in the form of front and rear walls plus thick ribs which divide the coolant region into multiple separate flow channels.

The coolant tube ends from the breeding zone are connected directly to the front wall of the manifold region. Individual welds of the two tubes at

each end of the tube assembly provide two separate pressure boundaries against leakage of the coolant into the breeder zone.

The manifold region for the inboard blanket modules is very similar to that described above, except that only a 7 cm total depth is neded because the total coolant flow through the inboard region is considerably less than for the outboard region.

9.4.2 Concept Evaluation Summary

The $LiAlO_2/H_2O$/FS/Be tokamak concept is ranked overall in the lowest group of the seven tokamak concepts. Despite its top rating in the area of economics, it is ranked near the bottom of the group in the engineering, safety, and R&D areas (see Chapter 3). The results of the evaluation of the concept are briefly summarized in this section.

9.4.2.1 Engineering

This concept ranks next to last in the Engineering Evaluation, scoring only ~66% of the score achieved by the top-ranked concept in this category. Its ratings in maintenance (11.3 of 15) and power load/surface load increase capability (7.5 of 10) are relatively good. However, the complexities resulting from use of a neutron multiplier, a separate purge system, and many small-diameter tubes of double wall construction, combined with the high pressure of the coolant, result in a low score of 10.7 out of 25 in the Engineering Complexity and Fabrication index. The relatively low 3-D tritium breeding ratio of 1.16 results in a low score of 8.3 out of 25 in the Tritium Breeding and Inventory index. Resources and Power Variation scores are also low.

9.4.2.2 Economics

The concept does very well in the economics area. It has the lowest cost of electricity (COE) of all the tokamak concepts. The cost of capacity, in $/kWe, is also lowest, and its annual plant operating cost is second lowest of the group. These results are achieved even though the concept's first wall/blanket cost (everything within the reactor envelope) is by far the highest of the group. The 90% ^6Li enrichment of the breeder and the complex first wall and coolant tube structure are significant cost elements. That cost is more than offset by the heat transfer system cost, nearly the lowest for the

group. Thermal power and net electric power were highest for the group, and thus the concept has also been helped in this comparison by economics of scale.

9.4.2.3 Safety and Environmental

The concept is ranked in the bottom group for this area, together with the nitrate-salt-cooled concept. The primary reason is tritium control, and the safety risks and potential health hazards associated with the permeation of relatively large quantities of tritium into the water coolant. Activation of the aluminum in the breeder, the toxicity of Be, and the perceived greater risk of leaks associated with the high pressure of the coolant are also important factors.

Any future improvement in this area would probably be the result of development of much more effective tritium barriers, and/or much more efficient methods of removing the tritium from the solid breeder. The use of another ternary ceramic breeder with much lower activation, e.g., Li_4SiO_4, would slightly improve the safety rating. However, little can probably be done in other areas, given the high coolant pressure and the need to use Be.

9.4.2.4 Research and Development

The concept finishes next to last in this category. It has the second-worst potential flaws (development risk) rating of the tokamak group, and together with the other ternary oxide solid breeders is in the highest "cost" group in terms of R&D resource requirements (money, facilities and time). The primary factors are the perceived relatively high risks and resource requirements for development of adequate tritium control measures, sphere-pac Be and solid breeder, and breeder-to-structure interface control methods.

9.4.3 Design Details and Related Issues

The following subsections present brief discussions of some of the more important issues involved in selection of design details for the $LiAlO_2/H_2O$/FS/Be tokamak blanket concept.

For the solid breeder water-cooled (SB/H_2O) blankets in general, the rationale for selections of (1) modular instead of monolithic approach,

(2) breeder-out-of-tube (BOT) instead of breeder-in-tube (BIT) or layered approach, and (3) sphere-pac breeder fabrication instead of sintered product were discussed in the Interim Report[1] and will not be repeated here.

9.4.3.1 Mechanical and Structural Design

Module Configuration - There are a number of important factors in determining whether the lobular and rectangular shape is a better overall choice for the module configuration:

- o Void fraction for "nose" region
- o Reaction of loads due to plasma disruption
- o Overall structural fraction
- o Containment of coolant pressure in accident
- o End wall configuration (toroidal direction)
- o Degree of load sharing between adjacent modules

The relative increase in void space for the lobular module because of its semi-cylindrical front region is equivalent in "lost" blanket depth to ~21% of the lobe radius, or ~3 cm for the 15-cm radius in the reference design. To get performance equivalent to a rectangular module in terms of breeding and thermal energy recovery, the lobular module must be deeper than the rectangular module by an amount roughly equal to 21% of the nose radius.

The reaction of loads due to actual or equivalent blanket internal pressure was an important factor in comparing module configurations. Disruption loads for the tokamak blankets were calculated to be much higher than for previous studies[2,3]. These loads act on the first wall to push it toward the plasma. The loads were estimated to act as an equivalent pressure internal to the blanket, uniformly distributed over a flat first wall but distributed according to a cosine function over a semi-cylindrical first wall (Sec. 5.1). The tokamak disruptions were assumed to be relatively frequent, and thus these loads would have to be taken as normal operating loads so that the structure would not be plastically deformed, which would require reactor shutdown and replacement of all first wall/blanket sectors.

A second important source of internal pressure is coolant pressure within the breeding zone in the event of a coolant tube large-scale leak or rupture. If that pressure ruptures the module walls, then Be, breeder and steam

could be ejected into the plasma chamber, markedly complicating cleanup and recovery operations. If the pressure is contained within the module, then only removal and replacement of a single sector would be required, with no cleanup needed. This would be both a safety and an economic advantage.

A third pressure source is the helium purge gas within the module. For sphere-pac Be and breeder, thermal conductivity is a strong function of helium gas presure over the range of ~0.1 to 6 atm (~0.01 to 0.6 MPa). The maximum pressure would be an important consideration, except for the disruption (normal) and coolant pressure (accident) loads which are much more influential.

The trade-off study to determine disruption load reaction capabilities for the two module approaches is described in Sec. 9.8.2. The results indicated that for the tokamak concept, the internal pressure loads are more efficiently reacted by the lobular module. The internal supports required for the rectangular module are an important additional consideration. These supports would be in contact with the breeder or SB/Be mixture, and would therefore require active cooling. Also, since their spacing would be < 10 cm for the loads considered, the graded coolant tube spacing laterially at any depth in the module would be impacted by the presence of the supports. The net effect of these supports would be a significant increase in th relative amounts of structure and coolant within the breeding zone and a significant reduction in tritium breeding ratio. Structurally connecting the supports to the first wall and the back wall, and connecting the coolant channels of the supports to the manifolds, represents further complications.

The degree to which internal pressure loads acting on the module side wall (in the poloidal direction) can be reacted by equal and opposite loads on the walls of the neighboring modules, takes on major importance when large-magnitude pressure levels are involved. This was not the case for the Li_2O/-H_2O/FS concept in the Interim Report[1], where the maximum internal load considered was the 1-atm helium purge gas pressure. If adjoining module side walls are not in full contact along their flat surfaces, then closely-spaced internal supports would be required within each module to connect its two side walls to make the load self-reacting. Increasing the side wall structural thickness instead, is structurally far less efficient. These supports, again

actively cooled, would be normal to the coolant tube axes and would significantly complicate the design problems.

The end walls (in the toroidal direction) are subjected to the same internal purge gas pressure (normal) and coolant pressure (emergency) levels as the other walls. In addition, they experience torques during disruptions resulting from electromagnetic loads, and must transmit these loads to the major sector structure in the manifold region. For rectangular modules, the internal pressure loads are reacted by the first wall, back wall, side walls and the internal supports connecting the first and back walls. For lobular modules, the internal supports would not be present, but the end wall can be tapered in thickness and "cantilevered" from the back wall, with local large load-carrying gussets added if needed to connect the inside surfaces of the back wall and end wall (as with the helium-cooled blanket concepts, Chapter 8).

The lobular module configuration was finally selected for the $LiAlO_2$/-H_2O/FS/Be tokamak concept (as well as for the other SB/H_2O tokamak concepts) primarily on the basis of:

- o structural efficiency in reacting disruption loads, and coolant pressure loads in accidents; and
- o relative simplicity of breeding zone mechanical design.

Double Wall Tubes (DWT) - The perceived need for double walled coolant tubes for SB/H_2O concepts to achieve acceptable reliability against leaks into the breeder zone was discussed in Sec. 9.3.1.1. Some important considerations in determining the DWT design details are:

- o Sizing of individual tube diameters and wall thicknesses
- o Contact of annular surfaces
- o Pressure of oxide films on annular surfaces
- o Gas or vacuum condition of annulus
- o Tube end weld configuration
- o Tube fabrication

The primary design objective of the DWT approach is to create two separate barriers for the coolant, such that both barriers in any given DWT assembly would have to be breached before water could come into contact with the breeder surrounding the tube assembly. The two boundaries should be as independent as possible so that failure of one does not increase the likelihood of

failure of the other. The two tubes should therefore each be designed so that primary stresses from the 15.2 MPa coolant design pressure are at or below the allowable stress level, S_{mt}. For the DWT in the reference design, the highest stress is ~116 MPa (outer tube), 5.75 mm inner radius and 0.75 mm thickness, which is below the 125 MPa allowable for HT-9 ferritic steel at 350^0C, in the tube near the first wall. Load sharing in this composite tube assembly is not considered.

Heat transfer across the annular region is a function of the % contact area and contact pressure, between the two surfaces, and of the pressure and thermal conductivity of any gas present in the annulus. Adequate heat transfer will occur even if the contact area (mutually contacting asperities on a microscopic scale) is only a few percent of the total annular surface area[6], and resulting temperature drops across the annulus would be $\lesssim 10^0$C for typical blanket conditions if gaseous helium at ~1 atm pressure is present. Minimizing the contact area is considered important because there may be increased tritium migration from the outer to inner tube at points of contact due to the possible reduction or absence of natural oxide films.

Leak detection for the annular region is not important for this application. Reactor shutdown would not be necessary until water was detected in a module breeder zone, meaning one of the DWT had developed a leak in both tubes. Since the presence of water in the annulus would mean only that the inner tube of one or more assemblies was leaking, the detection of leaks in this region is not relevant to reactor operation. Purging of the annulus, using helium gas with 1% O_2 added flowing through shallow grooves set in to the outer tube's inner surface, was also considered as a means of removing nonoxidized tritium (T_2 or HT) that had migrated through the outer tube. However, calculations of oxidation kinetics (Sec. 6.6) indicate that the reaction is very slow and would not substantially reduce overall tritium permeation into the blanket coolant unless purge gas volumetric flow rates or flow velocities were at levels so high as to be unworkable. Therefore, for the reference design, the annular region is sealed by the tube end welds, with helium at 1 atmosphere contained to enhance heat transfer across the annulus.

There are several important considerations in selecting the configuration and location of the welds for the ends of the DWT. The coolant path between the inner tube and the manifold channel must be unobstructed. The purge gas

tube at the outer surface of each DWT must connect to the shallow helium purge gas plenum at the back wall. Finally, the welds for inner and outer tubes should be as independent as possible to minimize the chances for common-mode or related failures. Of the various options considered (Fig. 9.4-3), the simplest, Option 3, was selected for the reference design.

Discussions and previous work on DWT fabrication indicate it is state-of-the-art or better for the requirements of SB/H_2O blanket concepts. Achieving the desired amount of contact area between tubes, even down to a few percent, would not be a problem.[7] Tube bending to form the U-shaped assemblies is not difficult if bend radii are adequate ($\gtrsim$10 x tube radius).[7] The added costs for DWT, over and above the costs for two single wall tubes, are only a very small fraction of total blanket costs (Sec. 3.2). It should be noted that the LMFBR program developed and qualified three vendors to produce DWT of similar size and materials for the double wall tube steam generator.[8]

Manifold Configuration - For the manifold region at the rear of the blanket, the two approaches considered were separate large-diameter tubes and an integral manifold with coolant channels of rectangular cross section.

It was desired to have two separate primary coolant loops within each blanket module as in the Starfire[2] and DEMO[3] SB/H_2O blankets, to provide redundant capability to remove first-wall/blanket afterheat in the event one circuit had to be shut down due to a failure or scheduled maintenance on some component.

The depth of the blanket was constrained to be 70 cm or less. From sector coolant flow rates and manifold flow velocity requirements (6 m/s maximum, from Ref. 3), it was determined that the equivalent thickness of coolant in the manifold region would be a maximum of ~13.5 cm, for the tokamak outboard blanket configuration. From the neutronics standpoint, the water-to-steel volume ratio in the manifold is not critical. Based on structural considerations, a 3:1 ratio was selected which results in ~4.5 cm equivalent thickness of ferritic steel. For the integral manifold, this structure includes the ribs between adjacent coolant channels (at essentially equal pressures) together with the front and back walls. Overall, the integral manifold is structurally very rigid, and little additional structural mass would be necessary behind the module for completing the overall sector structure.

For either configuration, the coolant tubes within the breeder zone are routed to terminate at specific channels. The exact routing, and specification of tube/channel hookup combinations, would be determined through detailed calculations and layouts, with the most important considerations being (1) assuring adequate cooling of the breeder in the rear of the blanket at all points, and (2) achieving uniform coolant mass flow rates in inlet and outlet channels for both circuits.

A manifold using large-diameter tubes would require considerably more depth than an integral manifold, because of the large void areas required around each tube for welding clearance and access and for supporting structure. The complexity of welding the small-diameter (~1 cm) blanket coolant tubes to the large-diameter (~30 cm) manifold tubes, and of maintaining pressure boundary integrity at the back wall of the breeding zone, would be considerably greater than for the integral manifold. Since it is not feasible to have the large-diameter tubes act as overall sector structure, a separate structural framework would be needed for support of the manifold tubes and modules and to provide sector structural integrity.

Based on these considerations, the integral manifold configuration was adopted for the tokamak concept reference design.

First Wall - A first wall configuration using rectangular cross section flow channels was selected over the corrugated panel approach used for Starfire and DEMO SB/H_2O blankets (see Sec. IX.3.4.2 of Ref. 1). Subsequently, the principal first wall considerations for the $LiAlO_2/H_2O$/FS/Be tokamak concept were:

- o Orientation of flow channels (poloidal vs. toroidal)
- o Integration with lobular module configuration

For the initial SB/H_2O blanket design,[1] the first wall flow direction was toroidal. Since the modules can extend the full width of the sector in that direction, the flow path is long, ~4 to 6 m. First wall flow velocity is limited to $\leq$8 m/s,[3] and the allowable coolant temperature increase is fixed at 40^0C. The resulting channel depth for a given heat load (surface heat flux plus nuclear heating) is thus inversely proportional to the channel length over which the heat is absorbed. Structural and coolant equivalent thicknesses increase roughly in direct proportion to channel depth. Because adequate tritium breeding became a more critical problem due to the use of double

wall coolant tubes and the incorporation of very low thermal conductivity values for irradiated solid breeders, it became much more important to minimize the amount of steel struxture and water coolant in the first wall.

For the first wall of a lobular module, the flow path length in the poloidal direction is shorter than for the toroidal direction by a factor of ~4 to 10, depending on lobe radius and module width. The same hold true for rectangular modules since they can be made to arbitrary widths poloidally. The choice of poloidal or toroidal flow direction makes little difference from the mechanical design standpoint. In either case, flow distribution and collection plenums connecting the first wall to the manifold are needed at the inlet and outlet ends. Also, flow direction has no effect on first wall structural requirements except that more structural area and cross section moment of inertia are automatically provided by the deeper channels for the larger toroidal flow paths.

Based on these arguments and the results from the thermal-hydraulics and structural analyses (Sec. 9.8.1 and Sec. 9.8.2), the poloidally-oriented flow direction was selected for the lobe-shaped first wall.

Inboard Blanket - The inboard vertical module for the Starfire and DEMO SB/H_2O blankets was designed in both cases without manifolds, to minimize total blanket depth for reduced reactor size and capital costs. The coolant flow direction for the first wall and blanket coolant tubes was vertical; flow distribution/collection plenums were located behind the large "canted" module at either end of the vertical module, where space could be provided with much less impact on reactor size. This approach is not considered feasible for the lobular modules chosen for the present concept. Integration of the modules for the vertical inboard section, regardless of orientation, with the modules in the upper and lower canted regions of the sector would be very difficult and complex, both structurally and mechanically, if no manifold were used. Therefore, the reference design concept uses an inboard blanket very similar in overall configuration to the outboard blanket, except that manifold depth is reduced to only 7 cm (vs. 18 for the outboard blanket) by configuring the overall sector flow paths so that coolant mass flow rates are minimized.

9.4.3.2 Thermal-Hydraulics

Most of the important design issues for the SB/H_2O concept that are related to thermal-hydraulics were reported on in Ref. 1 and will not be discussed further in this report. Among these are:

- o First wall integral with blanket instead of separate
- o Use of sphere-pac breeder instead of sintered product form
- o Breeder-out-of-tube approach (BOT) instead of breeder-in-tube (BIT) or layered approaches.

A number of lesser issues were investigated. Several of these related to the effects of radiation damage and the pressure of helium purge gas on breeder or Be/breeder mixture thermal conductivity. These effects influence the minimum and maximum temperature limits that the concept must be designed to achieve under normal conditions.

Breeder Zone Tube Spacing - The most important requirement in determining coolant tube spacing within the breeder zone was maintaining breeder temperature at all points within the range between minimum and maximum allowable temperatures. The design approach used was to first size a theoretical cylinder of breeder around each tube according to the local nuclear heating rate, q_n, such that the temperature at the outer radius equalled the maximum allowable temperature (Fig. 9.4-6). This cylinder was then assumed to circumscribe a square cell of breeder, so that only the four corners of the square would be at the maximum temperature. The sides of the square cell were d = (0.707) x (cylinder diameter). Thus, lateral spacing of tubes in any bank (equal q_n values) was equal to the value of d. Radial spacing between tube centers of banks i and j was set equal to $(d_i + d_j) \div 2$. Resultant tube spacing for all banks within the breeding zone of the reference design is shown in Table 9.4-2. The square cell approach was described and compared to other possible approaches in Sec. IX.3.3.1 of Ref. 1.

Breeder Minimum Temperature - The minimum allowable temperature for the $LiAlO_2$ breeder is 350^0C, based on tritium inventory considerations (Sec. 6.3). Since the minimum coolant temperature is 280^0C and the nominal temperature difference across the double wall tube assembly is only 30 to 40^0C, some additional thermal resistance is necessary over most of the tube length between the breeder and the outer tube surface (see Sec. 9.8.1). Conceptually, this could be accomplished in one of several ways:

1. Obtain or estimate $\dot{q}_N'''$ versus depth into blanket.
2. Generate curve of r_o (or d) versus $\dot{q}_N'''$.
3. Use results of (2) to generate volume fractions for each breeder zone material as function of $\dot{q}_N'''$.
4. Beginning at first wall depthwise through blanket, use the two curves to estimate maximum size of breeder element for which temperature limits are not violated at the average $\dot{q}_N'''$ predicted for the element midpoint depthwise.
5. Perform neutronics analysis using results of (4).
6. Compare $\dot{q}_N'''$ curve from (5) to that assumed in (1). If necessary, use the new curve in successive iterations of steps (4) through (5) until reasonable agreement (within 5 to 10%) of "old" and "new" $\dot{q}_N'''$ curves is obtained.
7. Final breeder sizing is given by results of (3) and (5) for the final iteration.

(a) General Approach to Sizing Breeder Elements

BOT APPROACH

For $\frac{dT}{dr} = 0$ @ r_o, $T = T_{min}$ @ r_i:

$$(T_{max}-T_{min}) = \frac{\dot{q}_N''' r_o^2}{4k_\beta} - 1 - 2 \ln \frac{r_i}{r_o} + \frac{r_i^2}{r_o}$$

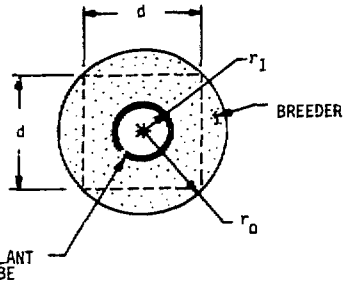

NOMENCLATURE

- T_{max} = Breeder maximum temperature, K
- T_{min} = Breeder minimum temperature, K
- r_o, r_i = Breeder cylinder outer and inner radius, mm
- $\dot{q}_N'''$ = Local average nuclear heating rate, W/mm^3
- k_T = Breeder thermal conductivity, W/mm-K
- d = $(r_D) \times 2 \times .707$ = cell side

(b) Equations for determining cell size.

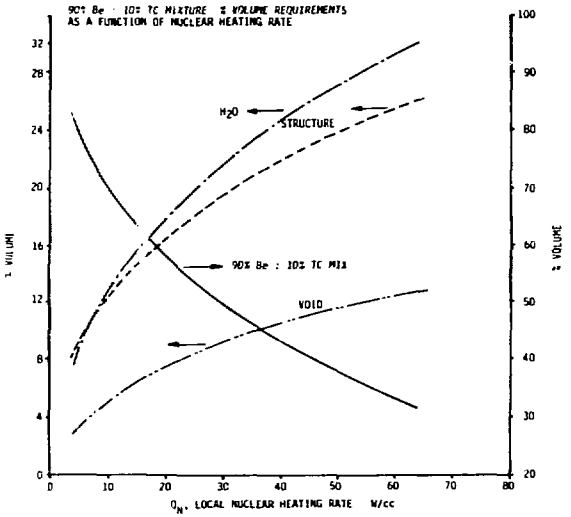

(c) % Volume vs q_n for Blanket Materials

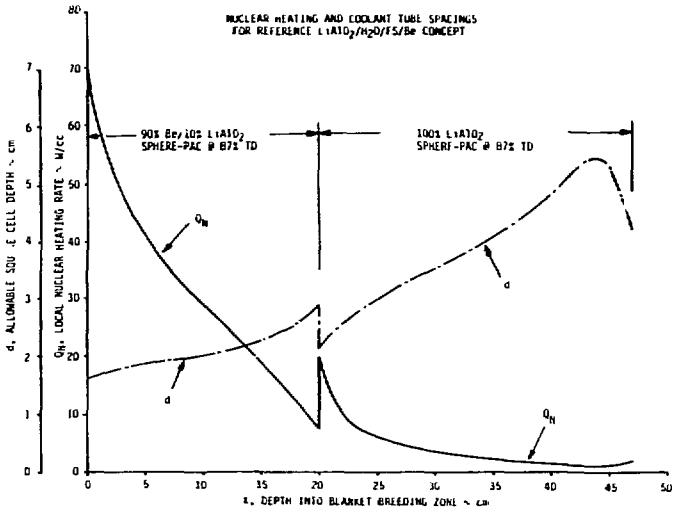

(d) q_n and d (allowable) vs Depth into Blanket.

Fig. 9.4-6. Methodology for Determining Cell Sizing/Tube Spacing

TABLE 9.4-2. COOLANT TUBE SPACING FOR REFERENCE DESIGN $LiAlO_2/H_2O/FS/Be$ CONCEPT (TOKAMAK, TMR)

TUBE BANK	DEPTH INTO BLANKET	RADIAL SPACING[a]	LATERAL SPACING	(TUBES/m)[a]	ZONE
1	0.00 cm	1.65 cm	1.65 cm	60.6	
2	1.65	3.4	1.75	57.1	
3	3.4	5.2	1.8	55.5	90% Be: 10% $LiAlO_2$ SPHERE-PAC @ 87% TD
4	5.2	7.05	1.85	54.0	
5	7.05	9.0	1.95	51.3	
6	9.0	11.0	2.00	50.0	
7	11.0	13.05	2.05	48.8	
8	13.05	15.2	2.15	46.5	
9	15.2	17.55	2.35	42.5	
10	17.55	20.0	2.45	40.8	
11	20.0	22.4	2.4	41.7	
12	22.4	25.2	2.8	35.8	
13	25.2	28.35	3.15	31.7	100% $LiAlO_2$ SPHERE-PAC @ 87% TD
14	28.35	31.85	3.50	28.6	
15	31.85	35.80	3.95	25.3	
16	35.80	40.30	4.50	22.2	
17	40.30	45.55	5.25	19.0	
18	45.55	47.0	(b)		
				Σ = 711	

[a] Tubes per meter poloidally, per sector (4 m avg. length).

[b] Cooled by conduction to back wall.

- Addition of an alumina (Al_2O_3) coating applied in graded thicknesses by plasma spraying
- A thin metallic felt with very high porosity (~80-85%)
- Revising the DWT annulus conditions to a vacuum (instead of He gas) and/or even lower % contact area.

Because the $LiAlO_2$ tritium inventory for this concept is strongly influenced by the minimum operating temperature (Sec. 6.3), future studies should evaluate the desirability of increasing the design minimum breeder temperature to decrease tritium inventory, which would be accomplished at the expense of tritium breeding ratio unless design maximum temperature was also increased by an equal amount.

Effect of Helium Pressure on Sphere-Pac Thermal Conductivity - One of the disadvantages to water-cooled solid breeder designs has been the difficulty in accommodating changes in reactor operating power level while maintaining breeder temperature within the allowable range. The use of the sphere-pac fabrication approach for the breeder and the Be/breeder mixture, together with the helium purge gas which fills the breeding zone, permits the reactor operator to adjust the sphere-pac bulk thermal conductivity by adjusting helium purge gas pressure between ~1 and 6 atm. Lower gas pressures result in lower k_t values. Since breeder maximum temperature during operation is inversely proportional to k_t but directly proportional to neutron wall load, helium gas pressure can be varied in accordance with a predetermined relationship (Fig. 9.4-7) so that breeder maximum and average temperatures remain at nominal design levels as reactor power level is reduced, thus preventing blanket tritium inventory from rising above the normal level. The topic of variable k_t for sphere-pac is discussed further in Sections 6.3 and 9.8.1.

Accommodating Radiation Damage Effects - For in situ solid breeder blankets, it is necessary to design such that the breeder is maintained within allowable temperature limits from beginning of life (BOL, zero fluence) to end of life (EOL, maximum fluence). Because the bulk k_t value for sphere-pac $LiAlO_2$ breeder is dominated by conduction through the helium gas, the effects of irradiation on sphere-pac k_t are not as severe as for sintered product (Sec. 6.3 and Fig. 9.4-8). The ratio of k_{BOL}/k_{EOL} varies little with helium purge gas pressure, 1.08 at 1 atm to 1.14 at 6 atm. A complicating factor for both initial design and for blanket operation is the difference between k_t at

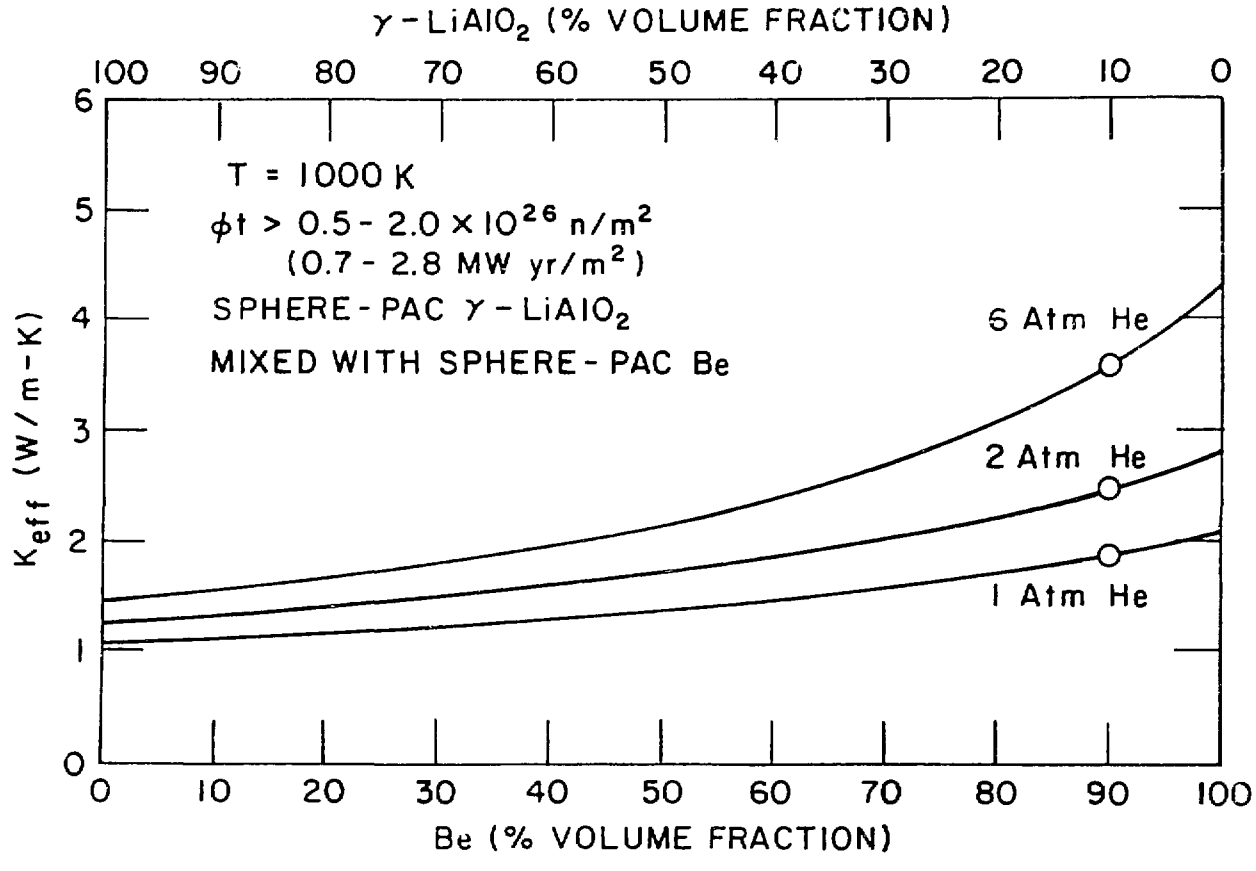

Figure 9.4-7. Effective thermal conductivity of a mixture of sphere-pac γ-$LiAlO_2$ and Be.

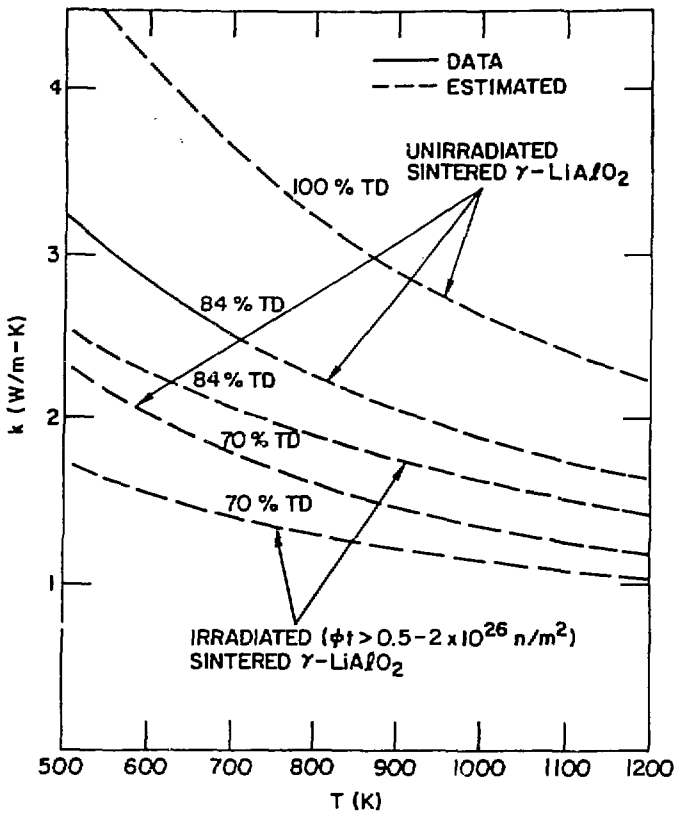

Figure 9.4-8a. Thermal conductivity of sintered γ-$LiAlO_2$ as a function of temperature.

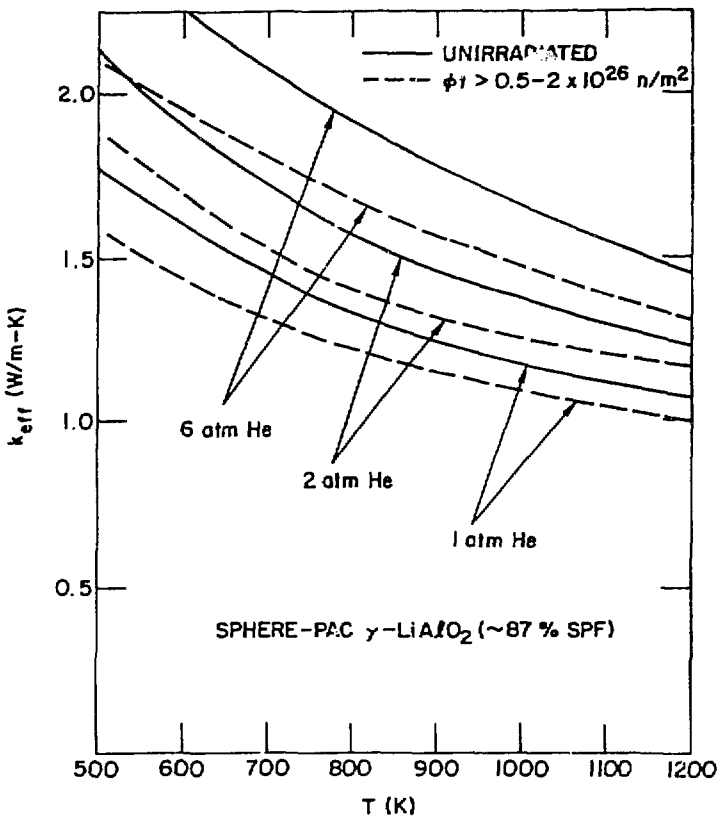

Figure 9.4-8b. Thermal conductivity of sphere-pac γ-$LiAlO_2$ as a function of temperature and helium fill-gas pressure.

the back of the blanket (low fluence) and at the front of the blanket (high fluence). Since helium pressure must be uniform throughout the blanket, it is not possible to achieve a uniform k_t everywhere by simply changing helium pressure. Since k_t decreases with fluence until the predicted saturation value ($0.7\text{-}2.8 \times 10^{22}$ n/cm^2) is reached, actual breeder maximum temperatures in regions for which fluence was below the saturation value would be less than the maximum design temperature. However, breeder minimum temperature--the most critical operating parameter influencing tritium inventory--would vary very little regardless of the local bulk k_t. Thus, the overall effect on blanket performance of the varying k_t values throughout the breeding zone would not be significant.

9.4.3.3 Neutronics

The neutronics analyses performed for the $LiAlO_2/H_2O$/FS/Be concept, and for the other SB/H_2O concepts, are discussed in detail in Sec. 9.8.4. The design details most influenced by the neutronics results were:

- Amount, location and fabrication form of Be neutron multiplier
- Radial depth of Be, SB/Be and SB regions in breeding zone

The location of a region of pure Be between the first wall and the solid breeder region results in high local q_n values for the breeder, as much as 100 to 120 W/cm^3 for the reference 5 MW/m^2 neutron wall load. Maximum TBR is obtained if a thin layer of breeder precedes the Be, but in this case q_n is even higher. Design difficulties are encountered in trying to space the cooling tubes closely enough to adequately cool these regions, because the tube outer surfaces nearly touch each other and there is virtually no room for any purge gas flow channels near the tubes.

The most desirable solution overall was to mix the $LiAlO_2$ breeder and the Be together, with both in sphere-pac form, in some predetermined volume ratio. This reduced the maximum q_n near the first wall to ~70 W/cm^3, which is a manageable value in conjunction with the $k_{t(eff)}$ and temperature limits assumed for the mixture. The conductivity of the mixture is a function of helium purge gas pressure and of the volume ratio (Fig. 9.4-7). For any mixture ratio, $k_{t(eff)}$ is much closer to the k_t value of pure breeder than to that of pure Be, which again illustrates the dominant role of conduction through the helium for sphere-pac. Temperature limit for the mixture was set

at 650°C minimum based on minimizing Be radiation damage effects (swelling). Compatibility of the Be and $LiAlO_2$ at these temperatures is not considered to be a problem (Sec. 6.5).

Based on results of the neutronics analysis (Sec. 9.8.3), the SB/Be region depth was selected to be 20 cm, with the Be/SB volume ratio at 90:10. The remaining 32 cm of depth is all $LiAlO_2$ breeder. In order to maximize TBR for any combination of Be and breeder thicknesses, the $LiAlO_2$ breeder was enriched with ^6Li to the 90% level. Further increases in TBR could be obtained by increasing the thickness of the SB/Be zone, but TBR appears to peak at a zone depth of ~30 cm. Detailed evaluations would be required to find the economically optimum combination of $\%^6Li$, zone depth, and volume ratio, but this was not done because the effects on blanket costs and energy production to a first order would not be significantly changed.

9.4.3.4 Tritium Control

The control of tritium within the first-wall/blanket module represents the largest uncertainty at present in assessing the feasibility of the $LiAlO_2/H_2O$/FS/Be tokamak concept. The major risks are in these areas:

- o Radiation damage effects on tritium release
- o High diffusive inventory
- o High inventory at grain surfaces
- o Tritium permeation into water coolant

There has been little definitive experimental work to date to help determine the severity of the problems. The design-related issues are briefly discussed below.

Radiation Damage Effects - This topic is discussed in detail in Sec. 6.3. For design purposes, it has been assumed that use of $LiAlO_2$ in sphere-pac form at ~86% packing density (with the individual spheres each at ~100% of theoretical density), with maximum temperature $\leq 1000^0C$ would ensure that the original tritium release rates for non-irradiated material would be maintained throughout the blanket lifetime (~4 to 5 calendar years). If sintering of the spheres or closure of open porosity within spheres were to occur at these conditions, the design maximum temperature would have to be reduced. Conversely, it is possible that future experiments might show that design maximum

temperature could be increased above 1000°C. This could enable a large reduction in tritium inventory by simply raising design minimum temperature by the same amount that design maximum temperature is raised, since ~86% of the reference design's tritium inventory is in the coldest ~50°C zone of breeder around each coolant tube.

High Diffusive Inventory - Tritium inventory in the breeder at steady state that is related to diffusion effects within the grains is high for the $LiAlO_2$, over 2 kg. If present estimates of the diffusion coefficient at low temperatures under irradiated conditions (Sec. 6.3) are much lower than the real value, the resulting inventory could be unacceptable from the safety standpoint. Increasing the minimum operation temperature for the breeder or significantly reducing the diameter of only the largest of the three sphere-pac ball sizes--presently 1200 μm--would significantly reduce calculated inventories. However, either measure would also reduce TBR if no other changes were made because the total volume of breeder relative to the structure and coolant volumes would decrease because of the reduced allowable temperature range in the first case, and reduced smear density in the second case.

High Inventory at Grain Surfaces - Based on present interpretations of the TRIO experiment results (Sec. 6.3), the addition of 1% dry hydrogen to the helium purge gas is considered sufficient to "swamp" the breeder grain surfaces with hydrogen, so that the tritium atoms at the grain surfaces form HT molecules which are then relatively easily removed from the surface into the helium purge gas. Thus, predicted adsorption-related tritium inventory for the reference design is very low. However, further experiments to corroborate the TRIO results/interpretations are considered necessary, and this area must be considered a significant uncertainty until further data are available.

Tritium Permeation Into Water Coolant - This concern has the largest uncertainty of all those discussed in this section. There are only three natural oxide barriers on the steel tube surfaces to retard permeation into the primary coolant of tritium in the helium purge gas within the blanket: one on each of the annular surfaces of the double wall tube deposited prior to joining of the two tubes, and one on the inside surface of the inner tube at the water coolant. The outer surface of the outside tube is in contact with the helium purge gas, where any oxide layer would be reduced by the 1% H_2

added to facilitate tritium removal. Only one oxide layer, that at the coolant channel inner surface, is present at the first wall to retard tritium permeating through the structure from the plasma.

In calculating the rate of tritium permeation into the water coolant, each layer was considered to represent a "barrier factor" of 100 (Sec. 6.6). Tests indicate this value may be at the high end of the range achievable for ferritic steels, and that factors of 20 or less may be more realistic. Such factors would drastically raise the rate of tritium permeation into the water coolant. The steady-state level of tritium in the water was set at 1 Ci/liter, which results in a 100 Ci/day loss to the environment if steam generator leakage is the assumed 100 liter/day (all leakage to the secondary side is assumed to be lost to the environment). Water processing costs to remove tritium were based on INTOR work,[9] and are considered fairly uncertain. In theory, one could remove tritium from the water at almost any rate to hold the contamination to very low levels, but in reality there will be some maximum level beyond which the size, cost and capacity requirements for the processing are economically not reasonable.

Before tritium contamination of the primary water coolant can be resolved as a feasibility issue, quantitative data must be developed in the following areas:

- o Allowable tritium concentration in primary coolant
- o Realistic steam generator primary coolant leakage/loss rates
- o Realistic permeation rates through natural oxide layers
- o Processing equipment capital and operating costs as functions of flowrate and tritium concentration.

9.5 $LiAlO_2/H_2O/FS/Be$ Concept - TMR (R=1)

This section describes the tandem mirror reactor blanket concepts that uses $LiAlO_2$ solid breeder, pressurized water coolant, ferritic steel structure, and beryllium as a neutron multiplier. Because the concept and the reference design are identical or very similar in most respects to that already discussed in detail in Sec. 9.4, only those areas where differences exist between the tokamak and TMR concepts will be discussed. Generic differences between tokamak and TMR configurations for water-cooled solid breeder blanket concepts were previously discussed in Sec. 9.3.2.

9.5.1 Reference Blanket Design Configuration

General Description - The reference design for the $LiAlO_2/H_2O$/FS/Be TMR concept (summarized in Table 9.5-1) is basically identical to that shown in Fig. 9.4-1 for the tokamak version of the concept. The major difference is that the total blanket depth including manifolds is 70 cm all around the plasma chamber, since there are no separate inboard or outboard regions as in the tokamak.

First Wall - The first wall is very similar to that for the tokamak version of the concept, with the exception that erosion thickness allowance can be reduced to ~0.4-0.5 mm, or 0.1 mm/yr of blanket life. As discussed in Sections 9.3.2.2 and 9.8.2, active cooling for first walls of TMR solid breeder blankets was found to be necessary. Given the other requirements and goals for SB/H_2O blanket concepts in addition, the conclusion was made that the basic TMR first wall configuration should be the same as for the tokamak concept.

Manifold Region - The manifolds for the concept are located immediately behind the breeding zone and extend the full length of the module. Depth of the zone is 18 cm. As discussed in Sec. 9.3.2.4, in-depth analysis with consideration of MARS or advanced MARS rector configurations and cell length/magnet size requirements could lead to some changes in an optimized manifold region, but these are not considered significant for purposes of concept comparative evaluations within the BCSS.

9.5.2 Concept Evaluation Summary

The results of the evaluation of the $LiAlO_2/H_2O$/FS/Be concept for TMR's are briefly summarized in this section. A summary listing of the major parameters and features of the blanket concept and the associated power conversion system is presented in Table 9.5-1.

Engineering - The concept finishes last in this evaluation category, although it is relatively considerably closer in numerical ranking to the top concept than was the case for the tokamak concept. The only significant change in the concept's point score was due to the increase in tritium breeding ratio compared to the tokamak concept; this was due principally to the differences in reactor configuration.

TABLE 9.5-1.
MAJOR PARAMETERS AND FEATURES OF
$LiAlO_2/H_2O$/FS/Be CONCEPT - TMR

General Description	
Materials	
Coolant	Pressurized H_2O
Breeder	γ-$LiAlO_2$ @ 86% TD; 90% ^6Li
Neutron Multiplier	Be @ 86% TD
Structure	HT-9 Ferritic Steel
Purge Gas	Helium
Major Design Parameters	
Reactor blanket thermal power, MW_{th}	3417
Average neutron wall load, MW/m^2	5.0
Average first wall surface heat flux, MW/m^2	0.05
Coolant	
Inlet/Outlet temperature, $^0C/^0C$	280/320
Maximum pressure, MPa	15.2
Breeder	
Minimum/maximum temperature, $^0C/^0C$	350/1000[c]
Maximum pressure, MPa	~0.6 (Purge Gas)
Structure	
First wall/blanket maximum temperature, $^0C/^0C$	~381[f]/340
Minimum/maximum temperature at:	
Coolant interface, $^0C/^0C$	~290/330
Breeder interface, $^0C/^0C$	~350/350
Neutronics	
Tritium breeding ratio	
1-D, 100% coverage	1.26
Net (3-D with all geometrical details and penetration)[a]	1.22
Maximum nuclear heating rates	
Be/breeder, W/cc	70
Breeder zone, W/cc	19
Structure, W/cc	66
Energy (1-D calculation)	
Multiplication factor	1.394
Deposited in heat recovery zone, MeV	1.386
Deposited in heat loss zone, MeV	0.008
First Wall/Blanket Design Description	
Thickness (including manifolds), m	0.70
Manifold thickness, m	0.18
Percent structure/percent coolant in manifold region	25/75
Coolant ΔP (total), MPa	0.2
Primary coolant loop pumping power, MW_e	27.5
First Wall	
Description	Welded; rect. x-sec. channels
Minimum/maximum coolant temperature, $^0C/^0C$	280/320
Maximum structure temperature, ^0C	~381[f]

TABLE 9.5-1 (Continued)

Blanket	
Description	Lobular module. Double wall coolant tubes within Be/breeder (first 20 cm) or breeder (last 32 cm), in sphere-pac form.
^{6}Li enrichment, %	90
Minimum/maximum coolant temperature, $^{0}C/^{0}C$	280/320
Maximum structure temperature, ^{0}C	~340
Tritium removal from breeder	
Method	Purge gas flow
Power loss (thermal), % total	~0
Steady-state breeder tritium inventory, g	1500
Purge gas	
Material	He
Temperature, ^{0}C	~350-400
Pressure, MPa	0.1-0.6[d]
Tritium barriers	Natural oxides
Power Conversion System	
Thermal storage provision	
Technique	Circulating liquid
Storage medium	Pressurized water
Steam generator	
Type	Once-through horizontal
Single or double wall tubes	Single
Steam	
Inlet/outlet temperature, $^{0}C/^{0}C$	240/299
Maximum pressure, MPa	6.9
Tritium barriers	Natural oxides
Thermal efficiency	
$\eta = \frac{(MW_e)_{out} - (MW_e)_{pump}}{MW_{th\ TOTAL}}$, %	34.9
Gross (MW_e/MW_{th}), %	35.7
Steady-State Tritium Losses, Ci/d	100[e]

[a] As calculated by Tritium Breeding Task Group

[b] Neutron energy multiplication only.

[c] 650^{0}C maximum for Be/$LiAlO_2$ mixture.

[d] Variable, for changing breeder bulk k_{th}.

[e] Assumes 1 Ci/l in primary coolant, with 10% l/day losses to secondary side of steam generator.

[f] Occurs at back side of first wall at interface with Be/breeder mixture.

Economics - The concept does well in economics, finishing third out of nine, within a few percent of the top concept in this category. It has the lowest annual cost and lowest total capital cost, but has nearly the lowest net electric output which reflects its relatively low thermal convesion efficiency.

Safety and Environmental - As with the tokamak concept, the TMR concept is ranked next-to-last in this category, just above the nitrate-salt-cooled blanket (see Sec. 9.4.2.3). The primary reason is tritium control, and the safety risks and potential health hazards associated with the permeation of relatively large amount of tritium into the water coolant.

Research and Development - The concept finishes third from the bottom in this category, just ahead of the LiPb/LiPb/V and $LiAlO_2$/NS/FS/Be concepts and almost 40% below the top concept. It has the second-worst potential flaws rating (development risk) and is tied for the highest resource requirements rating. The rationale for these rankings is essentially the same as that presented for the tokamak concept in Sec. 9.4.2.4.

9.5.3 Design Details and Related Issues

The primary issues and considerations involved in selecting design details for the TMR version of the $LiAlO_2/H_2O$/FS/Be concept were discussed in detail for the tokamak concept in Sec. 9.4.3. Because nearly all of those apply equally to the TMR and tokamak concepts, the discussion will not be repeated here. The principal differences between tokamaks and TMR's relating to the attractiveness of SB/H_2O blankets were listed in Table 9.3-1 and discussed in Sec. 9.3.2.

9.6 Concepts Ranked R=2A - Tokamak and TMR

9.6.1 Li_2O/H_2O/(STRUC)/Be (R=2A)

The water-cooled blanket concept using lithium oxide (Li_2O) solid breeder, Be neutron multiplier, and PCA, ferritic steel, or vanadium alloy as structural material is described and discussed in this section.

The concept was not given a complete comparative evaluation because it was not ranked R=1. The reference design for the concept, whether for tokamak

or TMR, is very similar to that for the $LiAlO_2/H_2O$/FS/BE concepts described in Sections 9.4 and 9.5. Many of the issues and concerns are the same for those concepts as well, principally because the breeder characteristics are similar except for allowable temperature limits and thermal conductivity values. The primary differences between the breeders relate to concerns for radiation effects on Li_2O and its greater potential for compatibility problems with Be and structural materials. These differences will be discussed in the following subsections.

9.6.1.1 Concept Reference Design

The reference design for the concept was not developed as completely as that for the concept with $LiAlO_2$, since effort was halted at the time the R=2A ranking was given. However, the reference design would almost certainly be nearly identical to that for the $LiAlO_2/H_2O$/FS/Be concept (Fig. 9.4-1). Major features and parameters for the concept are presented in Table 9.4-1. The key differences compared to the concept with $LiAlO_2$ breeder are the allowable temperature limits and the $\%^6Li$ enrichment of the breeder. Features such as the helium purge system details and the use of Be with the Li_2O in a sphere-pac mixture at the front of the blanket would likely have been updated to be the same as those for the concept with $LiAlO_2$ had further work been performed.

9.6.1.2 Key Issues

Li_2O Radiation Damage - The FUBR irradiation test results (Sec. 6.3) indicate substantial swelling of Li_2O can take place under neutron irradiation. The swelling rate appears to be temperature dependent to some extent. Lithium aluminate in the same tests exhibited virtually no swelling.

The observed swelling of Li_2O leads to major concerns in two related areas: (1) interaction with structure and/or contacting materials such as Be; (2) effects on tritium inventory/tritium release rates. The degree to which the breeder and structure would each undergo radiation-induced creep, which could partially relieve stresses due to Li_2O swelling, is not known. Analyses indicate that, in the absence of any relief by creep, the stresses in the structure could be extremely high (Sec. 6.3). The ~14% void area within the sphere-pac form of Li_2O would likely accommodate some of the swelling, but this would close up the pathways for the helium purge gas which removes the

TABLE 9.6-1. MAJOR PARAMETERS FOR Li_2O/H_2O BLANKET CONCEPT PRELIMINARY REFERENCE DESIGN

PARAMETER	VALUE
Materials	
Coolant	H_2O
Breeder	Li_2O (sphere-pak; ~86% TD)
Neutron Multiplier	Be
Structure	HT-9 Ferritic Steel
Purge Gas	Helium
Coolant	
Inlet/Outlet Temperature, ^0C	280/320
Inlet/Outlet Pressure, MPa	15.2/15.0
Pumping Power, % Thermal Output	< 1%
Breeder	
Minimum/Maximum Temperature, ^0C	410/800
Maximum Pressure, MPa	0.6 (purge gas)
Structure	
Maximum Temperature	550^0C
Neutronics	
Energy Multiplication Factor	~1.27
Energy Loss to Shield, % Total Thermal	~0.2
Geometry	
Inboard Blanket Thickness, m	0.30
Outboard Blanket Thickness, m	0.70
First Wall Erosion	
Thickness Allowance,mm	3.0[a]
Design Life, yr (1-mm/yr erosion)	3

[a]Maximum allowable thickness is ~4 mm at 100 W/cm^2 surface heat flux.

tritium from the solid breeder. Breakup of some of the microspheres as they are pushed together is also possible, which would likely affect the ability of the sphere-pac bed to maintain good thermal contact with the blanket coolant tubes.

Given the present experimental results for Li_2O and $LiAlO_2$, and the absence of any definitive information on the effects of Li_2O radiation damage on blanket integrity or performance, the use of Li_2O in water-cooled blankets must be considered a major uncertainty and risk. This was the principal reason for the R=2A ranking given to the concept.

Compatibility - In tests with solid breeders and candidate structural materials in flowing helium gas at temperatures of interest, only Li_2O was found to react with structural materials to form corrosion scales (Sec. 6.3). Thicknesses of the total scale and internal penetration were similar for Type 316 austenitic stainless steel and HT-9 ferritic steel. Increasing H_2O content in the helium carrier gas caused increased corrosion. In addition, LiOH (as LiOT) can form in Li_2O during blanket operation which could affect both blanket structure and purge system/tritium recovery components. Li_2O mass transfer tests under conditions considered realistic for water-cooled Li_2O blankets will be needed to determine the importance of these concerns.

9.7 Concepts Ranked R=2B and R=3 - Tokamak and TMR

The water-cooled concepts discussed in this section are those which were given a final ranking of R=3: not acceptable, or R=2B: having severe fundamental flaws or disadvantages relative to higher-ranked concepts. Both liquid breeder and solid breeder concepts are included.

For some of these concepts, the bulk of the design, analysis and evaluation work was performed during the first part of the study and reported in the BCSS Interim Report[1]. For the remainder, the concept was considered to be not acceptable on the basis of first-order qualitative evaluation. As a result, the discussions for each concept in the following subsections will be limited to the key issues and concerns that led to its R=2 or R=3B ranking.

9.7.1 LiPb/H_2O/(STRUC) Concept (R=2B)

This concept uses 17Li-83Pb liquid breeder (LiPb; Sec. 6.4) and water coolant, with PCA, ferritic steel, or vanadium alloy as the structural material. Initial work on this concept was reported in Sec. VII.2.2 of Ref. 1. The R=2B ranking for the concept results primarily from two major concerns:

- o Reactions of LiPb and pressurized high temperature steam in tests simulating power reactor blanket conditions
- o The relatively high rate of tritium permeation through the blanket coolant tubes into the water coolant.

Blanket Configuration - The conceptual design used lobular modules or pods ~30 cm in width, filled with molten LiPb breeder. Each of the U-shaped coolant tubes is thus surrounded by the LiPb. Tritium is recovered by processing the LiPb which is circulated into and out of the blankets at a low mass flowrate. The first wall is water-cooled, but the configuration was not defined.

LiPb/H_2O Compatibility - Tests were performed at HEDL to react 17Li-83Pb with steam at conditions similar to those for power reactor blankets using pressurized water coolant. The results (Sec. 3.3) indicate a high degree of incompatibility. The steam (350^0C, 10 atm) reacted violently with the 500^0C LiPb, forcing termination of the tests after only 4 minutes. Based on these results, the use of molten LiPb and high temperature water coolant within the same blanket is considered probably unacceptable.

Tritium Contamination of Water Coolant - Calculations to determine the magnitude of this problem were presented in Sec. VII.2.2 of Ref. 1. The results indicated the permeation rate into the coolant could be as much as 7000 Ci/day for ferritic steel tubes if tritium partial pressure in the LiPb is 10^{-4} torr. The presence of natural oxide coatings on the steel (water side) or in the annulus of a double walled tube could reduce this rate significantly. However, tritium permeation rates would increase if the tritium partial pressure could not be held to levels as low as 10^{-4} torr. In combination with tritium permeating through the first wall, ~3000 Ci/day, removal of the tritium from the water coolant at rates of 10^4 Ci/day or higher might be necessary. This could be a severe economic penalty for the concept.

9.7.2 Li_2O/H_2O/(STRUC) Concept (R=2B)

This concept was the focus of most of the effort on SB/H_2O concepts during the first year of the study (Sec. IX.3 of Ref. 1). The reference configuration developed (tokamak only) is generally similar to that for the $LiAlO_2/H_2O$/FS/Be concept described in Sec. 9.4.

Further work on the concept led to the conclusion that the concept was considerably more of a risk from the standpoint of fuel self-sufficiency than the Li_2O/H_2O/FS/Be concept. Several specific developments made this concept look much less attractive than before:

- o Low bulk thermal conductivity for irradiated sphere-pac Li_2O
- o Incorporation of double-wall tubes to increase reliability against water leaks into the breeder
- o Observations of Li_2O swelling in the FUBR test (Sec. 9.6.1.2)

Bulk thermal conductivity for sphere-pac Li_2O had initially been assumed to be 3.4 W/m-K at 1000 K, the same as for unirradated Li_2O in sintered product form at ~15% porosity. Subsequent calculations indicated the effective k_t for irradiated sphere-pac Li_2O would range from 1.10 to 1.65 W/m-K (1000 K) for helium gas pressures of 1 and 6 atm respectively. (The reduction in k_t of sintered product Li_2O due to irradiation would not have been as severe.) The result of this change was to drastically reduce the volume of breeder that could be placed around each coolant tube, since for a given allowable breeder temperature range (ΔT) and nuclear heating rate (q_n), the allowable breeder volume is roughly inversely proportional to k_t. This caused a very sharp increase in the relative amounts of coolant and structure, which significantly reduced TBR. The addition of a second coolant tube around each of the existing single wall coolant tubes, to form double wall tube assemblies, also increased the amount of structure in each breeder "cell," further decreasing TBR.

Neutronics calculations using 1-D models of the resulting reference design indicated that TBR values calculated with 3-D models would very likely fall below the 1.05 level considered to be the minimum acceptable for consideration of any concept (Sec. 5.1). The combination of this result and the observation of Li_2O swelling under irradiation were considered sufficient to justify the concept's ranking of R=2B.

The two principal areas where significant positive developments would be needed before a higher ranking would be deserved are (1) successful resolution of the swelling/interaction/tritium release concerns discussed in Sections 9.6.1.2 and 6.3, and (2) improvements in allowable ΔT and/or bulk k_t for the breeder.

9.7.3 $Li_8ZrO_6/H_2O/(STRUC)$ Concept (R=2B)

The breeder for this water-cooled concept is octa-lithium zirconate. Structural materials considered were PCA, ferritic steel, and vanadium alloy.

The initial attractiveness of this breeder was due to its presumed stability (compared to Li_2O) and its relatively high lithium atom fraction. The zirconium acts as a neutron multiplier, and thus the compound is one of the few solid breeder alternative to Li_2O that potentially could provide net tritium breeding without requiring the use of a separate neutron multiplier.

Subsequent evaluation (Sec. 6.3) indicated, however, that there were major concerns for both the compound's stability and for its ability to achieve net tritium breeding. SEM analyses indicated the occurrence of a phase transformation in the breeder occurring at ~660°C. The thermal conductivity (unirradiated) for Li_8ZrO_6 was indicated by tests to be much lower than for Li_2O at the same theoretical densities and temperatures. Thus even less Li_8ZrO_6 breeder could be placed around each coolant tube than for Li_2O. This is a severe disadvantage, since even on an equal-volume basis the TBR for Li_8ZrO_6 would be lower than for Li_2O. As an additional disadvantage, the Li_8ZrO_6 breeder would have significant waste management problems, resulting primarily from the long-lived ^{93}Zr isotope formed by transmutation of the zirconium.

Overall, the concept was judged to be no better than the $Li_2O/H_2O/FS$ concept in terms of risk and performance, and was therefore ranked R=2B.

9.7.4 $Li_8ZrO_6/H_2O/(STRUC)/Be$ Concept (R=2B)

This concept is very similar to that discussed in Sec. 9.7.3, except that Be is added as a neutron multiplier, to add to the multiplication effect already provided by the zirconium in the breeder. Although the problems in achieving adequate TBR are minimized, the other major concerns of stability

and waste mangement remain. The addition of Be to the concept significantly increases its complexity from the engineering and fabrication standpoints. In addition, there is no information at present on the tritium release characteristics of Li_8ZrO_6.

On balance, this concept is judged to be less attractive than the Li_2O/H_2O/(STRUC) concepts with or without Be, and is ranked R=2B.

9.7.5 $LiAlO_2/H_2O$/(STRUC)/Pb Concept (R=2B)

This water-cooled concept evaluated during the early part of the study (Sec. IX.5 of Ref. 1), used lead in liquid form as a neutron multiplier with lithium aluminate as the breeder. Figure 9.7-1 illustrates the preconceptual design configuration. PCA was used as the structural material for the reference design. Ferritic steel and vanadium alloy were not examined in depth but should also be acceptable.

The concept was given the equivalent of an R=2B ranking during the first year and no further work was done. There are a relatively large number of difficult design issues, most of which stem from the proximity of the Pb melting point (327^0 C) to the desired water coolant operating temperature range (280 to 320^0 C). Operator action would likely be required following shutdown to keep the lead from freezing around the colder areas of the water coolant tubes. This could entail either draining of the Pb from the pod or raising the water temperature to $\gtrsim 330^0$ C through use of the main coolant pumps or the pressurizer. Coolant tube reliability concerns (Sec. 9.3.1.1) would probably force the use of double wall coolant tubes to obtain very low rates of failures involving coolant leakage into the molten Pb. For PCA structural material, LME embrittlement and corrosion at temperatures in the range of the Pb/coolant tube interface temperature are serious concerns. The mechanical design configuration of the module would be perhaps the most complex of all the concepts examined. It would require a separate water-cooled first wall, a network of purged $LiAlO_2$ breeder tubes, a separate system of coolant tubes connected to a manifold region, and a Pb piping system for draining and filling of the modules.

- Li_2O OR TERNARY OXIDE SOLID BREEDER ($LiAlO_2$), WATER COOLANT, LIQUID LEAD NEUTRON MULTIPLIER
- RANKING: R=2B (ALL STRUCTURAL MATERIALS)
- CONFIGURATION:

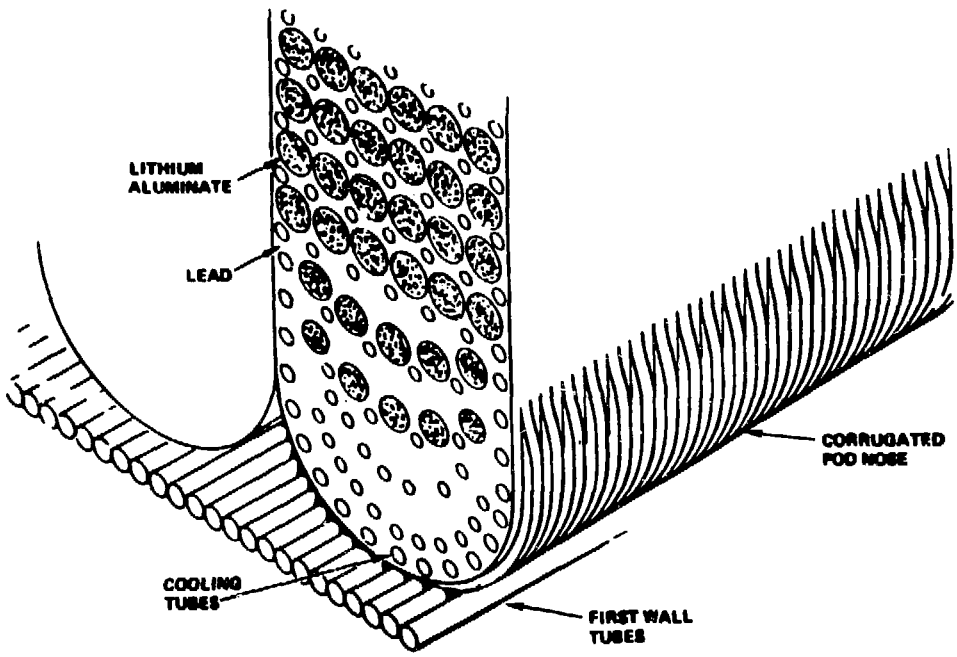

Fig. 9.7-1. General configuration for water-cooled solid breeder blanket concepts with Pb neutron multiplier

9.7.6 $Li_2O/H_2O/(STRUC)/Pb$ Concept (R=2B)

This concept is the same as that discussed in Sec. 9.7.5 except that Li_2O would be substituted for the $LiAlO_2$ solid breeder. This concept's ranking is also R=2B. The use of Li_2O gives no significant advantage over $LiAlO_2$ in this application. In addition, the concern for Li_2O radiation damage would be introduced, in addition to the problems discussed in Sec. 9.7.5 for the concept using $LiAlO_2$.

9.7.7 $LiAlO_2/H_2O/(STRUC)$ Concept (R=3)

There is no neutron multiplier in this concept. Many previous neutronics studies have conclusively determined that net tritium breeding with ternary oxide ceramics is not possible without the use of neutron multipliers, regardless of the design configuration or ^6Li enrichment level employed. Therefore the concept was given an R=3 ranking and received no effort within the study.

9.7.8 $Li/H_2O/(STRUC)$ Concept (R=3)

This concept uses liquid lithium breeder with water coolant, and PCA, ferritic steel, or vanadium alloy as the structural material. Because of the well-documented incompatibility of liquid lithium and high-temperature water, the concept was judged not acceptable from the safety standpoint. A ranking of R=3 was given, and no work was performed on the blanket concept within the study.

9.8 Special Issues Analyses

9.8.1 Thermal Hydraulics - Design Considerations For Solid Breeder Blankets

9.8.1.1 Introduction

Thermal hydraulic design considerations for blanket concepts using Li_2O and γ-$LiAlO_2$ solid breeders using pressurized water are presented in this section. An examination of the various design concepts for the exponentially decaying nuclear heating profile indicates that the thermal hydraulic analysis of solid breeder blankets can be very complex. Hence, the parametric design studies have been carried out using simple one-dimensional models which assume that the breeding blanket can be divided into a number of cylindrical unit cells,[2,3,10] each surrounded by an adiabatic boundary. A composite of the individual unit cell analysis represents the overall blanket performance. The analytical procedure adapted for this study is similar to that of Ref. 10, except that the results are presented either in terms of the nuclear heating profile or the blanket thickness rather than presenting the data for specific blanket regions.

9.8.1.2 Analytical Approach

For the purposes of parametric studies, let us consider the temperature distribution in a unit cylindrical cell (hollow heat-generating cylinder cooled convectively at the inner boundary, and adiabatic outer boundary):

$$T_{max} = T_{ex} + \frac{q_b R_3^2}{4 k_b}\left[\left(\frac{R_2}{R_3}\right)^2 - 2 \ln \left(\frac{R_2}{R_3}\right) - 1\right] + \frac{q_r R_3^2}{2}\left[1 - \left(\frac{R_2}{R_3}\right)^2 \quad \frac{1}{k_s} \ln \frac{R_2}{R_1} + \frac{1}{R_1 h_f}\right] + \frac{q_b}{2 R_2 H_g}\left[R_3^2 - R_2^2\right], \qquad [9.8\text{-}1]$$

where T_{max} = maximum temperature in breeder at the adiabatic boundary between two adjacent unit cells

T_{ex} = coolant exit temperature

q_s = nuclear heating rate in breeder

R_1 = coolant channel radius

k_b, k_s = thermal conductivity of breeder and structure, respectively

h_f = convective heat transfer coefficient (HTC)

H_g = interfacial gap conductance.

The following design and operating conditions have been used for parametric studies by using Eq. [9.8-1]:

Coolant inlet/outlet temperature (T_{in}/T_{out}), ^0C	280/320
Solid breeder material	Li_2O, γ-$LiAlO_2$
Coolant tube diameter, mm	8-10
Cladding thickness, mm	0.75-1.0
Nuclear (volumetric) heating rate (q_b), W/cc	1-60
Temperature drop (ΔT_b) across breeder region for each unit cell, ^0C	200, 390, 600

The major part of the analyses presented herein is for the H_2O-cooled concept with Li_2O, with $\Delta T = 390^0 C$. Since a typical blanket module cannot accommodate a fixed number of unit cylindrical cells, each with an adiabatic boundary, it was necessary to present the analytical results in terms of either q_b or blanket thickness. This enabled a large number of parametric studies to be carried out without being limited by the characteristics of individual cells or specific blanket regions.

As the various terms in Eq. [9.8-1] represent temperature drops (ΔT's) associated with the breeder (ΔT_b), cladding (ΔT_s), coolant film (ΔT_f), and interfacial gap between breeder and cladding (ΔT_g), Eq. [9.8-1] may be rewritten as

$$T_{max} = T_{ex} + \Delta T_b + \Delta T_s + \Delta T_f + \Delta T_g \qquad [9.8\text{-}2]$$

Since the above ΔT's are interdependent quantities, thermal hydraulic analysis of a solid breeder blanket requires simultaneous consideration of the temperature differences and their functional dependencies as discussed below.

Operating temperature limits (T_{max} and T_{min}) have been imposed on all lithium ceramic breeder materials. The lower operating temperature limits stem from the need for maintaining the breeder above a certain temperature to reduce tritium inventory, and (in the case of Li_2O) to minimize the chemical interactions between the bred tritium and the ceramics. The upper limit is due to the concerns over thermal sintering, especially under neutron irradiation, and high mass transfer rates of the breeder materials. The following temperatures and temperature differences (ΔT) have been used in the parametric studies:

T_{max}, ^0C	800-1000 (represents Li_2O, $LiAlO_2$ limits)
T_{min}, ^0C	400
ΔT_b, ^0C	200, 390, 600

For a given ΔT and q_s, the breeder region size (R_3, see Eq. [9.8-1]) essentially depends on k_b. Hence, k_b and the uncertainties associated with it due to microstructure, thermal and nuclear irradiation play a prominent role in the blanket designs. Similarly, for a given k_b and ΔT_b the size of the breeder region associated with each coolant channel depends on q_s. Therefore, the heat flux over each coolant channel depends on the location of the coolant channel in the depthwise direction of the blanket. This leads to each coolant tube requiring a different coolant velocity for the same coolant inlet/outlet conditions. From this brief discussion one can visualize the interdependency of many physical and operating parameters. An assessment of the role of these parameters on blanket designs is given in the following sections.

9.8.1.3 The Role of Thermal Conductivity

The thermal conductivity of lithium ceramics (k_b) such as Li_2O and γ-$LiAlO_2$ depends on many factors such as microstructure, porosity, morphology (e.g., sintered pellets and sphere-pac), temperature and nuclear irradiation. The experimental thermal conductivity data for many ceramics indicate significant degradation of this property due to nuclear irradiation. As discussed in Sec. 6.3, k_b can decrease by ~25-40% or more due to

nuclear irradiation. Therefore, blanket designs based on the estimated values of k_b are susceptible to large uncertainties. In order to show the effect of k_b on blanket designs, the thermal conductivity values of Li_2O and γ-$LiAlO_2$ as given below were used in the parametric studies.

	Li_2O		γ-$LiAlO_2$	
	Unirradiated	Irradiated	Unirradiated	Irradiated
Thermal Conductivity (W/m-K)	2.60	1.56	1.43	1.18

Using the above data, the volume fraction of the breeder was calculated and the results are summarized in Fig. 9.8-1. Since the tritium breeding

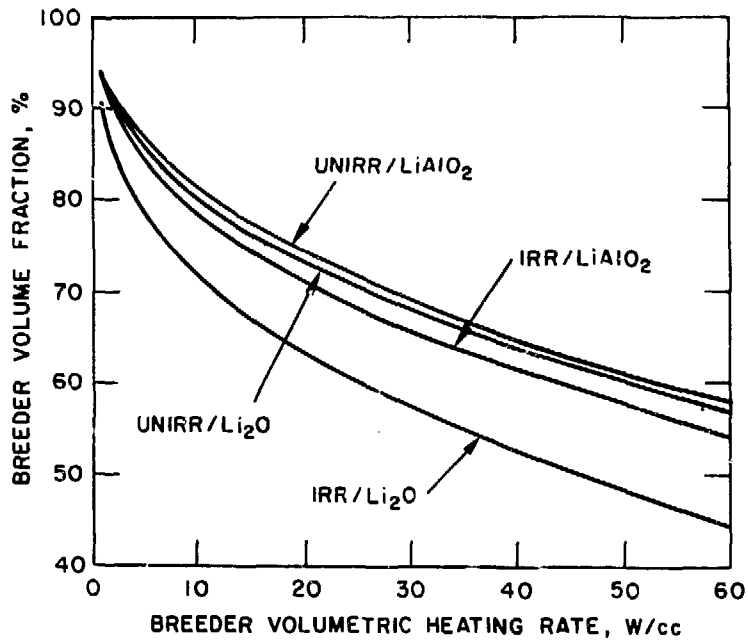

Fig. 9.8-1. Breeder volume fractions for irradiated and unirradiated Li_2O and γ-$LiAlO_2$

ratio (TBR) depends on the volume fraction of the breeding material, significant reduction in TBR would result for designs based on k_b of irradiated material. Figure 9.8-1 shows that the percent performance degradation for the γ-$LiAlO_2$ blanket is not as severe as that for Li_2O since nuclear irradiation appears to have less adverse effect on γ-$LiAlO_2$ (see the above tabular data).

The thermal conductivity data of sphere-pac fission reactor fuels (UO_2 and PuO_2) indicate strong dependence of the effective thermal conductivity (k_{ef}) on both the nature and the pressure of the fill gas. For example, k_{ef} was found to increase by more than 60% when the helium fill gas pressure was increased from 1 atm to 6 atm. If the fill gas is assumed to have similar effect on lithium ceramics, then a mechanism is available to vary the thermal conductivity of the solid breeder by changing the purge gas pressure. The implication of this mechanism is discussed in a later section.

9.8.1.4 The Role of Temperature Window

Blanket Performance - From the standpoint of blanket performance, it would be desirable to have no limits at all on T_{min} and T_{max}. However, temperature windows are necessary and designs must be based on T_{max} and T_{min} for the chosen ceramic. Pending experimental verification of these limits, parametric investigations were carried out to study blanket performance for three different values of temperature window. The results are summarized in Figures 9.8-2 and 9.8-3. As expected, the breeder volume fraction depends strongly on the temperature window. Hence, one of the primary objectives of an experimental program to study the thermophysical properties of lithium ceramics would be to establish the allowable T_{max} and T_{min}.

Coolant Velocity - For a fixed temperature window, the size of the breeder region associated with each coolant channel increases in the depthwise direction of the blanket. The breeder region profile for a typical design is shown in Fig. 9.8-4. There is an almost 15-fold increase in the breeder volume associated with coolant channels located near the reflector/shield region compared to those located near the first wall. However, due to the exponential power profile, the heat flux (Q/A) over each coolant channel decreases as the blanket segments are located further and further away from the first wall. Hence, for the same coolant inlet/outlet temperature, the

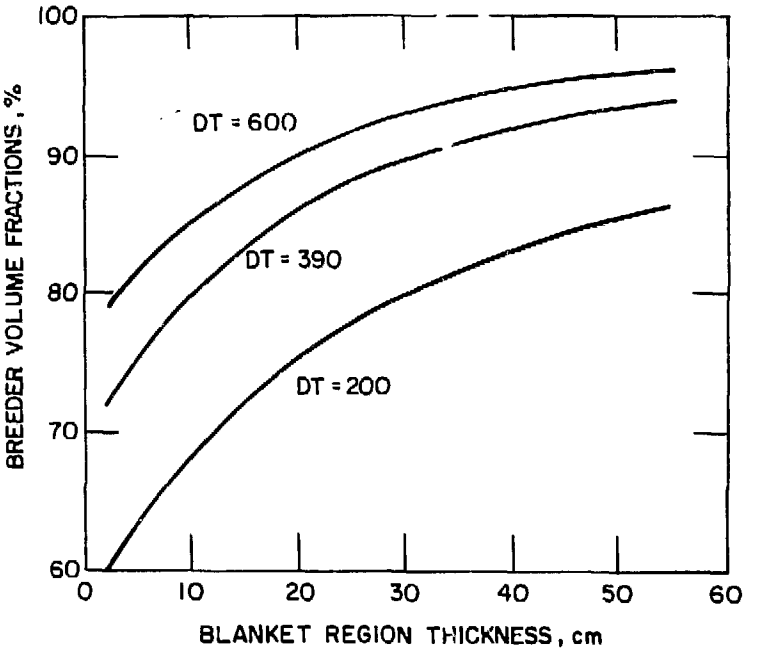

Fig. 9.8-2. Dependence of breeder volume fraction on the temperature window as a function of depth into breeding zone

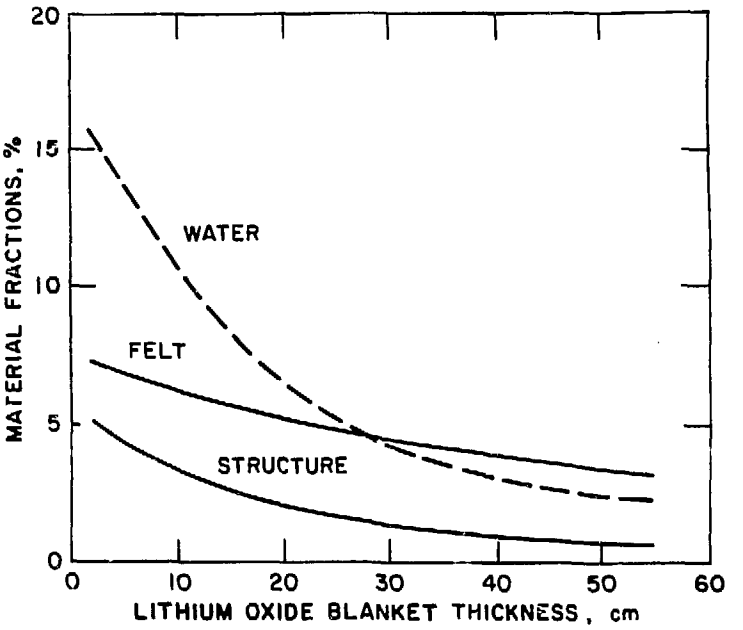

Fig. 9.8-3. Material volume fractions for Li_2O blanket as a function of depth into blanket

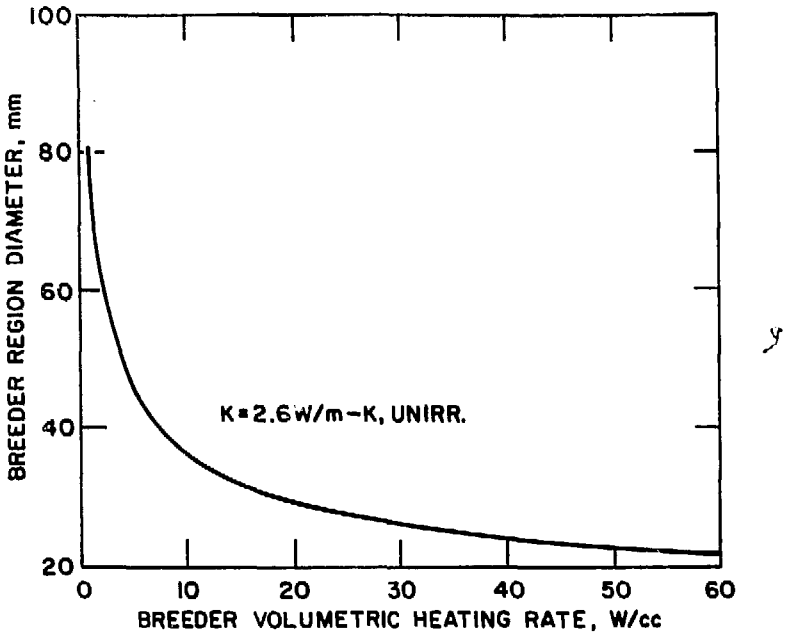

Fig. 9.8-4. Dependence of breeder region diameter on nuclear heating rate

corresponding coolant velocities become smaller and smaller. The coolant velocities are plotted in Fig. 9.8-5. The heat flux and the heat transfer coefficients (HTC) are shown in Fig. 9.8-6. Figure 9.8-5 shows that the temperature drop across the coolant film (i.e., the temperature difference between the bulk fluid and the inner wall of the coolant channel) is of the order of only 20^0C (divide Q/A by HTC). For the nuclear heating rates used in this analysis, the coolant velocities are quite modest (~7 m/s). If all of the coolant channels are to be connected to the same inlet and outlet headers, it would be necessary to provide a means of coolant velocity distribution. This can be done by orificing each tube, although it introduces a design complexity.

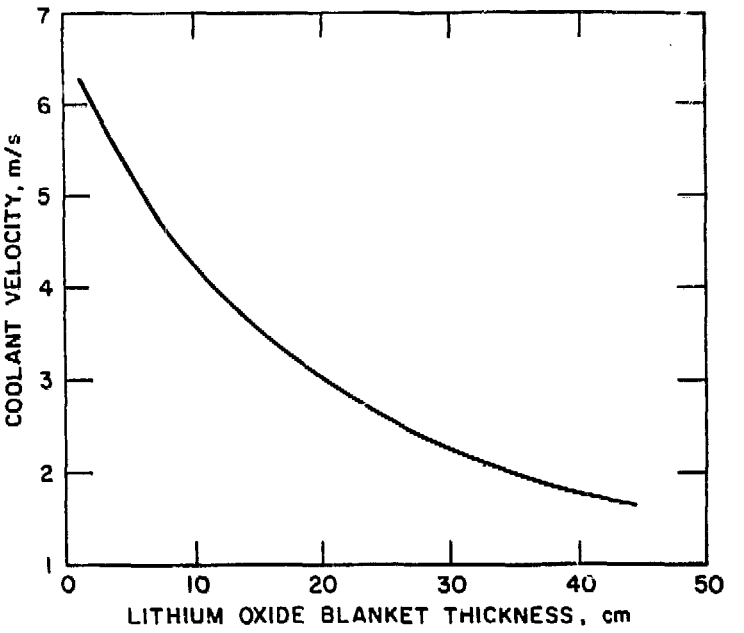

Fig. 9.8-5. Variation of coolant velocity in depth-wise direction of blanket

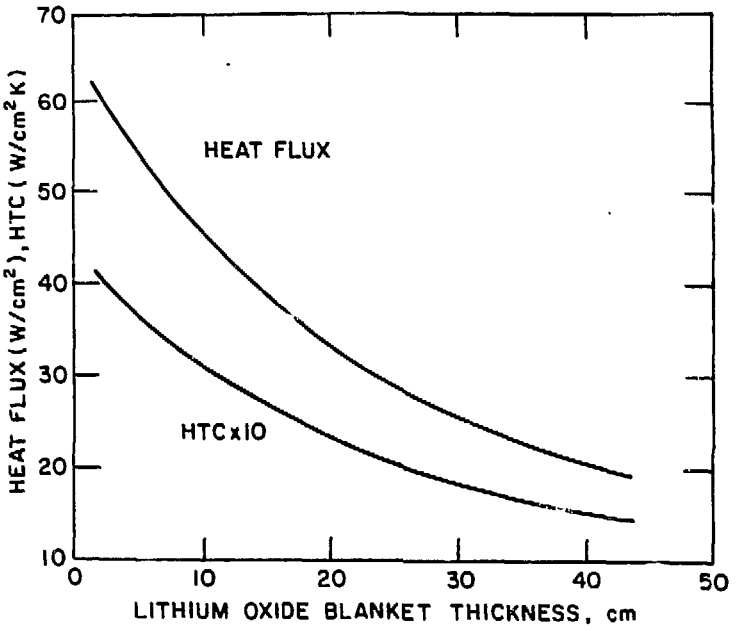

Fig. 9.8-6. Variation of heat flux and heat transfer coefficient (HTC) in cooling channels

9.8.1.5 The Role of Interfacial Contact Resistance

An examination of the heat flux (Q/A) over the coolant channels shows that for the 0.75-1.0 mm thick cladding, the temperature drop across the coolant tube wall (ΔT_s) is of the order of 15-45^{0}C. Hence, the interface temperature (T_I) between the cladding and the breeder (assuming no interfacial contact resistance, $T_I = T_{min}$) is approximately equal to

$$T_I = 260 + 20 + 15 = 295^0C$$

The expected minimum temperature for the solid breeder is therefore significantly lower than the T_{min} for the analyses (~400^{0}C). In order to provide the required T_{min}, it would be necessary to tailor the interfacial contact resistance between the cladding and the solid breeder. A number of methods of providing the needed thermal barrier have been considered,[10] including helium gas gap via double wall tubes, high-porosity stainless steel felt sleeves over the coolant tubes, and a low conductance ceramic coating such as Li_2ZrO_3. The required thickness of these three thermal barriers is shown in Fig. 9.8-7. Several observations may be made from the data:

1. It does not seem practical to provide a tightly controlled gas gap varying from 0.5 mm to <2.0 mm. The manufacturing tolerances are expected to be of the same order of magnitude.

2. The required thickness of the stainless steel felt (~70-80% porous) can be larger than 3 mm. This will increase the structural material fraction and thus degrade TBR.

3. The required Li_2ZrO_3 coating thickness is quite modest. In addition, since Li_2ZrO_3 is a tritium breeder, a thermal barrier based on Li_2ZrO_3 may not have adverse effect on TBR. However, no data exist on how such coatings can be applied and the long-term integrity of Li_2ZrO_3 coatings.

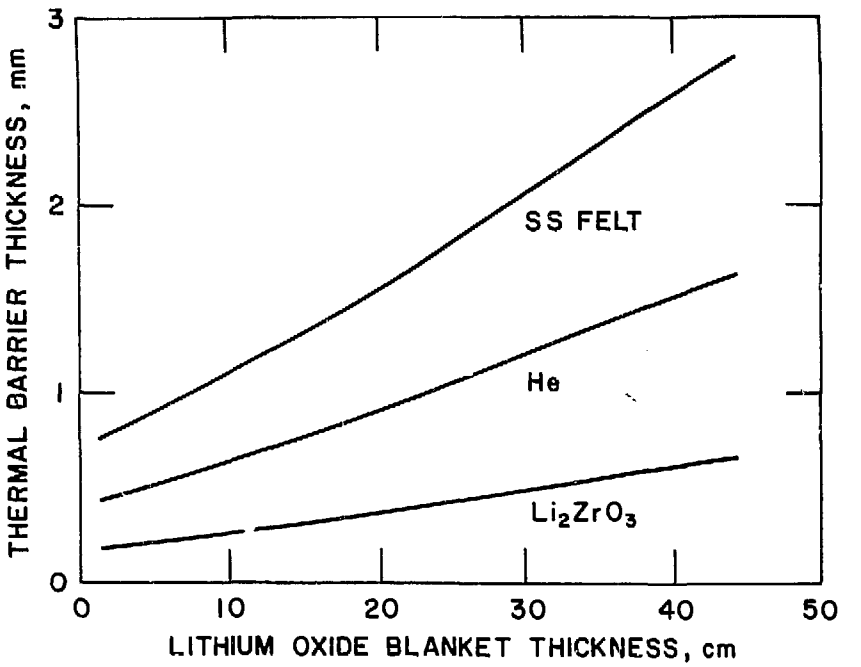

Fig. 9.8-7. Thermal barrier thickness for Li_2O breeding blanket

4. As the thickness of the thermal barrier depends on the location of the coolant channel, the coolant tubes in each bank will require a different thickness of the thermal barrier. Since all of the blanket modules are not expected to be all the same size, this will introduce added complexities into the blanket design. In addition, it would be necessary to vary the thickness of the thermal barrier continuously or step-wise between the coolant inlet and coolant outlet to account for the coolant temperature rise.

It should be noted that there will be some ΔT between the tube outer surface and the breeder due to interfacial contact resistance. This will lessen the importance of the problem, but has not been included here.

9.8.1.6 Sphere-Pac Concept

The problems associated with gap conductance/thermal barrier as discussed above have led to consideration of solid breeders in the form of sphere-pac. The sphere-pac solid breeders are considered to possess thermophysical and thermomechanical properties that are more suitable for use in liquid-cooled blankets compared with those of sintered solid breeder pellets. Also, the interfacial contact resistance between the cladding and the sphere-pac material is considered to be more predictable. Hence, consideration is being given to blanket designs based on sphere-pac materials with and without an added thermal barrier. The implication of this design is discussed below.

The sphere-pac concept is based on using a mixture of microspheres (100% dense) of several sizes which can yield fairly high smear densities (~86%). A mixture of three microspheres with a diametral ratio of 1:10:40 (for example, 30, 300, and 1200 μm diameter particles, consisting approximately of 20% by weight fine and medium size particles and 60% by weight coarse particles) are considered for this study. The sphere-pac concept further assumes that the void space in the material is filled with a gas possessing high thermal conductivity, such as helium. A detailed discussion of the sphere-pac concept is given in Sec. 6.3.

The measured gap conductance (H_g) for U and UO_2 pellet and sphere-pac fuels as reported by Fitts and Miller[11] are 0.73 and 1.93 W/cm^2-K, respectively. From the measurements of the gap conductance between UO_2 and zircaloy cladding, Ross and Stoute[12] found the gap conductance to vary from <1.0 to ~5 W/cm^2-K in helium gas atmosphere. Thermal analysis of TRIO-01 data[13] indicates the gap conductance between $LiAlO_2$ pellets and stainless steel tubing to be approximately 0.50 W/cm^2-K. Since the gap conductance is strongly dependent on the contact pressure between the ceramic and the cladding, surface finish, material hardness, etc., selection of a gap conductance for design purposes is difficult. Hence, a range of values of H_g varying from 0.25 to 2.0 W/cm^2-K was used in the parametric study. The minimum temperature of the breeder, which occurs at the coolant inlet end of the blanket, is plotted in Fig. 9.8-8 for unirradiated $LiAlO_2$. A significant volume of the blanket will remain below 400^{0}C for all values of gap conductance included in this study (see Fig. 9.8-8). For the Li_2O blanket one observes similar thermal behavior (see Fig. 9.8-9). Since the steady state tritium inventory in

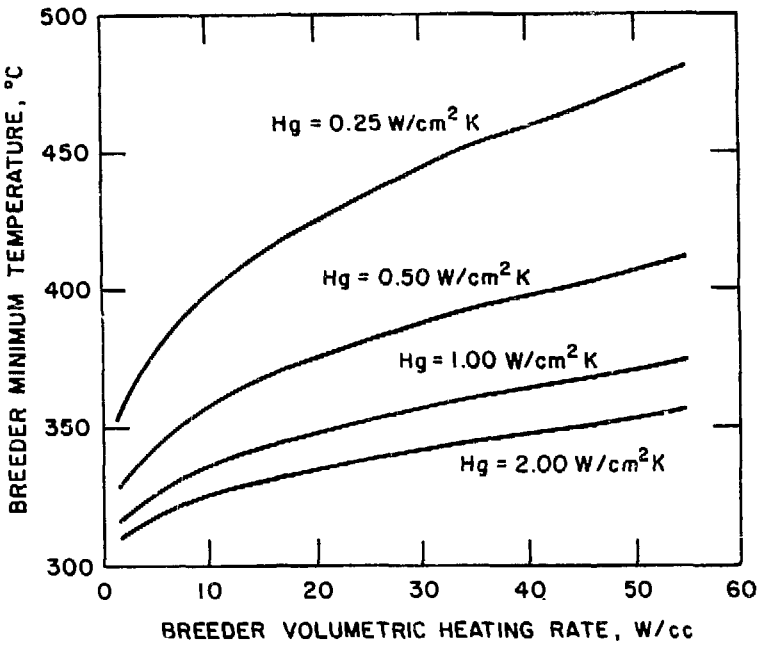

Fig. 9.8-8. Breeder minimum temperature dependence on gap conductance (γ-$LiAlO_2$)

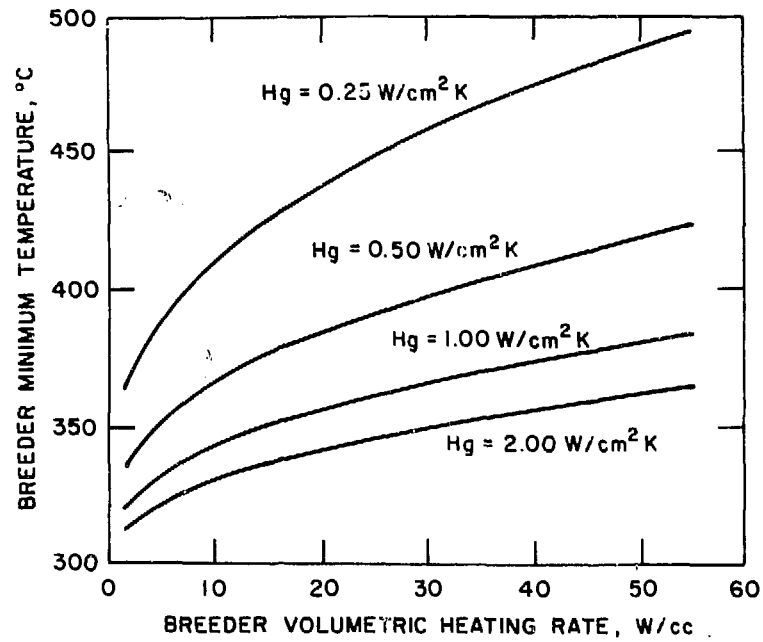

Fig. 9.8-9. Breeder minimum temperature dependence on gap conductance (Li_2O)

the breeding blanket is a function of the temperature distribution, designs based on sphere-pac materials will require development of effective thermal barriers which have minimal impact on TBR, to avoid high tritium inventories as discussed below.

9.8.1.7 Tritium Inventory

The radial temperature distribution in the breeder region associated with each coolant channel may be expressed by

$$T_1 = T_{max} - \frac{q_b R_3^2}{4 k_b} \left[\left(\frac{r_1}{R_3}\right)^2 - 2 \ln \left(\frac{r_1}{R_3}\right) - 1 \right], \qquad [9.8\text{-}3]$$

where T_1 is the breeder temperature at radial distance r_1.

As there are more data for tritium diffusion characteristics in γ-$LiAlO_2$,[13] a breeding blanket based on γ-$LiAlO_2$ breeder was analyzed for tritium inventory calculations. The blanket was divided into ten independently-cooled regions, and the steady state temperature distribution in each region was calculated using Eq. [9.8-3]. The diffusion coefficient of tritium in γ-$LiAlO_2$ as estimated from TRIO-01 data in conjunction with the temperature distribution was used to estimate the tritium inventory for each region. Since there are no data on gap conductance (defined as inverse of interfacial contact resistance) for the sphere-pac lithium ceramics, a range of H_g values was used to assess how the tritium inventory depends on the gap conductance. The tritium inventory for a 4000 MWt (STARFIRE-size) reactor for $T_{max} = 850^0$C was estimated. The results are plotted in Fig. 9.8-10. From the data shown, it can be stated that in order to obtain a tritium inventory of 10 kg or less, the gap conductance must be of the order of 0.5 W/cm^2-K. The data of Fitts and Miller indicate that an additional thermal barrier between the cladding and the solid breeder is required for acceptable designs. While designs based on sphere-pac materials may alleviate mechanical problems such as cracking, such designs may also lead to large tritium inventories. Therefore, the question of gap conductance for sphere-pac materials needs further scrutiny.

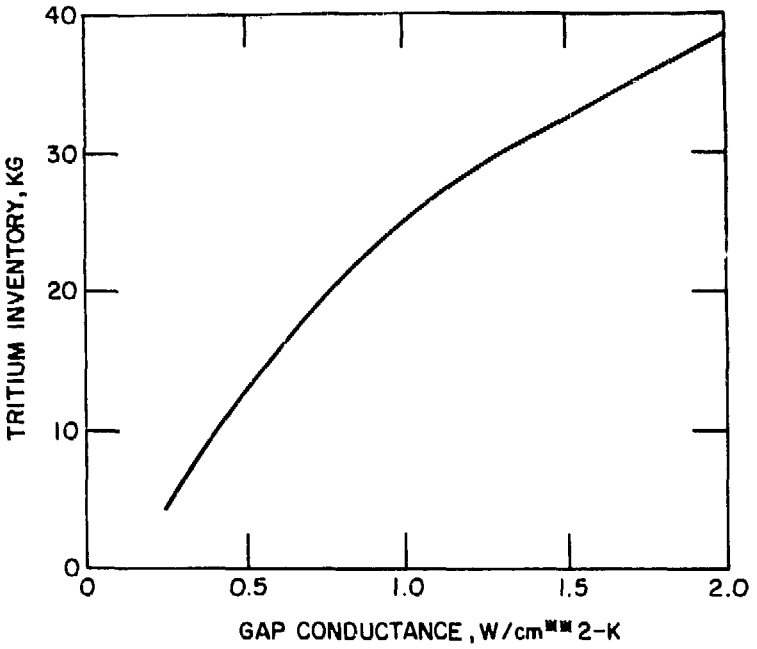

Fig. 9.8-10. Dependence of tritium inventory on gap conductance for γ-$LiAlO_2$ blanket (4000 MW_{th} reactor)

9.8.1.8 Partial Power Operation

Unlike fossil and fission reactor (LWR) power plants, low power or partial power operation of fusion reactors which use lithium ceramic breeder blankets (such as Li_2O and γ-$LiAlO_2$) has special implications. The method of maintaining the required temperature window during partial power operation is not obvious. Throttling of the coolant flow rate provides very little flexibility for temperature control due to the small coolant temperature rise (40^0C) for the water-cooled blankets. However, blanket designs based on sphere-pac lithium ceramics can provide some flexibility for reactor power variation.

As indicated in an earlier section and discussed fully in Sec. 6.3, the effective thermal conductivity of both pellet fuels and sphere-pac fuels

depends on the pressure of the fill gas. For example, the thermal conductivity of sphere-pac Li_2O and γ-$LiAlO_2$ can be increased by more than 60% by increasing the helium fill gas (purge gas) pressure from 1 atm to 6 atm. Since there are no supporting data on the effect of the purge gas (helium) pressure on the effective thermal conductivity of lithium ceramics, calculations were carried out for k_{ef} values varying from 1 to 3 W/m-K.

In order to calculate the operating power level as a function of the expected thermal conductivity of the sphere-pac breeder blanket, three blanket regions (100%, 25%, and 5%, where 100% refers to blanket region near the first wall and 5% refers to blanket region near the reflector/shield) were selected. The operating power level which will not alter the breeder temperature distribution (i.e., which will provide the same temperature window) is shown in Fig. 9.8-11 for the 100% power region as a function of the expected effective thermal conductivity of sphere-pac Li_2O. The calculated results for the

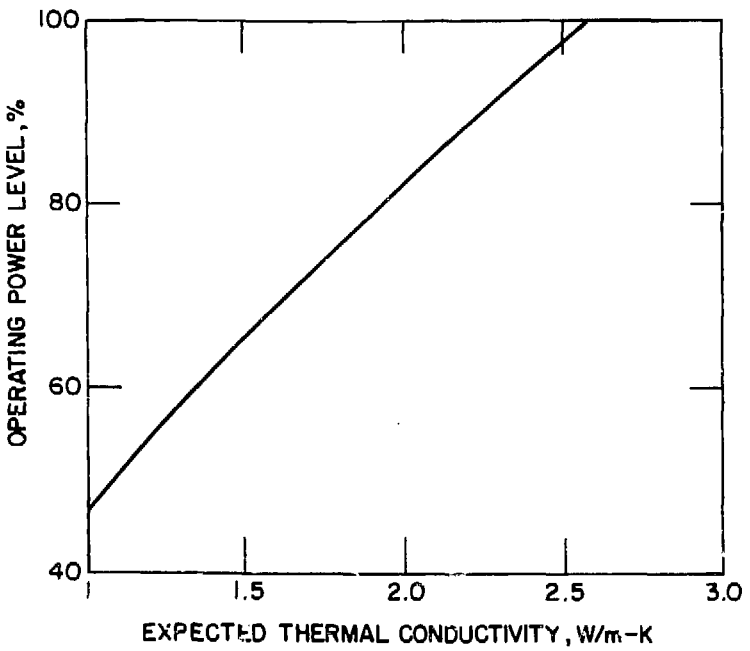

Fig. 9.8-11. Operating power level variation due to change in thermal conductivity

25% and 5% power regions are similar to the data shown in Fig. 9.8-11. An inspection of the effect of helium purge gas pressure on the effective thermal conductivity of unirradiated Li_2O shows that k_{ef} can increase from ~1.5 to 2.6 W/m-K. By taking into account the above variation of k_{ef} and referring to Fig. 9.8-11, one can see that is is possible to obtain a power variation between ~65% and 100% while maintaining the temperature distribution essentially constant.

9.8.1.9 Summary

An assessment of the role of the design and operating parameters on performance of solid breeder blankets based on lithium ceramics (Li_2O and-γ-$LiAlO_2$) was carried out. The results indicate that the thermophysical properties and the uncertainties associated with the property data base are major design-limiting factors. The operating conditions such as the upper and the lower temperature limits, the choice of breeder materials either in the form of sintered pellets or in sphere-pac form, the interfacial contact resistance between the coolant channels and the solid breeder, and the diffusion characteristics of tritium and chemical interactions between tritium and the solid breeder also play prominent roles in blanket designs. Accounting for the expected degradation of the thermophysical properties due to irradiation in designs leads to higher coolant and structural material fractions, and thus lower tritium breeding ratios. The relatively low temperature of water coolant and the necessity of maintaining a certain minimum operating temperature dictate the need for a thermal barrier between the cladding and the solid breeder. Uncertainties in contact thermal resistance for sphere-pac lithium ceramics need to be minimized using experimental results to avoid the possibility of high tritium inventories. A firmer data base for the operating temperature limits, thermophysical properties and gap conductances are necessary to carry out more realistic fusion reactor blanket designs based on lithium ceramics.

9.8.2 Thermal Hydraulics - First Wall

Thermal analyses were performed for both TMR and tokamak first wall (FW) concepts. The objective was to determine the thermal feasibility of the lobe-shaped FW design concept for both TMR and tokamak heating conditions.

Because of the relatively low 5 W/cm^2 surface heat flux of the TMR, it was thought that the FW might possibly be cooled passively--i.e., by conduction of heat through the breeder to the first row of cooling tubes in the blanket breeding zone (Fig. 9.8-12). The first task was to determine what breeder thickness in this sort of geometry would produce acceptable FW temperatures. The second task was similar except the FW was assumed to be water cooled, and the required coolant flow conditions and FW temperatures were determined for both TMR and tokamak heating conditions. The $Li_2O/H_2O/FS$ blanket was used as the reference design; results would be very similar for other SB/H_2O concepts.

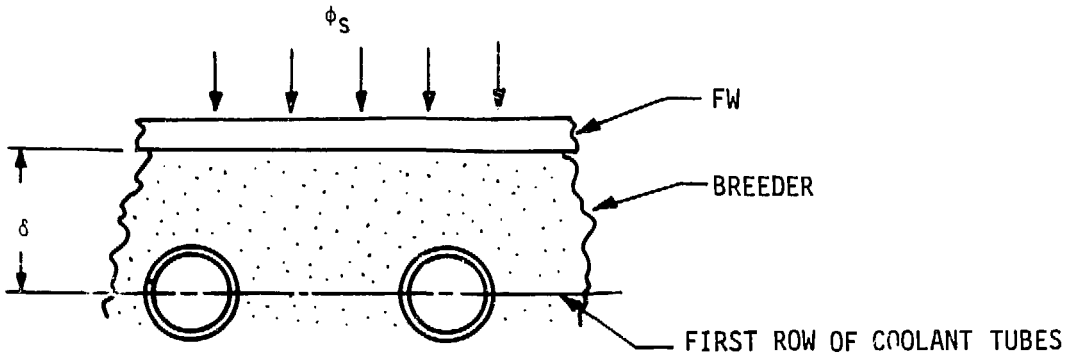

Fig. 9.8-12. Passively cooled FW geometry - conceptual model

9.8.2.1 Analytical Approach

Finite difference models of the geometry for each approach were constructed. Table 9.8-1 presents a summary of thermal properties and heating rates used in these analyses. For the passively cooled FW, the primary thermal constraints were the 550^0C maximum temperature for the ferritic steel FW and the 410^0C minimum temperature for the Li_2O breeder. The stainless steel compliant layer shown conceptually in Fig. 9.8-13 is a possible design option which serves to isolate the breeder displacement from the FW displacement.

TABLE 9.8-1. THERMAL PROPERTIES AND HEATING RATES

FIRST WALL NUCLEAR HEATING	60 W/cm^3
BREEDER NUCLEAR HEATING EQUATION	$Q = 60-7.5X$, W/cm^3 (X=depth, cm)
FIRST WALL SURFACE HEATING	5 W/cm^2 (TMR)
	100 W/cm^2 (TOKAMAK)
THERMAL CONDUCTIVITY	
HT-9 FIRST WALL	0.27 W/cm-K
STAINLESS COMPLIANT LAYER	0.013 W/cm-K
BREEDER	.02, .027, .034 W/cm-K
BREEDER ALLOWABLE T_{MIN}	410^0 C
HT-9 ALLOWABLE T_{MAX}	550^0 C

Figure 9.8-13 shows the unknown breeder thickness, t_{BR}, for the actively cooled FW. The approach for this task was to first determine t_{BR} from the known heating rate and temperature limit information. This breeder thickness was then used in computing a heat flux to the breeder side of the FW, assuming one-half the breeder thickness was cooled by the FW and the other half was cooled by the first row of tubes. The back side FW heating was then summed with the surface and volumetric heating of the FW itself to determine the total heat load to FW coolant. This process was repeated for each of three assumed values for breeder conductivity. For a given flow channel geometry, values for convective coefficients were computed and comparisons made with critical heat fluxes to ensure that adequate cooling was being provided. Temperature distributions within the first wall were then computed using the finite difference code, STEDROM.

9.8.2.2 Discussion of Results

Results for the passively cooled FW for the TMR appear in Fig. 9.8-14. The plot shows that this cooling approach is not feasible. The low thermal

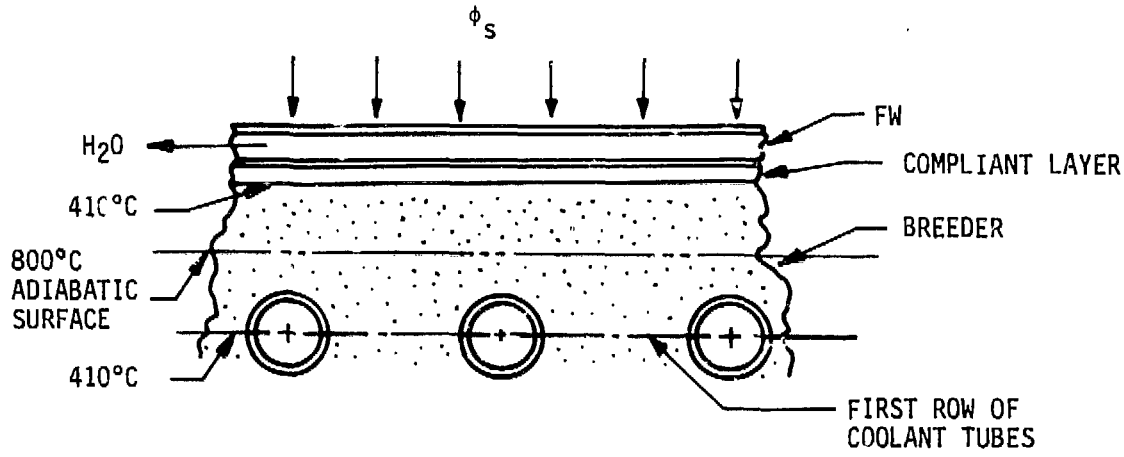

Fig. 9.8-13. Actively cooled FW geometry - conceptual model

conductivity values of the breeder and the small allowable ΔT ($550^0C-410^0C = 140^0C$) make it impossible to have a reasonable thickness of breeder even for a 2 mm thick FW without exceeding the maximum temperature for HT-9. Therefore, this FW concept was not considered further.

Results for the actively cooled lobe-shaped FW appear in Table 9.8-2. These results indicate that a breeder thickness of ~1 to 1.5 cm, depending on thermal conductivity, would be possible with an actively cooled FW. These breeder thicknesses are limited by Li_2O breeder T_{max} and T_{min} of 800^0C and 410^0C, respectively. Coolant flows per channel of 0.02 and 0.04 kg/s for TMR and tokamak heat fluxes, respectively, were adequate to prevent hydraulic burnout. Coolant velocities for the minimum flow channel heights were $\lesssim$8 m/s. From the finite difference model, maximum allowable thicknesses for the plasma-facing structure were established based on the 550^0C HT-9 maximum structural temperature constraint and a 320^0C coolant temperature. For the TMR, this allowable thickness is >1.0 cm, while for the tokamak it is ~0.5 cm. Temperature distributions produced by this analysis were also used to determine thermal stresses in the FW; these studies are reported in Sec. 9.8.3.

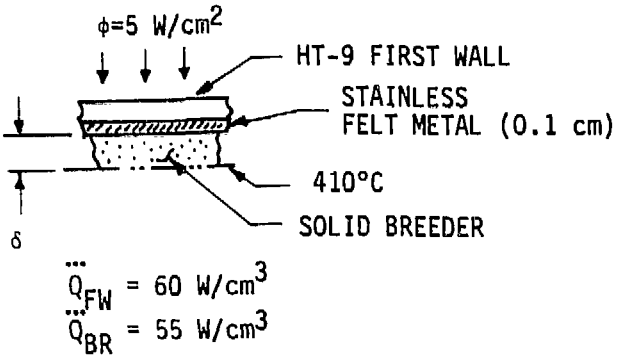

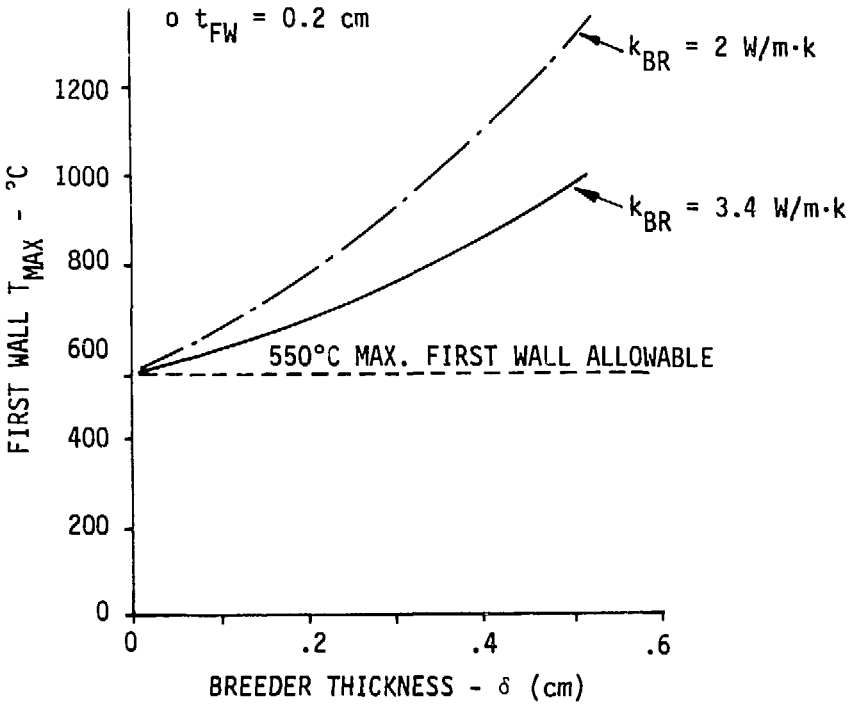

Fig. 9.8-14. Allowable breeder thickness behind passively cooled first wall

TABLE 9.8-2. ALLOWABLE FIRST LAYER BREEDER THICKNESSES AND MINIMUM COOLING CHANNEL HEIGHTS FOR ACTIVELY COOLED FIRST WALL

DEVICE	Φ_s (W/cm^2)	MAX. ALLOWABLE BREEDER THICKNESS[a] 0.020 W/cm-K	0.027	0.034	MASS FLOW RATE (kg/s)	MIN. FLOW CHANNEL HEIGHT
TANDEM MIRROR	5	1.12 cm	1.30 cm	1.46 cm	0.02	1.0 mm
TOKAMAK	100				0.04	2.0 mm

[a]Thickness of breeder layer behind first wall which will yield breeder T_{MAX} and T_{MIN}, for various values of breeder thermal conductivity.

9.8.3 Structural Analyses

9.8.3.1 Introduction and Summary

A trade study was conducted to compare a flat first wall with a lobe shaped first wall of the blanket module for both a tokamak and a tandem mirror reactor. Loading on the blanket module resulted from the vacuum pressure, internal pressurization of blanket module, and plasma disruption or sudden-loss-of-plasma (TMR). The lobe shaped first wall can carry a load that is a factor of five higher than the flat first wall can carry for the same spacing of internal supports or side walls. In addition, the lobe shaped first wall can carry the blanket internal pressurization loads more efficiently. Thermal stresses in the TMR version are not a problem because of the low surface heat flux. For the tokamak version, the first wall structural thickness cannot exceed 2.4 mm.

9.8.3.2 Applied Loads and Design Allowables

Loads acting on the first wall of the blanket module result from internal pressurization of the blanket module, forces resulting from sudden-loss-of-plasma, and a surface heat flux of 100 W/cm^2. The steady-state blanket module pressurization is 6 atm (helium purge gas). Forces resulting from a sudden-loss-of-plasma in a tokamak result in an equivalent distributed pressure of 0.6 MPa (88 psi) acting inward toward the plasma. For a flat first wall, this loading is simply distributed as a uniform pressure loading. For a lobular first wall, the forces resulting from a sudden-loss-of-plasma produce a cosine pressure distribution load with an average load equavalent to that from the 0.6 MPa uniform pressure loading. In a TMR, forces caused by toroidal eddy currents produce an equivalent distributed pressure of ~.02 MPa (2.4 psi) acting inward toward the plasma.

Allowable stresses for the ferritic steel first wall/blanket module are based on the ASME Boiler and Pressure Vessel Code, Section III. Allowable stress levels are given in Section 6.7. Irradiated material design allowables (S_{mt}) were used for stresses resulting from the coolant pressure, internal blanket pressurization and thermal stresses. For stresses resulting from sudden-loss-of-plasma, design allowables are based on unirradiated material properties because the loads are of very short duration, i.e., creep is not a factor. However, these loads are treated as normal operating loads.

9.8.3.3 Comparison of Flat First Wall With a Lobe Shaped First Wall

A ribbed coolant panel with internal rectangular-shaped coolant channels was used for the first wall, as shown in Fig. 9.8-15. Coolant passages in the first wall have a square cross-section 3.81 mm by 3.81 mm. The support ribs between coolant passages are 1.27 mm wide. Because of the length of the blanket module, internal supports are required for the first wall to keep stresses below design allowables.

Two geometries for the first wall, flat and lobe-shaped, were considered in this study. These two geometries are shown in Fig. 9.8-15.

Based on symmetry of the first wall and applied loads about the internal supports, the first wall cannot rotate about the internal supports. Therefore, stresses in the flat first wall design were calculated using equations

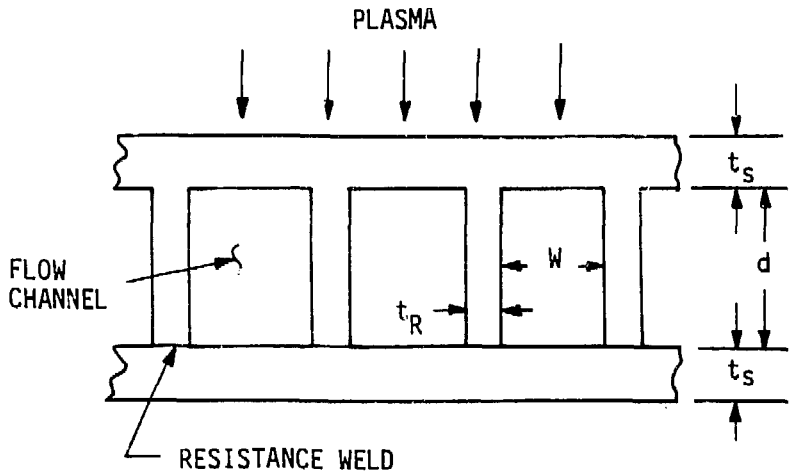

FIRST WALL CROSS SECTION

RECTANGULAR MODULE - FLAT FIRST WALL

LOBULAR MODULE - SEMICYLINDRICAL FIRST WAL

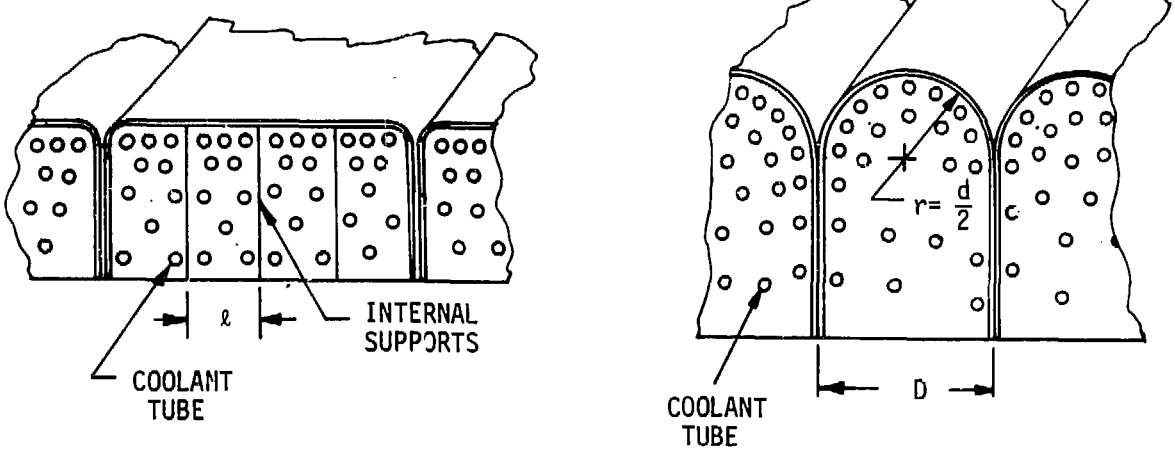

Fig. 9.8-15. General configuration for rectangular and lobular modules

that represent a beam with fixed edges. Stresses in the lobe-shaped first wall were calculated in a similar fashion. Since the first wall cannot rotate about the internal support, equations that represent a ring with fixed edges were used to calculate stresses in the lobe-shaped first wall.

For the flat first wall, a study was conducted to determine the effects of internal support spacing and skin thickness on the allowable pressure that the first wall can withstand. Results of this study are shown in Fig. 9.8-16. As internal support spacing decreases and skin thickness increases, the allowable pressure increases. At an internal support spacing of 10 cm, the allowable pressure for a skin thickness of 1.27 mm is 1.00 MPa. By increasing the skin thickness to 2.54 mm, the allowable pressure increases to 2.16 MPa. These values are based on an allowable stress level of 1.5 S_{mt} (primary membrane plus bending stresses). Increasing the internal support spacing to 20 cm from 10 cm decreased the allowable pressure to 0.25 MPa from 1.00 MPa.

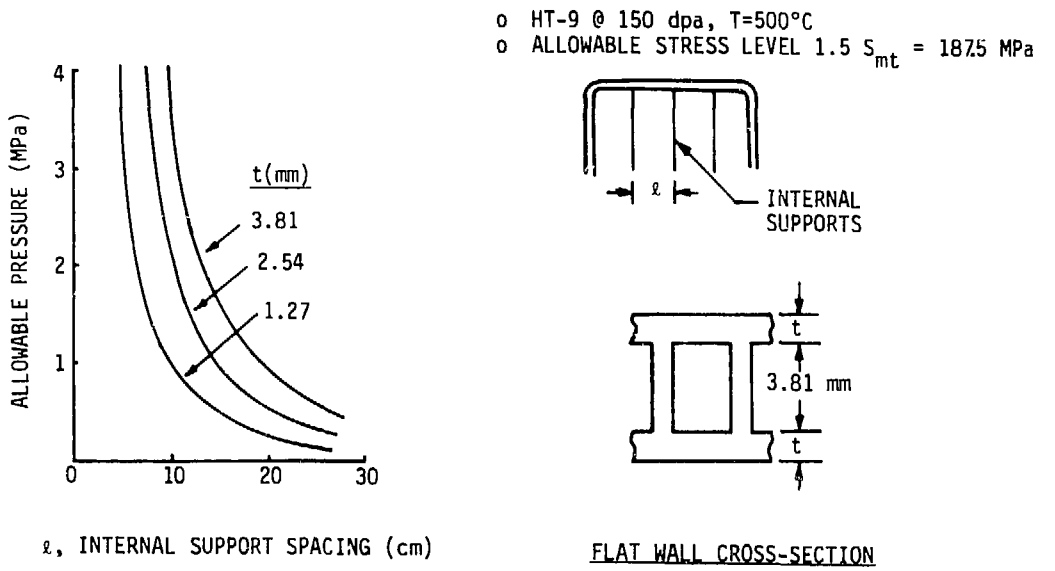

Fig. 9.8.16. Allowable pressure for rectangular module as function of internal support spacing

A similar study was conducted for the lobe-shaped first wall with an applied uniform load. Lobe diameter and skin thickness were varied. For a 40 cm lobe diameter, the allowable pressure is 2.31 MPa for a skin thickness of 1.27 mm. Increasing the skin thickness to 2.54 mm increases the allowable pressure to 4.53 MPa. These results are shown in Fig. 9.8-17.

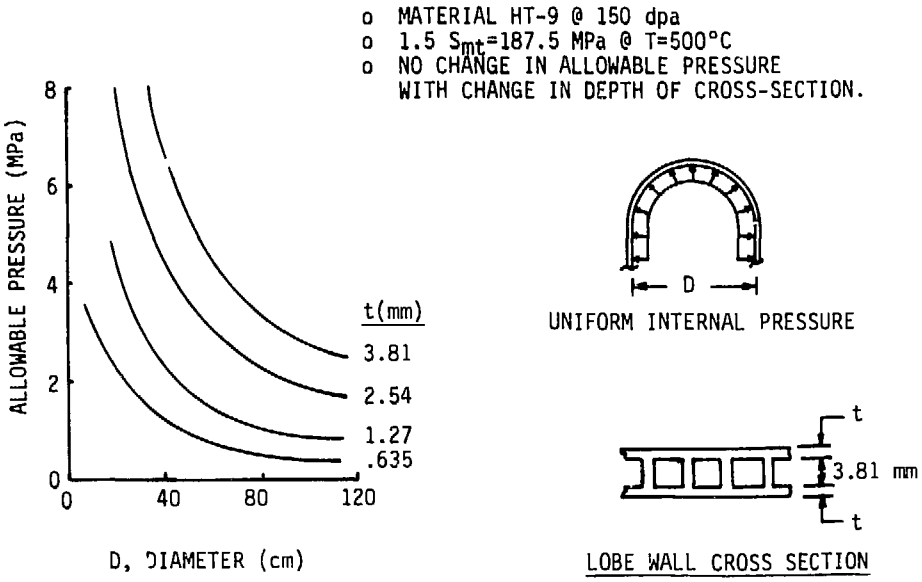

Fig. 9.8-17. Allowable pressure for lobular module

For the lobe-shaped first wall, the loads resulting from a plasma disruption or sudden-loss-of-plasma were applied as a cosine distribution load. For a lobe diameter of 20 cm, the allowable pressure is 1.12 MPa for a skin thickness of 1.27 mm. Increasing the skin thickness to 2.54 mm increases the allowable pressure to 3.00 MPa.

A comparison of the flat first wall and the lobe-shaped first wall with both the cosine distributed loading and a uniform loading are shown in Fig. 9.8-18 and Fig. 9.8-19. For a lobe-shaped first wall, the allowable pressure can be increased by approximately a factor of 5 for the same spacing/diameter

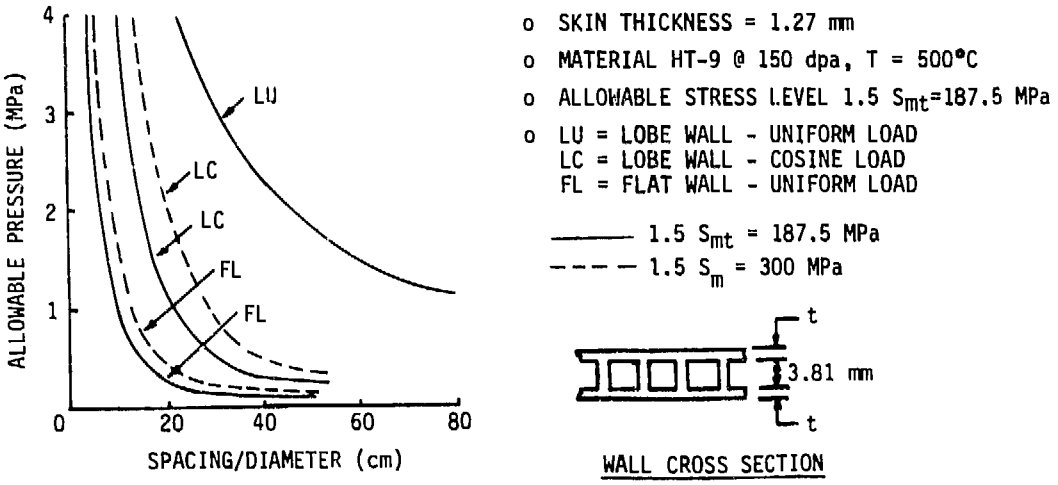

Fig. 9.8-18. Comparison of allowable pressures--t_s = 1.27 mm

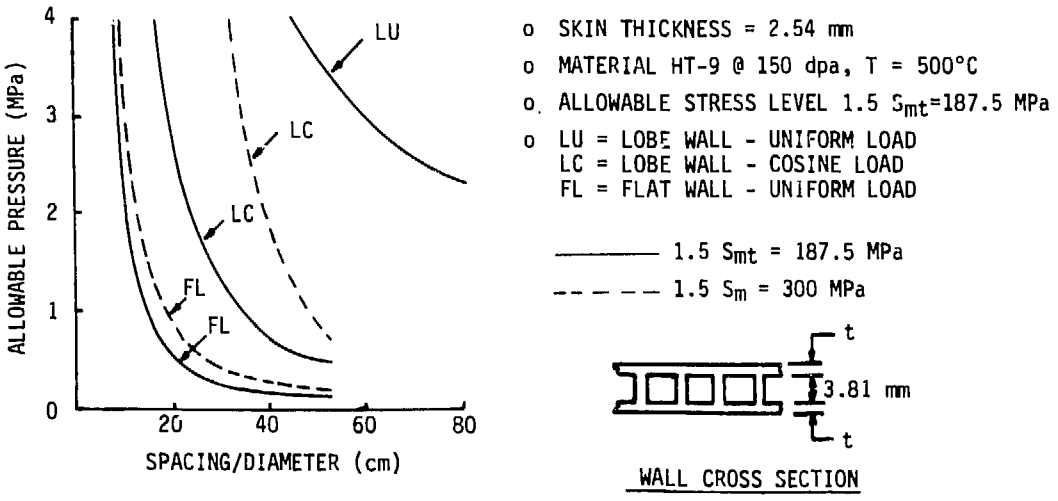

Fig. 9.8-19. Comparison of allowable pressures--t_s = 2.54 mm

value. For the same applied loading, the spacing of internal supports for the lobe-shaped first wall can be approximately double the required spacing for a flat first wall.

Also shown in Fig. 9.8-18 and Fig. 9.8-19 is the effect of allowing stresses resulting from a sudden-loss-of-plasma to be based on 1.5 S_m instead of 1.5 S_{mt}. Because of the very short time that the loads are applied, 1.5 S_m can be used and the allowable applied pressure increases by ~80%.

For the flat first wall, the design allowables can be met with an internal support spacing of 10 cm and a skin thickness of 1.27 mm. This is based on applied loads of 6 atm blanket pressurization, 0.607 MPa loading from sudden-loss-of-plasma, and a surface heat flux of 100 W/cm^2. By going to a lobe-shaped first wall, internal support spacing can be increased to 30 cm. Spacing can be increased because the lobe-shaped first wall can carry the blanket internal pressurization and loads resulting from sudden-loss-of-plasma more efficiently than a flat first wall. Stresses resulting from the 6 atm blanket pressurization are 36 MPa for a 30 cm span for the lobe-shaped first wall compared to 130 MPa for a 10 cm span on the flat first wall.

9.8.3.4 Thermal Stresses for TMR and Tokamak First Walls

A study was conducted to determine the maximum allowable skin thickness of the first wall based on thermal stresses. The design allowables for thermal stresses were based on the ASME Boiler and Pressure Vessel Code. For combined primary plus bending plus secondary (thermal) stresses, the design allowable is 3.0 S_{mt}. The design allowable for primary plus bending stresses only is 1.5 S_{mt}. Therefore, the minimum allowable for thermal stresses is 1.5 S_{mt}. This allows the remaining 1.5 S_{mt} of the 3 S_{mt} to be utilized for loads resulting from the blanket module pressurization loads and loads resulting from sudden-loss-of-plasma.

Thermal stresses increase with increasing first wall skin thickness, for both the tokamak and TMR, as shown in Fig. 9.8-20. The applied surface heat flux for a mirror machine is a factor of 20 less than the 100 W/cm^2 surface heat flux on a tokamak machine. The maximum allowable structural thickness for the tokamak is 2.40 mm. For the TMR, the maximum allowable thickness is 11.0 mm. Therefore, thermal stresses will not be a problem for a mirror machine.

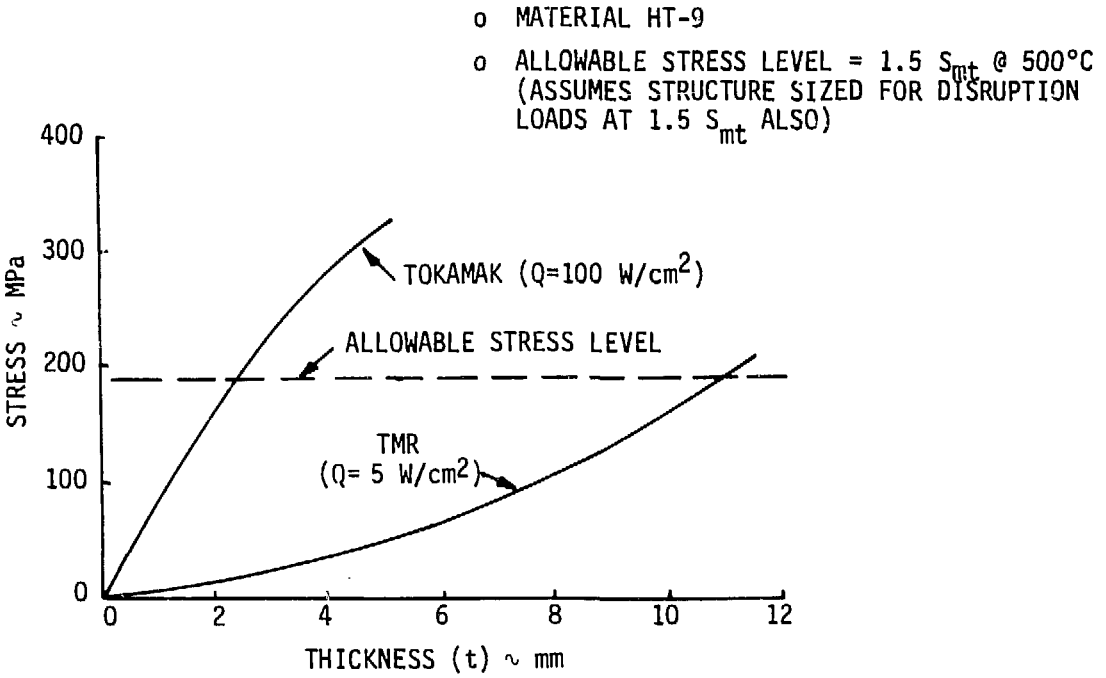

Fig. 9.8-20. First wall thermal stresses for TMR and tokamak conditions

9.8.3.5 Electromagnetic Forces on the First Wall/Blanket Due to Plasma Disruption or Loss of Plasma

For a tokamak, the plasma disruption induces currents in the first wall which result in an equivalent pressure of 0.6 MPa on the outboard first wall. This pressure acts inward, toward the plasma. An additional inward pressure of 0.16 MPa acts on the outboard first wall due to loss of plasma diamagnetism. This results in a total pressure of 0.76 MPa (Sec. 5.1).

A lobe-shaped first wall with a skin thickness of 1.27 mm and a radius of 15 cm results in a stress of 225 MPa. The resulting margin-of-safety is -0.17. Margin-of-safety is the ratio of allowable load divided by the applied load minus one. Increasing the skin thickness to 2.54 mm, the reference design value, decreases the stress level to 112.5 MPa. The resulting margin-of-safety is 0.67.

If the blanket sectors are electrically connected further back than the first wall, currents will be induced in the sides of the blanket sectors. Currents on opposite sides of the blanket are in opposite directions. Therefore, a net torque about a radial axis is produced. The allowable torque on the blanket module was calculated for a 1.0-m-square module. The walls of the blanket module were assumed to be the same as the first wall, i.e., the double wall configuration with a skin thickness of 1.27 mm. The resulting allowable torque for the blanket module is 126,000 N-m.

9.8.3.6 Seismic Loads on First Wall/Blanket Module

The first wall/blanket module must withstand a seismic event that results in accelerations applied simultaneously in all three directions. The very conservative ±4.4 g acceleration assumed (Sec. 5.1) is based on an equivalent static acceleration per RDT Standard F9-2T[14]. This equivalent static design acceleration for supported equipment and components of ±4.4 g's is applied simultaneously in two horizontal and the vertical directions.

Based on the 4.4 g equivalent static design acceleration, the equivalent pressure acting on the first wall is ~0.06 MPa. The resulting stress in the lobe-shaped first wall, assuming this total load acts with a cosine distribution, results in an additional stress of 18 MPa (<3 ksi). This stress is easily within the design allowables when combined with other stresses due to normal loads.

9.8.3.7 Magnetic Loads on the Ferritic Steel Lobe-Shaped First Wall

Since HT-9 is ferromagnetic, the first wall blanket will be subjected to magnetic forces. A check was made for the HT-9 first wall/blanket module to determine what effect these loads will have. The magnitude of these loads depend on the location of the module along the major radius of the sector. These loads and position of the blanket modules are shown in Fig. 9.8-21.

All modules experience a load in the y-direction (toroidal direction). This load is approximately six times the HT-9 weight. Modules under the magnet are in compression, while those between magnets are in tension. The resulting stress in the module structure is 0.10 MPa, an extremely low value.

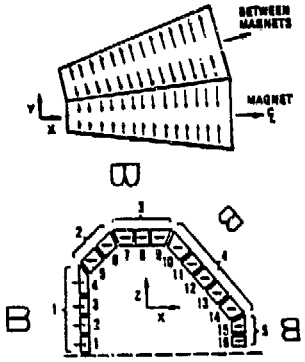

Schematic showing position and forces on blanket modules: (a) shows forces in Y-direction, and (b) shows forces in X-direction. Brackets indicate full blanket modules while small numbers refer to elements used in GFUN calculation.

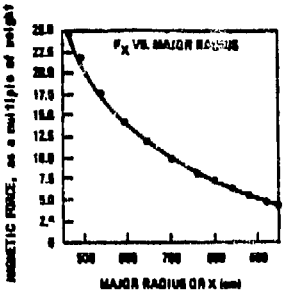

The force distribution in the direction of major radius on blanket module.

Fig. 9.8-21. Ferromagnetic forces and directions for FS first wall/ blanket modules

The modules also experience a load in the x-direction (radial) pulling the modules towards the center of the tokamak. Modules located closest to the reactor center see the highest field gradient; therefore, they experience the greatest loading.

Modules 1-4 experience a load that is equal to 25 times the HT-9 weight. This magnetic load puts the module in compression. This loading puts an equivalent pressure of 0.031 MPa on the lobe-shaped first wall. Using the cosine load distribution, the resulting stress in the first wall is 5.0 MPa (<1 ksi).

On modules 15 and 16 the loading is similar to the loading on modules 1-4. However, the modules are in tension and the magnitude of the loading is only 5 times the HT-9 weight. Therefore, these magnetic loads will present no problems.

The magnetic loads on module 8 produce a shearing load on the module which is similar to the dead weight loading on modules 1 and 16. This magnetic load on the first wall is approximately 10 times the HT-9 weight. The load must be carried by the side wall of the module. The resulting stress is 5.5 MPa.

The load on modules 10-14 is in the range of 5 to 10 times the HT-9 structure weight. These loads are reacted by a combination of tension on the first wall and shear on the side walls of the module. The magnitude of the resulting stresses will be on the same order of magnitude as those shown for the other modules.

All of these stresses due to ferromagnetic loads for the reference design $LiAlO_2/H_2O$/FS/Be tokamak concept are very easily accommodated along with other stresses due to normal operating loads, and all stress limits are met.

9.8.4 Nuclear Analysis

This section presents the nuclear analysis for a series of water-cooled solid-breeder blanket designs. The breeding materials investigated include Li_2O and gamma-phase $LiAlO_2$ (γ-$LiAlO_2$) as a representative breeder for the general group of ternary ceramic breeders such as Li_2SiO_3, Li_2TiO_3, Li_2ZrO_3, etc.

The analysis presented in this section is grouped into two categories; (1) 1-D and 3-D design scoping study which has eventually led to a design of the reference γ-$LiAlO_2/H_2O$ blanket; and (2) the 3-D nuclear analysis for the reference design. In terms of the reactor concept, both a TMR based on the MARS design and a tokamak reactor based on the STARFIRE design are considered for the reference system analysis.

All scoping study has been performed using multi-group nuclear data libraries based on EDNF/B-IV. Regarding the transport calculation, 1-D ANISN (with the S_8-P_3 approximation) and 3-D MORSE-CG (with the P_3 approximation) codes were utilized. For the final reference blanket analysis, a continuous energy Monte Carlo code, MCNP, was employed with its associated data library based on the latest ENDF/B-V version.

9.8.4.1 Evolution of the $LiAlO_2/H_2O$/FS/Be Reference Blanket Design

The water-cooled solid-breeder blanket designs have been revised several times during the course of the study to cope with changes in structural/mechanical design and/or breeding material properties such as the thermal conductivity and the maximum/minimum breeder temperatures. Concept changes from the flat-shape first-wall design to lobular-shape first-wall design, and from sintered breeders to sphere-pac breeders, all necessitated design iterations. The evolution of concept ranking has also forced design changes such as those from use of PCA structure to use of HT-9 structure. From the neutronics standpoint, these design changes generally resulted in substantial increases of structural-material volume and decreases of breeder volume, as shown in Table 9.8-3.

TABLE 9.8-3. EVOLUTION OF γ-$LiAlO_2/H_2O$/(FS or PCA)/Be DESIGN PARAMETERS

System	k_t (W/m-^{0}K)	T_{min} (^{0}C)	T_{max} (^{0}C)	ΔT (^{0}C)	Volume % at 50 MW/m^3 Heating		
					HT9	H_2O	$LiAlO_2$
NOV 83	2.2	300	1200	900	20 (PCA)	20	55[a]
FEB 84	1.6	410	1200	790	22	20	47[b]
APR 84	1.45	350	1000	650	27	25	35[b]

[a]Sintered γ-$LiAlO_2$: 85% T.D.

[b]Sphere-pac γ-$LiAlO_2$: 86.6% S.P.F.

In addition, safety considerations for use of the high-pressure (~15 MPa) water coolant with lithium-containing solid-breeders necessitated the use of a double-wall coolant tube (DWT) concept as opposed to the single-wall coolant tube (SWT) concept previously considered, resulting in an even higher structure fraction (and a lower breeder fraction) in the blanket. For example, Fig. 9.8-22 compares the DWT-Li_2O/H_2O blanket designs without neutron multiplier in terms of the breeding performance as a function of neutron wall

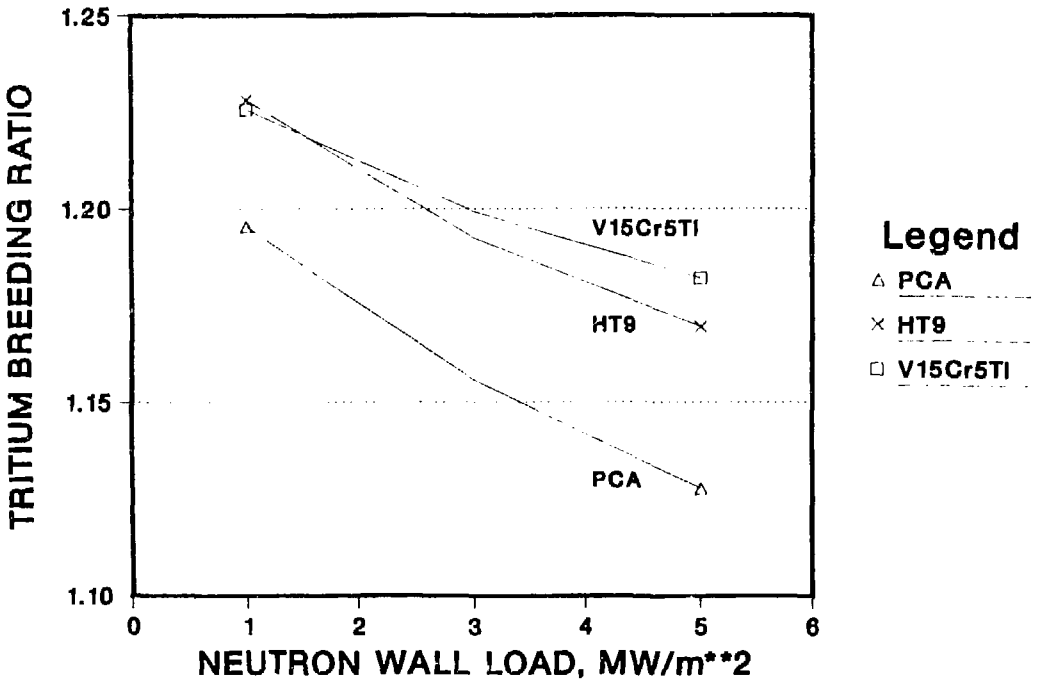

Fig. 9.8-22. Effects of structural materials and neutron wall load on tritium breeding performance for DWT Li_2O/H_2O blanket design

loading, for several candidate structural materials. It is evident that the breeding performance shown is substantially lower than those reported earlier (generally TBR's $\gtrsim$ 1.25), particularly at high neutron wall loads. Given present design assumptions and BCSS design guidelines, it seems impossible to design Li_2O/H_2O blankets without multiplier that result in a TBR > 1.2 on a full-breeding basis when the DWT approach is taken. Note that the breeding performance is significantly enhanced, in such high-structure-content designs, by using HT9 instead of PCA. This is due to the lack of strong neutron absorption of nickel in HT9.

Table 9.8-4 lists the 1-D TBR's and the associated design parameters used, for a series of water-cooled Li_2O blanket designs. The breeding loss of ~0.05 in Design 3 relative to Design 2 is apparently caused by an increased neutron absorption of HT9 in Design 3, as expected from the following average blanket compositions:

Design 2: 9% HT9 + 8% H_2O + 79% Li_2O + 4% void
Design 3: 11% HT9 + 10% H_2O + 74% Li_2O + 5% void

In the first few centimeters behind the first wall, the compositional difference is more evident:

Design 2: 17% HT9 + 16% H_2O + 60% Li_2O + 7% void
Design 3: 22% HT9 + 20% H_2O + 47% Li_2O + 11% void

TABLE 9.8-4. TRITIUM BREEDING PERFORMANCE OF Li_2O/H_2O BLANKET DESIGNS[a]

Design No.	First Wall Shape	Form of Li_2O	Thermal Conductivity, W/m-°K	Structural Material	Neutron Multiplier	1-D TBR
1	Flat	Sintered	3.4	PCA	---	1.098[b] (1.136)[c]
2	Flat	Sintered	3.4	HT9	---	1.142 (1.180)
3	Lobe	Sphere-pac	2.6	HT9	---	1.098 (1.128)
4	Lobe	Sphere-pac	2.6	HT9	Be(5.7 cm)[d]	1.405 (1.420)

[a]Based on ANISN/VITAMIN-C/MACKLIB-IV calculation with STARFIRE (major radius) model. Li_2O at 85% of T.D. with natural lithium.

[b]$T_6 + 0.85\ T_7$

[c]$T_6 + T_7$

[d]Beryllium is placed behind a 2.4-cm thick first breeder zone.

Use of a neutron multiplier makes the Li_2O/H_2O designs more viable in terms of sufficient breeding margin for such high-structure-content blankets. As shown in Design 4 for example, ~6 cm of beryllium can enhance the breeding by more than 0.3/DT provided that the beryllium region is sandwiched between the two adjacent breeding zones near the first wall. Design 4 includes more water coolant and structure than Design 2, in order to remove higher nuclear heating caused by the beryllium use.

Table 9.8-5 shows some of the γ-$LiAlO_2/H_2O$/Be blanket designs studied. The general trend is similar to those indicated in Table 9.8-4 for the Li_2O designs, i.e., breeding improvements reflecting the use of HT9 instead of PCA and the sandwich-type use of beryllium as opposed to a conventional multiplier design (Design 2).

One of the most important considerations for the nuclear design of ternary ceramic breeders in general is how to cope with high nuclear heating rates stemming from use of neutron multipliers (see Sec. 9.4.3.2). For instance, Design 4 (shown in Table 9.8-5) yields a maximum nuclear heating rate of ~120 MW/m^3 in the breeder region behind the first wall for a neutron wall load of 5 MW/m^2. Lowering the ^6Li enrichment can ameliorate the design problem for the heat-removal system. Unfortunately, however, a relatively high ^6Li enrichment must be used in order to mitigate the lithium burn-up effect and make the blanket system durable over the whole period of operation.

Use of an $LiAlO_2$/Be mixture in a sphere-pac mode, especially an $LiAlO_2$-lean mixture, has two strong design incentives from the neutronics standpoint. They are suppression of high nuclear heating and enhancement of the Be(n,2n) potential. For example, use of a 90:10 Be/SB sphere-pac mixture reduces the maximum nuclear heating rate to ~70 MW/m^3 from ~120 MW/m^3, leading to an easily manageable average zone heating rate of ~30 MW/m^3.

As listed in Table 9.8-6, the thermal conductivity of the $LiAlO_2$/Be mixture is relatively high (~3.0 $W/m-^0K$) compared to the $LiAlO_2$ sphere-pac. This reflects the high thermal conductivity of beryllium. However, the $LiAlO_2$/Be design is not much different from the previous $LiAlO_2$ sphere-pac design with slab Be from the viewpoint of the blanket materials compositions. This is due to the narrow temperature window caused by the relatively low maximum allowable temperature of beryllium, i.e., 650^0C instead of 1000^0C for $LiAlO_2$ alone. The high structure and coolant volume fractions

TABLE 9.8-5. TRITIUM BREEDING PERFORMANCE OF γ-$LiAlO_2/H_2O$/Be BLANKET DESIGNS[a]

Design No.	First Wall Shape	Form of γ-$LiAlO_2$	Thermal Conductivity W/M-^{0}K	Structural Material	Beryllium Thickness (cm)	1D-TBR	
1	Flat	Sintered	2.2	PCA	5.7[d]	1.253[b]	(1.259)[c]
2	Flat	Sintered	2.2	PCA	5.7[e]	1.141	(1.146)
3	Flat	Sintered	2.2	HT9	5.7[d]	1.313	(1.319)
4	Lobe	Sphere-pac	1.6	HT9	5.8[f]	1.300	(1.304)

[a]Based on ANISN/VITAMIN-C/MACKLIB-IV calculation with STARFIRE (major radius) model. γ-$LiAlO_2$ at 85% of T.D. with 30% ^6Li enrichment.

[b]$T_6 + 0.85\ T_7$

[c]$T_6 + T_7$

[d]Beryllium is placed behind a 1.5 cm first breeder zone.

[e]Beryllium is placed behind the first wall.

[f]Beryllium is placed behind a 1.9 cm first breeder zone.

TABLE 9.8-6. COMPARISON OF γ-$LiAlO_2$ AND γ-$LiAlO_2$/Be MIXTURE DESIGN PARAMETERS

	γ-$LiAlO_2$ (Sphere-pac)	γ-$LiAlO_2$/Be Mixture (Sphere-Pac)
k_{th} (W/m-K)	1.45	3.0
T_{min} (^{0}C)	350	350
T_{max} (^{0}C)	1000	650 (Be)
ΔT (^{0}C)	650	300
Volume % at 50 MW/m^3 Nuclear Heating		
HT9	27	27
H_2O	25	25
γ-$LiAlO_2$ (or /Be)	35	34

observed here led to a design requirement for high enrichment of ^{6}Li to compete with the strong neutron absorption of HT9.

Figure 9.8-23 illustrates the neutron multiplication rate by beryllium and the resulting TBR as a function of γ-$LiAlO_2$/Be mixture zone thickness. The analysis was performed for a tokamak system with total breeding zone thicknesses of 47 cm in the outboard region and of 27 cm in the inboard region. The blanket compositions have been determined based on the material properties shown in Table 9.8-6. Two cases of ^{6}Li enrichment, 60% and 90%, are considered for $LiAlO_2$ throughout the blanket. Both cases result in about the same Be(n,2n)/DT rate, but the 90% enrichment case generates more tritons per DT-fusion. The implication is that the primary function of ^{6}Li enrichment for $LiAlO_2$ is to compete with the parasitic neutron loss in HT9 rather than affecting the performance of neutron multiplication. With a mixture zone of ~20 cm and a ^{6}Li enrichment of ~90%, one can expect a 1-D TBR of greater than 1.2.

Another important parameter that governs the breeding performance in the γ-$LiAlO_2$/Be blanket design is the mixing ratio of γ-$LiAlO_2$ to Be. As

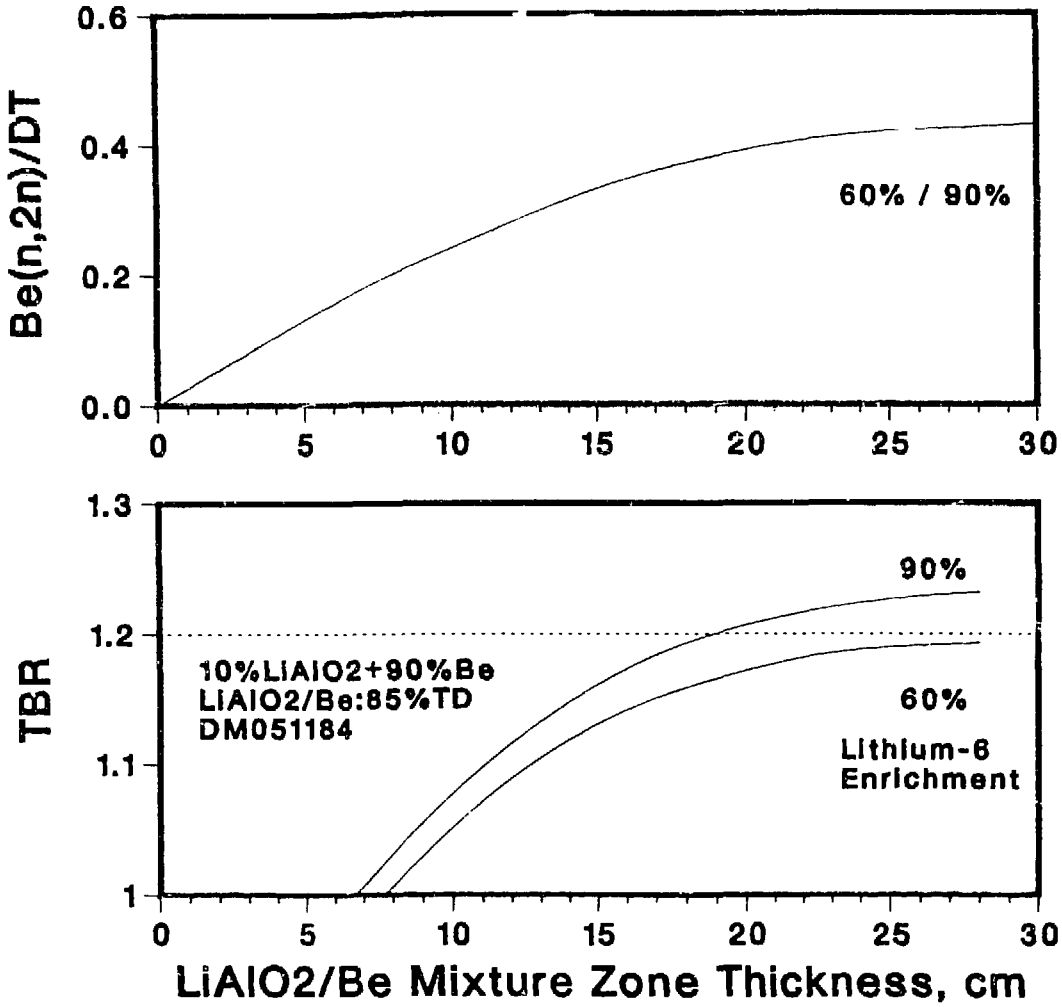

Fig. 9.8-23. Effect of ^{6}Li enrichment on tritium breeding performance

indicated in Fig. 9.8-24, the $LiAlO_2$-lean mixture substantially improves the breeding performance due to the higher potential of the Be(n,2n) reaction. For the 10% $LiAlO_2$ + 90% Be mixture, a minimum mixture zone thickness is ~8 cm for a 1-D TBR $\gtrsim$ 1.0 and is ~20 cm for a 1-D TBR $\gtrsim$ 1.2.

The reference γ-$LiAlO_2/H_2O$ blanket (Sections 9.4 and 9.5) which will be analyzed in more detail in Sec. 9.8.4.4, has thus been designed to have a 20-cm 90:10 SB/Be mixture zone surrounding the first wall, with the breeder being enriched to 90% ^{6}Li.

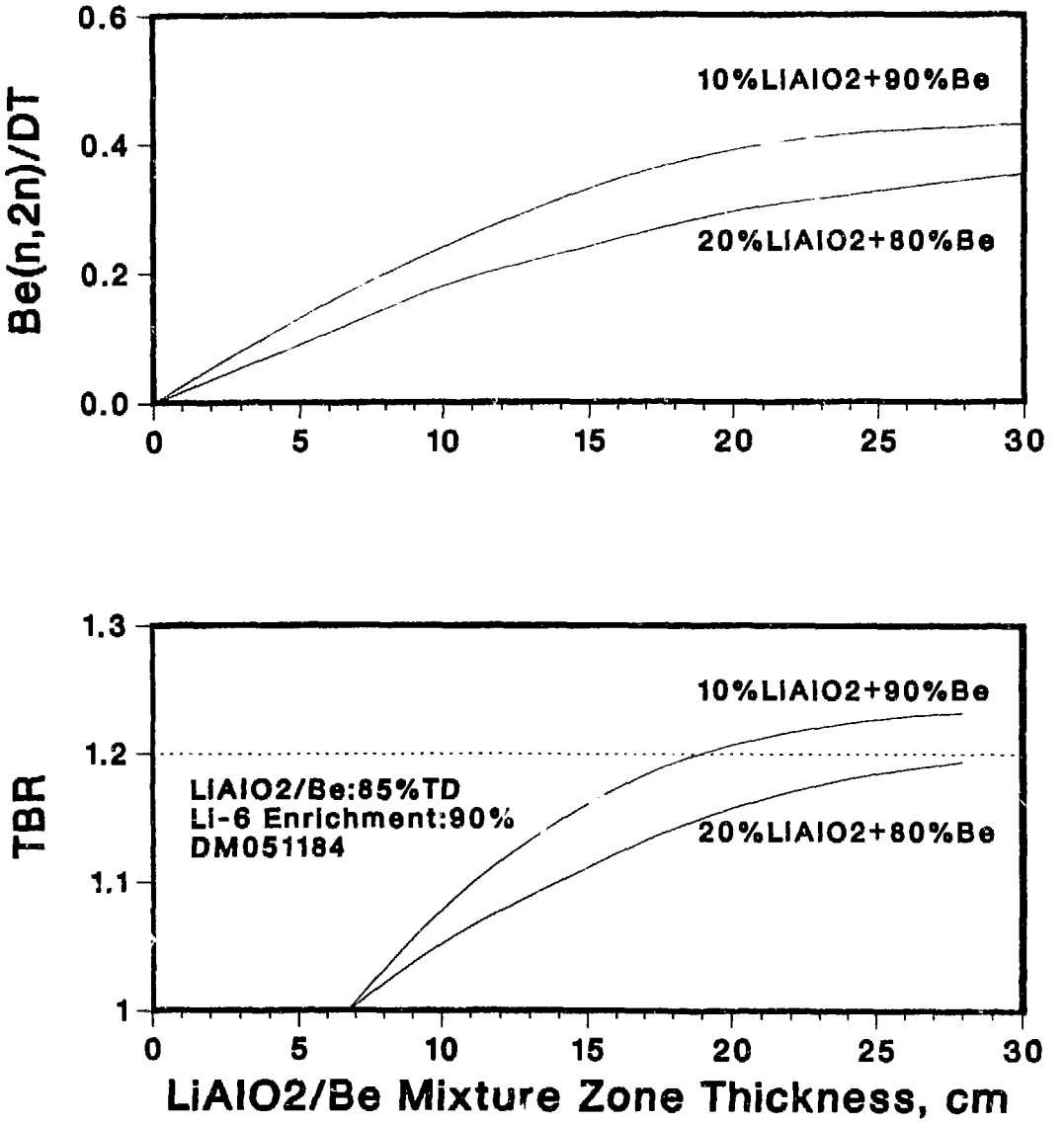

Fig. 9.8-24. Effect of $LiAlO_2$/Be zone thickness and mixture ratios on tritium breeding performance

The economic penalty for the relatively high ^6Li enrichment should be compensated for by the advantages of the resulting smaller inventories of lithium and beryllium. In fact, the effective beryllium thickness required for the reference design is only ~7.7 cm and the corresponding total γ-$LiAlO_2$ thickness is ~2.7 cm in the inboard blanket and ~18.9 cm in the outboard. In the case of the reference TMR design, the respective Be and $LiAlO_2$ thicknesses come to ~8.0 cm and ~19.8 cm. These multiplier and breeder thicknesses appear to be appreciably small considering the very high coolant and structure volume fractions in the reference blanket designs.

However, a related potential problem for the $LiAlO_2/H_2O$/FS/Be concept is a significant reduction in both TBR and nuclear heating rates over the life of the blanket, caused by high burnup rates of ^6Li in regions near the first wall. This concern, discussed in more detail in Sec. 9.3.1.6, came about after the reference designs had been "frozen," and thus the severity of the problem and possible design solutions could not be investigated. However, further work in this area is necessary for any future water-cooled solid breeder blankets using neutron multipliers.

9.8.4.2 Multi-Dimensional Analysis of Water-Cooled Solid-Breeder Blanket Designs

Prior to the detailed nuclear analysis of the reference blanket designs, a neutronics study was conducted to understand the general multi-dimensional effects on tritium breeding, using a 3-D Monte Carlo code, MORSE-CG. The effects investigated include non-uniform source neutron distribution generated by the MHD plasma shift and breeding perturbation due to the limiter penetration, both of which are of concern for the tokamak system analysis.

As described in detail in Section 6.10, the reference source neutron distribution assumed for all tokamak designs ranked R=1 has a form

$$f(r) \propto \left[1 - \left(r/r_m\right)^{C_1}\right]^{C_2} ,$$

with parametric equations,

$$Z_b = a\,\kappa\,\sin t$$

and

$$\rho_b = R_m + a \cos(t + d \sin t) \quad ,$$

where Z_b = boundary contour height in the direction perpendicular to the reactor midplane;

ρ_b = boundary contour major radius;

a = plasma minor radius (1.94 m);

κ = plasma elongation factor (1.6);

d = plasma triangularity factor (0.5);

C_1, C_2 = plasma shaping factors ($C_1 = C_2 = 2$);

r_m = plasma boundary radius measured from the shifted plasma center, which is 7.59 m, i.e., the major radius R_m (7.0 m) plus the shift distance S_m (0.79 m).

Table 9.8-7 summarizes the 3-D TBR's obtained for a variety of neutron distribution functions that were parametrically changed. All results are compared to the reference TBR of 1.104 for the SWT Li_2O/H_2O design selected from Ref. 1. The limiter is assumed to be constructed of a water-cooled Ta-5W heat sink located at the bottom.

It is concluded that the source distribution has little effect on the breeding performance provided that the overall source distribution is confined to the D-shaped plasma region. The conclusion is valid not only for the reference Li_2O/H_2O blanket design but also for relatively hard neutron spectrum systems such as the helium-cooled Li_2O blanket and the self-cooled lithium blanket studied.

Table 9.8-8 examines the effect of a series of limiter designs considered during the course of the BCSS study. Three different types of limiter are considered:

(1) Cu alloy heat sink limiter with 10 mm of beryllium coating;

(2) V-15Cr-5Ti alloy heat sink limiter with 10 mm of beryllium coating; and

(3) Ta-5W alloy heat sink limiter without beryllium coating.

TABLE 9.8-7. MULTIDIMENSIONAL EFFECTS OF SOURCE NEUTRON DISTRIBUTIONS ON TRITIUM BREEDING

(A) Effect of Source Shape Parameters

Case	A1	A2	A3	A4	A5
C_1	2	2	2	2	3
C_2	0	1	2	4	3
TBR	1.106	1.104	1.104	1.099	1.099

(B) Effect of Source Shifting

Case	B1	B2	B3
S_m (m)		0.0	0.79	1.50
TBR	1.102	1.104	1.102

(C) Effect of Source Triangularity

ase	C1	C2	C3
	0.0	0.50	0.75
BR	1.109	1.104	1.105

(D) ombined Effects of Source Distribution Functions

Case D1	[C_1 = 2, C_2 = 4, S_m = 1.5 m]		
Blanket	Li_2O/H_2O	Li_2O/He	Li/Li
TBR 1.104	1.119	1.158	

Case D2	[C_1 = 2, C_2 = 2, S_m = 0.79 m]		
Blanket	Li_2O/H_2O	Li_2O/He	Li/Li
TBR 1.109	1.115	1.157	

TABLE 9.8-8. EFFECT OF LIMITER DESIGN ON TRITIUM BREEDING[a]

System	Case A	Case B	Case C	Case D	Case E
A) Li_2O/H_2O					
Inbd. Blanket (cm)	28.8	28.8	28.8	28.8	28.8
Outbd. Blanket (cm)	33.1	33.1	48.1	48.1	48.1
Limiter					
• Type	None	STARFIRE	STARFIRE	STARFIRE	FED/INTOR[b]
• Coolant	(Full	H_2O	H_2O	H_2O	H_2O
• Position	Breeding)	Midplane	Midplane	Midplane	Midplane
TBR	1.112	1.050	1.104	1.115	1.141
B) Li_2O/He					
Inbd. Blanket (cm)	56.8	56.8	56.8	56.8	56.8
Outbd. Blanket (cm)	47.8	47.8	47.8	47.8	47.8
Limiter					
• Type	None	STARFIRE	STARFIRE	STARFIRE	STARFIRE
• Coolant	(Full	He	H_2O	He	H_2O
• Position	Breeding)	Midplane	Midplane	Bottom	Bottom
TBR	1.186	1.141	1.088	1.144	1.109
C) Li/Li					
Inbd. Blanket (cm)	28.1	28.1	28.1	28.1	
Outbd. Blanket (cm)	48.1	48.1	48.1	48.1	
Outbd. Reflector (cm)	20.7	20.7	20.7	20.7	
Limiter					
• Type	None	STARFIRE	STARFIRE	STARFIRE	FED/INTOR[c]
• Coolant	Full	Li	H_2O	H_2O	Li
• Position	Breeding)	Midplane	Midplane	Bottom	Bottom
TBR	1.235 (1.360)[d]	1.190	1.131	1.157	(1.347)d

[a]Based on MORSE-CG with 10,000 neutron histories; typical deviation $\lesssim \pm 1\%$.
[b]Be/Cu.
[c]Be/V-15Cr-5Ti.
[d]Inboard blanket 40 cm; inboard reflector 20 cm; outboard blanket 60 cm; outboard reflector 30 cm.

The coolant is assumed to be variable in this study. The first two designs are based on the 1982 FED/INTOR Phase 2A study[9] and the third one is based on the STARFIRE design[2].

Several important observations can be made from the results shown in Table 9.8-8. First of all, the effect of the limiter's presence on tritium production is not excessive when the blanket and the limiter possess a close proximity in terms of the material compositions, e.g., the Li_2O/H_2O blanket with the water-cooled limiter. By comparing Case A to Case B one finds the breeding loss for such designs due to the limiter is more or less proportional to the size of limiter opening, which is ~3 to 4% of the total first wall area. Second, the bottom limiter slightly improves the breeding as compared to the midplane limiter design, because the source neutrons are most populated near the outboard midplane of torus due to the MHD plasma shift. Third, the most adverse effect of the limiter on tritium production is caused when the water-cooled limiter is used for the hard spectrum blanket designs such as the Li_2O/He and Li/Li designs. As addressed in Sec. 6.10, this is due to the drastic spectrum softening in the limiter, leading to a substantial neutron loss in the heat sink materials. Lastly, as noticed from comparisons between Cases A and E, the FED/INTOR type limiter design has the least detrimental effect on tritium breeding, particularly if the same coolant is employed both for the blanket and the limiter. Such a result is apparently brought about by the use of the beryllium coating in the limiter system.

9.8.4.3 Nuclear Analysis of the Reference $LiAlO_2/H_2O$/FS/Be Blanket Design

The scoping study presented in the previous sections has led to the reference blanket designs for the TMR and tokamak concepts, as shown in Figs. 9.8-25 and -26. The material compositions assumed in the present analysis are listed in Table 9.8-9. As described in Section 6.10, the analysis for the reference designs has been performed using a continuous-energy Monte Carlo code, MCNP, with the associated ENDF/B-V cross section libraries. The number of neutron histories generated in each case is 10,000. The tokamak reactor model used is shown in Fig. 9.8-27 after the STARFIRE design[2]. The limiter is modeled based on the FED/INTOR study[9], i.e., a bottom limiter constructed of Cu-2Be heat sink, H_2O coolant and 1 cm of beryllium coating.

TANDEM MIRROR/ TMRANL4/γ-$LiAlO_2$-H_2O-HT9-Be

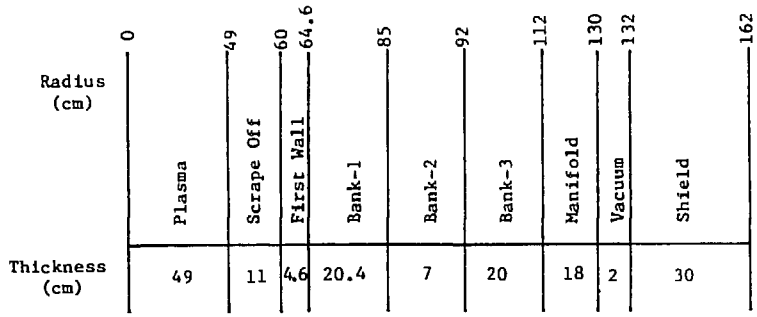

Material Compositions (vol-%)

	HT9	H_2O	γ-$LiAlO_2$*	Be**
First Wall	22	8	---	---
Bank-1	19.5	21.5	5(4.35)	45(39.15)
Bank-2	12.5	11.5	70(60.9)	---
Bank-3	7	4	84(73.08)	---
Manifold	33	67	---	---
Shield	80 (Fe1422)	20		

*γ-$LiAlO_2$ density = 87% of T.D.; ^6Li enrichment = 90%.

**Be density = 87% of T.D.

Fig. 9.8-25. System description of the TMR γ-$LiAlO_2$/H_2O/HT-9/Be design

TOKAMAK/TOKANL4/γ-$LiAlO_2$-H_2O-HT9-Be (H_2O/Cu-2Be Limiter)

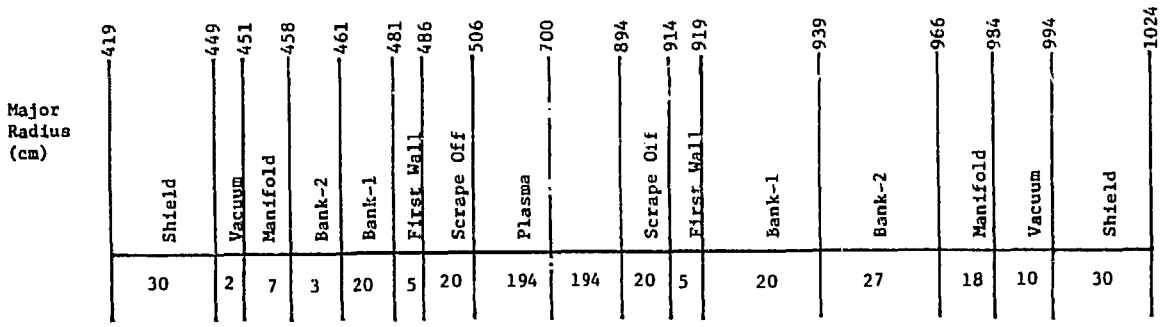

Material Compositions (vol-%)

	Inboard				Outboard			
	HT9	H_2O	γ-$LiAlO_2$*	Be**	HT9	H_2O	γ-$LiAlO_2$*	Be**
First Wall	32	7	---	---	32	7	---	---
Bank-1	19.5	21.5	5(4.35)	45(39.15)	19.5	21.5	5(4.35)	45(39.15)
Bank-2	12.5	11.5	70(60.9)	---	8.5	6.0	80(70.04)	---
Manifold	33	67	---	---	33	67	---	---
Shield	80 (Fel422)	20			80 (Fel422)	20 (H_2O)		

*γ-$LiAlO_2$ density = 87% of T.D.; ^6Li enrichment = 90%.

**Be density = 8% of T.D.

Fig. 9.8-26. System description of the tokamak design

TABLE 9.8-9. MATERIAL COMPOSITIONS

Material @ 100% T.D.	Element	Atom/b-cm
γ-$LiAlO_2$ (90% ^6Li enrichment)	^6Li	2.098-2
	^7Li	2.311-3
	Al	2.331-2
	O	4.661-2
HT-9	Fe	7.058-2
	Cr	1.070-2
	Mo	4.833-4
Fe1422	Fe	7.028-2
	Mn	1.219-2
	Cr	1.849-3
	Ni	1.581-3
Cu-2Be	Cu	7.639-2
	Be	1.099-2
H_2O	H	6.686-2
	O	3.348-2
Beryllium	Be	1.236-1

Tables 9.8-10 and 9.8-11 summarize the resulting nuclear performance in these reference systems, and Fig. 9.8-28 shows the nuclear heating rates throughout the reference design blanket. The TBR of 1.26 obtained for the TMR design before adjustment is close to that from the 1-D scoping study (see Fig. 9.8-23 or -24). In fact, the 1-D ANISN (ENDF/B-IV) calculation for the reference system yields a TBR (T_6 + 0.85 T_7) of 1.28, which favorably compares to the MCNP result within the statistical error of ~ ±1%. Note that the MCNP calculation accounts for neutron leakage through the end cells, which is estimated to be 0.011/DT (within ±9.5%) in the present case. The blanket energy deposition of 18.3 MeV estimated by MCNP is the second highest among the nine R=1 TMR designs investigated (see Table 6.10-5 in Sec. 6.10). This stems from the combination of the large neutron multiplication by beryllium (~0.54/DT) and the very strong spectrum softening due to the water coolant. The favorable blanket performance is also evident from the trivial neutron

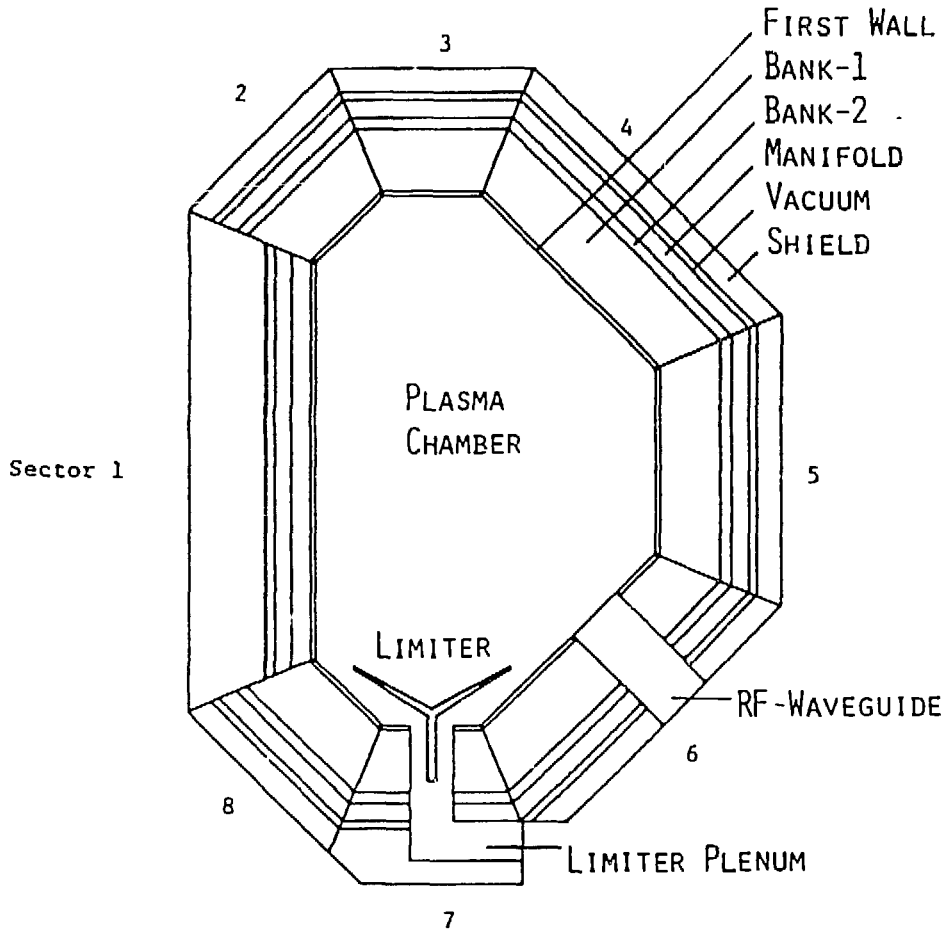

Fig. 9.8-27. A vertical cross-section of tokamak design

TABLE 9.8-10. NUCLEAR PERFORMANCE[a] OF THE REFERENCE TMR γ-$LiAlO_2/H_2O$ BLANKET DESIGN

Region	Tritium Breeding Ratio		Energy Deposition (MeV/DT)	
First Wall	---		1.59	(±1.3%)
Bank - 1	0.969	(±1.1%)	12.97	(±0.8%)
Bank - 2	0.166	(±2.6%)	1.69	(±2.0%)
Bank - 3	0.120	(±2.8%)	1.57	(±2.6%)
Manifold	---		0.43	(±5.5%)
Shield	---		0.10	(±11%)
Total	1.255	(±1.1%)	18.35	(±0.8%)
T_6	1.253	(±1.1%)		
T_7	0.002	(±1.1%)		
$(T_6 + T_7)$[b]	1.217	(±1.1%)		

[a]Based on MCNP/ENDF/B-V with 10,000 neutron histories.

[b]-3% adjustment for end cell fusion and neutron losses in choke coils and for start-up heating penetration.

leakage into the shield. For example, the shield energy deposition of ~0.1 MeV/DT for this design compares to 2.0 MeV/DT for the extremely "leaky" helium-cooled γ-$LiAlO_2$ design shown in Table 6.10-5.

The relatively low TBR of 1.16 for the reference tokamak design is due to the limiter and rf waveguide penetrations, predominantly the former. As shown in Table 9.8-11, most of the breeding loss relative to the full breeding coverage case takes place in the bottom Sector 7 where the limiter resides, and the two adjacent Sectors 6 and 8. However, the breeding loss is not excessive and is more or less proportional to the limiter/rf opening size at the first wall (~4%). As far as the full breeding ratio is concerned, the previous scoping study again indicates good agreement to the present result (TBR ~1.21). In spite of the sizeable blanket penetrations of limiter and rf

TABLE 9.8-11. NUCLEAR PERFORMANCE[a] OF THE REFERENCE TOKAMAK γ-$LiAlO_2/H_2O$ BLANKET DESIGN

Region	TBR, Full Breeding		TBR With Limiter/rf		Energy Deposition, MeV/DT	
First Wall	---		---		2.18	(±3.8%)
Bank-1	0.982	(±1.1%)	0.948	(±1.1%)	12.01	(±2.9%)
Bank-2	0.227	(±2.4%)	0.211	(±2.5%)	2.45	(±5.6%)
Manifold	---		---		0.44	(±12.5%)
Shield	---		---		0.33	(±7.2%)
RF-Waveguide	---		---		0.18	(±9.6%)
Limiter	---		---		1.07	(±3.4%)
Sector-1	0.189	(±3.0%)	0.186	(±3.1%)	2.80	(±2.5%)[b]
Sector-2	0.059	(±6.1%)	0.052	(±6.0%)	0.77	(±5.2%)[b]
Sector-3	0.069	(±5.2%)	0.078	(±5.2%)	1.14	(±4.5%)[b]
Sector-4	0.262	(±2.7%)	0.270	(±2.6%)	4.08	(±2.2%)[b]
Sector-5	0.249	(±2.9%)	0.265	(±2.8%)	3.93	(±2.3%)[b]
Sector-6	0.257	(±2.7%)	0.239	(±2.8%)	3.52	(±2.4%)[b]
Sector-7	0.073	(±5.4%)	0.028	(±8.1%)	0.31	(±7.4%)[b]
Sector-8	0.052	(±6.1%)	0.040	(±6.7%)	0.52	(±6.3%)[b]
Total	1.209	(±1.1%)	1.159	(±1.1%)	18.66	(±0.8%)
T_6	1.207	(±1.1%)	1.158	(±1.1%)		
T_7	0.0017	(±1.1%)	0.0016	(±1.2%)		

[a]Based on MCNP/ENDF/B-V with 10,000 neutron histories.

[b]Limiter, rf openings and shield not included.

waveguides, the reference system maintains about the same amount of net neutron multiplication (a multiplication factor of ~1.60) as that for the full breeding coverage case (~1.61) because of the beryllium coating on the limiter. The implication is that an increased fraction of neutrons is lost in the limiter materials, particularly in the Cu-2Be heat-sink material. As a result, the overall energy performance of the tokamak design is as good as or even better than the TMR design case. As for the TMR design, the blanket energy deposition of 18.3 MeV/DT for the tokamak design is the second largest among the seven R=1 designs studied.

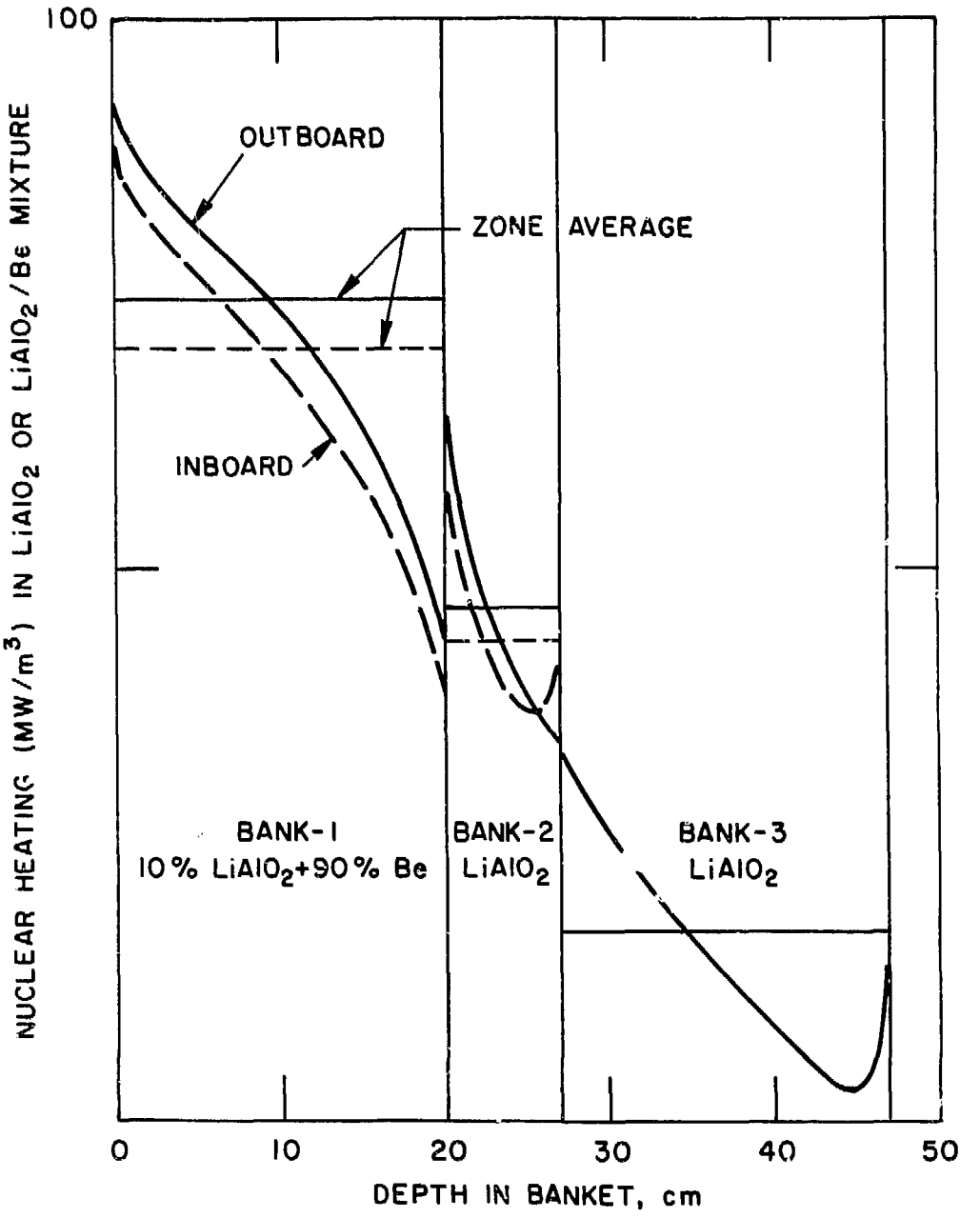

Fig. 9.8-28. Nuclear heating in $LiAlO_2/H_2O$/FS/Be reference design blanket

REFERENCES - CHAPTER 9

1. M. A. Abdou et al., "Blanket Comparison and Selection Study," report ANL/FPP-83-1 (Vols. I and II), Argonne National Laboratory (October 1983).

2. C. C. Baker et al., "STARFIRE - A Commercial Tokamak Fusion Power Plant Study," report ANL/FPP-80-1, Argonne National Laboratory (September 1980).

3. M. A. Abdou et al., "A Demonstration Tokamak Power Plant Study (DEMO)," report ANL/FPP/82-1, Argonne National Laboratory (September 1982).

4. "Mirror Advanced Reactor Study Final Design Report," report UCRL-53480, Lawrence Livermore National Laboratory (July 1984).

5. J. S. Herring et al., "The Consequences of a Tube Rupture in a Fusion Breeder Reactor," EG&G Idaho, presented at 1982 Annual Meeting of the American Institute of Chemical Engineers (November 1982).

6. J. J. Henry, "Thermal Contact Resistance," A.E.C. report No. MIT-2079-2, U.S. Atomic Energy Commission (June 1964).

7. Private communication, R. L. Heestand (ORNL) to G. D. Morgan (McDonnell Douglas Corporation), November 1983.

8. C.C. Stone et al., "Experience With Liquid-Metal Fast Breeder Reactor Steam Generators - U.S. Design," Nuclear Technology 55, pp. 60-87 (October 1981).

9. W. Stacey et al., "U.S. FED-INTOR Critical Issues," report U.S.A. FED-INTOR/82-1, Georgia Institute of Technology (1982).

10. B. Misra, R. G. Clemmer, and D. L. Smith, "An Assessment of Critical Thermal-Hydraulic Problems in a Deuterium-Tritium Solid Breeder Blanket," Nuclear Technology/Fusion, 4, No. 2, Part 1 (1983).

11. R. B. Fitts and F. L. Miller, "A Comparison of Sphere-Pak and Pellet $(U,Pu)O_2$ Fuel Pins in Low-Burnup Instrumented Irradiation Tests," Nuclear Technology, 21, p. 26 (1974).

12. A. M. Ross and R. L. Stoute, "Heat Transfer Coefficient Between UO_2 and Zircaloy-2," Report No. AECL-1552, Atomic Energy of Canada (1962).

13. R. G. Clemmer, et al., "The TRIO Experiment," ANL-84-55, Argonne National Laboratory (1984).

14. "Seismic Requirements for Design of Nuclear Power Plants and Test Facilities," RDT Standard F9-2T, Division of Reactor Research and Development, U.S. A.E.C. (January 1974).

BLANKET COMPARISON AND SELECTION STUDY

CHAPTER 10 - MOLTEN SALT COOLED BLANKET CONCEPTS

10. MOLTEN SALT COOLED BLANKET CONCEPTS

TABLE OF CONTENTS

LIST OF FIGURES FOR CHAPTER 10

LIST OF TABLES FOR CHAPTER 10

10. MOLTEN SALT COOLED BLANKET CONCEPTS

10.1 Introduction

Two characteristics of blanket coolants that are highly desirable in a fusion reactor are the ability to operate at low pressure with high temperature and a high heat transfer coefficient. These characteristics are best met by molten salt coolants. For these two reasons, molten salt coolants emerged from the BCSS Alternate Concepts task performed in FY'83 for consideration as a principal blanket coolant with liquid metals, helium and water. Specifically, we considered the family of nitrate and nitrate/nitrite salts. This coolant allows good tritium breeding and high energy multiplication, is relatively non-corrosive, has a low cost heat transport system and assists in tritium containment. The many desirable features of molten salt coolants are mitigated by some undesirable features (most notable is a very high level of induced radioactivity) and by several uncertainties that cannot be resolved without experiments. In this section, we will present the advantages, disadvantages and uncertainties associated with molten salt coolants as well as specific design concepts applicable to tokamaks and tandem mirrors.

We chose to select one generic blanket type and specify the salt composition without a detailed study of alternatives. This was done to complete a design that could be evaluated against other blanket concepts. As much as possible, we will discuss the generic properties of salt cooled blankets. However, the specific designs that were implemented are those which have been evaluated. Other design concepts may rank better or worse than our initial concept selection.

The salt selected was an equimolar mixture of $NaNO_3$ and KNO_3 known as draw salt. The reasons for its selection are the data base established from its use in the Solar Program, its high temperature stability and the hope that thermal stability would also result in radiation stability. The fact that nitrate salts have a higher melting point than nitrate/nitrite mixtures was deemed a small penalty when compared to their higher temperature limits. Most other characteristics are essentially the same for these types of salts.

Preliminary analyses were performed for several breeder and structural materials and a "best" concept selected. These analyses were far from

complete and should be revisited in future studies. Molten salt coolants are compatible with both austenitic and ferritic steel structural materials. We selected ferritic steel (typically HT-9) because of its increased radiation resistance. In addition, if molten salts were used with a lithium lead breeder or with a liquid lead multiplier, ferritic steels would be preferred for increased corrosion resistance to the liquid metal. Molten salts, because they are highly oxidizing, are believed to be incompatible with vanadium and vanadium-based alloys.

Several breeders were investigated. These were 17Li-83Pb, Li_2O and $LiAlO_2$ with lead and beryllium multipliers. We selected $LiAlO_2$ with a beryllium multiplier because of its good performance and relatively simple design. Also, we were encouraged by initial tests performed at LLNL that showed minimal reactions between draw salt and a beryllium wire at 500°C[1]. The designs with a 17Li-83Pb breeder also looked attractive and had good performance characteristics. They were not pursued because of a concern about 17Li-83Pb compatibility with the salt. Scoping tests have been performed at HEDL [2]. The results of these tests show that there is a moderate energy release rate and that the reaction is more vigorous when there is excess 17Li-83Pb. We believe that no overall conclusion can be reached from these first tests; however, the reaction is less vigorous than sodium and water. If additional experiments and analysis shows that the draw salt/17Li-83Pb combination is acceptable from a safety point of view, than designs of this type are expected to be slightly better than the $LiAlO_2$/Be/HT-9 design. The HEDL experiment is discussed in more detail in Section 5. Use of Li_2O without a separate multiplier proved to be a marginal breeder and is not recommended. A lead multiplier is less desirable than beryllium based on engineering and economics but does result in a feasible design. It could be pursued if beryllium is eliminated from consideration for any reason.

In summary, we have selected a concept that uses a nitrate salt (draw salt) coolant, HT-9 ferritic steel structure, a beryllium multiplier and an enriched $LiAlO_2$ breeder. The specific designs for tokamak and mirror reactors are presented in Section 10.4. The summary of the ranking of these concepts is discussed in Section 10.2. Major issues associated with molten salt coolants are presented in Section 10.3. Discussions of concepts with other breeders and configurations are given in Sections 10.6 and 10.7. Finally, a

recommended research program for salt-cooled blankets is presented in Section 10.8.

10.2 Evaluation of Salt-Cooled Blankets

The nitrate salt-cooled blanket was found to be the top ranked blanket in economics and the second ranked blanket in engineering feasibility. However, this blanket ranked last in both safety and R&D requirements. The reasons for these rankings will be briefly discussed.

Good economic performance is an inherent feature of the salt-cooled blanket. This occurs because the combination of blanket inlet and outlet temperatures, no intermediate coolant loop, low pumping power and low pressure make the heat transport system relatively inexpensive and efficient. In addition, the use of beryllium combined with the coolant as a neutron moderator results in a thin blanket and shield. The designs have a moderately high value of energy multiplication which allows a reduction in the fusion power. For the tandem mirror, the efficient, low cost heat transport system and the energy multiplication are the drivers for low cost of electricity. For the tokamak, the relative thinness of the blanket and shield is an additional key factor. The tokamak economics could be further improved by thinning the inboard blanket while thickening the top, bottom and outboard areas. The excellent economics is expected to occur in salt-cooled blankets with other breeders.

The engineering feasibility evaluation of this blanket had both good and bad points. The score was helped by excellent tritium breeding, low pressure and the ability to handle operation at various power levels. Areas where the blanket scored low were use of beryllium resources, need for multiple pressure boundaries and welds, multiple regions, and difficulty in cleaning up a coolant spill. In retrospect, the value of low pressure may not have received sufficient weight in the scoring. The salt-cooled design ranked second among the seven tokamak concepts. It was significantly below lithium/vanadium but significantly above all of the other concepts. Among the nine TMR designs, the salt blanket ranked first. However, seven of the designs were closely grouped near the top with the differences less than the precision of the method. The use of salt cooling with a liquid breeder would raise the engineering feasibility score by simplifying the mechanical configuration.

One generic characteristic of nitrate salt coolants caused the design to be poorly ranked in safety. This is the very high induced activation in the coolant that affects many of the safety indices. Sodium-22 is produced by 14 MeV neutrons and sodium-24 by thermal neutrons. The half-lives of 2.6 years and 15 hours together with the penetrating gamma radiation emitted by these isotopes makes the primary loop extremely hazardous. The creation of gaseous radioactivity, argon from potassium and carbon from nitrogen, compounds these problems. The safety methodology properly gives a high weighting to radioactive source terms and effluent control. Thus, with this type of methodology, the low ranking is generic to this coolant class and independent of the specific design. If a full probabilistic risk assessment were performed for a safety ranking, one might reach a different conclusion. However, such an analysis must be based on much more detailed designs and on test data. We do not believe that molten salt-cooled blankets would result in unsafe reactors. They would result in reactors that have a high radioactive inventory. Release of this inventory can be made improbable by design. However, the stigma of high source terms is inherent and must be both accepted and mitigated for these blankets to be carried further. In summary, based on the best evaluation that can be performed today, the molten salt cooled blankets rank last in safety for both the tokamak and TMR. Their scores are significantly below those of all other blankets except the water-cooled designs.

The salt-cooled blankets require relatively more R&D than the other designs for two reasons. First, molten salt coolants have received less attention in the past than the other coolants being considered. Thus, there has been less breadth and depth in design and little or no data generated. The data that is available is from the solar program and does not include nuclear radiation and fusion relevant materials. Second, the design concept selected uses beryllium, $LiAlO_2$ and HT-9 as well as the coolant. Each of these materials has its own set of R&D needs. Thus, we must address the individual data needs of each of four primary materials and possible interactions among the materials. An example of the latter is compatibility between the coolant and beryllium in the sphere-pac breeder in the event of a coolant tube failure.

10.3 Major Issues

There are several major issues associated with the nitrate salt coolant and with the design concept that must be resolved by future experiments. These issues are briefly enumerated below. General issues related only to HT-9, $LiAlO_2$ or beryllium are not included in this section.

1. Salt Stability

   The thermal stability of the salt is relatively well understood from the Solar Program. There is effectively a total void in our understanding of salt stability in the blanket radiation environment. Clearly, the combined effects of temperature and radiation are unknown. If radiation causes excessive decomposition of the salt or results in the operating temperature limit being reduced significantly, the concept could be disqualified. Additionally, if large chemical reprocessing facilities are required to reconvert alkali and gas formed by radiolytic decomposition back to the original constituency, then this is a significant economic and practical disadvantage. Two experiments have been performed with conflicting results. The first experiment was at ORNL prior to 1960 [3]. This was indirectly reported but showed that the irradiated samples were rendered more hygroscopic by radiation and underwent some breakdown yielding, in part, gaseous decomposition products. More recently, experiments were conducted at ANL to investigate the radiolytic stability of salts to gamma radiation [4,5]. They were exposed to 8 x 10^8 rads of ^{60}Co radiation while being heated to above 530°C. No radiolytic decomposition was observed but thermal decomposition was found above 530°C.

2. Activation Product Control

   In Section 10.2, we discussed the effect of high coolant activity on the safety evaluation. The key issue is activation product control and safe removal of gaseous products, A and CO_2, from the system. Emission control appears feasible at an acceptable cost. This would be performed in a slip stream in conjunction with tritium removal. Vacuum degassing is the preferred technique. However, if the generation rate of gaseous radioactive products is significantly

higher than expected, then the costs of chemical reprocessing may become prohibitive.

3. Tritium Control

The salts are expected to rapidly oxidize T_2 to T_2O for easy containment. The kinetics of oxidation are not sufficiently well known to validate this assertion. Additionally, the removal of T_2O from the salt by vacuum degassing must be validated. Based on the very limited data available, these salts appear to be excellent from the points of view of both tritium containment and inventory.

4. Voltage Enhanced Corrosion

The salts are somewhat conducting and, when moved through a magnetic field, will generate a voltage which can cause disassociation of the salt. Increasng the ionic content of the salt will increase the corrosion of the structure. We presently estimate that a flow velocity of 6 m/s in a 1 cm channel would not cause corrosion enhancement. This restriction is not severe and indicates that there is no problem. However, this is based primarily on data for fluoride salts which itself is sparse. Thus, there is an issue that the effects are worse and that restrictions on flow channel size and flow velocity would ensue.

5. Chemical Compatibility

The chemical compatibility of molten salts with candidate blanket materials in the forms that they would be used is an uncertainty. For the specific designs implemented, compatibility of the salt with beryllium powder in the sphere-pac is the only issue. As discussed earlier, compatibility with 17Li-83Pb is not yet resolved.

10.4 Lithium Aluminate, Nitrate Salt, Beryllium Blanket Concepts

10.4.1 Overview

This section describes the nitrate salt-cooled tokamak and tandem mirror blanket designs developed in this study. The major goals of this effort were to develop a feasible design and to optimize performance in key areas. Most

of the design optimization work, which is by no means complete, was done to maximize tritium breeding and energy multiplication, and to simplify the mechanical design. The resulting design appears to serve its major purposes of pointing out the issues and R&D needs with nitrate salt cooling and providing a representative design for comparative evaluation. Performance parameters for the designs are given in Table 10-1.

TABLE 10-1. NITRATE SALT COOLED BLANKET PERFORMANCE PARAMETERS

	Tokamak	Tandem Mirror
Tritium Breeding Ratio*	1.24	1.29
Energy Multiplication*	1.323	1.316
Coolant Inlet/Outlet (^{o}C)	330/405	375/450
Coolant Pressure (MPa)	0.4	0.4
Pumping Power (%)	0.2	0.2
Gross Thermal Cycle Efficiency	.375	.40
Blanket/Shield Thickness (cm)	111	110

*From 3-D Neutronics.

Results of the mechanical design, neutronics analysis, heat transfer and thermalhydraulics analyses, and the design issues are discussed below.

10.4.2 Mechanical Design

Tokamak Pod Configuration

A pod concept was chosen for the tokamak blanket to contain the pressure with the minimum amount of structure, and to reduce thermal and swelling stresses (see Fig. 10-1). Although the operating pressure is low (4 atm), confining it with a flat plate or composite flat plate first wall would require additional structure. The pod configuration will also tolerate higher pressures (over 3.2 MPa or 8 times the operating pressure at end-of-life

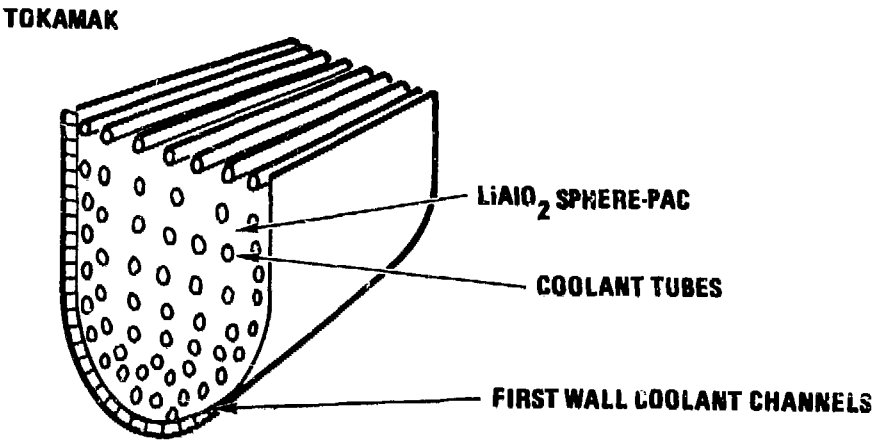

Figure 10-1. Nitrate Salt Cooled Tokamak Blanket Pod

allowable stress) during off-normal conditions. Hoop stress during normal operation is 12.5 MPa. In choosing the pod over the flat plate, we have in effect traded more void space (the space lost around the pod noses) for less structure. The choice was made as a judgment; a more rigorous study would compare neutronics performance and analyze off-normal pressure conditions. However, the breeding is sufficiently high to accommodate this void space.

Tandem Mirror Blanket Containment and First Wall

The tandem mirror blanket has a composite cylindrical first wall loaded in compression, to contain the sphere-pac breeder and multiplier and the helium purge gas. The first wall is connected to the back of the blanket at the module ends by semi-eliptical toroidal end caps (see Fig.10-2). The composite structure of the first wall (Fig.10-3) increases the moment of inertia, and thus the buckling strength of the first wall. Buckling analysis indicates that the first wall is not near the critical stress value (first wall hoop stress is 60 MPa); however, buckling under irradiation creep is not a well-characterized phenomena. No sacrificial erosion layer is required for the TM first wall.

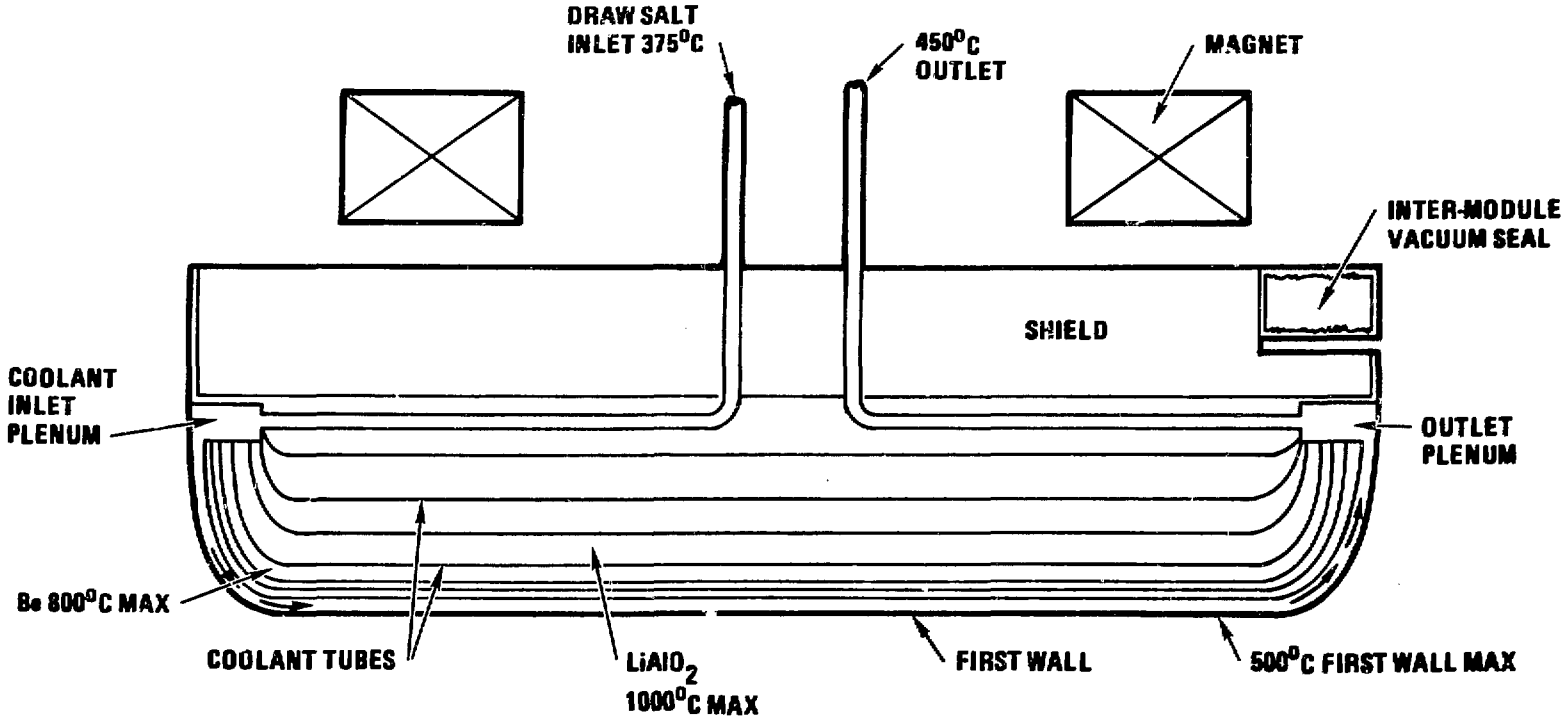

Figure 10-2. Nitrate Salt Cooled Tandem Mirror Blanket

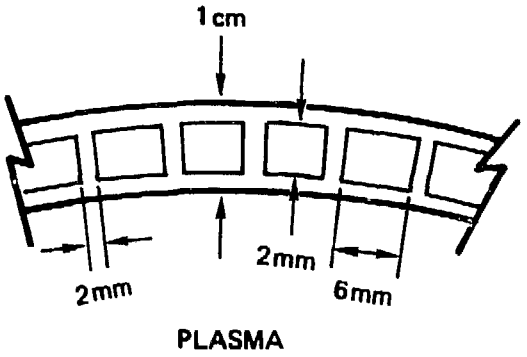

Figure 10-3. Tandem Mirror First Wall Concept

Coolant Tubes

The nitrate salt is contained in tubes because it is parasitic neutronically, and to minimize MHD-induced voltage which can cause decomposition and voltage-enhanced corrosion. Designs with the solid breeder and beryllium in tubes with nitrate salt circulation on the outside were briefly considered. The tubes must be spaced so that the salt can flow between them, resulting in a 15-20% minimum nitrate salt fraction in the blanket. This higher salt fraction significantly reduces tritium breeding potential. Spacing the tubes one to two millimeters apart results in difficult support and flow problems because a small relative deflection of a tube may cause a flow imbalance, leading to hot spots.

As was discussed, a voltage is induced across a channel filled with flowing salt in a magnetic field. The magnitude of the voltage is proportional to the velocity and the channel width. Tubes provide small channels and therefore allow higher velocities (and thus better cooling) for a given voltage limit. One volt is expected across a 1 cm tube at a velocity of 6 m/s. This is believed to be sufficiently low to avoid voltage enhanced corrosion.

Flow in the tokamak pods is axial from one end to the other for design simplicity. Thermal hydraulics considerations result in desirable cooling tube lengths of approximately 6 meters, or 2 pod lengths. Tubes could be routed back and forth within the pods to achieve this length; however,

temperature control and manufacturing simplicity suggest that axial flow through two adjacent pods in series is a better design choice.

The tandem mirror coolant tube are routed similarly to the tokamak coolant tubes; but the 6.32 m tandem mirror module length does not require that the coolant pass through more than one module as it must in the ~ 3 m tokamak pods.

The primary support for the cooling tubes within the blankets is expected to come from the sphere-pac solid breeder itself. This may present problems if settling and/or sintering occurs. Supporting the tubes with conventional tube sheets is difficult because of the very high temperatures (~ 1000°C) occurring in the solid breeder between tubes. If further support is needed, it may be feasible to cool a tube support structure by internal conduction if it is insulated from the solid breeder. Adequate tube support is a potential problem in this design. Hoop stress in the tubes from the 4 atm maximum coolant pressure is negligible at 2 MPa.

Two independent coolant loops are provided by manifolding and crossing over tubes at the back of the blanket such that alternate tubes are supplied by one coolant loop. This allows removal of afterheat in the event of failure of one of the loops. One of the loops also includes the first wall, and the pod wall cooling in the case of the tokamak. Figure 10-4 indicates schematically how the tubing is arranged.

Tokamak First Wall

The first wall and pod sidewalls require active cooling. This is accomplished by making one side and the first wall of each pod a coolant panel, as indicated in Fig. 10-1. Flow is axial as it is for the cooling tubes. The major drawback of this approach is the complexity in venting the coolant channels at the module ends. Orificing of the first wall and sidewall coolant channels, as well as for the tubes, is required for temperature control.

The composite first wall structure is shown in Fig. 10-5. The 5 mm sacrificial erosion layer is grooved to reduce thermal stresses. A two-millimeter minimum wall thickness was chosen to simplify handling and manufacturing, not because of stress limitations. The first wall hoop stress with the pod at the 4 atm coolant pressure is 12.5 MPa.

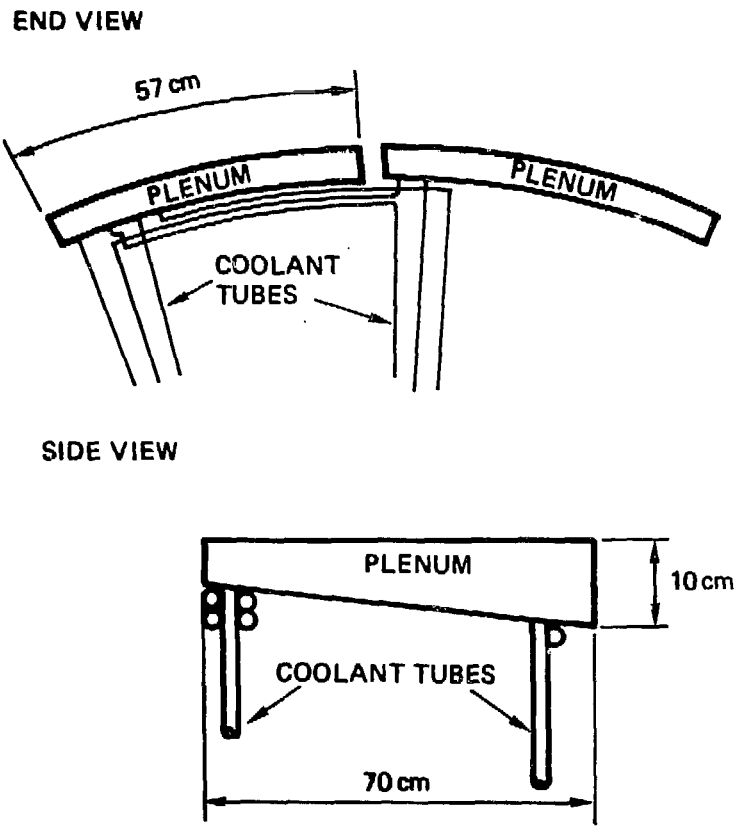

Figure 10-4. Dual Coolant Loop Schematic

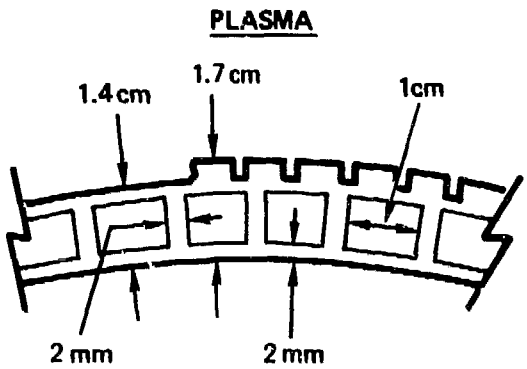

Figure 10-5. Nitrate Salt Cooled Tokamak First Wall

Tritium Purge System

The tritium purge system consists of an inlet plenum at the front and an outlet plenum at the back of the blanket which supply the sphere-pac bed with a 1 cm/s flow of helium. The pressure drop through the bed is 0.9 atm. Purge flow and tritium removal characteristics are discussed in Section 10.4.5. The plena consist of 300 mesh screens held about 1 cm away from the first wall and back wall of the blanket (see Fig. 10-6). Tungsten screen may be required for the first wall plenum because of hot spots. Double screens may be prudent to prevent the sphere-pac from entering a plenum in the event of a tear. Flowing the purge directly through the sphere pac results in minimum structure and maximum design simplicity.

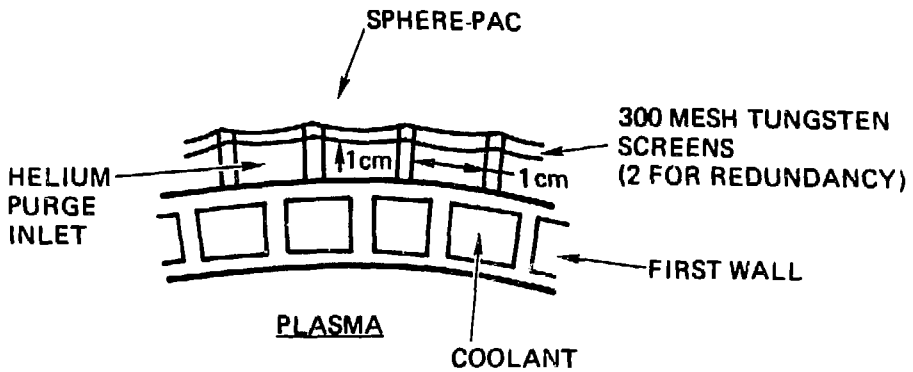

Figure 10-6. Tritium Purge Inlet Plenum

Blanket Supports

A vacuum gap between the blanket and water-cooled shield is required for tritium control. Supports for the blanket in this region require some mobility to take up differences in thermal expansion without stressing and distorting the blanket. No work has been done on blanket supports, but radiation damage is low at the back of the blanket and analogous problems have been solved with present day technology in other blanket designs.

10.4.3 Neutronics

Simple 1-D neutronics calculations were performed and used iteratively with the thermal hydraulics analysis to arrive at a first approximation for tritium breeding and heat generation in a tandem mirror blanket. Although TART [6] was employed as the primary neutronics tool, comparative results were generated with ANISN [7]. A discrepancy in heat generation was resolved in favor of the ANISN calculations as TART includes only prompt energy production.

Five homogenized breeding zones were used in the TART calculations. The first two of these contained beryllium. The breeding zones were sandwiched between a 1 cm first wall and a 30 cm shield. The thicknesses of these zones plus their material volume fractions and the local neutronics are presented in Table 10-2. The beryllium and lithium aluminate were considered to be at 70% and 85% of theoretical density. The lithium is 50% enriched in ^{6}Li.

Substantial neutron moderation is obtained in regions 2 and 3 that contain beryllium. This allows for important reductions in the blanket radial dimensions. Further increases in the effective thickness of beryllium will not result in appreciable reductions in blanket dimensions. It is beneficial to allow the beryllium and lithium aluminate to be interspersed to cause more uniform burnup.

Global neutronics results indicated a TBR of around 1.30 for the full coverage tandem mirror blanket. This was modified to 1.29 by three-dimensional calculations. A slight reduction to a TBR of 1.24 for the tokamak occurs because of the necessary increase in the first wall thickness and

TABLE 10-2. LOCAL NEUTRONICS RESULT FOR NS/$LiAlO_2$/Be BLANKET (50% ENRICHED ^6Li)

Zone	Plasma	Void	1	2	3	4	5	6	80% Fe-1422 + 20% H_2O Magnet Shield
Radial Dimension	46	60	61	69	79	91	101	111	141
Volume Fractions: HT-9			.55	.12	.10	.10	.08	.06	
Volume Fractions: Draw salt			.45	.16	.11	.11	.06	.04	
Volume Fractions: Be (70% TD)			-	.53	.58	-	-	-	
Volume Fractions: $LiAlO_2$ (85% TD)			-	.19	.21	.79	.86	.90	
Nuclear Performance: Tritium breeding/n			-	.37	.35	.36	.14	.10	
Nuclear Performance: $\dot{Q}$ (W/cm^3)			-	26.4	13.2	8.6	3.0	1.5	

larger void space. The blanket energy multiplication is 1.323 for the tokamak and 1.316 for the mirror.

10.4.4 Heat Transfer and Thermal Hydraulics

Heat transfer and thermal hydraulics analyses have been performed to determine tube spacing, film drop temperatures, and maximum and minimum temperatures in the breeding material and structure. Heat generation rates averaged over zones were given in Table 10-2. Coolant tube spacing is determined by finding the radius (R_o from Fig. 10-7) corresponding to a 300°C temperature rise from the tube wall in the breeding zones that contain

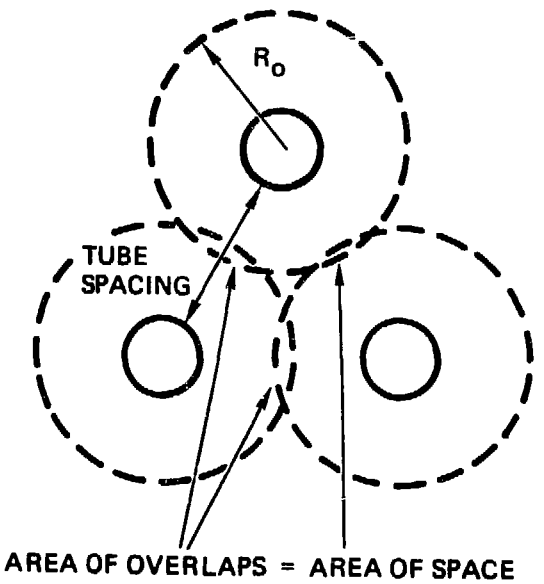

Figure 10-7. Coolant Tube Spacing Model

beryllium. The 300°C temperature rise was chosen for the calculations to keep the maximum temperature in beryllium below 800°C. This results in temperature margins of approximately 75°C in the tokamak and 30°C in the tandem mirror. The 1-D cylindrical conduction equation was solved using constant properties. The distance between tubes is found by assuming that the R_o (or +300°C) boundaries from adjacent tubes would overlap enough so that the total area cooled by each tube equals the area of the circle formed by R_o. This results in small areas that are overcooled where the circles overlap and small areas that are undercooled between the circles. The undercooled areas will be within 20°C of the intended value due to this approximation. A 500°C temperature rise to a maximum 1000°C is allowed in the regions not containing beryllium. This limit is based on $LiAlO_2$ sintering. In these regions there are temperature margins of 75°C and 30°C in the tokamak and mirror, respectively.

Table 10-3 gives the tube spacings and resulting fractions of steel and nitrate salt in the blanket. These are compared with the values used in the neutronics model to find the heat generation rates, and show that the process has converged. Also included is the equivalent surface heat flux on the coolant tubes. The first beryllium containing region has an equivalent 42 W/cm^2 heat flux on the coolant tubes.

TABLE 10-3. COOLANT TUBE SPACING PARAMETERS FOR THE NITRATE SALT COOLED BLANKET

Zone*	R_o, cm	Tube v/o	$\dot{Q}_v$ W/cm^3	q" W/cm^2
2	1.26	22.5	26.4	41.9
3	1.51	16.0	13.2	30.1
4	1.53	16.0	8.6	20.1
5	2.11	9.0	3.0	13.4
6	2.55	5.0	1.5	9.8

*See Table 10-2.

The coolant tubes are routed such that they cool approximately 6 m, axially, of blanket. In the tandem mirror the 6.32 m module length is compatible with the required flow path length, but in the tokamak the coolant is routed in series through to adjacent pods to achieve the 6 m length. Assuming a 6 m length and a maximum coolant velocity of 5 m/s (to reduce the pressure drop and emf voltage) results in a coolant ΔT of 73.4°C. The maximum film drop temperature is 27°C. The pumping power at the operating velocity is approximately 0.2% of the blanket energy which is much lower than is obtained for other coolants.

Maintaining a constant coolant exit temperature while preserving a maximum temperature in the breeding material requires control of the coolant velocity as a function of depth in the blanket. The coolant flow will be slower at increasing depths in the blanket. The radially dependent velocity is shown in Table 10-4. The velocity differences lead to pressure drop variations that must be equalized. Single orifices at the entrance of each coolant tube provide the additional pressure drop needed for equalization. Typical orifice sizes for the 1 cm ID tubes are also listed in Table 10-4. An alternative approach is to orifice both ends of the coolant tube thus increasing the required orifice size.

TABLE 10-4. COOLANT FLOW PARAMETERS FOR THE NITRATE SALT COOLED BLANKET

Zone*	Coolant Velocity, cm/s	Reynolds Number	Film Drop, °C	Pressure Drop, kPa	Orifice Radius, cm
2	500	46100	27.3	290	0.5
3	359	33119	25.8	150	0.32
4	240	22128	24.1	67	0.24
5	159	14700	22.5	29	0.20
6	116	10733	21.4	16	0.16

*See Table 10-2.

10.4.5 Tritium Inventories

Structure

The structural tritium inventory was calculated based on an experimental value of 2.5×10^{-2} moles T_2/cm^3 for hydrogen in steel at 500°C and 3.2×10^{-5} atm partial pressure. Pressure dependence was taken to be proportional to the square root of the HT partial pressure (5.2×10^{-6} atm); a hydrogen (H_2) dilution factor of 35 was assumed. The calculated inventory values are 0.3 g for the tandem mirror and 0.5 g in the tokamak. The difference is a result of the different geometries and reactor sizes.

Coolant

The coolant inventories of 26 g in the tokamak and 14 g in the TM are based on experimental values for water solubility in draw salt (see Section 6). Assuming that these values are applicable to tritium (HTO) at low partial pressures, it is possible to keep the coolant inventory to these levels in the tokamak and tandem mirror coolant loops. This can be accomplished by drying a 500°C, 2% slipstream at 25% efficiency.

Purge Gas

The helium purge gas inventory at 5.2×10^{-6} atm HT partial pressure is approximately .033 g in the TM and 0.036 g in the tokamak, assuming that most of the tritium is in the form of HT. The purge gas volumes have been scaled from the solid breeder volumes for the tandem mirror and tokamak. The purge gas tritium inventories given here are meant to be used as order-of-magnitude values. Temperature variations have been neglected, and the purge gas process loop outside the blanket, which is expected to contain most of the purge gas and tritium, has not been designed.

Solid Breeder

As discussed above for the water-cooled designs, the solid breeder tritium inventory is dependent on the temperature and the presence of 100 wppm of excess hydrogen in the purge stream. The diffusive tritium inventories are 2 kg in the tokamak and 0.25 kg in the tandem mirror blankets as calculated by the method discussed in Section 6. The much lower value in the tandem mirror solid breeder inventory is primarily due to the higher minimum temperature.

Because of the presence of the excess hydrogen, there is minimal tritium inventory in surface adsorption. These inventories are summarized in Table 10-5.

TABLE 10-5. TRITIUM INVENTORIES

	Tandem Mirror (g)	Tokamak (g)
Structure	0.3	0.5
Coolant	14	26
Purge Gas	.033	.036
Solid Breeder	250	2000

To maintain a low tritium partial pressure and inventory, the helium purge stream will flow through the sphere pac from the front wall to the back. The purge stream is necessary because calculations indicate that if just a diffusion mechanism is relied on, substantial partial pressures of tritium would develop and thus lead to high permeation rates of tritium out of the reactor. Diffusion resistance within the sphere-pac particles is included in the inventory calculations discussed above. The mechanism of tritium transport considered here is thus the forced convective flow of the purge stream. Mass balance on a differential segment of the blanket volume can be made, and an equation derived which can be used to estimate steady-state tritium concentrations. This was done, with the additional assumption being made that the geometry can be reasonably modeled with a flat plate configuration (this will overestimate the tritium concentration and thus provide some margin of safety). The concentration of tritium in the blanket is a function of the radial distance from the first wall, and is given by the following equation:

$$C = \frac{Q_v}{2V} [r - r_o] \qquad [10-1]$$

where C is the tritium concentration in g/cm^3, Q_v is the volumetric production rate in g/cm^3-s), V is the linear velocity of the purge stream gas in cm/s, r is the radius of the outer wall in cm and r_o is the radius of the first wall in cm.

The maximum concentration of tritium is achieved at the back wall of the reactor. The tritium partial pressures and tritium permeation rates were calculated for two design cases. A hydrogen dilution factor of 35 is assumed. The values of the parameters used for these calculations are listed in Table 10-6. For the first case, a tandem mirror reactor design at 475°C, the maximum partial pressure of HT which develops is 5.2×10^{-6} atm. The permeation rate at this partial pressure and temperature is 1.0×10^{-10} Ci/cm^2-s. For the second case, a tokamak reactor at 400°C, the maximum concentration of HT which develops is 4.6×10^{-6} atm. The permeation rate at this partial pressure and temperature is 4.2×10^{-10} Ci/cm^2-s. This results in a permeation to the coolant of 200 Ci/day in the tandem mirror and 290 Ci/day in the tokamak blanket based on estimates of the coolant tube surface areas.

TABLE 10-6. PARAMETRIC VALUES FOR TRITIUM PERMEATION

Parameters	Value
r_o	100 cm
r_{max}	150 cm
Q_v	1×10^{-11} g/cm^3-s
V	1 cm/s

The pressure drop of the helium purge stream across the sphere-pac bed, which has a porosity of 0.15, was calculated from the Ergun equation for the two design cases. For the tandem mirror reactor at 475°C and a purge stream velocity of 1 cm/s, the pressure drop is 0.9 atm across a 50 cm bed. For the tokamak reactor the pressure drop is also 0.9 atm. Pumping power is less than 1 MW for the purge system.

The purge inlet pressure is maintained at 4 atm, equal to the coolant pressure. Excess (100 wpm) hydrogen is added for isotopic dilution of the tritium which eliminates the surface inventory on the breeder.

10.4.6 Design Issues

This section discusses issues which are specific to the design or to the analysis methods used. Issues generic to the use of nitrate salts as coolants are discussed in Section 10.4.3 above. The issues considered below apply to both the tokamak and tandem mirror blankets.

Sphere-Pac Settling

As mentioned earlier, the only support for the coolant tubes within the blanket comes from the sphere-pac itself. If significant settling or shrinkage of the sphere-pac occurs it could lead to premature tube failure. Tube sheets or other supports may be difficult to design because of the high (up to 1000°C) temperatures in the solid breeder, and because forces from shifting of the sphere-pac may be large. It may be necessary to separate the sphere-pac into smaller compartments. This will tend to increase the structural fraction and probably the coolant fraction as the added structure will require cooling.

Another problem that will arise if settling of the sphere-pac occurs is temperature control. The sphere-pac will pull away from the lower side of horizontal surfaces, introducing a low conductivity gap. If this occurs, more cooling tubes will be required to keep the solid breeder within temperature limits, thus further increasing the coolant and structure fractions. Small regions where the temperature limits are exceeded may be tolerated with a minor increase in tritium inventory.

Calculations

One-dimensional heat transfer calculations can only give a first order approximation of coolant tube spacing requirements in the actual complex geometry of the blanket. A two-dimensional calculation and optimization would probably result in slightly higher than calculated coolant and structure fractions due to spatially varying heat fluxes and interactions with the containing walls.

Another factor that affects neutronic performance is the degree of heterogeneity in the model used for the neutronics calculations. Blankets with beryllium tend to have soft spectra, and therefore parasitic captures in the coolant and structure can be underestimated with homogeneous models.

The issues mentioned so far all have a potential effect on neutronic performance from increased parasitic capture in the structure and coolant. Increased parasitics in the front zones of the blanket can decrease both the tritium breeding ratio and the energy multiplication since a neutron that may have been multiplied in beryllium is lost. However, most of the neutrons absorbed in the steel and nitrate salt will be low energy, and thus below the threshold of the beryllium (n,2n) reaction. In this case, and in the back of the blanket where no beryllium is present, neutrons captured parasitically will tend to increase energy multiplication at the expense of the tritium breeding ratio. Thus the issues discussed above have the overall effect of reducing the calculated tritium breeding ratio and increasing the energy multiplication factor.

Manufacturing

Manufacturing of the nitrate salt blanket has not been addressed. The pod ends (or module ends in the tandem mirror) consist of two plates connected by (nearly) parallel webs forming cooling channels, with the whole composite curving in three dimensions. Construction and adequate flow control in adjacent cooling channels may be difficult. Other potential manufacturing problems occur at the back of the blanket, where the pods connect with the back of the blanket and the inlet and outlet plena. Changes in material thicknesses may be required in this location, and stress concentrations will occur without careful design and manufacturing. We do not see any potential feasibility issues in this design, but manufacturing difficulties exist and may require design changes.

Coolant Handling/Freezing

Draw salt expands reversibly approximately 4.5% on melting at 222°C. This can cause tubes or other components to burst if the salt were to freeze and remelt, depending on the configuration and the distribution of the melting. Dilution with water to lower the melting point is used for filling and draining nitrate salt systems, but this would complicate tritium control

in a fusion system. Water dilution and flushing can be used for emergencies and at final shutdown. The helium purge system can be used to preheat the blanket and to keep the salt molten during an extended shutdown. Afterheat will cause the draw salt temperature to increase, rather than decrease after a few days or less of operation. Freezing does not appear to pose any major problems, but will be an operating consideration.

10.5 Summary

Based on the conceptual design work and the evaluations performed, nitrate salt cooled, lithium aluminate blankets with beryllium multipliers are excellent in economic performance, engineering feasibility and tritium breeding for both tandem mirror and tokamak reactors. A pod containment design with the coolant in tubes and the lithium aluminate and beryllium in sphere-pac form was chosen for the tokamak to provide structural strength, good heat transfer characteristics, and good tritium breeding. In the tandem mirror, a cylindrical containment was selected to minimize void space with the rest of the blanket and its performance being very similar to the tokamak. A unique approach was taken in the tritium purge system. A plenum immediately behind the first wall supplies helium purge gas directly to the sphere pac. The purge gas flows through the sphere pac at 1 cm/s to an exit plenum at the back of the blanket. This simple design keeps the permeation to an acceptable level, has a low pressure drop and eliminates large amounts of plumbing.

The performance of salt-cooled blankets with other breeders may equal or exceed that of the blanket described in this paper. Of particular interest is 17Li-83Pb breeder if the chemical reaction between the breeder and coolant is deemed acceptable in the event of a tube failure.

The two principal advantages of salt cooling are low pressure and economics. We could not quantify all of the advantages of low pressure in the BCSS. We would expect them to become evident in blanket reliability and safety if the designs were implemented and tested. The properties of molten salt coolants should result in the lowest cost of electricity of any of the blankets studied.

The critical disadvantage of this coolant is the intensely radioactive primary loop. The system will contain large radioactive source terms which have an adverse effect on both the actual and perceived safety of these

blankets. The radioactivity will also constrain reactor operational procedures because the primary loop must be shielded.

There are several uncertainties associated with nitrate salt coolants that must be resolved by experiment. The most important of these is salt stability under irradiation because it affects the feasibility of the concept. Design issues remain which may either improve or detract from performance; these do not appear to be feasibility issues. A substantial experimental program would be needed to resolve these issues and to generate additional design data.

10.6 Concepts Set Aside for Possible Future Consideration

The most promising nitrate salt-cooled blankets, other than the ferritic steel/lithium aluminate/beryllium blankets discussed in this section are: lithium lead, lithium oxide with no multiplier, and ternary oxide with a lead multiplier. Ternary oxides other than lithium aluminate are expected to perform similarly, and the conclusions and recommendations for lithium aluminate are intended to extrapolate to the other ternary ceramics. Ferritic steel appears to offer the most promise as a structural material. Vanadium is incompatible with the heavily oxidizing salt and austenitic steels appear to offer less radiation and corrosion resistance.

As mentioned above, nitrate salt-cooled lithium lead blankets look very promising if the two liquids do not have an unacceptable energy release rate and if the oxidation kinetics of tritium in nitrate salt are favorable. However, they would have the highest level of induced radioactivity of any blanket considered in BCSS. Lithium lead/nitrate salt reactions are currently being studied at HEDL. The preliminary results of this work are not conclusive. Favorable tritium oxidation kinetics in the nitrate salt can be used to overcome the difficult tritium control problems with lithium lead. The very low solubility of tritium in lithium lead results in high tritium partial pressures, and therefore high permeation rates. In a proper nitrate salt-cooled lithium lead design, some tritium would permeate into the coolant where it would oxidize, halting permeation through subsequent boundaries. The kinetics of the oxidation process are presently unknown. Oxidation would have to occur within a few seconds to adequately prevent permeation. Tritium can be removed from the nitrate salt by drying.

Nitrate salt-cooled lithium oxide, with no neutron multiplier, offers a simple solid breeder blanket but has marginal tritium breeding potential. Neutronics scoping studies indicate a TBR between that of helium-cooled lithium oxide, which is discussed in Section 9, and water-cooled lithium oxide, which was rejected because of poor tritium breeding. Since issues generic to lithium oxide and issues generic to nitrate salts are being considered in this study, we feel that the principal R&D requirements for nitrate salt-cooled lithium oxide blankets are being addressed implicitly. If the TBR is found to be sufficient and the outstanding nitrate salt issues are resolved favorably this breeder/coolant combination would warrant further study.

A water-cooled, ternary oxide blanket with a liquid lead multiplier was studied during the first year of BCSS. The concept was eliminated from the study because of difficulties with possible lead freeze up and the necessity of operating within the liquid metal embrittlement temperature range. Draw salt is more promising as a coolant in this regard since the coolant inlet temperature can be kept well above the lead melting point, and possibly above the LME range. Difficulties with freezing and LME during startup, shutdown and off-normal conditions remain. If the beryllium multiplier is eliminated, a lead multiplier would be worth further consideration.

Several alternate mechanical configurations are possible for the lithium aluminate, nitrate salt, beryllium blanket. The concepts explored here were chosen for good performance and in an attempt to illuminate the generic issues. Better concepts probably exist.

10.7 Concepts Judged to be Less Promising or Clearly Inferior

As mentioned above, austenitic steels were considered inferior to ferritic steels because of less resistance to radiation damage and corrosion. Lithium oxide with lead and beryllium multipliers was considered less promising than the ternary ceramic breeders. With the multiplier present, the advantage of higher lithium atom density in lithium oxide for tritium breeding is lost. The ternary ceramics appear to have wider operating temperature windows and less severe problems with burnup chemistry. Lithium zirconate does not appear to offer a better tritium breeding potential than

lithium oxide, and has a lower thermal conductivity. These factors, together with safety problems from zirconium activation, make lithium zirconate an inferior choice.

10.8 Recommended Research

The R&D needs for the nitrate salt are discussed in this section. We have emphasized issues that are unique to this blanket and not those that apply to ferritic steel or $LiAlO_2$ in general.

10.8.1 Excessive Salt Decomposition

As discussed in Section 6, nitrate and nitrate/nitrite salts decompose at high temperatures and may decompose under neutron and gamma irradiation. Some of the decomposition products are insoluble while others are gaseous. Typical reactions are:

$$2\ NaNO_3 \rightarrow 2\ NaNO_2 + O_2$$

$$5\ NaNO_2 \rightarrow 3\ NaNO_3 + Na_2O + N_2$$

Depending on the salt, an appropriate cover gas is used to drive the reactions to the left. Air is the best choice for the cover gas. If excessive decomposition occurs, a large clean-up system may be needed. During a temperature excursion, decomposition may affect safety.

The required data are:

a. Decomposition rates and reactions at temperatures from 400°C to 600°C at 25°C intervals and to 800°C at 50°C intervals.

b. Decomposition rates and reactions in a combined radiation and temperature field at temperatures from 400°C to 550°C and radiation dose rates from 5×10^5 to 5×10^6 rad/s at 25°C intervals and two intermediate radiation dose rates.

c. Tests of decomposition in a temperature excursion from an initial temperature of 450°C at heat input rates from .01 to 1 W/cm^3.

d. The effects, if any, of cover gas pressure on decomposition rates should be investigated and the pressure increase in the gas measured.

There is a reasonable data base on thermal decomposition from the solar and other programs. However, it is incomplete and the data on radiation-induced decomposition is effectively nil.

We recommend near term testing of radiation-induced decomposition. This issue could eliminate nitrate salts from consideration, and small sample experiments could be done quickly and inexpensively and would be adequate to determine if there is a major problem. The next step would be to test combined radiation and temperature effects and to include testing at higher fluxes.

10.8.2 Excessive Chemical Reactivity

Nitrate and nitrite salts are good oxidizing agents. This can result in a high rate of energy release when put in contact with an active reductant. For the specific blanket design, leakage of draw salt into the sphere pac mixture of Be and $LiAlO_2$ powder is the largest concern. Reactions with other potential blanket materials, such as 17Li-83Pb, are also a concern. This is primarily a safety issue.

The following tests are recommended:

a. Tests of NS with powdered Be/$LiAlO_2$ with the NS at 450, 500 and 550°C and the solid at 600 to 800°C. Monitor temperature and pressure response and chemical reaction products.

b. Tests of NS with 17Li-83Pb with the NS at 450, 500 and 500°C and the 17Li-83Pb at 50 to 100°C higher temperature than the NS. Injection of NS into 17Li-83Pb and 17Li-83Pb into NS should both be done to simulate a blanket and an IHX. Same measurements as in a.

c. Screening tests of NS with other blanket materials and material forms. These include Li_2O, other ternary ceramics, Be, graphite, SiC, lead at 500°C.

Much of the currently available data comes from manufacturers and should be validated by well-characterized tests under fusion blanket conditions. Preliminary 17Li-83Pb tests have been run at HEDL. The results showed a moderate reaction and leaves the compatibility in doubt. However, the reaction is milder than that of sodium/water which is considered acceptable.

10.8.3 Excessive Activation Products from NS

The salt will be highly activated in the fusion blanket. The key concern is determining the form of the products and our ability to contain normal emissions. Of particular importance are the gaseous products, argon and CO_2, especially the former.

The data required to resolve this issue are:

a. Validate activation calculations by neutronics experiments on Na, K, N, and O. This can be done on NS, elements or other compounds.

b. Determine chemical form of products. This must be performed with NS and at temperatures from 350°C to 500°C.

c. Develop methods and test gaseous product removal and control. This may be done in conjunction with tritium recovery.

Basic activation cross sections exist and are relatively quite good for these elements. Only a simple validation is needed. Whether carbon forms a gaseous product, CO or CO_2, is unknown. Both CO_2 and carbonates have been predicted. The kinetics are not known. No work has been done on argon or CO/CO_2 removal from NS or on containment.

10.8.4 Tritium Control

Nitrate salts are expected to rapidly oxidize tritium to T_2O to prevent leakage from the system. In addition, the removal of T_2O from NS by vacuum degassing needs to be validated. Of importance are the rates of diffusion to determine slip stream size, pool area and whether additional agitation is required. These data are needed to evaluate the tritium inventory in the primary loop.

The required data are:

a. The oxidation kinetics of tritium in NS should be measured at temperatures from 350 to 550°C at 50°C intervals. Hydrogen can be used in place of tritium with a one-point comparison.

b. Diffusion rates of T_2O in NS at temperatures from 350 to 550°C.

c. Vapor pressure and solubility of T_2O in NS from 350 to 550°C.

d. Development of techniques for T_2O recovery from NS and experimental validation of methods.

The only data that currently exist are for H_2O solubility in NS as a function of temperature and water vapor pressure above the salt. No data exist for tritium.

Oxidation kinetics of tritium is of fundamental importance in the consideration of NS as a blanket coolant. If tritium oxidizes rapidly in NS, excellent tritium control is possible. If oxidation is slow, tritium control with NS may be as difficult as it is with other coolants, and one of the main motivations for using NS is eliminated. We recommend that a high priority be given to the study of the oxidation kinetics of tritium in NS.

10.8.5 Corrosion Effects

The NS is a conducting fluid that when pumped through a magnetic field will develop an induced voltage. This voltage depends on the fluid velocity, field strength and pipe size. The induced voltage causes breakdown of the salt which in turn enhances corrosion of the structure.

The required data are:

a. Salt breakdown as a function of applied potential for voltages between 0.1 and 2 V at temperatures between 350 and 500°C at 50°C intervals. Measurements to be made include ionic content of the salt and chemical form of the salt.

b. Corrosion rates of ferritic steel in a static system and in a forced convection loops at 75 and 150°C ΔTs at T_{OUT} between 400 and 500°C and an applied voltage of between 0.1 and 2V.

c. Validation of induced voltage in NS by flow through a magnet field. Three values of field between 3 and 7 T, 3 values of coolant velocity between 0.5 and 5 m/s, and 3 values of tube diameter between 0.5 and 2 cm should be included in the matrix. These should be performed at temperatures between 350 and 550°C. The size of this test matrix will depend on the importance of voltage enhanced corrosion determined in data need b) above.

At present, there are no data on NS for allowable voltage level or on corrosion with magnetic field effects. Theory exists for estimating the induced voltage. We are using extrapolations based on fluoride salt data in this study to estimate allowable voltage. The data on fluoride salts are quite sparse.

10.8.6 Solid Breeder Temperature Control

The temperature of the breeder sphere pac must be maintained in the proper temperature range for tritium recovery. Because no gaps are required, the key issue becomes the breeder losing contact with the coolant tubes which may cause overheating. Validation of this need requires, at least, a full thermal simulation of a blanket mockup including temperature cycling and long term operation. Simple tests can be done on a single element but these are not conclusive.

The data needed are:

a. Settling and change of thermal properties for a sphere-pac element with a cooling tube.

b. Breeder temperature distribution after multiple thermal cycles with full simulation of temperature and geometry conditions.

No data base currently exists for this issue. Some extrapolations can be made from fission elements.

10.8.7 Beryllium Reprocessing

Beryllium reprocessing (including refabrication) must be low loss (~ 1-2% per recycle) to avoid resource limitations. The reprocessing must also be done remotely because the beryllium will be radioactive. For the particular NS blanket design, this includes separating Be from $LiAlO_2$ microspheres and remanufacturing. Chemical purification may also be needed. Other Be forms such as balls, rods and blocks should also be investigated to help determine the best mechanization of the design concept.

Required data are:

a. Develop and validate methods for remote manufacturing of Be microspheres.

b. Develop and validate methods for remote separation of Be from $LiAlO_2$ microspheres at high efficiency.

c. Develop and validate methods for remote, low loss reprocessing and refabrication of other Be forms that may be used in NS blankets.

There is considerable expertise in remote fabrication in the beryllium industry based on powder metallurgy technology. This is done remotely because of toxicity of BeO. Processes would have to be upgraded for full remote operation because of induced radioactivity. Significant study of reprocessing and refabrication of Be balls was done for the Fusion Breeder Program. To our knowledge, no work has been done on microspheres.

REFERENCES

1. R. MOIR and W. HELM, LLNL, Private Communication, March 1984.

2. S. PIET, EG&G INEL, Private Communication, September 1984.

3. H. W. HOFFMAN, S. I. COHEN, "Fused Salt Heat Transfer Part III: Forced Convection Heat Transfer in Circular Tubes Containing the Salt Mixture $NaNO_2$ - $NaNO_3$ - KNO_3", Oak Ridge National Laboratory, ORNL-2433 (1960).

4. S. R. BREON, N. R. CHELLEW, R. G. CLEMMER, "Gamma Irradiation of Nitrate-Based Salts", Argonne National Laboratory, ANL/FPP/TM-129, (1980).

5. Internal correspondences from PAT FINN to VIC MARONI at Argonne National Laboratory on 07/02/80 and 02/09/83.

6. E. PLECHATY and J. KIMLINGER, "TARTNP: A coupled Neutron-Photon Monte-Carlo Transport Code," LLNL Report UCRL-50400, Vol. 14, (1976).

7. "ANISN-ORNL," RSIC Code Package CCC-254, Radiation Shielding Information Center, Oak Ridge National Laboratory, Oak Ridge, TN, (1979).

DISTRIBUTION FOR ANL/FPP-84-1

Internal:

C. Baker
M. Billone
J. Brooks
Y. Cha
R. Clemmer
D. Diercks
D. Ehst
K. Evans
Y. Gohar
D. Gruen
A. Hassanein
P. Finn
A. Fischer
C. Johnson
J. Jung
R. Leonard
Y. Liu
B. Loomis
S. Majumdar
R. Mattas
B. Misra
B. Picologlou
D. L. Smith
D. K. Sze
S. W. Tam
L. Turner
S. Vogler
S. Yang
FPP Files (53)
ANL Contract File
ANL Libraries
ANL Patent Dept.
TIS Files (6)

External:

DOE-TIC (27)
Manager, Chicago Operations Office, DOE
University of Chicago Special Committee for the Fusion Program:
S. Baron, Burns and Roe, Inc.
H. Forsen, Bechtel Group, Inc.
J. Maniscalco, TRW, Inc.
G. Miley, University of Illinois-Urbana
P. Reardon, Brookhaven National Laboratory
P. Rutherford, Princeton University
D. Steiner, Rensselaer Polytechnic Institute
K. Symon, University of Wisconsin-Madison
K. Thomassen, Lawrence Livermore National Laboratory
S. Abdel-Khalik, University of Wisconsin-Madison
M. A. Abdou, University of California-Los Angeles (6)
J. Anderson, Los Alamos National Laboratory
W. Bauer, Sandia Laboratories
S. Berk, U.S. Department of Energy/Office of Fusion Energy
D. H. Berwald, TRW, Inc.
R. Bourque, GA Technologies Inc.
W. Bjorndahl, TRW, Inc.
G. Carlson, Lawrence Livermore National Laboratory
F. Carre, , CEN-Saclay, FRANCE
G. Casini, Joint Research Centre, Ispra Establishment, ITALY
E. Cheng, GA Technologies Inc.
D. Cohn, Massachusetts Institute of Technology
R. Conn, University of California-Los Angeles
L. Creedon, GA Technologies Inc.
J. Crocker, EG&G Idaho, Inc.
J. W. Davis, McDonnell Douglas Astronautics Company
S. O. Dean, Fusion Power Associates
D. DeFreece, McDonnell Douglas Astronautics Co.
J. DeVan, Oak Ridge National Laboratory
R. Dowling, U.S. Department of Energy/Office of Fusion Energy
T. Drolet, Ontario Hydro, CANADA
C. Flanagan, Fusion Engineering Design Center/Oak Ridge National Laboratory

J. V. Foley, Princeton University
K. Furuta, University of Tokyo, JAPAN
F. Garner, Hanford Engineering Development Laboratory
J. Garner, TRW, Inc.
N. Ghoneim, University of California-Los Angeles
J. D. Gordon, TRW, Inc.
R. A. Gross, Columbia University
R. Hancox, Culham Laboratory
C. Henning, Lawrence Livermore National Laboratory
S. Herring, EG&G Idaho, Inc.
M. Hoffman, Lawrence Livermore National Laboratory
N. Hoffman, Energy Technology Engineering Center
G. Hollenberg, Hanford Engineering Development Laboratory
M. Kazimi, Massachusetts Institute of Technology
I. A. Knobloch, Max-Planck-Institute fur Plasmaphysik, WEST GERMANY
R. Krakowski, Los Alamos National Laboratory
G. Kulcinski, University of Wisconsin-Madison
T. Lechtenberg, GA Technologies Inc.
J. D. Lee, Lawrence Livermore National Laboratory
R. Little, Princeton University
G. Logan, Lawrence Livermore National Laboratory
P. S. Lykoudis, Purdue University
S. Malang, Kernforschungszentrum Karlsruhe, Federal Republic of Germany
R. C. Maninger, Lawrence Livermore National Laboratory
H. Mantz, McDonnell Douglas Astronautics Co.
L. Masson, EG&G Idaho, Inc.
I. Maya, GA Technologies Inc.
C. Maynard, University of Wisconsin-Madison
R. Micich, Grumman Aerospace Corporation
R. Moir, Lawrence Livermore National Laboratory
D. B. Montgomery, Massachusetts Institute of Technology
G. D. Morgan, McDonnell Douglas Astronautics Co.
D. Moyer, Technical Support Services Staff
L. Muhlestein, Hanford Engineering Development Laboratory
G. R. Nardella, U.S. Department of Energy/Office of Fusion Energy
W. S. Neef, Jr., Lawrence Livermore National Laboratory
A. L. Opdenaker, III, U.S. Department of Energy/Office of Fusion Energy
S. Piet, EG&G Idaho, Inc.
T. Reuther, U.S. Department of Energy/Office of Fusion Energy
F. Ribe, University of Washington
M. Rogers, Monsanto Research Corporation
D. Rowe, Rowe and Associates
D. E. Ruester, McDonnell Douglas Astronautics Co.
R. Ryder, GA Technologies Inc.
M. Sawan, University of Wisconsin-Madison
J. Schmidt, Princeton Plasma Physics Laboratory
K. Schultz, GA Technologies Inc.
F. R. Scott, Electric Power Research Institute-Palo Alto
J. Scott, Oak Ridge National Laboratory
T. Shannon, Fusion Engineering Design Center, Oak Ridge National Laboratory
A. E. Sherwood, Lawrence Livermore National Laboratory
K. Shin, University of California-Los Angeles
W. M. Stacey, Jr., Georgia Institute of Technology
W. G. Steele, TRW, Inc.

K. Sumita, Osaka University, JAPAN
I. Sviatoslavsky, University of Wisconsin-Madison
A. Tobin, Grumman Aerospace Corporation
T. Tomabechi, Japan Atomic Energy Research Institute, JAERI
P. Tortorelli, Oak Ridge National Laboratory
C. Trachsel, McDonnell Douglas Astronautics Co.
W. Verbeeck, CEC, Belgium
Prof. Vetter, Kernforschungszentrum Karlsruhe und Verwaltung, GERMANY
G. Vieider, Max-Planck-Institut fur Plasmaphysik, GERMANY
E. Vold, University of California-Los Angeles
L. Waganer, McDonnell Douglas Astronautics Co.
K. Wenzel, Massachusetts Institute of Technology
F. W. Wiffen, Oak Ridge National Laboratory
C. P. C. Wong, GA Technologies Inc.
G. L. Woodruff, University of Washington
L. Yang, GA Technologies Inc.
M. Z. Youssef, University of California-Los Angeles
Bibliothek, Max-Planck-Institute fur Plasmaphysik, WEST GERMANY
C.E.A. Library, Fontenay-aux-Roses, FRANCE
Librarian, Culham Laboratory, ENGLAND
Library Laboratorio Gas Ionizati, ITALY
Thermonuclear Library, Japan Atomic Energy Research Institute, JAPAN